Thesis presented to the University of Oxford

for the Degree of Doctor of Philosophy.

PALAEOCLIMATIC SIGNIFICANCE OF OPEN-MARINE CYCLIC SEQUENCES.

LIBRARY OXFORD
DEPOSITED
16 VII 87

VOLUME 2

GRAHAM PETER WEEDON B.Sc., A.R.S.M.

Linacre College

and Department of Earth Sciences,

Hilary Term, 1987.

CONTENTS OF VOLUME 2 - FIGURES

PAGE

Chapter 1

1.1A Location of the lithostratigraphic units listed in Table 1A. 1
1.2A The nature of cyclic changes in orbital obliquity. 2
1.2B The nature of cyclic changes in orbital eccentricity. 3
1.2C The nature of cyclic changes in orbital precession. 4

Chapter 2

2.1A Map of basal Lias localities. 5
2.1B Field photo of limestone nodule in Lang's bed 36, Lyme Regis. 6
2.1C Field photo of limestone nodules in light marl bed passing laterally into a continuous limestone bed. 6
2.1D Field photo illustrating the different rock types. 7
2.1E Field photo illustrating the different rock types. 7
2.1F Field photo of *Chondrites* burrow-mottles in a light marl and limestone bed. 8
2.1G Field photo of *Diplocraterion* burrow-mottle in a limestone underneath a dark marl bed. 8
2.1H Field photo of burrow-mottling in a dark marl and limestone bed. 9
2.1I Field aspect of the basal Lias at Lyme Regis, Dorset. 9
2.1J Field aspect of the basal Lias at Watchet, Somerset. 10
2.1K Field photo of Palmer's beds C56-C82 near Blue Ben, Watchet. 10
2.1L Field photo of Trueman's beds 9-33, Pre-*planorbis* beds - *planorbis* zone, Lavernock Point, Glamorgan. 11
2.1M Field aspect of the basal Lias at Nash Point, Glamorgan. 12
2.1N Field photo of Trueman's beds 1-7, *conybeari* subzone, *bucklandi* zone, Nash Point. 12
2.1O Field photo of Clement's *et al.*'s beds 17k-23g, *angulata* zone, Long Itchington, Warwickshire. 13
2.2A The Sutton Stone overlying the Carboniferous Limestone at Southerndown, Glamorgan. 14
2.2B Close-up of the Southerndown beds at Southerndown, Glamorgan. 14
2.2C The Brockley Down Stone overlying the Carboniferous Limestone at Lulsgate, Avon. 15
2.2D Loose blocks of Brockley Down Stone at Lulsgate Quarry. 15
2.2E Thin section photomicrograph of limestone. 16
2.2F Thin section photomicrograph of limestone. 16
2.2G Thin section photomicrograph of limestone. 17
2.2H Thin section photomicrograph of limestone. 17
2.2I Thin section photomicrograph of *Gryphaea*. 18
2.2J Thin section photomicrograph of *Gryphaea*. 18
2.2K Thin section photomicrograph of light marl. 19
2.2L Thin section photomicrograph of light marl. 19
2.2M Thin section photomicrograph of dark marl. 20
2.2N Thin section photomicrograph of dark marl. 20

PAGE

2.2O	Thin section photomicrograph of laminated shale.	21
2.2P	Thin section photomicrograph of laminated shale.	21
2.2Q	Thin section photomicrograph of beef calcite.	22
2.2R	Thin section photomicrograph of beef calcite.	22
2.2S	Thin section photomicrograph of laminated limestone.	23
2.2T	Thin section photomicrograph of laminated limestone.	23
2.3A	XRD trace for laminated shale whole-rock powder.	24
2.4A	SEM photomicrograph of limestone.	25
2.4B	SEM photomicrograph of light marl.	25
2.4C	SEM photomicrograph of light marl.	26
2.4D	SEM photomicrograph of dark marl.	26
2.4E	SEM photomicrograph of dark marl.	27
2.4F	SEM photomicrograph of dark marl.	27
2.4G	SEM photomicrograph of dark marl.	28
2.4H	SEM photomicrograph of laminated shale.	28
2.4I	SEM photomicrograph of laminated shale.	29
2.4J	SEM photomicrograph of laminated limestone.	29
2.5A	Relative thickness changes in the basal Lias studied.	30
2.5B	Field photo of limestone surface dominated by *Gryphaea*.	31
2.5C	Field photo of limestone containing limestone intraclasts.	31
2.5D	Field photo of isolated dark marl burrow-mottles.	32
2.5E	Photo of cut and polished block of limestone showing encrusted and bored surface.	33
2.5F	Photo of cut and polished block of limestone showing encrusted and bored surface.	33
2.5G	Negative prints of acetate peels from the encrusted and bored limestone surface.	34
2.5H	Negative prints of acetate peels from the encrusted and bored limestone surface.	34
2.8A	Stratigraphic variations in the average proportions of different rock types.	35
2.8B	Stratigraphic variations in the average proportions of different rock types.	36
2.8C	Correlation of %light marl/limestone with number of limestone beds and nodule horizons.	37
2.8D	Correlation in the basal Lias.	38
2.8E	Possible lithostratigraphic correlation for the lower part of the basal Lias.	39
2.8F	Possible lithostratigraphic correlation for the upper part of the basal. Lias.	40

Chapter 3

3.2A	Lower Lias whole rock composition according to rock type.	41
3.2B	TOC/$CaCO_3$ relationship at Watchet and Lyme Regis.	42
3.2C	Clay/FeS_2CaCO_3 relationship at Watchet and Lyme Regis.	43
3.3A	Variations in whole rock composition at Watchet.	44
3.4A	Detailed geochemical profiles through Lang's beds 13-20 Upper *angulata* zone, Seven Rock Point, Lyme Regis.	45

PAGE

3.4B	Field photo of Lang's beds 13-20, *angulata* zone, Seven Rock Point, Lyme Regis.	46
3.4C	Interpretation of S/DOP/Fe/TOC plots	47
3.4D	S/DOP/Fe/TOC relationships Upper *angulata* zone, Lyme Regis.	48
3.4E	Fe/S and S/TOC relationships at Watchet and Lyme Regis.	49
3.4F	Stable isotopes of carbonate from the *angulata*-*bucklandi* zone, Lyme Regis.	50
3.4G	Previously published stable isotopes from the Pre-*planorbis* beds-*semicostatum* zone, Lyme Regis.	51
3.4H	Stable isotopes in *Gryphaea arcuata* specimen BLG33.	52
3.4I	Stable isotopes in a limestone nodule from Lang's bed 37 *bucklandi* zone, Seven Rock Point, Lyme Regis.	53

Chapter 4

4.2A	Walsh power spectral estimates.	54
4.2B	The effect of hiatuses upon a perfectly regular time series.	55
4.2C	Time series: 16cm cycle plus 'random' gaps, for Fig 4.2B.	56
4.2D	Time series generated with random numbers.	57
4.2E	Spectrum of random time series.	58
4.2F	Time series generation.	59
4.2G	Choosing sample intervals.	60
4.2H	Testing the significance of spectral peaks.	61
4.2I	Harmonics.	62
4.3A	Basal Lias, Lyme Regis time series.	63
4.3B	Basal Lias, Lyme Regis power spectra.	64
4.3C	Basal Lias, Watchet time series.	65
4.3D	Basal Lias, Watchet time series.	66
4.3E	Basal Lias, Watchet time series.	67
4.3F	Basal Lias, Watchet power spectra.	68
4.3G	Basal Lias, Lavernock Point time series.	69
4.3H	Basal Lias, Lavernock Point power spectra.	70
4.3I	Basal Lias, Nash Point time series.	71
4.3J	Basal Lias, Nash Point power spectra.	72
4.3K	Basal Lias, Long Itchington time series.	73
4.3L	Basal Lias, Long Itchington power spectra.	74

Chapter 5

5.1A	Relationship between number of cemented horizons and zone thickness.	75
5.3A	Sea-level changes in the Early Jurassic in Britain.	76
5.4A	Productivity model.	77
5.4B	Stagnation model.	78
5.5A	General environmental model for the latest Triassic and earliest Jurassic in South Britain.	79
5.5B	Palaeogeography in the Hettangian and Early Sinemurian.	80

PAGE

Chapter 6

6.2A	Field aspect of the Boom Clay Formation, Terhagen, near Antwerp.	81
6.2B	Boom Clay Formation time series.	82
6.2C	Boom Clay Formation power spectra - using five codes.	83
6.2D	Boom Clay Formation power spectra - using two codes.	84
6.3A	Field aspect of the Upper Kimmeridge Clay Formation, near Freshwater Steps, Kimmeridge, Dorset.	85
6.3B	Kimmeridge Clay Formation time series.	86
6.3C	Kimmeridge Clay Formation upper section power spectra.	87
6.3D	Kimmeridge Clay Formation lower section power spectra.	88
6.4A	Measured sections within the stratigraphy of Breggia Gorge, Ticino, Switzerland.	89
6.4B	Field aspect of the Toarcian section, Breggia Gorge.	90
6.4C	Breggia Gorge Toarcian section time series.	91
6.4D	Breggia Gorge Toarcian section power spectra.	92
6.4E	Field aspect of the Upper Pliensbachian section Breggia Gorge.	93
6.4F	Breggia Gorge Upper Pliensbachian section time series.	94
6.4G	Breggia Gorge Upper Pliensbachian section power spectra.	95
6.4H	Field aspect of the Middle Pliensbachian section Breggia Gorge.	96
6.4I	Breggia Gorge Middle Pliensbachian section time series.	97
6.4J	Breggia Gorge Middle Pliensbachian section power spectra.	98
6.5A	Field aspect of the Belemnite Marls, Charmouth, Dorset.	99
6.5B	Belemnite Marls time series.	100
6.5C	Belemnite Marls power spectra.	101
6.6A	Field aspect of the 'Siliceous Shales', Robin Hood's Bay, Yorkshire.	102
6.6B	'Siliceous Shales' time series.	103
6.6C	'Siliceous Shales' power spectra.	104
6.7A	Field aspect of the Upper Birkhill Shales, Dob's Linn, Dumfries and Galloway.	105
6.7B	Upper Birkhill Shales time series.	106
6.7C	Upper Birkhill Shales power spectra.	107

CONTENTS OF VOLUME 2 - APPENDICES

PAGE

For Chapter 2 - Stratigraphic logs for the basal Lias sections

Key to stratigraphic logs.
2.1 Stratigraphic log for the basal Lias at Lyme Regis. 108
2.2 Stratigraphic log for the basal Lias at Watchet. 115
2.3 Stratigraphic log for the basal Lias at Lavernock Point. 138
2.4 Stratigraphic log for the basal Lias at Nash Point. 145
2.5 Stratigraphic log for the basal Lias at Long Itchington. 149

For Chapter 3 - Geochemical methodology

3.1 Bulk sample preparation. 156
3.2 *Gryphaea* specimen preparation. 156
3.3 Determination of %$CaCO_3$, %TOC, and % FeS_2. 157
3.4 Determination of %Fe/R and DOP/R. 158
3.5 Determination of $\delta^{18}O$ and $\delta^{13}C$. 160
3.6 Reproducibility. 161

For Chapter 4 - Computer Program for illustrating time series and generating Walsh power spectra

4.1 Listing of Program WPSPEC. 163

For Chapter 5 - Publications

5.1 Weedon 1985. 168
5.2 Weedon 1986. 169
5.3 Weedon 1987. 184

For Chapter 6 - Time series for various formations

6.1 Time series for the Boom Clay Formation. 186
6.2 Time series for the Upper Kimmeridge Clay Formation. 188
6.3 Time series for the Toarcian section at Breggia Gorege. 190
6.4 Time series for the Upper Pliensbachian section at Breggia Gorge. 193
6.5 Time series for the Middle Pliensbachian section at Breggia Gorge. 195
6.6 Time series for the Belemnite Marls. 196
6.7 Time series for the 'Siliceous Shales'. 197
6.8 Time series for the Upper Birkhill Shales. 198

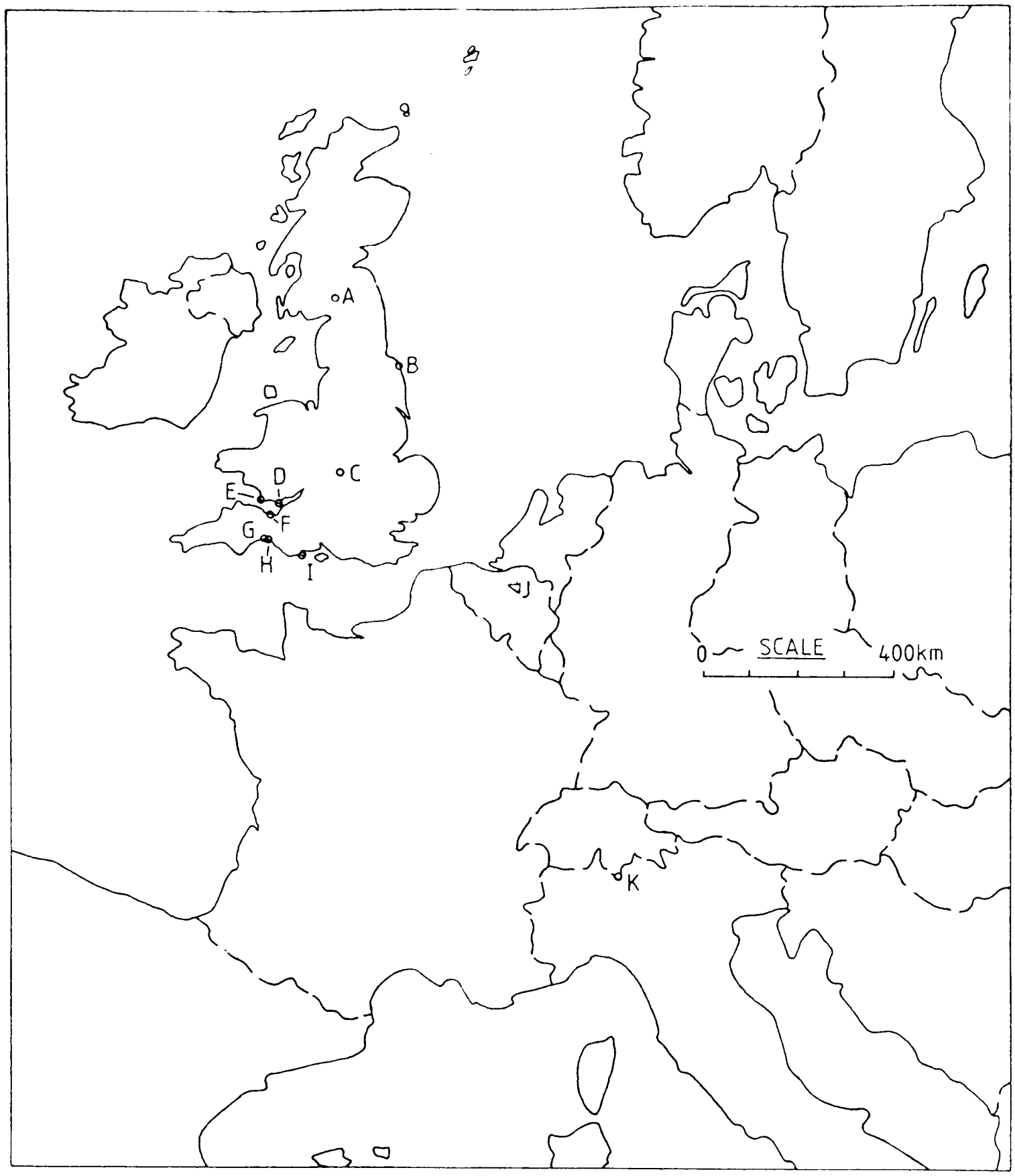

A DOB'S LINN
B ROBIN HOOD'S BAY
C LONG ITCHINGTON
D LAVERNOCK POINT
E NASH POINT
F WATCHET
G LYME REGIS
H CHARMOUTH
I KIMMERIDGE BAY - CHAPMAN'S POOL
J ANTWERP AND FOUR PITS WITHIN 19km
K BREGGIA GORGE

FIG 1.1A LOCATION OF THE LITHOSTRATIGRAPHIC UNITS LISTED IN TABLE 1A

Fig 1.2A The Nature of Cyclic Changes in Orbital Obliquity (Tilt).

OBLIQUITY: Dominant Period = 41kyr, Minor Periods = 29kyr & 54kyr, Period on Power spectra = 41kyr.

Oblique View of Orbit:

a) Obliquity = Minimum

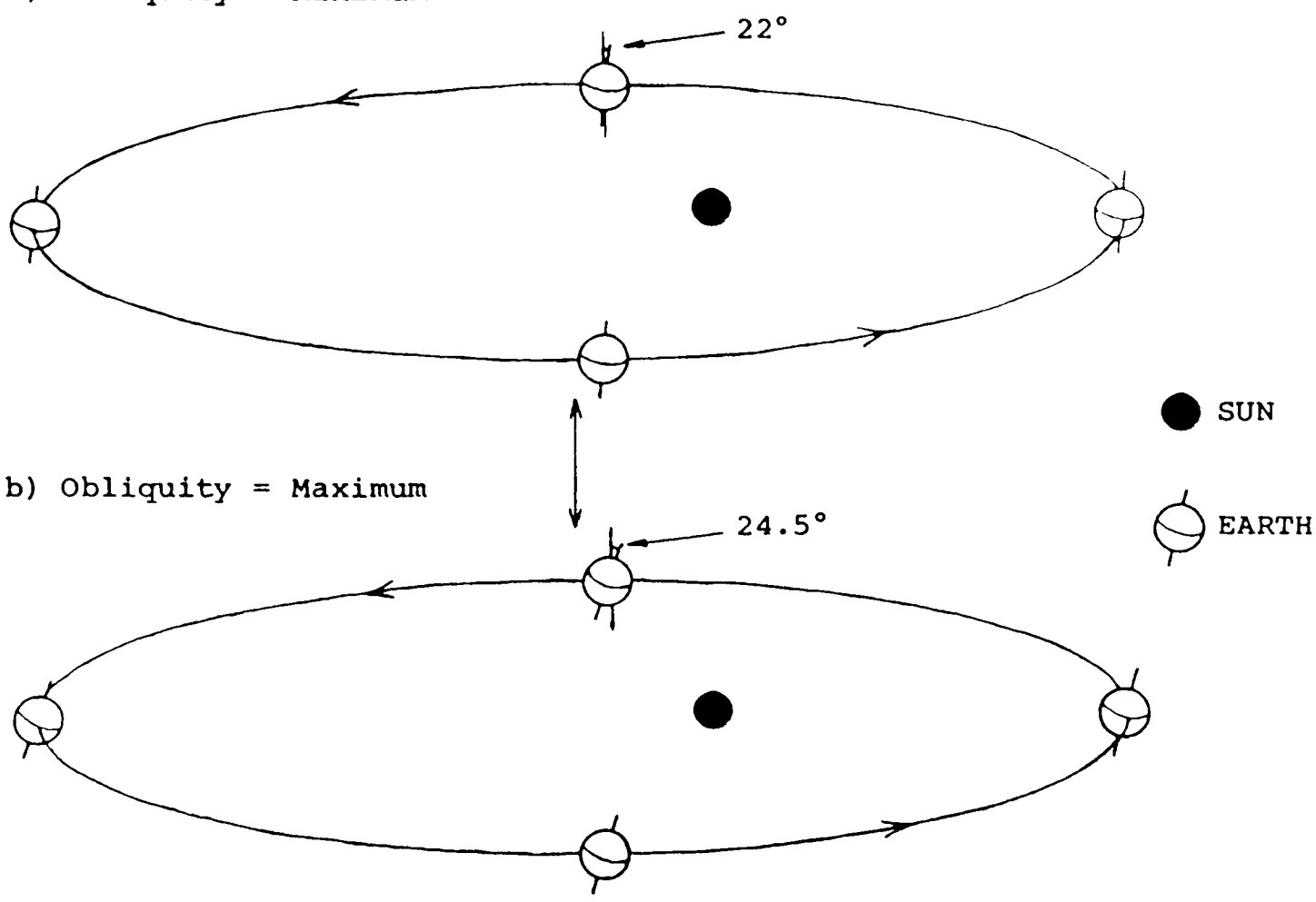

b) Obliquity = Maximum

Radiation Levels - for 45°N with circular orbit:

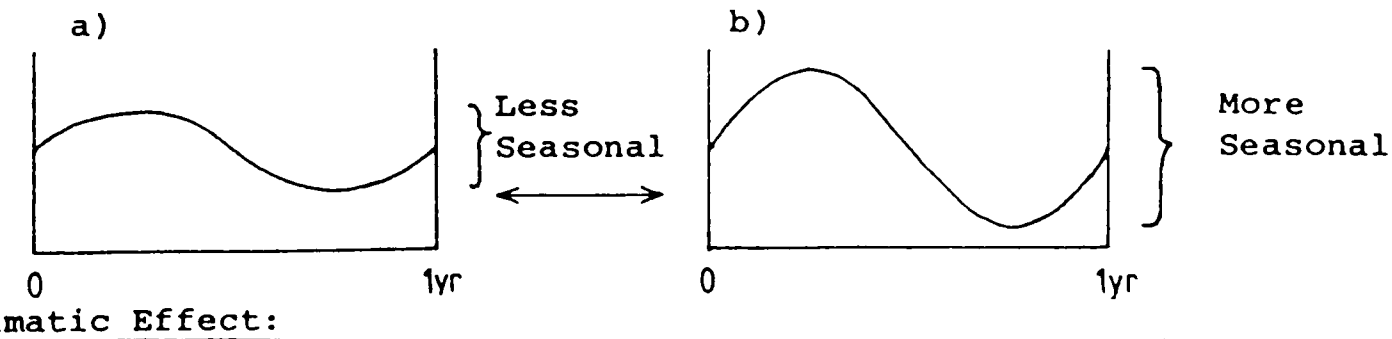

Climatic Effect:

Changes degree of seasonality. Nb. if Obliquity = 0° then there would be no seasons.

(Diagrams are schematic. Based on data from Berger 1980 & 1984.)

Fig 1.2B The Nature of Cyclic Changes in Orbital Eccentricity.

ECCENTRICITY: Dominant Periods = 95kyr, 100kyr, 120kyr & 410kyr,
Periods on Power Spectra = 100kyr & 410kyr.

Plan View of Orbit:

a) Eccentricity = Minimum
(ε = 0.0005)

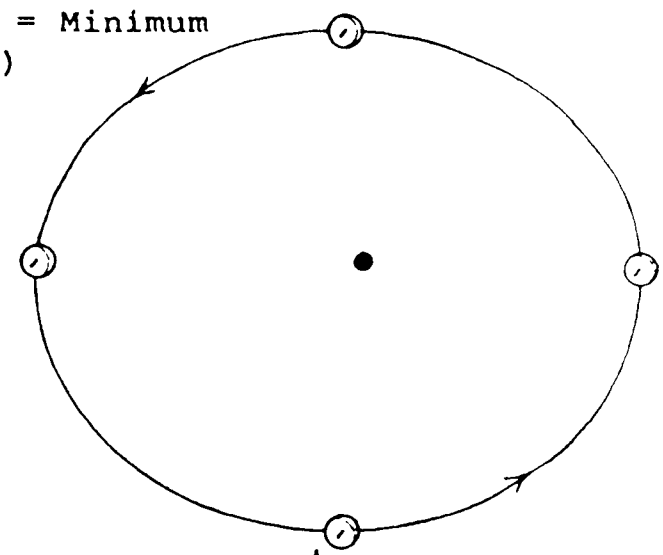

b) Eccentricity = Maximum
(ε = 0.0607)

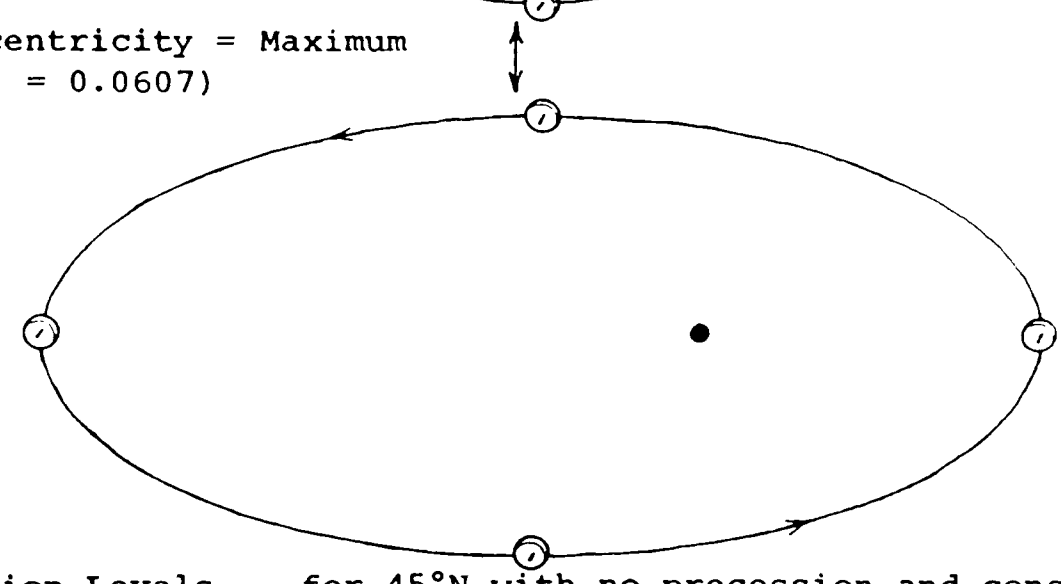

● SUN

⊙ EARTH

Radiation Levels - for 45°N with no precession and constant obliquity

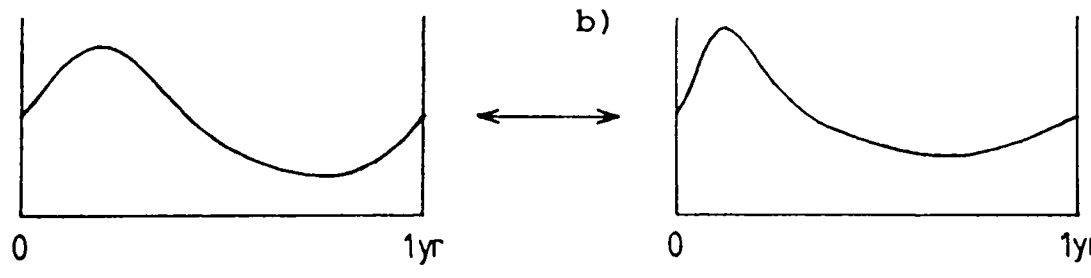

Climatic Effect:

Very small change in total insolation from year to year. Mainly controls the impact of precession upon climate (Fig 1.2C). Nb. if eccentricity = 0.0 (ie a circular orbit), then precession absent. Greater eccentricity leads to more important precession impact. Cause of asymmetry in the duration of summer compared to winter.

(Diagrams are schematic. Based on data from Berger 1980 & 1984.)

Fig 1.2C The Nature of Cyclic Changes in Orbital Precession.

PRECESSION: Dominant Periods = 19kyr & 23kyr,
Periods on Power Spectra = 19kyr & 23kyr or 21kyr only.

Oblique View of Orbit:
Nb. Summer occurs when the relevant hemisphere faces towards the Sun.

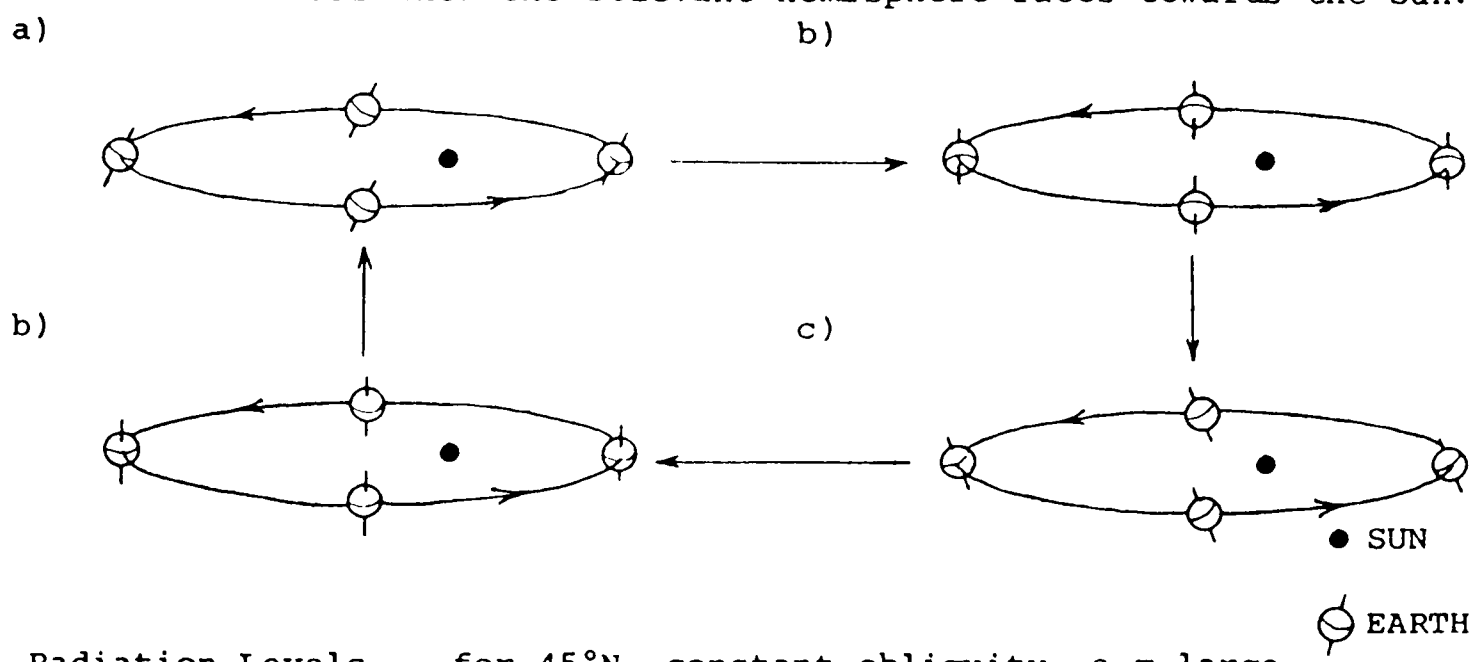

Radiation Levels - for 45°N, constant obliquity, ε = large

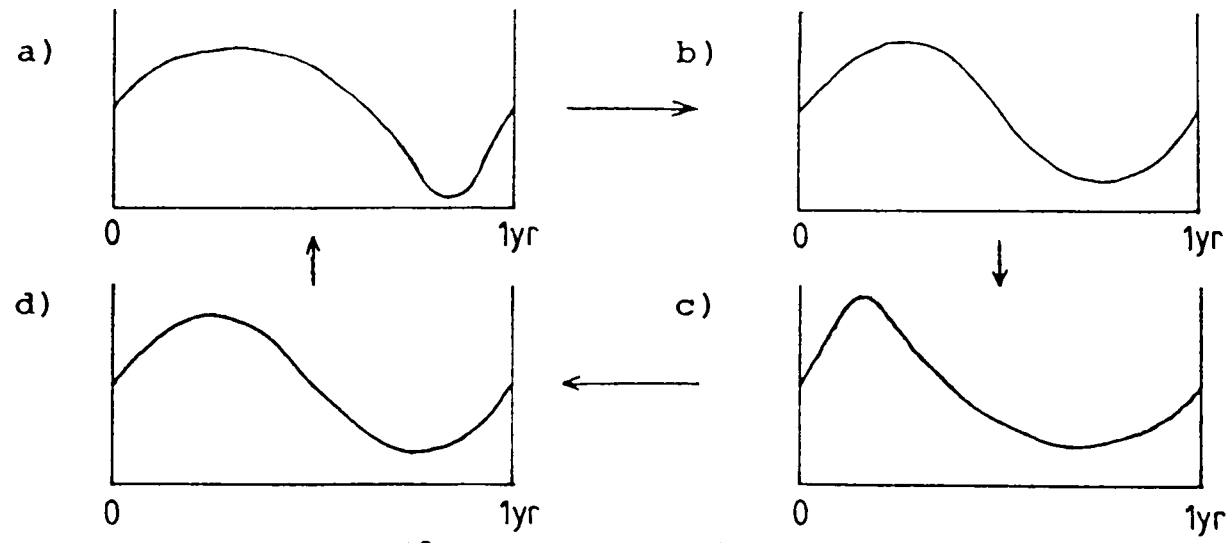

Radiation Levels - for 45°N, constant obliquity, ε = small

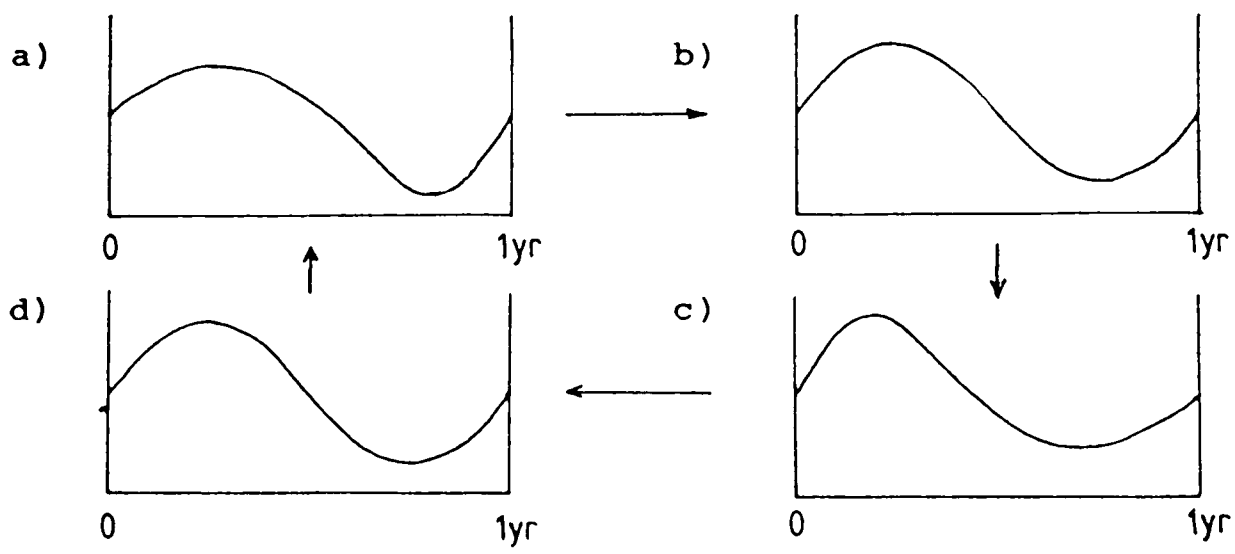

Climatic Effect:

Given season becomes alternately short & intense and long & weak. Size of impact controlled by eccentricity (Fig 1.2B). See Berger 1980 for a more precise description of precession. (Diagrams are schematic. Based on data from Berger 1980 & 1984.)

Fig 2.1A MAP OF BASAL LIAS LOCALITIES

Fig 2.1B

Limestone nodule in Lang's bed 36 at Lyme Regis. The nodule passes laterally into light marl. Nearby beds of laminated shale (brown), dark marl (dark blue/grey) and light marl (light blue grey) are compacted round the nodule. *bucklandi* zone, Lyme Regis. The hammer is 39cm long.

Fig 2.1C

Limestone nodules in a light marl passing laterally into a light marl bed. The nodules and continuous limestone bed can be seen just below Dr. H.C. Jenkyns waist and occur in Lang's bed 37, *bucklandi* zone, Lyme Regis.

Fig 2.1D

Illustration of different rock types. Laminated shale overlies light marl and dark marl. The light marl bed contains a limestone nodule. The light bed represents Lang's bed 15c, *angulata* zone, Lyme Regis. The lens cap is 5cm in diameter.

Fig 2.1E

Illustration of different rock types. A limestone bed overlies dark marl with burrow mottles. Under this a light marl bed contains a limestone and at the base in a laminated shale bed with a burrowed top. Lang's beds 18 and 19, *angulata* zone, Lyme Regis. The lens cap is 5cm in diameter.

MINOLTA

MINOLTA

Fig 2.1F

Chondrites burrow-mottles in a light marl and limestone bed. The mottles pass down from a dark marl bed. Lang's beds 17 and 18, *angulata* zone, Lyme Regis. Notice that the light marl/dark marl contact is sharp despite burrow-mottling. Lens cap is 5cm in diameter.

Fig 2.1G

Diplocraterion burrow-mottle in a limestone underneath a dark marl bed. The spreite are only poorly developed suggesting that most *Arenicolites* mottles observed were produced by the same organism which produced *Diplocraterion*. Lang's bed 19, *angulata* zone, Lyme Regis.

MINOLTA

Fig 2.1H

Burrow-mottles in a dark marl and limestone bed. Notice that *Chondrites* burrow occur within an *Arenicolites* or *Thalassinoides* burrow-mottle. Lang's bed 19, *angulata* zone, Lyme Regis.

Fig 2.1I

Field aspect of the basal Lias at Lyme Regis, West Cliff, Dorset. The section illustrated represents Lang's beds 1-49 - about 13m thick.

Fig 2.1J

Field aspect of the basal Lias at St. Audrie's Cliff, Watchet, Somerset. The average proportion of limestones was used by Palmer (1972) to divide the basal Lias into divisions A-F. Illustrated here are division A, B and the lowermost part of C. The photograph illustrates Palmer's beds A17-C11 representing about 32m (Pre-*planorbis* beds - lowest *angulata* zone). Cope *et al.* 1980 suggested that the base of the Jurassic be defined at Watchet above the second limestone bed in the section illustrated.

Fig 2.1K

Palmer's beds C56-C82 below Blue Ben, *angulata* zone Watchet. Small normal fault displaces the beds at the right of the photograph. The hammer is 39cm long.

Fig 2.1L

Trueman's beds 9-33, Pre-*planorbis* beds - *planorbis* zone, Lavernock Point, Glamorgan. Many laminated limestone beds are enclosed by laminated shale (Appendix Section 2.3). The section represents 10m of the basal Lias.

Fig 2.1M

Field aspect of the basal Lias at Nash Point, Glamorgan. The section represents about 27m. Notice the exceptionally high proportion of limestone and the very nodular contacts.

Fig 2.1N

Trueman's beds 1-7, *bucklandi* zone, Nash Point. The hammer is 39cm long.

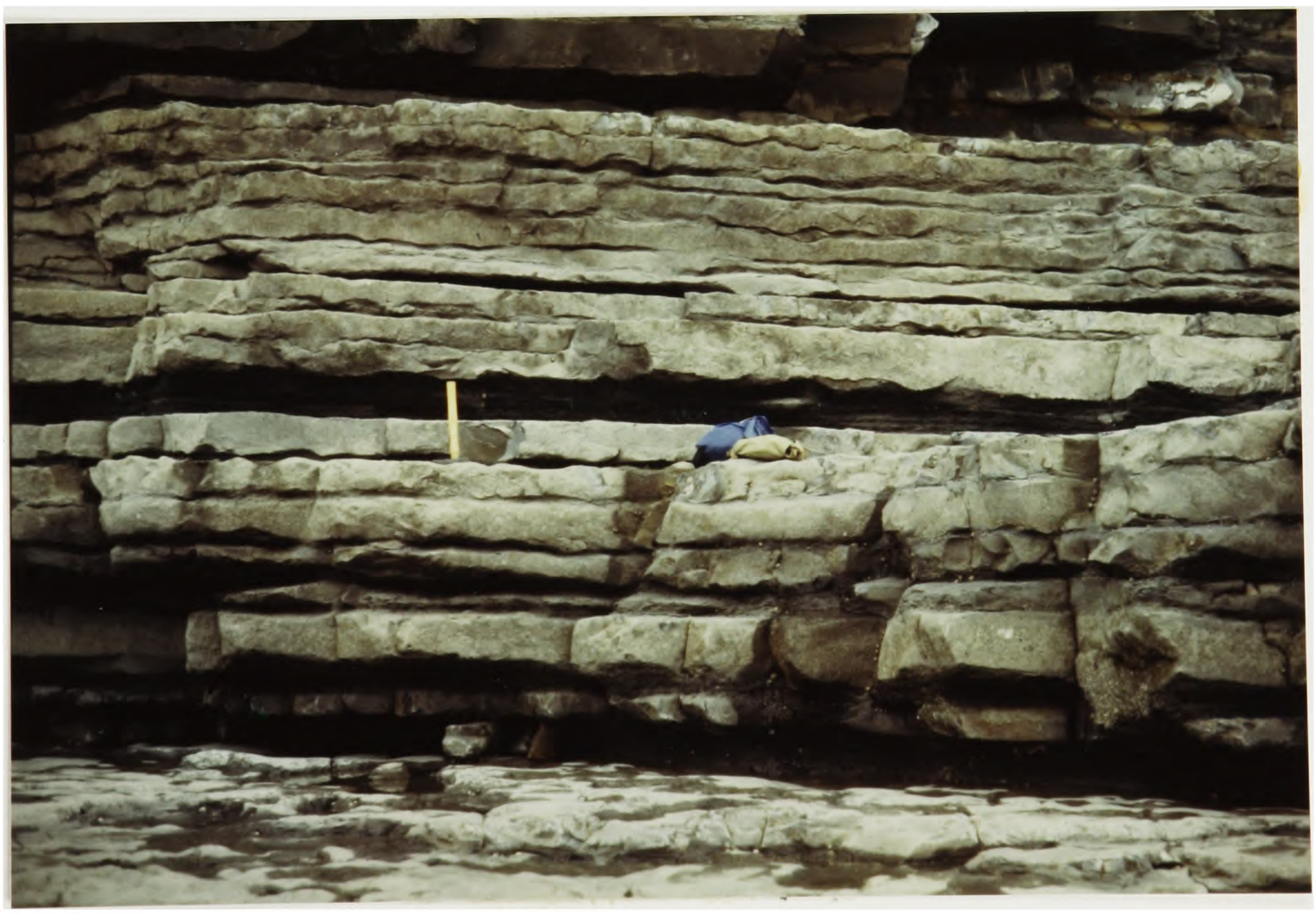

Fig 2.10

Clement's et al.'s (1975) beds 17k-23g, angulata zone, Long Itchington, Warwickshire. The section represents about 5m.

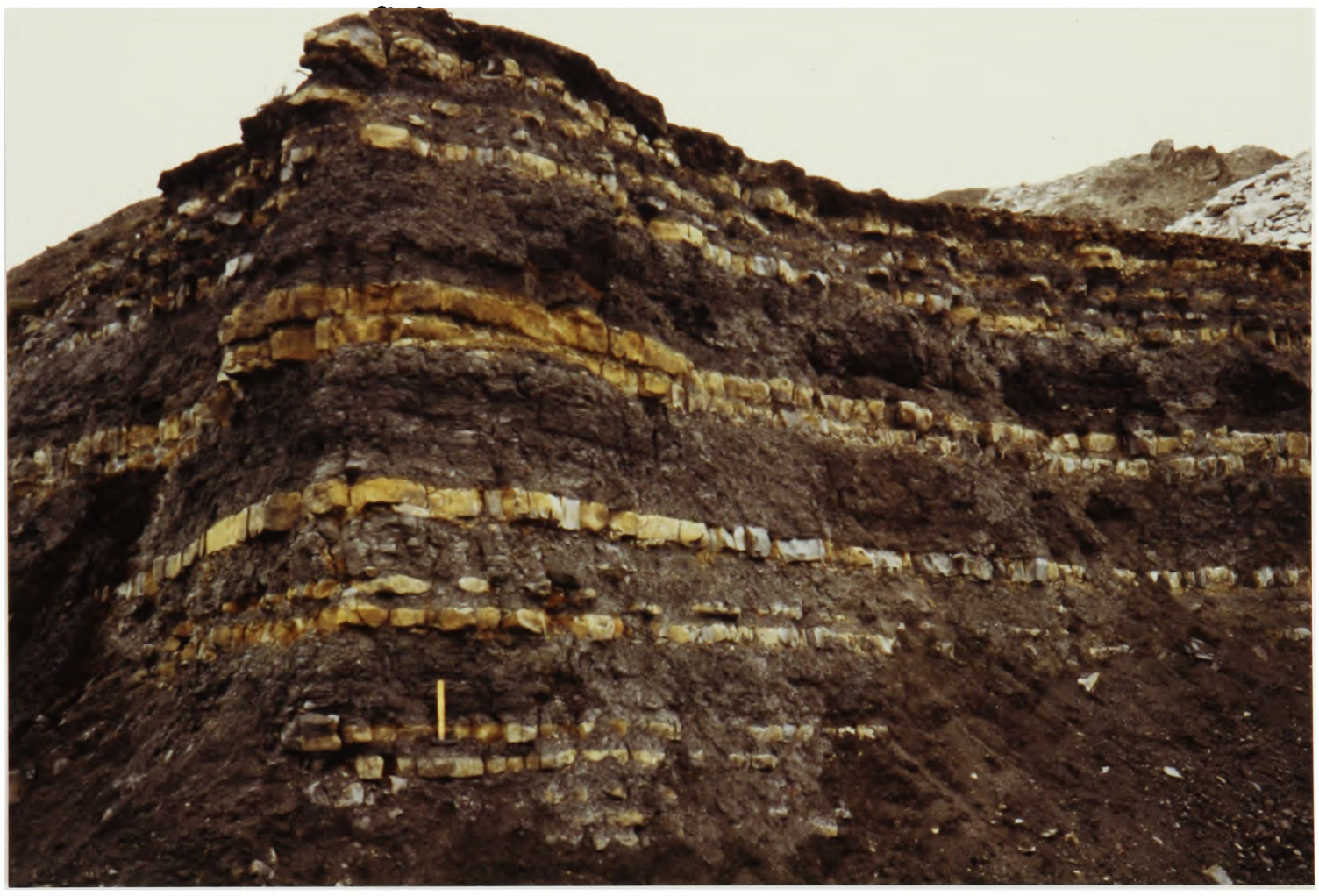

Fig 2.2A

The Sutton stone overlying the Carboniferous Limestone at Southerndown, Glamorgan. The hammer is 39cm long.

Fig 2.2B

Close-up of the Southerndown beds at Southerndown, Glamorgan. The lens cap (diameter 5cm) is leaning against a bed containing a relatively high proportion of clay and lithoclasts. Stylolites can be seen at the top of the section.

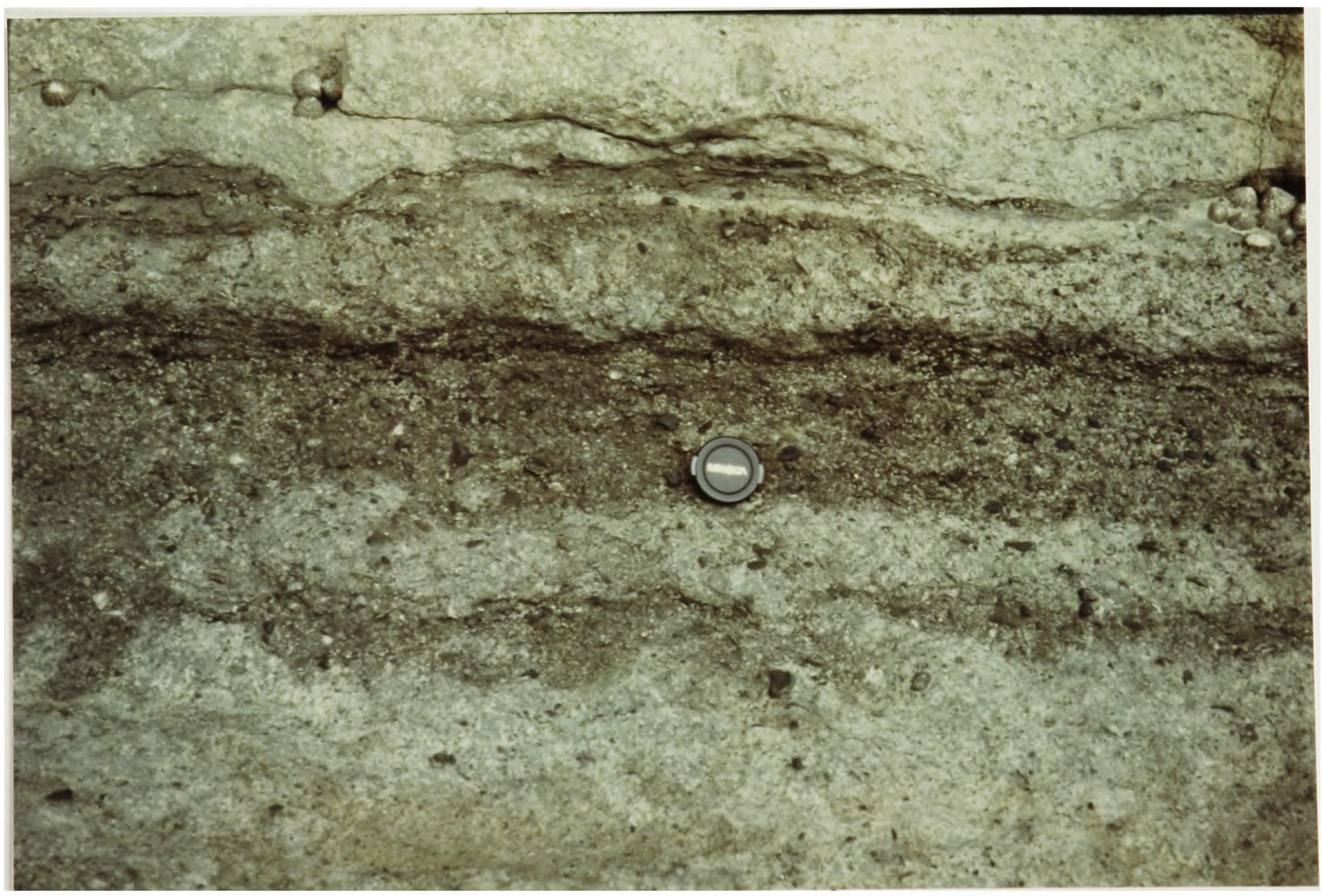

Fig 2.2C

The Brockley Down Stone overlying the Carbon iferous Limestone at Lulsgate, Avon. The Brocley Down Stone is about 14m thick in Lulsgate Quarry.

Fig 2.2D

Loose blocks of Brockley Down Stone, Lulsgate Quarry, containing Carboniferous Limestone lithoclasts.

Fig 2.2E

Thin section photomicrograph of limestone. Plane polarized light. The section is partly stained. The matrix consists of microspar and clay and contains a small benthonic foraminifera filled by glauconite, lower right. The large bioclast on the left represents the wall of an ammonite chamber composed of neomorphic spar. Sample BL103, bucklandi zone, Lyme Regis. The width of the photo represents 3mm.

Fig 2.2F

Thin section photomicrograph of limestone. Crossed polars. the whole section is stained. Neomorphic spar forms the uncrushed walls of an ammonite chamber. The centre of one chamber is filled by cavity filling spar - the blue tinged part is ferroan calcite, the rest is non-ferroan calcite. The matrix of microspar and clay appears to be pelleted. Sample BL105, fallen block, Lyme Regis. The field of view is 3mm across.

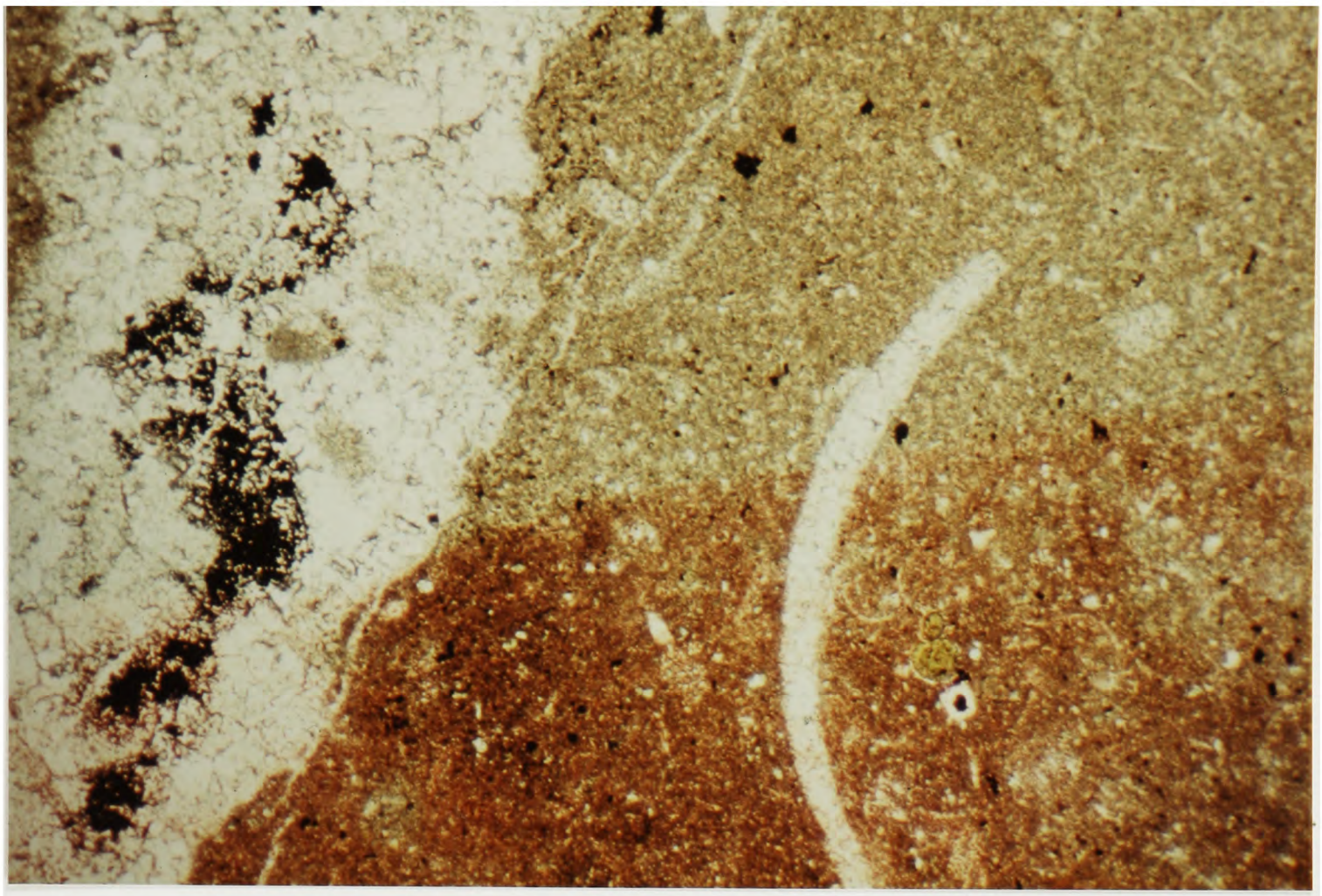

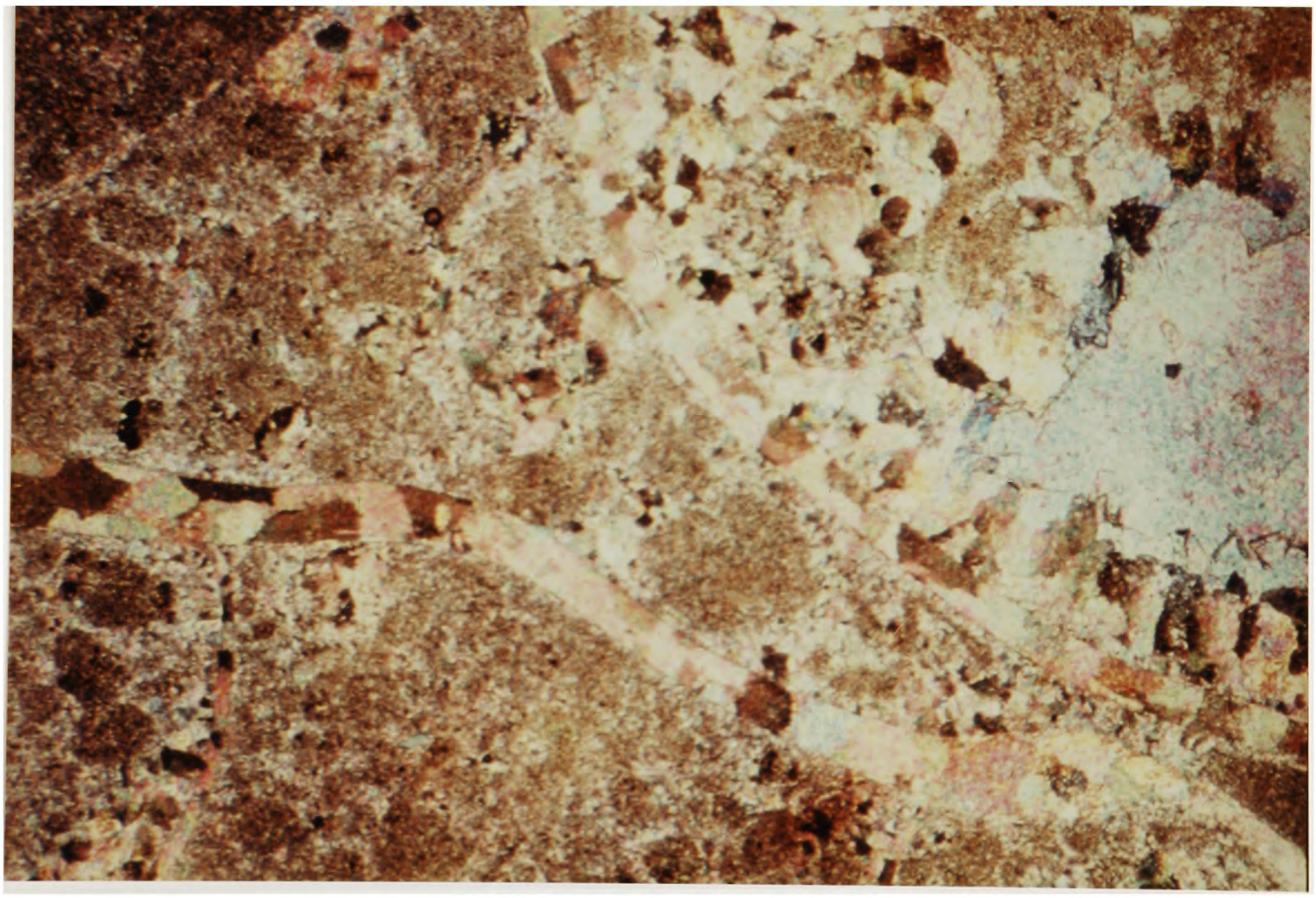

Fig 2.2G

Thin section photomicrograph of limestone. Crossed polars. Part of an ammonite set in a clay and microspar matrix. The black dots are pyrite framboids. Sample BL103, *bucklandi* zone, Lyme Regis. Field of view 3mm across.

Fig 2.2H

Thin section photomicrograph of limestone. Cathodoluminescence. Zoning in the neomorphic spar appears to indicate two phases of growth. The bivalve fragment lower right is unaltered and therefore not luminescent although it is overgrown by luminescent cement. The matrix microspar is uniformly luminescent. Quartz silt grains luminesce blue. Same area as Fig 2.2G.

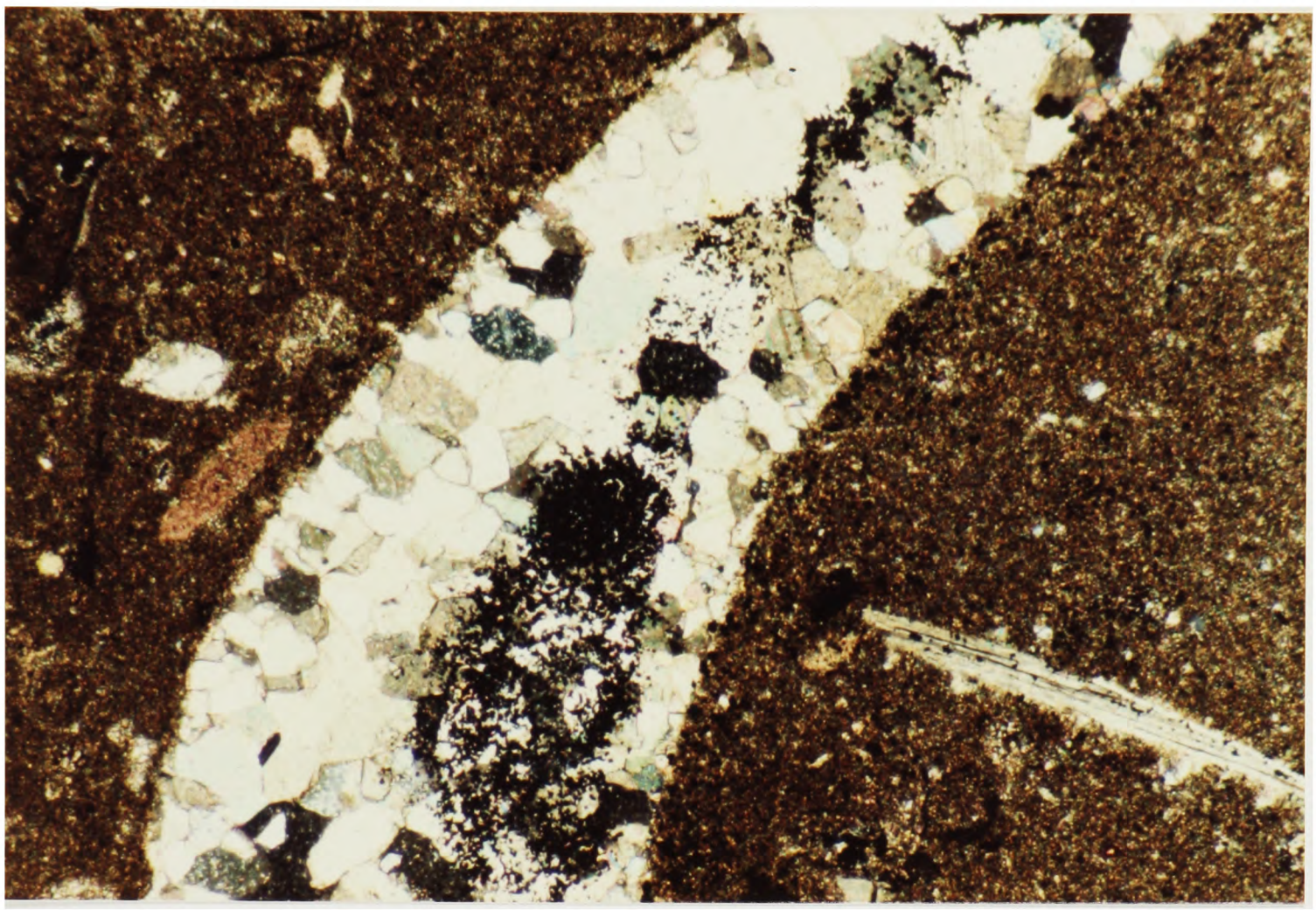

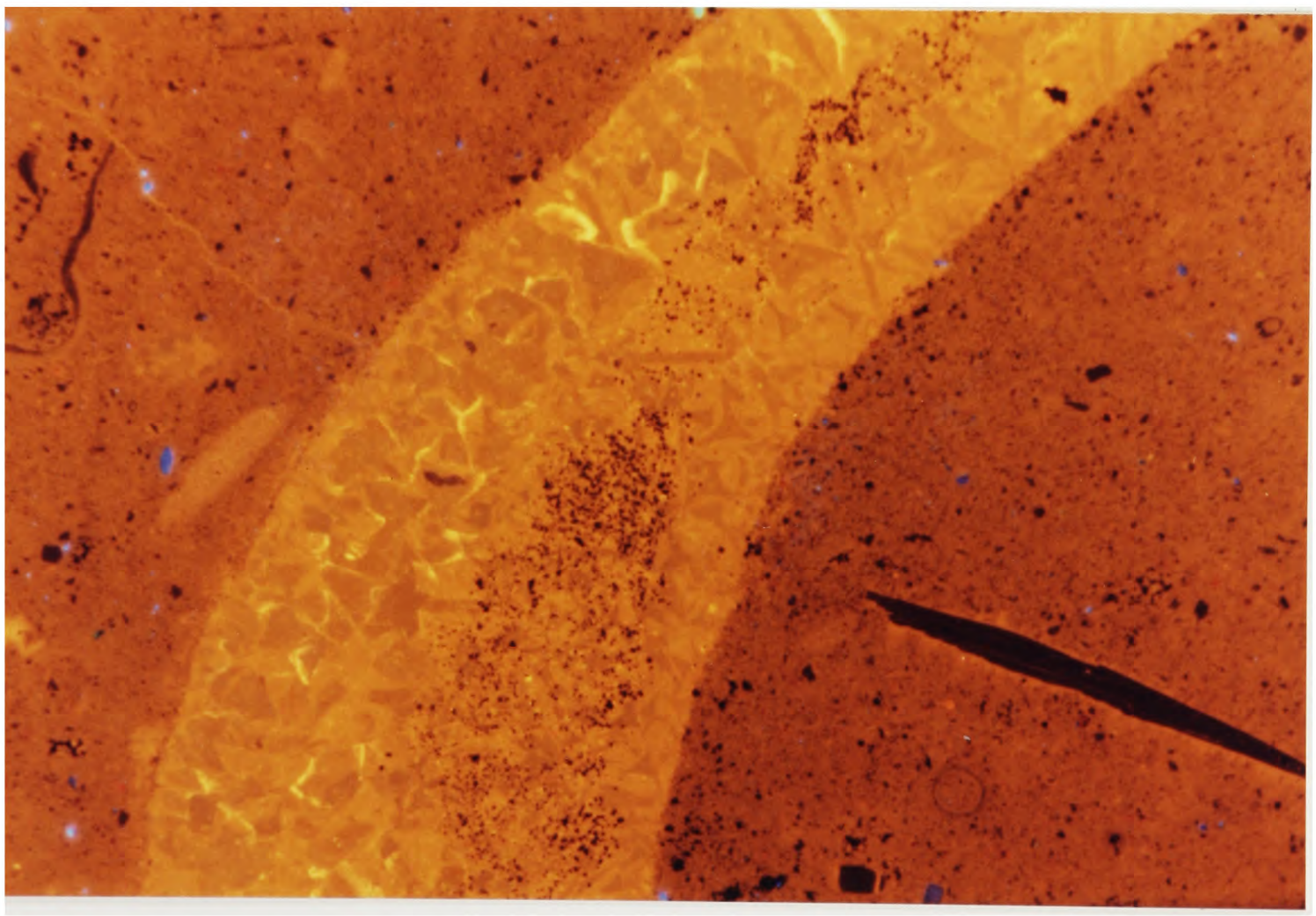

Fig 2.2I

Thin section photomicrograph of *Gryphaea*. Crossed polars. The original foliated texture appears to have been preserved. Sample BLG28, *angulata* zone, Lyme Regis. Field of view 8.5mm across.

Fig 2.2J

Thin section photomicrograph of *Gryphaea*. Cathodoluminescence. The bulk of the shell is unaltered and not luminescent. (Nb. photo overexposed). Cleavage and twin planes appear to be filled with luminescent cement. Same area as Fig 2.2I.

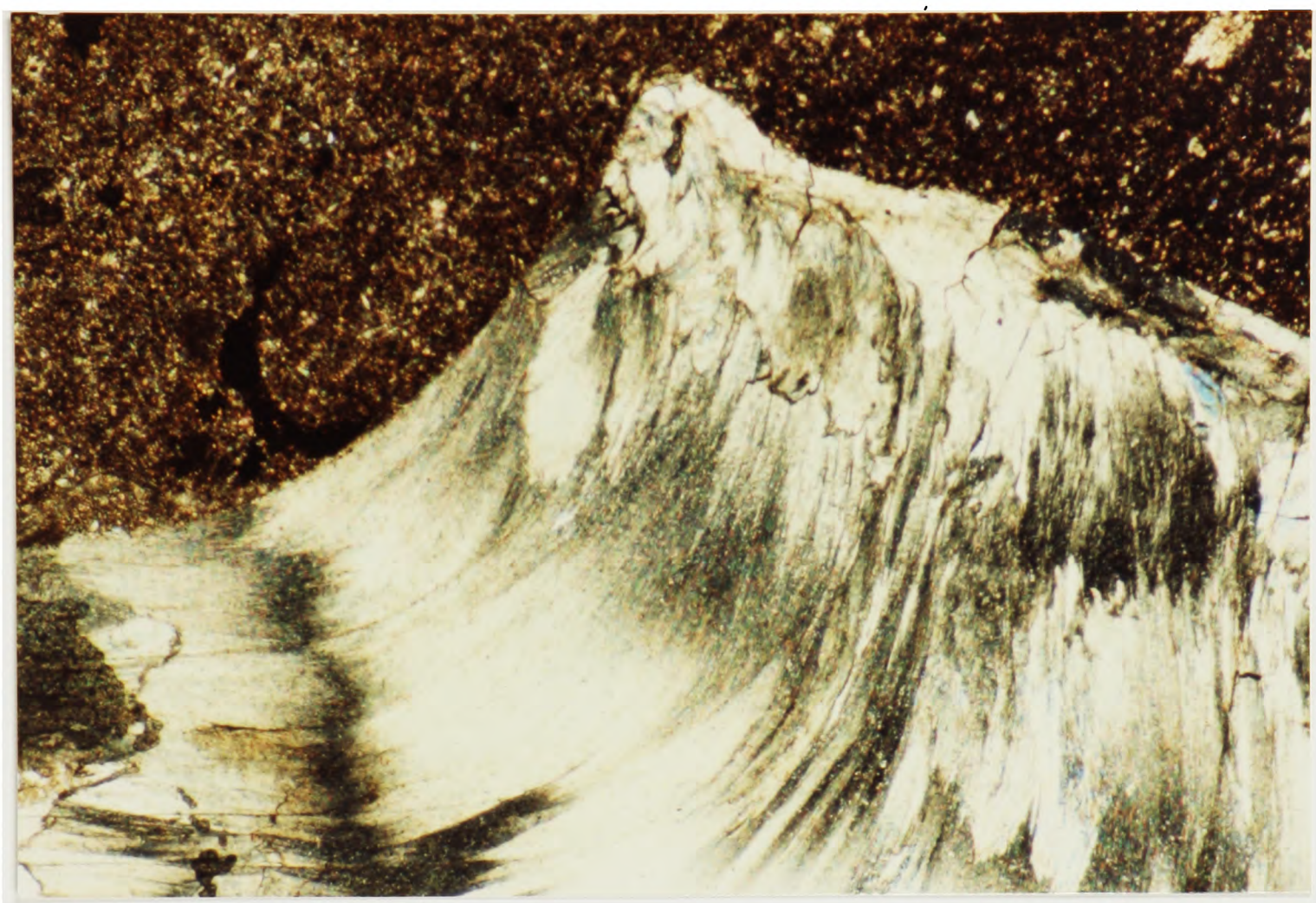

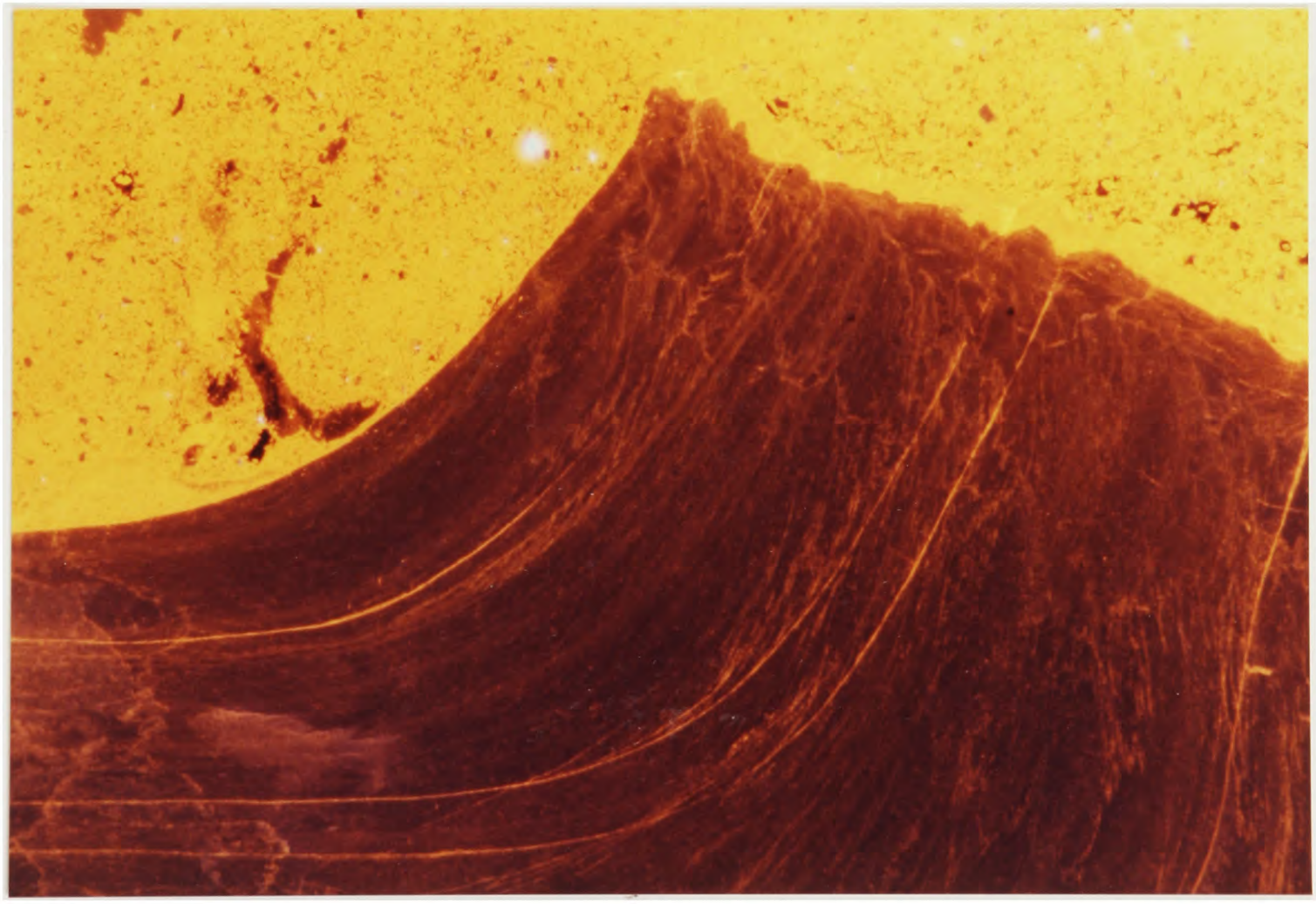

Fig 2.2K

Thin section photomicrograph of light marl. Plane polarized light. A large ostracod can be seen lower right. The matrix consists of intimately mixed microspar and clay with black patchs representing pyrite. Sample BW44, angulata zone, Watchet. The width of the photo represents 1.5mm.

Fig 2.2L

Thin section photomicrograph of light marl. Cathodoluminescence. The microspar matrix is more or less uniformly luminescent with a few silt grade quartz grains (blue). Same area as Fig 2.2K.

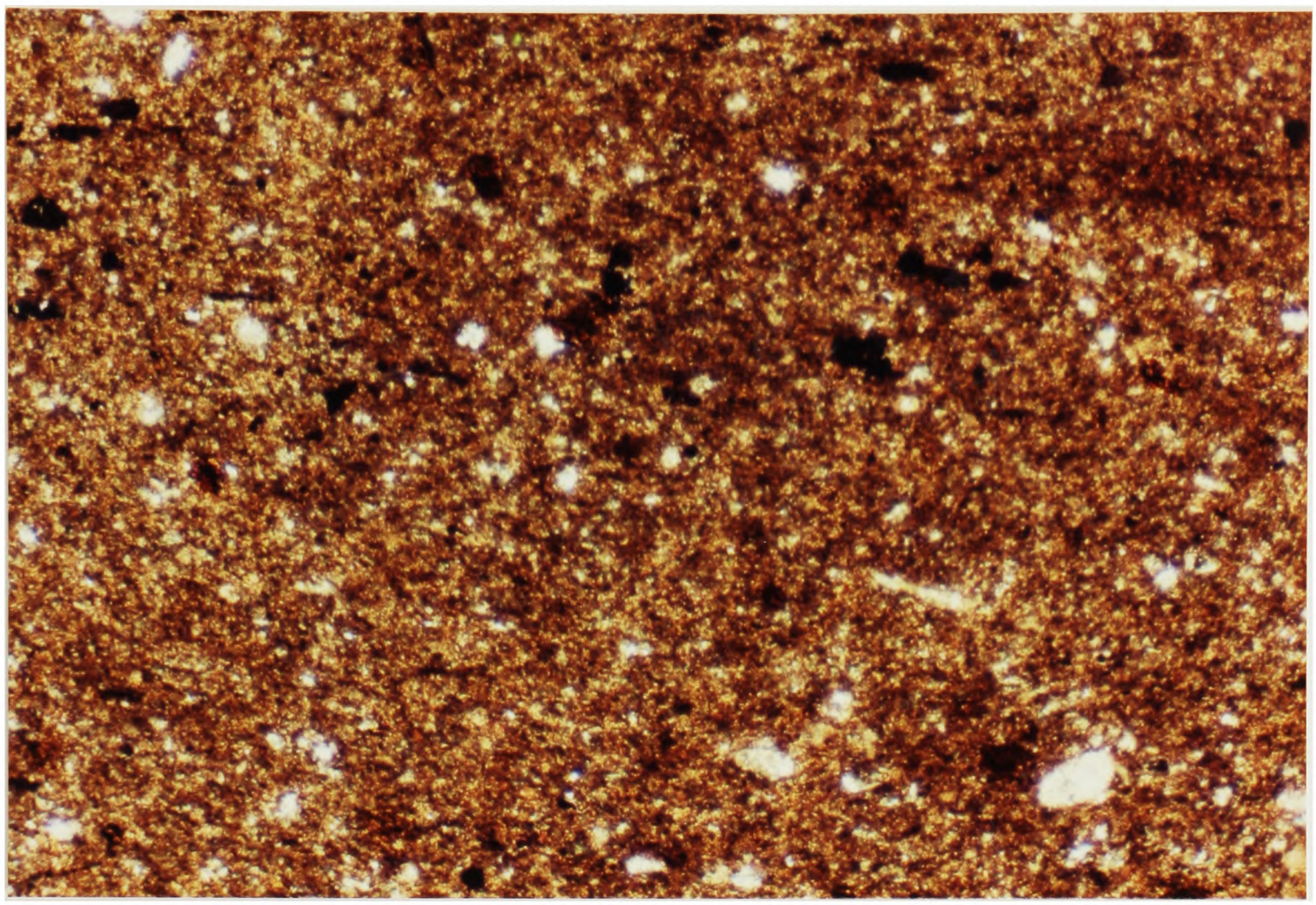

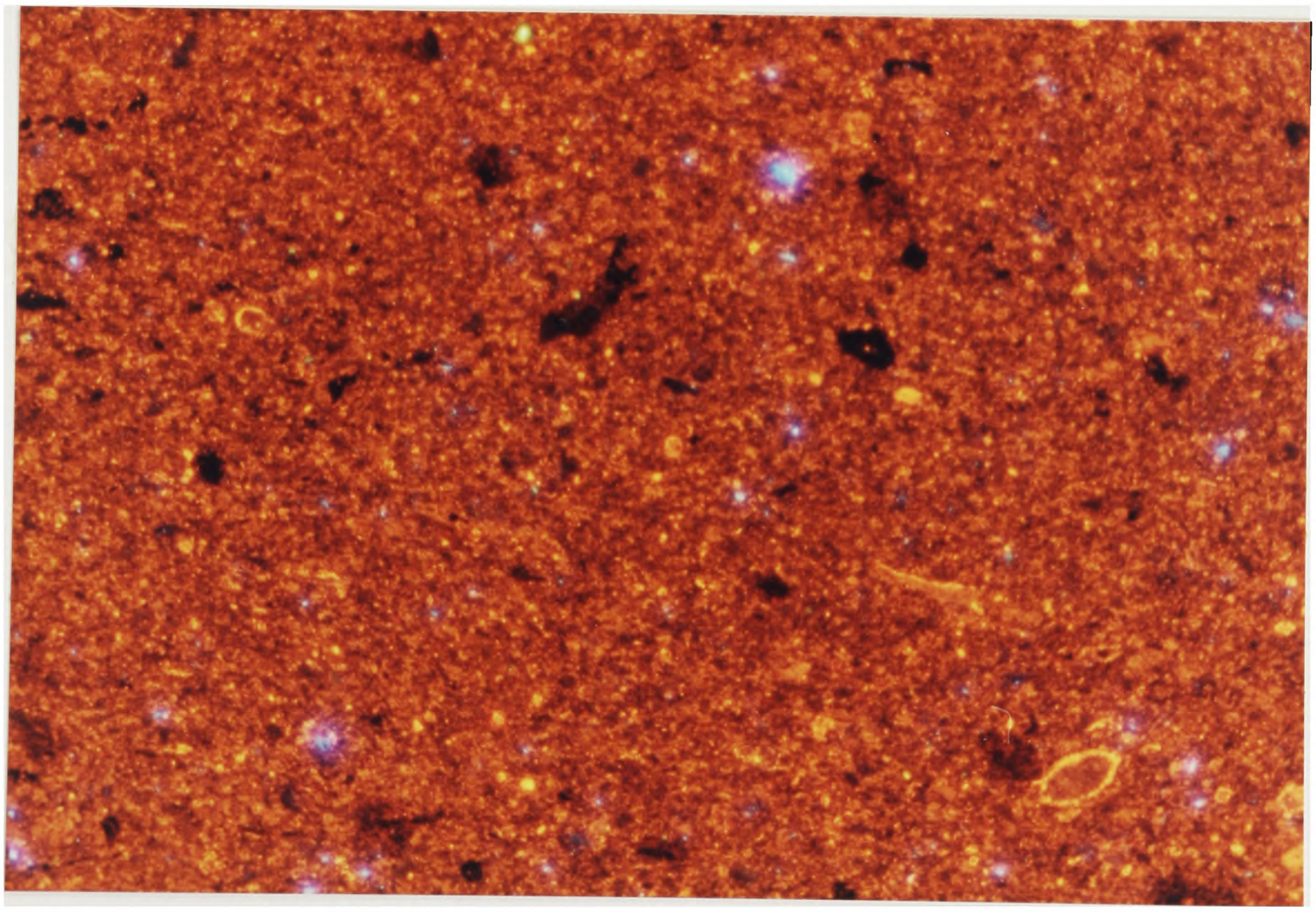

Fig 2.2M

Thin section photomicrograph of dark marl. Plane polarized light. The mat rix consists of clay and organic laminae with dispersed microspar 'blebs'. A bleb-rich horizon can be seen at the top of the photograph. A burrow is filled by light marl, lower left. Sample BL120, bucklandi zone, Lyme Regis. The width of the photo represents 3mm.

Fig 2.2N

Thin section photomicrograph of dark marl. Cathodoluminescence. The clay and organic matrix contains many small ostracods and some quartz silt grains. The microspar in the blebs luminesces yellow/orange whereas a few isolated microspar crystals (? microdolomite) are zoned and luminesce red/orange. A burrow-mottle, top right, is filled with light marl containing more ostracods. Sample BL120, bucklandi zone, Lyme Regis. Field of view 1.5mm across.

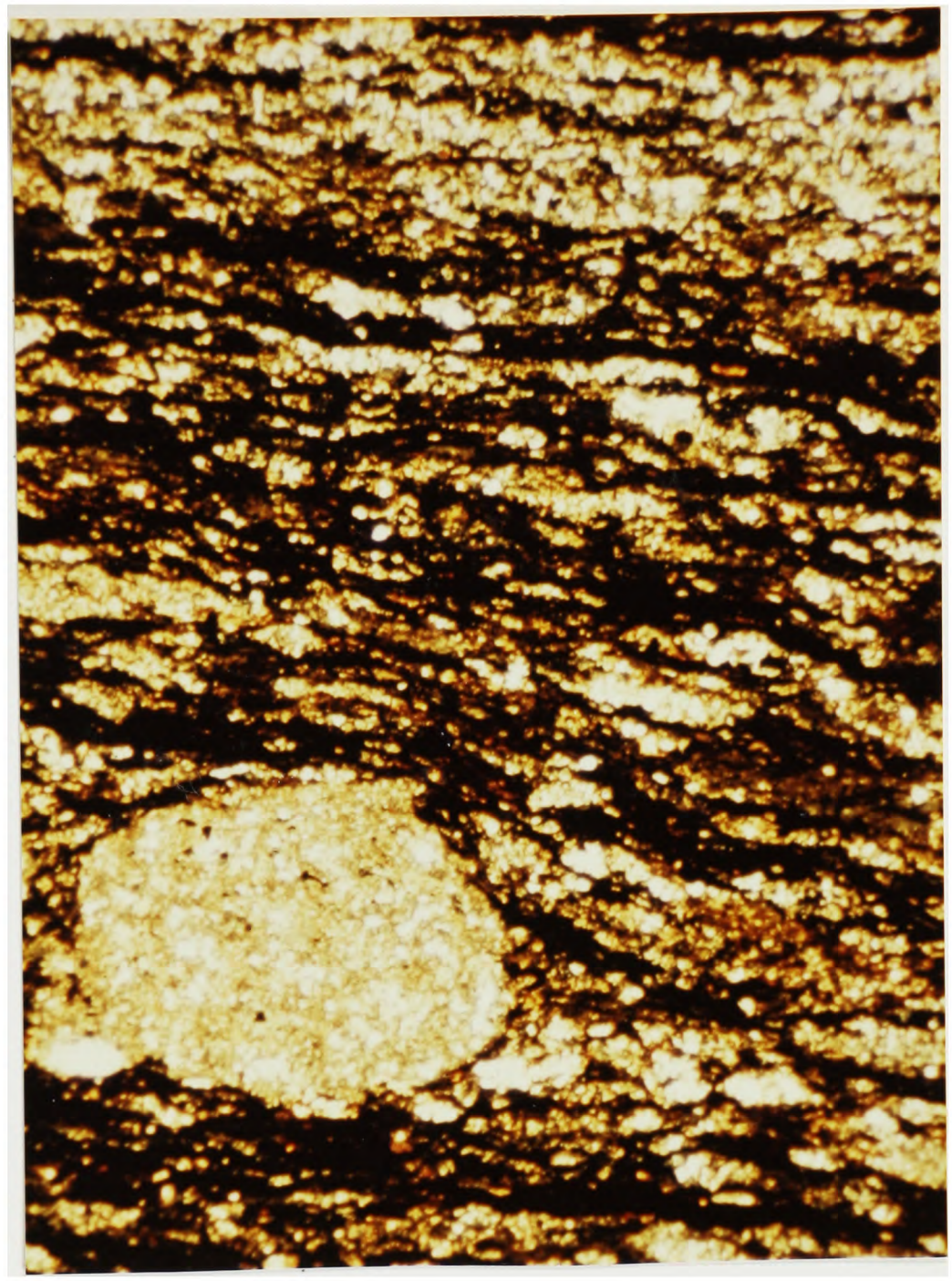

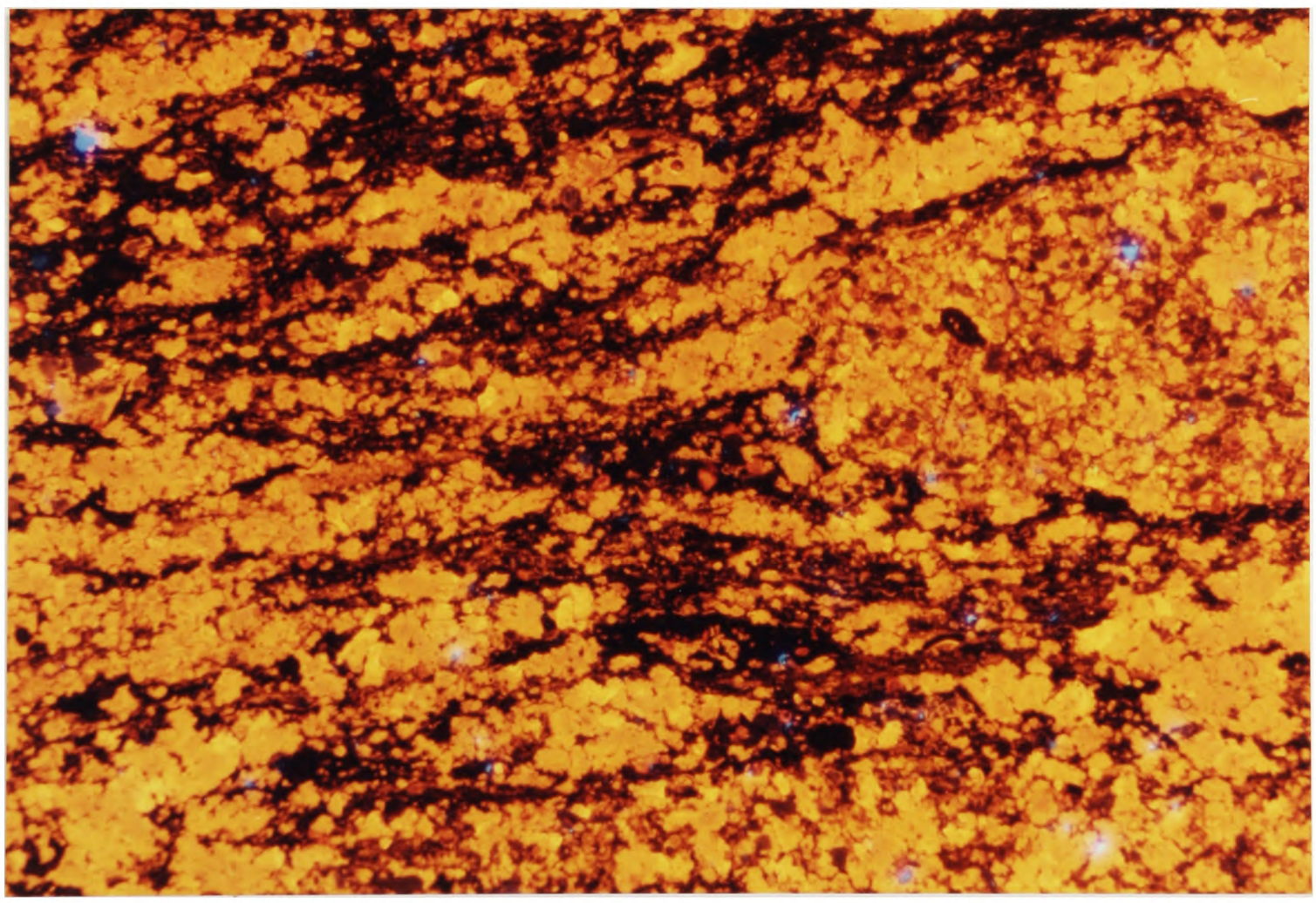

Fig 2.20

Thin section photomicrograph of laminated shale. Plane polarized light. The white material is calcite microspar often forming 'blebs'. Clay laminae are brown and organic laminae are black. Sample BL117, *bucklandi* zone, Lyme Regis. Field of view 4.5mm across.

Fig 2.2P

Thin section photomicrograph of laminated shale. Cathodoluminescence. Small ostracods are normally masked by clay and organic matter, but they can be picked out under cathodoluminescence. Notice the lamina of concentrated ostracods in the middle. Most carbonate appears to be ostracodal. A few isolated microspar crystals, eg. middle top and middle bottom, are zoned and euhedral - they may represent microdolomite. Silt grade quartz grains (blue) are scattered throughout. Sample BL117, *bucklandi* zone, Lyme Regis. Field of view 1mm across.

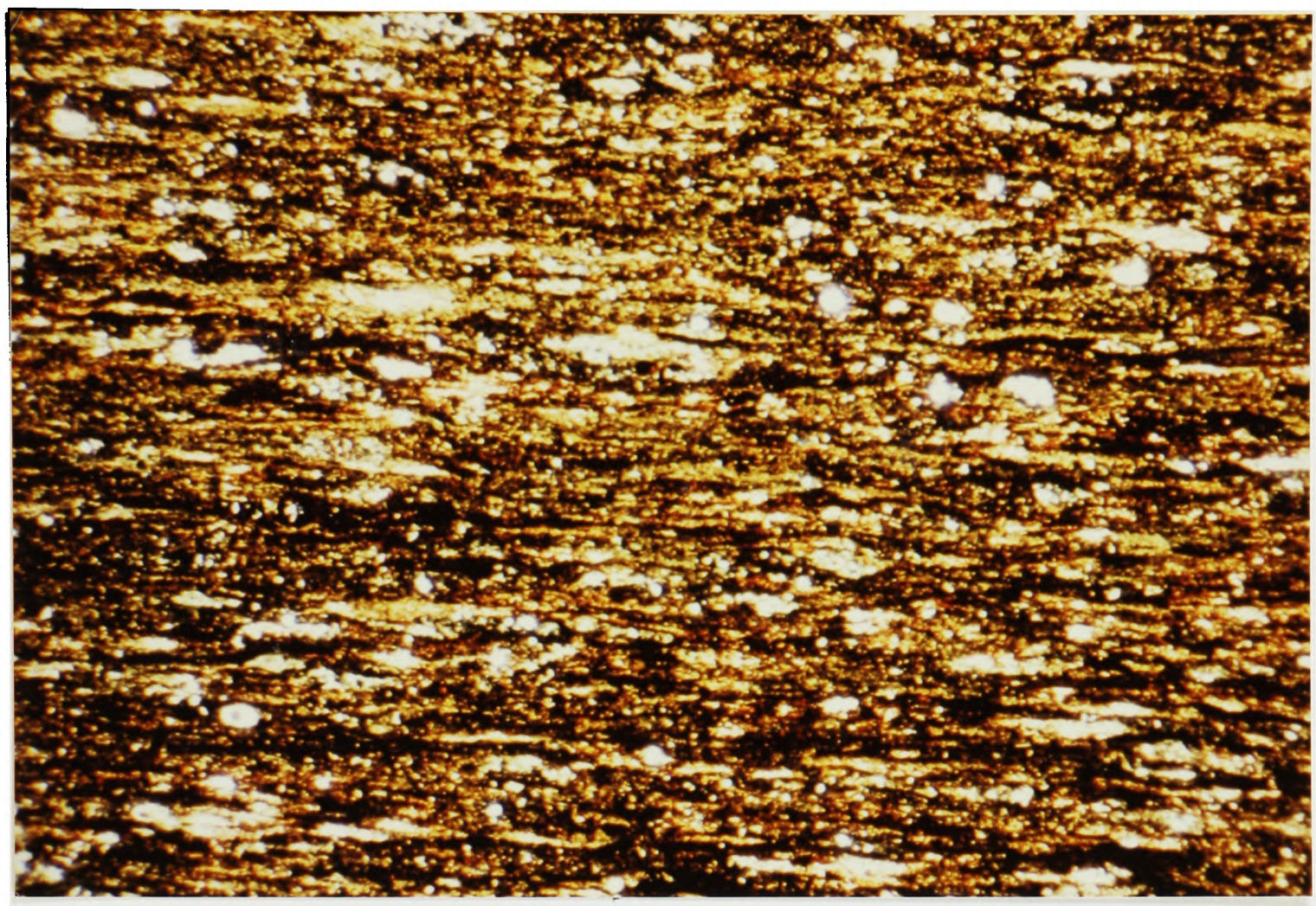

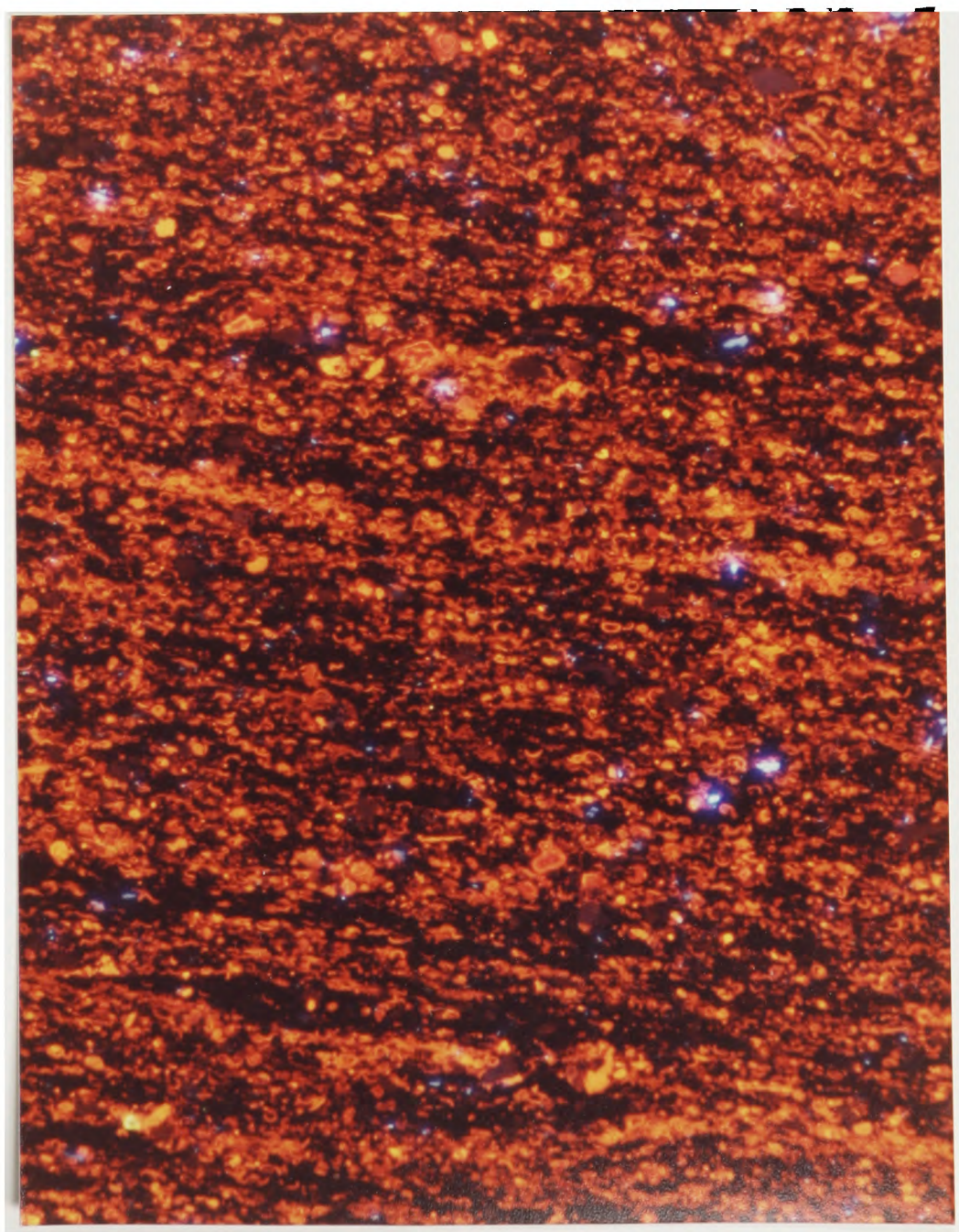

Fig 2.2Q

Thin section photomicrograph of beef calcite. Crossed polars. Laminated shale inclusions can be seen at the top. Crystal size increases away from the inclusion perhaps indicating growth from the inclusion upwards and downwards. Sample BL115, *bucklandi* zone, Lyme Regis. Field of view 1mm across.

Fig 2.2R

Thin section photomicrograph of beef calcite. Cathodoluminescence. Some zoning indicates some change in water chemistry or two or more stages of growth. Staining, however, shows that the ferroan-non-ferroan calcite contacts are bedding parallel and cut across the crystal boundaries. Same area as Fig 2.2Q.

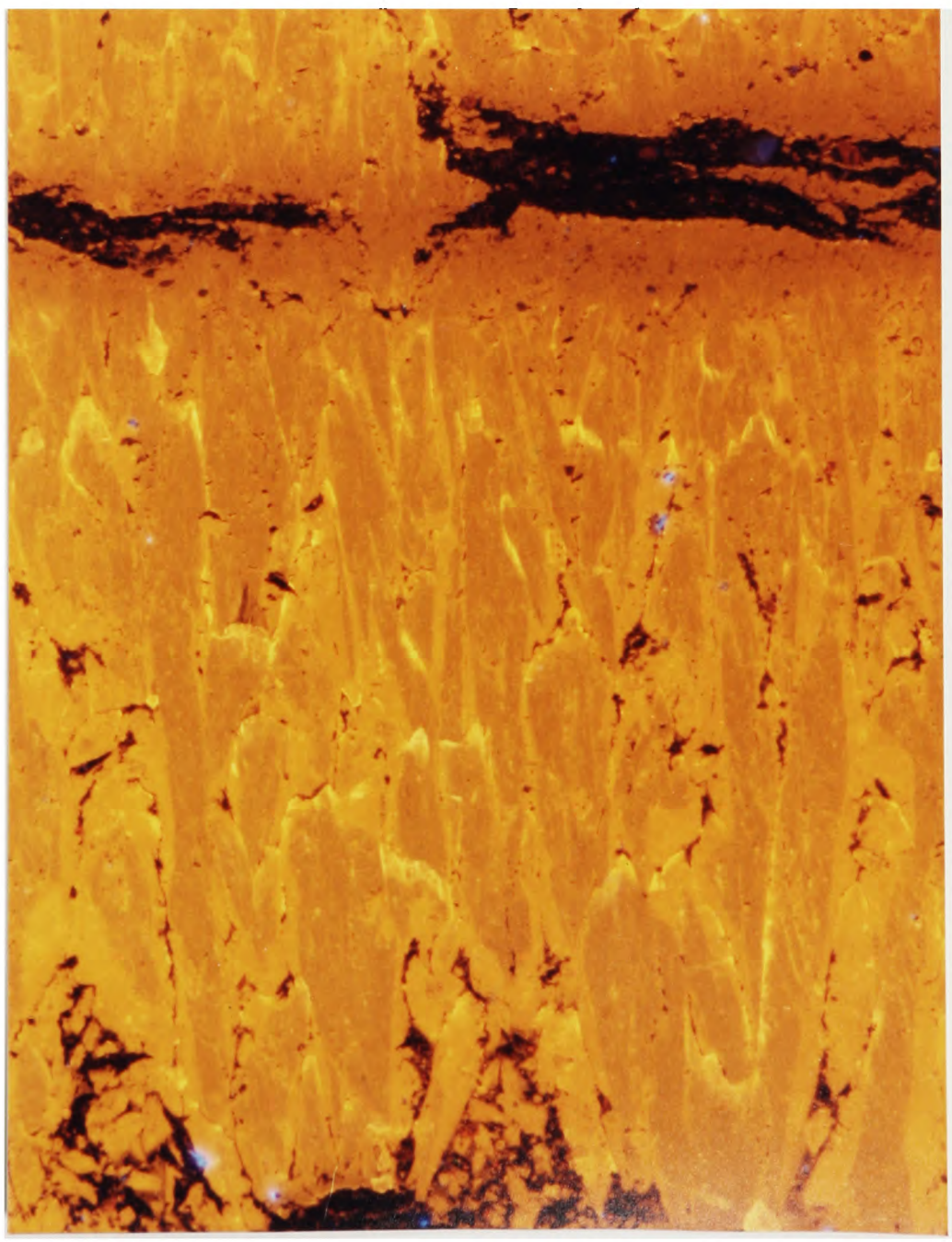

Fig 2.2S

Thin section photomicrograph of laminated limestone. Plane polarized light. Lighter and darker horizons might represent cemented bleb-rich and bleb-poor horizons (Fig 2.2M). Black areas represent pyrite. Matrix mainly consists of microspar with disseminated clay. Spherical structures might be large (60μm diameter) *Schizosphaerella* Sample LA39, bed 33, *planorbis* zone, Lavernock Point. Field of view 1mm across.

Fig 2.2T

Thin section photomicrograph of laminated limestone. Cathodoluminescence. The non-luminescent pyrite appears to be concentrated in the lighter (? originally bleb-rich) horizons. Scattered quartz grains luminesce blue. Same areas as Fig 2.2S.

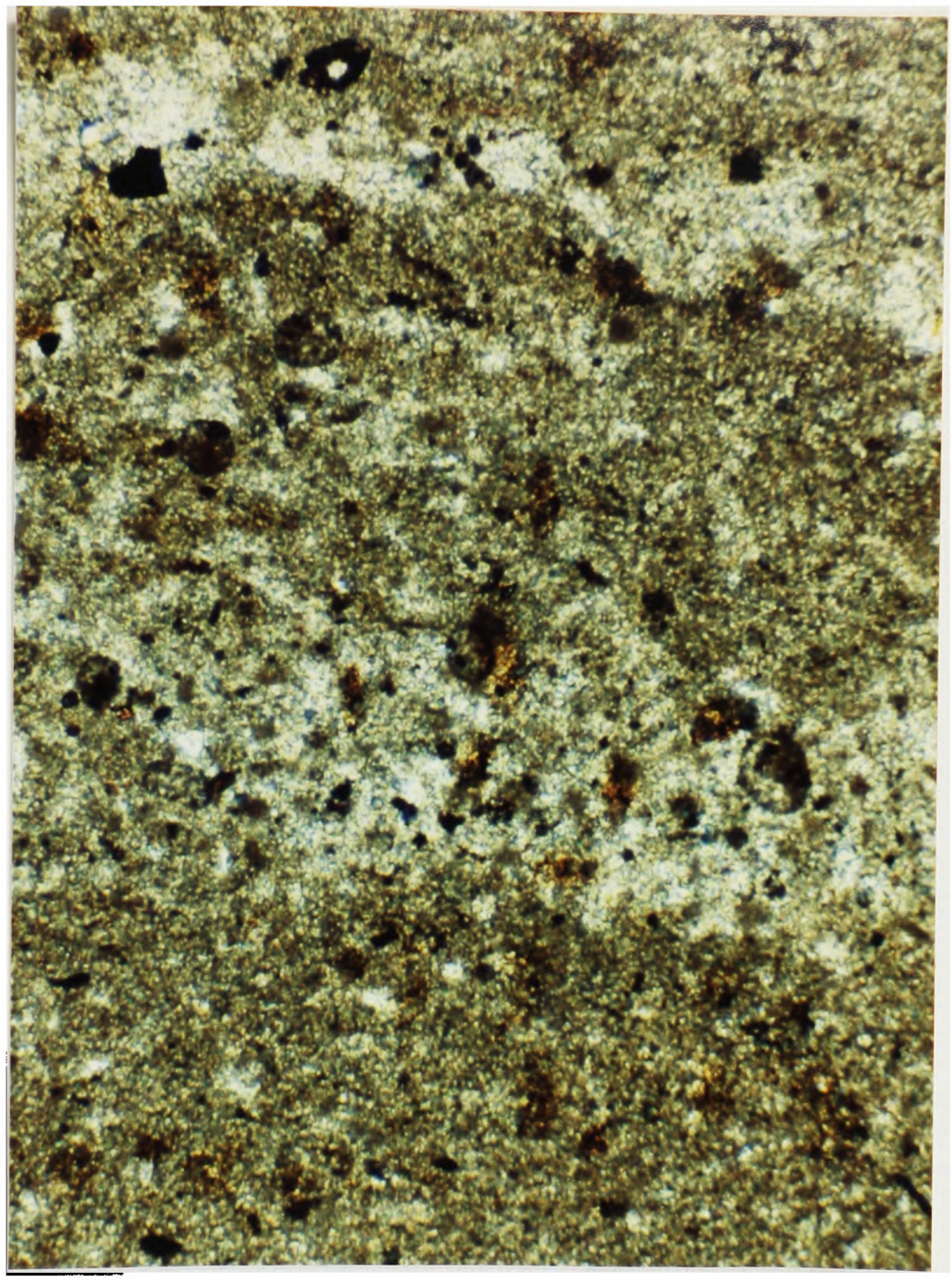

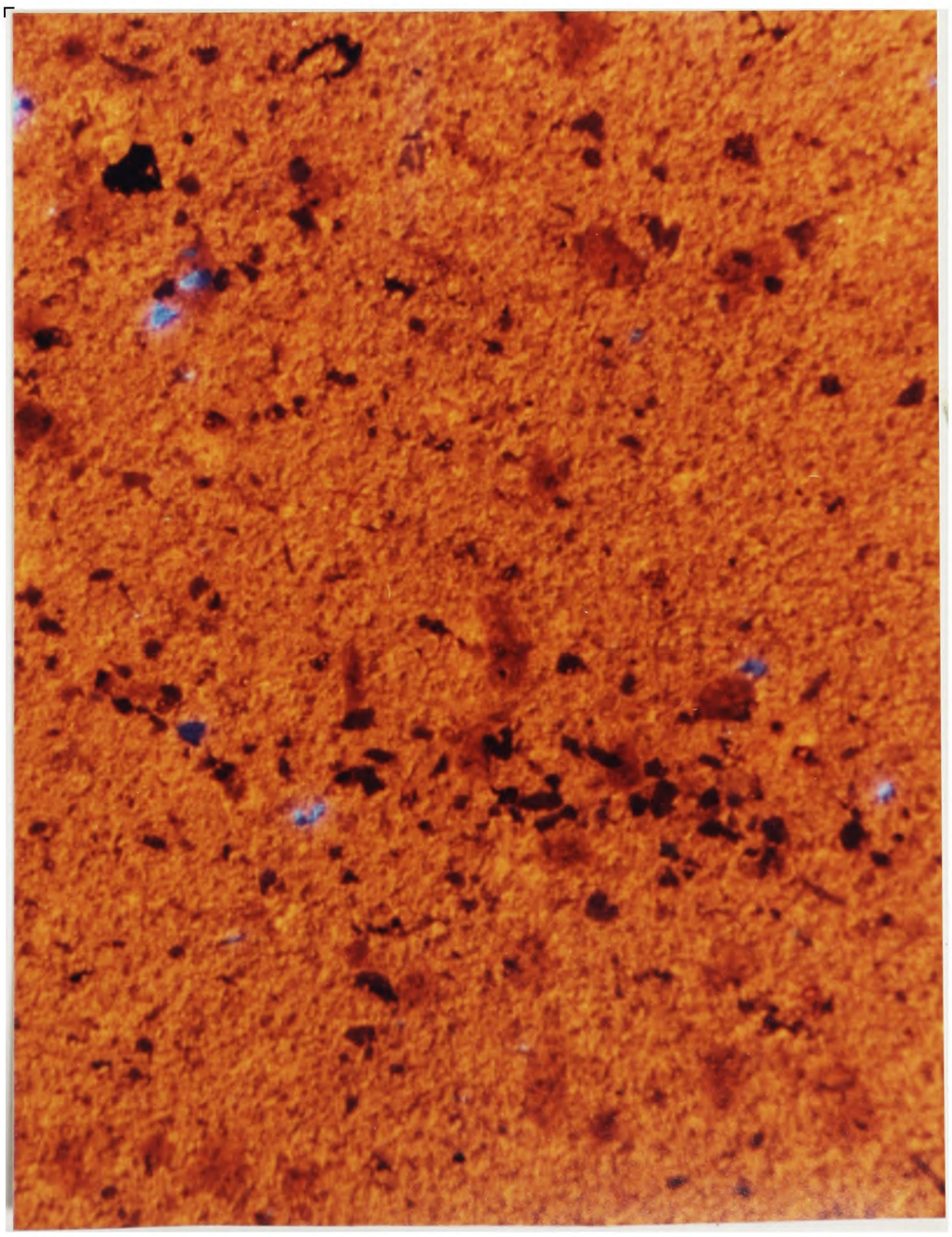

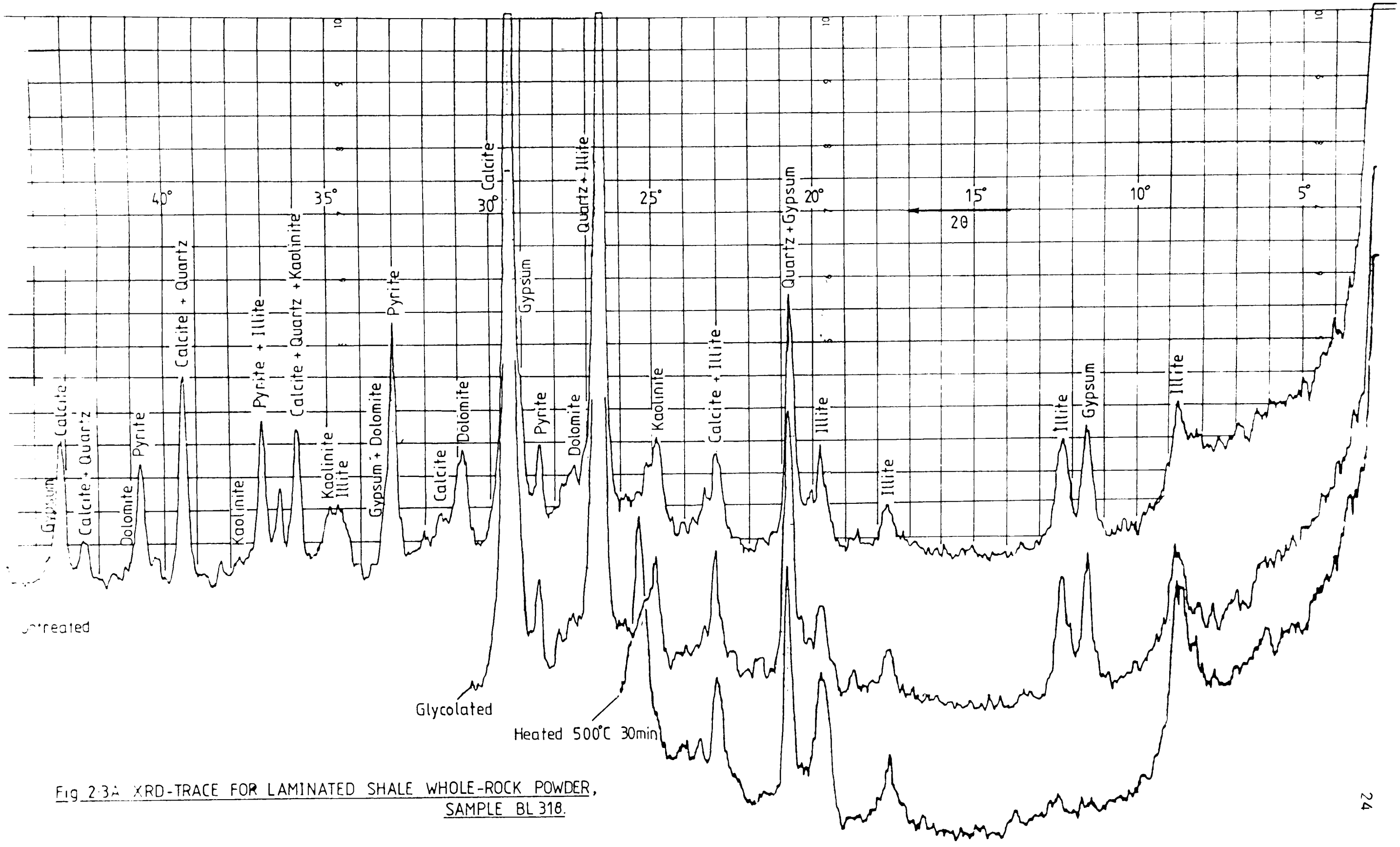

Fig 2.3A XRD-TRACE FOR LAMINATED SHALE WHOLE-ROCK POWDER, SAMPLE BL 318.

Fig 2.4A

SEM photomicrograph of limestone. A matrix of fused calcite microspar contains an elongate ring which appears to be a corroded coccolith considering its size and shape. Sample BL103, Lang's bed 29, *bucklandi* zone, Lyme Regis. Field of view 19μm across.

Fig 2.4B

SEM photomicrograph of light marl. Clay and microspar surround what appears to be a partially overgrown coccolith. Sample BW71 Palmer's bed C85, *angulata* zone, Watchet. Field of view 25μm across.

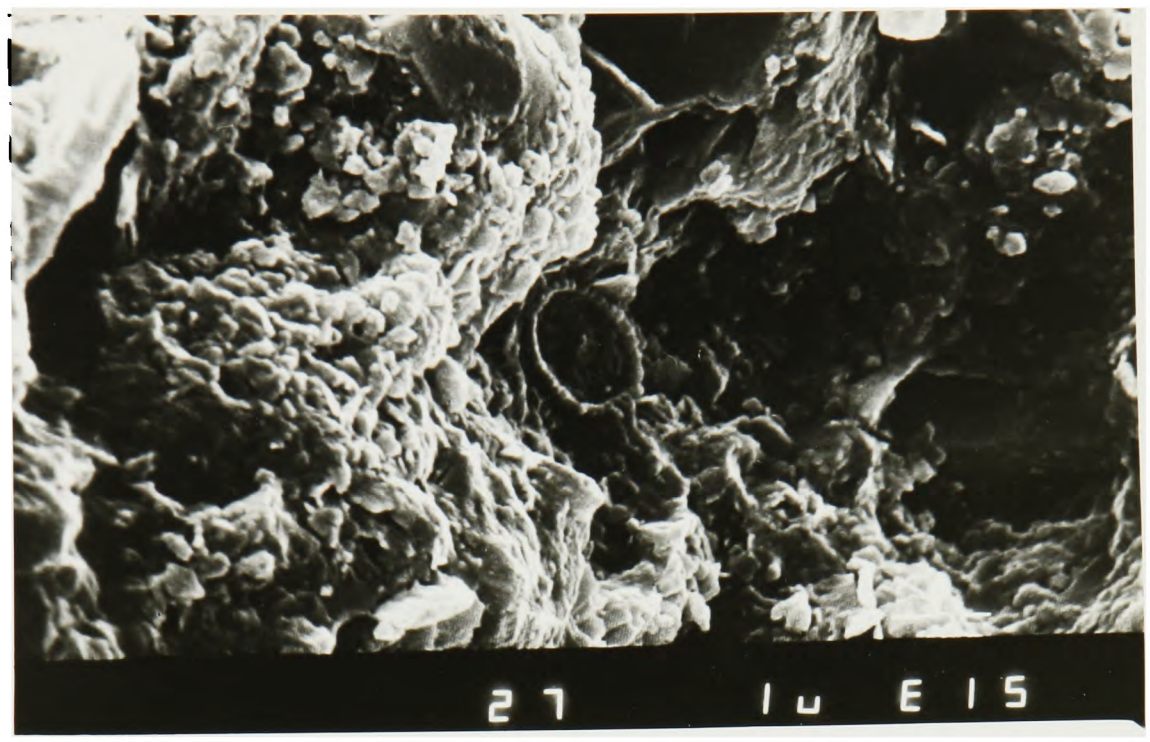
27 1u E15

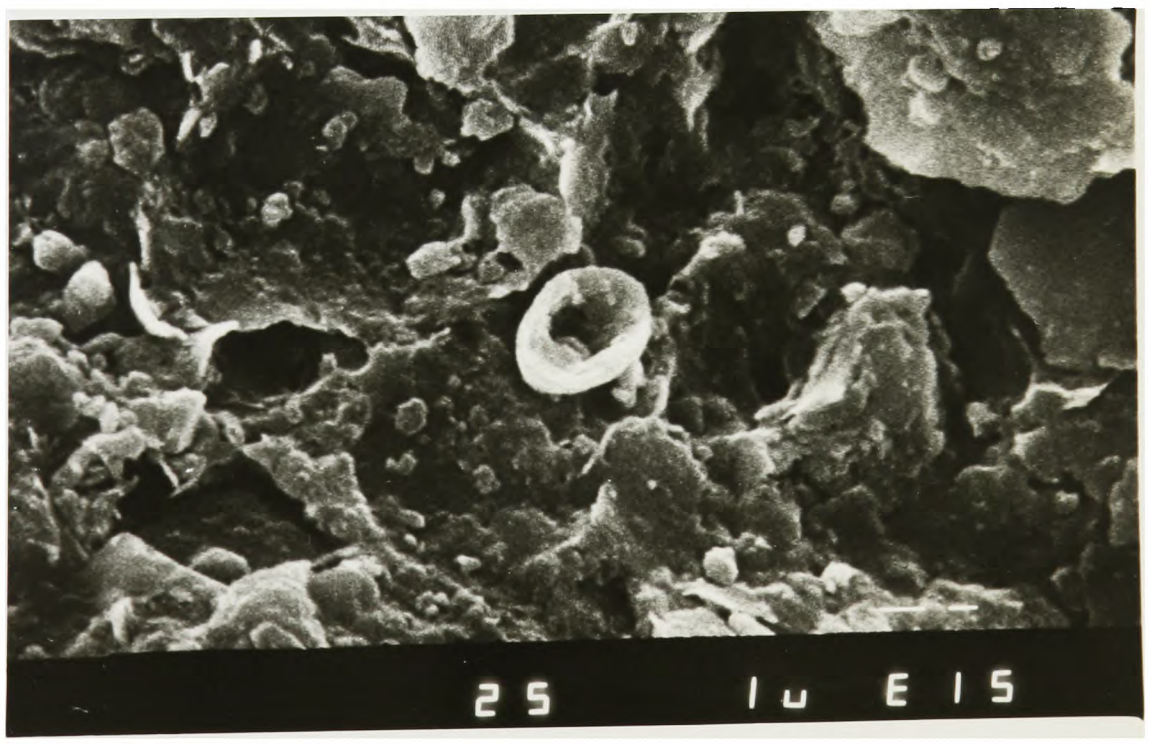
25 1u E15

Fig 2.4C

SEM photomicrograph of light marl. The spheres are Schizosphaerella punctulata - probably representing the calcified walls of a dinoflagellate (Kälin and Bernoulli 1984). The walls of this fossil were originally very porous (Fig 2.4H), but these examples are partially cemented. Sample BW71, Palmer's bed C85, angulata zone, Watchet. Field of view 78μm across.

Fig 2.4D

SEM photomicrograph of dark marl. A single valve of Schizosphaerella. The walls have been internally cemented producing a smooth outer surface. Sample LI28, Clements et al.'s bed 20d, angulata zone, Long Itchington. Field of view 38μm across.

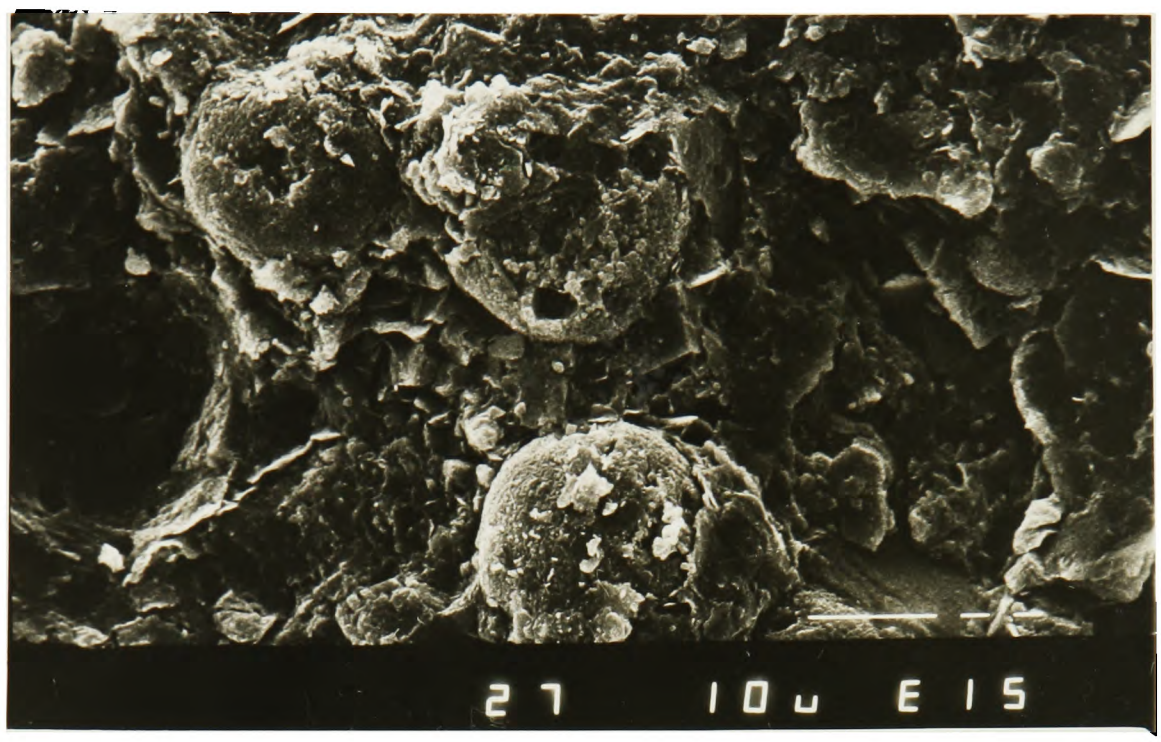
27 10u E15

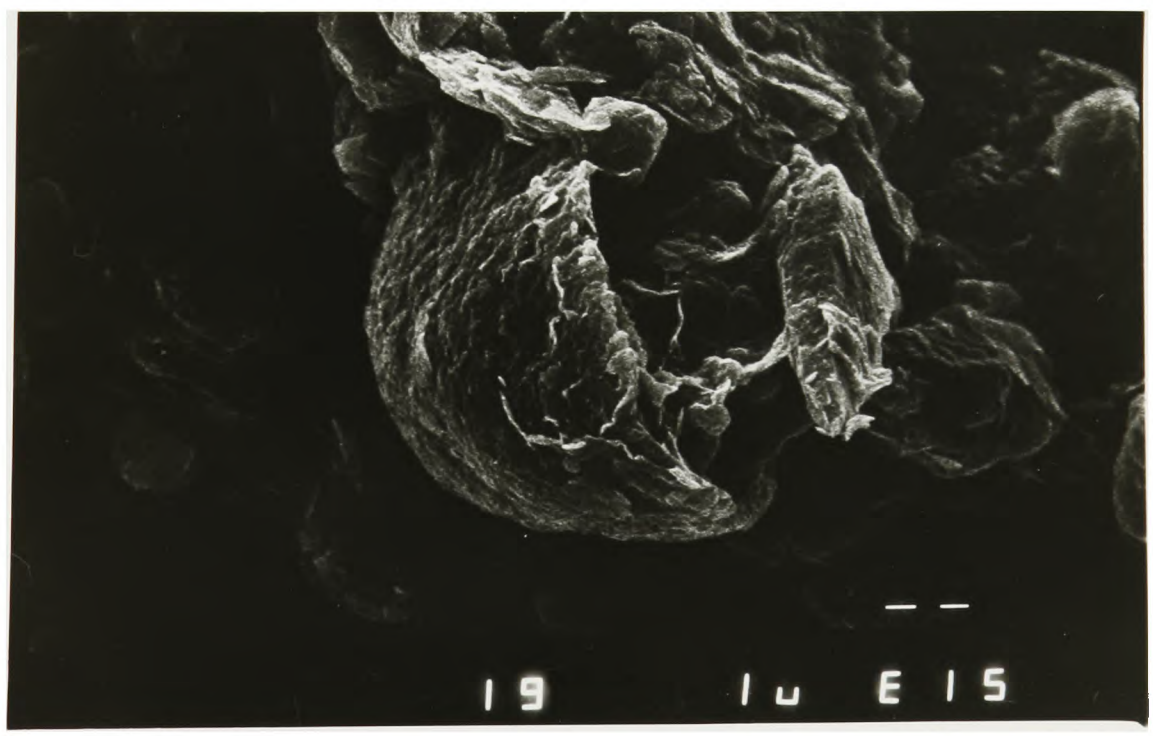
19 1u E15

Fig 2.4E

SEM photomicrograph of dark marl. A coccolith aggragate can be seen surrounded by clay and organic matter. Sample BL120, Lang's bed 32, *bucklandi* zone, Lyme Regis. Field of view 124μm across.

Fig 2.4F

SEM photomicrograph of dark marl. Close-up of the top part of the coccolith aggregate in Fig 2.4E. Notice that a variety of sizes and species of coccoliths are present (see Hamilton 1980 for identifications). Most of the aggregates appear to be free of clay, but microspar crystals appear to be engulfing some coccoliths (eg. middle centre, middle top and lower left). Sample BL120 as Fig 2.4E. Field of view 64μm across.

2 10u E15

3 1u E15

Fig 2.4G

SEM photomicrograph of dark marl. Part of a coccolith aggragate showing microspar overgrowths on coccoliths. Sample BL120, Lang's bed 32a, *bucklandi* zone, Lyme Regis. Field of view 45μm across.

Fig 2.4H

SEM photomicrograph of laminated shale. A matrix of clay and organic matter contains a sma ll coccolith aggregate (top left), *Schizosphaerella puntulata* (middle centre and middle right), and a euhedral microspar crystal. The calcite laths which make up the wall of *Schizosphaerella* can be seen in the left hand specimen, but they are larger and more fused than examples figured by Kälin and Bernoulli (1984). Lower right is an area of fibrous clay - probably authigenic illite. Sample BL117, Lang's bed 32, *bucklandi* zone, Lyme Regis. Field of view 75μm across.

8 1u E15

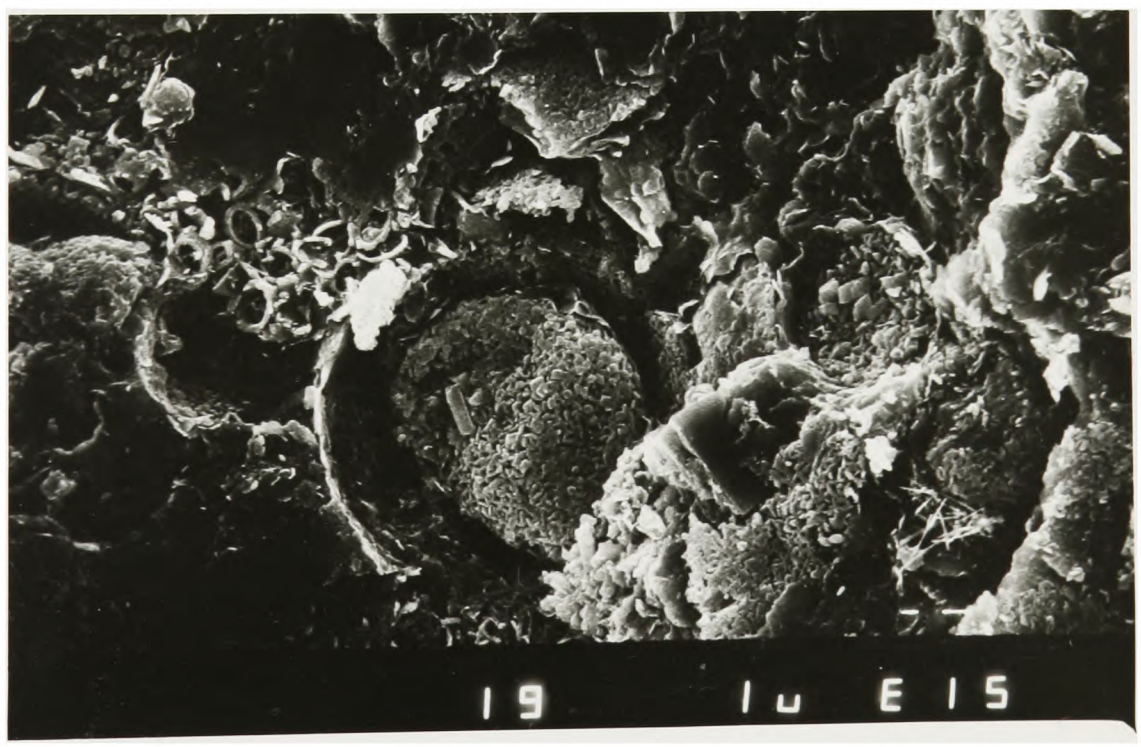
19 1u E15

Fig 2.4I

SEM photomicrograph of laminated shale. Three specimens of Schizosphaerella punctulata can be seen. The left hand specimen is surrounded by lightly fused microspar crystals, whereas the right hand specimens are embedded in fused microspar. Notice that the specimens are not surrounded by fringes of radial calcite spar (cf. Kälin & Bernoulli 1984). Specimen BW83, Palmer's bed C94, angulata zone, Watchet. Field of view 75μm across.

Fig 2.4J

SEM photomicrograph of laminated limestone. A microspar matrix encloses a Schizosphaerella specimen with a slightly pitted surface the walls appear to have been almost totally cemented (compare with Fig 2.4H). Sample BW86, Palmer's bed C94, angulata zone, Watchet. Field of view 75μm across.

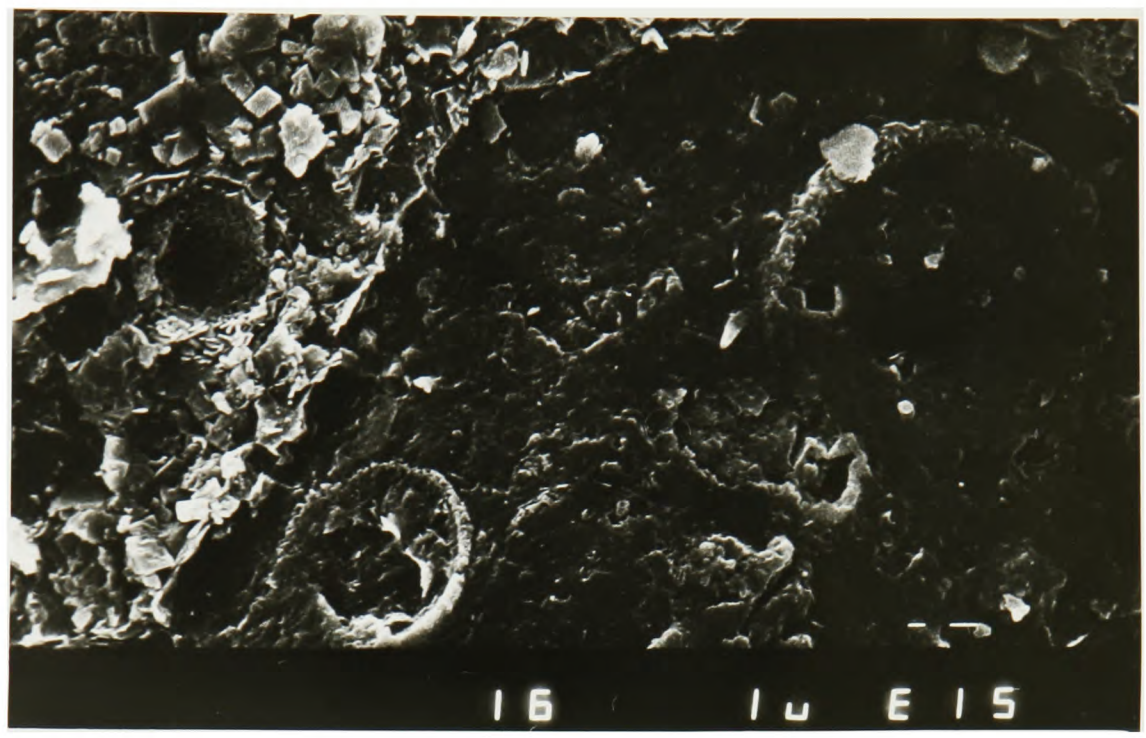
16 1u E15

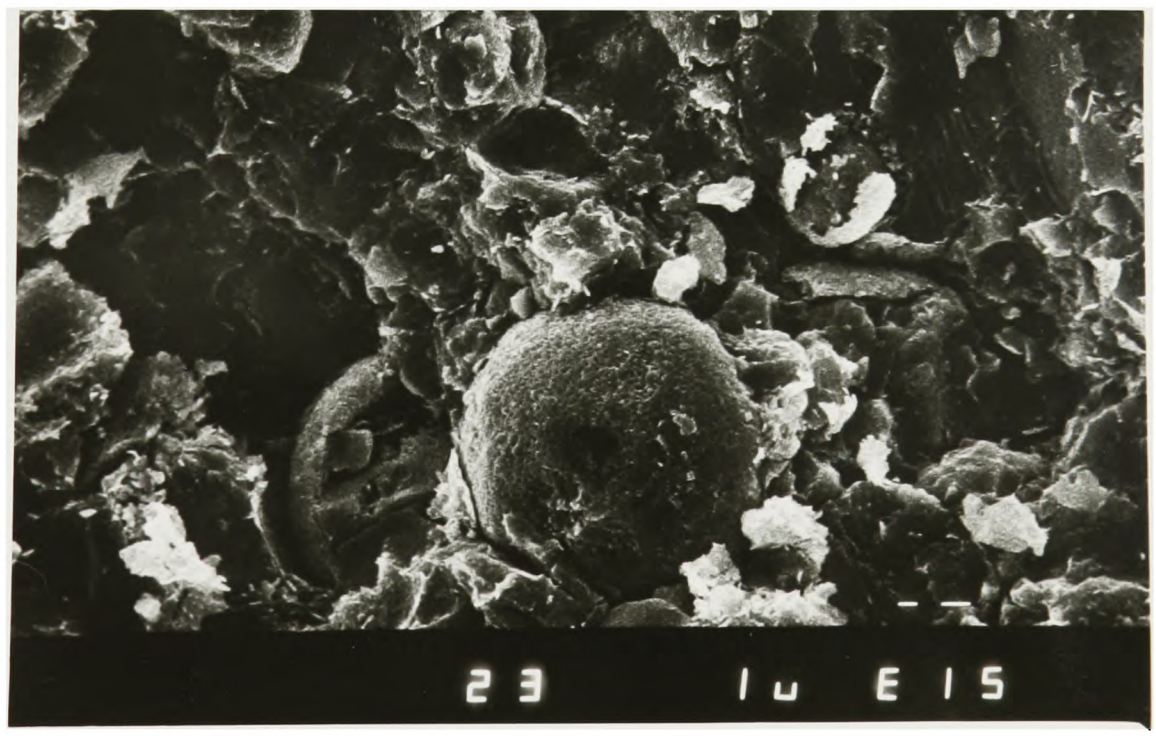
23 1u E15

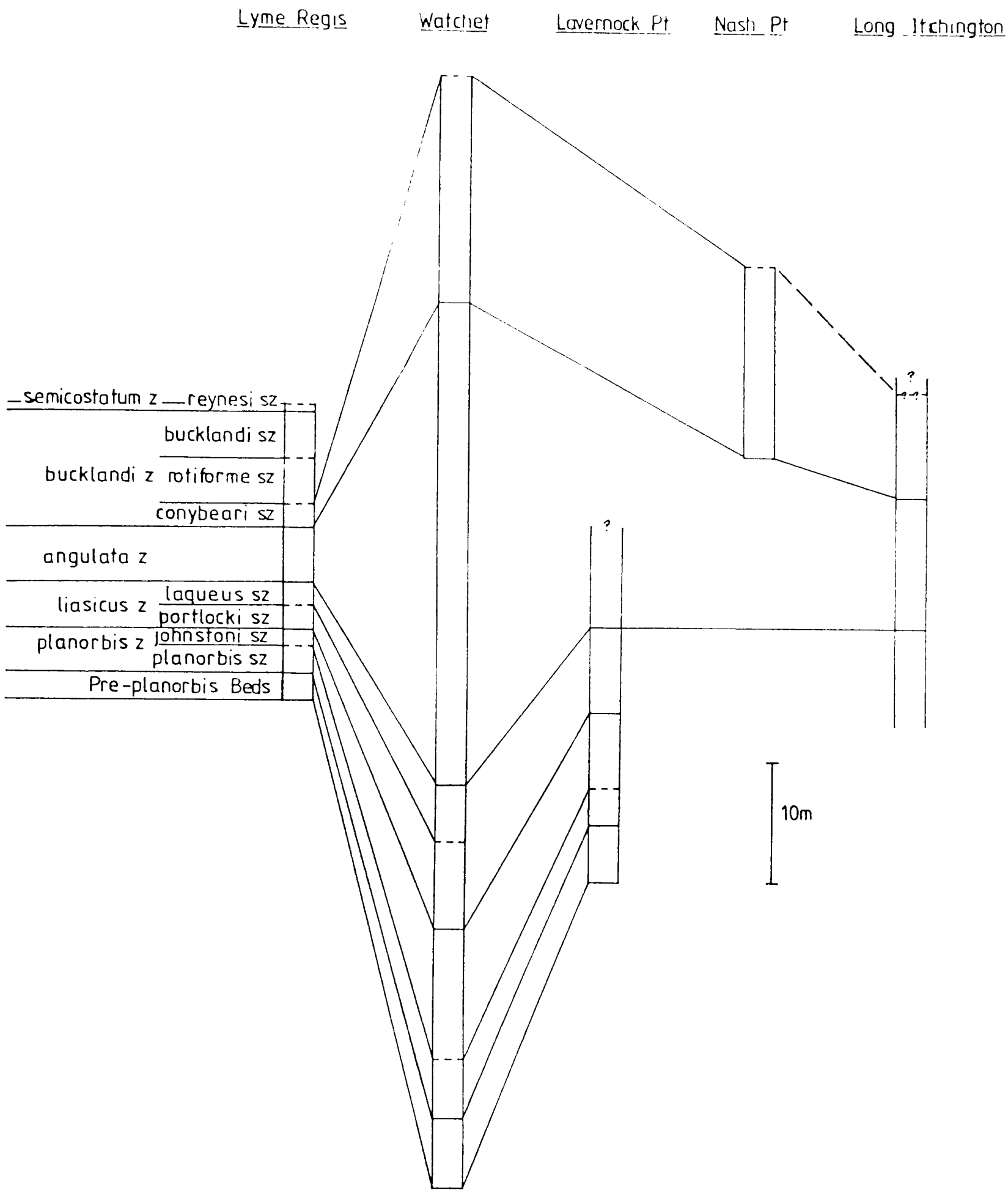

Fig 2·5A RELATIVE THICKNESS CHANGES IN THE BASAL LIAS STUDIED.

Fig 2.5B

Limestone surface dominated by Gryphaea. Other types of body fossils are rare, limestone beds dominated by one body fossil were ascribed to biological processes rather than winnowing. The specimens associated are unbroken and of much lower density than would be expected for a winnowed horizon. On the other hand the density of bioclasts is higher than in most limestones and the combination of low diversity 'high' density biota implies a restricted environment (there is some evidence for less than normal oxygenation for light marl (limestone) deposition (Section 5.2.2)). Palmer's bed C93, angulata zone, Watchet. The hammer is 39cm long.

Fig 2.5C

Limestone containing intraclasts. The intraclasts represent limestone and laminated shale and some contain worn bioclasts. The matrix limestone is dominated by dispersed crinoid fragments. Loose block, Lyme Regis. The lens cap is 5 cm in diameter.

MINOLTA

Fig 2.5D

Isolated dark marl burrow-mottles. In this limestone bed a continuous dark marl bed can usually be seen overlying the dark marl burrow-mottles (eg. Fig 2.1G and 2.1H). However, here the dark marl bed appears to have been removed by erosion, leaving the mottles, but not the sediment which filtered down into the originally open burrows. Lang's bed 19, angulata zone, Lyme Regis.

Fig 2.5E

Cut and polished block of limestone showing encrusted and bored surface. At the base of the block are intraclasts of lamniated shale. A dome shaped surface (left) is overlain by bioclastic packstone grading up into burrow-mottled carbonate mudstone. Lang's bed 25, *conybeari* subzone, *bucklandi* zone, Lyme Regis. Width of photo represents 25cm.

Fig 2.5F

Close-up of Fig 2.5E. The dome shaped surface is encrusted by *Liostrea*. At the centre bottom two sharp contacts between limestone of different colours appear to intersect. This suggests that the dome consists of limestone intraclasts. Just below the encrusted surface, centre right, is a truncated bioclast within what appears to be a triangular intraclast. Under the encrusted surface, top left, are a series of U-shaped *Trypanites* (? bivalve) borings. Width of photo represents 12cm.

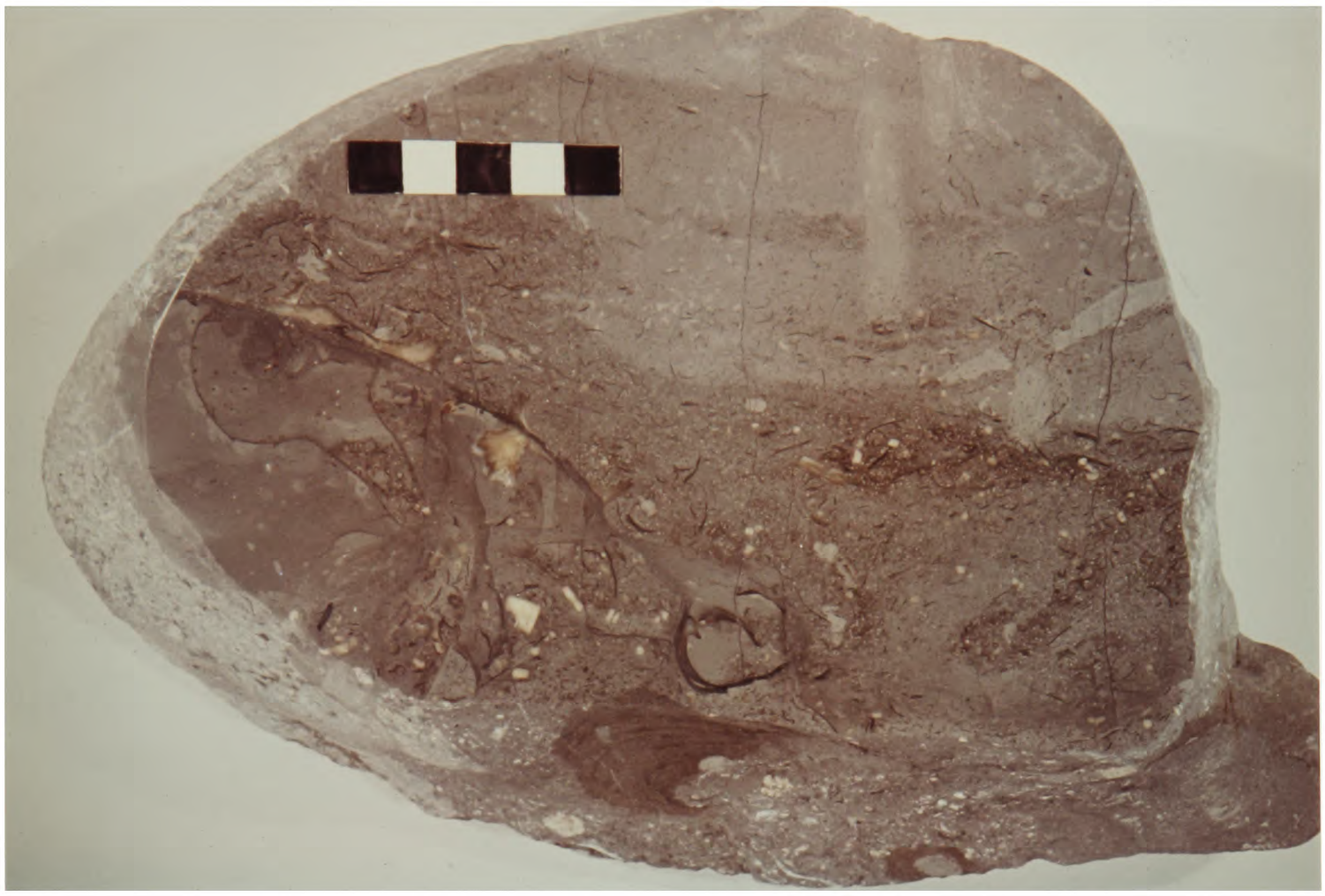

Fig 2.5G

Negative print of acetate peel from encrusted and bored limestone surface. Close-up of the top centre of Fig 2.5F (note this print is reverse sense to Fig 2.5F). The *Liostrea* specimen has borings of *Talpina ramosa* (? phoronid) and encrusts a limestone surface which also has *Talpina* borings. Very small dots and thin lines within the left part of the *Liostrea* may represent algal or fungal borings (Kennedy pers. comm. 1985). At the right of the print, about 1mm of 'light' coloured limestone overlies the bored limestone and underlies the *Liostrea* specimen. The limestone with *Talpina* borings forms a layer about 3mm thick on top of a flat surface of 'lighter' coloured limestone which is interrupted by *Trypanites* borings elsewhere (Fig 2.5F). The *Liostrea* specimen is overlain by bioclastic packstone/wackestone with many small gastropods and benthonic foraminifera. Width of print represents 1.7cm.

Fig 2.5H

Negative print of acetate peel from encrusted and bored limestone surface. Close-up of the top left of Fig 2.5F. The bored limestone surface has been bored and encrusted several times. The top part of the *Trypanites* borings of Fig 2.5F can be seen at the lower left. Width of print represents 2.5cm.

Fig 2·8A STRATIGRAPHIC VARIATION IN THE AVERAGE PROPORTIONS OF DIFFERENT ROCK TYPES

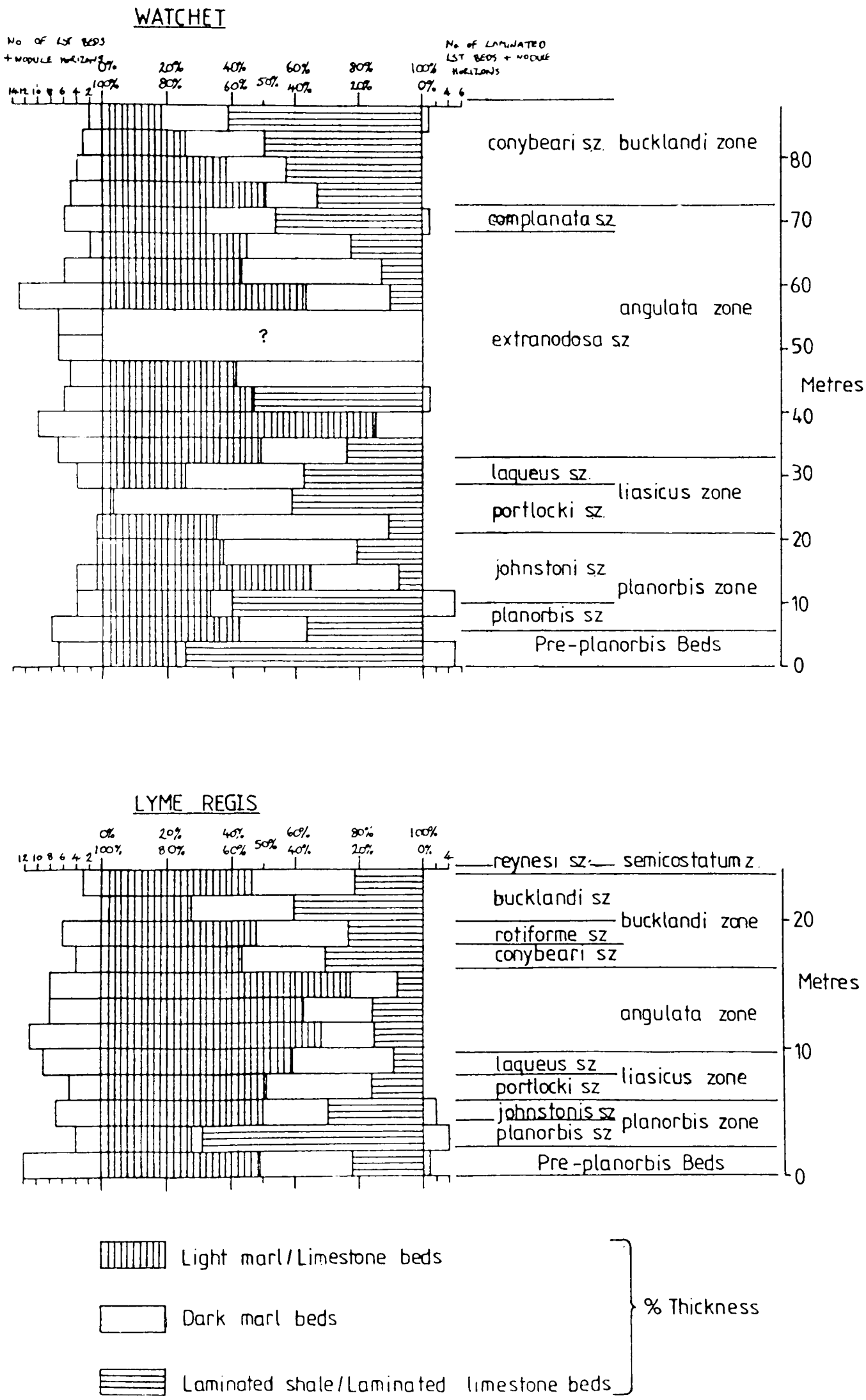

Fig 2.8B STRATIGRAPHIC VARIATION IN THE AVERAGE PROPORTIONS OF DIFFERENT ROCK TYPES

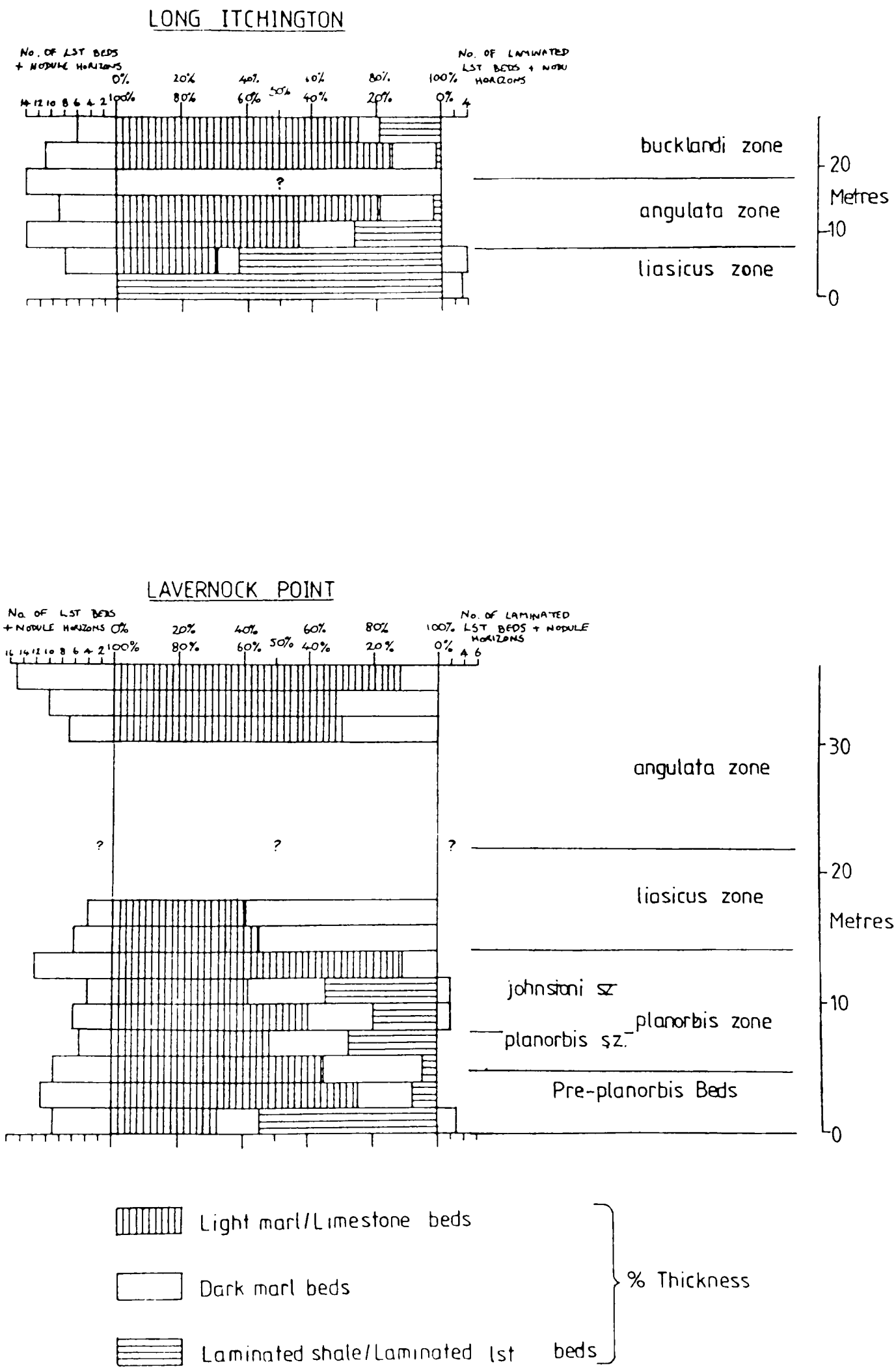

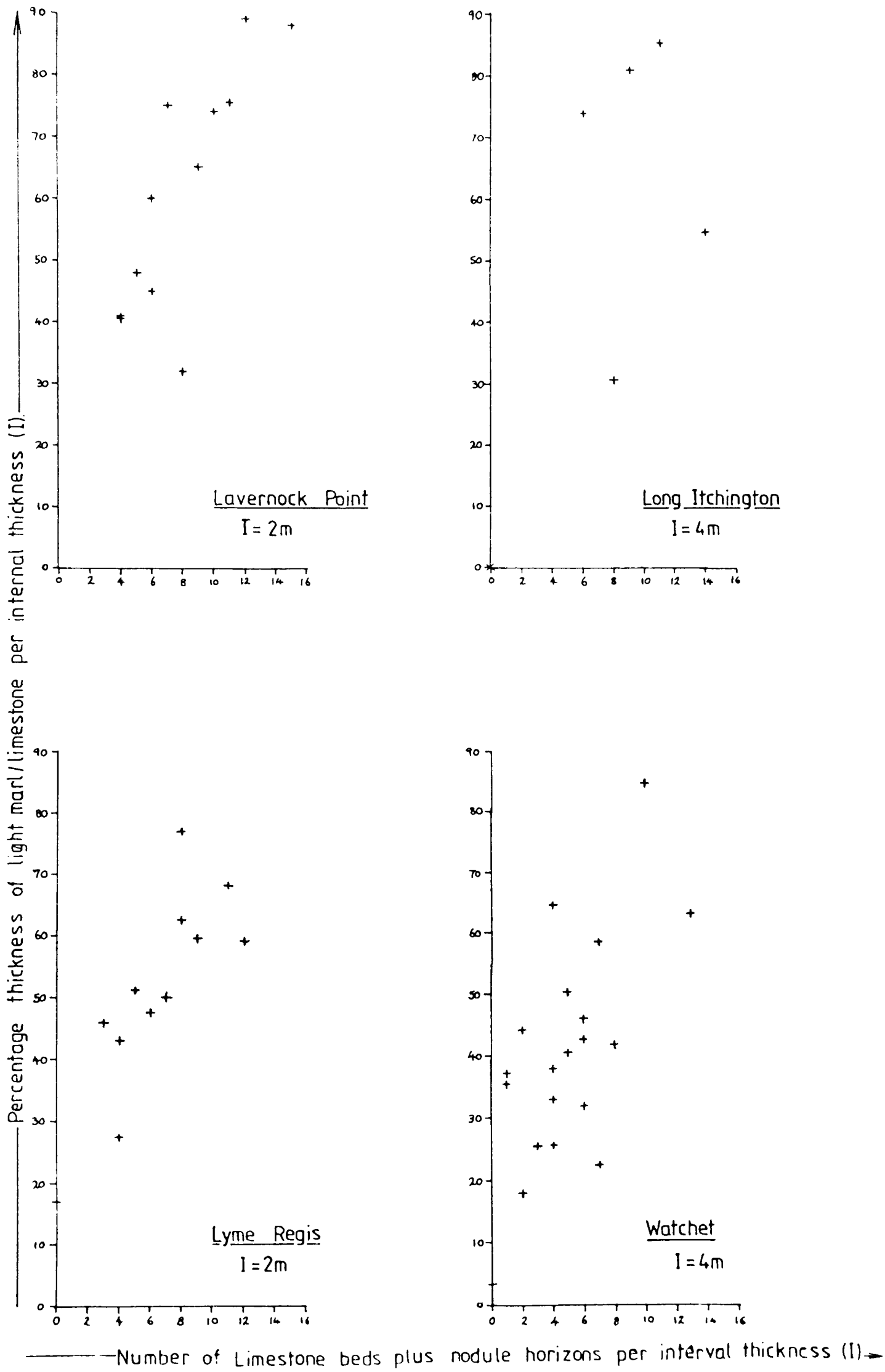

Fig 2·8C Correlation of %lM/L thickness with No. of L beds + nodule horizons

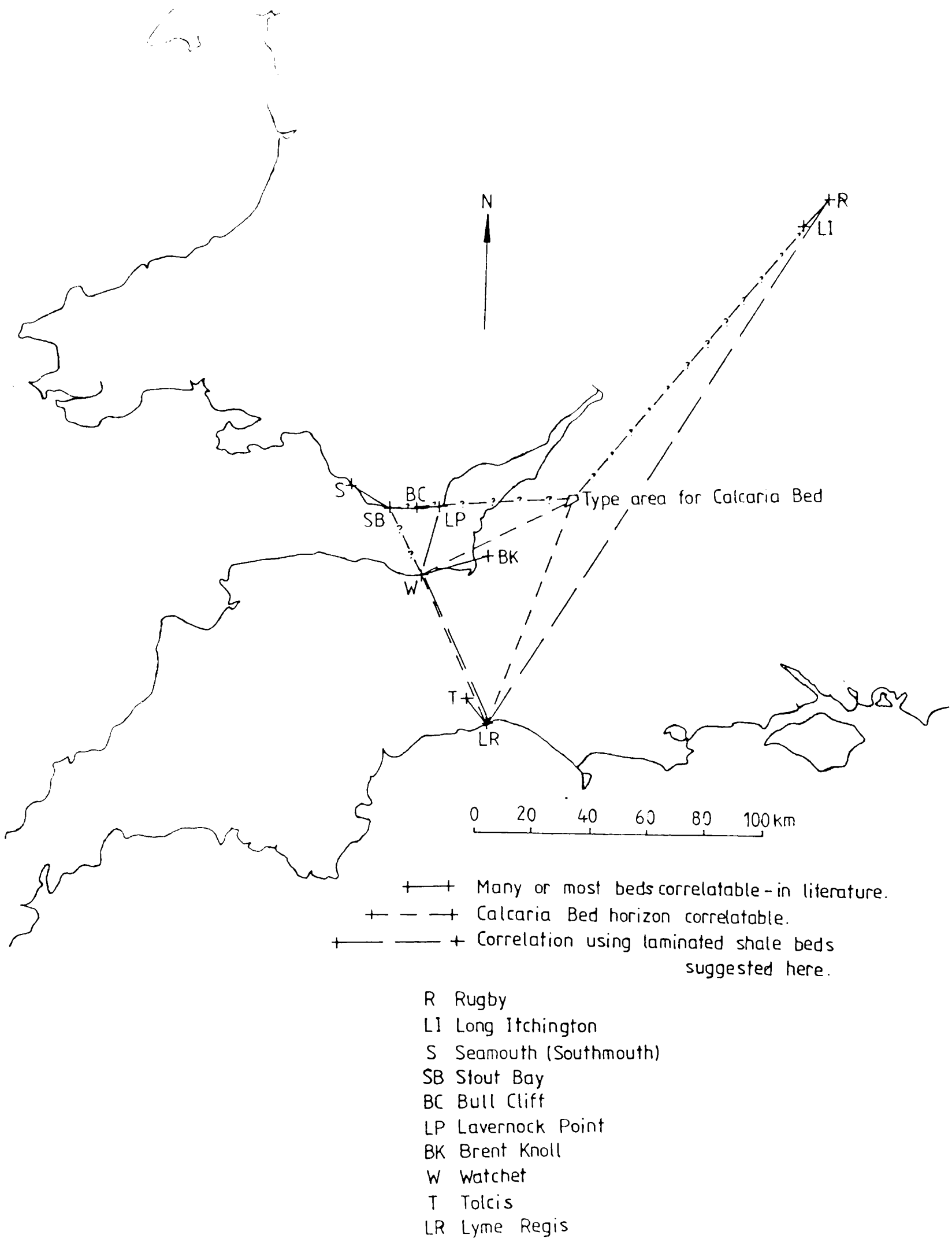

Fig 2·8D CORRELATION IN THE BASAL LIAS

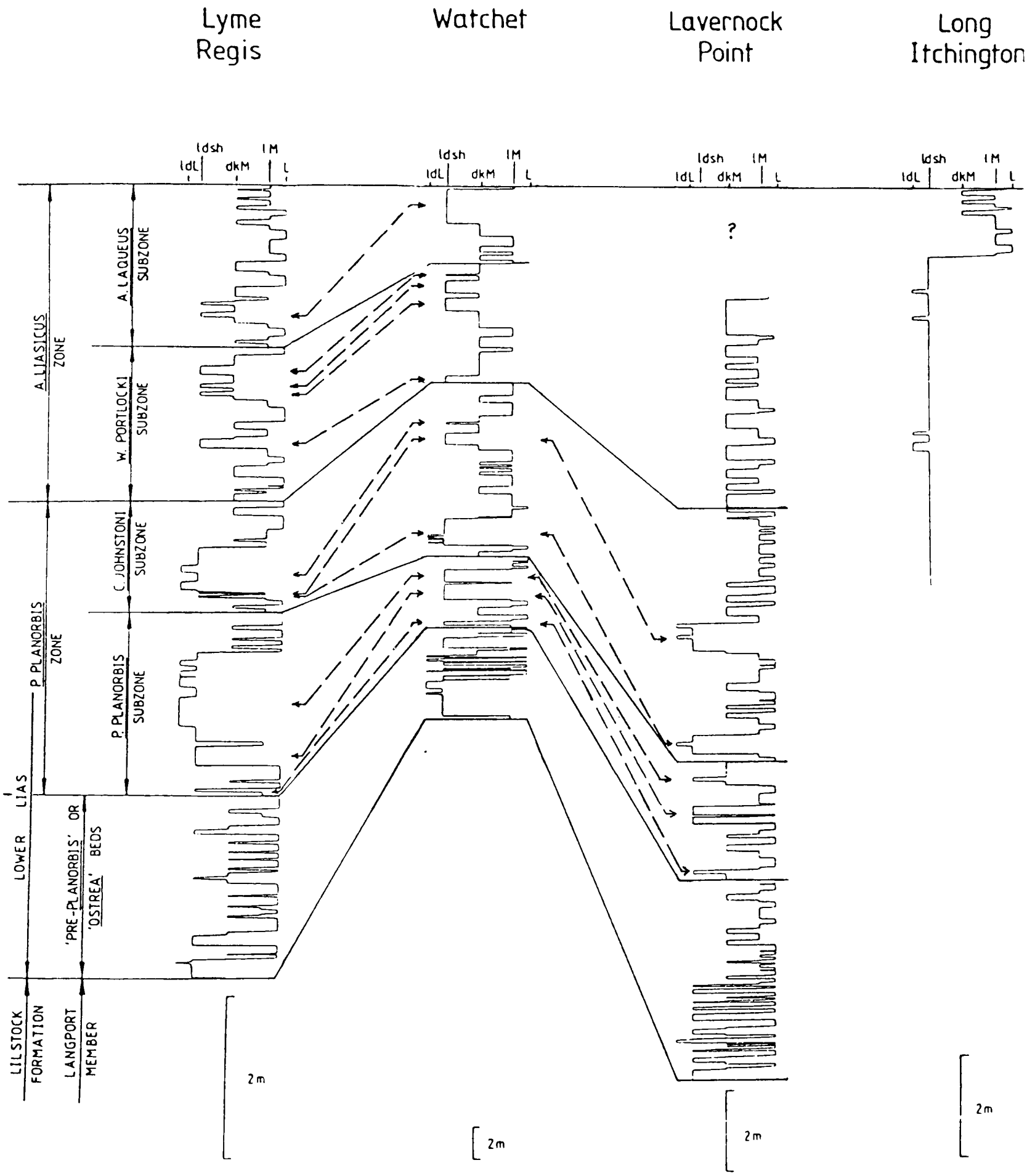

Fig 2·8E POSSIBLE LITHOSTRATIGRAPHIC CORRELATION FOR THE LOWER PART OF BASAL LIAS

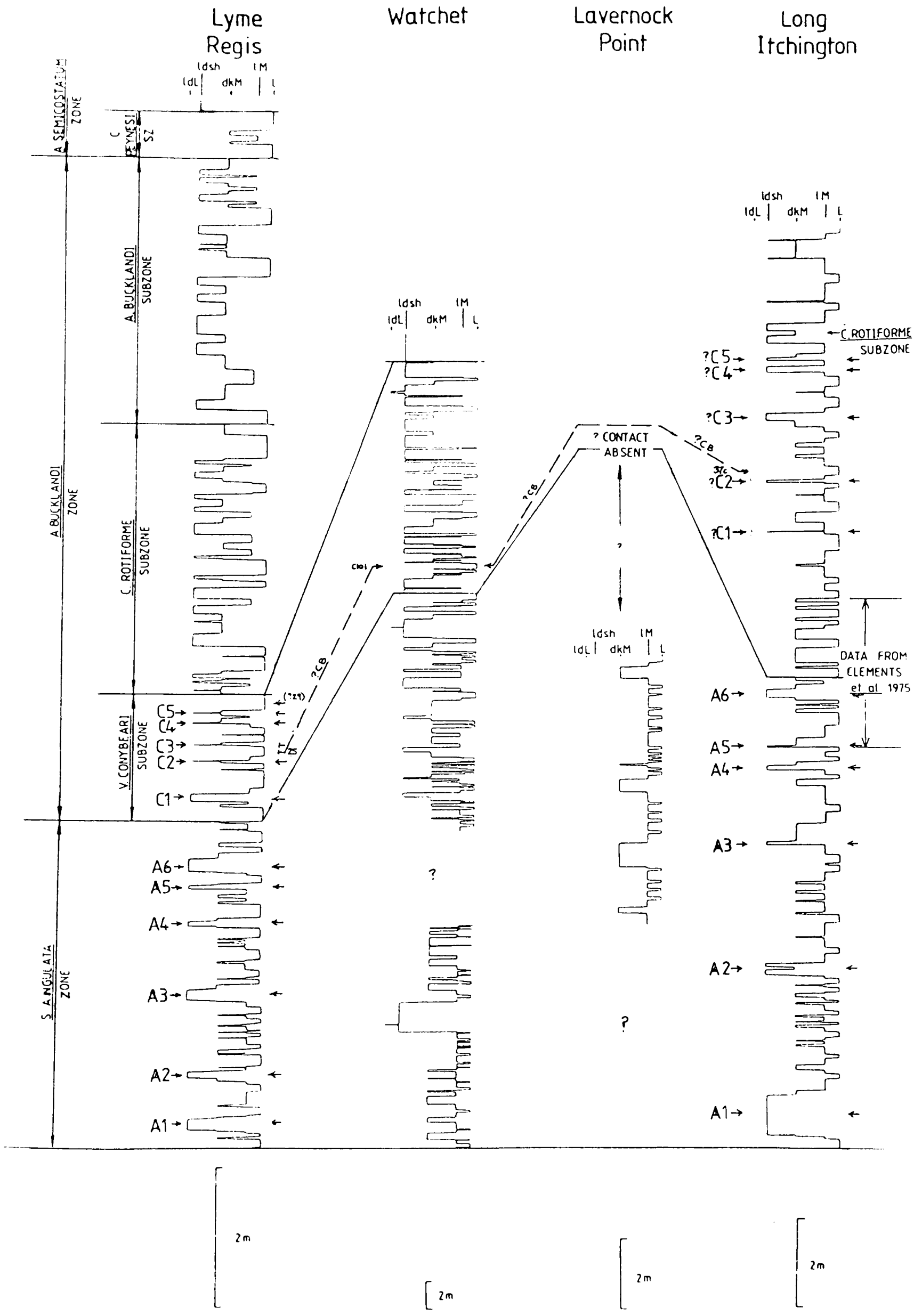

←(25) Calcaric Bed Equivalent and local bed number

Fig 2·8F POSSIBLE LITHOSTRATIGRAPHIC CORRELATION FOR THE UPPER PART OF BASAL LIAS

Fig 3 2A LOWER LIAS WHOLE ROCK COMPOSITION ACCORDING TO ROCK TYPE

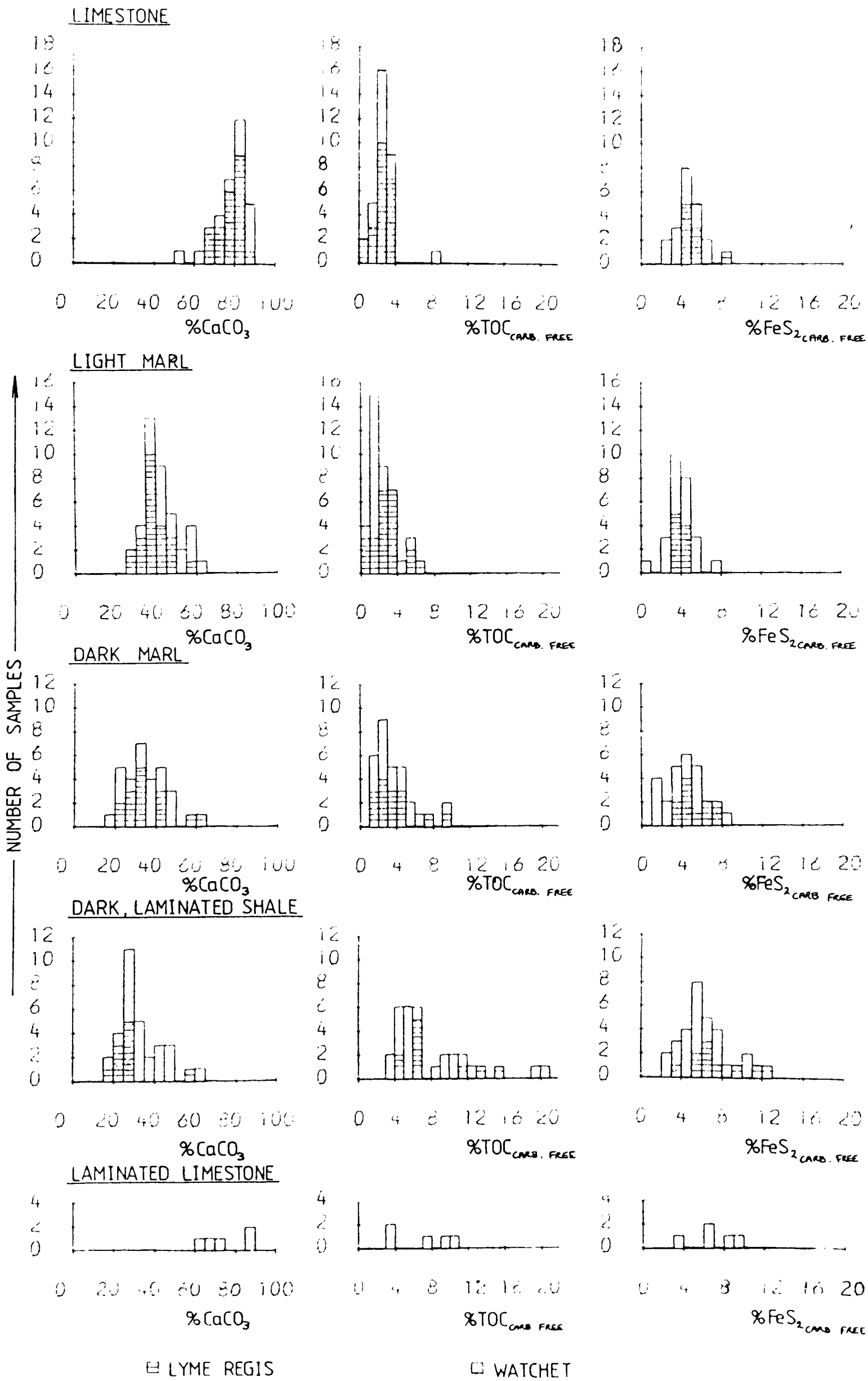

Fig 3·2B TOC / $CaCO_3$ RELATIONSHIP AT WATCHET AND LYME REGIS

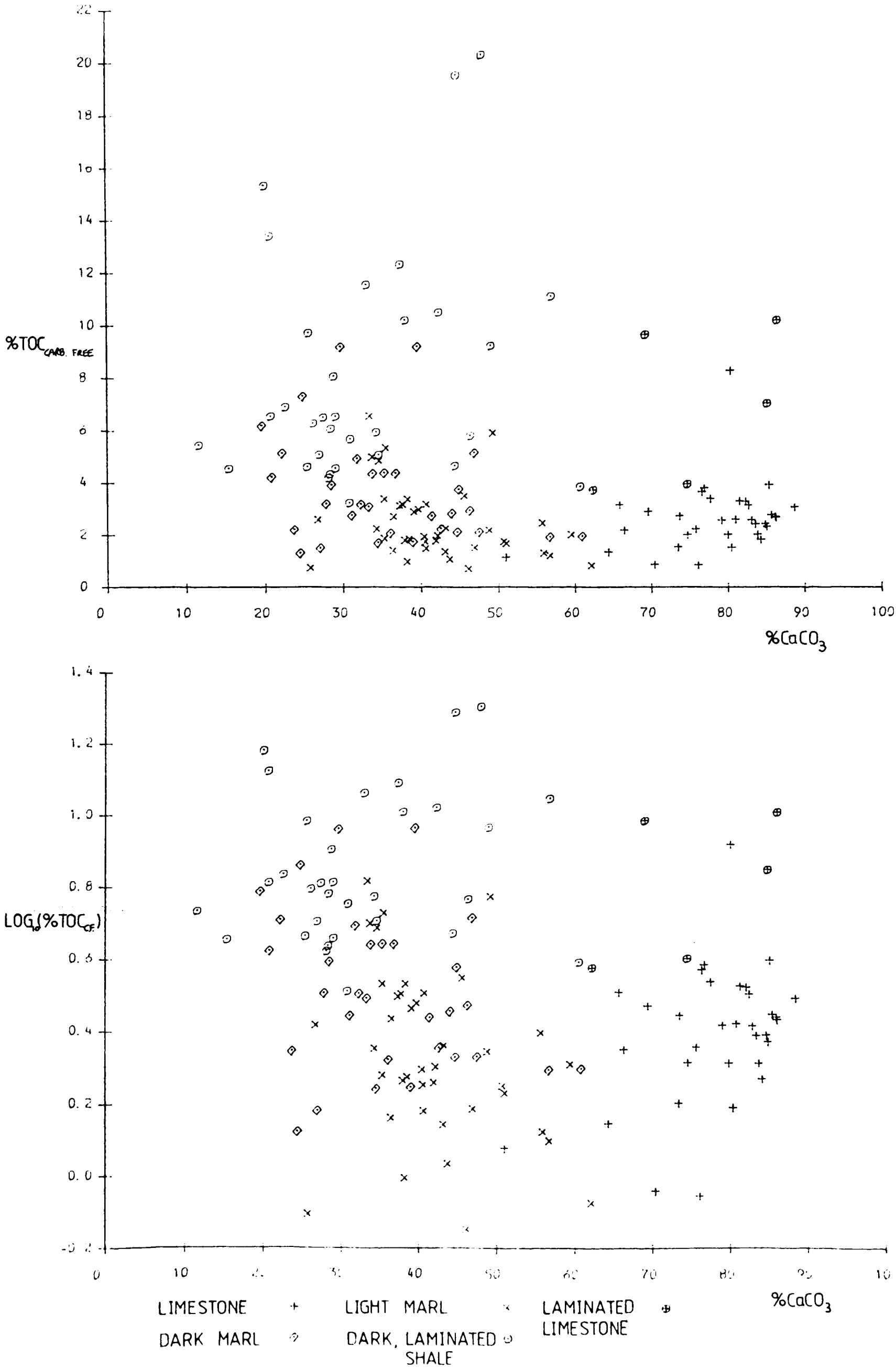

Fig 3·2C CLAY/ FeS_2/$CaCO_3$ RELATIONSHIPS AT WATCHET AND LYME REGIS

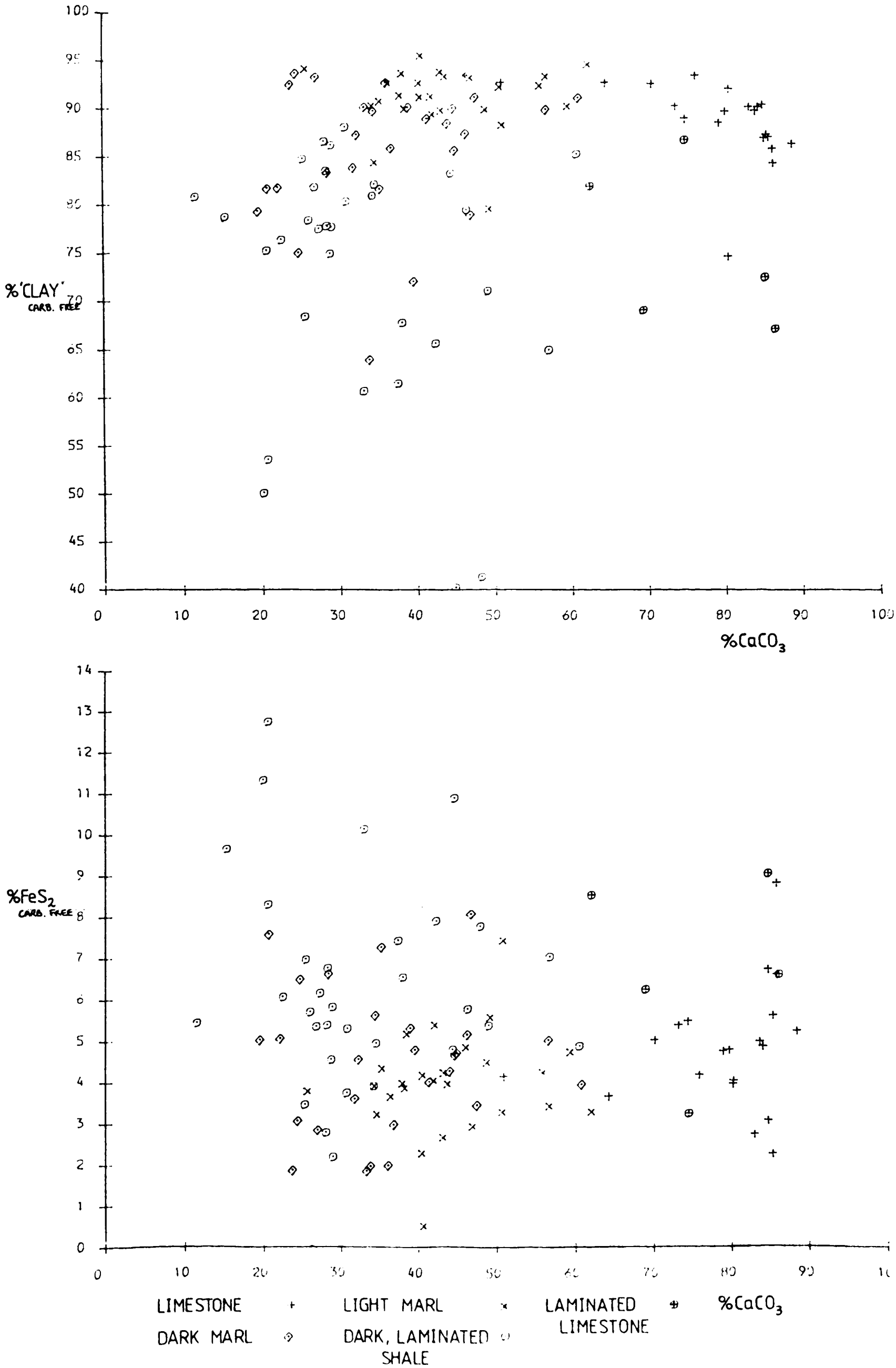

Fig 3·3A VARIATION IN WHOLE ROCK COMPOSITION AT WATCHET

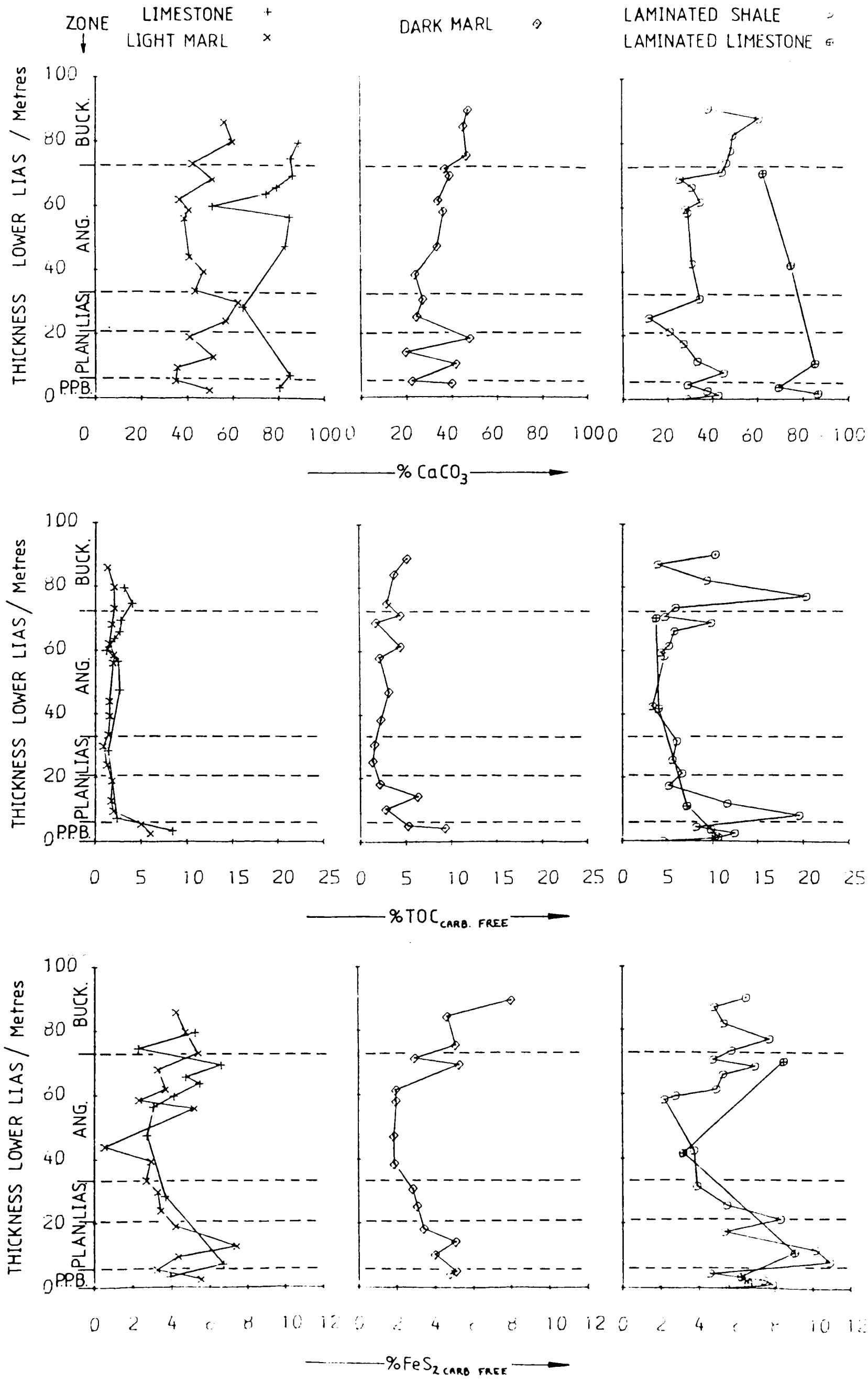

Fig 3·4A DETAILED GEOCHEMICAL PROFILES THROUGH LANG'S BEDS 13-20, UPPER S.ANGULATA ZONE, SEVEN ROCK POINT, LYME REGIS

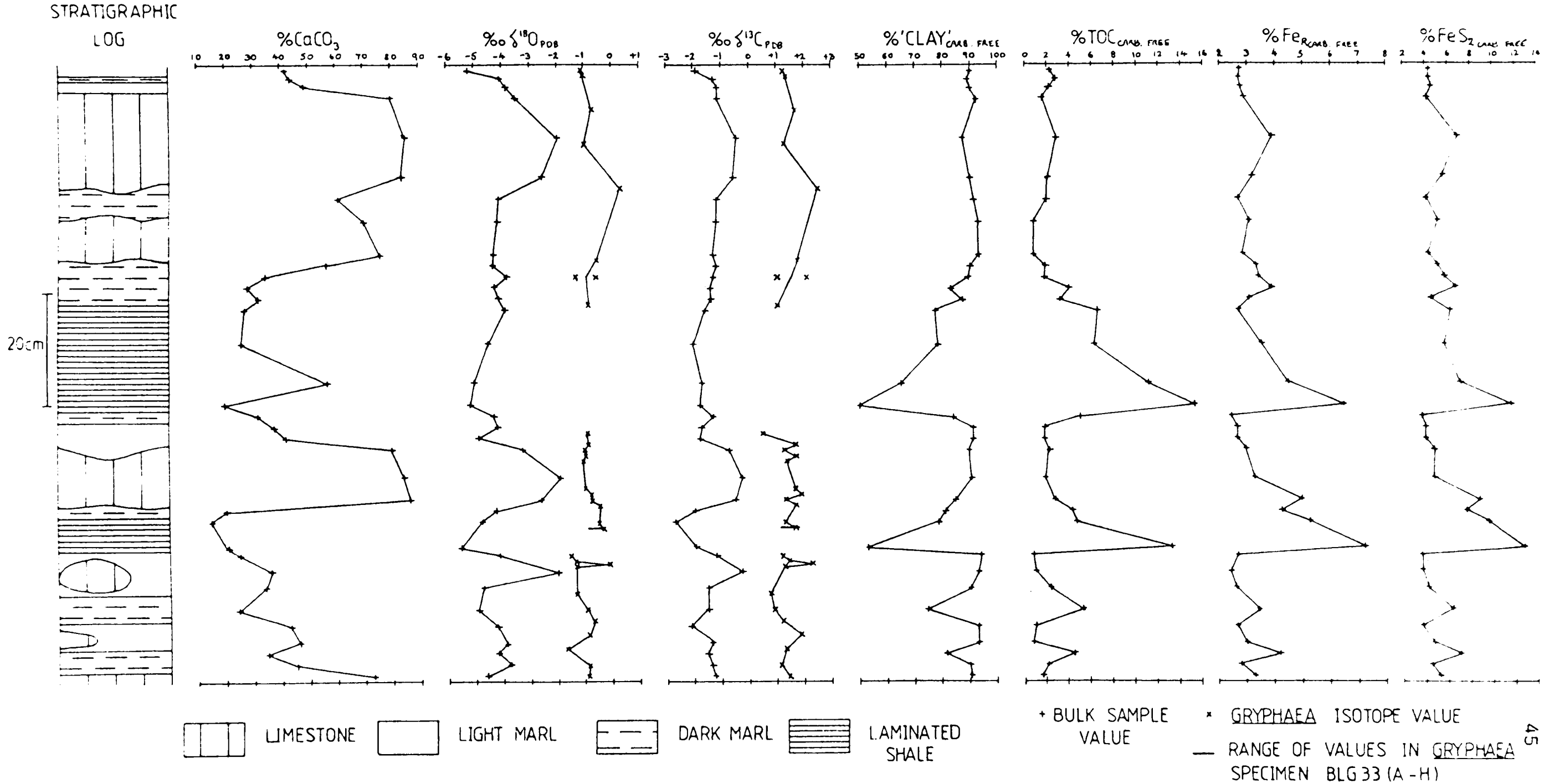

Fig 3.5B

Lang's beds 13-20, angulata zone, Seven Rock Point, Lyme Regis. Compare with Fig 3.4A and Appendix Section 2.1. A number of Gryphaea can be seen. The hammer is 39cm long.

Fig 3.4C INTERPRETATION OF S/DOP/Fe/TOC PLOTS

Results	Interpretation	Environment/Example
a) 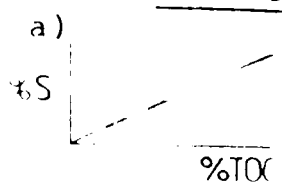	Pyrite forms only when organic matter present. Pyrite formation organic -limited.	
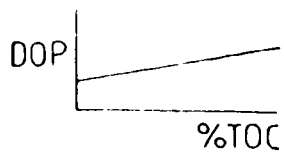	DOP controlled by H_2S production (controlled by %organic matter.	Normally oxygenated bottom-water.
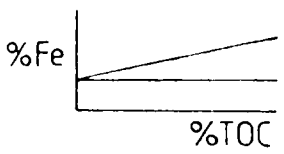	Iron deposition may or may not be linked to organic matter deposition.	
b) 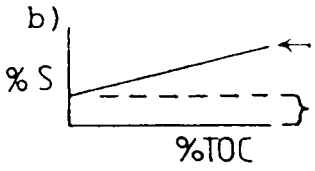	Pyrite formed diagenetically is organic-limited. Pyrite formed on seafloor is limited by the concentration of bottom-water H_2S (syngenetic).	
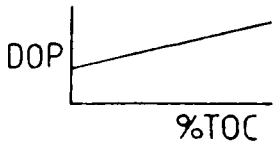	DOP controlled by H_2S production (controlled by %organic matter.	Anoxic bottom water. eg. Black Sea sediment
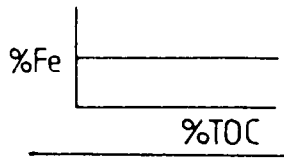	Iron and organic matter deposition linked.	
c) 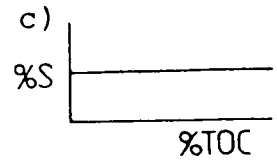	Pyrite formed diagenetically and is iron-limited.	
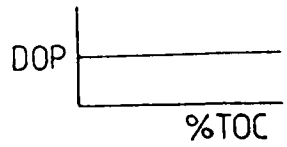	DOP not controlled by supply of H_2S as readily converted iron used up.	Poorly oxygenated, anoxic or fluctuating oxygenation of bottom -water.
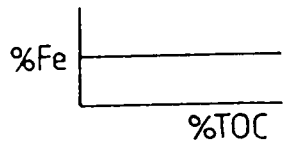	Iron deposition not linked to deposition of organic matter.	eg Black Ven Marls
d) 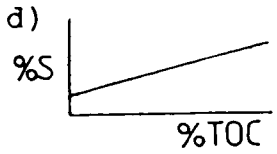	Pyrite formed diagenetically and is iron limited.	
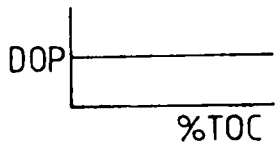	DOP not controlled by supply of H_2S as readily converted iron used up.	Poorly oxygenated, anoxia or fluctuating oxygenation of bottom -water.
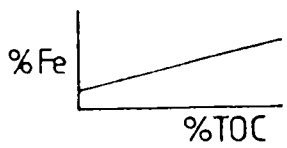	Iron and organic matter deposition linked.	eg Jet Rock

Plot	Use of plot for interpretation of pyrite formation.
%S v %TOC	Intercept=0 → Normal oxygenation, Int.=+ve → low oxygen levels or anoxia. Slope dependent on: DOP v %TOC plot if organic-limited, %Fe v %TOC plot if iron-limited.
DOP v %TOC	Slope=0 → Iron limited. Slope=+ve → Organic limited. DOP=low → Normal oxygenation. DOP=high → low oxygen levels or anoxia.
%Fe v %TOC	Slope=0 → Iron deposition independent of organic matter. Slope +ve → Deposition of organic matter and iron linked.

Based on Raiswell & Berner 1985.

Fig 3·4 D S/DOP$_R$/Fe$_R$/TOC RELATIONSHIPS UPPER ANGULATA ZONE LYME REGIS

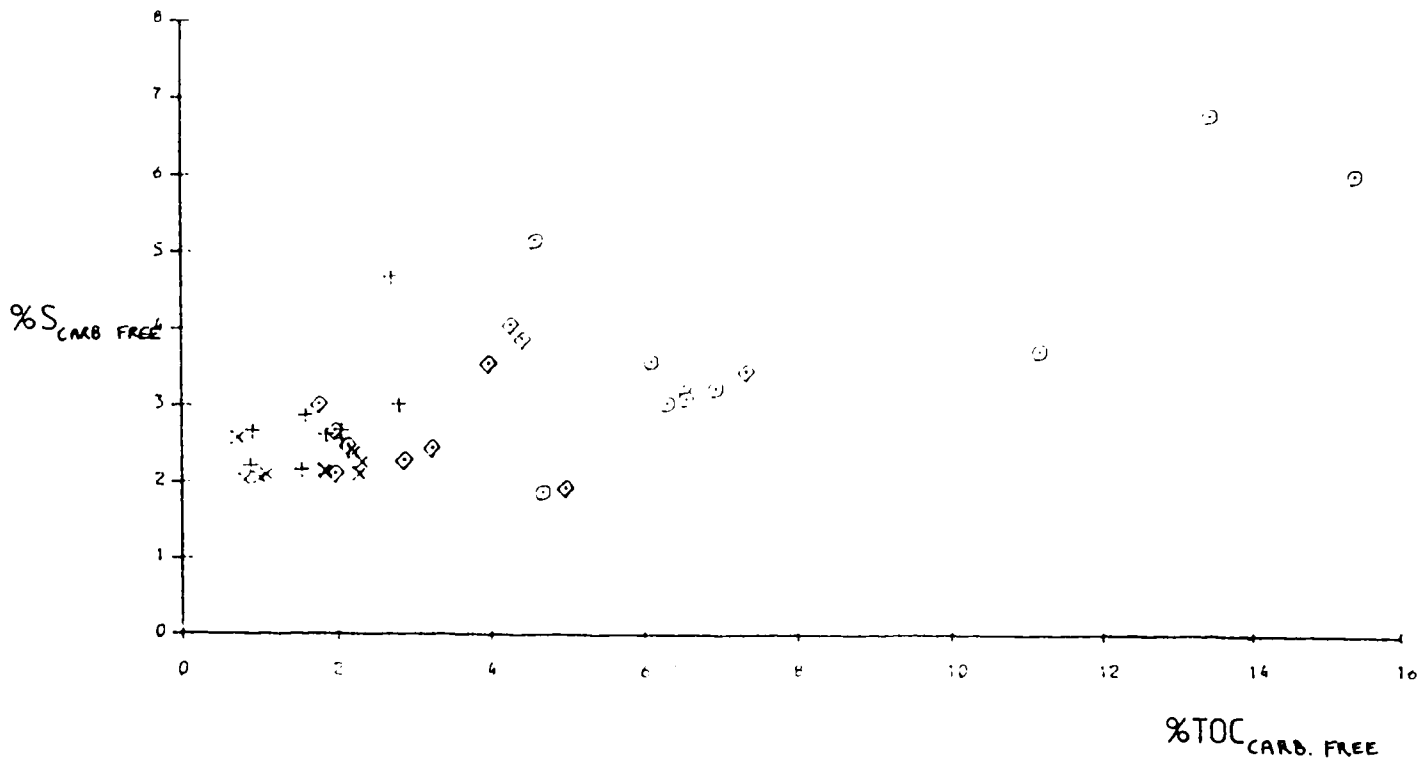

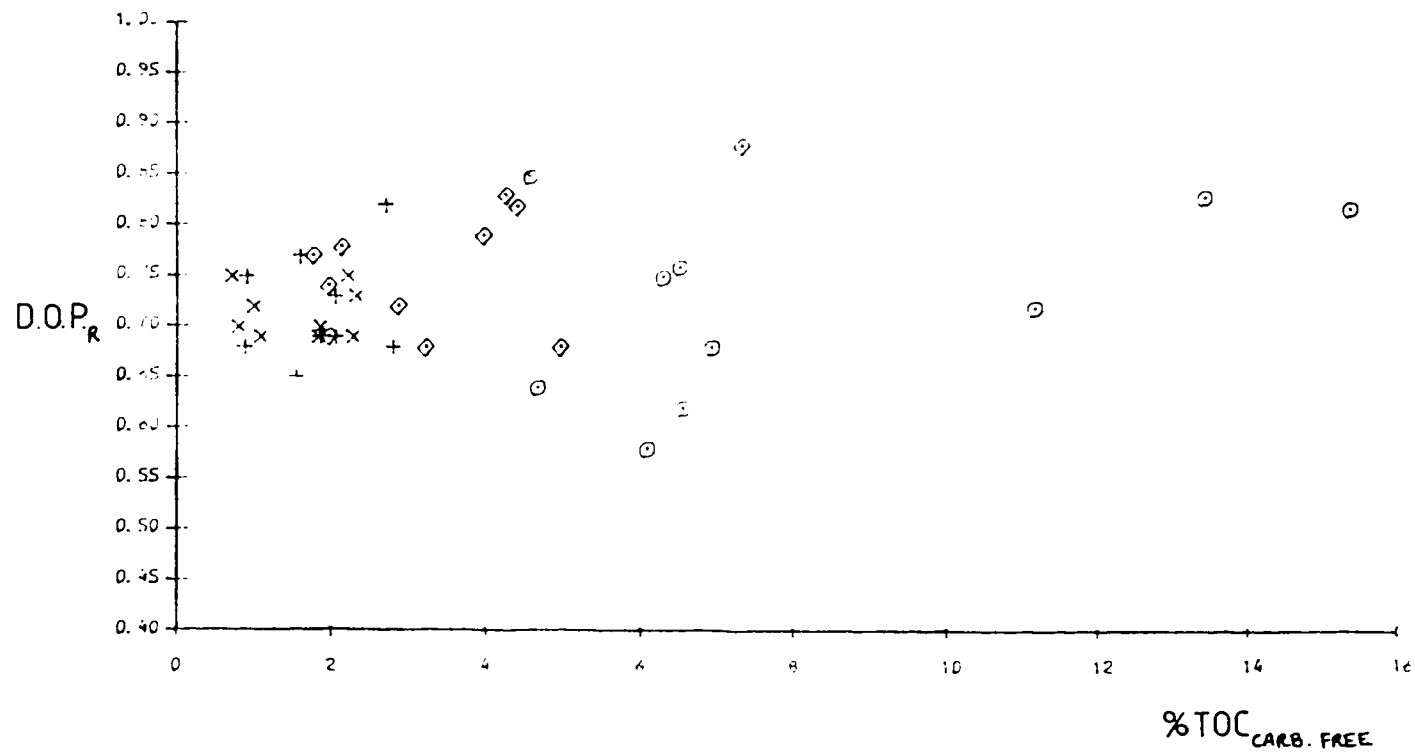

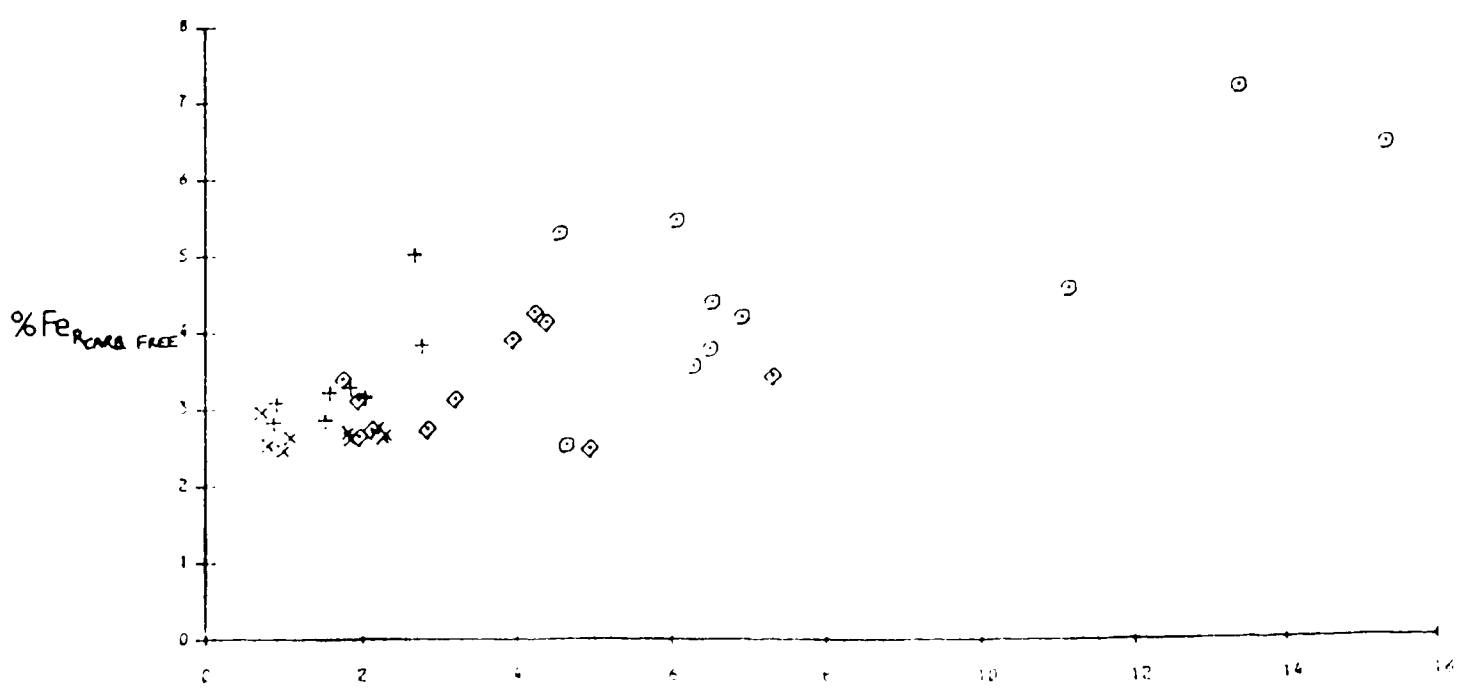

LIMESTONE + LIGHT MARL ×

DARK MARL ⊙ DARK, LAMINATED SHALE ⊙

Fig 3·4E Fe_R/S RELATIONSHIP UPPER ANGULATA ZONE, LYME REGIS

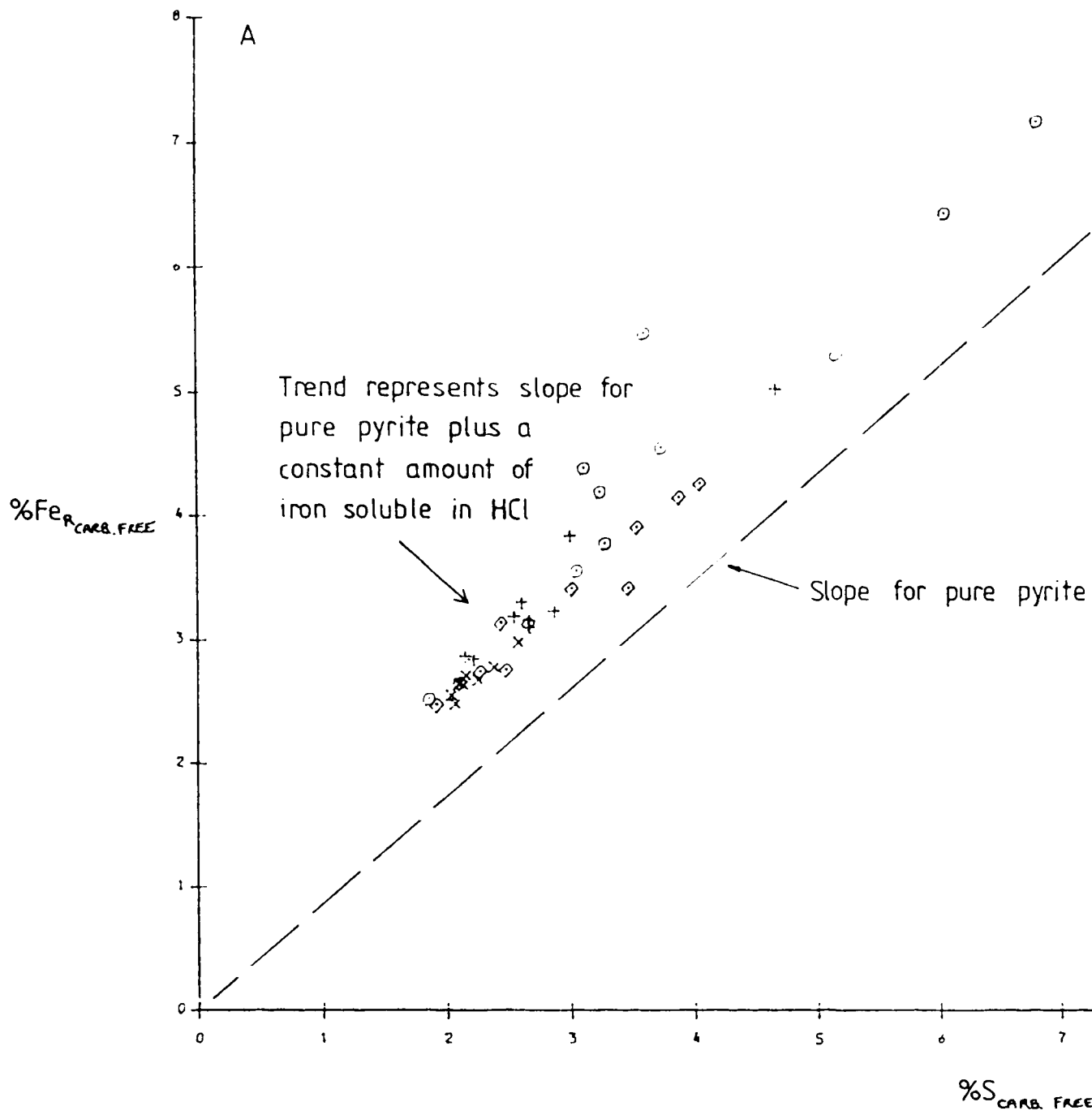

LIMESTONE + LIGHT MARL × LAMINATED LIMESTONE ⊕

DARK MARL ◇ DARK, LAMINATED SHALE ⊙

S/TOC RELATIONSHIP AT WATCHET AND LYME REGIS

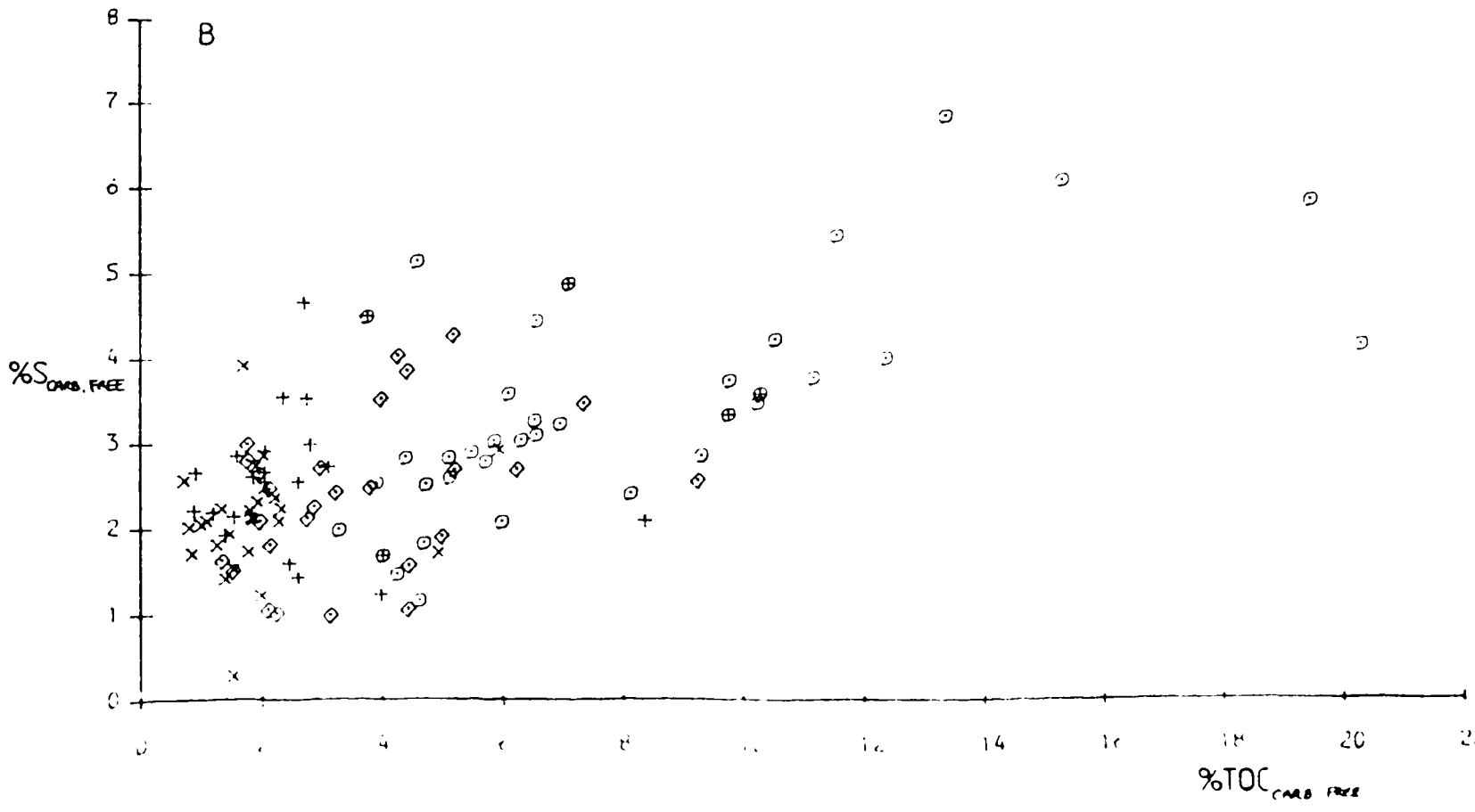

Fig 3·4F STABLE ISOTOPES OF CARBONATE FROM THE ANGULATA - BUCKLANDI ZONE LYME REGIS

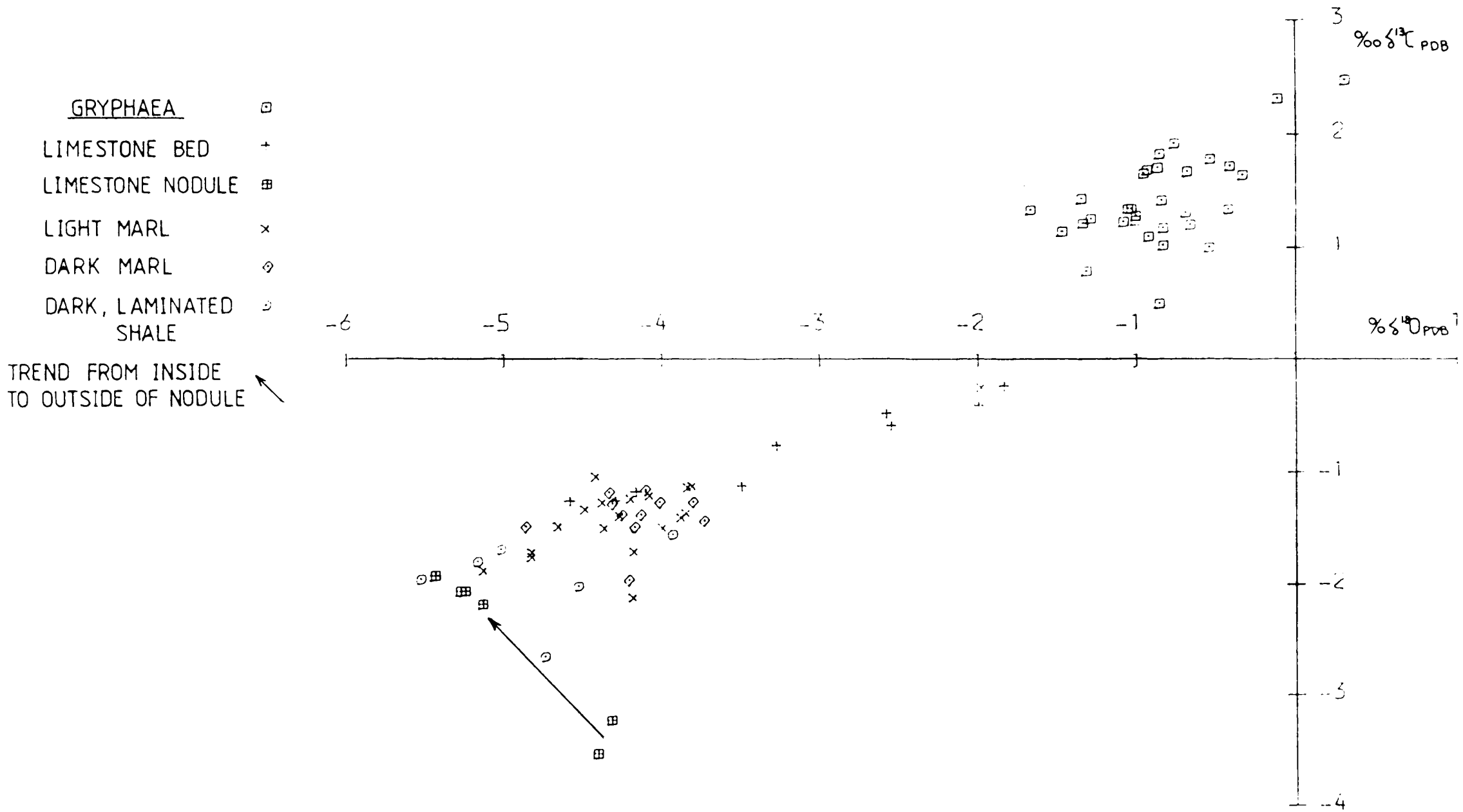

Fig 3·4G PREVIOUSLY PUBLISHED STABLE ISOTOPES OF CARBONATE FROM THE PRE-PLANORBIS BEDS - SEMICOSTATUM ZONE, LYME REGIS

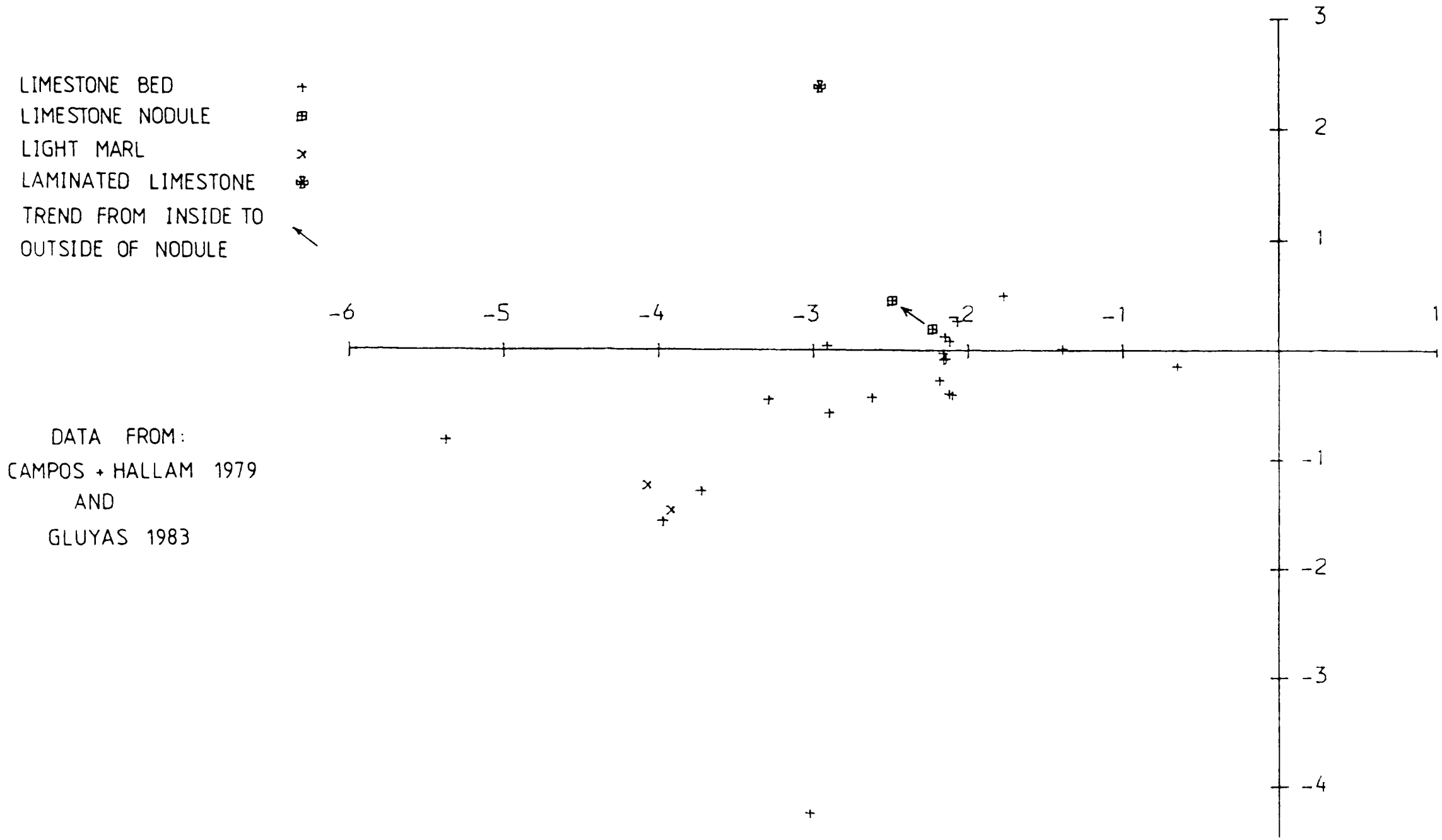

Fig 3·4H

GRYPHAEA ARCUATA SPECIMEN BLG 33 SAMPLE POINTS

‰ $\delta^{18}O_{PDB}$

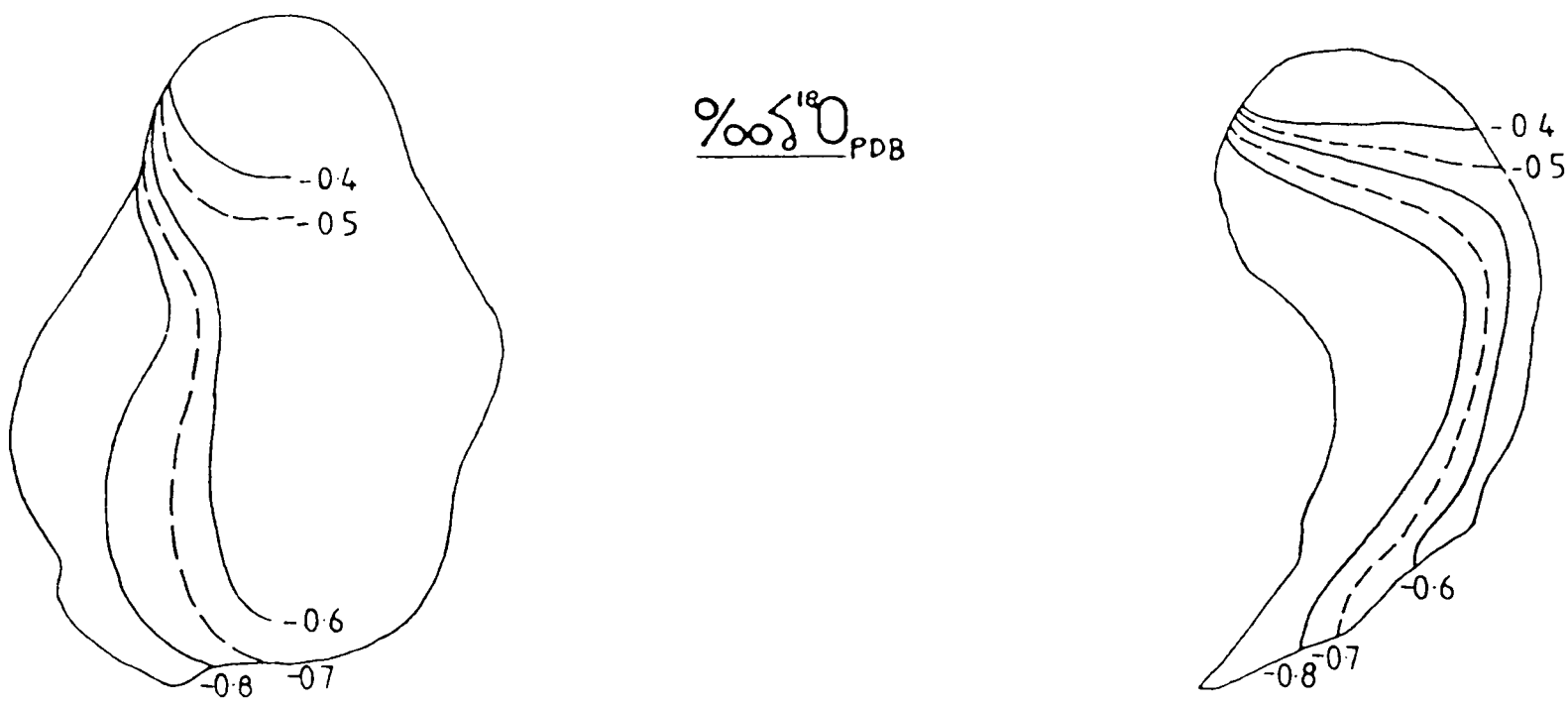

‰ $\delta^{13}C_{PDB}$

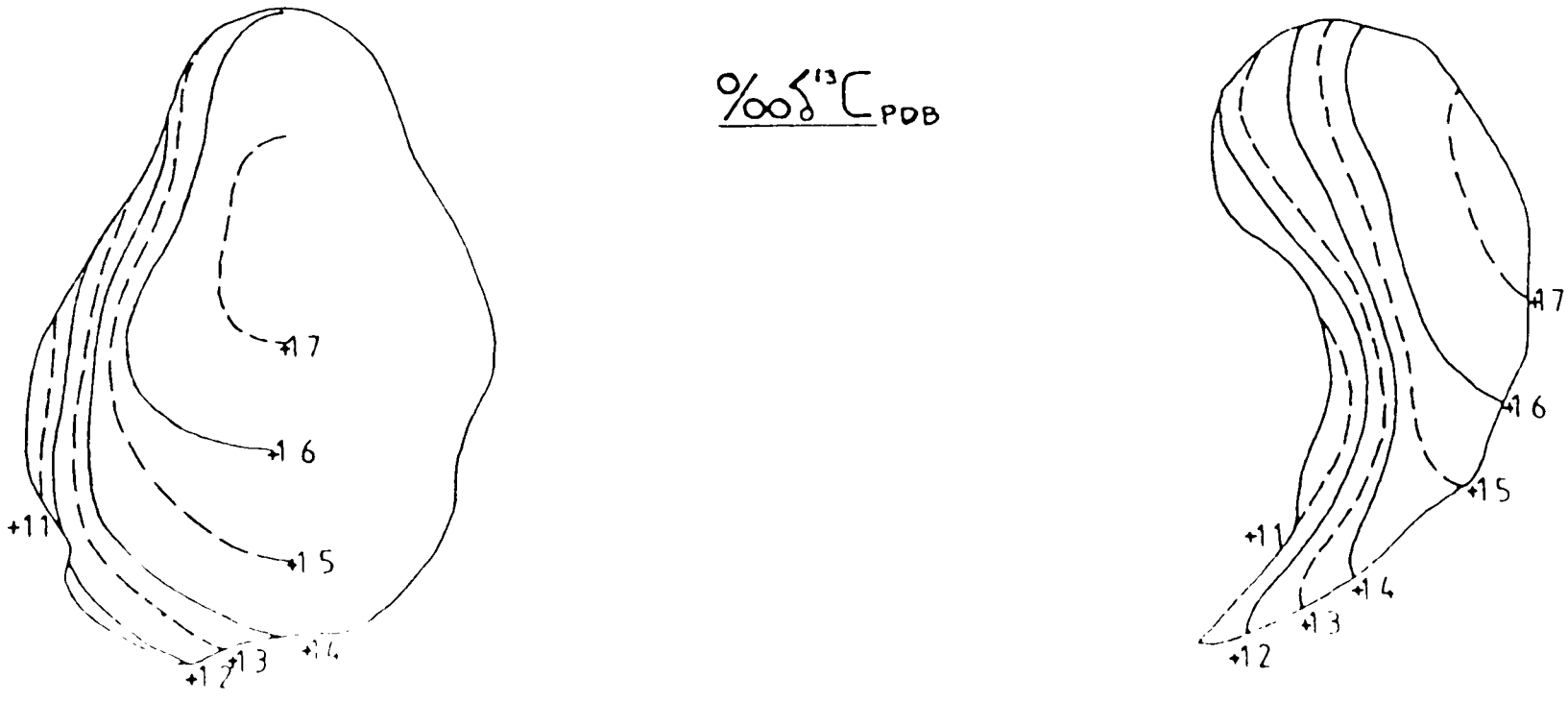

Fig 3·41 STABLE ISOTOPES IN A LIMESTONE NODULE FROM LANG'S BED 37, BUCKLANDI ZONE, SEVEN ROCK POINT, LYME REGIS

SAMPLE POSITIONS

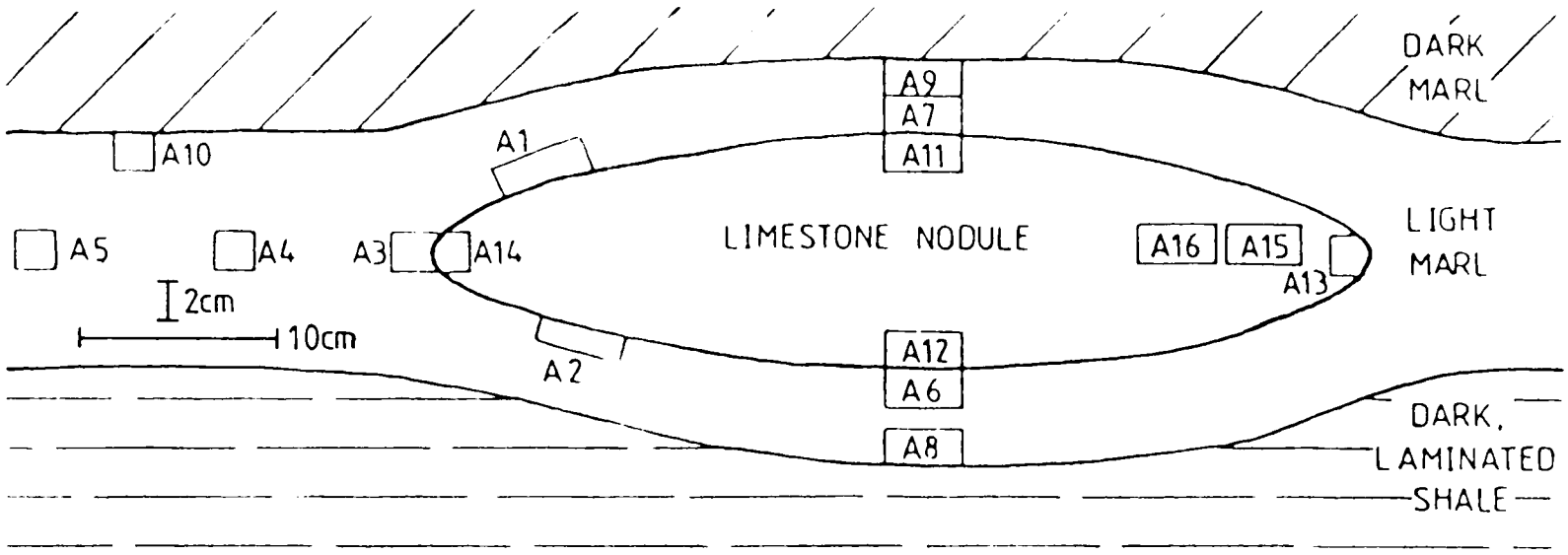

Positions of A15 and A16 projected to appear in the same plane as other samples.

‰ $\delta^{18}O_{PDB}$

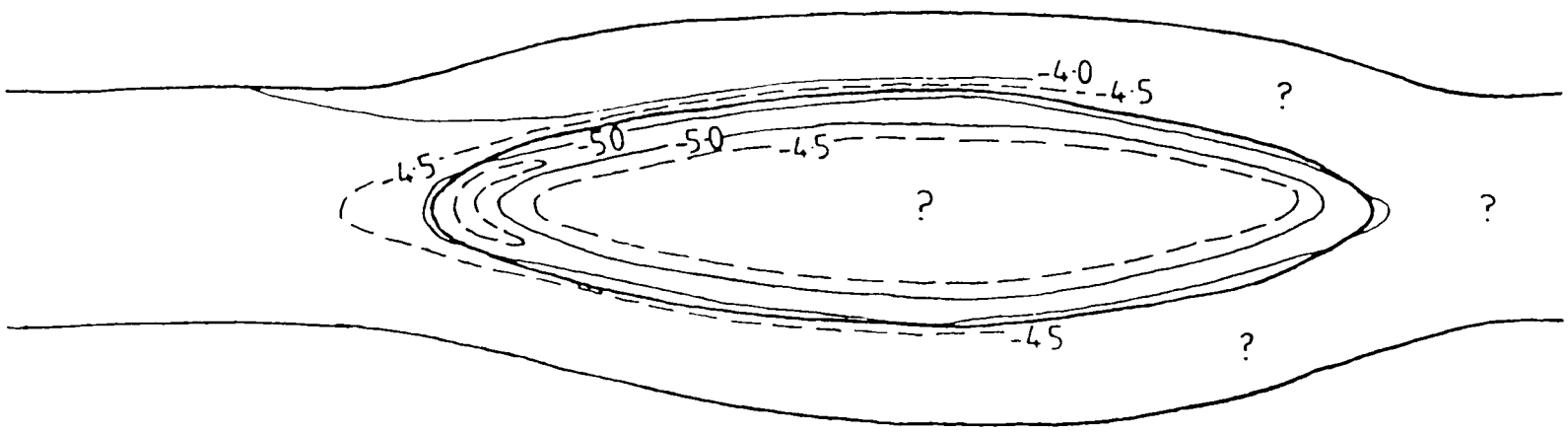

‰ $\delta^{13}C_{PDB}$

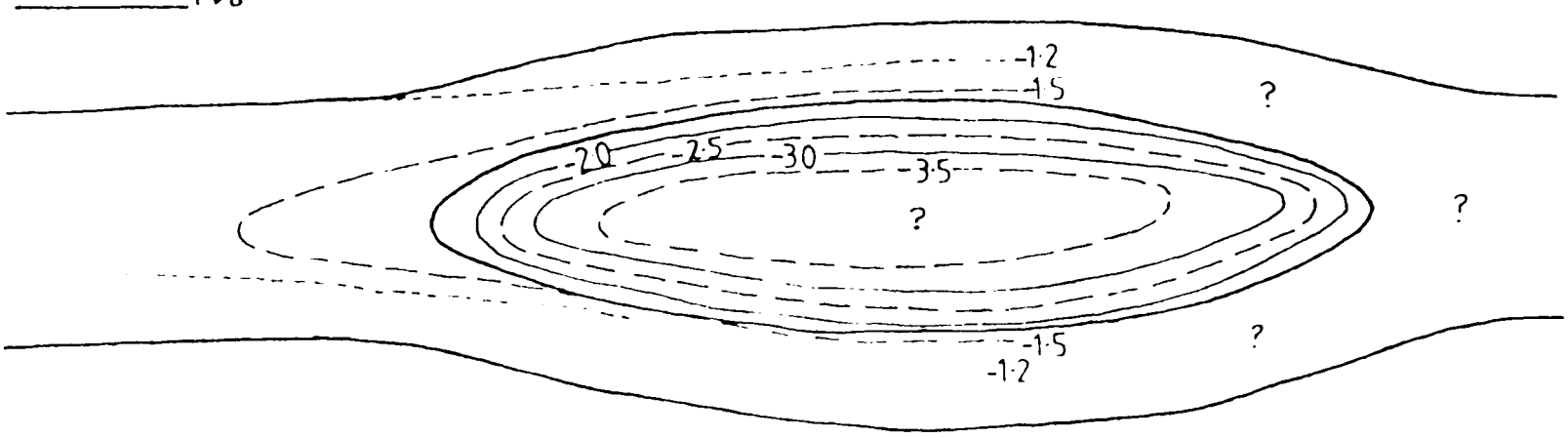

Fig 4·2A

WALSH POWER SPECTRAL ESTIMATION

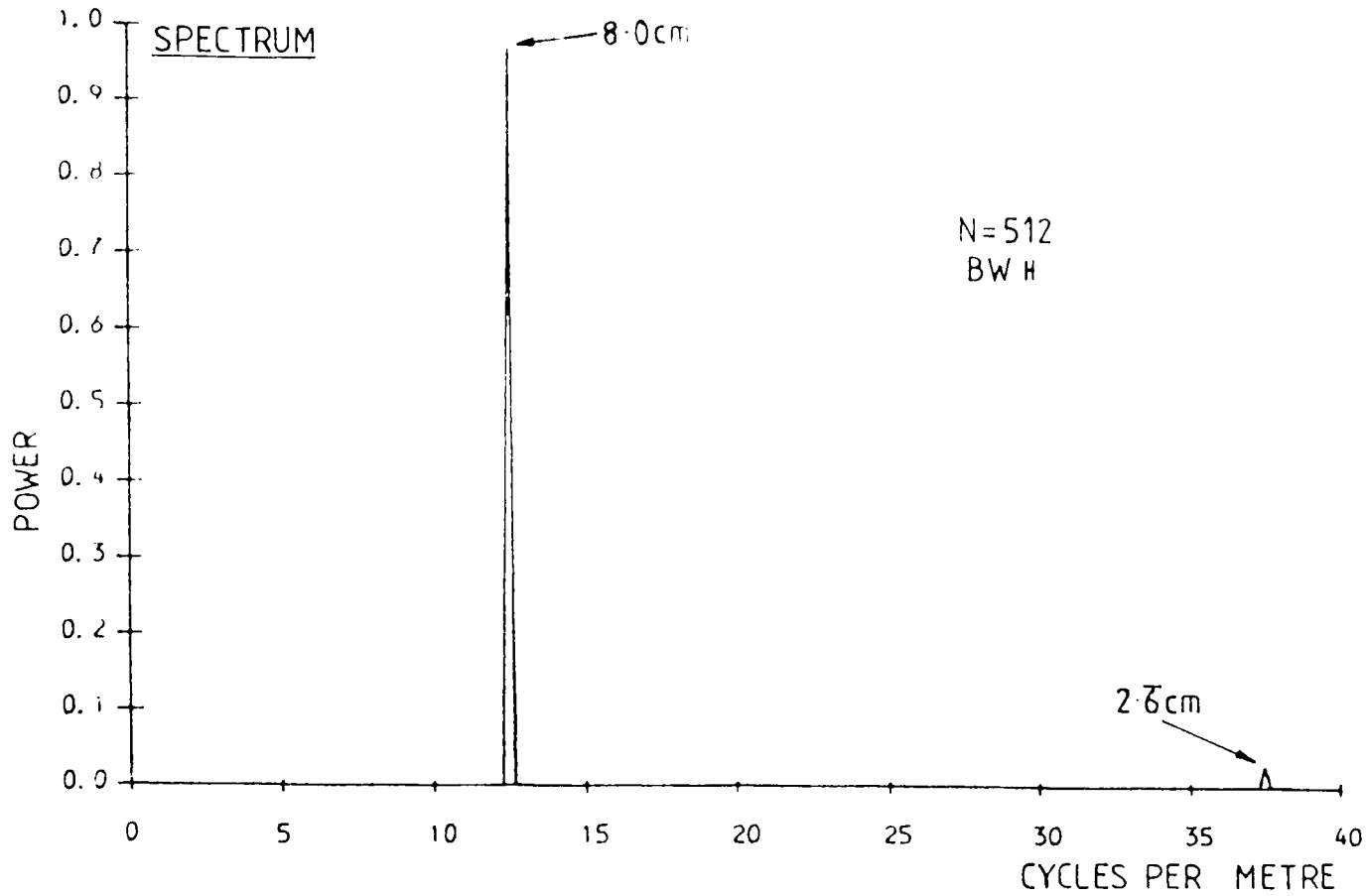

TIME SERIES ≃ SINE WAVE, TREATED AS THE SUM OF VARIOUS WALSH FUNCTIONS:

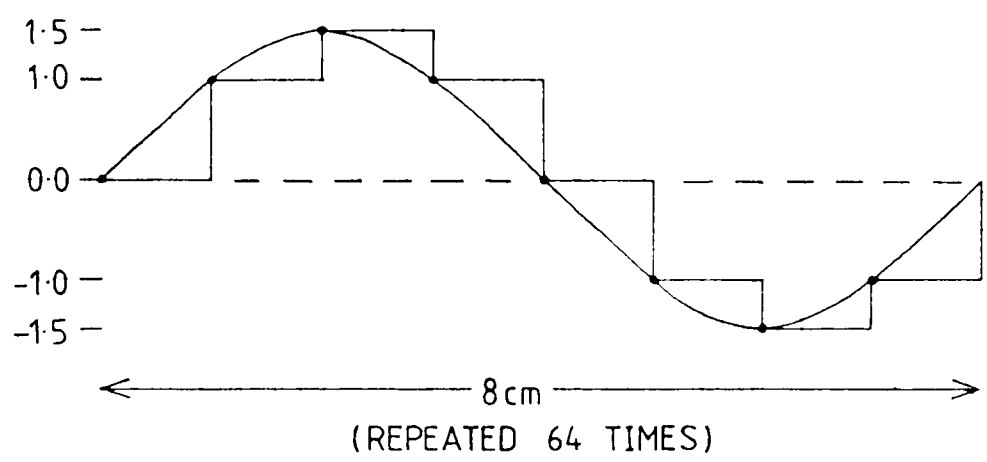

COMPONENT WALSH FUNCTIONS WITH RELATIVE AMPLITUDES, PHASE & WAVELENGTHS:

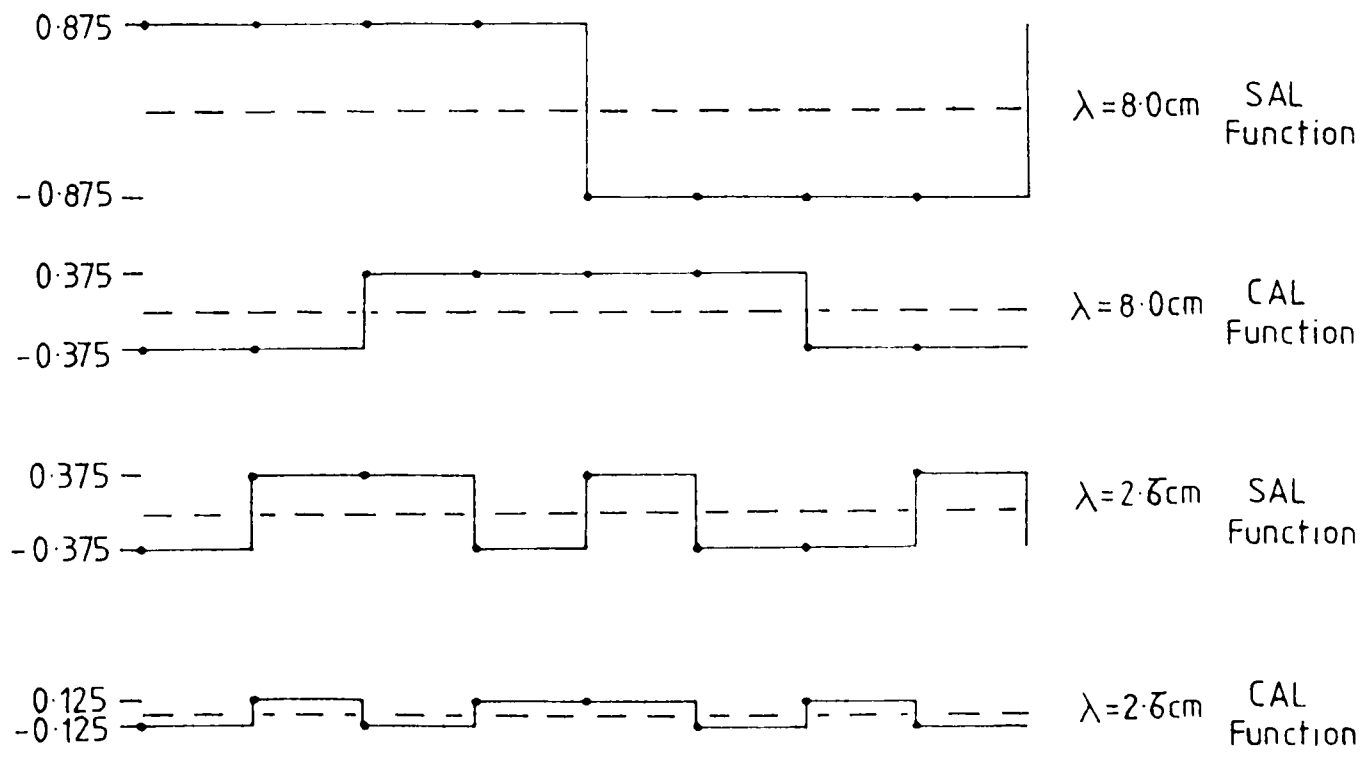

(MODIFIED FROM KANASEWICH 1981 FIG 23.2)

eg. Normalized Power for 8cm Peak $= 0.9711 = \dfrac{(0.875^2 + 0.375^2)^2}{(0.875^2 + 0.375^2)^2 + (0.375^2 + 0.125^2)^2}$

Power Term

Normalization Term (Section 4.2.4)

Fig 4·2B

THE EFFECT OF HIATUSES UPON A PERFECTLY REGULAR TIME SERIES

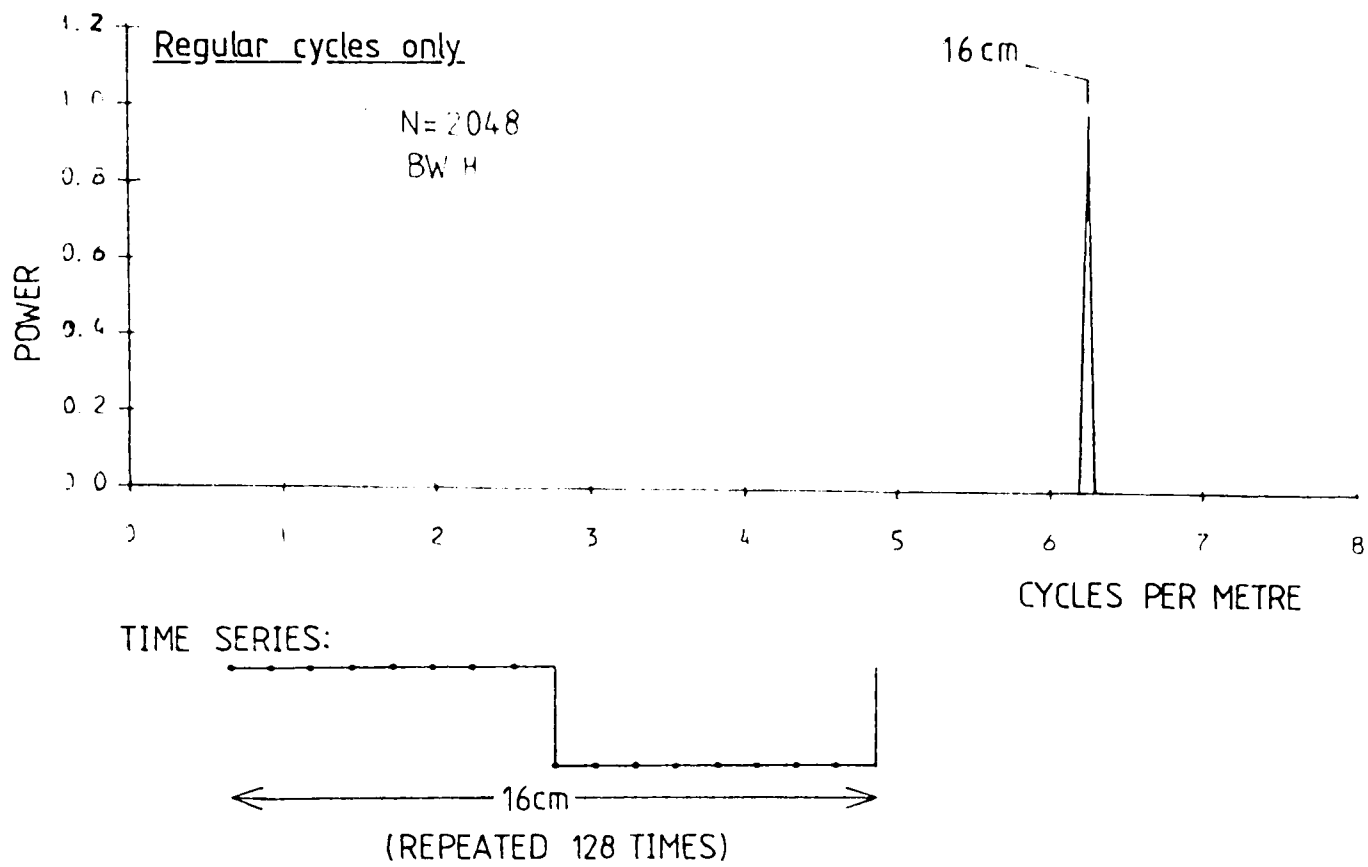

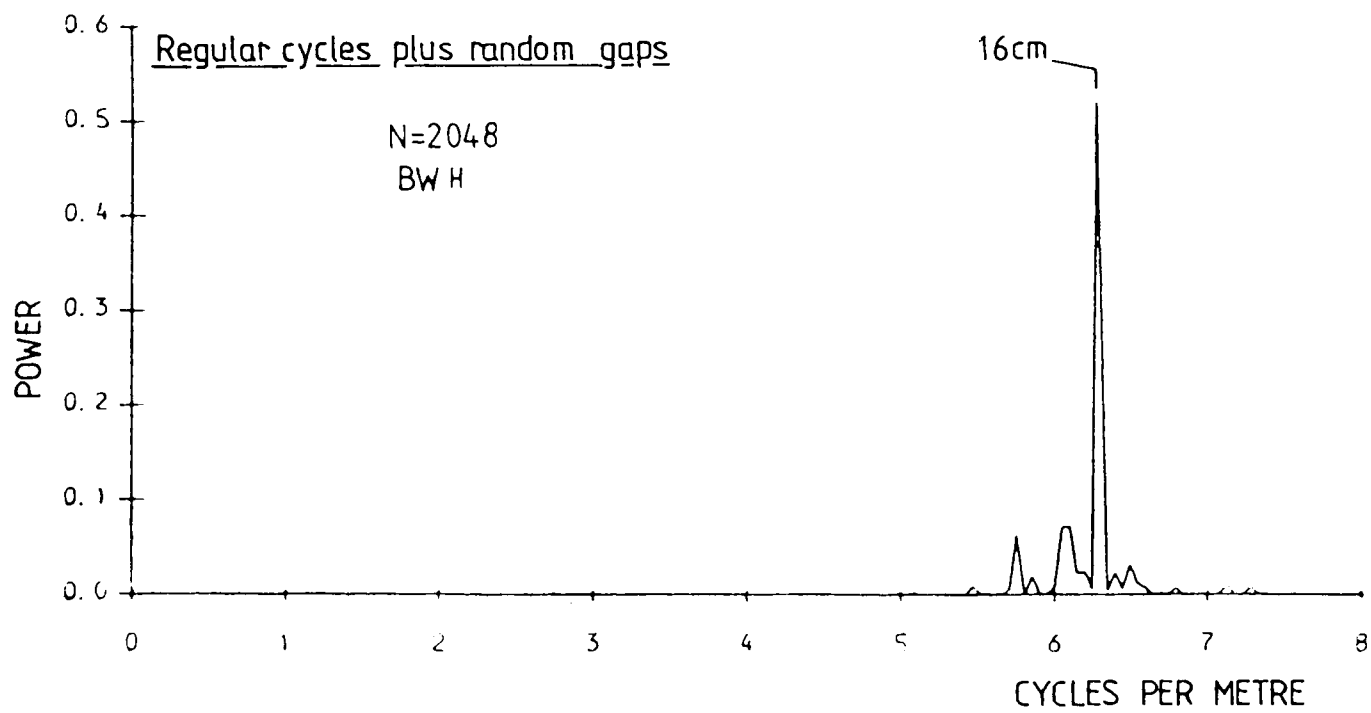

TIME SERIES = 16cm CYCLE PLUS 'RANDOM GAPS' (SEE FIG 4.2C)

GAPS:

RANDOM No. COLUMNS 1 + 2 (BOTH 00-99)

1 = SEPARTION OF GAPS

2 = THICKNESS LOSS AT EACH GAP

BW = BANDWITH = FREQUENCY RESOLUTION OF SPECTRUM

N = No. OF SAMPLE POINTS USED TO GENERATE SPECTRUM (= cm HERE)

Fig 4·2C

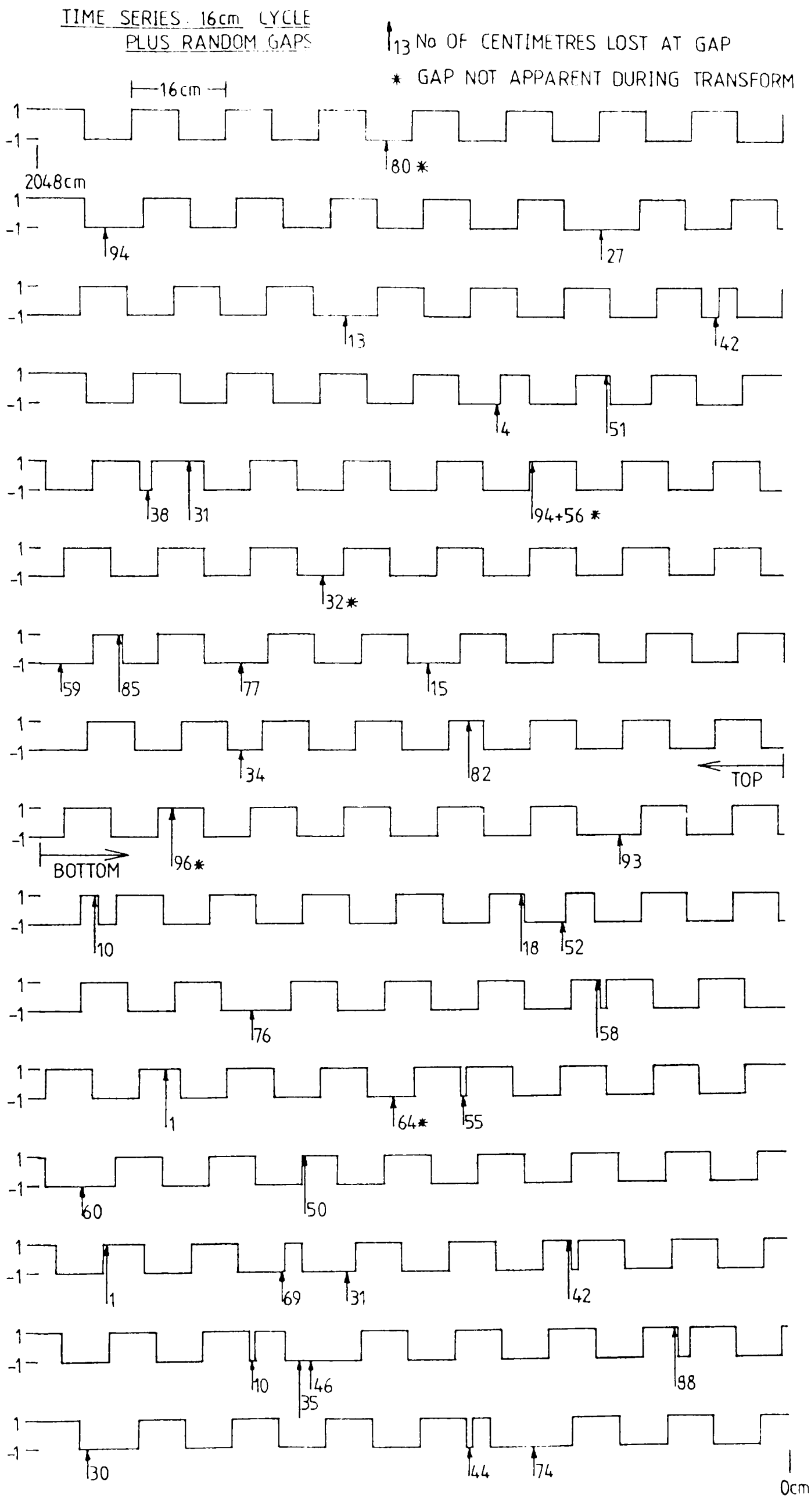
TIME SERIES. 16cm CYCLE
PLUS RANDOM GAPS
13 No OF CENTIMETRES LOST AT GAP
* GAP NOT APPARENT DURING TRANSFORM
16cm
2048cm
1
-1
80 *
94
27
13
42
4
51
38
31
94+56 *
32*
59
85
77
15
34
82
TOP
BOTTOM
96*
93
10
18
52
76
58
1
64*
55
60
50
1
69
31
42
10
46
35
98
30
44
74
0cm

Fig 4·2D

TIME SERIES GENERATED WITH RANDOM NUMBERS

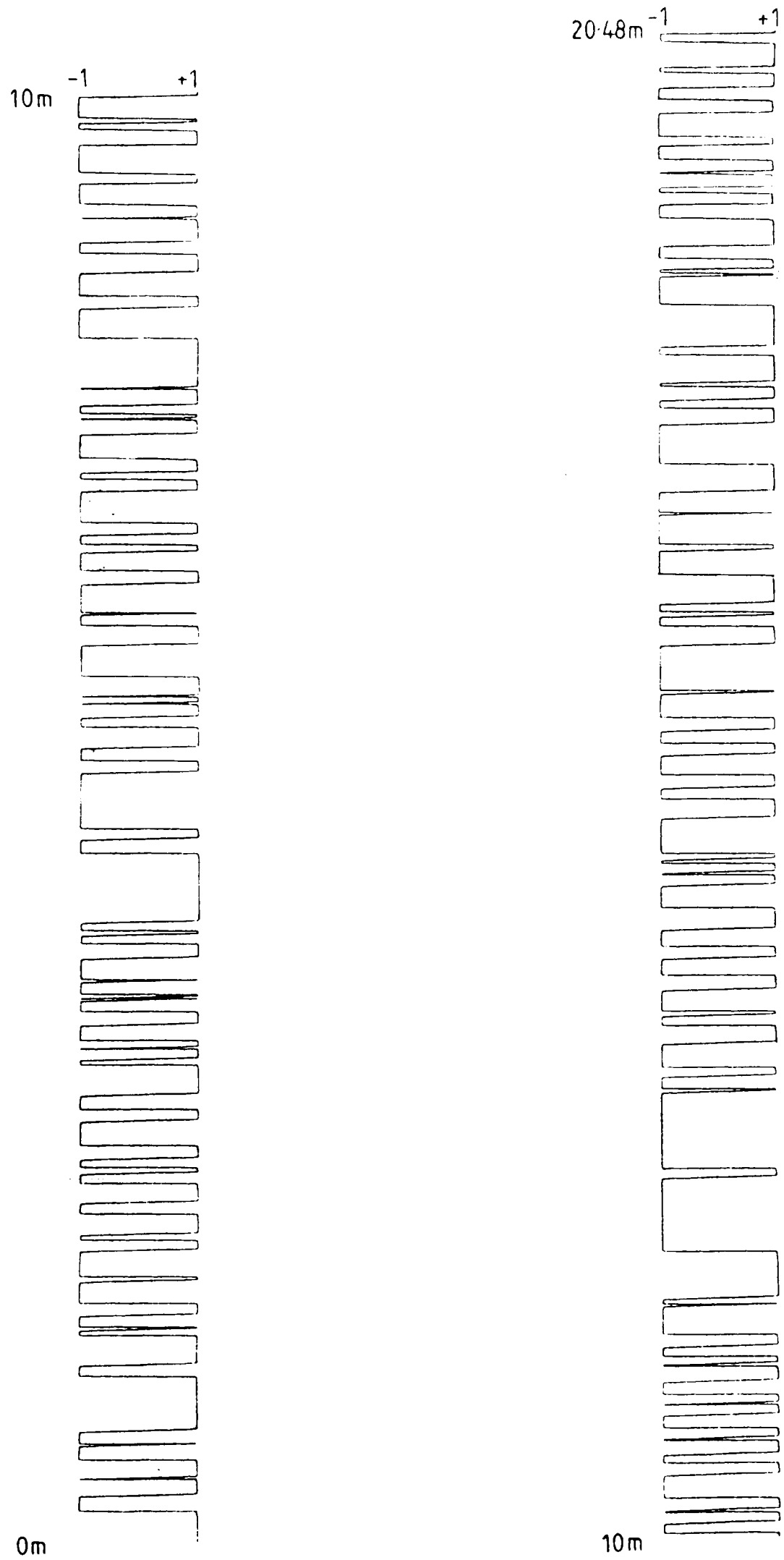

On random number table column 1 = bed thickness = 0-9cm
column 2 = rock type codes =+1 if even number
=-1 if odd number

Fig 4·2E

SPECTRUM OF RANDOM TIME SERIES

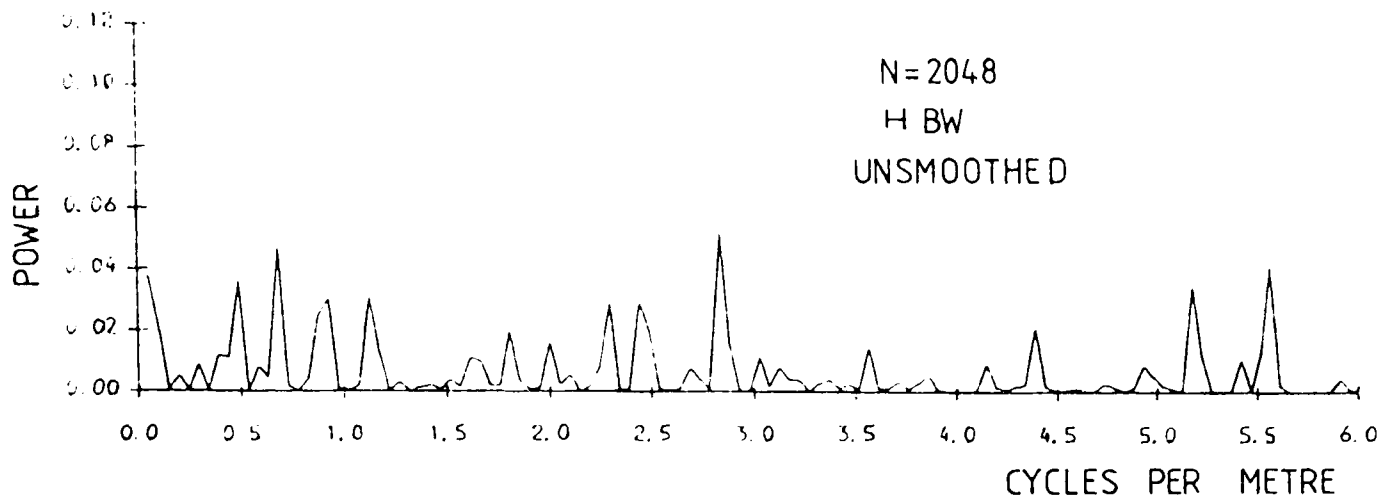

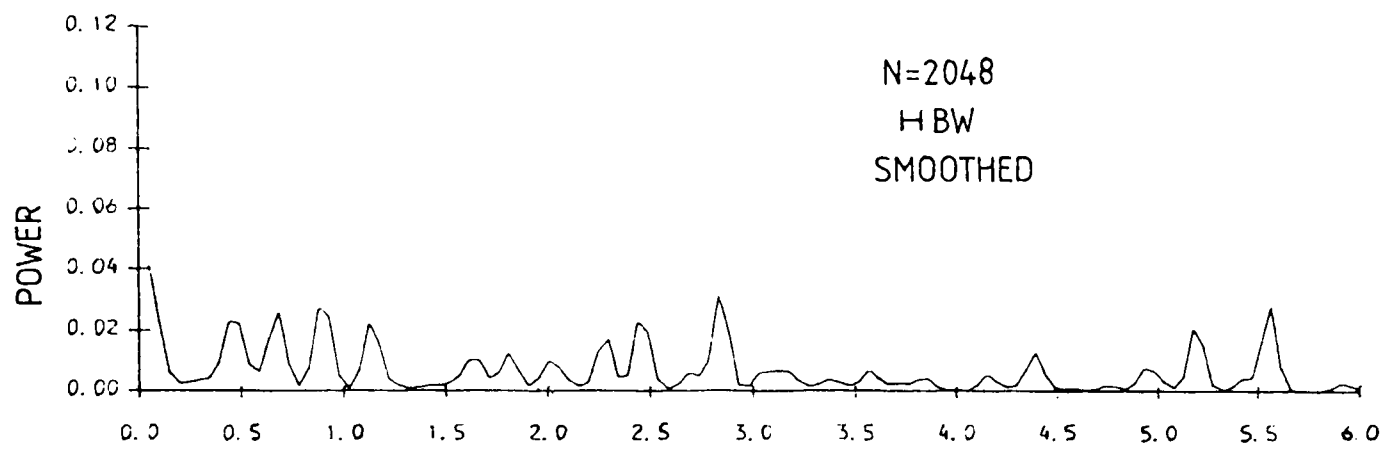

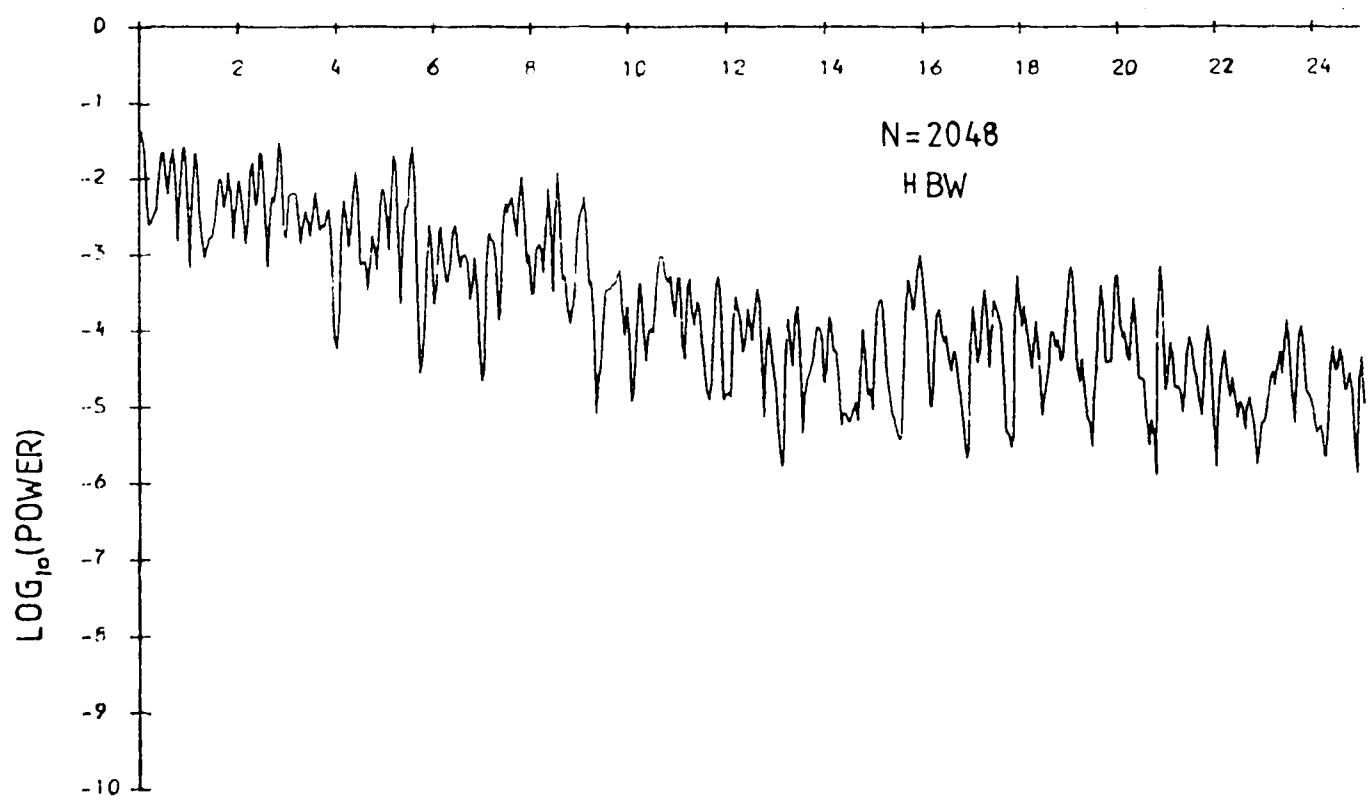

COMPARE FIG 4.3B (SAME SCALING)

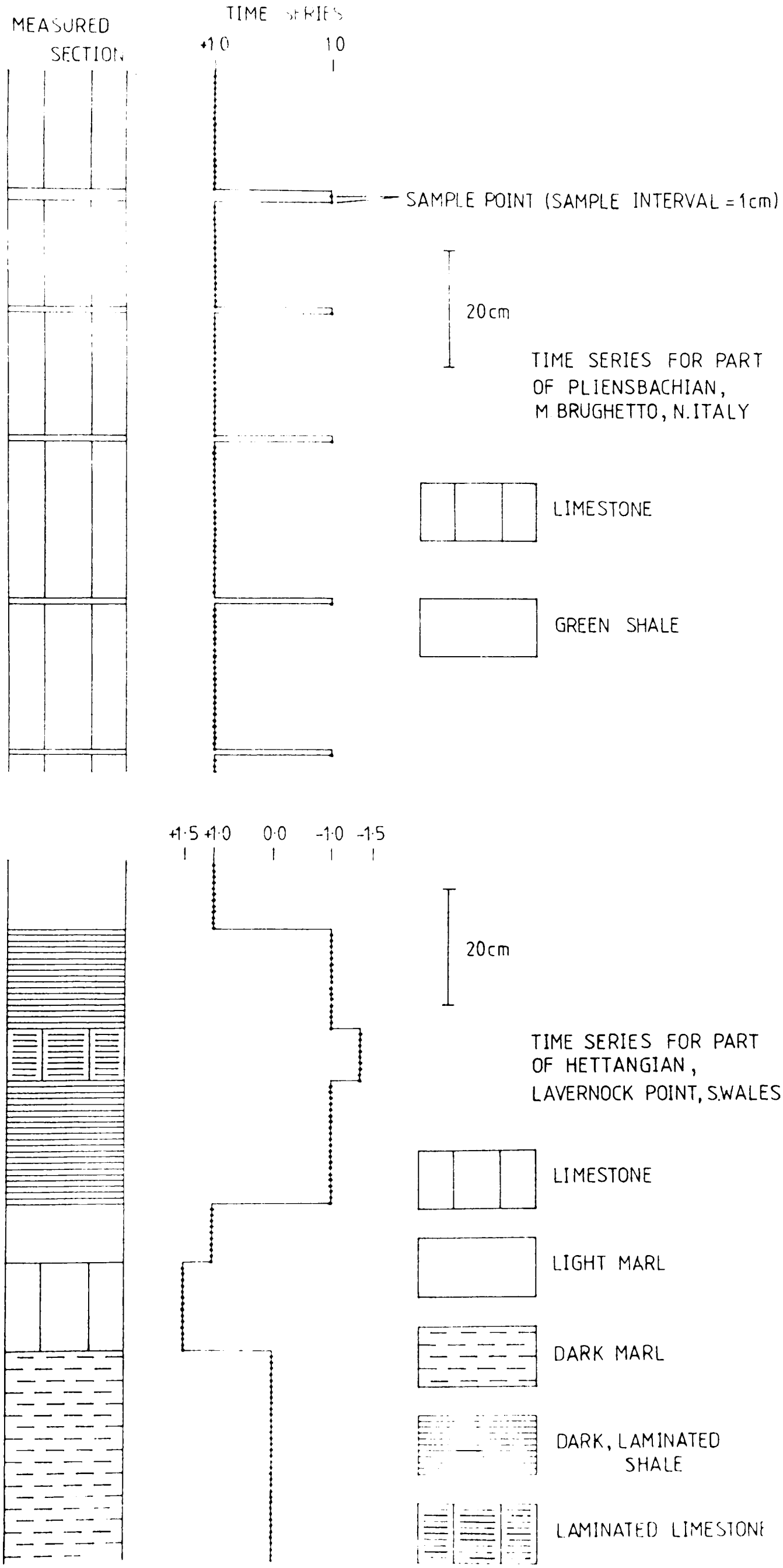
MEASURED SECTION
TIME SERIES
+1.0
1.0
SAMPLE POINT (SAMPLE INTERVAL = 1cm)
20cm
TIME SERIES FOR PART OF PLIENSBACHIAN, M BRUGHETTO, N.ITALY
LIMESTONE
GREEN SHALE
+1.5 +1.0 0.0 -1.0 -1.5
20cm
TIME SERIES FOR PART OF HETTANGIAN, LAVERNOCK POINT, S.WALES
LIMESTONE
LIGHT MARL
DARK MARL
DARK, LAMINATED SHALE
LAMINATED LIMESTONE

Fig 4·2G

CHOOSING SAMPLE INTERVALS:

SEQUENCE CONTAINS BEDS 1cm THICK

SAMPLE INTERVAL CHOSEN = 1·5cm

SAMPLED SEQUENCE.

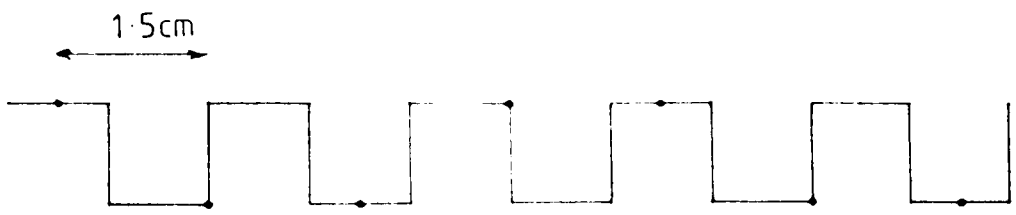

RECREATED TIME SERIES CONTAINS SPURIOUS LOW FREQUENCY COMPONENT:

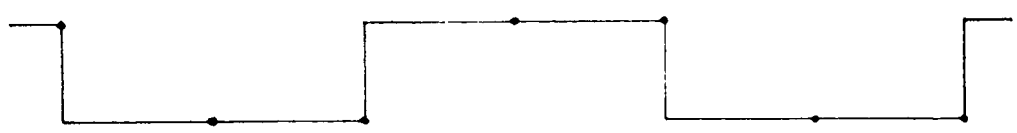

SAMPLE INTERVAL = 1·0cm

SAMPLED SEQUENCE:

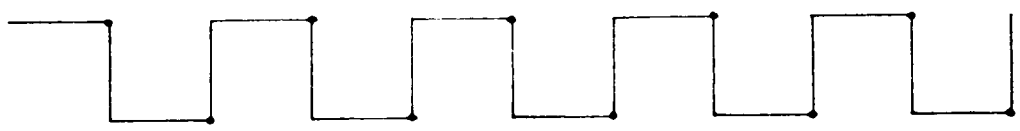

RECREATED TIME SERIES = CORRECT REPRESENTATION OF SEQUENCE:

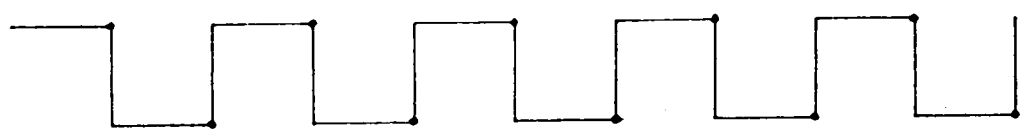

Fig 4·2H

TESTING THE SIGNIFICANCE OF SPECTRAL PEAKS

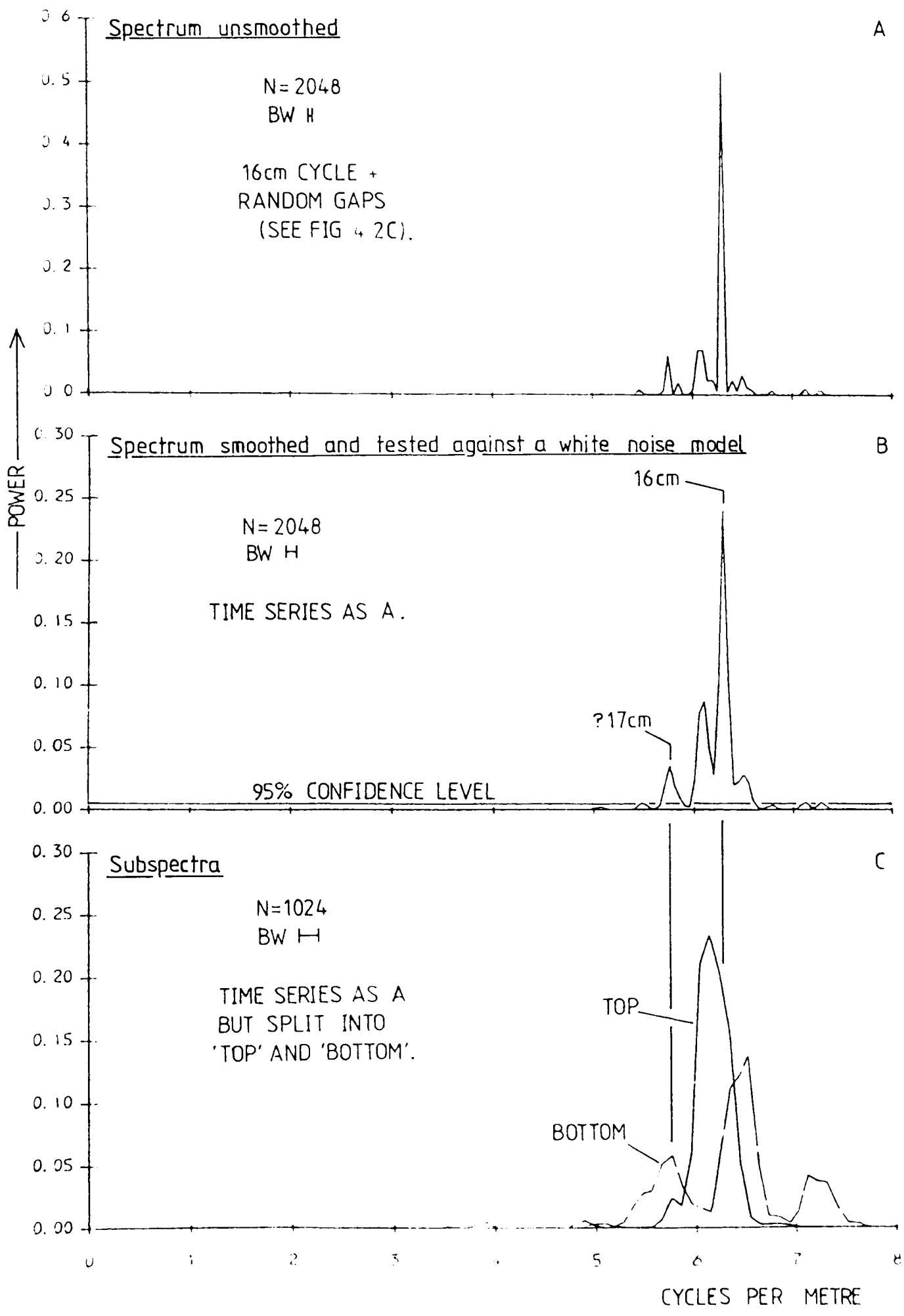

Fig 4·21

HARMONICS

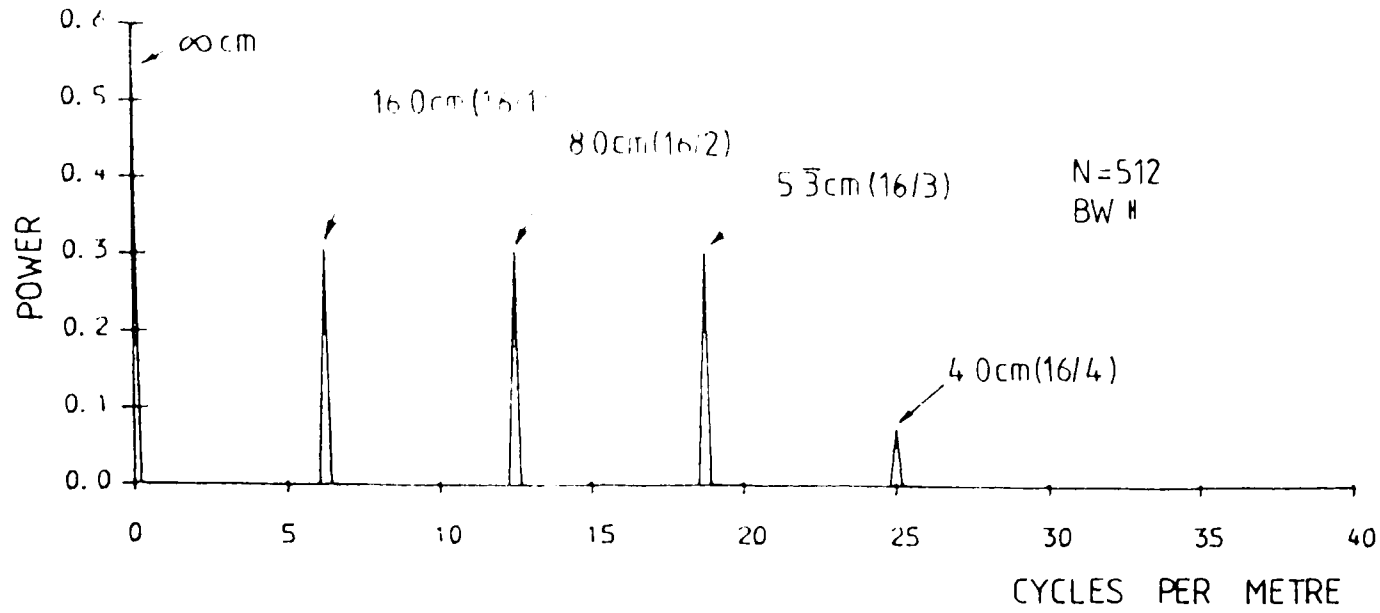

TIME SERIES IS REGULAR & ASYMMETRICAL (cf. LIMESTONE-SHALE SEQUENCES):

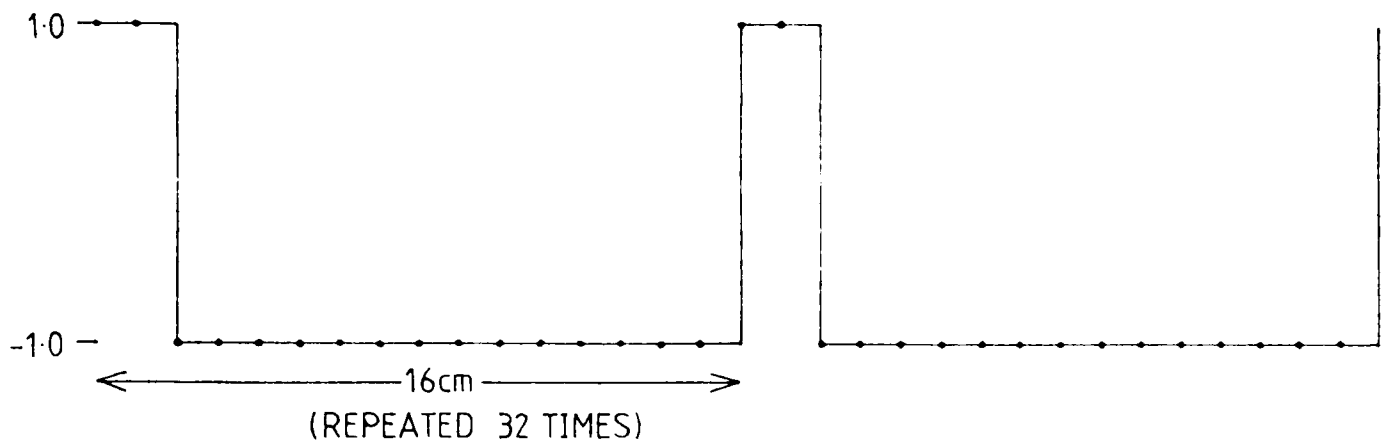

COMPONENT WALSH FUNCTIONS WITH RELATIVE AMPLITUDES, PHASE & WAVELENGTHS:

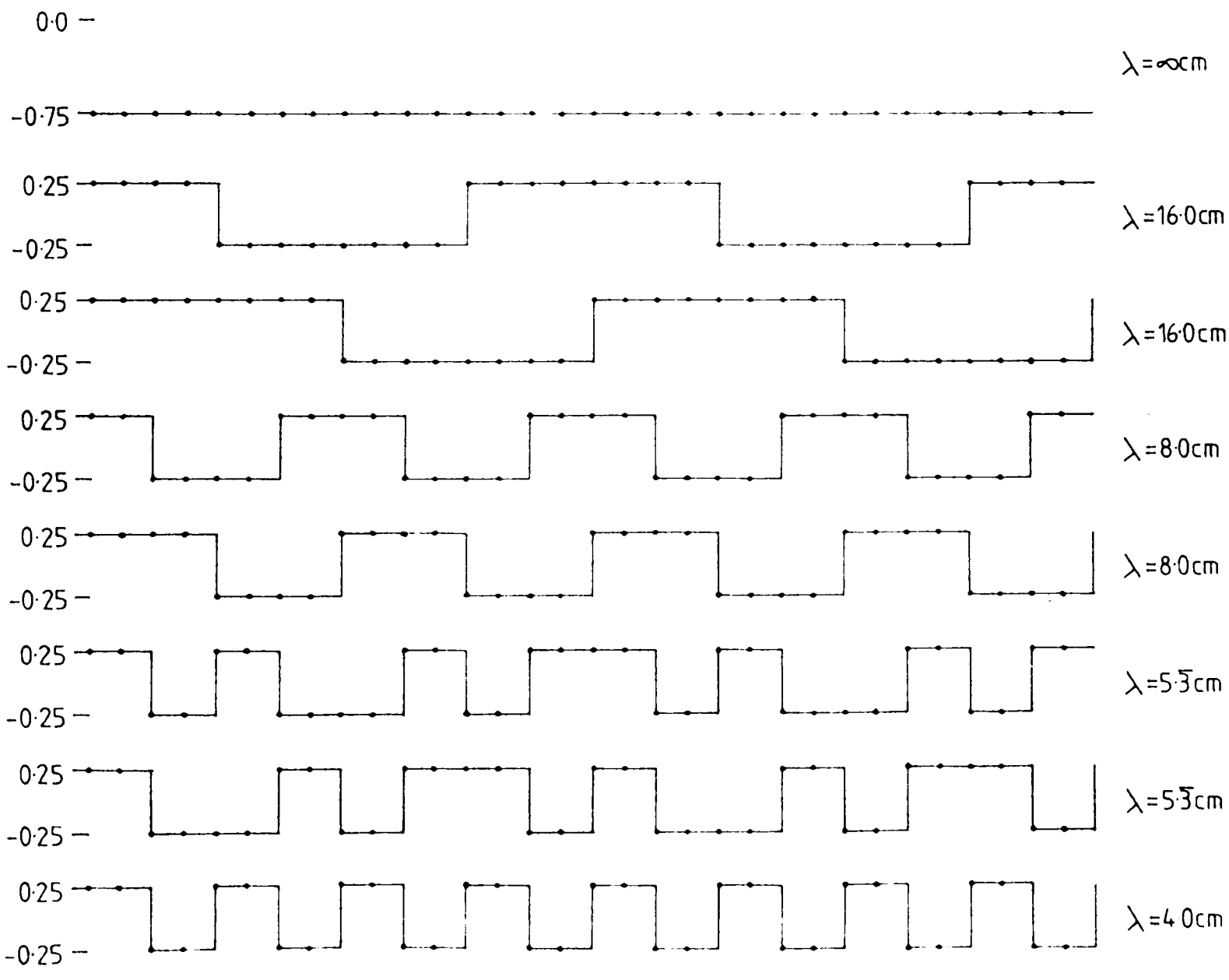

Fig 4·3A BASAL LIAS LYME REGIS TIME SERIES

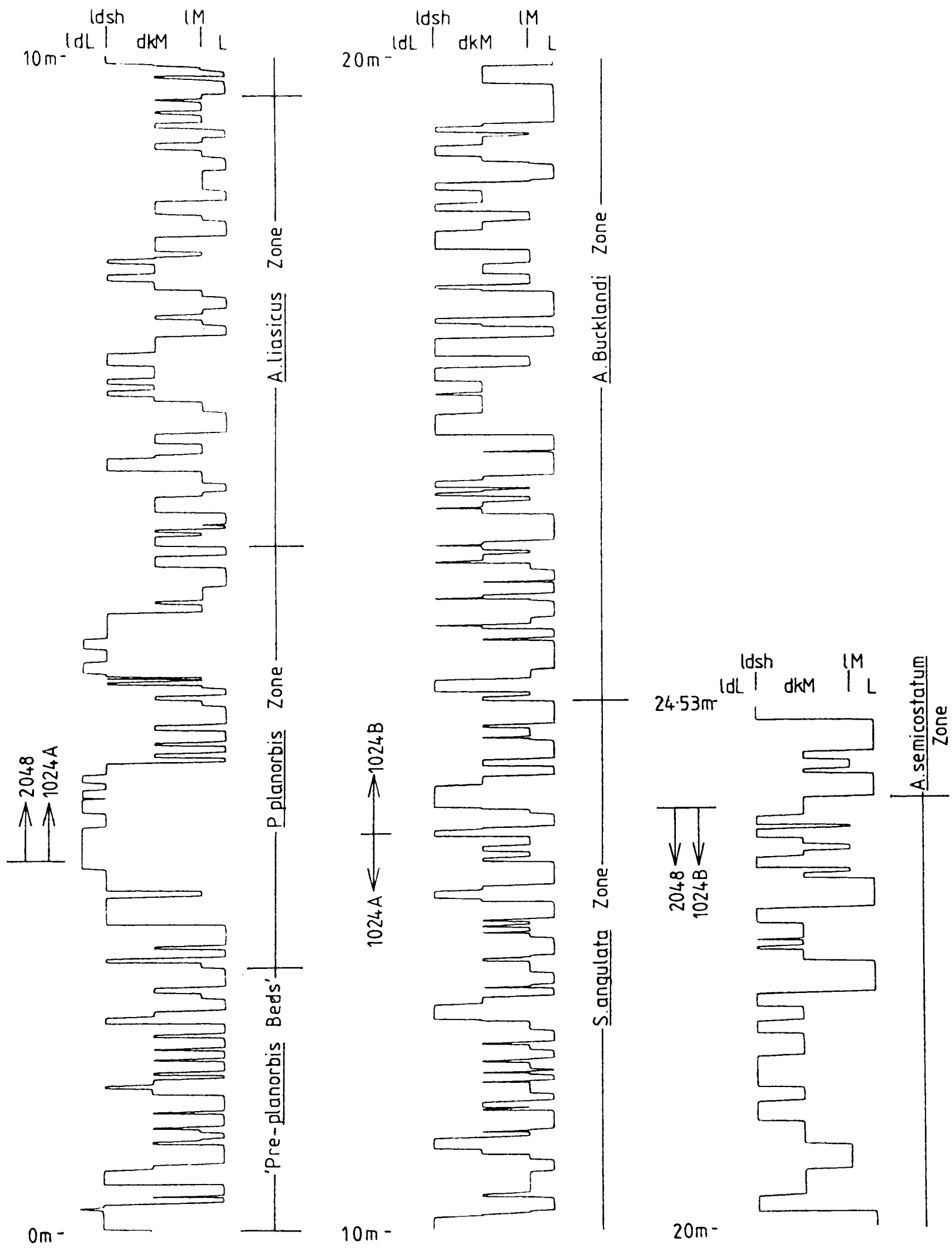

Biostratigraphy from Cope et al. 1980

Fig 4·3B BASAL LIAS, LYME REGIS POWER SPECTRA

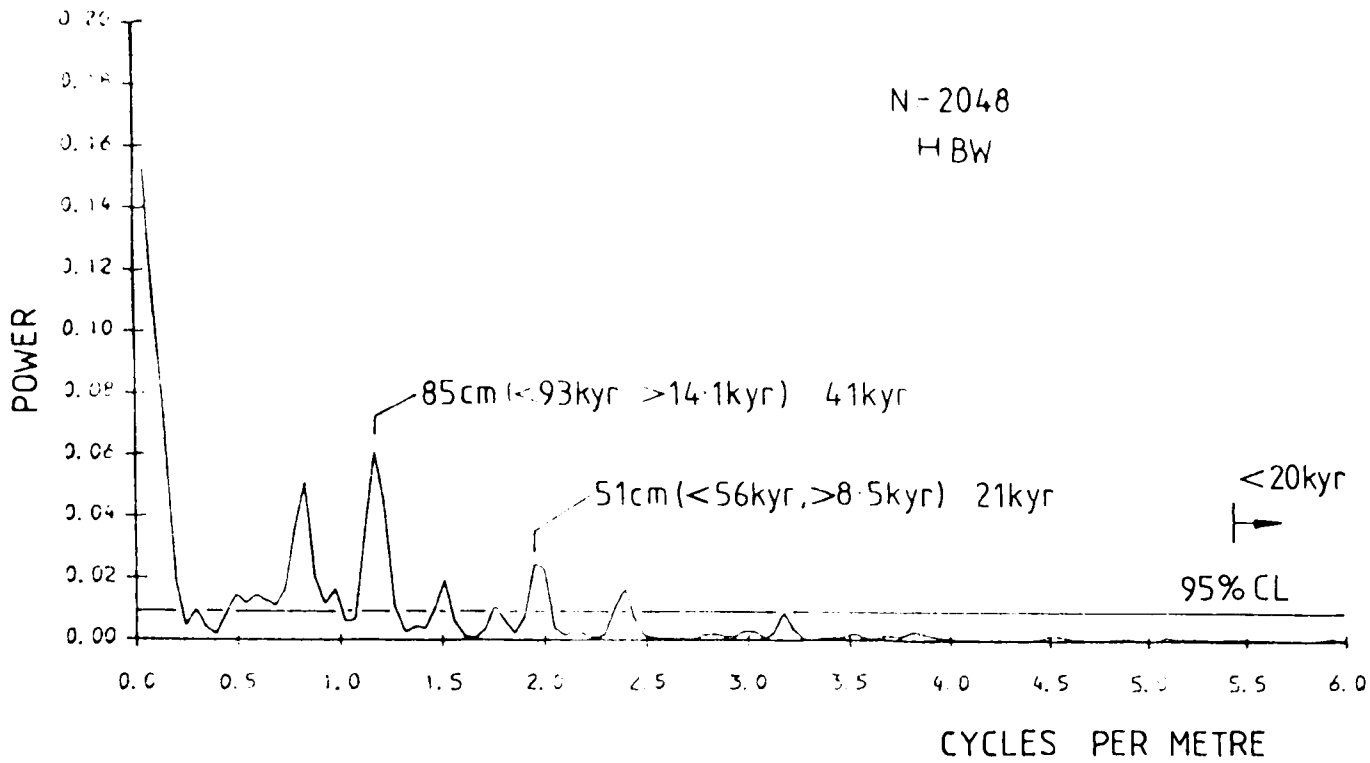

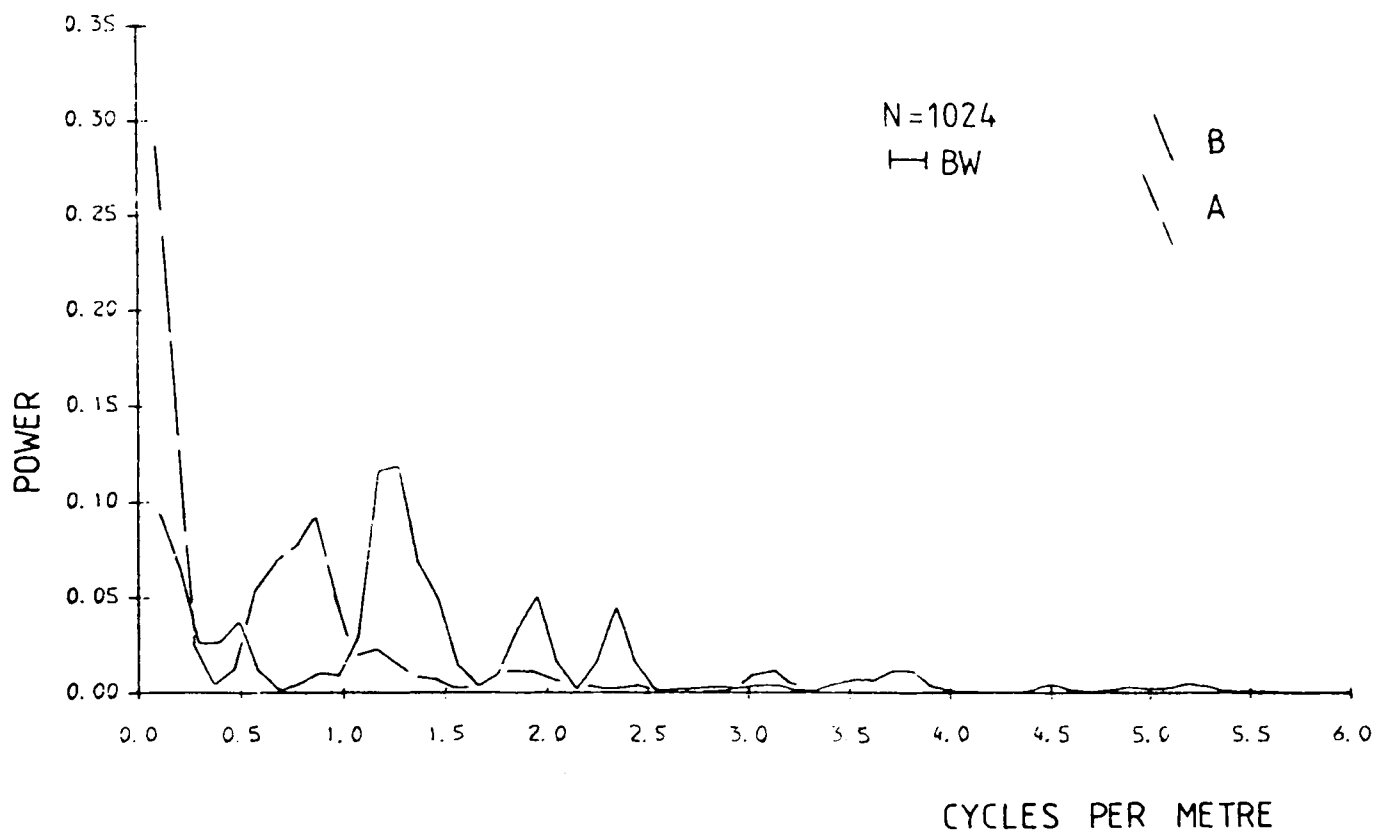

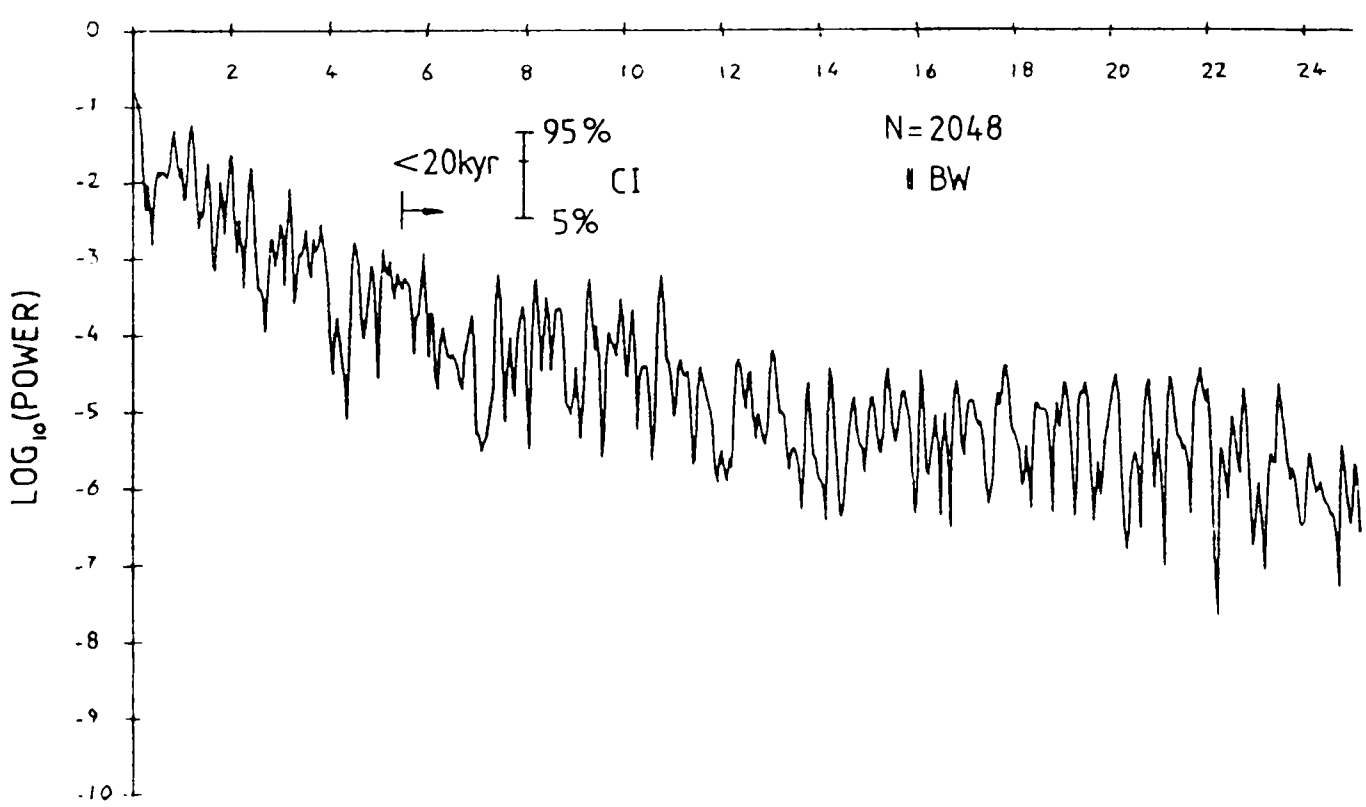

Fig 4.3C BASAL LIAS WATCHET TIME SERIES

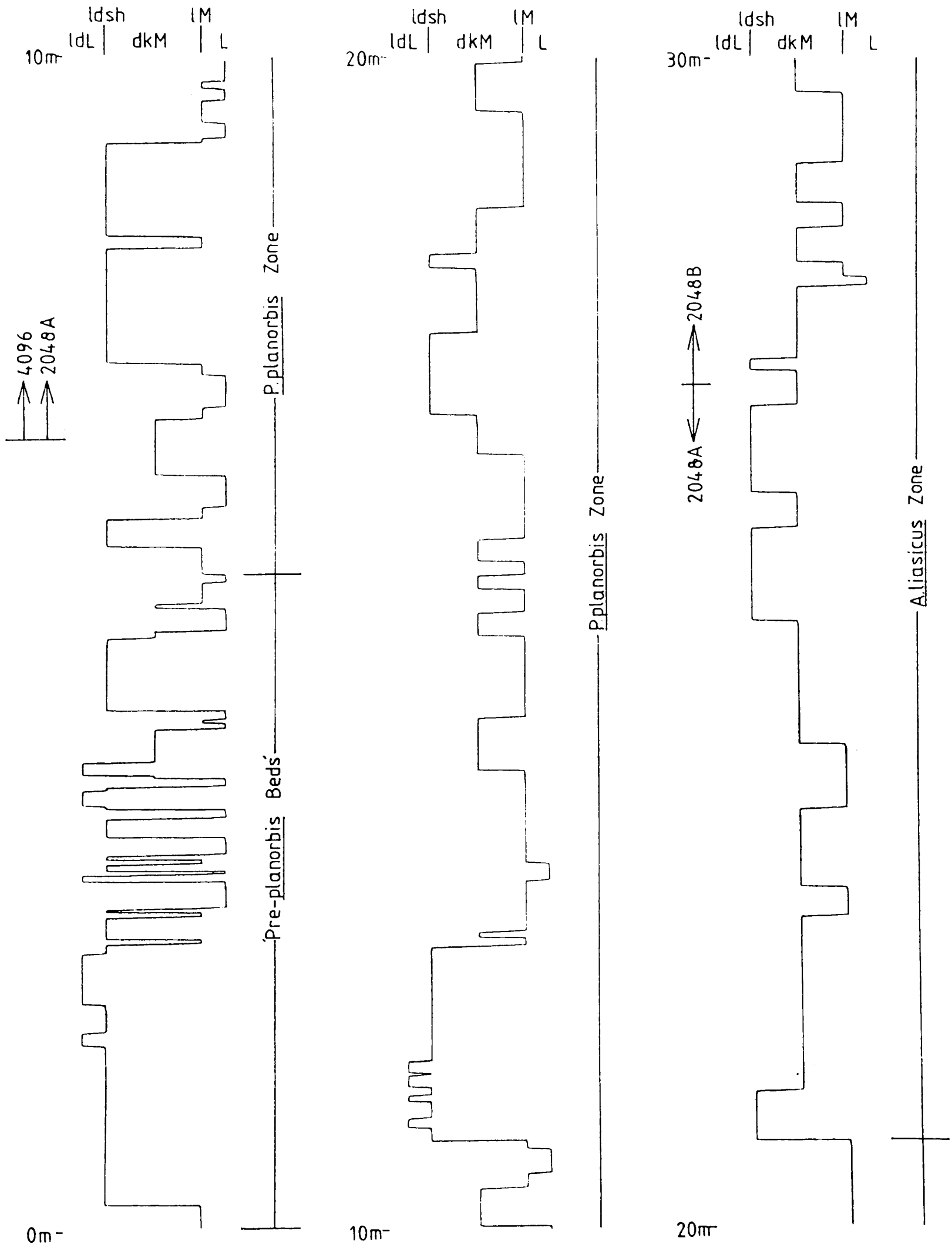

Biostratigraphy from Palmer 1972 + Cope et al 1980

Fig 4 3D BASAL LIAS WATCHET TIME SERIES

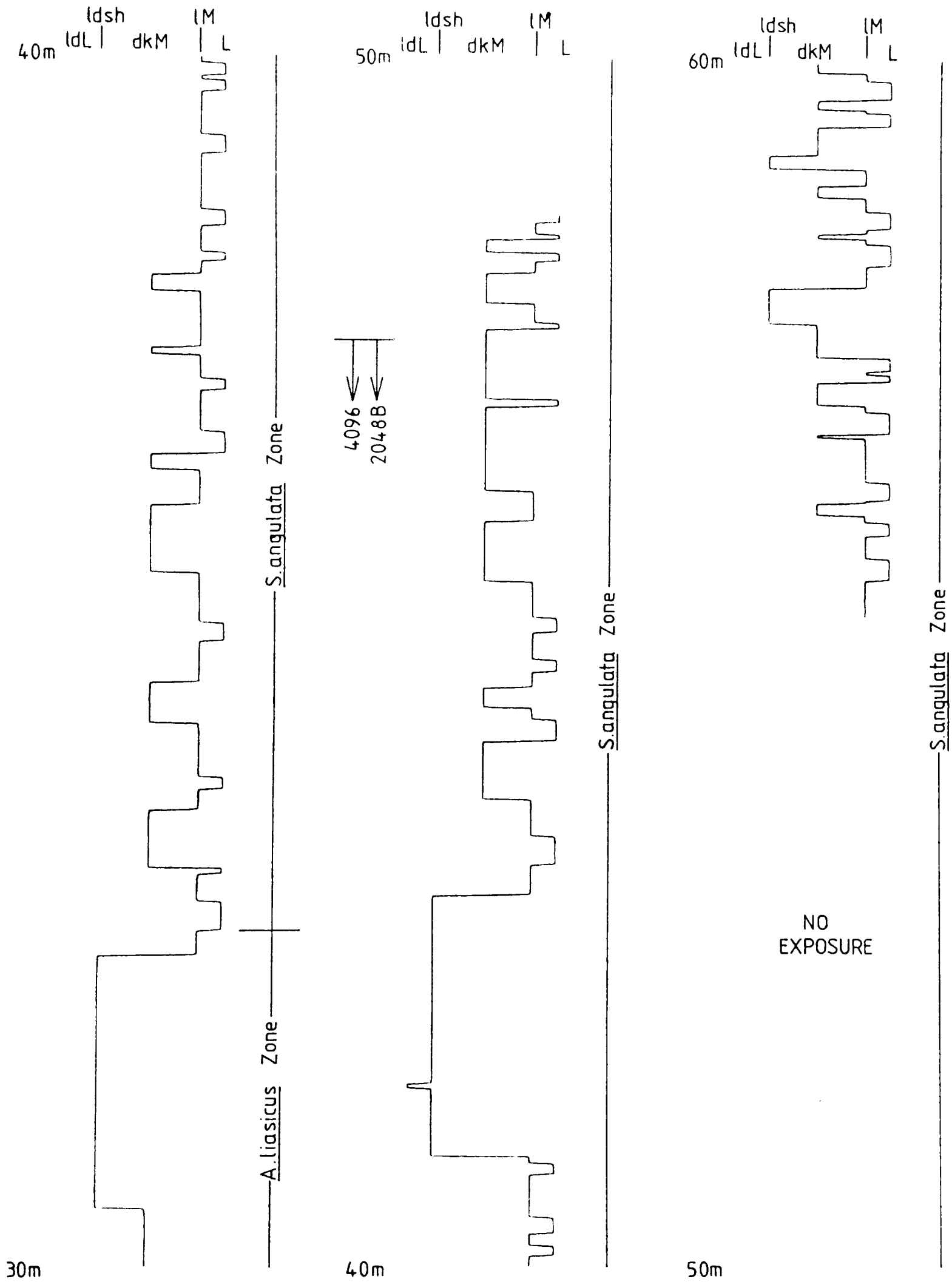

Fig 4·3E BASAL LIAS WATCHET TIME SERIES

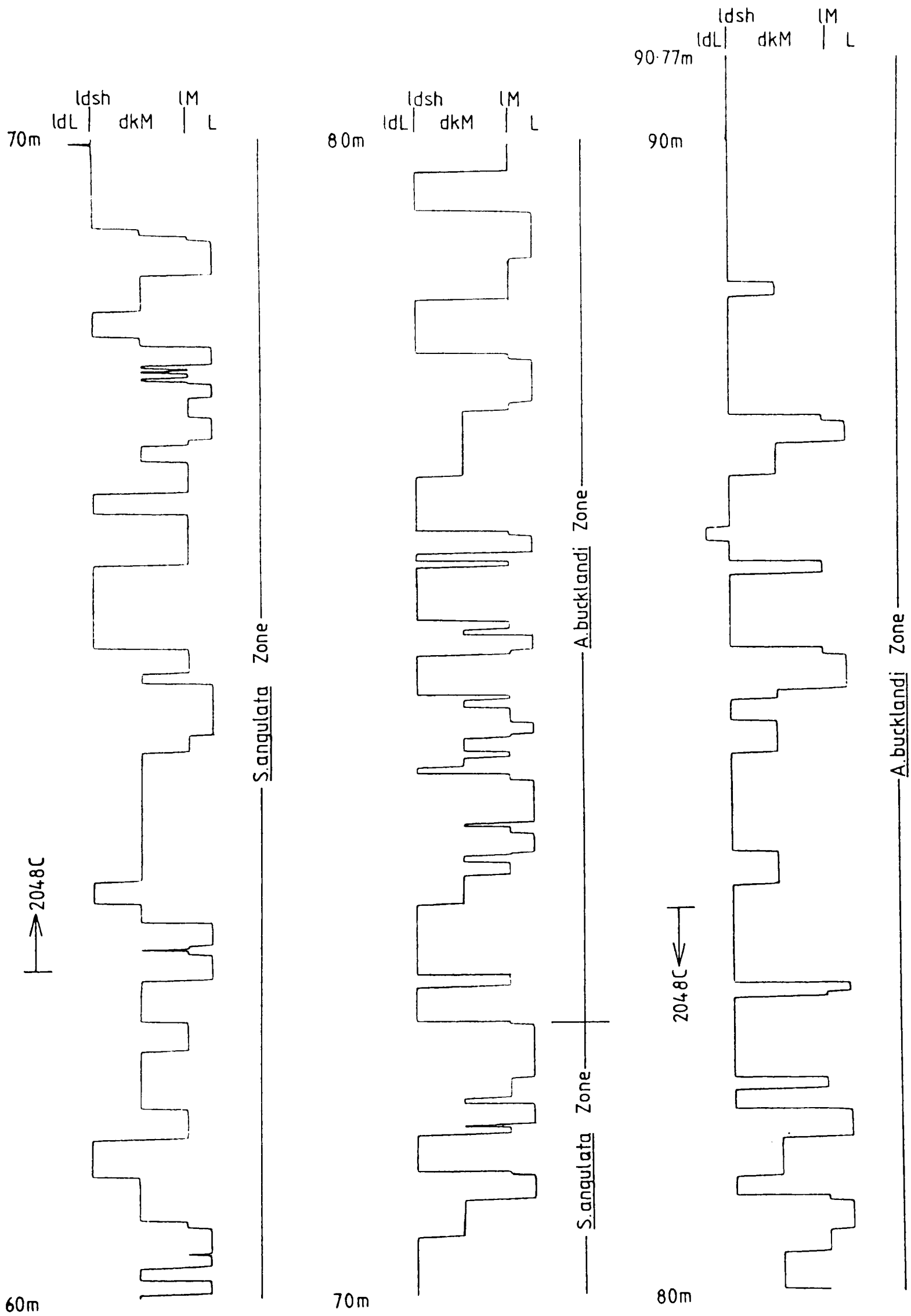

Fig 4·3F BASAL LIAS WATCHET POWER SPECTRA

Fig 4·3G BASAL LIAS LAVERNOCK POINT TIME SERIES

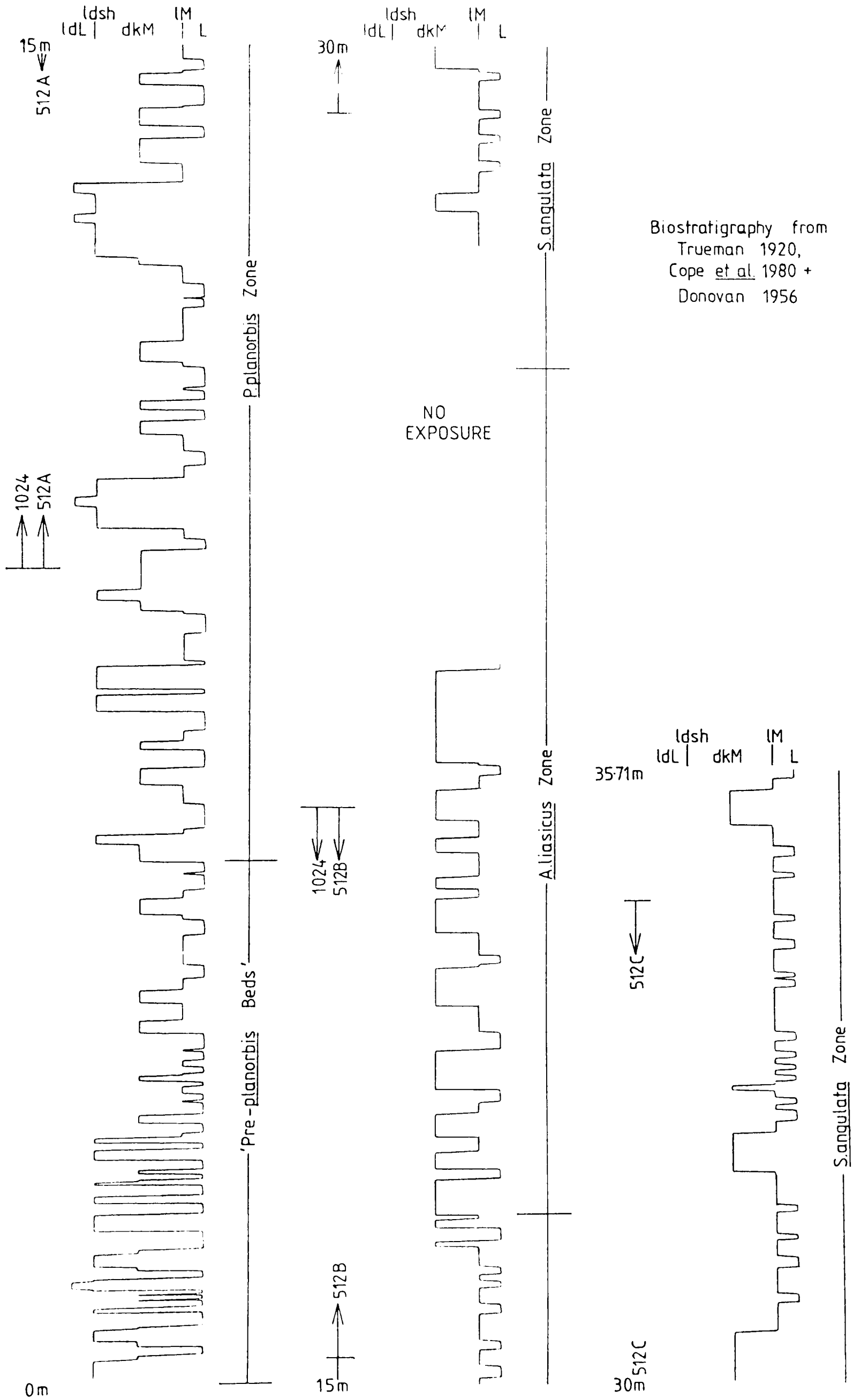

Biostratigraphy from
Trueman 1920,
Cope et al. 1980 +
Donovan 1956

Fig 4·3H BASAL LIAS LAVERNOCK POINT POWER SPECTRA

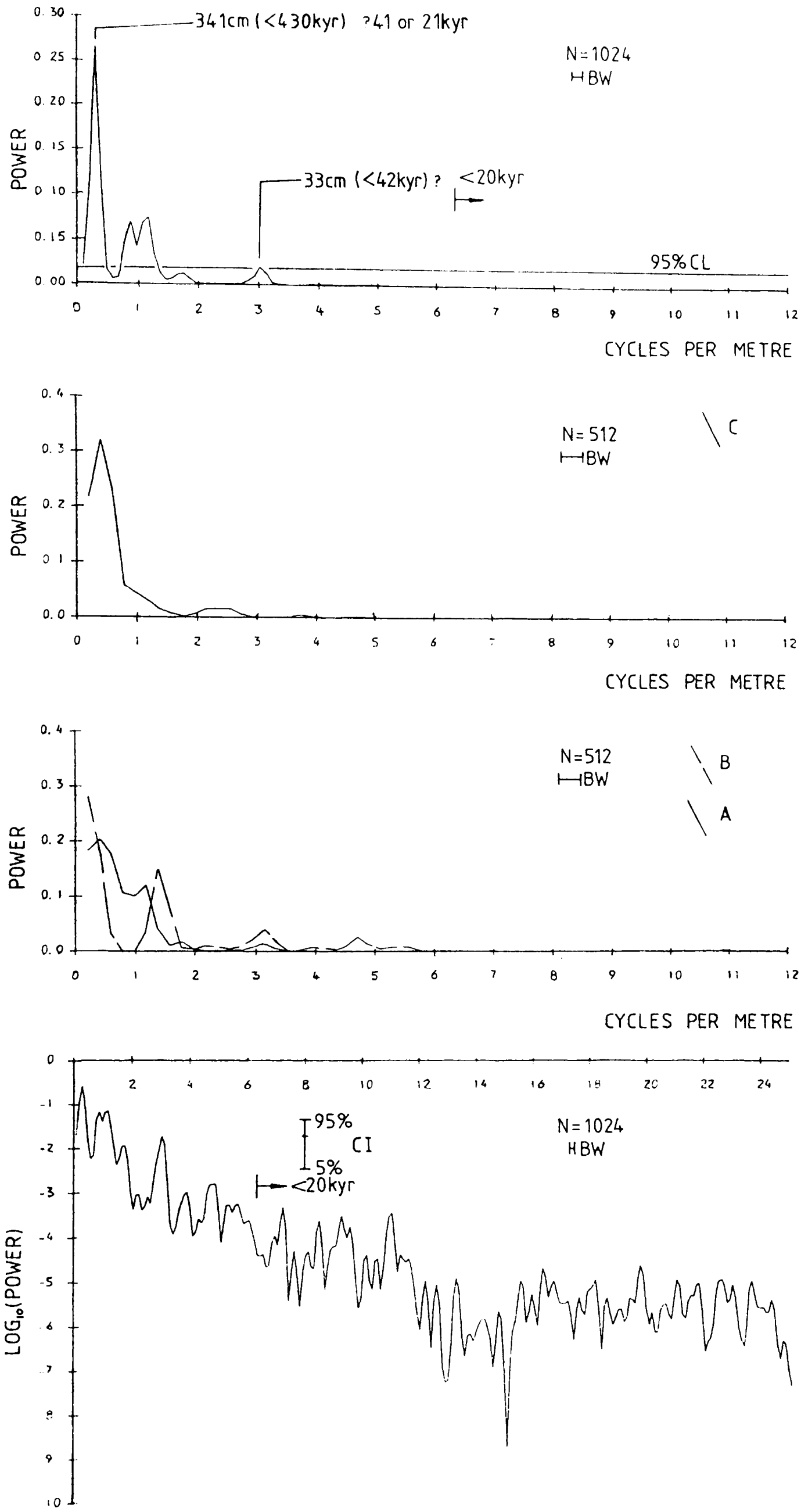

Fig 4·31 BASAL LIAS, NASH POINT TIME SERIES

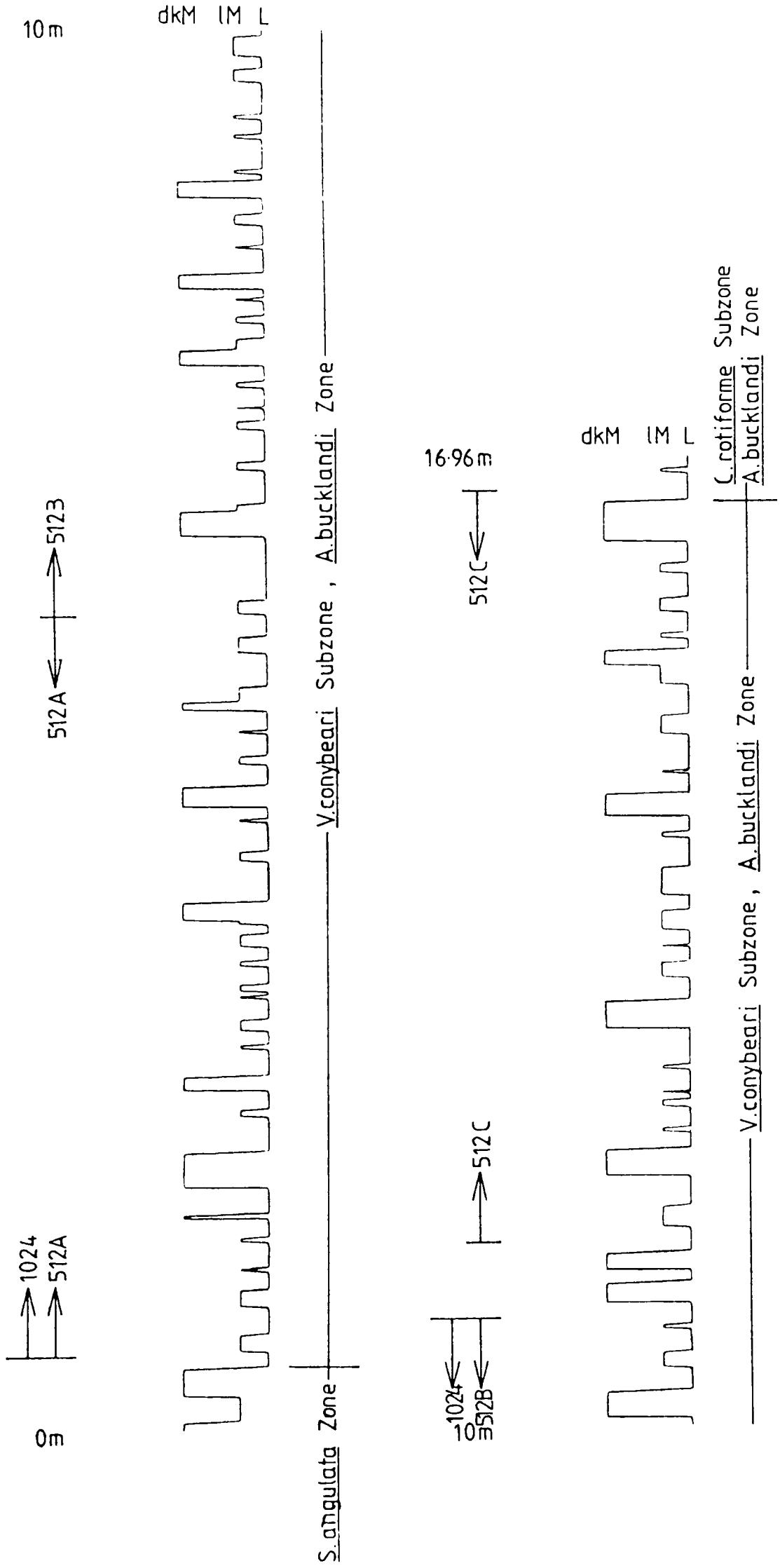

Biostratigraphy from Trueman 1930

Fig 4·3J BASAL LIAS, NASH POINT POWER SPECTRA

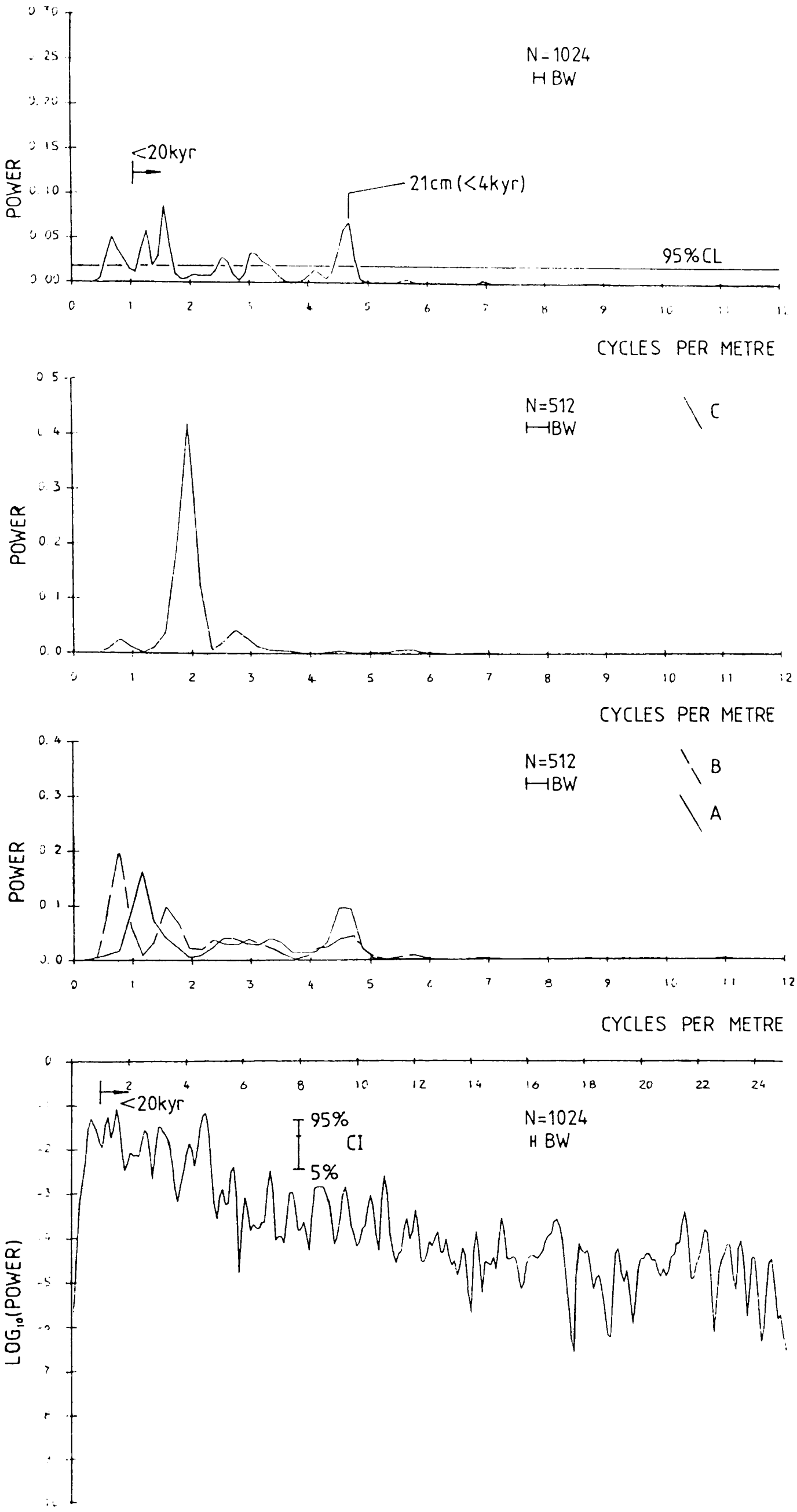

Fig 4·3K BASAL LIAS, LONG ITCHINGTON TIME SERIES

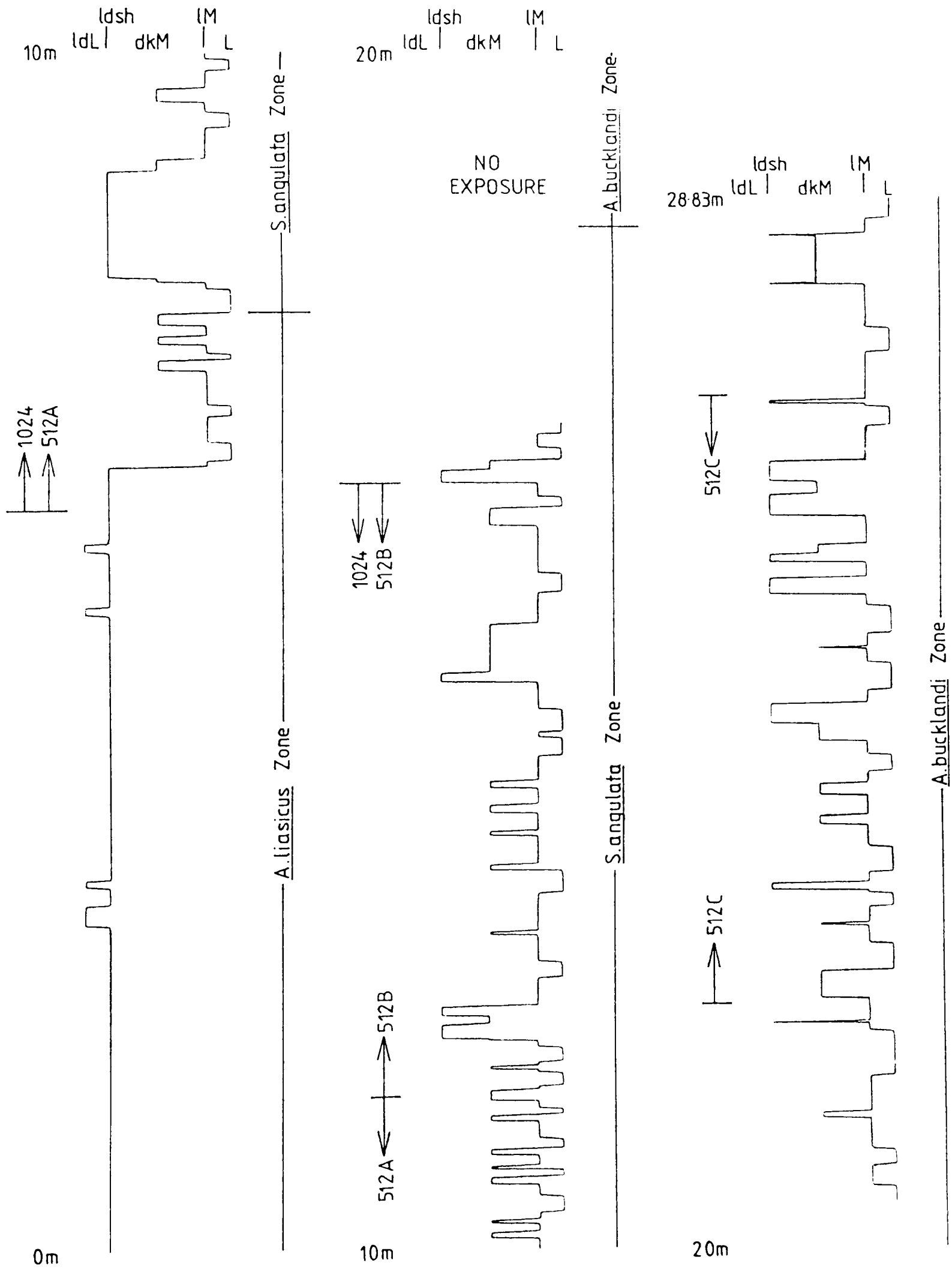

Biostratigraphy from Clements et al. 1975

Fig 4·3L BASAL LIAS, LONG ITCHINGTON POWER SPECTRA

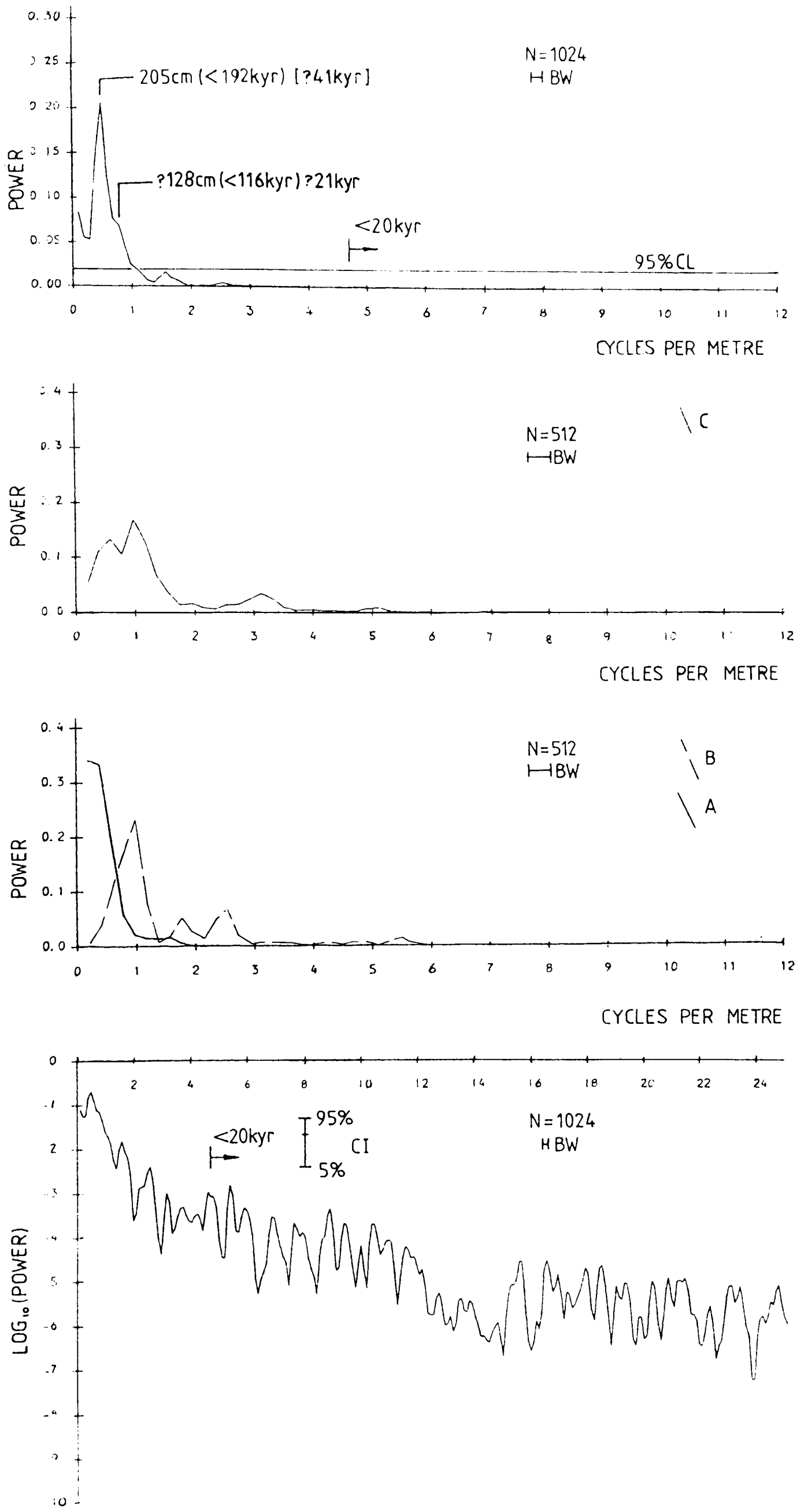

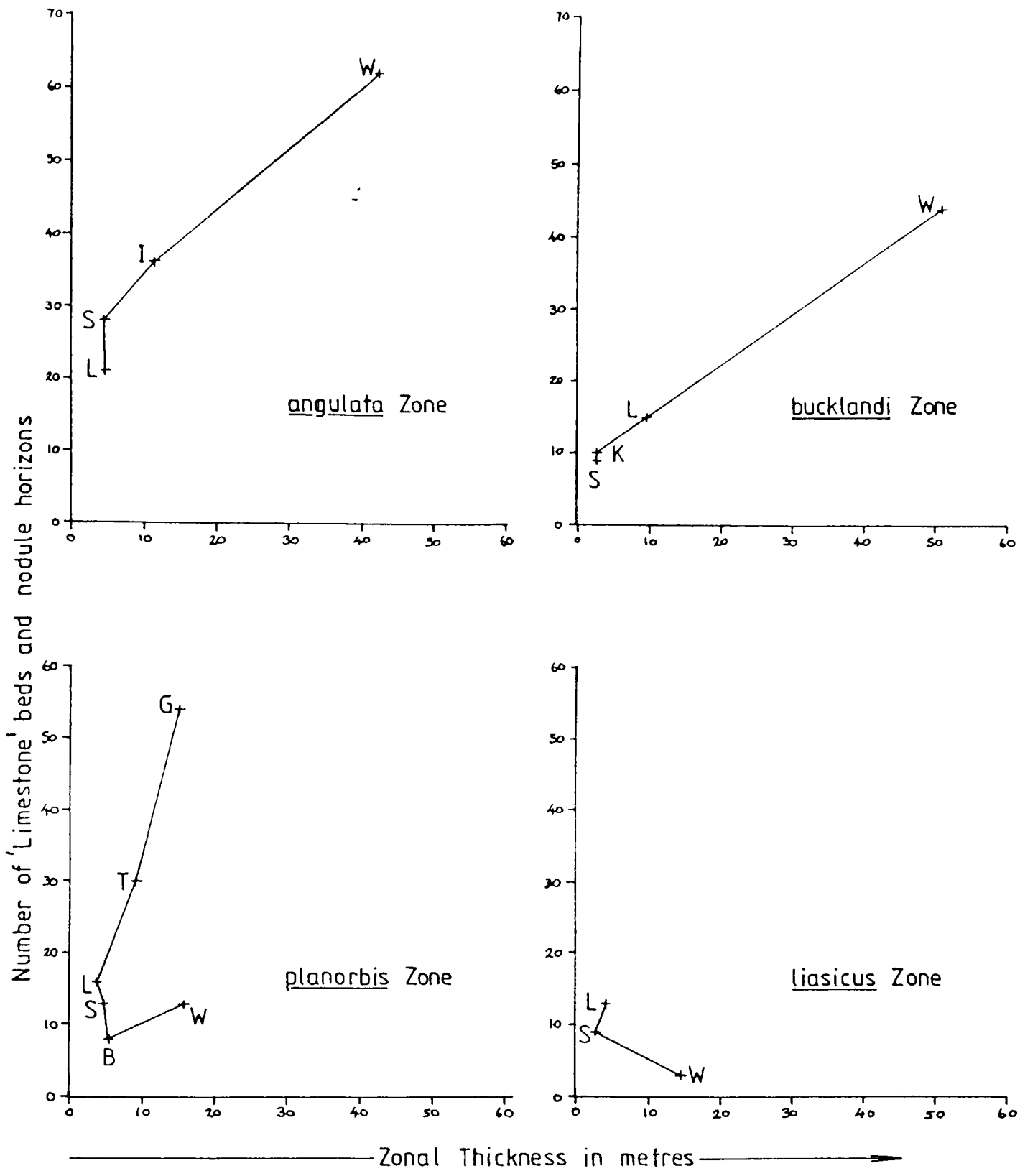

S	Saltford Cutting, Avon	Donovan 1956, Donovan + Kellaway 1984
K	Keeling's Quarry, Avon	
W	Watchet, Somerset	- Palmer 1972
L	Lyme Regis, Dorset	- Lang 1924
I	Long Itchington, Warwick	- Clements et al. 1975
T	Tolcis, Devon	Hallam 1960a
G	Glamorgan	
B	Barnstone, Nottingham.	- Kent 1937

Nb. here 'Limestone' = Homogeneous + Laminated Limestone

Fig 5·1A RELATIONSHIP BETWEEN NUMBER OF CEMENTED HORIZONS + ZONE THICKNESS

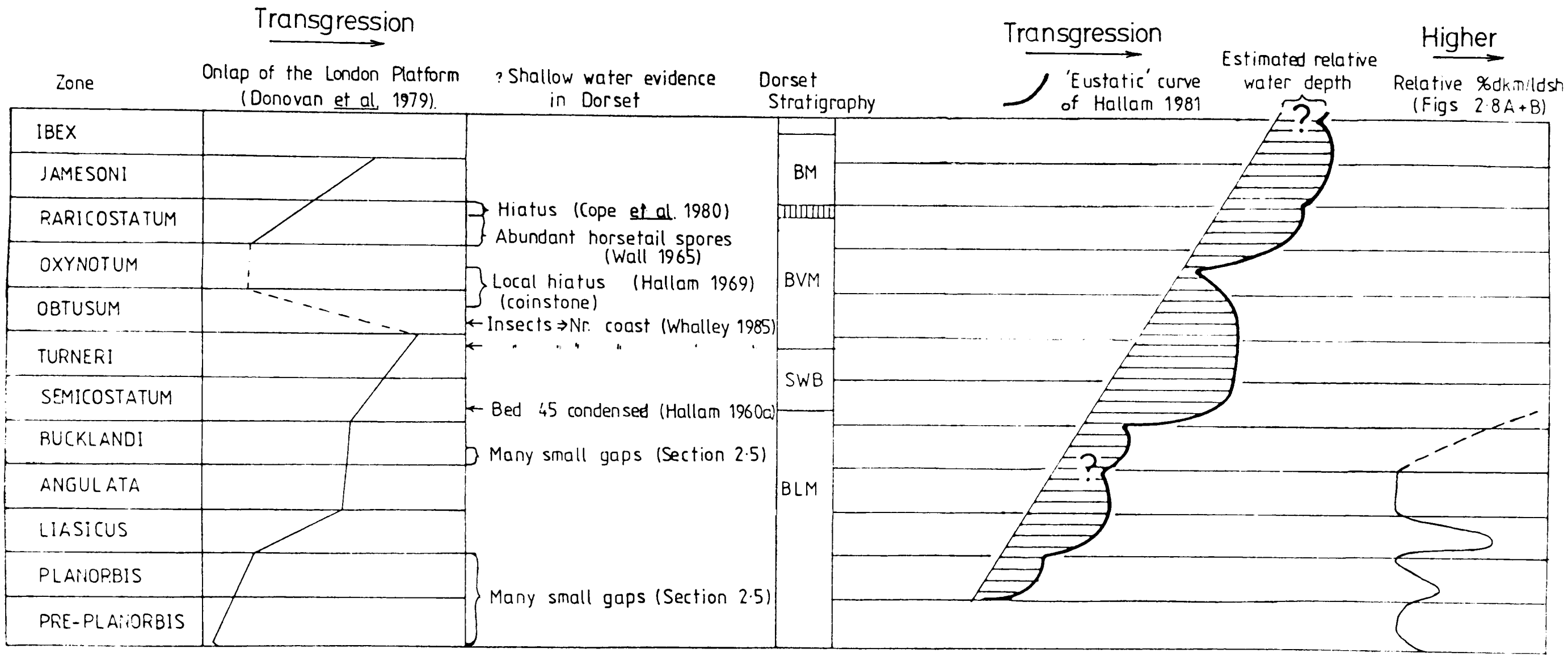

BM – Belemnite Marl BVM – Black Ven Marls SWB – Shales with beef BLM – Blue Lias Member

Fig 5·3A SEA-LEVEL CHANGES IN THE EARLY JURASSIC IN BRITAIN

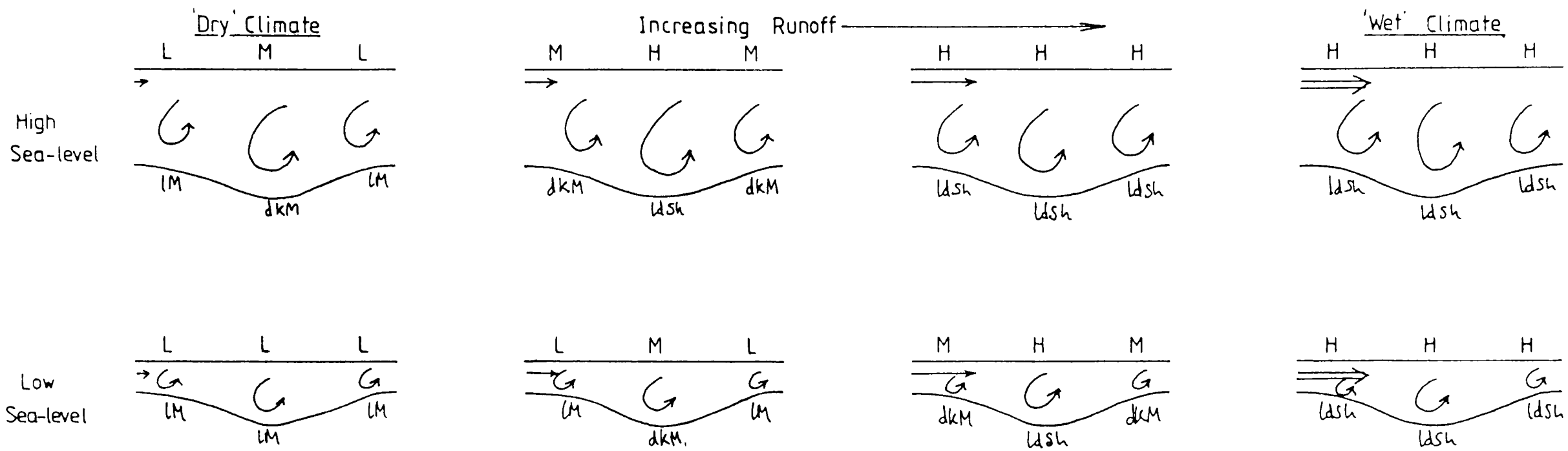

L Low
M Medium
H High
} Surface productivity proportional to supply of nutrients

$\frac{\%\text{Dinoflagellate}}{\%\text{Coccolithophore}} \propto$ Productivity

(High coccolith proportion ⇒ carbonate-rich sediment)

⟶ Nutrients supplied from runoff - size of arrows proportional to amount of nutrients

↺ " " " mixing - " " " " " " " "

Fig 5·4A Productivity Model.

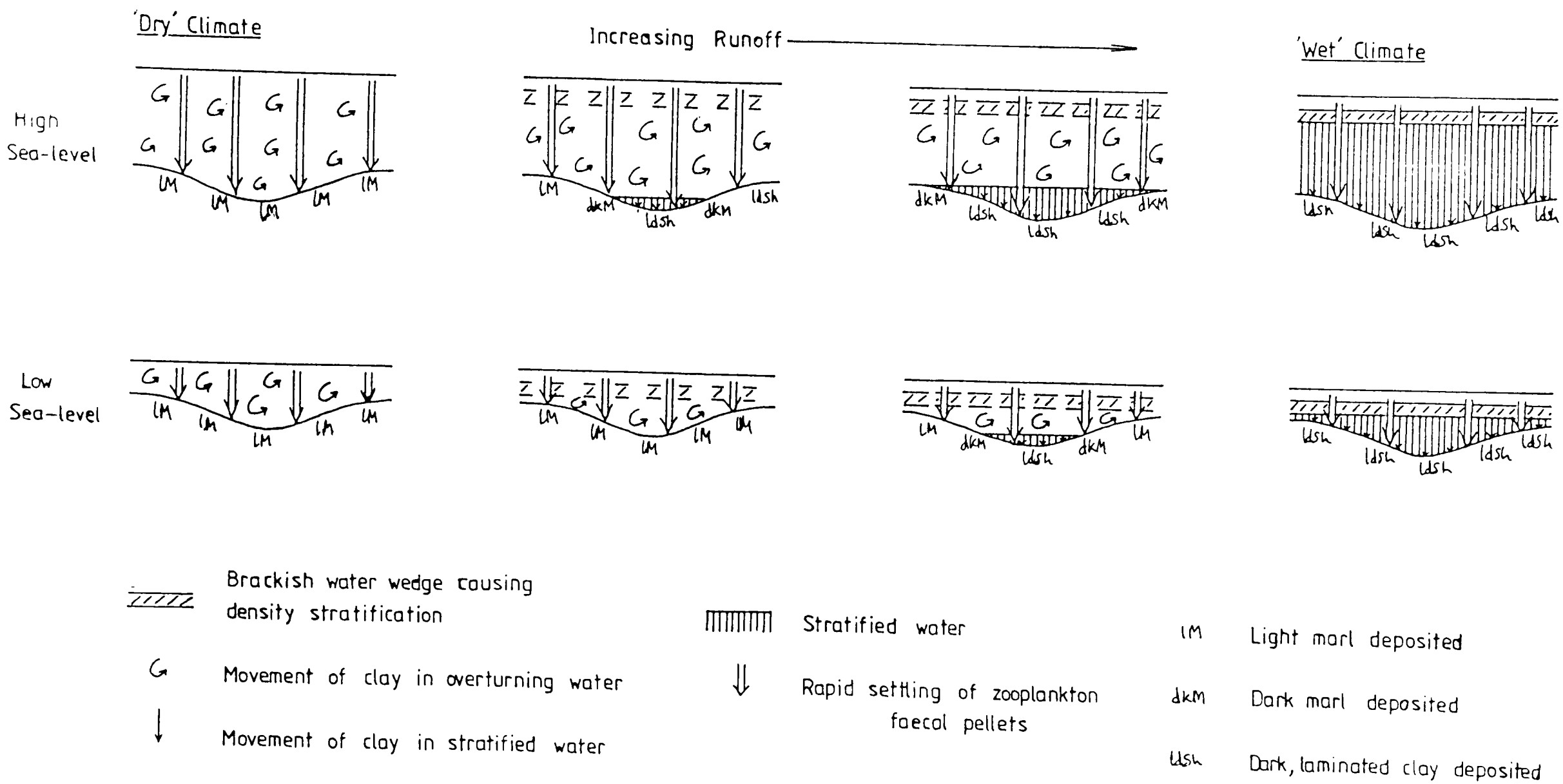

Fig 5·4B Stratification Model (based on Hallam + Bradshaw 1979 and Barron et al. 1985).

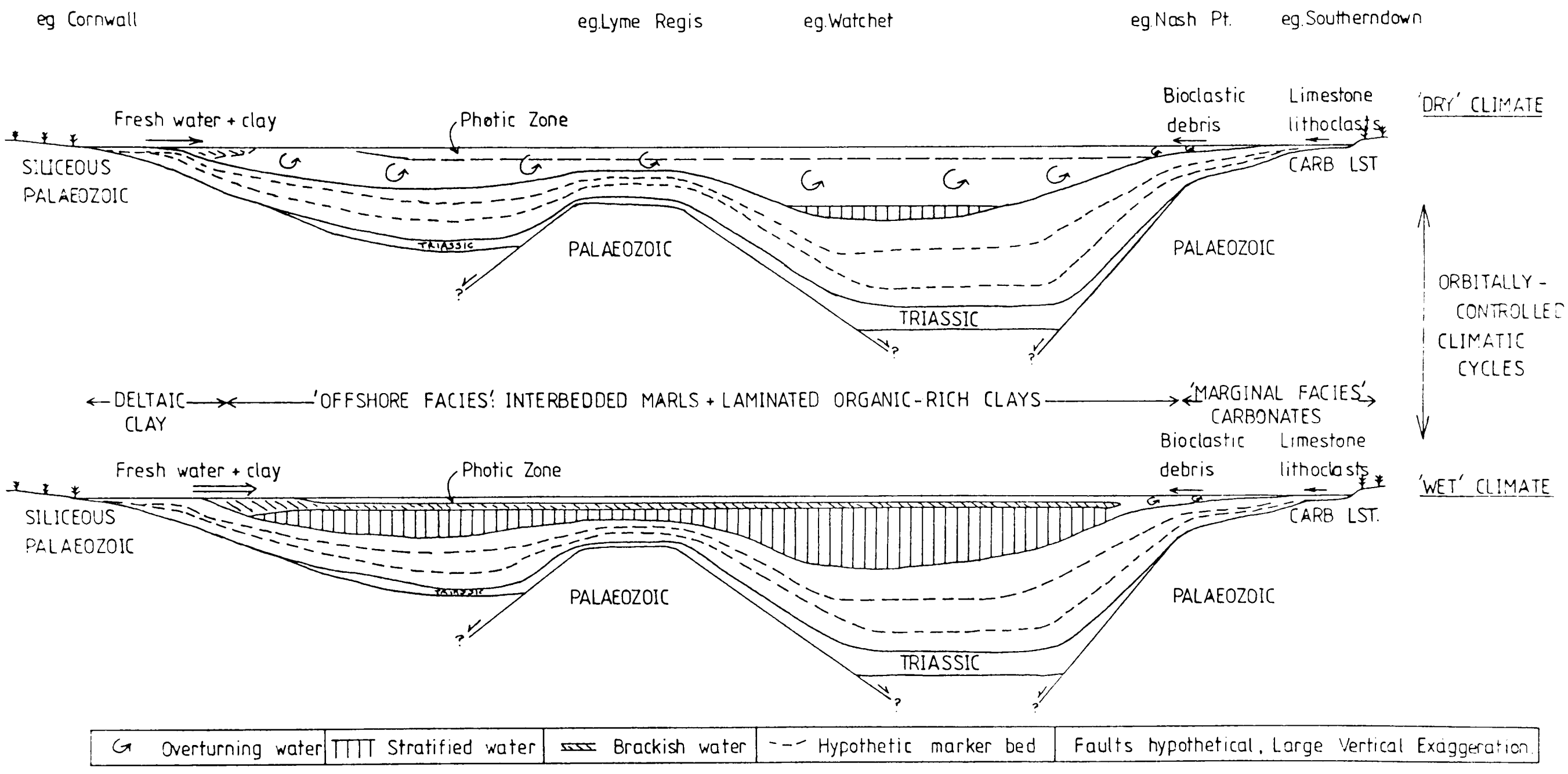

Fig 5·5A GENERAL ENVIRONMENTAL MODEL FOR THE LATEST TRIASSIC AND EARLIEST JURASSIC IN SOUTH BRITAIN (cf Figs 5·4B and 5·5B)

Fig 5.5B

References used for Palaeogeography:

Smith *et al.* 1981	Palaeocontinental positions.
Hallam 1975	Emergent areas.
Zeigler 1982	Islands and clastic influx.
Loughman 1982	N.W. Europe palaeogeography.
Bernoulli and Jenkyns 1974	S.European and N.African carbonate platforms.
Hay *et al.* 1982	N.Atlantic rift evaporites and lakes in the N.America.
Bloos 1982	German palaeogeography.
Troedsson 1951	Scandinavian clastic influx.
Batten *et al.* 1986	Clastics in East Scotland.
Hallam 1975	Clastics in West Scotland.

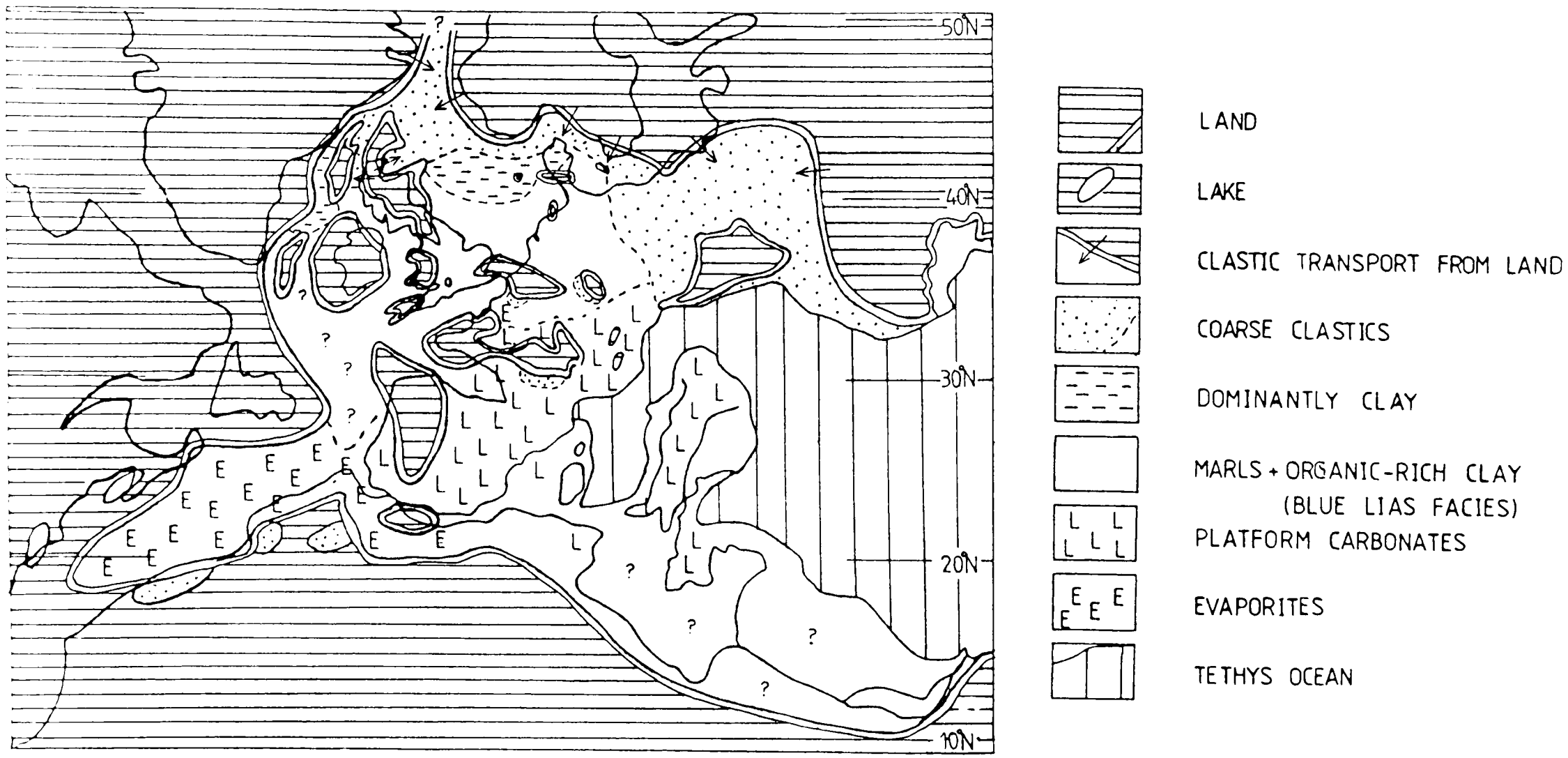

Fig 5·5B PALAEOGEOGRAPHY IN THE HETTANGIAN AND EARLY SINEMURIAN

Fig 6.2A

Field aspect of the Boom Clay Formation, Terhagen, near Antwerp.

Top:	Vandenberghe's beds 14-32	(10.6m)
Bottom:	Vandenberghe's beds 32-49	(7.7m)

Fig 6.2B BOOM CLAY FORMATION TIME SERIES

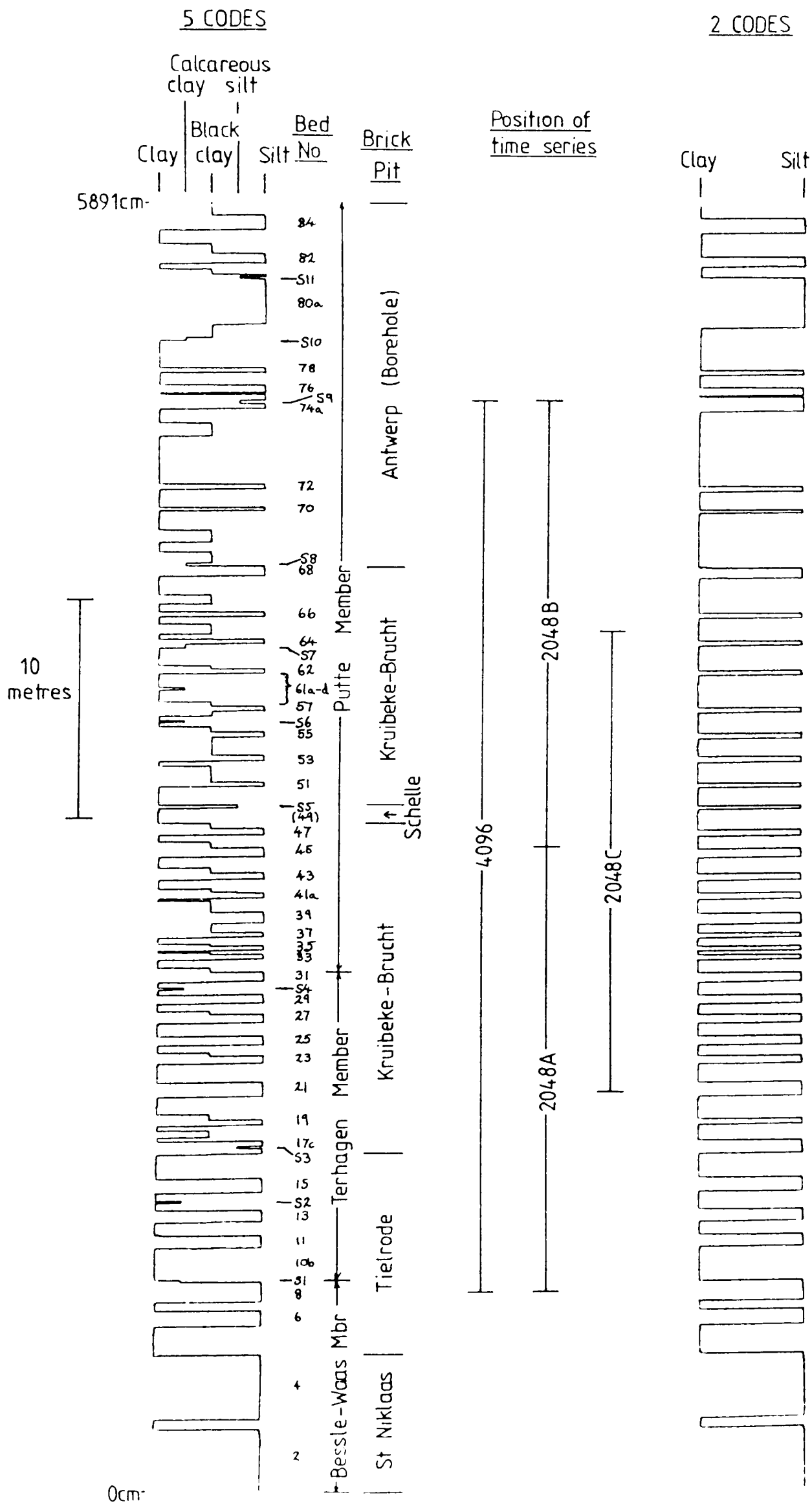

Fig 6.2C BOOM CLAY FORMATION POWER SPECTRA - Using 5 Rock Type Codes

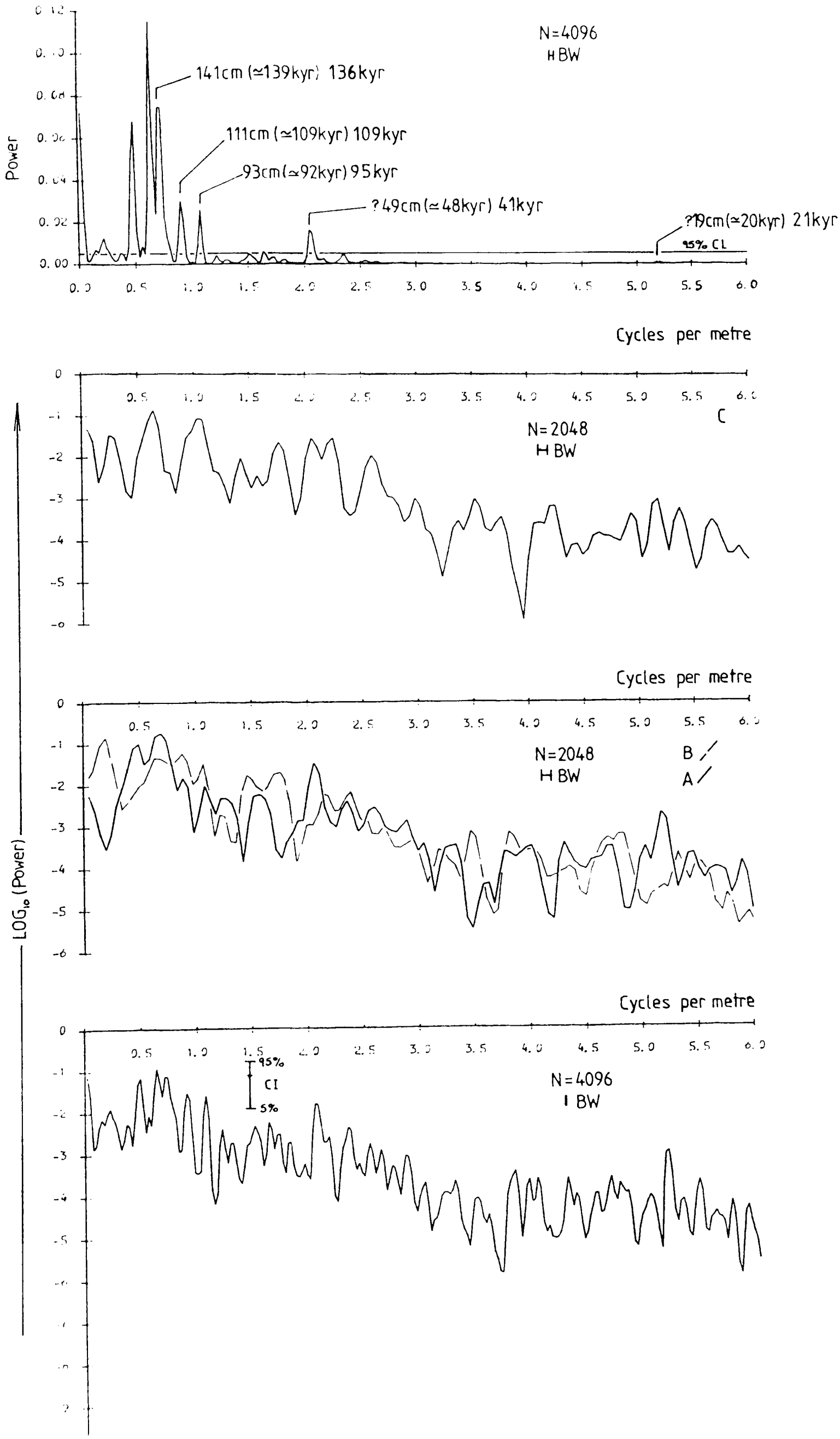

Fig 6.2D BOOM CLAY FORMATION POWER SPECTRA Using 2 Rock Type Codes

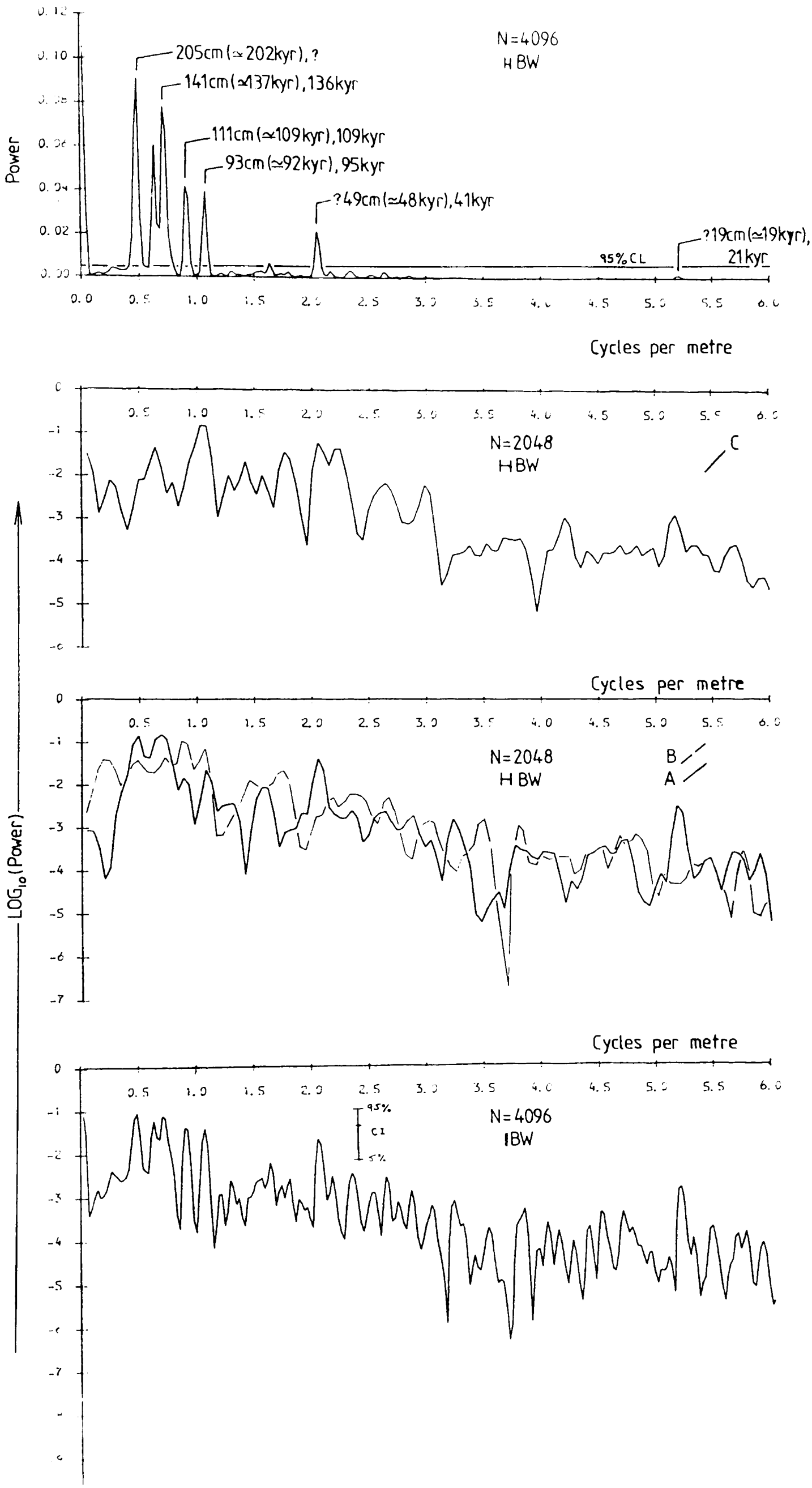

Fig 6.3A

Field aspect of the Kimmeridge Clay Formation, near Freshwater Steps, Kimmeridge, Dorset.

Top: The White Stone band near the top is a coccolith limestone. Underneath calcareous shale and oil shales are interbedded. The hammer is 39cm long.

Bottom: Close-up of the White Stone band coccolith limestone with an oil shale. Notice that both rock types are laminated. The oil shale appears to have suffered minor syn-compactional faulting. The lens cap is 5cm in diameter.

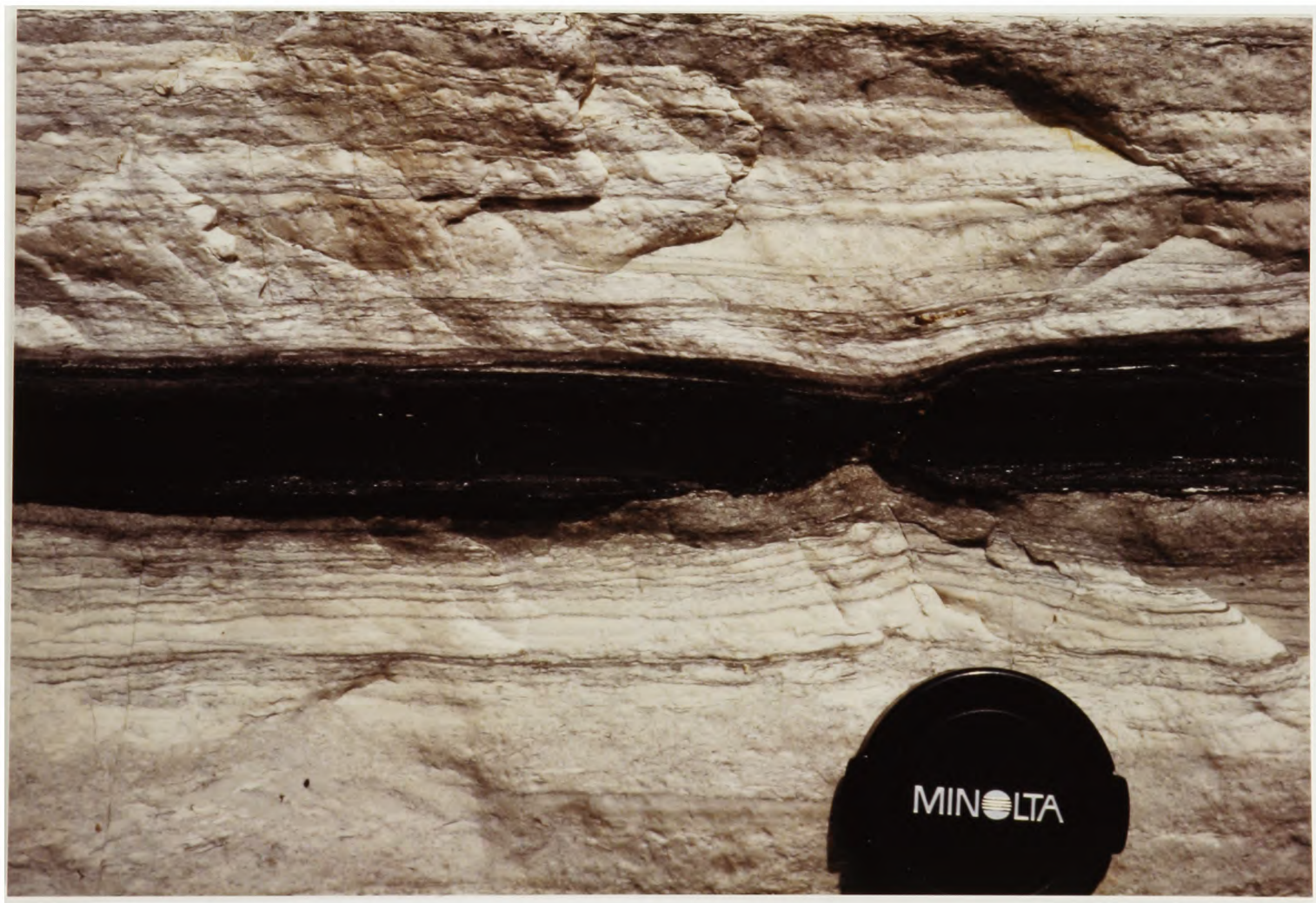
MINOLTA

Fig 6.3B Upper KIMMERIDGE CLAY TIME SERIES

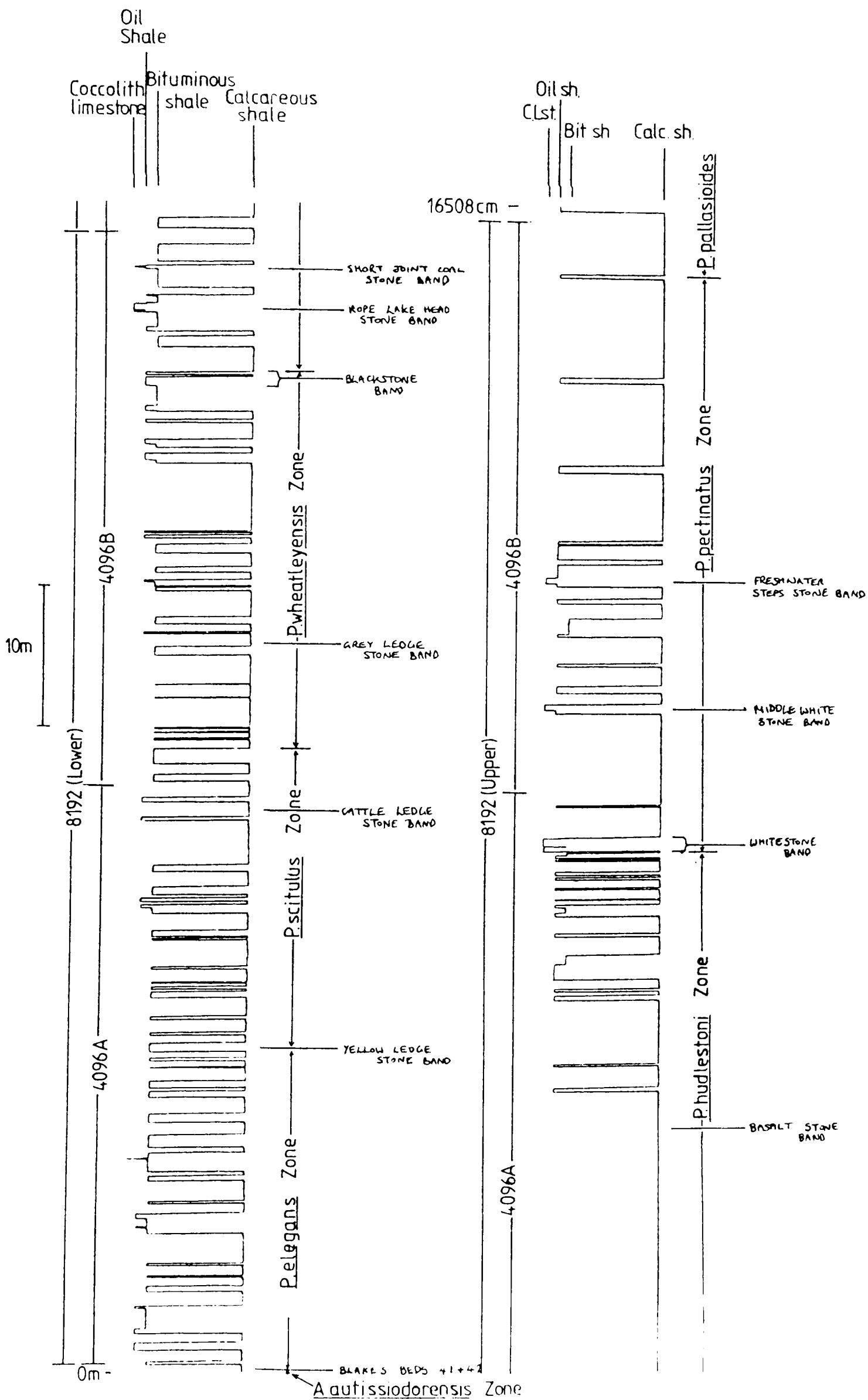

Fig 6.3C Upper KIMMERIDGE CLAY TOP SECTION POWER SPECTRA

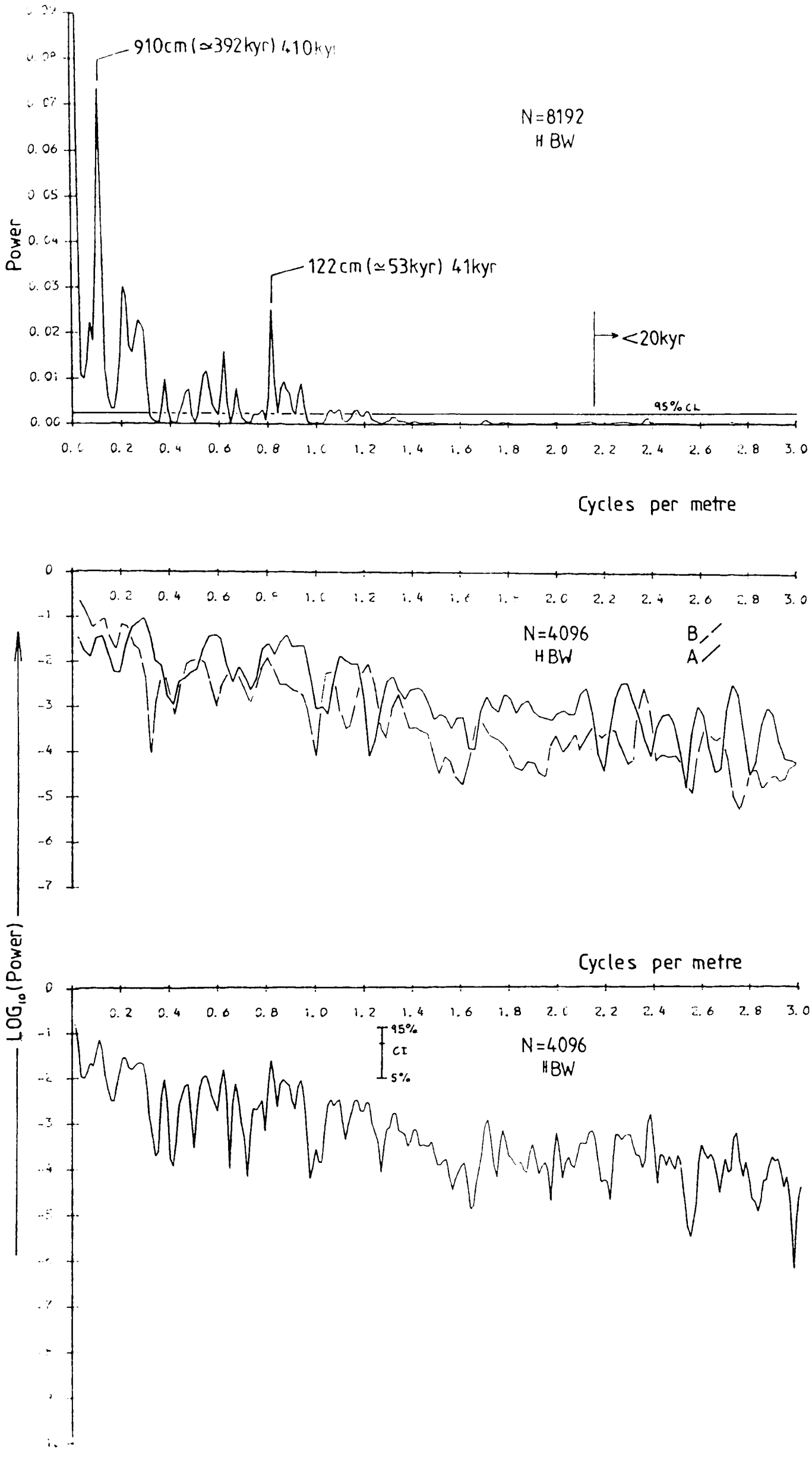

Fig 6 3D UKIMMERIDGE CLAY BOTTOM SECTION POWER SPECTRA

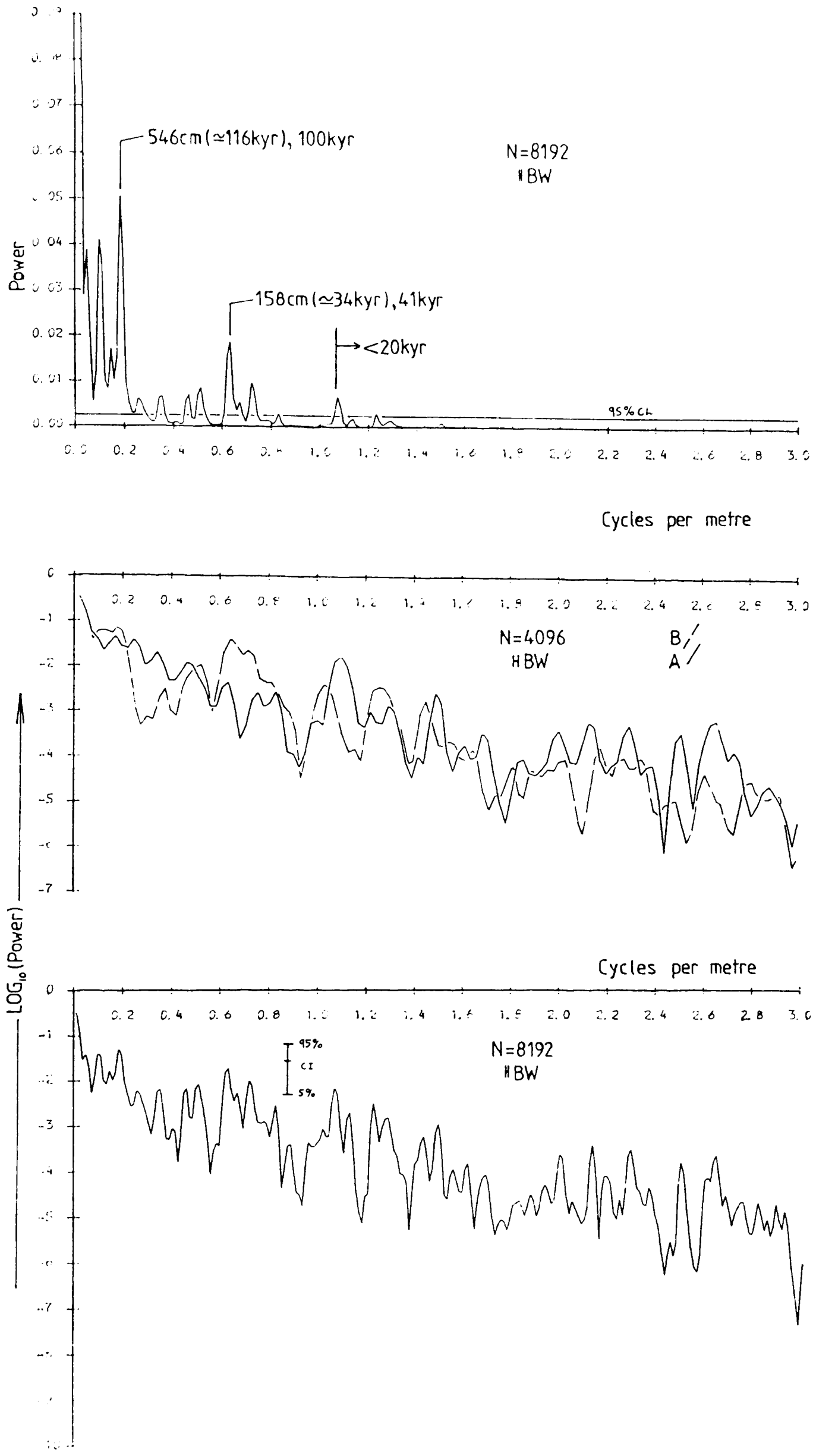

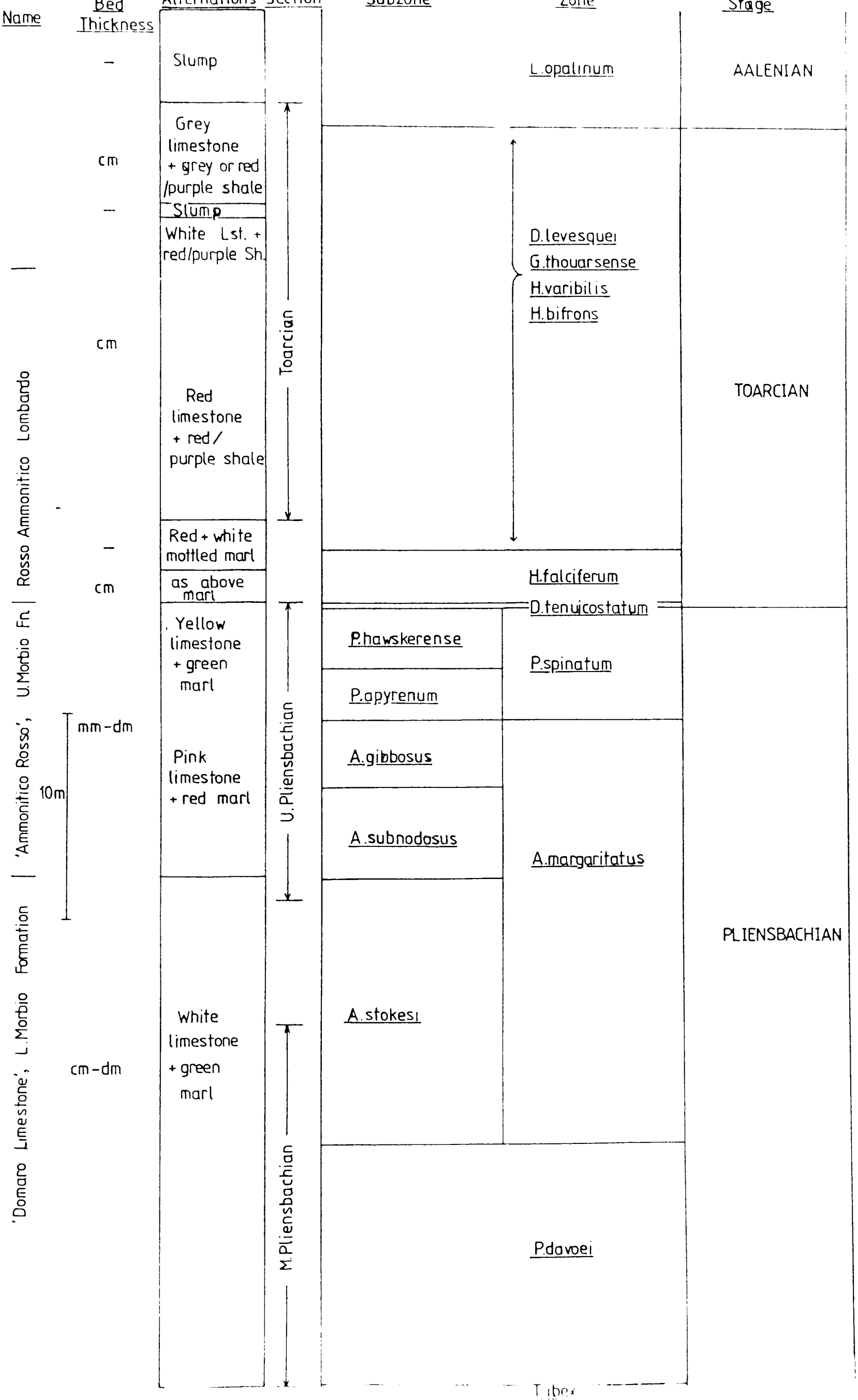

Fig 64A MEASURED SECTIONS WITHIN THE STRATIGRAPHY OF BREGGIA GORGE

Fig 6.4B

Field aspect of the Toarician section (Ammontico Lombardo), Breggia Gorge.

Top: Bernoulli's beds 1-5.
Bottom: Part of Bernoulli's bed 1. The hammer is 39cm long.

Fig 6.4C BREGGIA GORGE TOARCIAN SECTION TIME SERIES

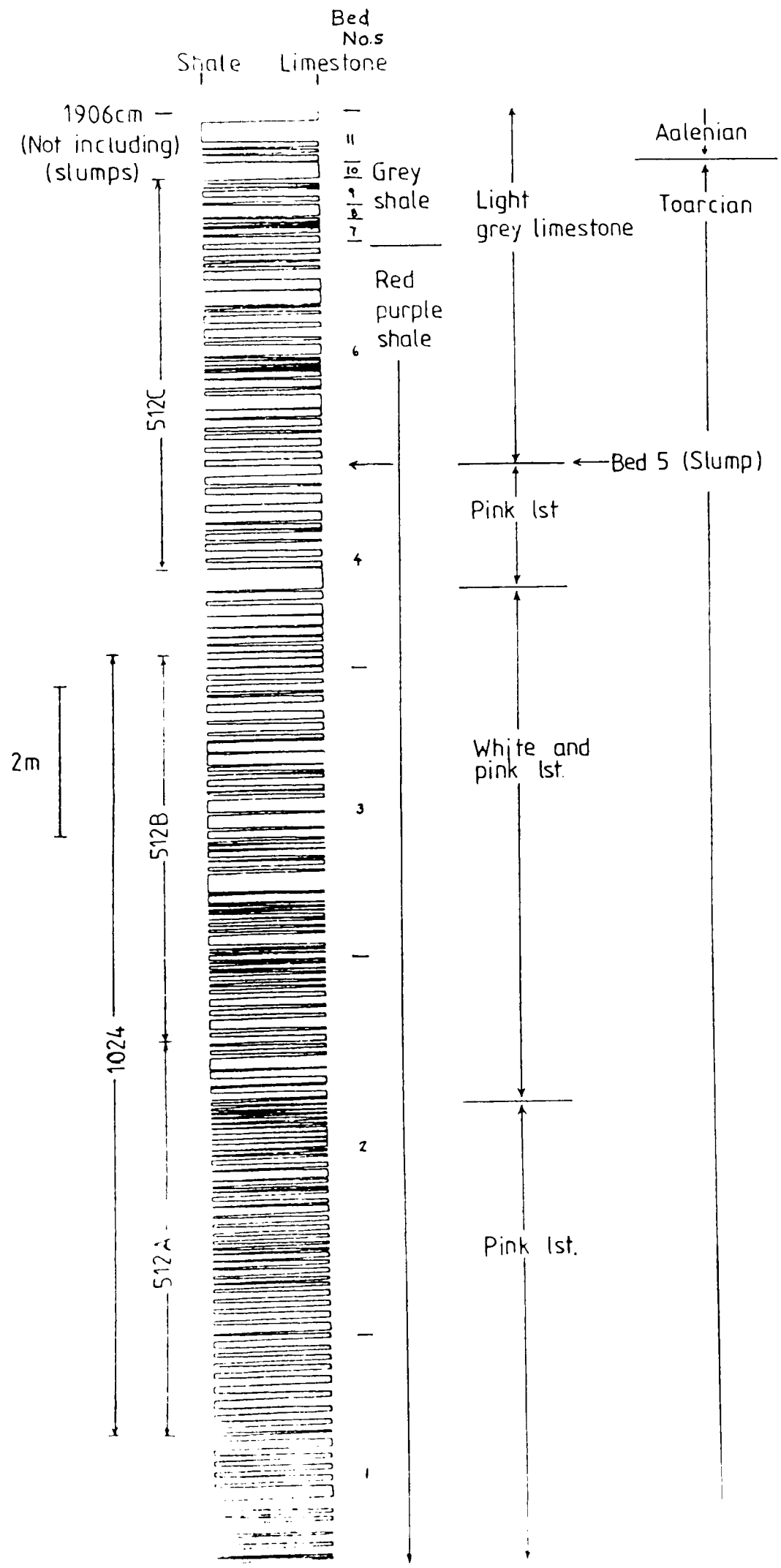

Fig 64D BREGGIA GORGE TOARCIAN SECTION POWER SPECTRA

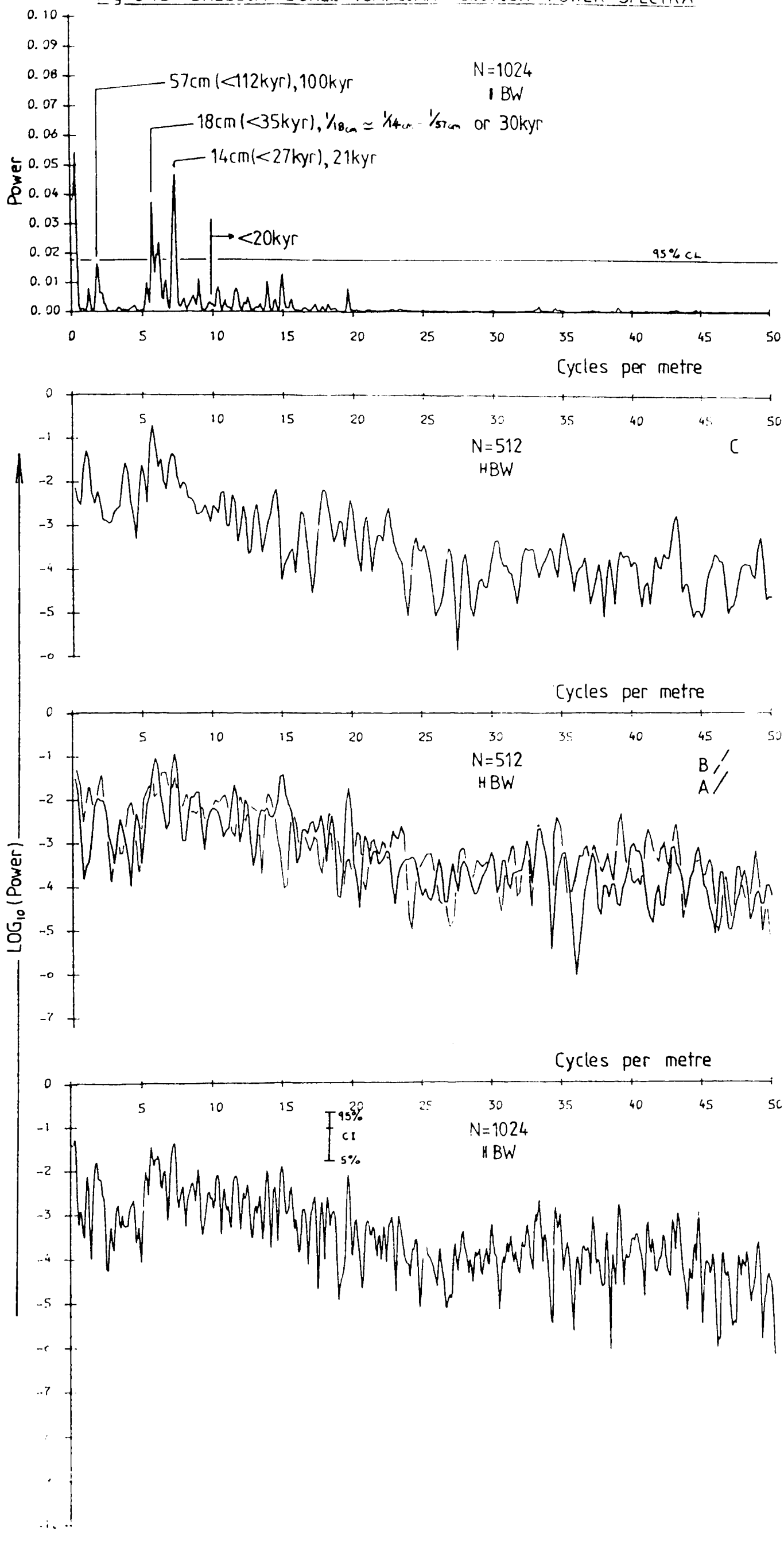

Fig 6.4E

Field aspect of the Upper Pliensbachian section (Upper Morbio Formation), Breggia Gorge.

Top: The section represents about 8m, younging to the left.

Bottom: The beds young to the right. The hammer is 39cm long.

Fig 6.4F BREGGIA GORGE Upper PLIENSBACHIAN SECTION TIME SERIES

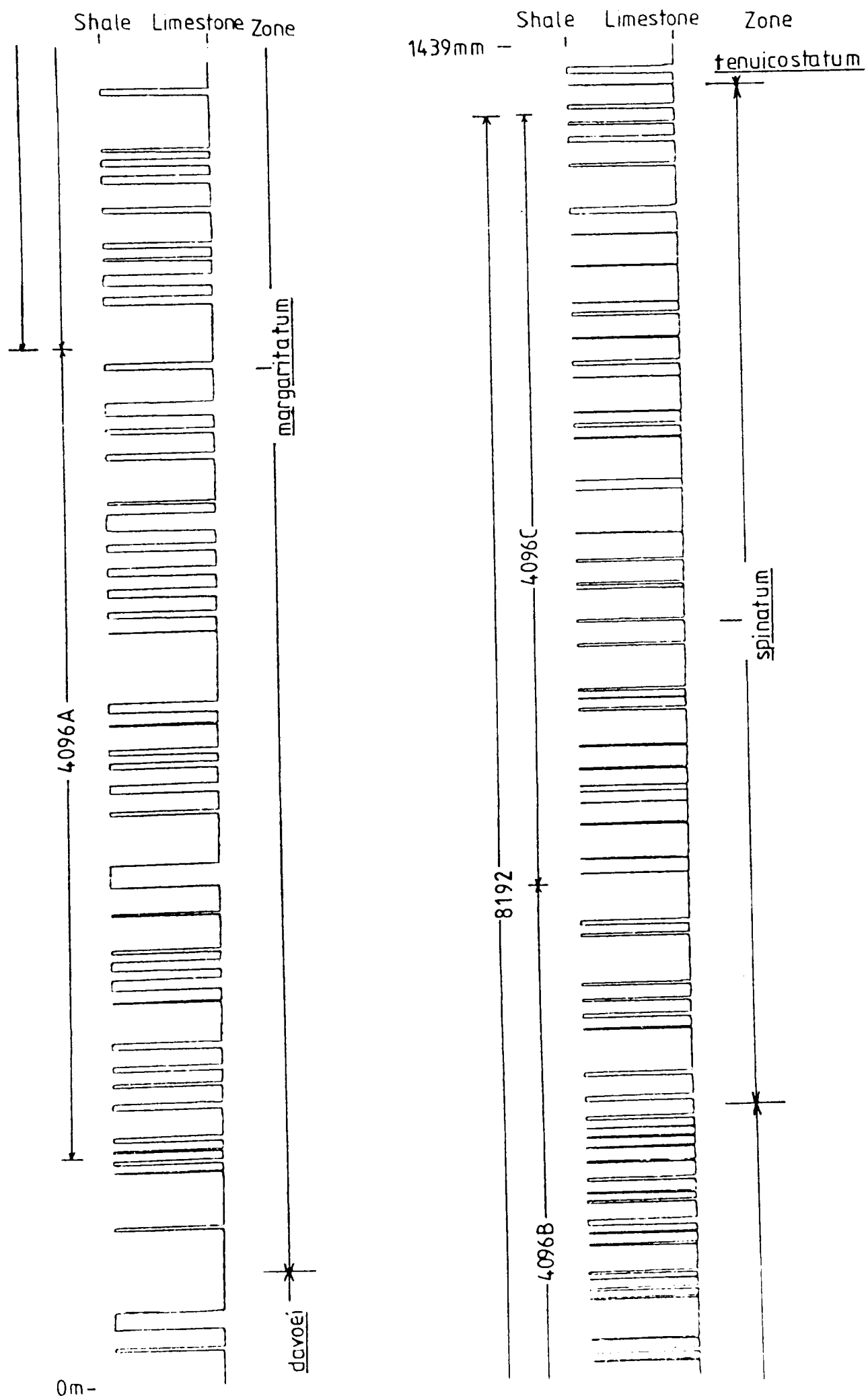

Fig 6.4G BREGGIA GORGE U.PLIENSBACHIAN SECTION POWER SPECTRA

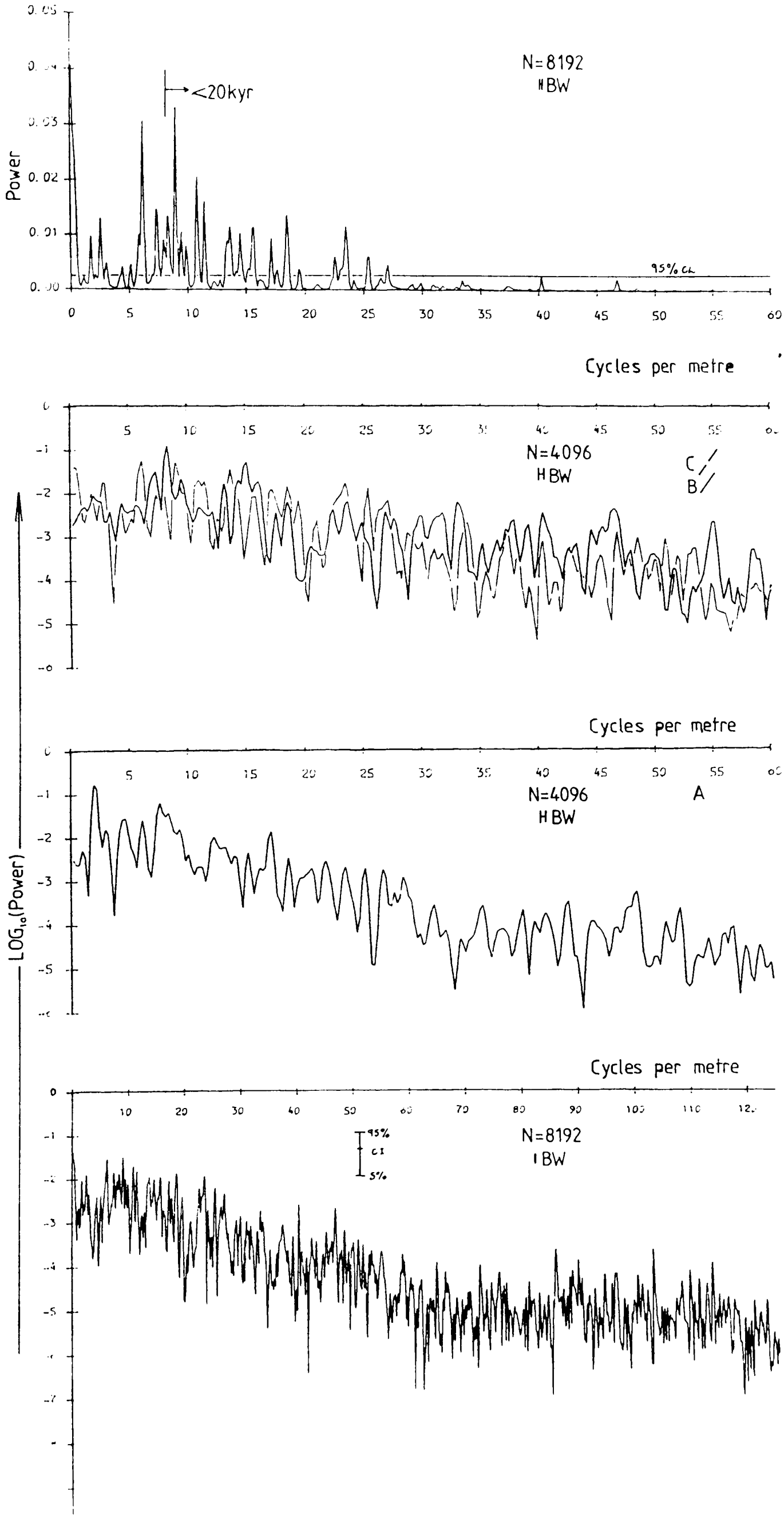

Fig 6.4H

Field aspect of the Middle Pliensbachian section (Lower Morbio Formation), Breggia Gorge.

Top: Wiedenmaryer's beds 974-966. On the far side of the stream, top right, is the section illustrated in Fig 6.4E. The hammer is 39cm long.

Bottom: Wiedenmayer's bed 944. In the middle nodular terminations to a limestone bed probably indicate that the limestones are secondary. The lens cap is 5cm in diameter.

Fig 6·41 BREGGIA GORGE Middle PLIENSBACHIAN SECTION TIME SERIES

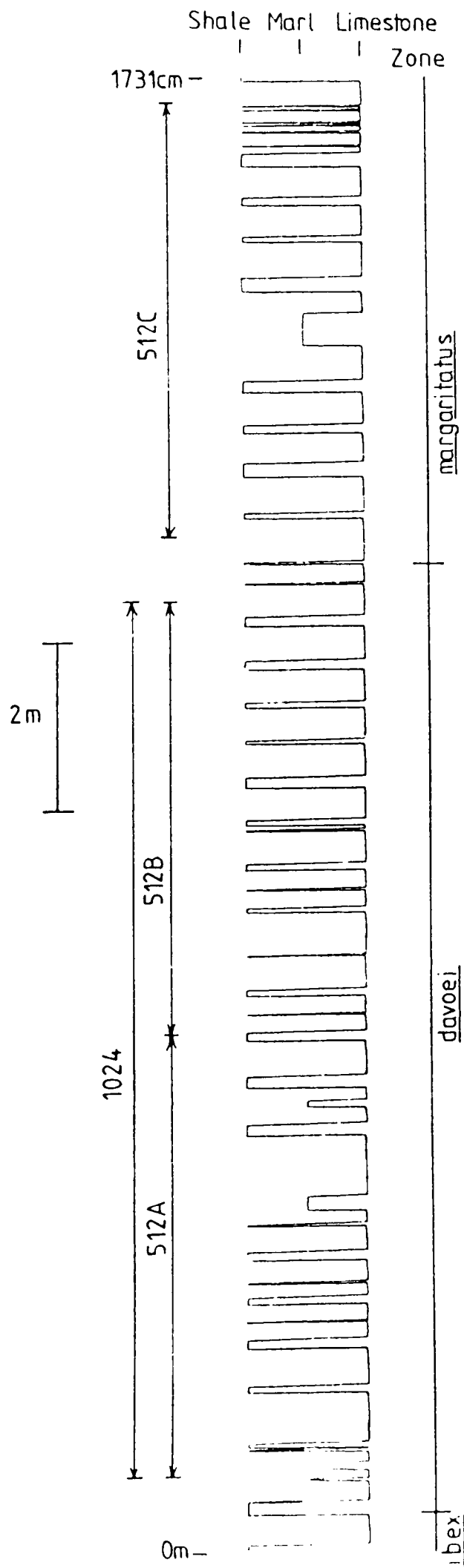

Fig 6.4J BREGGIA GORGE M. PLIENSBACHIAN SECTION POWER SPECTUM

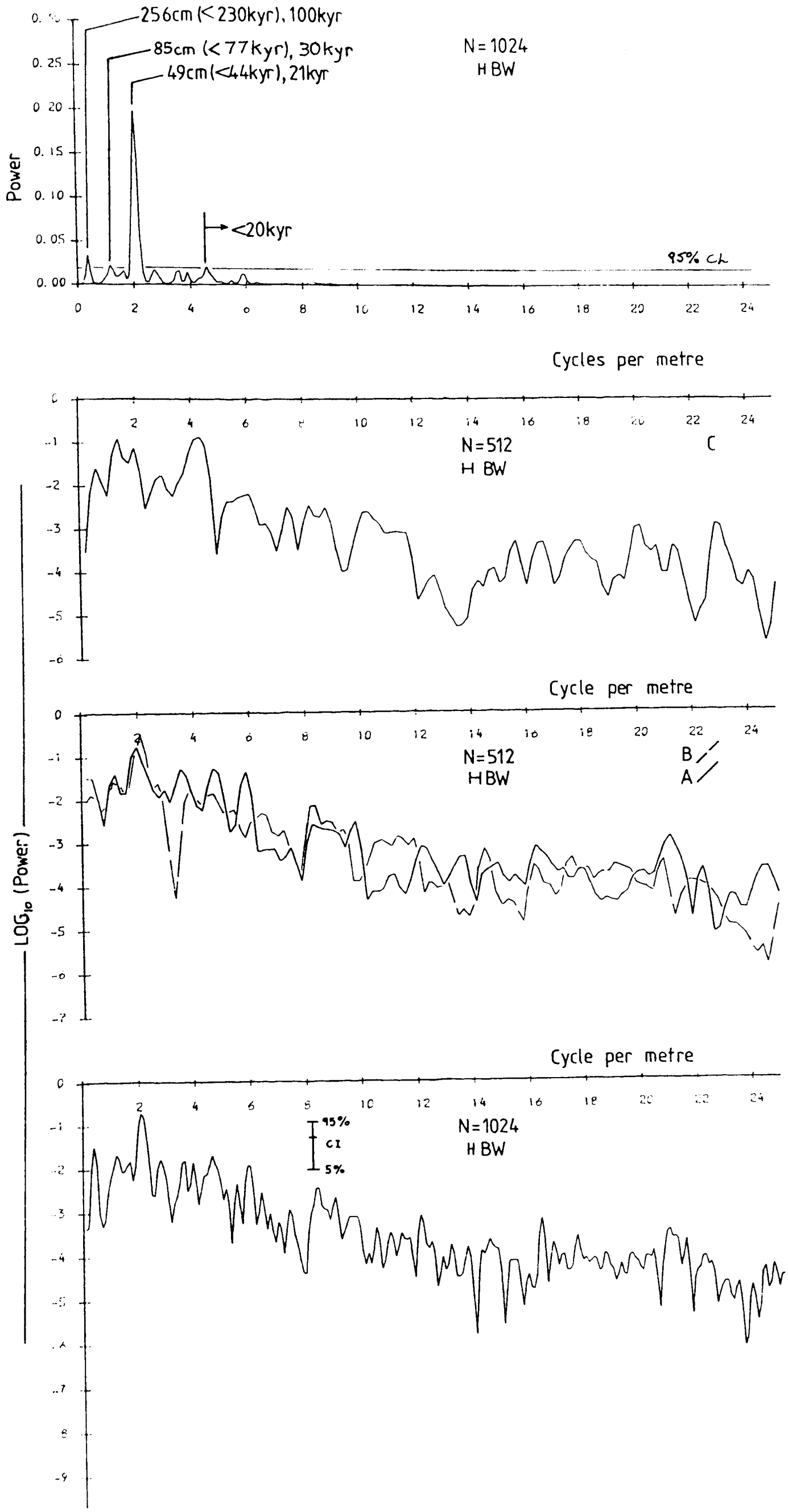

Fig 6.5A

Field aspect of the Belemnite Marls, Stonebarrow, Charmouth, Dorset.

Top: The whole of the Belemnite Marls is about 26m thick. The section clearly illustrates the characteristic interbedding. Beds Lang et al.'s beds 110a-118 used for the time series, occur in the middle and upper part where the measurements of bed thicknesses proved to be most reliable..

Bottom: Calcareous clay overlying argillaceous calcilutite with a burrow-mottled contact.

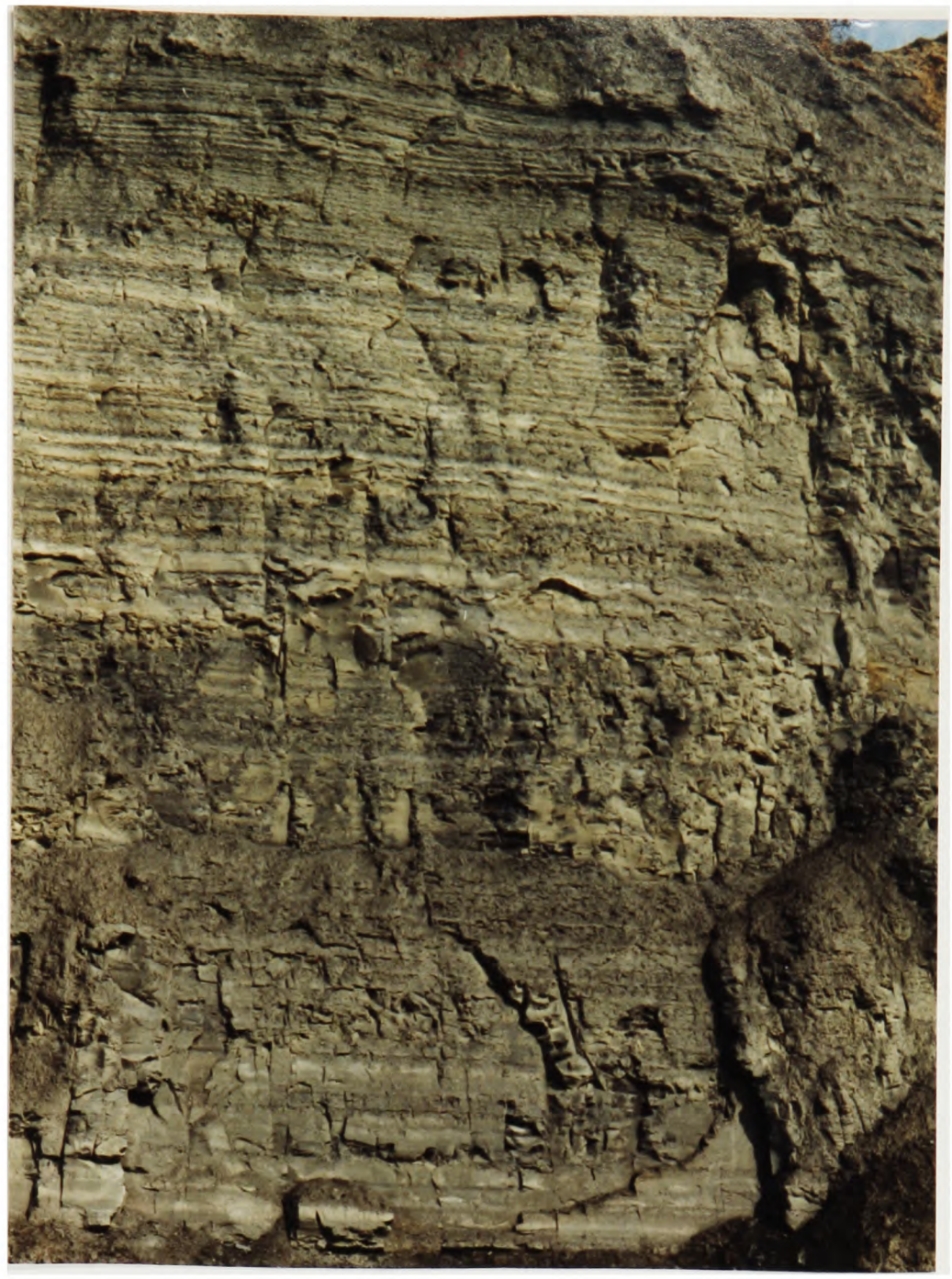

Fig 6.5B BELEMNITE MARLS TIME SERIES

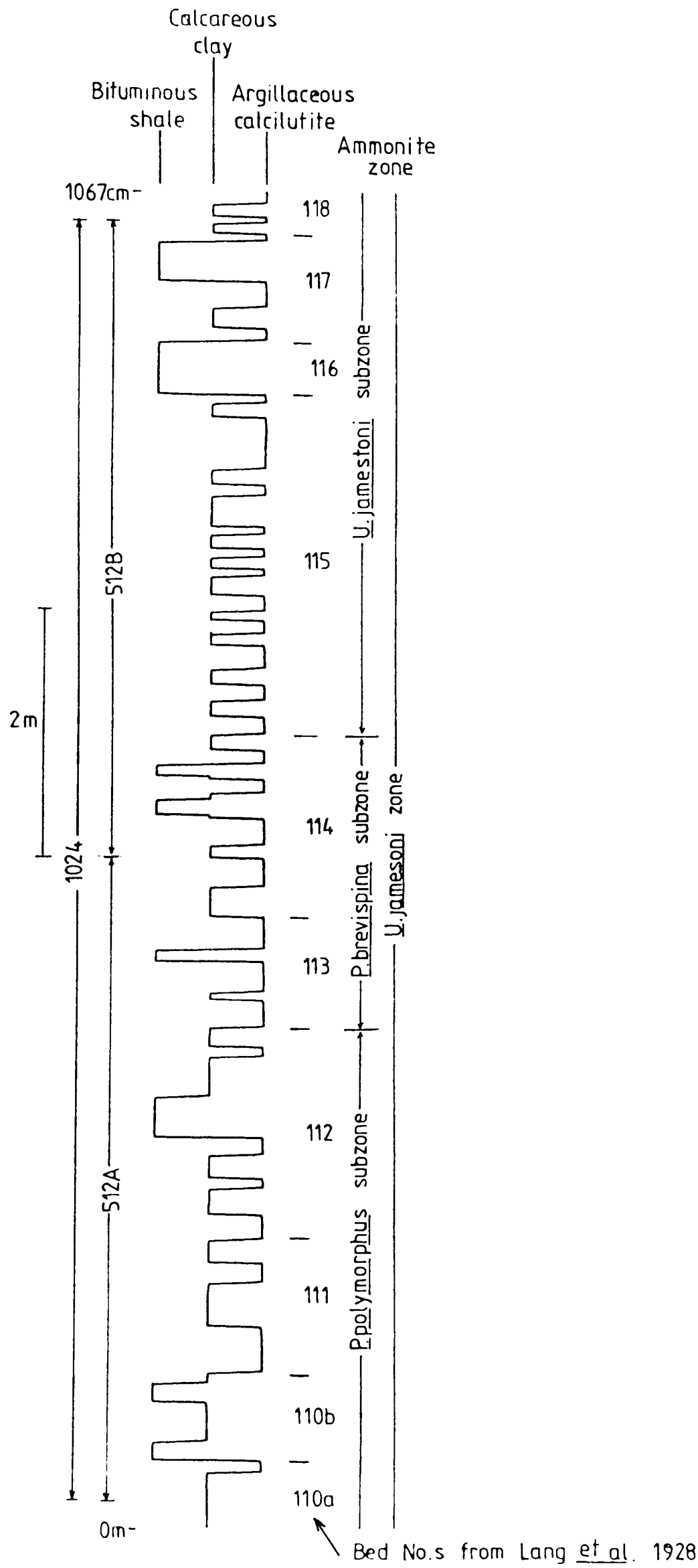

Fig 6 5C. BELEMNITE MARLS POWER SPECTRA

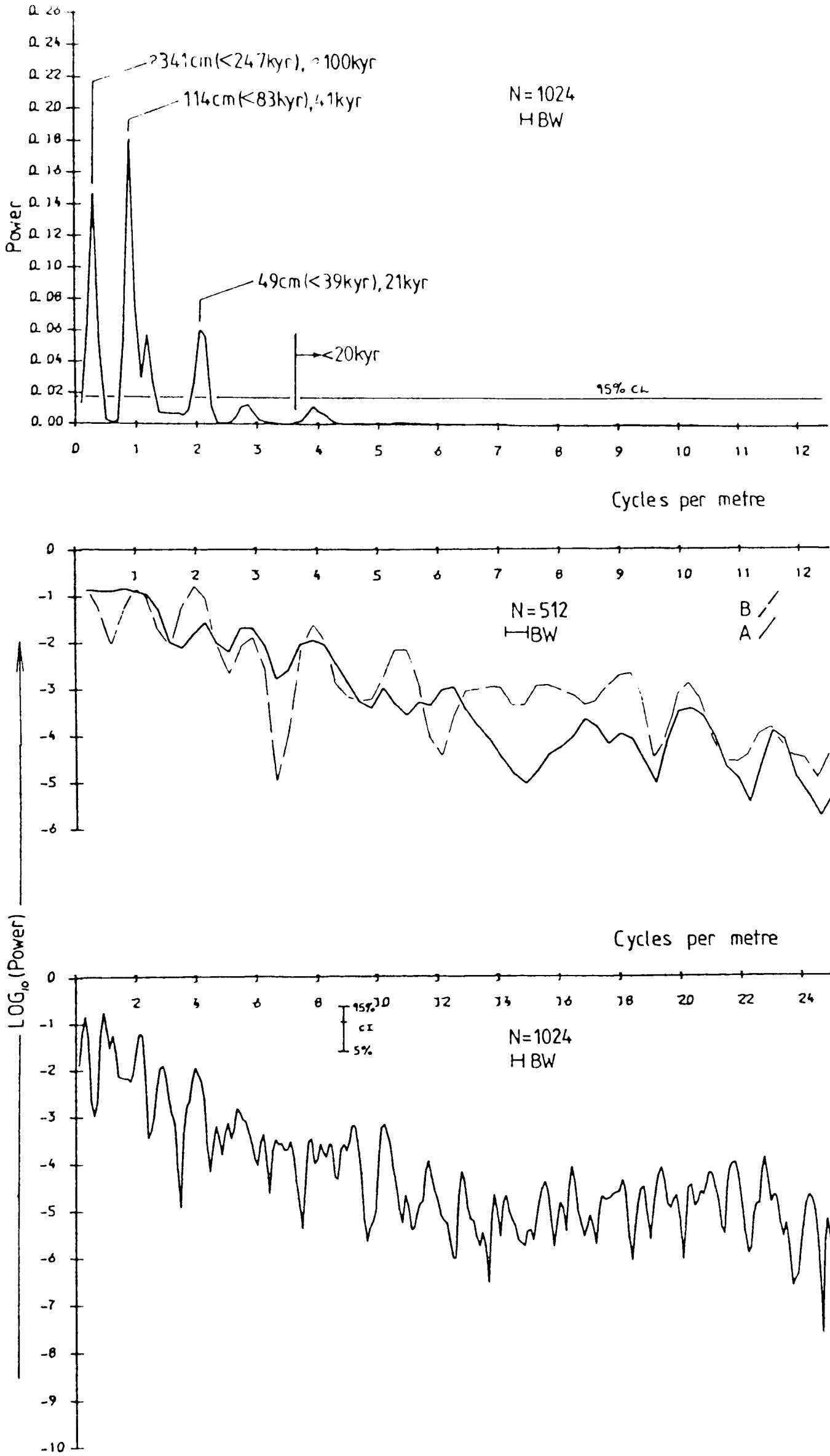

Fig 6.6A

Field aspect of the 'Siliceous Shales', Robin Hood's Bay.

Top: Sellwood's beds 3-7, alternating shale, shaley sandstone and sandstone.

Bottom: Large Storm scour, Sellwood's bed 3. The hammer is 39cm long.

Fig 6·6B 'SILICEOUS SHALES' TIME SERIES

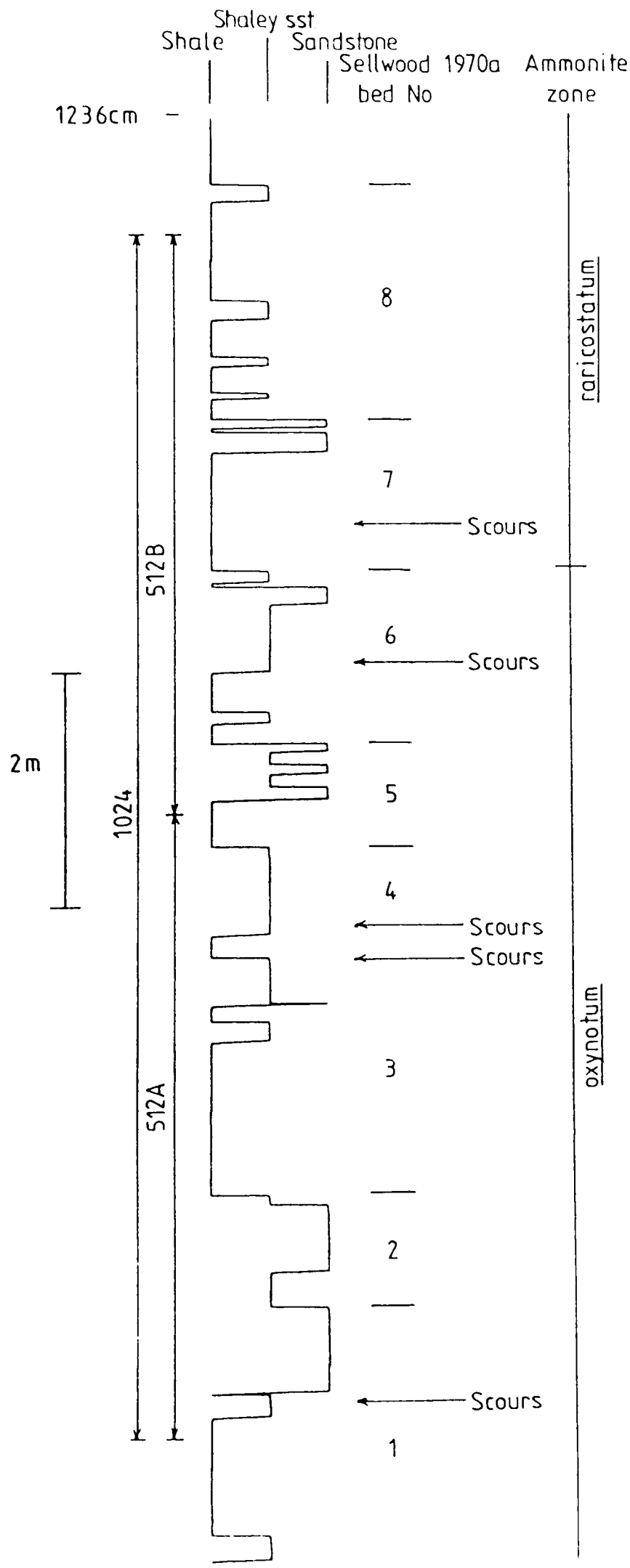

Fig 6 6C 'SILICEOUS' SHALES POWER SPECTRA

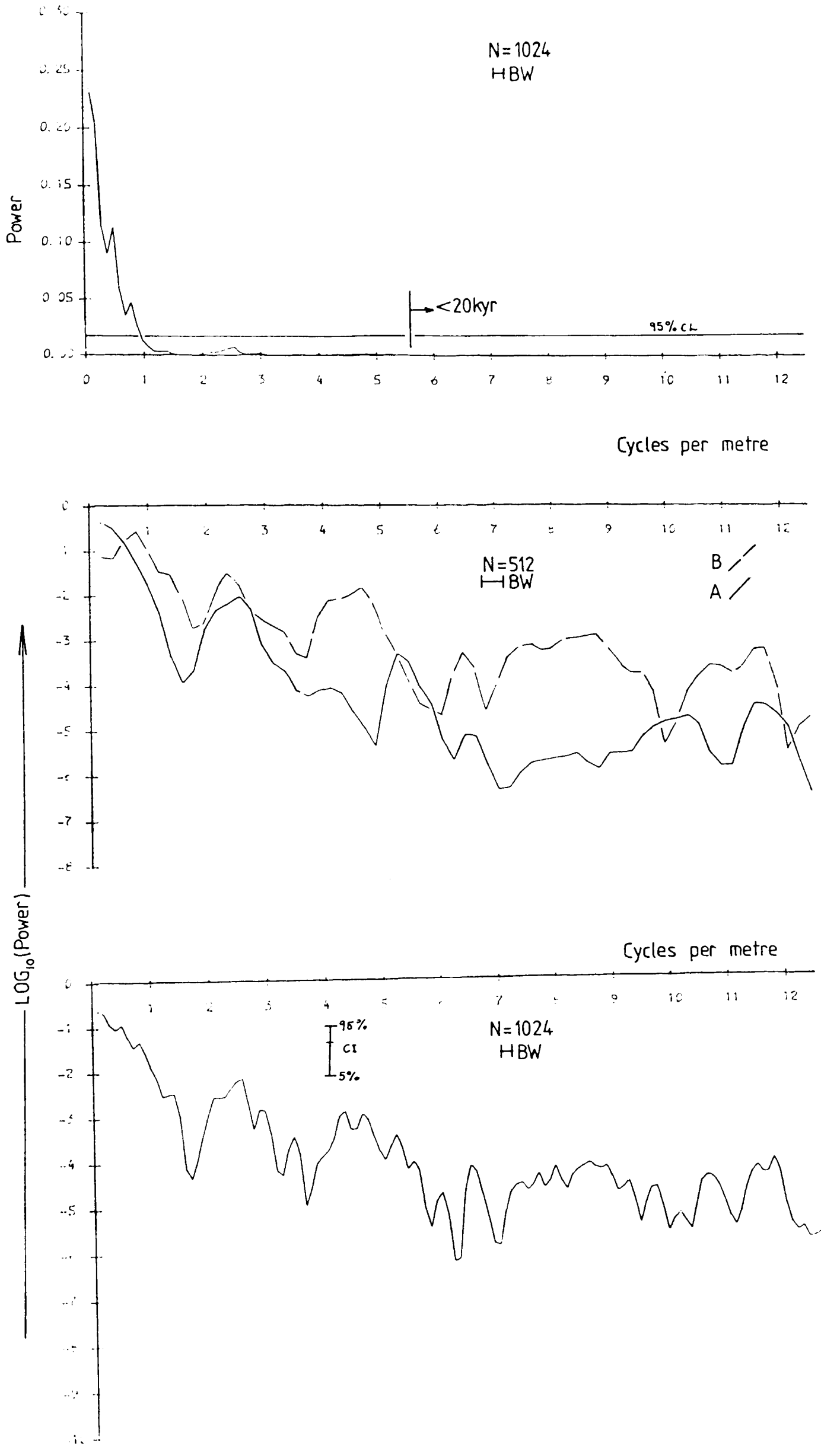

Fig 6.7A

Field aspect of the Upper Birkhill Shales, Dob's Linn. Three relatively thick black mudstone beds can be seen interbedded with grey mudstone in the left of the photograph. The hammer is 39cm long.

Fig 6.7B Upper BIRKHILL SHALES TIME SERIES

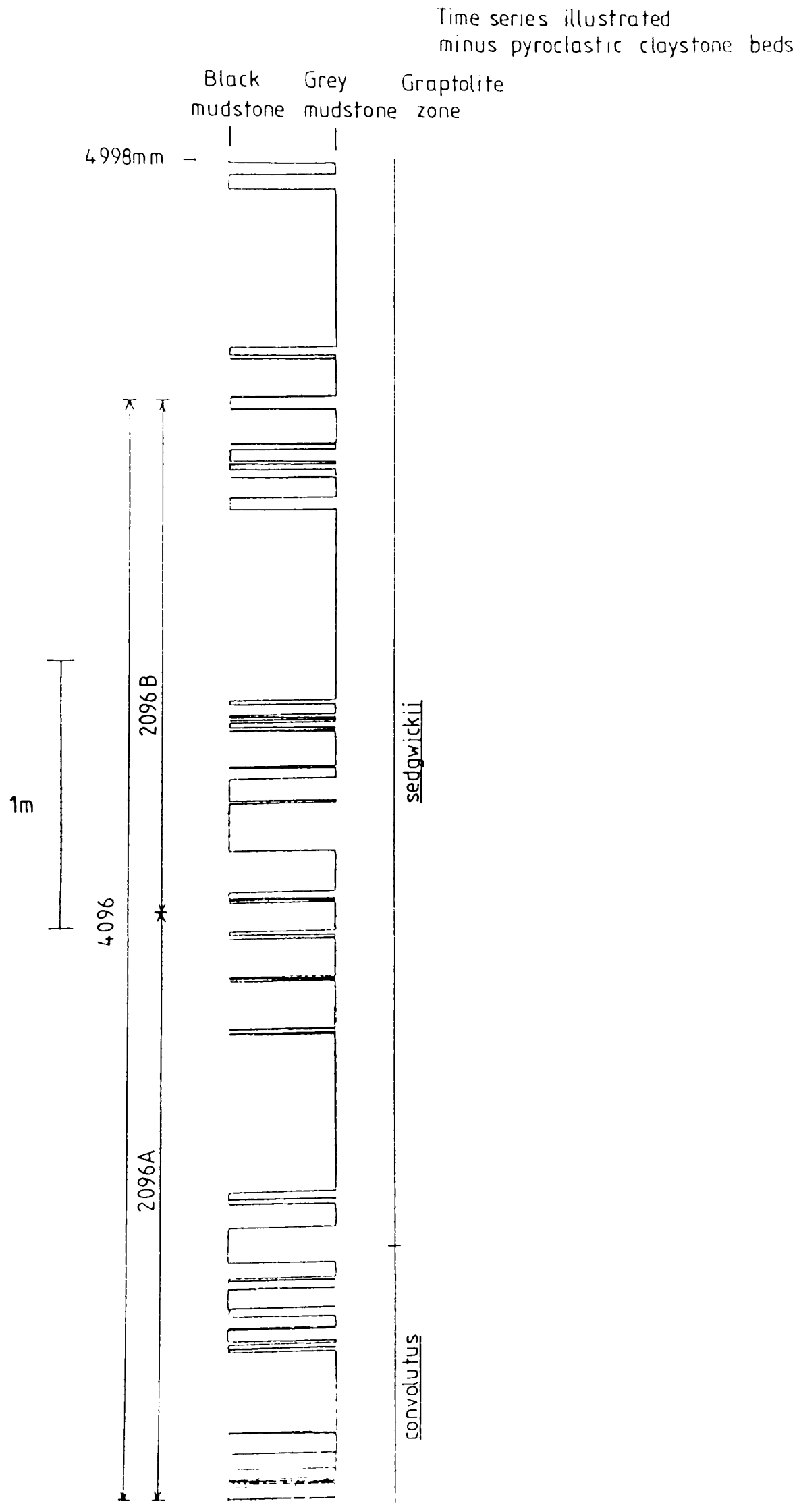

Fig 6.7C Upper BIRKHILL SHALES POWER SPECTRA

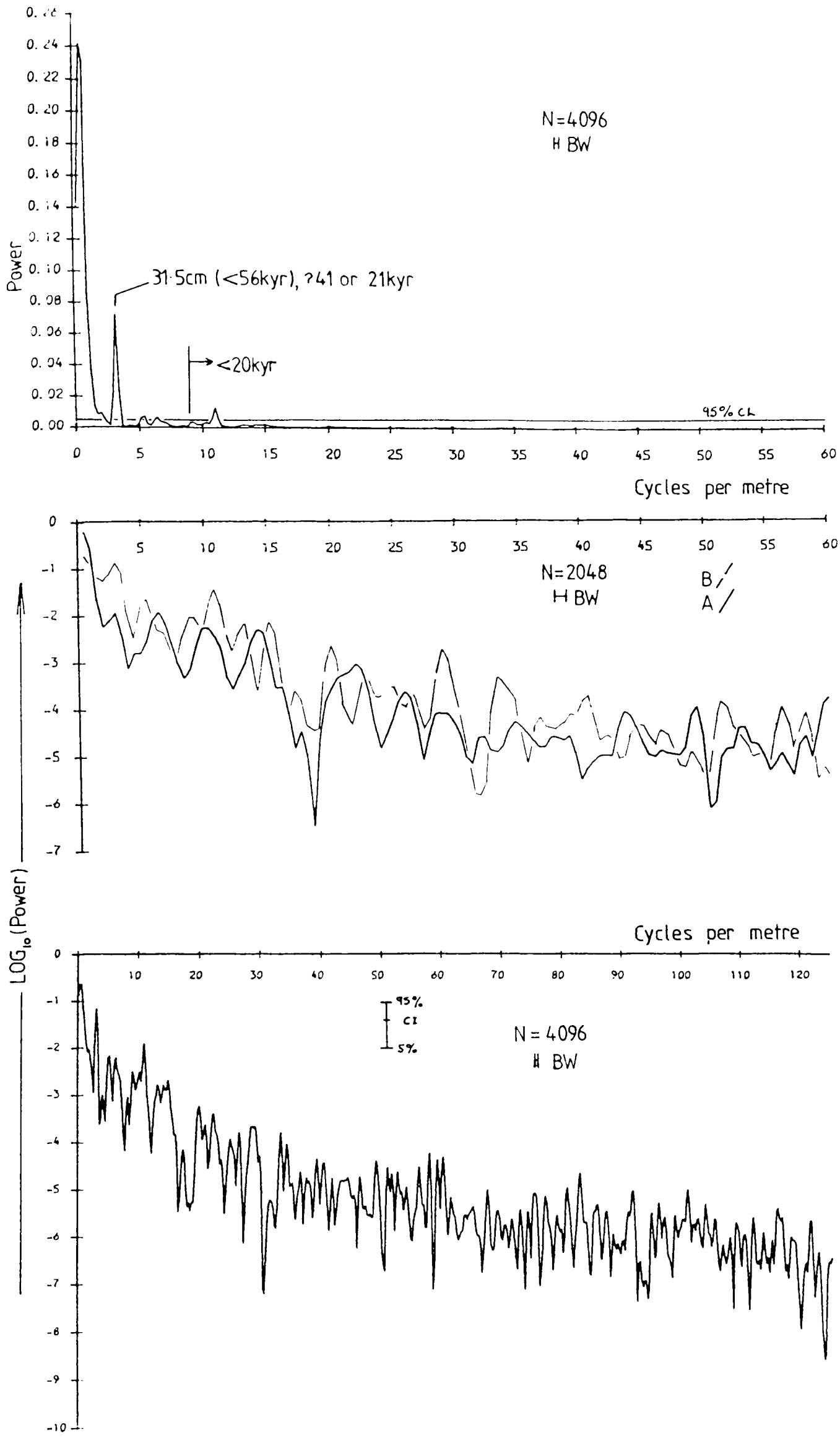

APPENDIX FOR CHAPTER 2

STRATIGRAPHIC LOGS FOR THE BASAL LIAS SECTIONS.

KEY TO STRATIGRAPHIC LOGS

o POSITION OF BURROW MOTTLES

BEEF CALCITE

LITHOLOGIES
- LIMESTONE
- LIGHT MARL
- DARK MARL
- DARK, LAMINATED SHALE
- LAMINATED LIMESTONE

BODY FOSSILS
- BIOCLASTIC FRAGMENTS - INDETERMINATE
- BIVALVES
- GASTROPODS
- AMMONITES
- BELEMNITES
- BRACHIOPODS
- ECHINOID FRAGMENTS - ESP. SPINES
- CRINOID FRAGMENTS - ESP. OSSICLES
- FISH SCALES
- ICHYTHYOSAUR VERTEBRAE
- SOLITARY CORALS
- ANNELID TUBES
- LIGNITE

TRACE FOSSILS
- CHONDRITES
- ARENICOLITES
- DIPLOCRATERION
- RHIZOCORALLIUM
- THALASSINOIDES

CONTACTS
- SHARP
- GRADATIONAL
- BURROW-MOTTLED
- PLANE
- WAVY

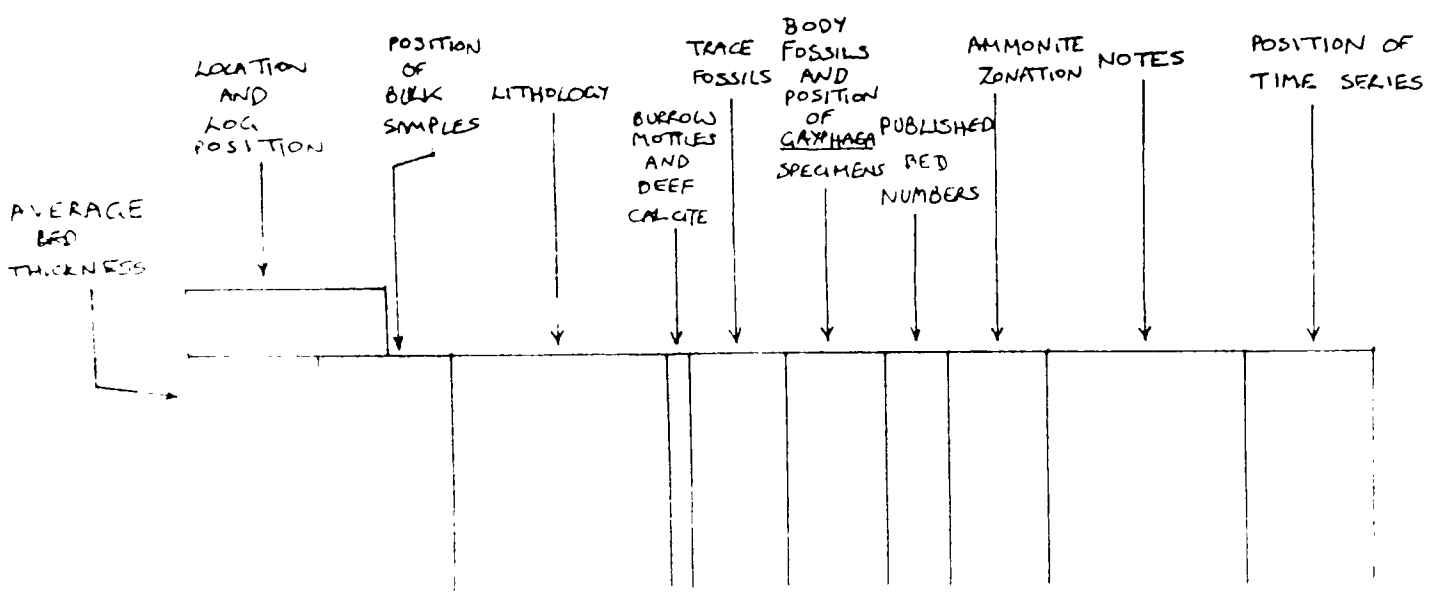

2.1 Stratigraphic log for the basal Lias at Lyme Regis.

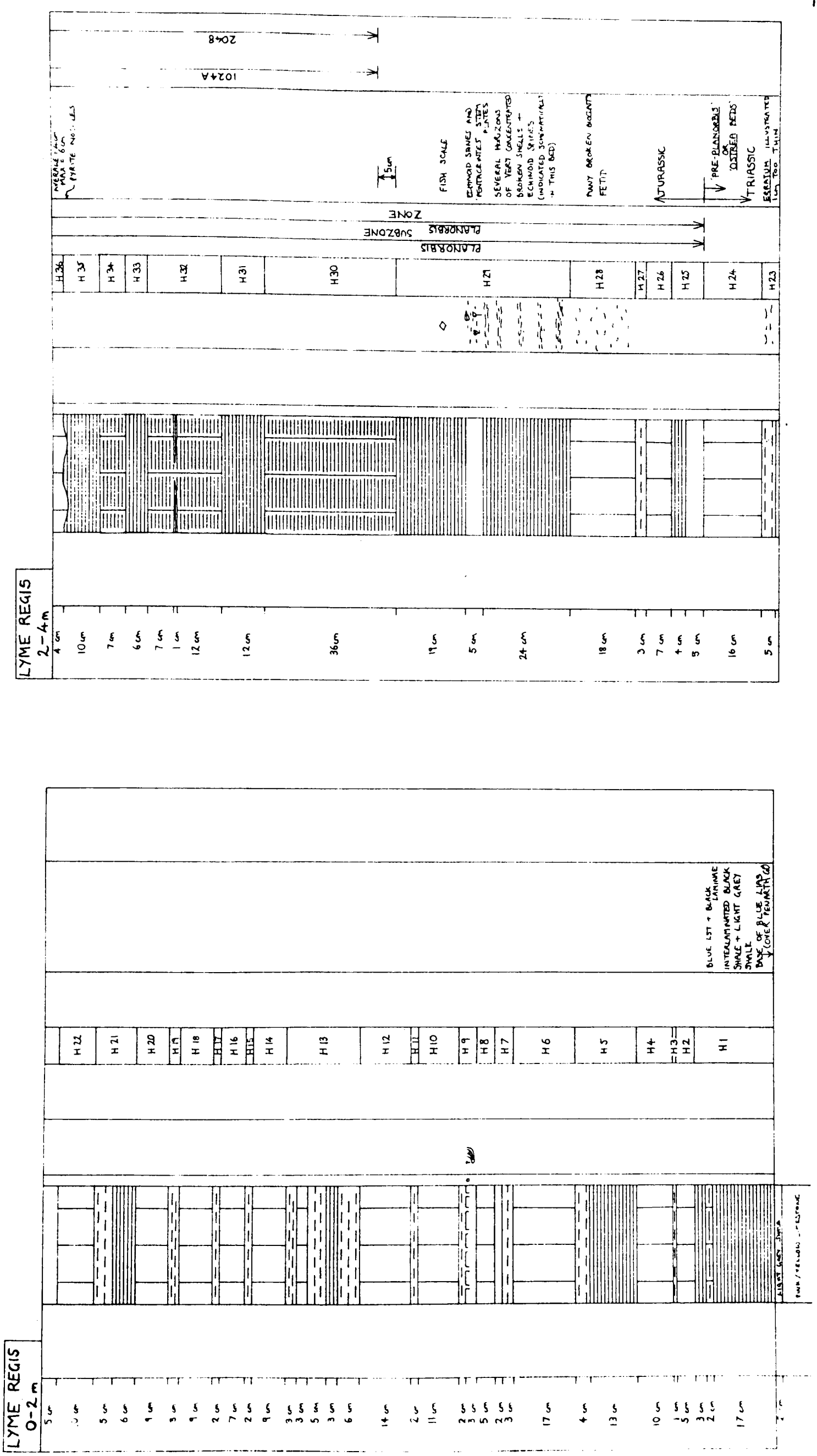

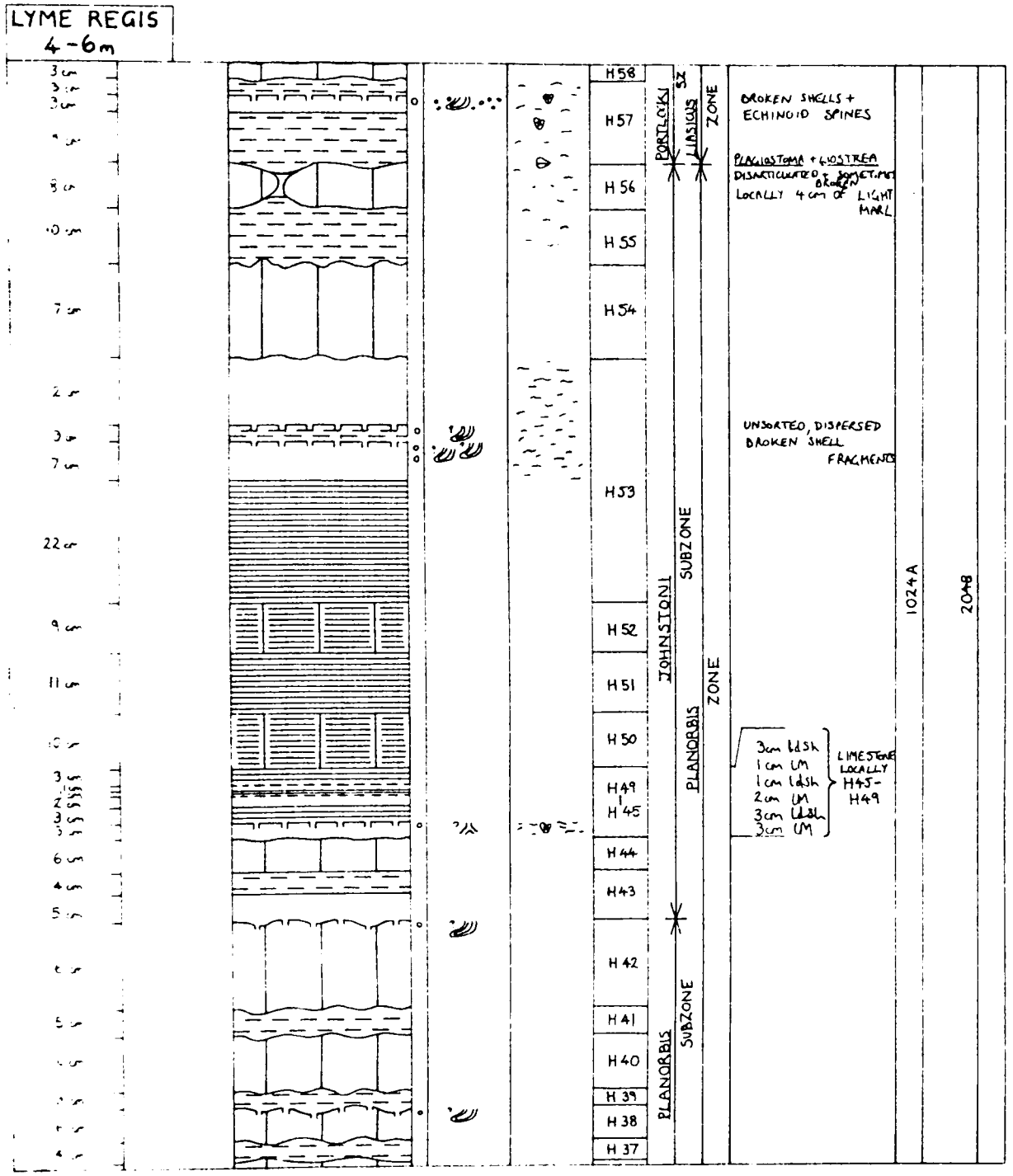
LYME REGIS
4-6m
H58
H57
H56
H55
H54
H53
H52
H51
H50
H49
H45
H44
H43
H42
H41
H40
H39
H38
H37
PORTLOCKI SZ
LIASICUS ZONE
BROKEN SHELLS + ECHINOID SPINES
PLAGIOSTOMA + GIOSTREA DISARTICULATED + SOMETIMES BROKEN
LOCALLY 4 cm OF LIGHT MARL
UNSORTED, DISPERSED BROKEN SHELL FRAGMENTS
JOHNSTONI SUBZONE
PLANORBIS ZONE
3cm LdSh
1cm LM
1cm LdSh
2cm LM
3cm LdSh
3cm LM
LIMESTONE LOCALLY H45-H49
PLANORBIS SUBZONE
1024A
2048

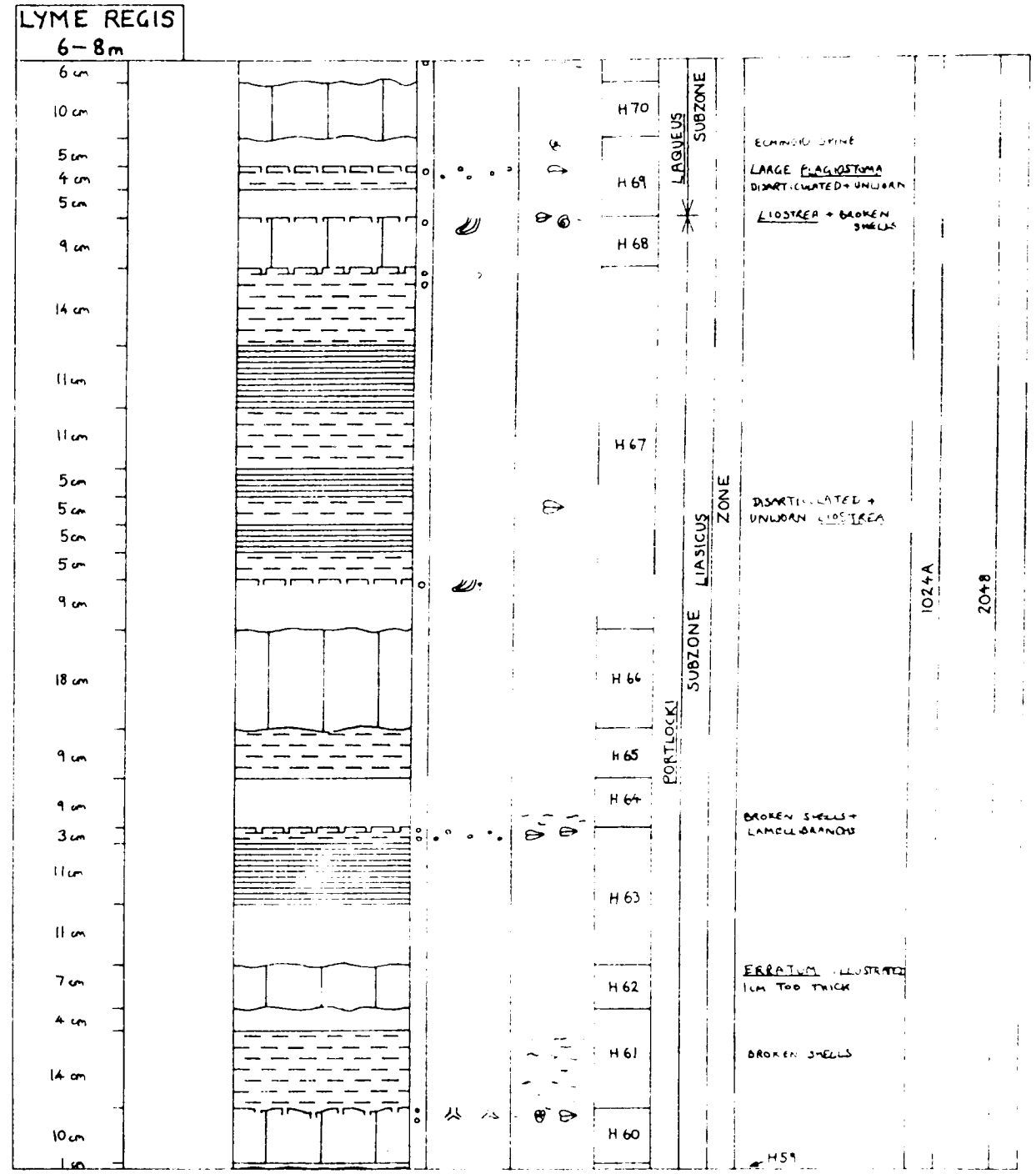
LYME REGIS
6-8m
H70
H69
H68
H67
H66
H65
H64
H63
H62
H61
H60
LAQUEUS SUBZONE
ECHINOID SPINE
LARGE PLAGIOSTOMA DISARTICULATED + UNWORN
LIOSTREA + BROKEN SHELLS
LIASICUS ZONE
DISARTICULATED + UNWORN GIOSTREA
PORTLOCKI SUBZONE
BROKEN SHELLS + LAMELLIBRANCHS
ERRATUM ILLUSTRATED 1cm TOO THICK
BROKEN SHELLS
H59
1024A
2048

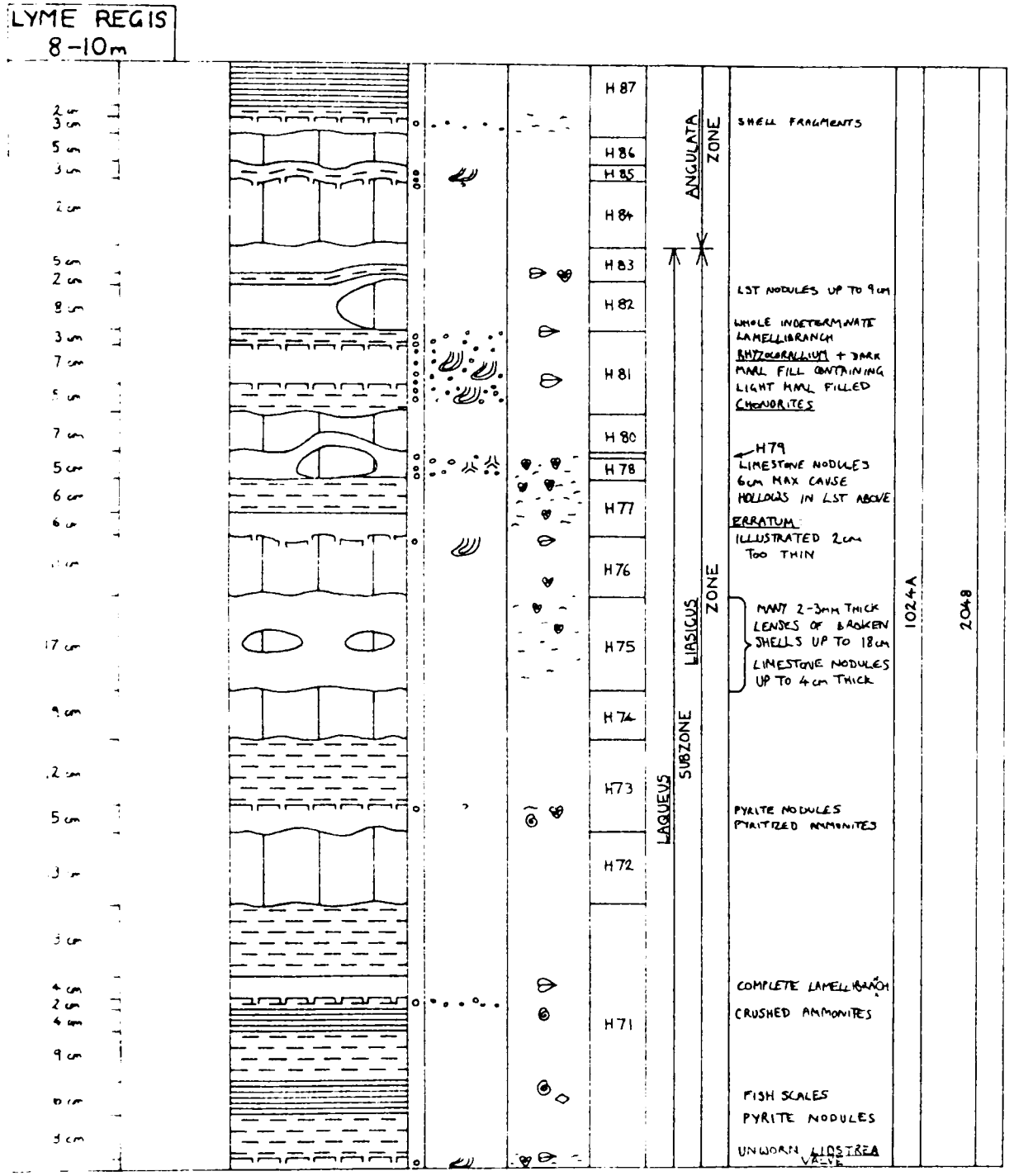
LYME REGIS
8-10m
H 87
H 86
H 85
H 84
H 83
H 82
H 81
H 80
H 78
H 77
H 76
H 75
H 74
H 73
H 72
H 71
ANGULATA ZONE
LIASICUS ZONE
LAQUEUS SUBZONE
SHELL FRAGMENTS
LST NODULES UP TO 9cm
WHOLE INDETERMINATE LAMELLIBRANCH
RHYZOCORALLIUM + DARK MARL FILL CONTAINING LIGHT MARL FILLED CHONDRITES
H79
LIMESTONE NODULES 6cm MAX CAUSE HOLLOWS IN LST ABOVE
ERRATUM:
ILLUSTRATED 2cm TOO THIN
MANY 2-3mm THICK LENSES OF BROKEN SHELLS UP TO 18cm
LIMESTONE NODULES UP TO 4cm THICK
PYRITE NODULES
PYRITIZED AMMONITES
COMPLETE LAMELLIBRANCH
CRUSHED AMMONITES
FISH SCALES
PYRITE NODULES
UNWORN LIOSTREA VALVE
1024A
2048

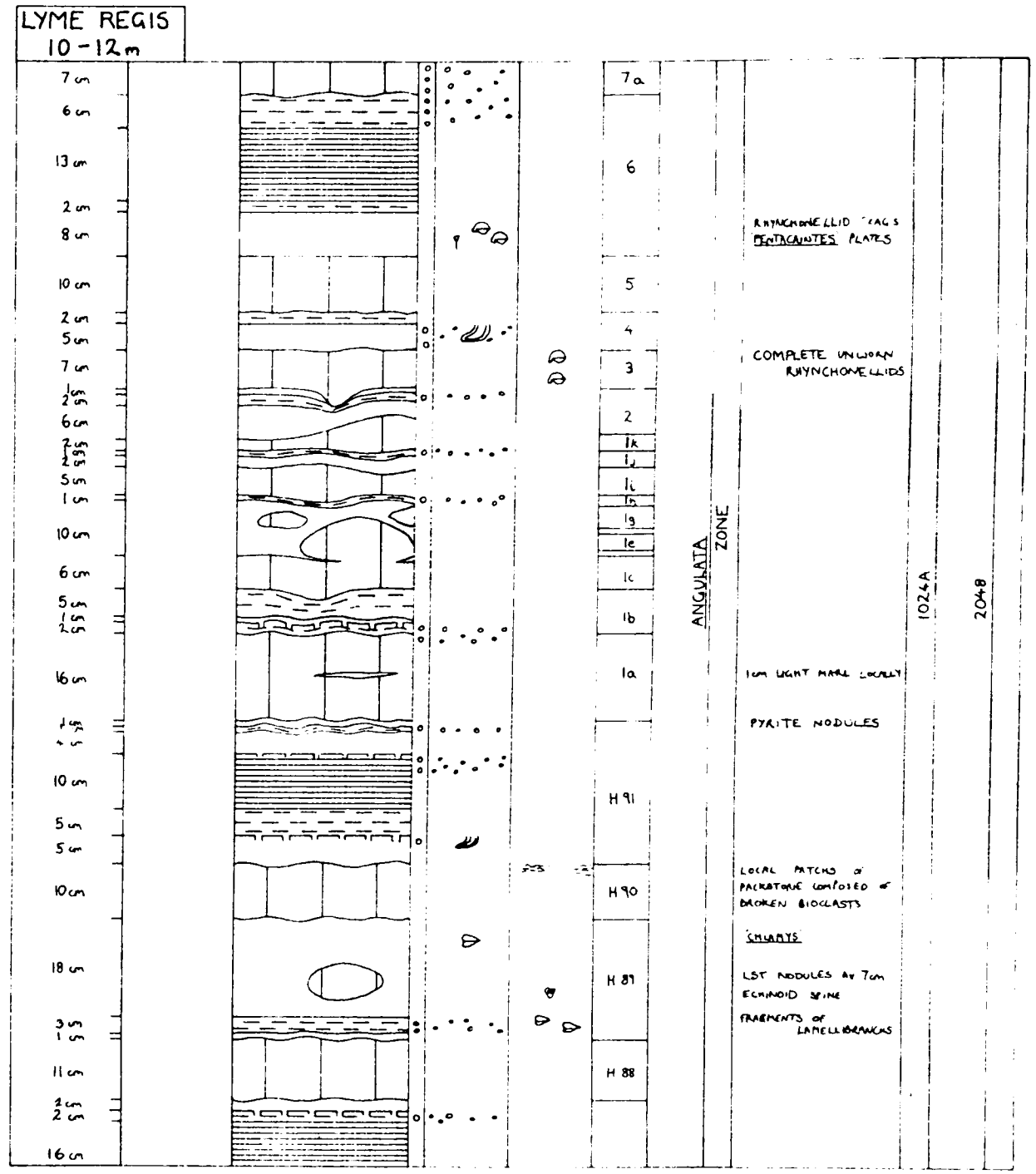
LYME REGIS
10-12m
7a
6
5
4
3
2
1k
1j
1i
1h
1g
1e
1c
1b
1a
H 91
H 90
H 89
H 88
ANGULATA ZONE
RHYNCHONELLID TRAGS
PENTACRINITES PLATES
COMPLETE UNWORN RHYNCHONELLIDS
1cm LIGHT MARL LOCALLY
PYRITE NODULES
LOCAL PATCHS OF PACKSTONE COMPOSED OF BROKEN BIOCLASTS
SMEARS
LST NODULES AV 7cm
ECHINOID SPINE
FRAGMENTS OF LAMELLIBRANCHS
1024A
2048

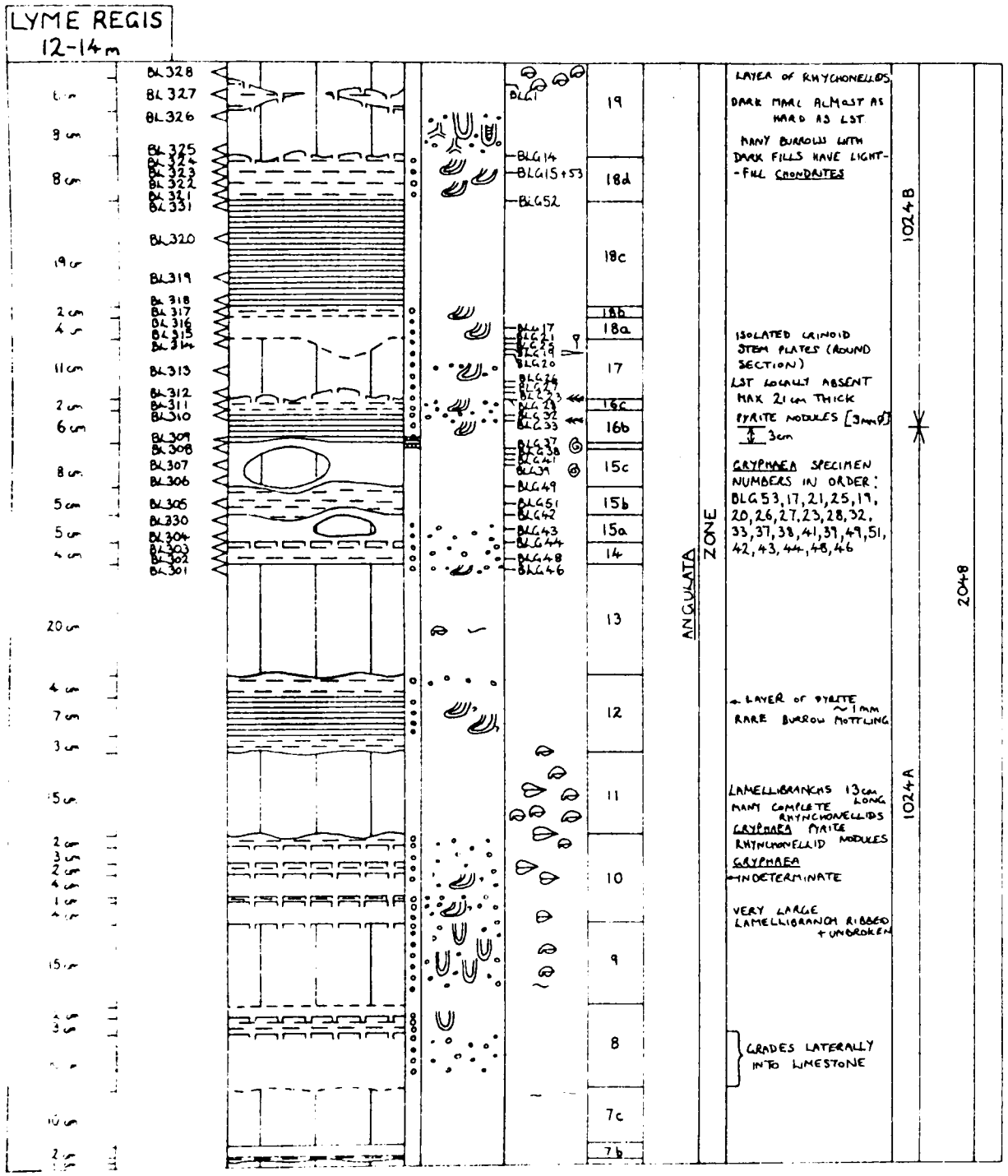
LYME REGIS
12-14m
BL328
BL327
BL326
BL325
BL324
BL323
BL322
BL321
BL331
BL320
BL319
BL318
BL317
BL316
BL315
BL314
BL313
BL312
BL311
BL310
BL309
BL308
BL307
BL306
BL305
BL330
BL304
BL303
BL302
BL301
BLG1
BLG14
BLG15+53
BLG52
BLG17
BLG21
BLG25
BLG19
BLG20
BLG24
BLG44
BLG23
BLG22
BLG32
BLG33
BLG37
BLG38
BLG41
BLG39
BLG49
BLG51
BLG42
BLG43
BLG44
BLG48
BLG46
19
18d
18c
18b
18a
17
16c
16b
15c
15b
15a
14
13
12
11
10
9
8
7c
7b
ANGULATA ZONE
1024B
2048
1024A
LAYER OF RHYCHONELLIDS
DARK MARL ALMOST AS HARD AS LST
MANY BURROWS WITH DARK FILLS HAVE LIGHT-FILL CHONDRITES
ISOLATED CRINOID STEM PLATES (ROUND SECTION)
LST LOCALLY ABSENT MAX 21cm THICK
PYRITE NODULES [3mm Ø]
3cm
GRYPHAEA SPECIMEN NUMBERS IN ORDER: BLG53, 17, 21, 25, 19, 20, 26, 27, 23, 28, 32, 33, 37, 38, 41, 39, 49, 51, 42, 43, 44, 48, 46
LAYER OF PYRITE ~1mm
RARE BURROW MOTTLING
LAMELLIBRANCHS 13cm LONG
MANY COMPLETE RHYNCHONELLIDS
GRYPHAEA
PYRITE NODULES
RHYNCHONELLID
GRYPHAEA
INDETERMINATE
VERY LARGE LAMELLIBRANCH RIBBED + UNBROKEN
GRADES LATERALLY INTO LIMESTONE

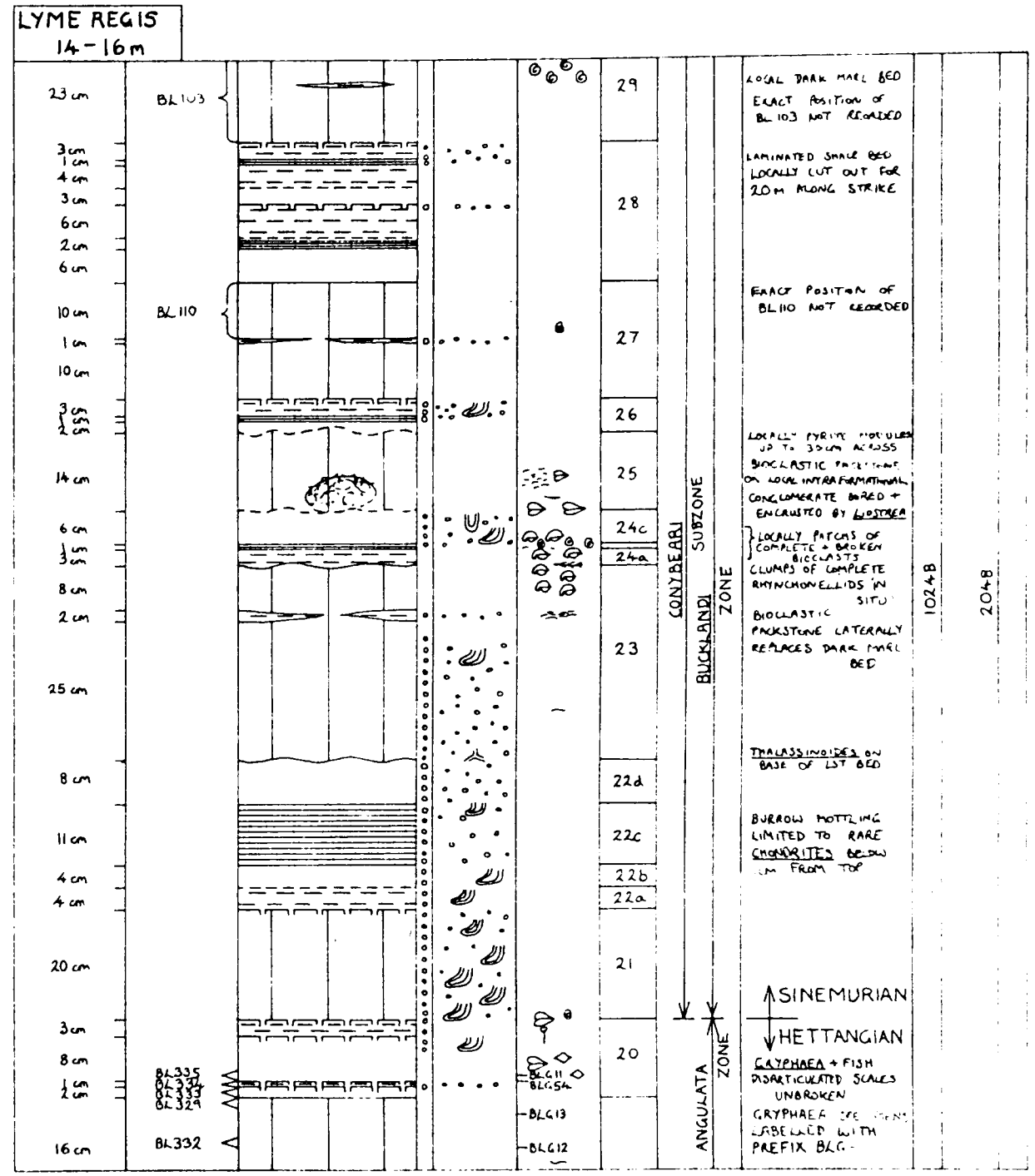
LYME REGIS
14-16m
BL103
BL110
BL335
BL334
BL333
BL329
BL332
BLG11
BLG54
BLG13
BLG12
29
28
27
26
25
24c
24a
23
22d
22c
22b
22a
21
20
CONYBEARI SUBZONE
BUCKLANDI ZONE
ANGULATA ZONE
1024B
2048
LOCAL DARK MARL BED
EXACT POSITION OF BL103 NOT RECORDED
LAMINATED SHALE BED LOCALLY CUT OUT FOR 20m ALONG STRIKE
EXACT POSITION OF BL110 NOT RECORDED
LOCALLY PYRITE NODULES UP TO 35cm ACROSS
BIOCLASTIC PACKSTONE ON LOCAL INTRAFORMATIONAL CONGLOMERATE BORED + ENCRUSTED BY LOSTREA
LOCALLY PATCHES OF COMPLETE + BROKEN BIOCLASTS
CLUMPS OF COMPLETE RHYNCHONELLIDS IN SITU
BIOCLASTIC PACKSTONE LATERALLY REPLACES DARK MARL BED
THALASSINOIDES ON BASE OF LST BED
BURROW MOTTLING LIMITED TO RARE CHONDRITES BELOW 1m FROM TOP
SINEMURIAN
HETTANGIAN
GRYPHAEA + FISH DISARTICULATED SCALES UNBROKEN
GRYPHAEA SPECIMENS LABELLED WITH PREFIX BLG-

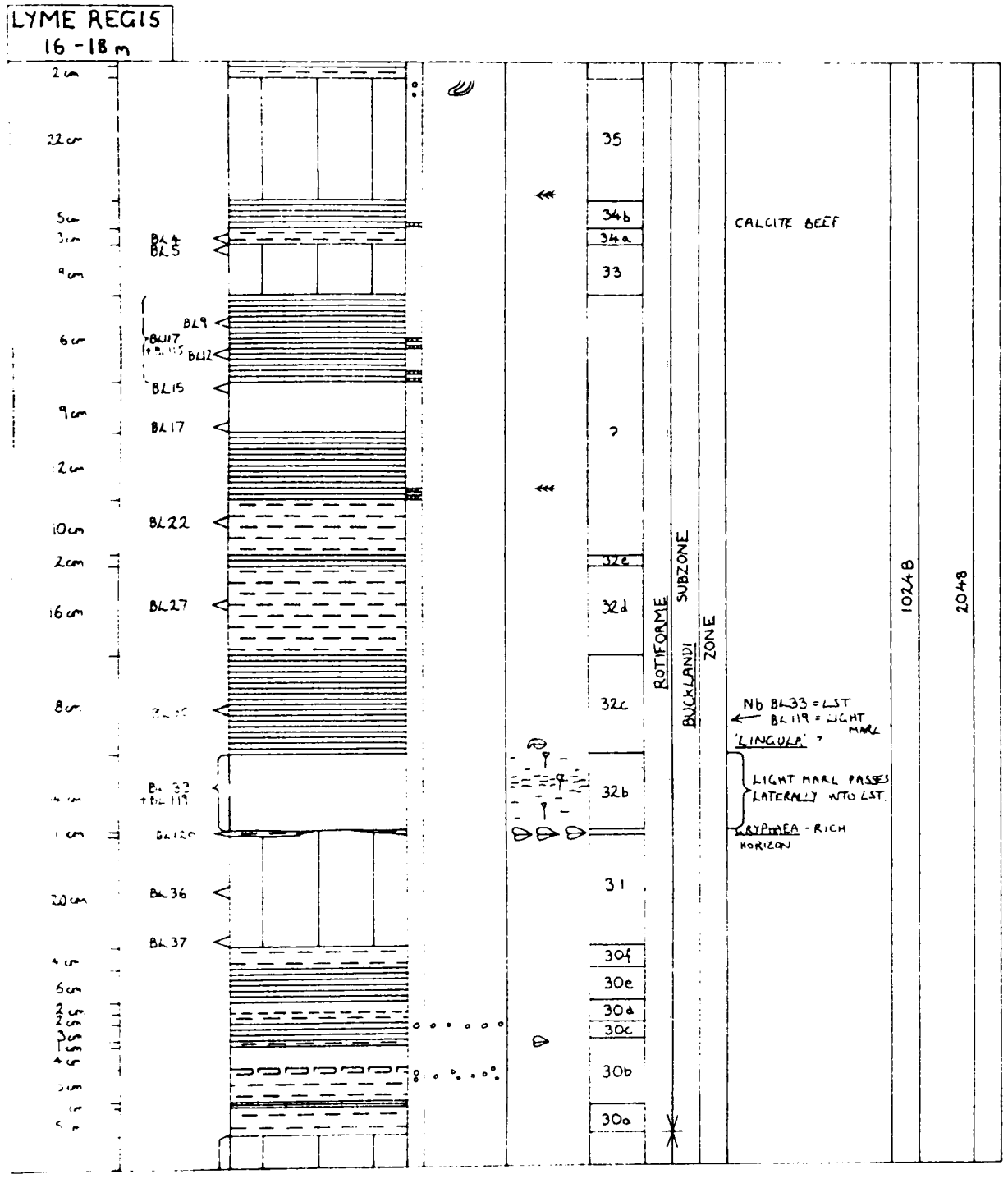
LYME REGIS
16 - 18 m
2 cm
22 cm
5 cm
3 cm
9 cm
6 cm
9 cm
2 cm
10 cm
2 cm
16 cm
8 cm
20 cm
BL 4
BL 5
BL9
BL17
BL12
BL15
BL17
BL22
BL27
BL 32
+BL 119
BL120
BL36
BL37
35
34b
34a
33
?
32e
32d
32c
32b
31
30f
30e
30d
30c
30b
30a
ROTIFORME SUBZONE
BUCKLANDI ZONE
CALCITE BEEF
Nb BL33 = LST
BL119 = LIGHT MARL
'LINGULA' ?
LIGHT MARL PASSES LATERALLY INTO LST.
GRYPHAEA - RICH HORIZON
1024B
2048

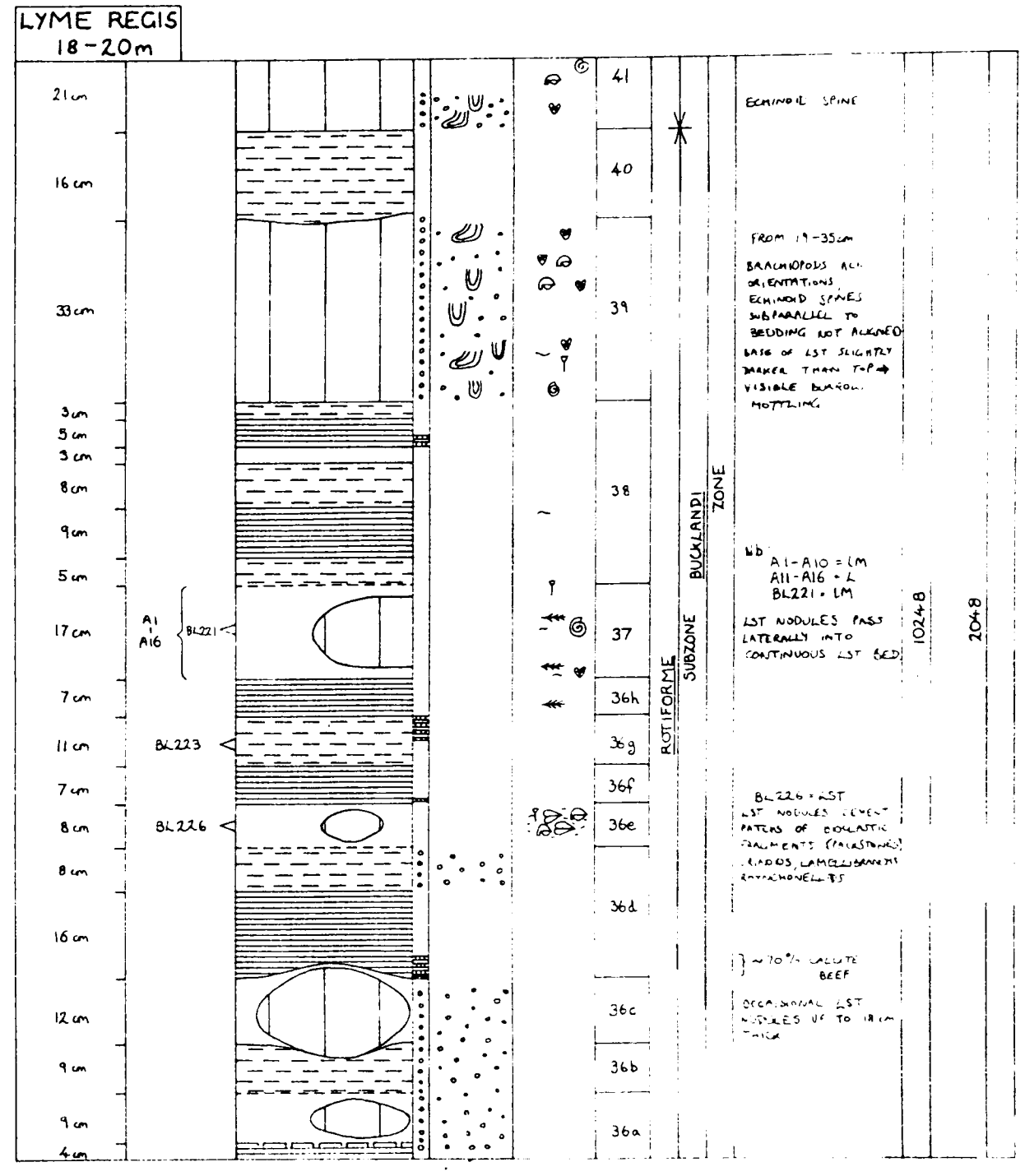
LYME REGIS
18 - 20m
21 cm
16 cm
33 cm
3 cm
5 cm
3 cm
8 cm
9 cm
5 cm
17 cm
7 cm
11 cm
7 cm
8 cm
8 cm
16 cm
12 cm
9 cm
9 cm
4 cm
A1 - A16
BL221
BL223
BL226
41
40
39
38
37
36h
36g
36f
36e
36d
36c
36b
36a
ECHINOID SPINE
FROM 19-35cm
BRACHIOPODS ALL ORIENTATIONS, ECHINOID SPINES SUBPARALLEL TO BEDDING NOT ALIGNED
BASE OF LST SLIGHTLY DARKER THAN TOP
VISIBLE BURROW MOTTLING
Nb
A1-A10 = LM
A11-A16 = L
BL221 = LM
LST NODULES PASS LATERALLY INTO CONTINUOUS LST BED
BL226 = LST
LST NODULES CEMENT PATCHES OF BIOCLASTIC FRAGMENTS (PALAESTINA?) (RADIOLARIA, LAMELLIBRANCHS, BRACHIOPODS, ECHINOIDS)
~70% CALCITE BEEF
OCCASIONAL LST NODULES UP TO 18cm THICK
ROTIFORME SUBZONE
BUCKLANDI ZONE
1024B
2048

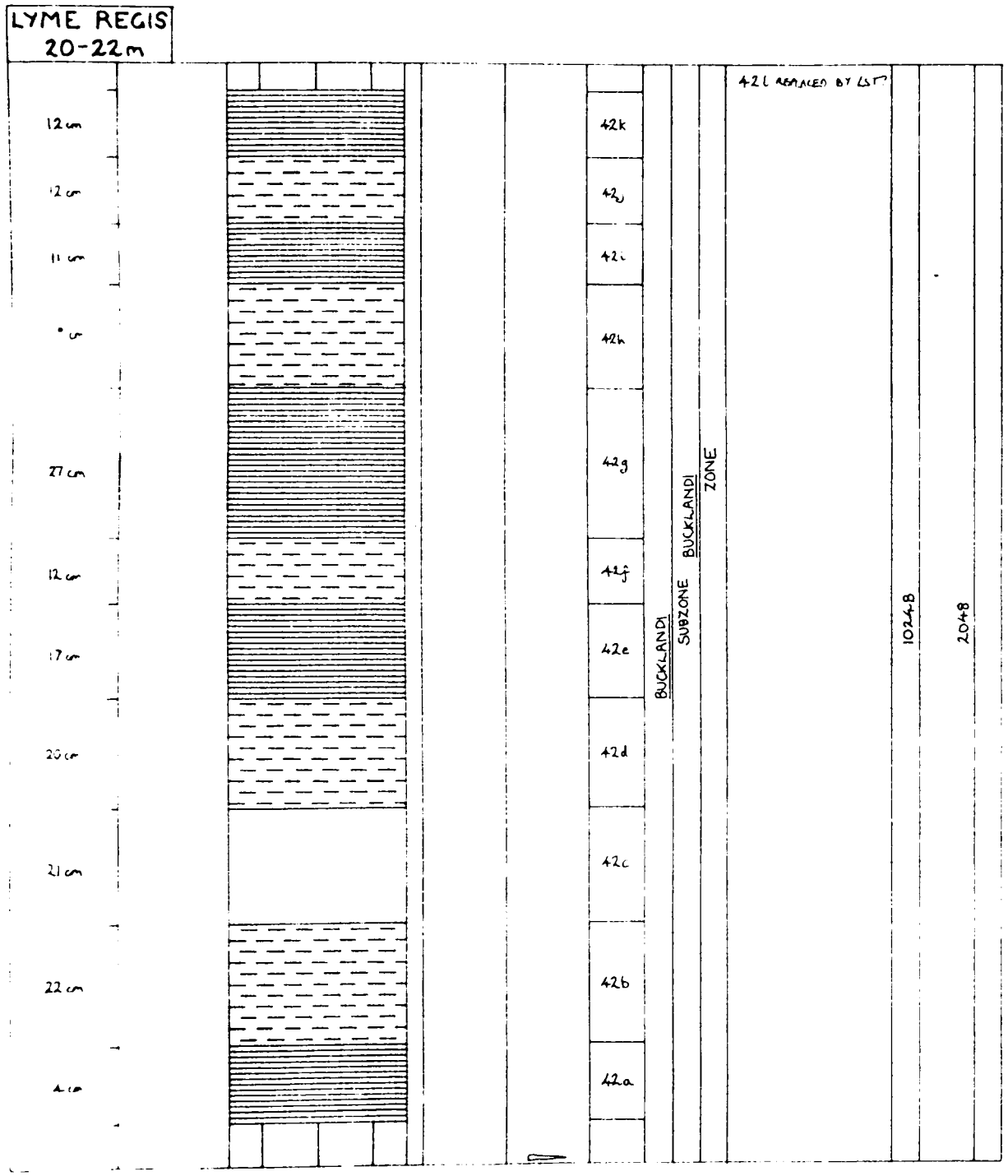
LYME REGIS
20-22m
12 cm
12 cm
11 cm
27 cm
12 cm
17 cm
20 cm
21 cm
22 cm
42k
42j
42i
42h
42g
42f
42e
42d
42c
42b
42a
BUCKLANDI SUBZONE
BUCKLANDI ZONE
42L REPLACED BY LST
1024B
2048

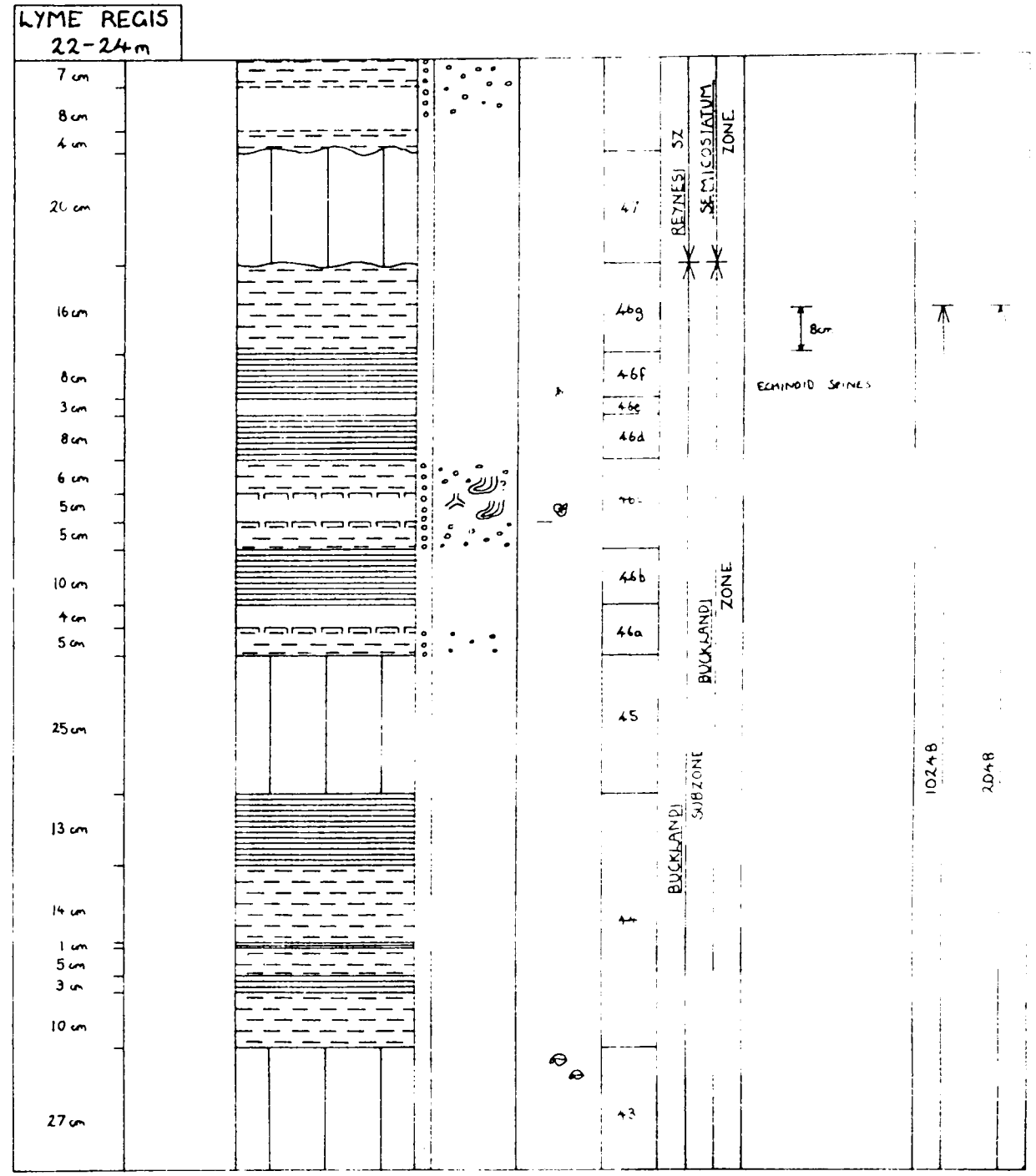
LYME REGIS
22-24m
7 cm
8 cm
4 cm
20 cm
16 cm
8 cm
3 cm
8 cm
6 cm
5 cm
5 cm
10 cm
4 cm
5 cm
25 cm
13 cm
14 cm
1 cm
5 cm
3 cm
10 cm
27 cm
47
46g
46f
46e
46d
46b
46a
45
43
REYNESI SZ
SEMICOSTATUM ZONE
BUCKLANDI ZONE
BUCKLANDI SUBZONE
8cm
ECHINOID SPINES
1024B
2048

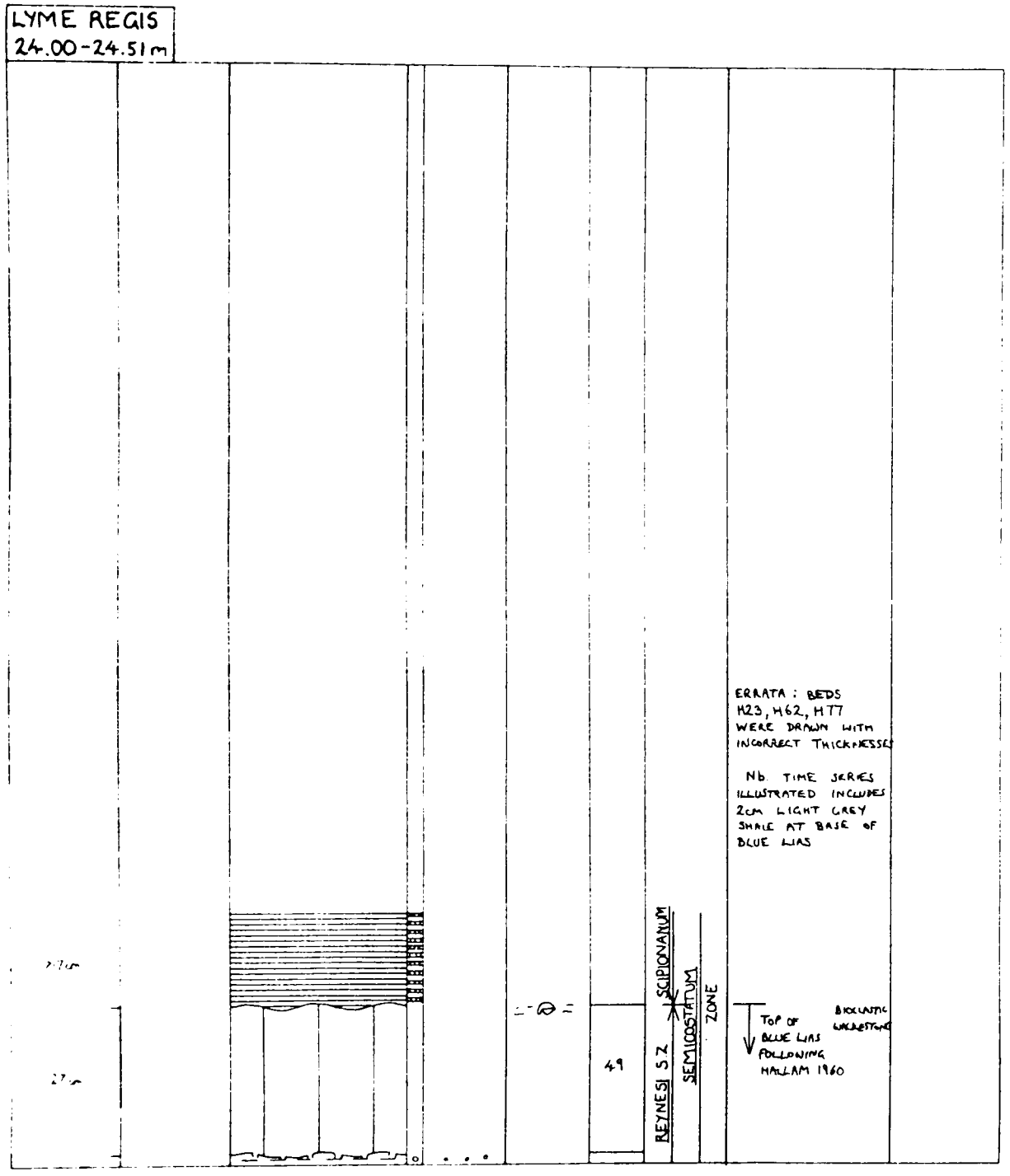
LYME REGIS
24.00-24.51m
ERRATA : BEDS
H23, H62, H77
WERE DRAWN WITH
INCORRECT THICKNESSES
Nb. TIME SERIES
ILLUSTRATED INCLUDES
2cm LIGHT GREY
SHALE AT BASE OF
BLUE LIAS
SCIPIONANUM
SEMICOSTATUM
ZONE
REYNESI S.Z.
49
TOP OF
BLUE LIAS
FOLLOWING
HALLAM 1960
BIOCLASTIC
LIMESTONE

2.2 Stratigraphic log for the basal Lias at Watchet.

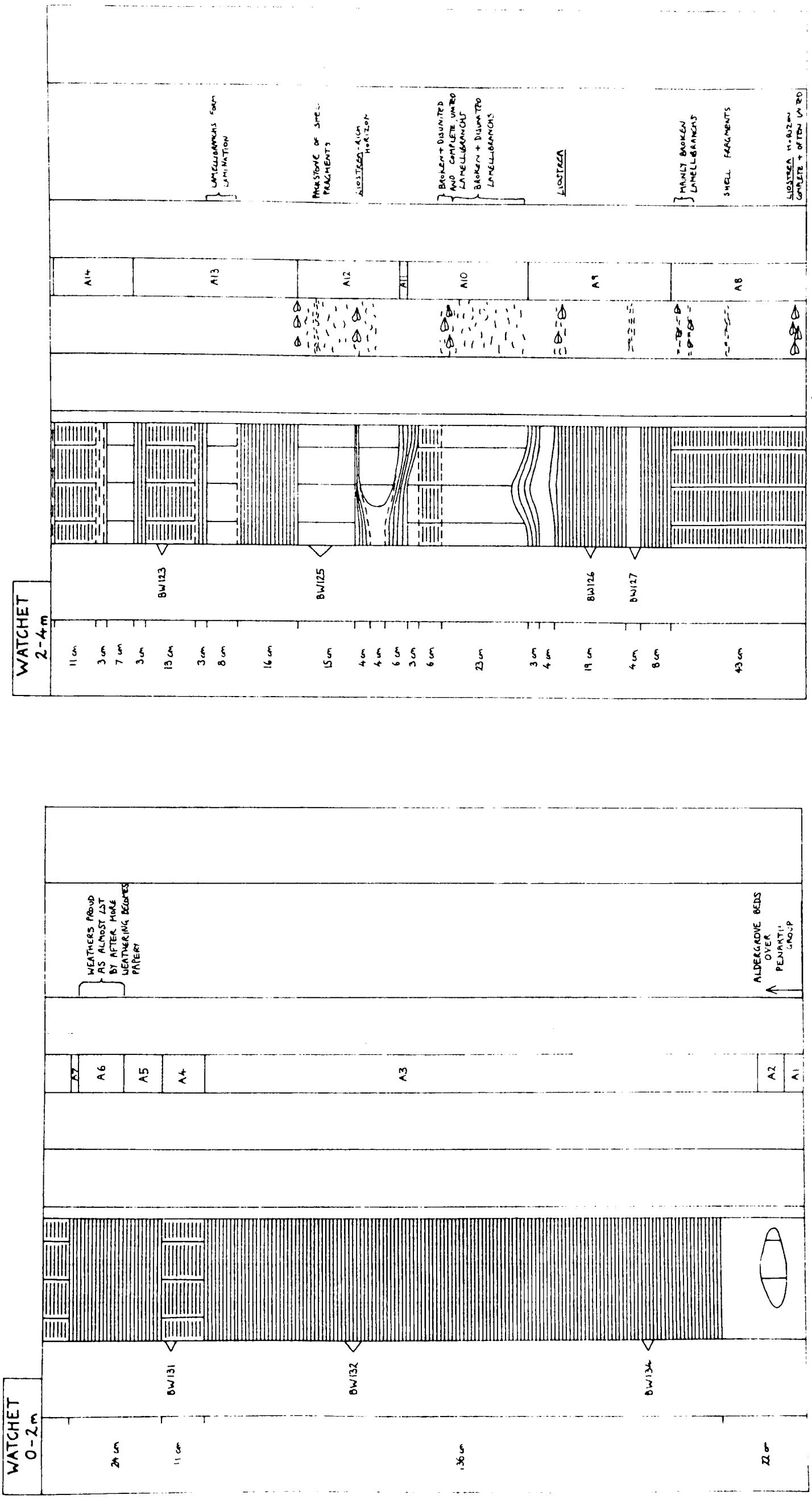

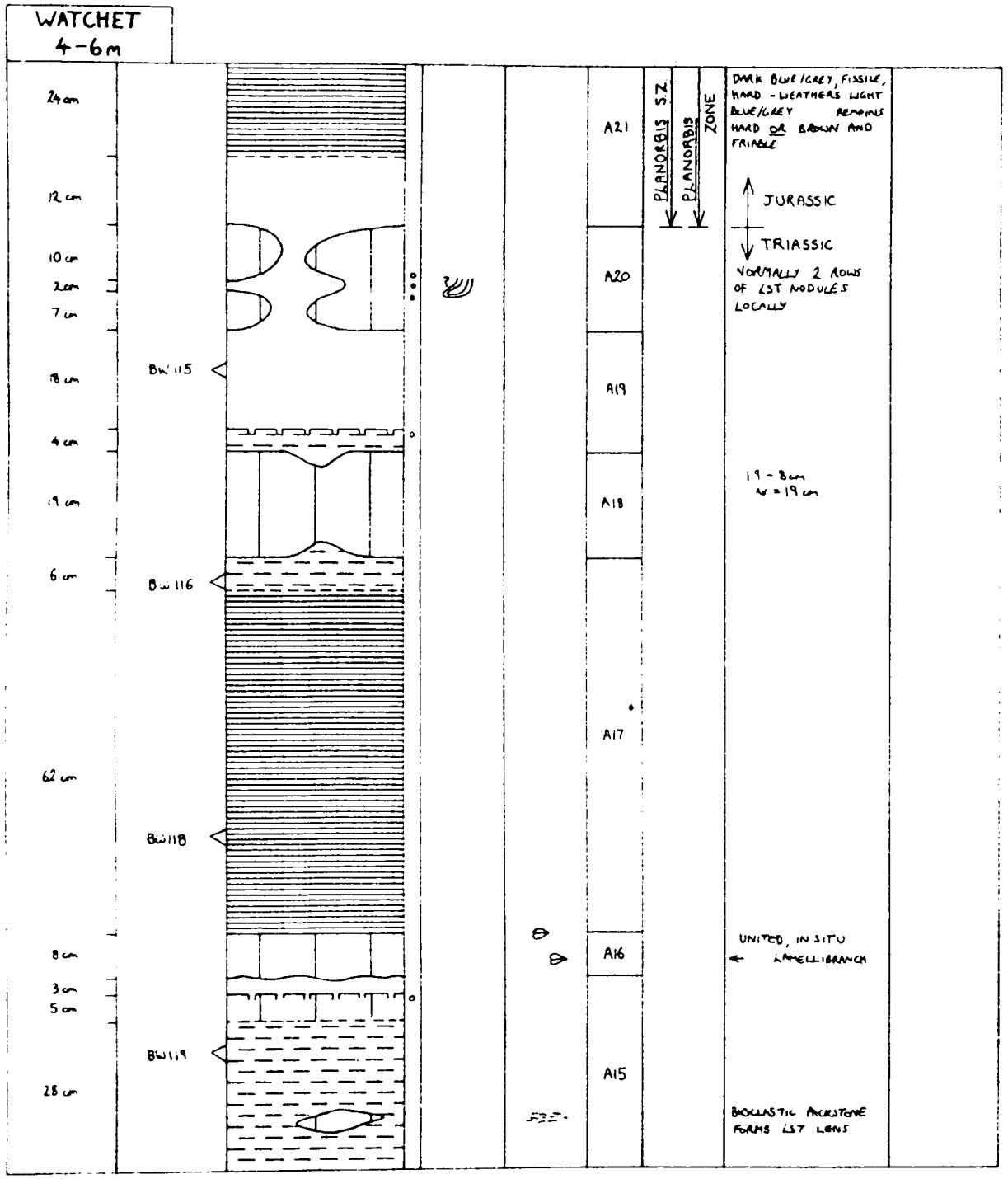
WATCHET
4-6m
24 cm
12 cm
10 cm
2 cm
7 cm
8 cm
4 cm
19 cm
6 cm
62 cm
8 cm
3 cm
5 cm
28 cm
BW 115
BW 116
BW 118
BW 119
A21
A20
A19
A18
A17
A16
A15
PLANORBIS S.Z.
PLANORBIS ZONE
DARK BLUE/GREY, FISSILE, HARD - WEATHERS LIGHT BLUE/GREY REMAINS HARD OR BROWN AND FRIABLE
JURASSIC
TRIASSIC
NORMALLY 2 ROWS OF LST NODULES LOCALLY
19 - 8cm
W = 19 cm
UNITED, IN SITU
LAMELLIBRANCH
BIOCLASTIC PACKSTONE FORMS LST LENS

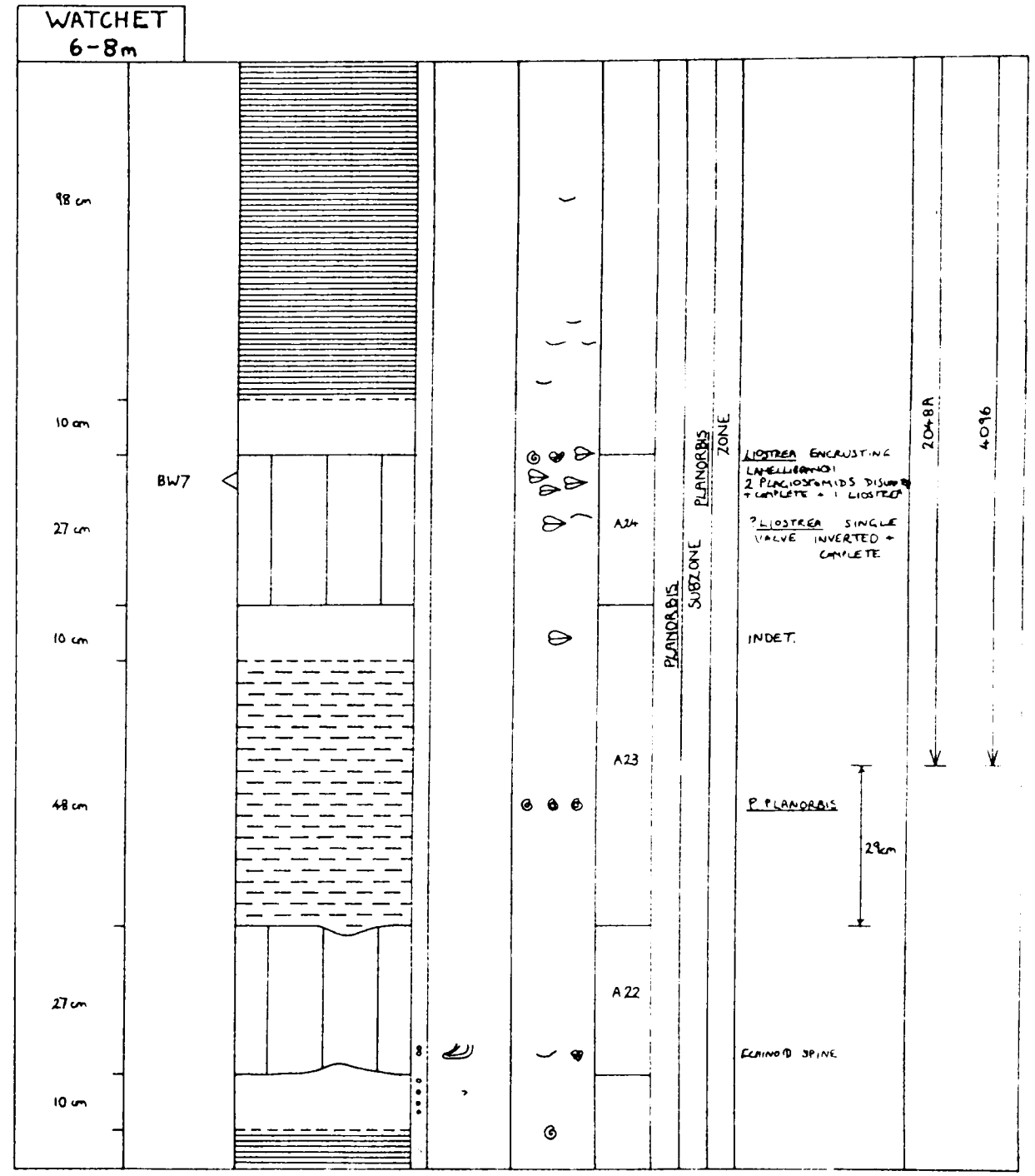
WATCHET
6-8m
98 cm
10 cm
27 cm
10 cm
48 cm
27 cm
10 cm
BW7
A24
A23
A22
PLANORBIS SUBZONE
PLANORBIS ZONE
LIOSTREA ENCRUSTING LAMELLIBRANCH
2 PLANIOSTOMIDS DISUNITED + COMPLETE + 1 LIOSTREA
?LIOSTREA SINGLE VALVE INVERTED + COMPLETE
INDET.
P. PLANORBIS
29cm
ECHINOID SPINE
2048A
4096

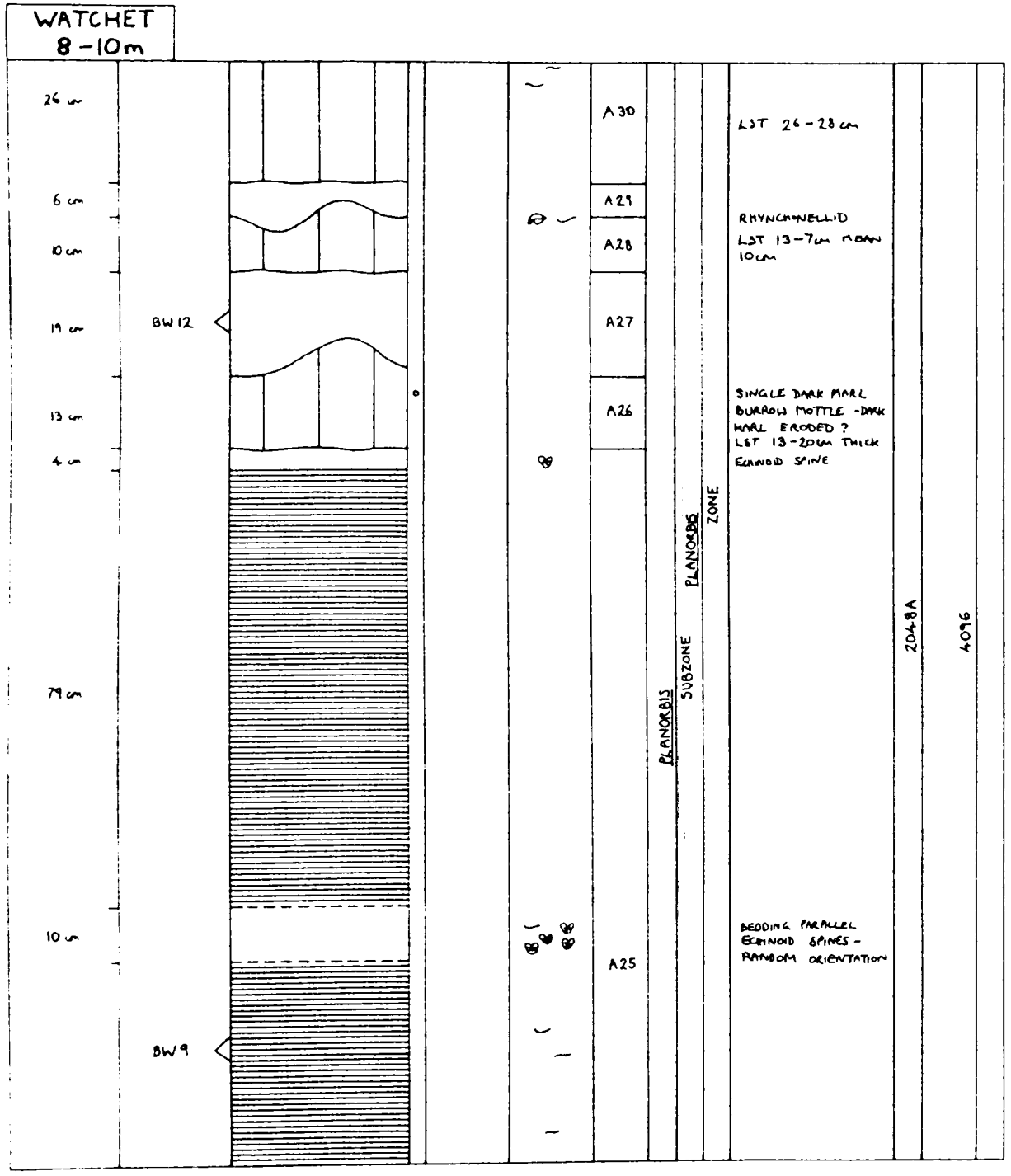
WATCHET
8 - 10m
26 cm
6 cm
10 cm
19 cm
13 cm
4 cm
79 cm
10 cm
BW12
BW9
A30
A29
A28
A27
A26
A25
PLANORBIS SUBZONE
PLANORBIS ZONE
LST 26 - 28 cm
RHYNCHONELLID
LST 13 - 7cm MEAN 10cm
SINGLE DARK MARL
BURROW MOTTLE - DARK MARL ERODED ?
LST 13 - 20cm THICK
ECHINOID SPINE
BEDDING PARALLEL ECHINOID SPINES - RANDOM ORIENTATION
2048A
4096

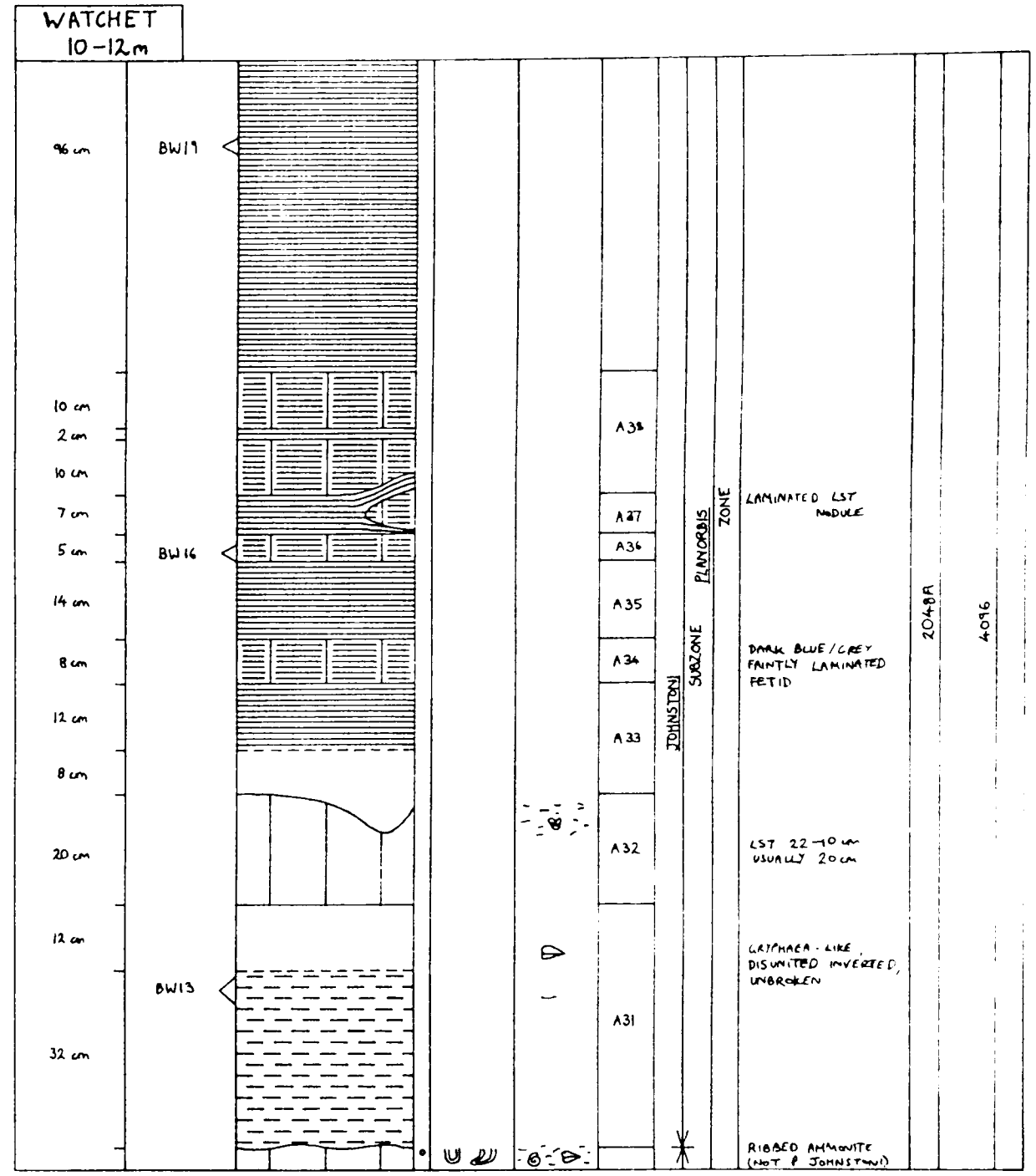
WATCHET
10 - 12m
96 cm
10 cm
2 cm
10 cm
7 cm
5 cm
14 cm
8 cm
12 cm
8 cm
20 cm
12 cm
32 cm
BW19
BW16
BW13
A38
A37
A36
A35
A34
A33
A32
A31
JOHNSTONI SUBZONE
PLANORBIS ZONE
LAMINATED LST MODULE
DARK BLUE / GREY FAINTLY LAMINATED FETID
LST 22 - 10 cm USUALLY 20 cm
GRYPHAEA - LIKE, DISUNITED INVERTED, UNBROKEN
RIBBED AMMONITE (NOT P. JOHNSTONI)
2048A
4096

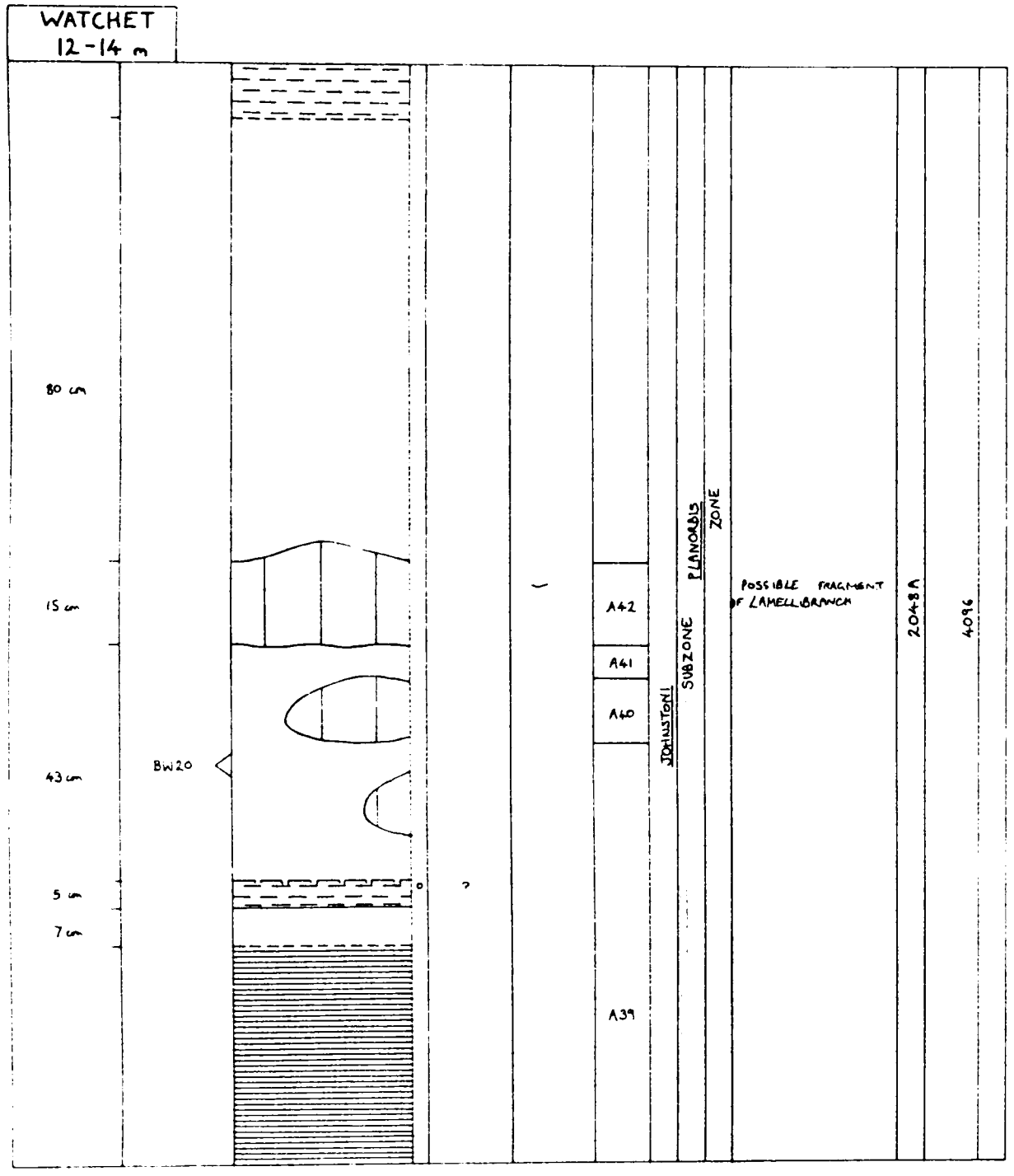
WATCHET
12-14 m
80 cm
15 cm
43 cm
5 cm
7 cm
BW20
A42
A41
A40
A39
JOHNSTONI SUBZONE
PLANORBIS ZONE
POSSIBLE FRAGMENT OF LAMELLIBRANCH
2048A
4096

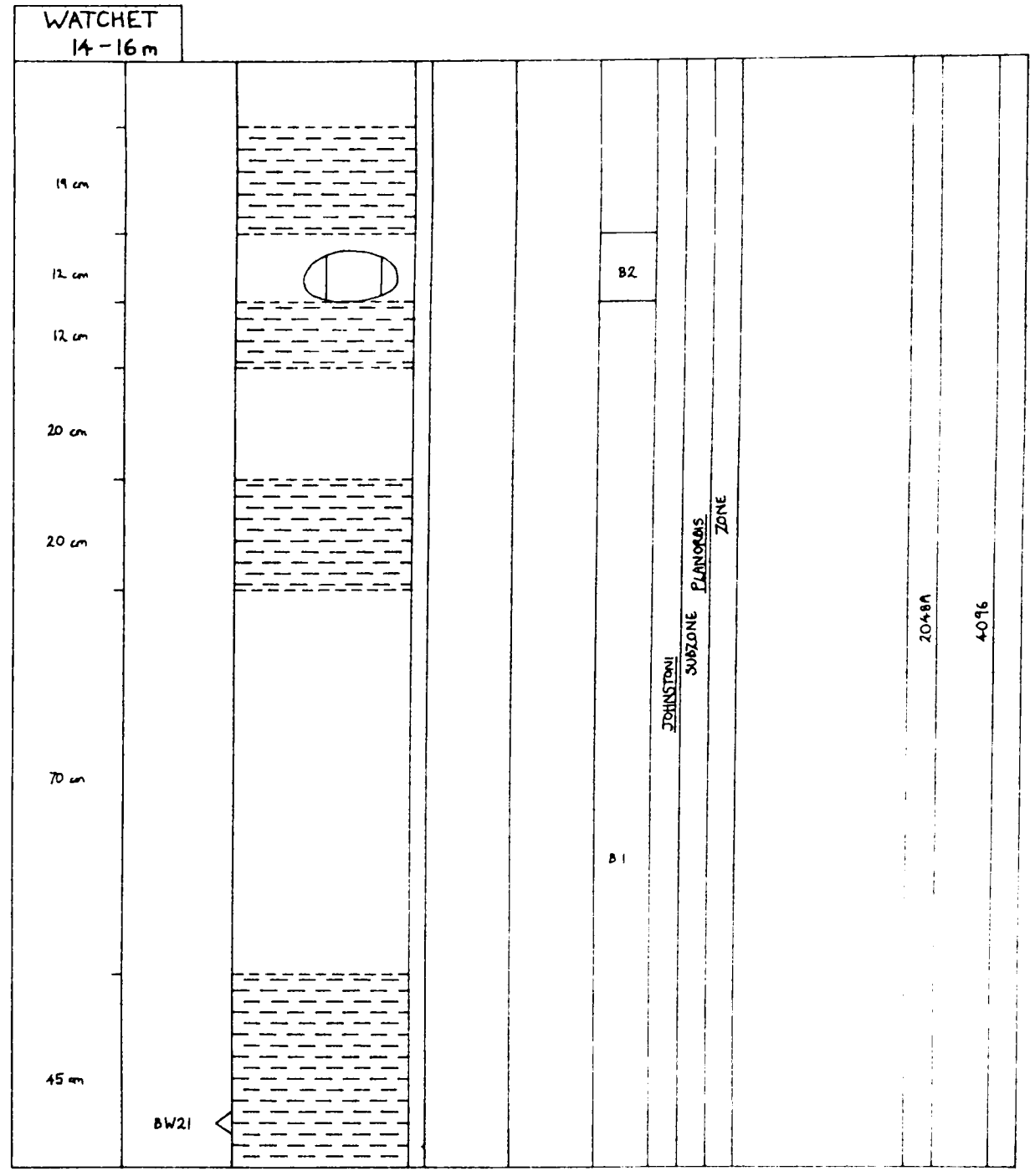
WATCHET
14-16 m
19 cm
12 cm
12 cm
20 cm
20 cm
70 cm
45 cm
BW21
B2
B1
JOHNSTONI SUBZONE
PLANORBIS ZONE
2048A
4096

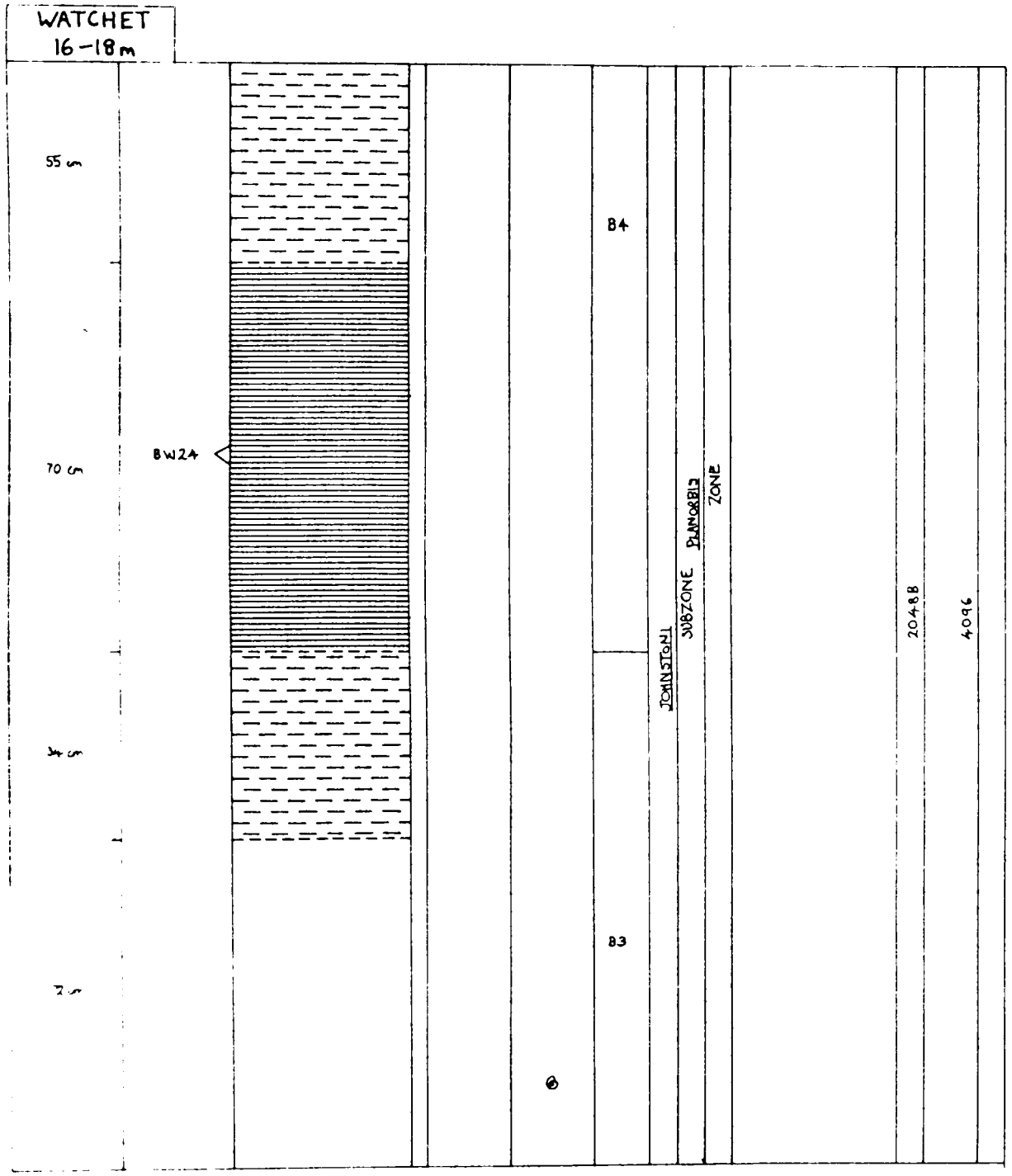
WATCHET
16-18m
55 cm
70 cm
BW24
B4
B3
JOHNSTONI SUBZONE
PLANORBIS ZONE
2048B
4096

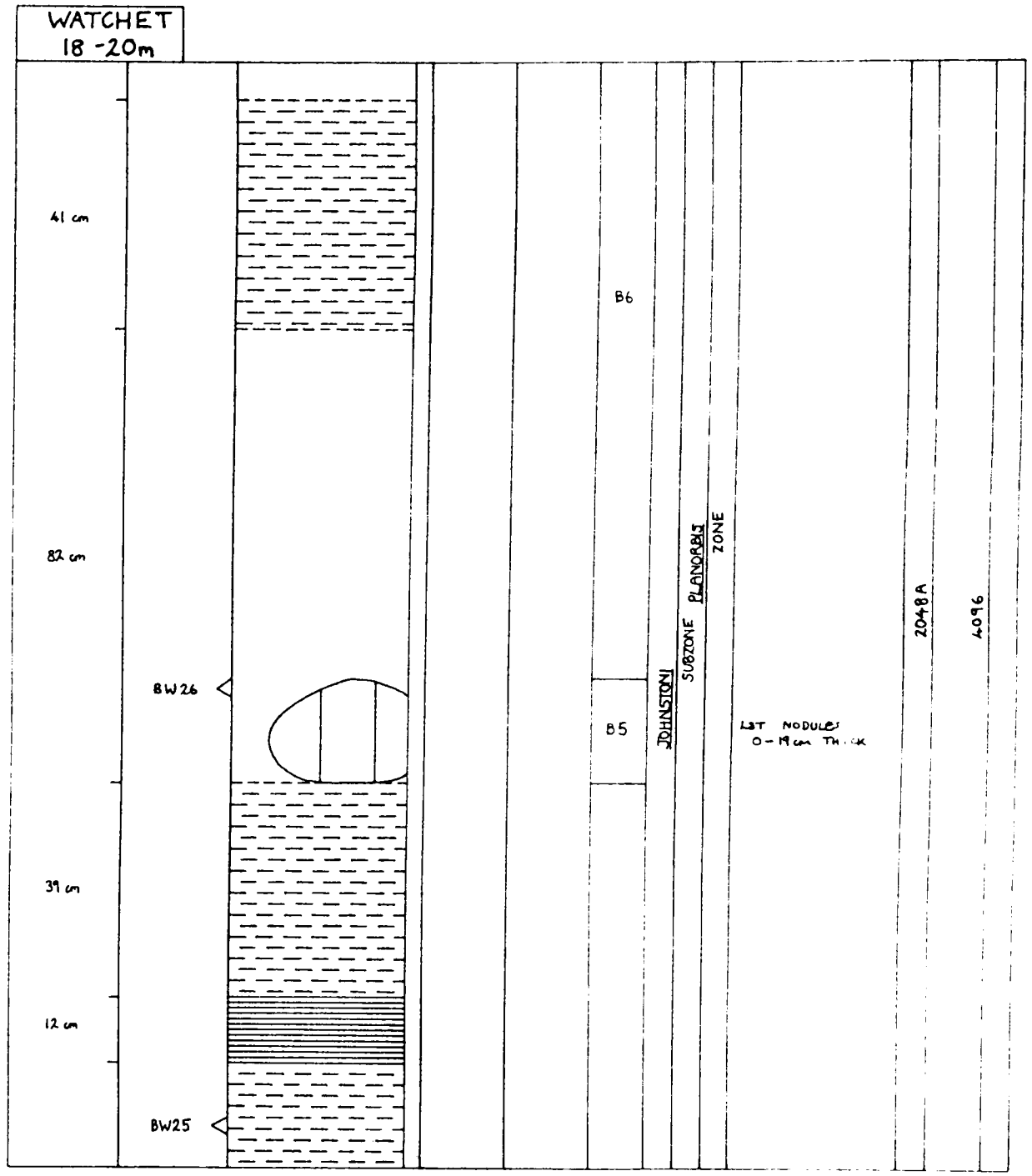
WATCHET
18-20m
41 cm
82 cm
39 cm
12 cm
BW26
BW25
B6
B5
JOHNSTONI SUBZONE
PLANORBIS ZONE
LST NODULES
0-19cm THICK
2048A
4096

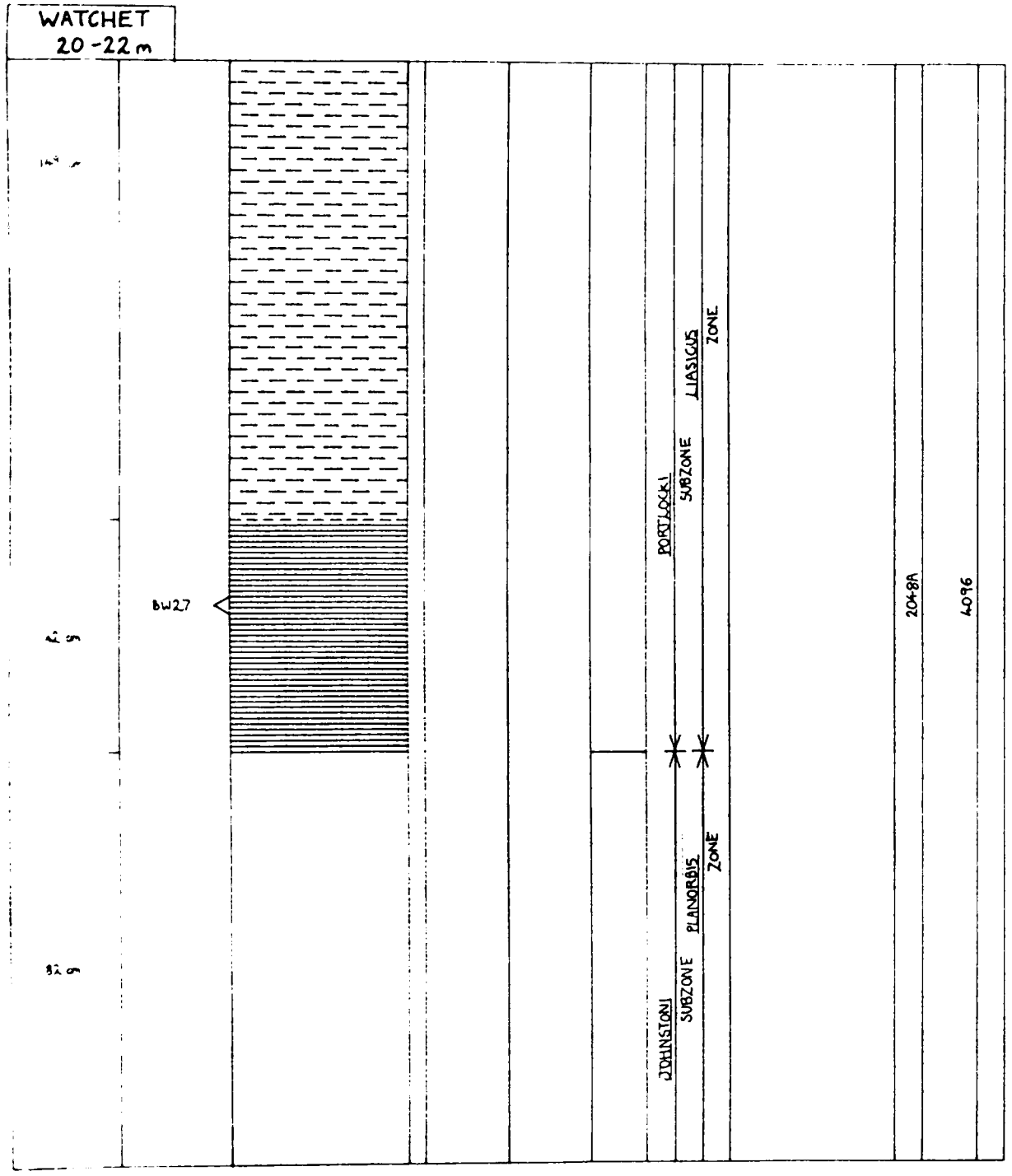
WATCHET
20 -22 m
BW27
PORTLOCKI
SUBZONE
LIASICUS
ZONE
JOHNSTONI
SUBZONE
PLANORBIS
ZONE
2048A
4096

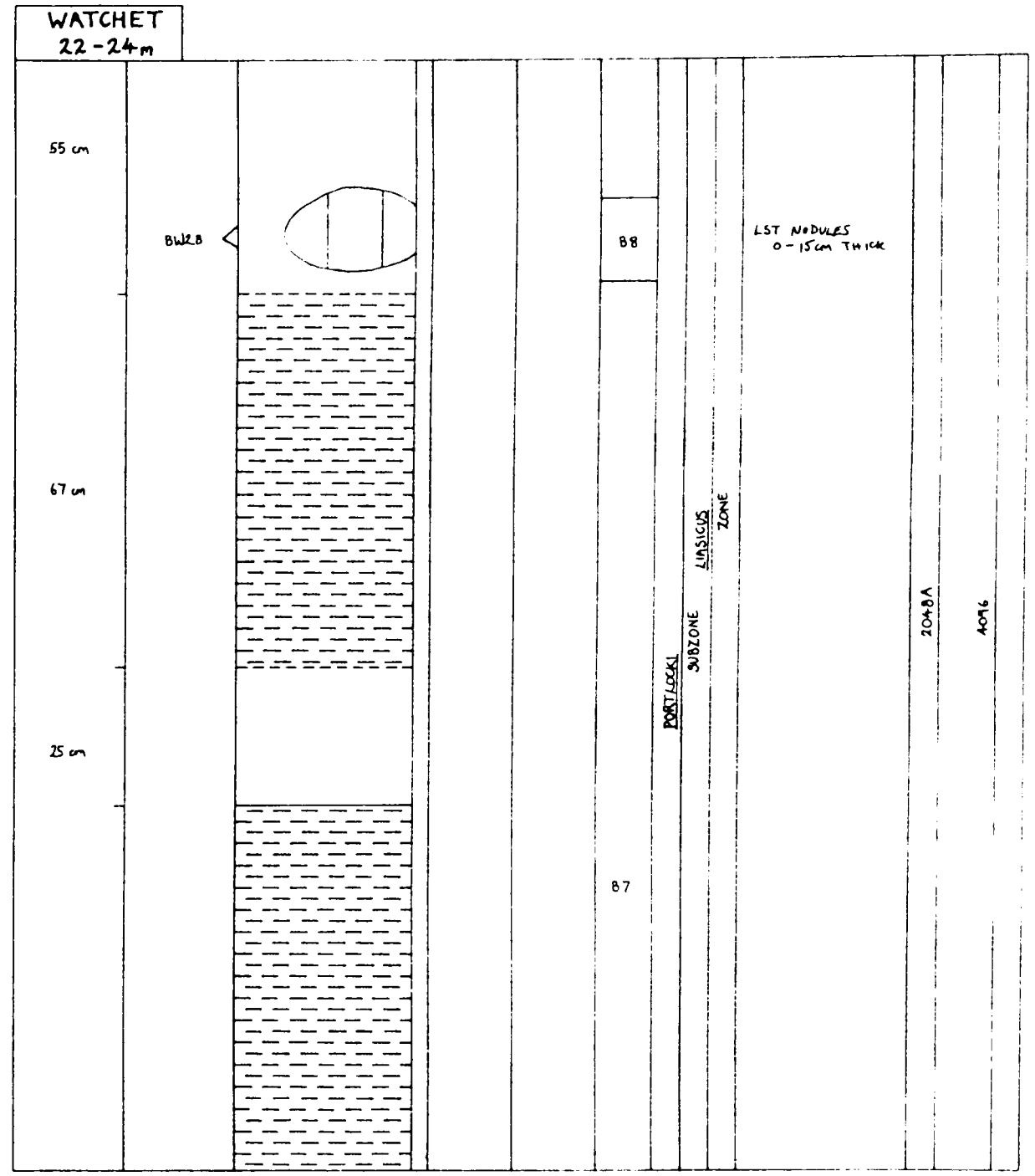
WATCHET
22 -24 m
55 cm
67 cm
25 cm
BW28
B8
B7
LST NODULES
0 - 15cm THICK
PORTLOCKI
SUBZONE
LIASICUS
ZONE
2048A
4096

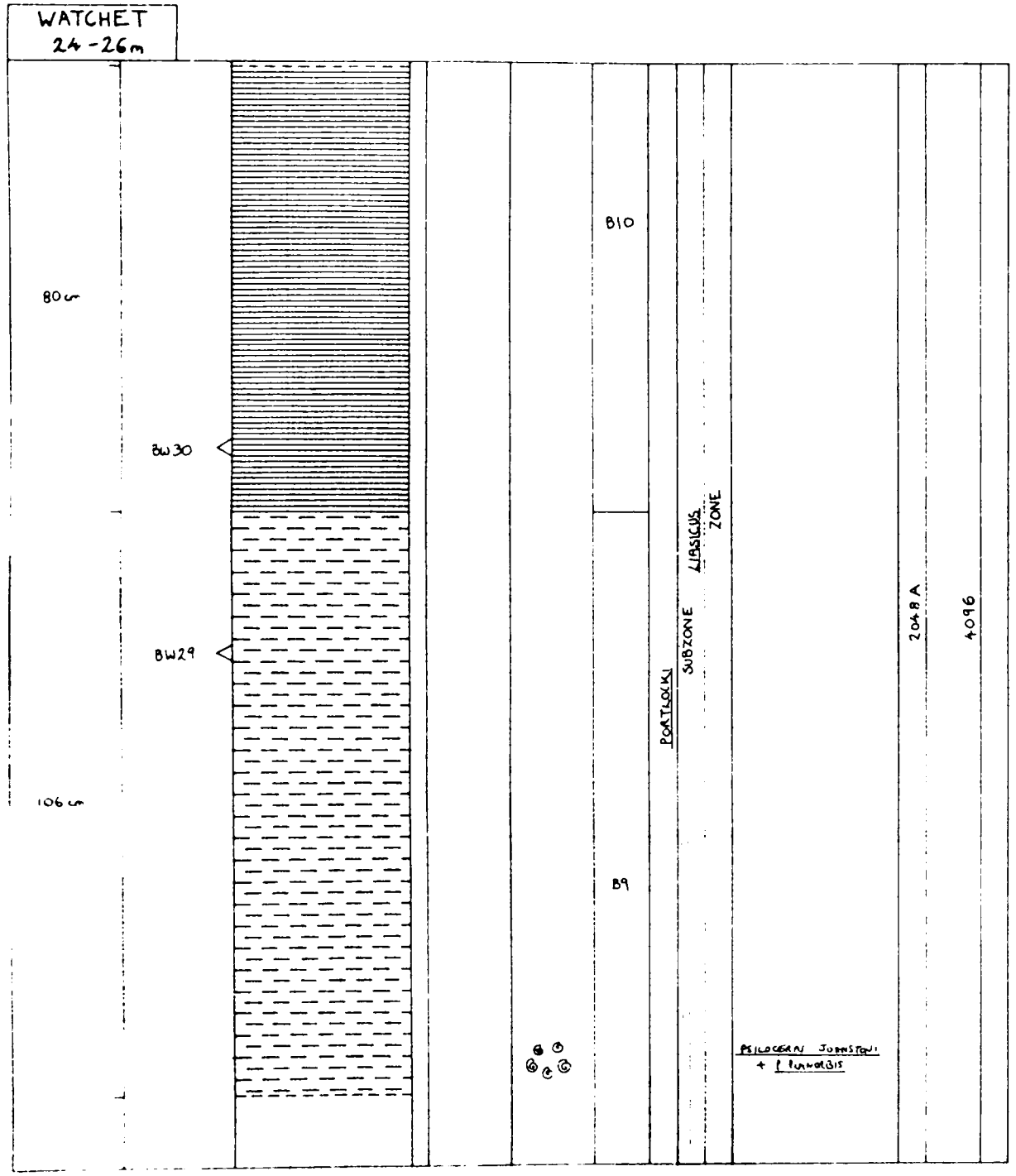
WATCHET
24 - 26m
80 cm
106 cm
BW30
BW29
B10
B9
PORTLOCKI
SUBZONE
LIASICUS
ZONE
PSILOCERAS JOHNSTONI
+ P. PLANORBIS
2048 A
4096

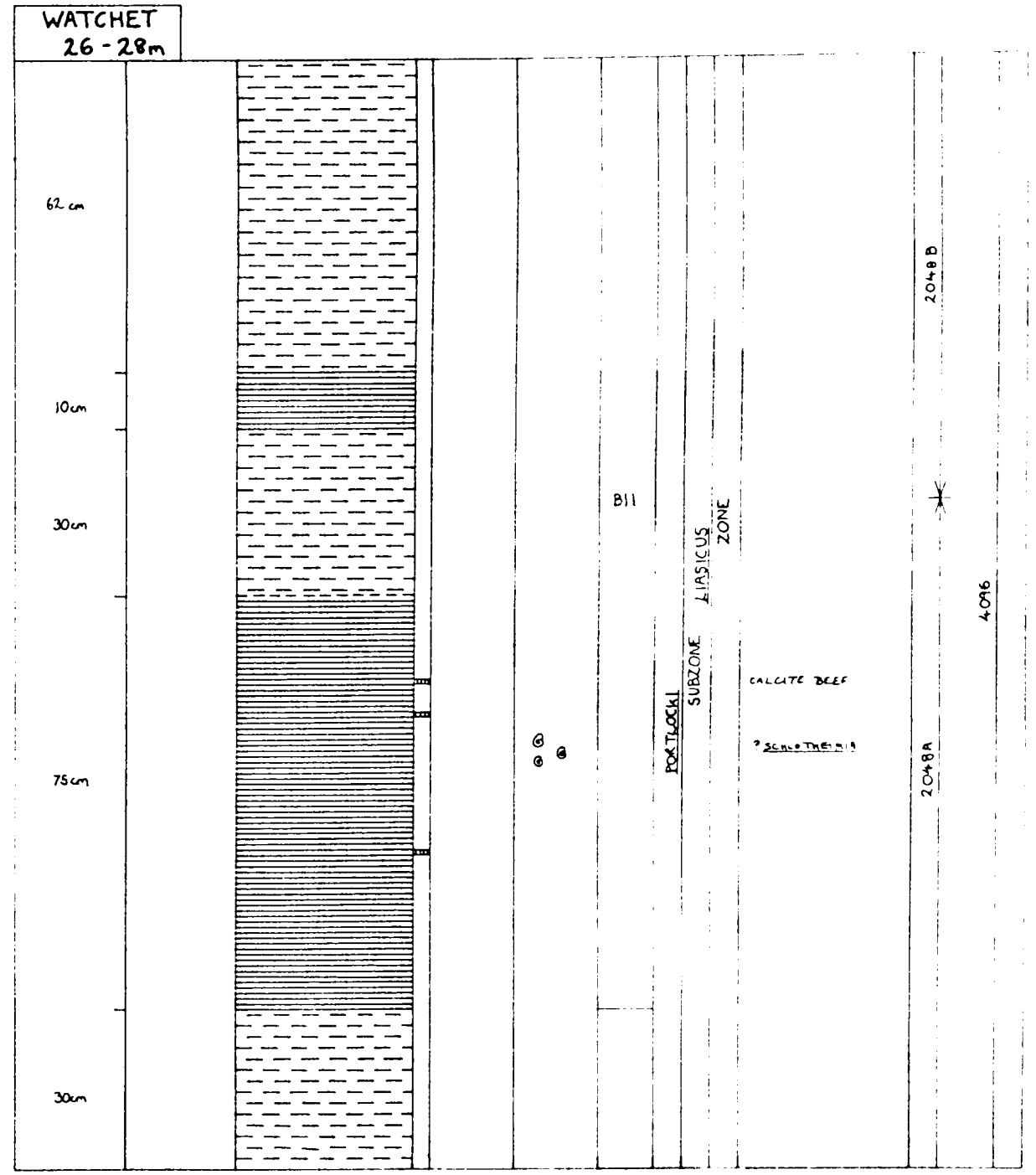
WATCHET
26 - 28m
62 cm
10cm
30cm
75cm
30cm
B11
PORTLOCKI
SUBZONE
LIASICUS
ZONE
CALCITE BEEF
? SCHLOTHEIMIA
2048 B
2048 A
4096

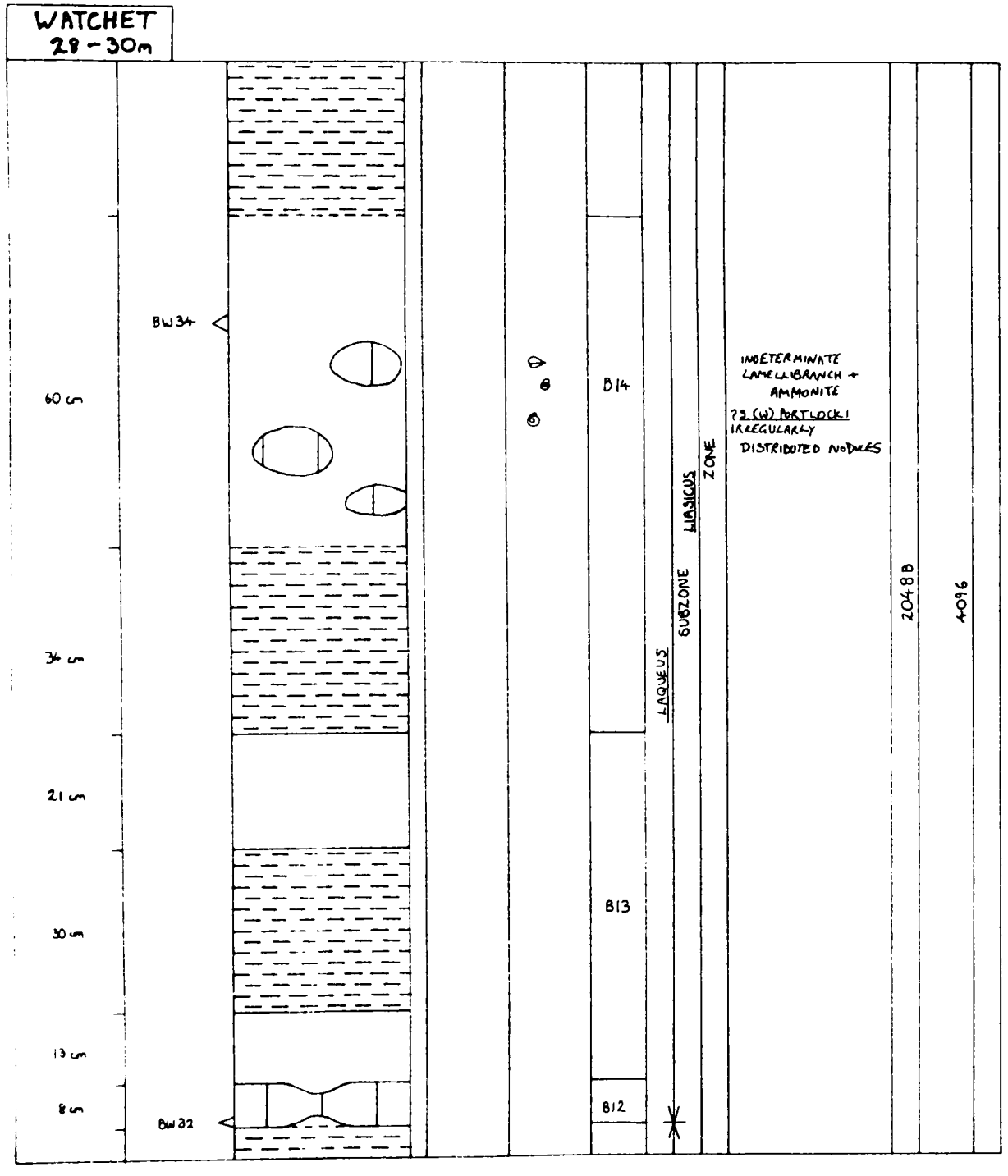
WATCHET
28 - 30m
60 cm
36 cm
21 cm
30 cm
13 cm
8 cm
BW34
BW32
B14
B13
B12
LIASICUS
ZONE
LAQUEUS
SUBZONE
INDETERMINATE
LAMELLIBRANCH +
AMMONITE
?? (W) PORTLOCKI
IRREGULARLY
DISTRIBUTED NODULES
2048B
4096

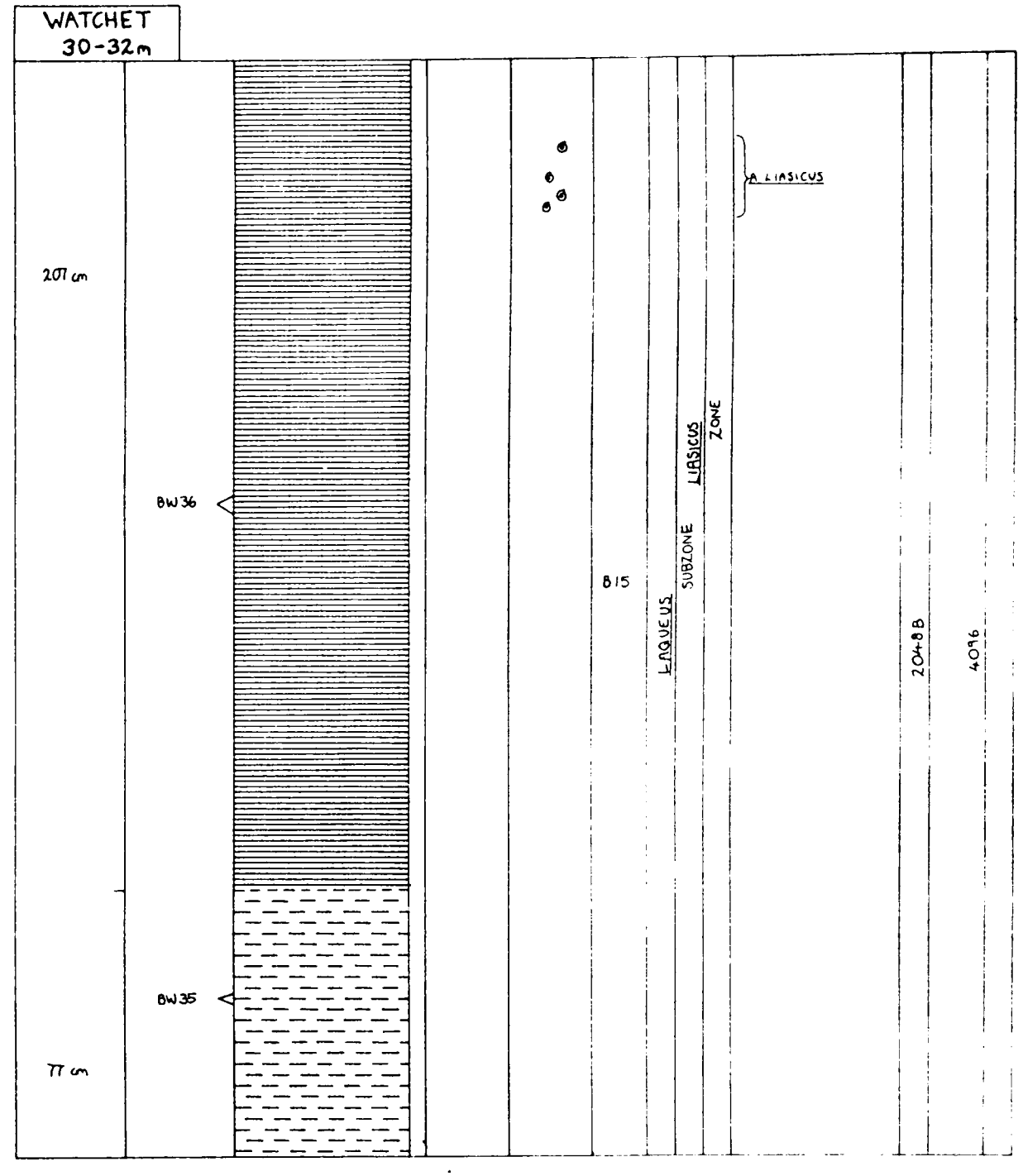
WATCHET
30-32m
207 cm
77 cm
BW36
BW35
B15
A. LIASICUS
LIASICUS
ZONE
LAQUEUS
SUBZONE
2048B
4096

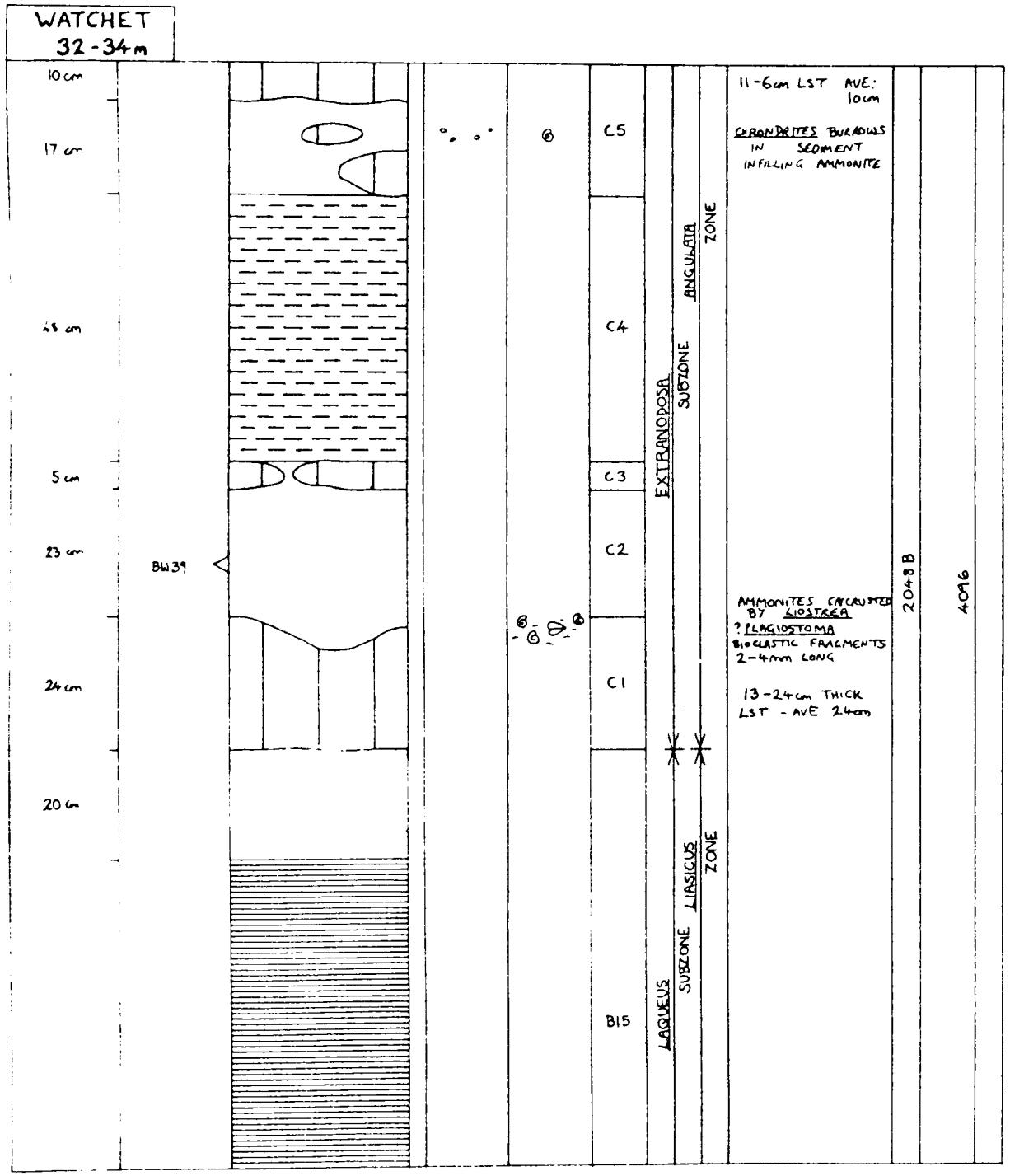
WATCHET
32-34m
10 cm
17 cm
25 cm
5 cm
23 cm
24 cm
20 cm
BW39
C5
C4
C3
C2
C1
B15
EXTRANODOSA SUBZONE
ANGULATA ZONE
LAQUEUS SUBZONE
LIASICUS ZONE
11-6cm LST AVE: 10cm
CHRONDRITES BURROWS IN SEDIMENT INFILLING AMMONITE
AMMONITES ENCRUSTED BY LIOSTREA
? PLAGIOSTOMA
BIOCLASTIC FRAGMENTS 2-4mm LONG
13-24cm THICK LST - AVE 24cm
2048 B
4096

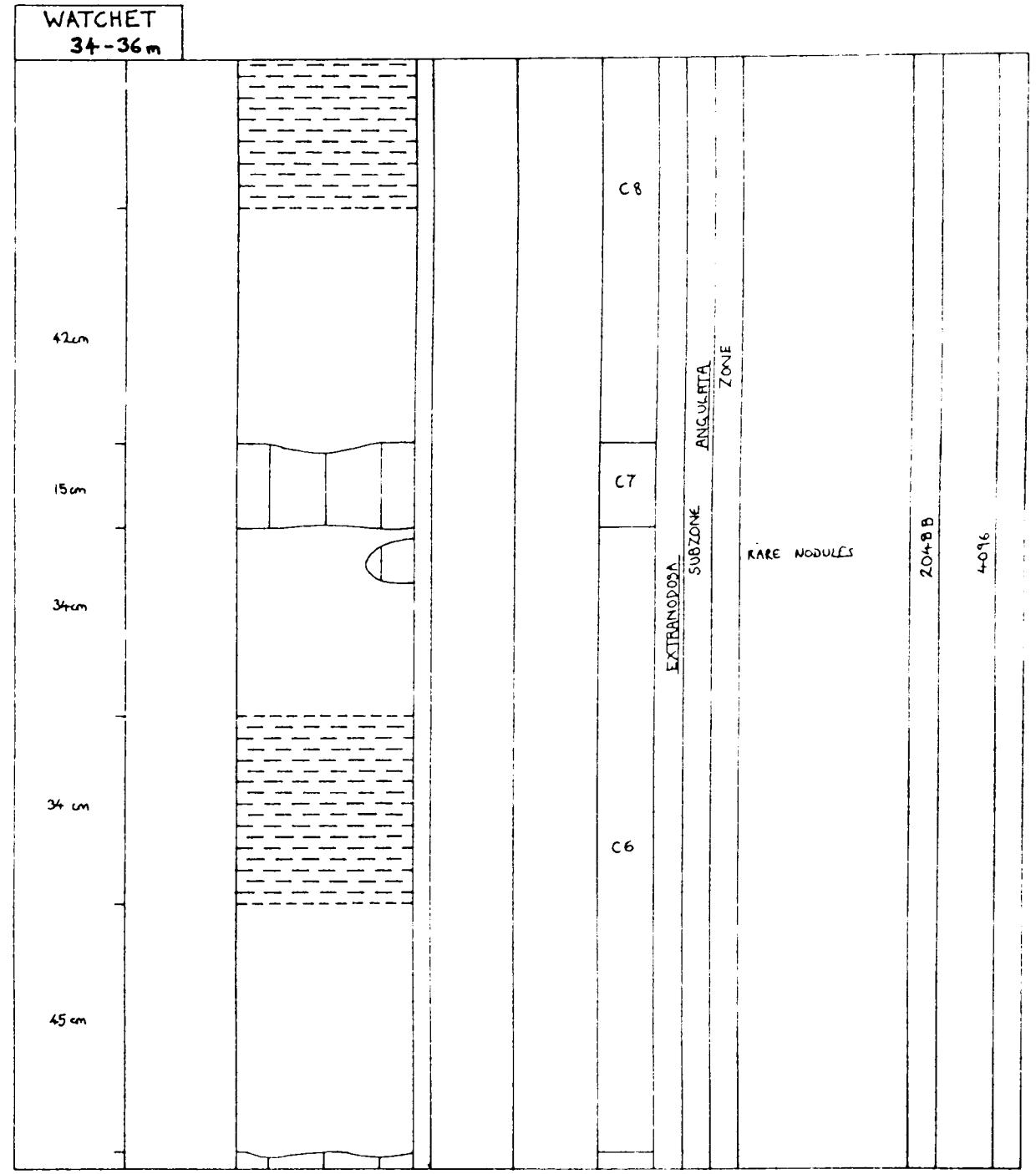
WATCHET
34-36m
42cm
15cm
34cm
34 cm
45 cm
C8
C7
C6
EXTRANODOSA SUBZONE
ANGULATA ZONE
RARE NODULES
2048 B
4096

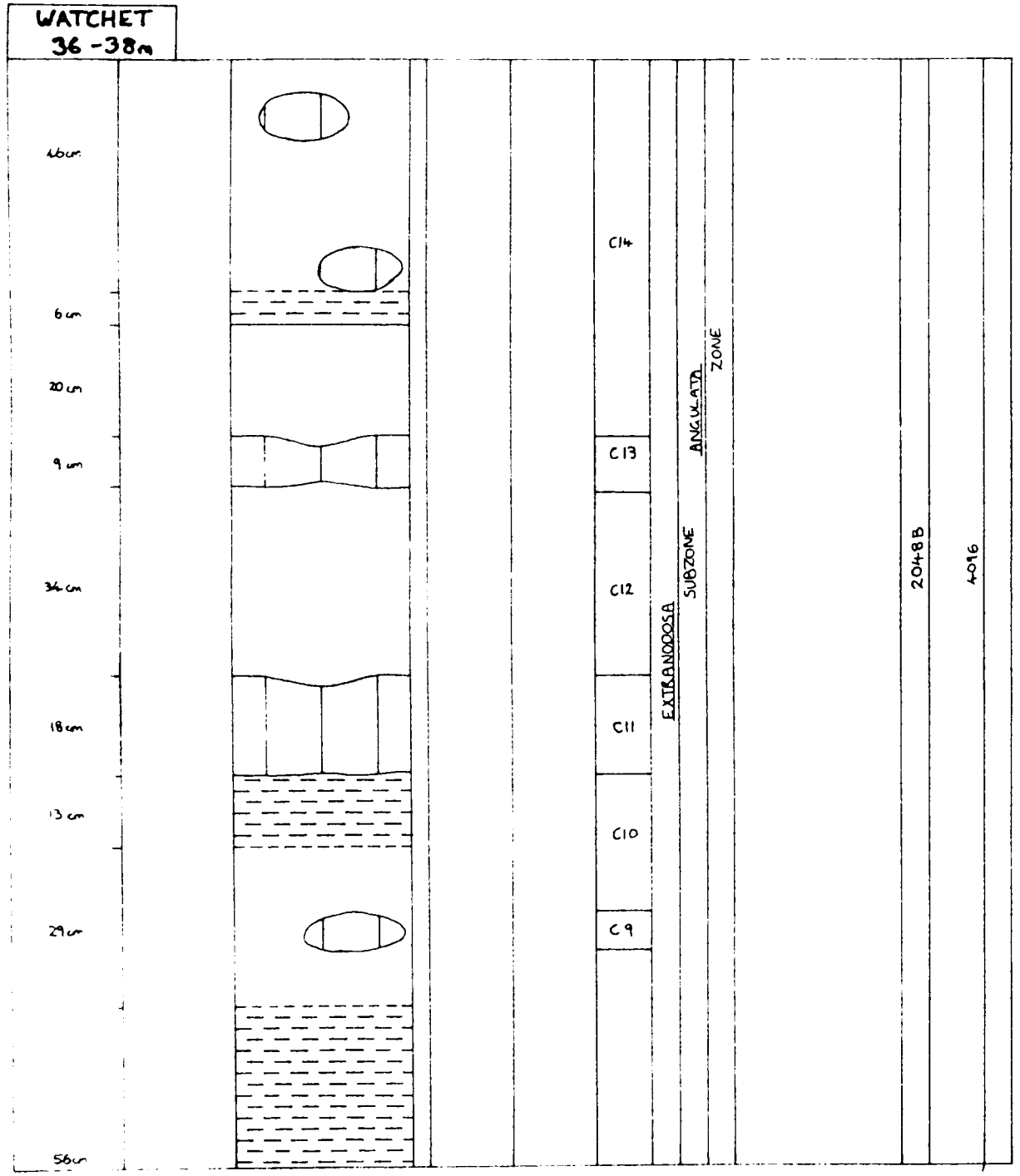
WATCHET
36 - 38m
4cm
6cm
20cm
9cm
36cm
18cm
13cm
29cm
56cm
C14
C13
C12
C11
C10
C9
EXTRANODOSA
SUBZONE
ANGULATA
ZONE
2048B
4096

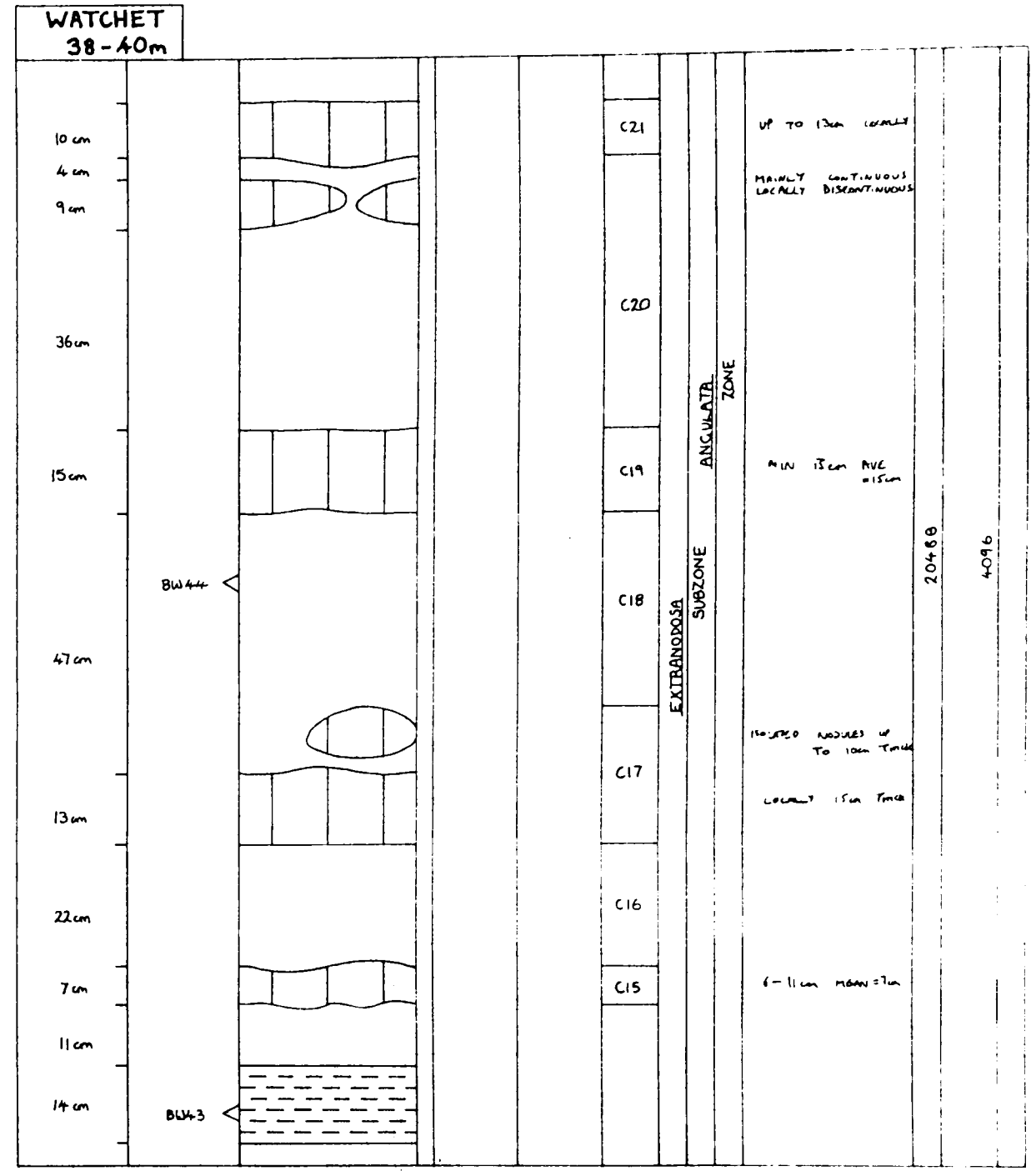
WATCHET
38 - 40m
10cm
4cm
9cm
36cm
15cm
47cm
13cm
22cm
7cm
11cm
14cm
BW44
BW43
C21
C20
C19
C18
C17
C16
C15
EXTRANODOSA
SUBZONE
ANGULATA
ZONE
UP TO 13cm LOCALLY
MAINLY CONTINUOUS
LOCALLY DISCONTINUOUS
MIN 13cm AVE =15cm
ISOLATED NODULES UP TO 10cm THICK
LOCALLY 15cm THICK
6-11cm MEAN=7cm
2048B
4096

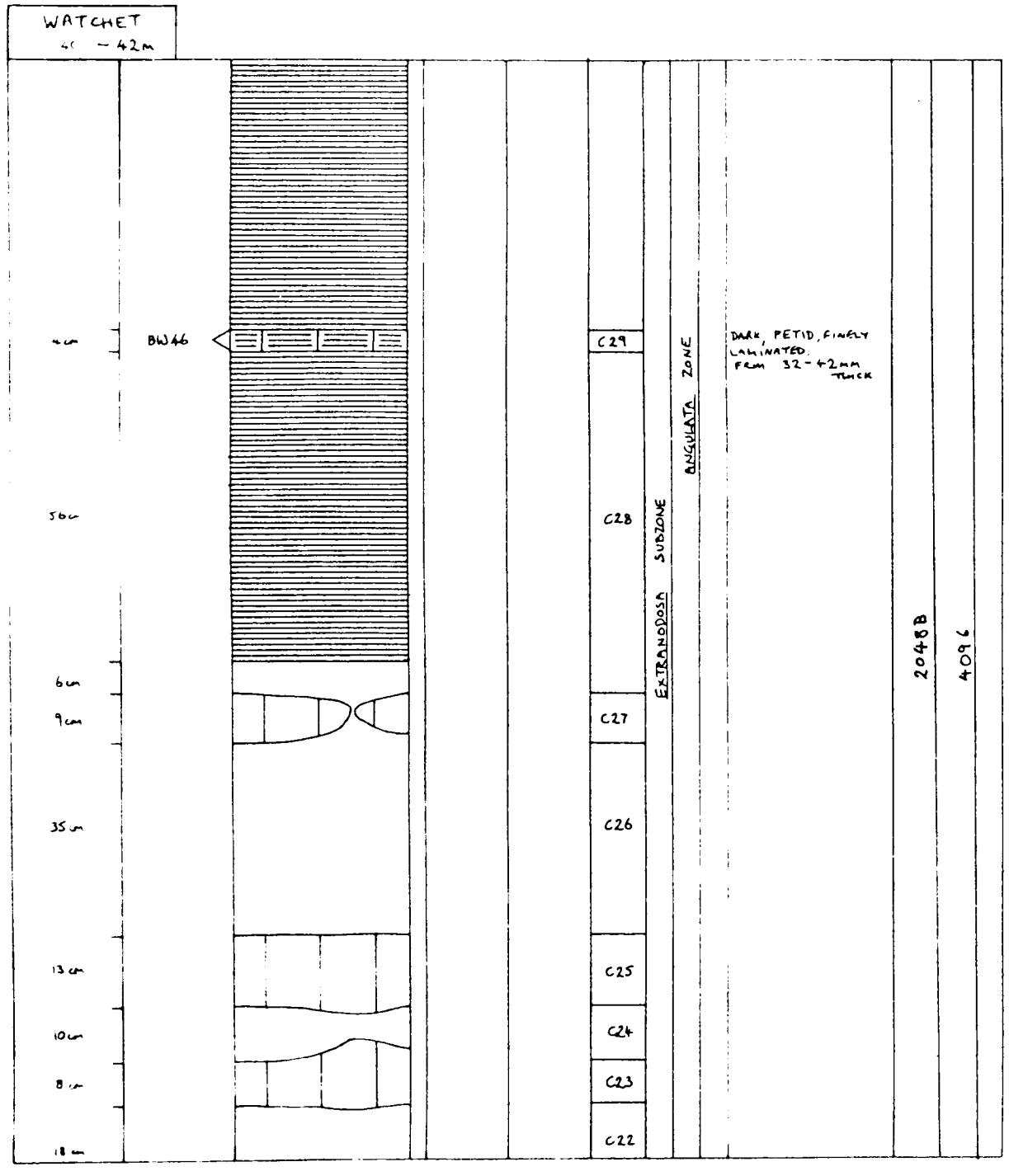
WATCHET
40 - 42m
BW46
C29
C28
C27
C26
C25
C24
C23
C22
EXTRANODOSA SUBZONE
ANGULATA ZONE
DARK, PETID, FINELY LAMINATED. FROM 32 - 42mm THICK
2048B
4096

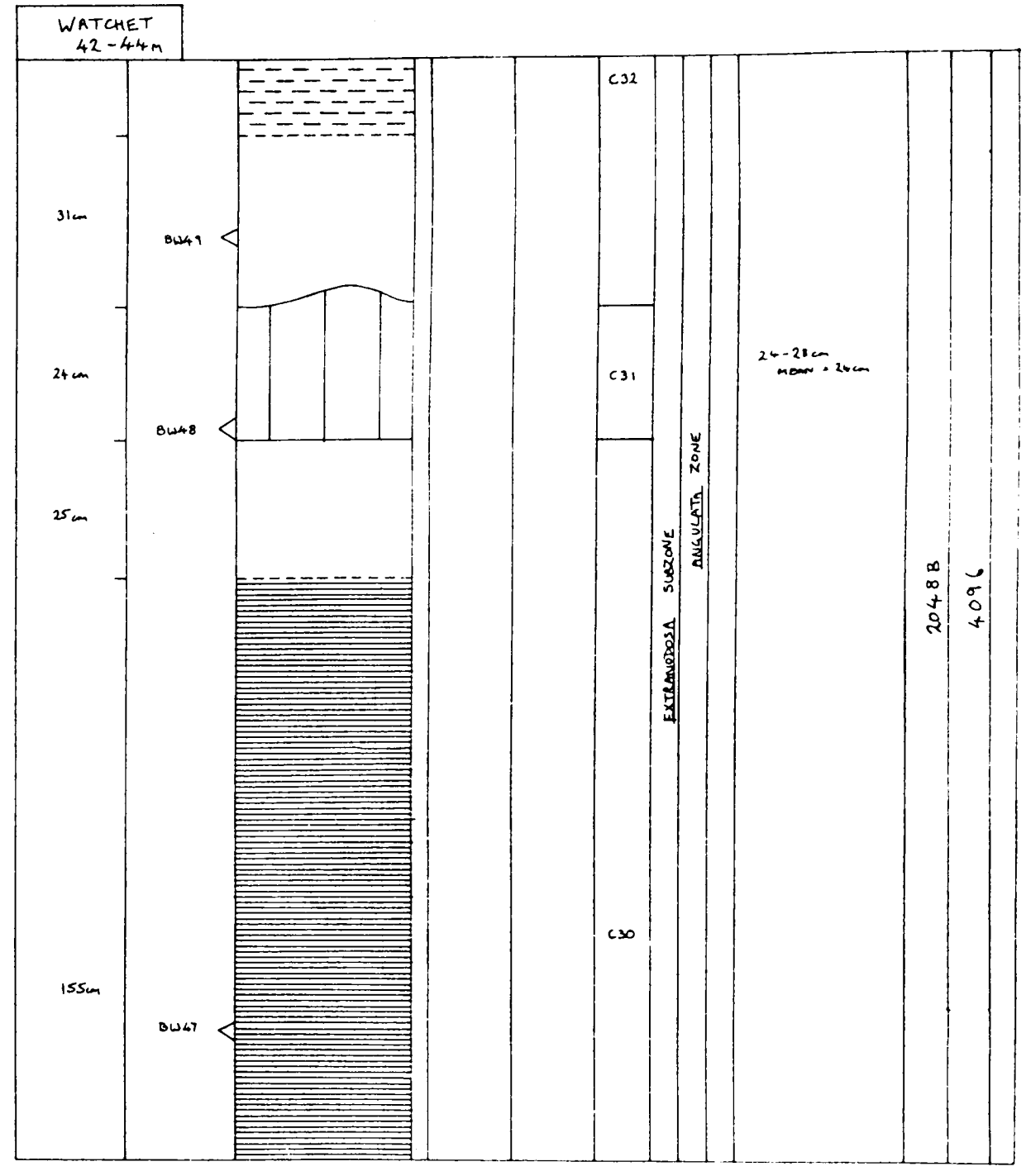
WATCHET
42 - 44m
31cm
24cm
25cm
155cm
BW49
BW48
BW47
C32
C31
C30
EXTRANODOSA SUBZONE
ANGULATA ZONE
24 - 28cm
MEAN = 26cm
2048B
4096

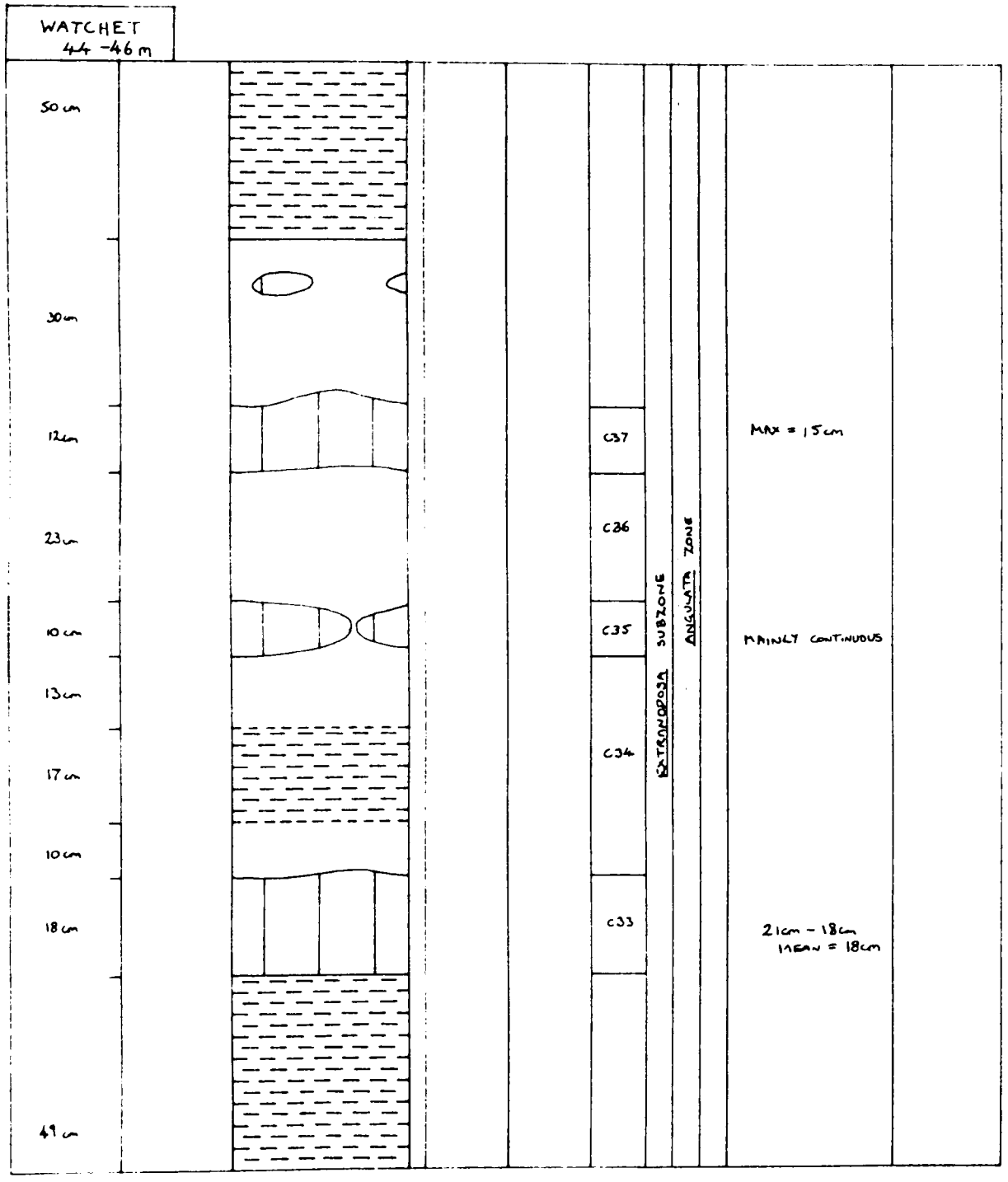
WATCHET
44 -46 m
50 cm
30 cm
12cm
23cm
10 cm
13 cm
17 cm
10 cm
18 cm
49 cm
C37
C36
C35
C34
C33
EXTRANODOSA SUBZONE
ANGULATA ZONE
MAX = 15cm
MAINLY CONTINUOUS
21cm - 18cm
MEAN = 18cm

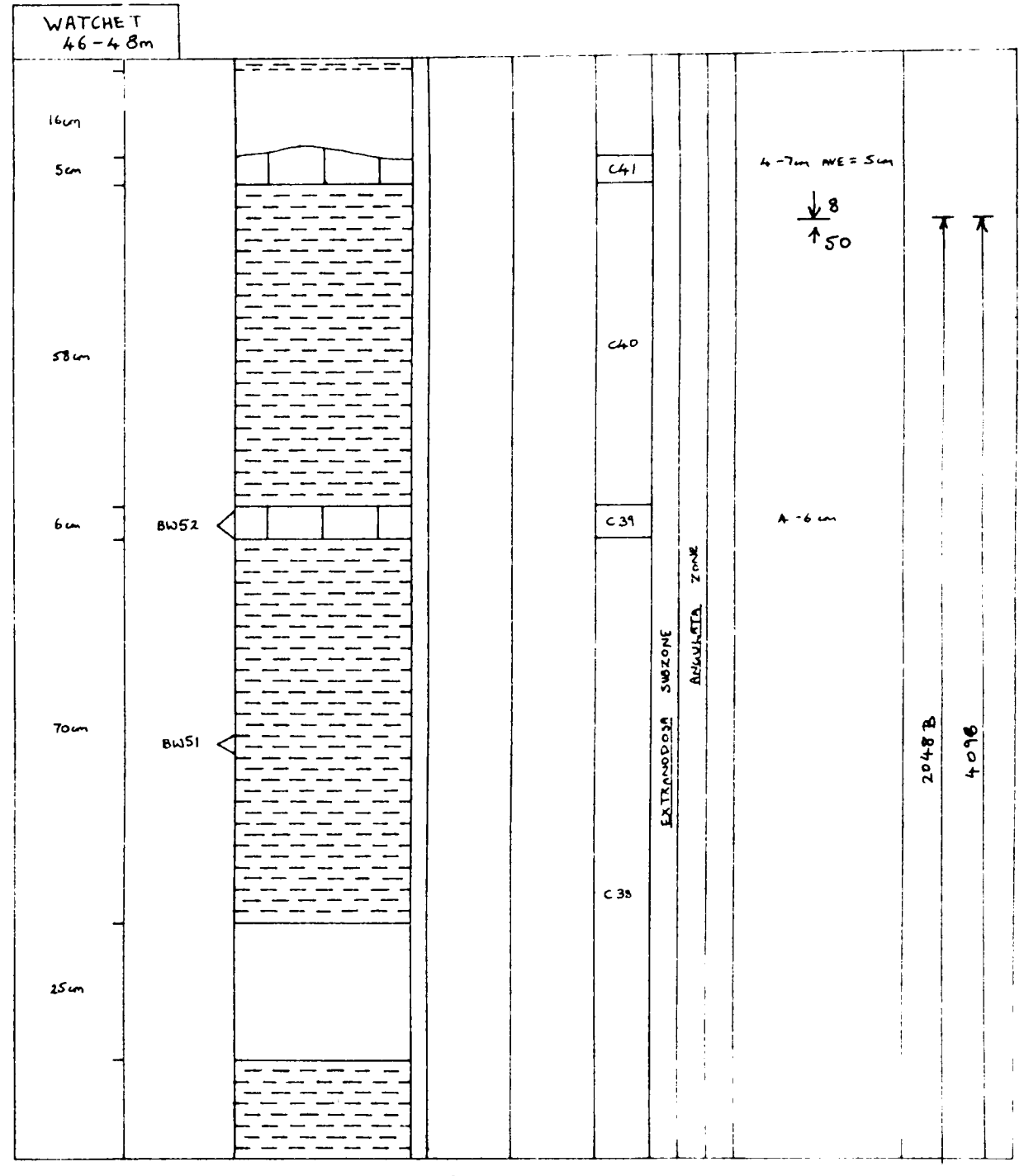
WATCHET
46 - 48m
16cm
5cm
58cm
6cm
70cm
25cm
BW52
BW51
C41
C40
C39
C38
EXTRANODOSA SUBZONE
ANGULATA ZONE
4 -7cm AVE = 5cm
8
50
A -6 cm
2048 B
4096

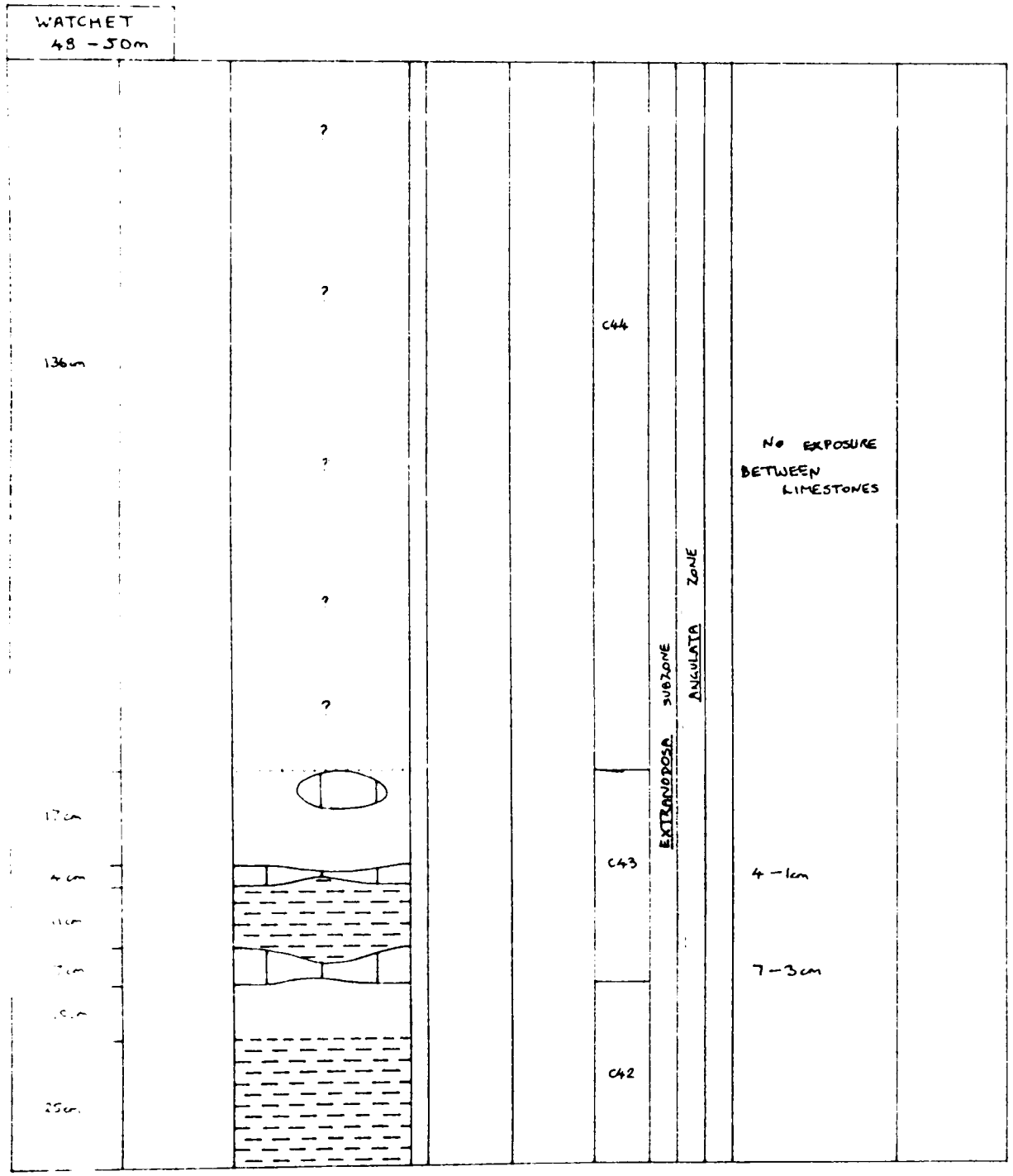
WATCHET
48 - 50m
136cm
17cm
4cm
25cm
C44
C43
C42
EXTRANODOSA SUBZONE
ANGULATA ZONE
NO EXPOSURE
BETWEEN
LIMESTONES
4 - 1cm
7 - 3cm

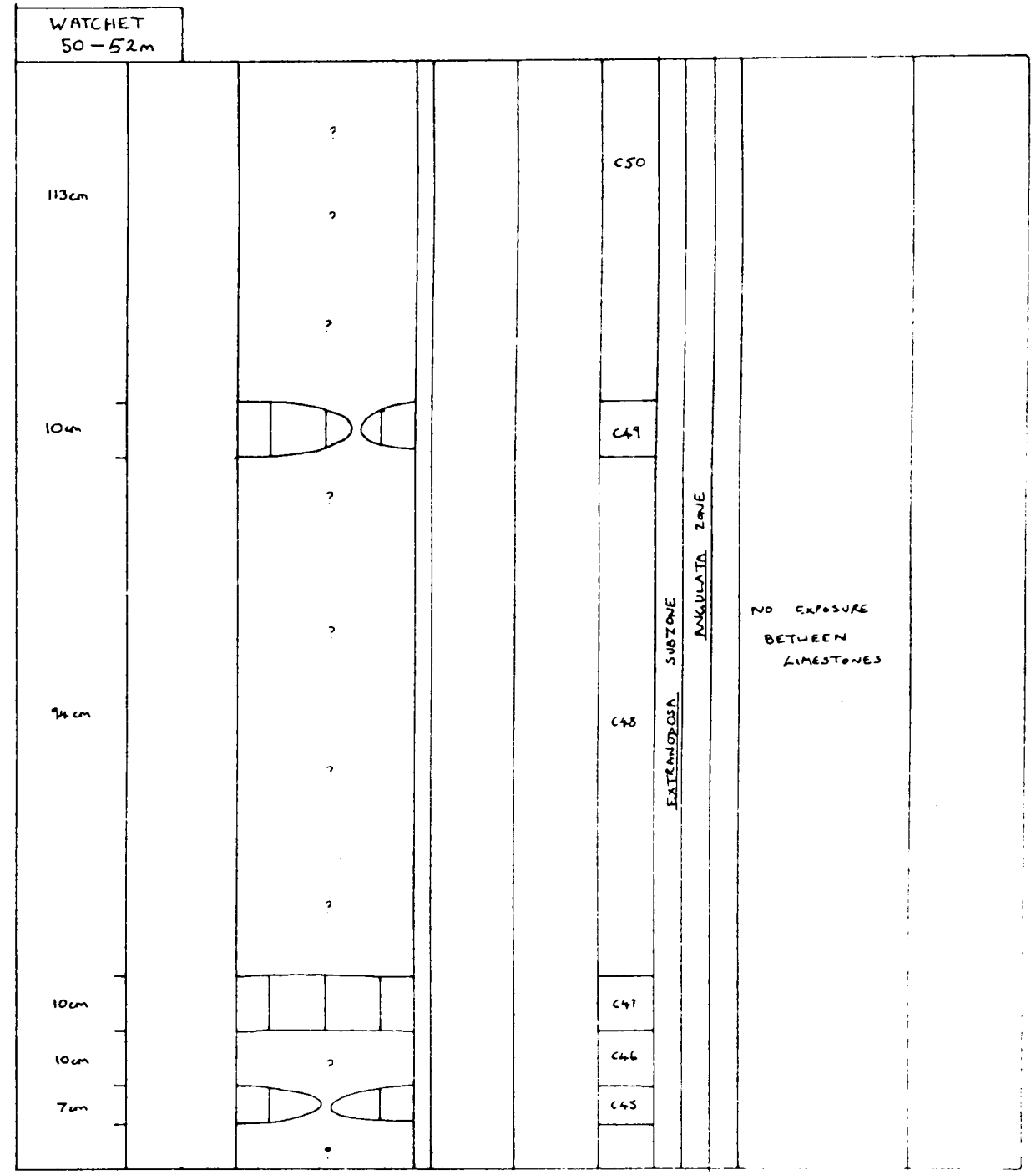
WATCHET
50 - 52m
113cm
10cm
94cm
10cm
10cm
7cm
C50
C49
C48
C47
C46
C45
EXTRANODOSA SUBZONE
ANGULATA ZONE
NO EXPOSURE
BETWEEN
LIMESTONES

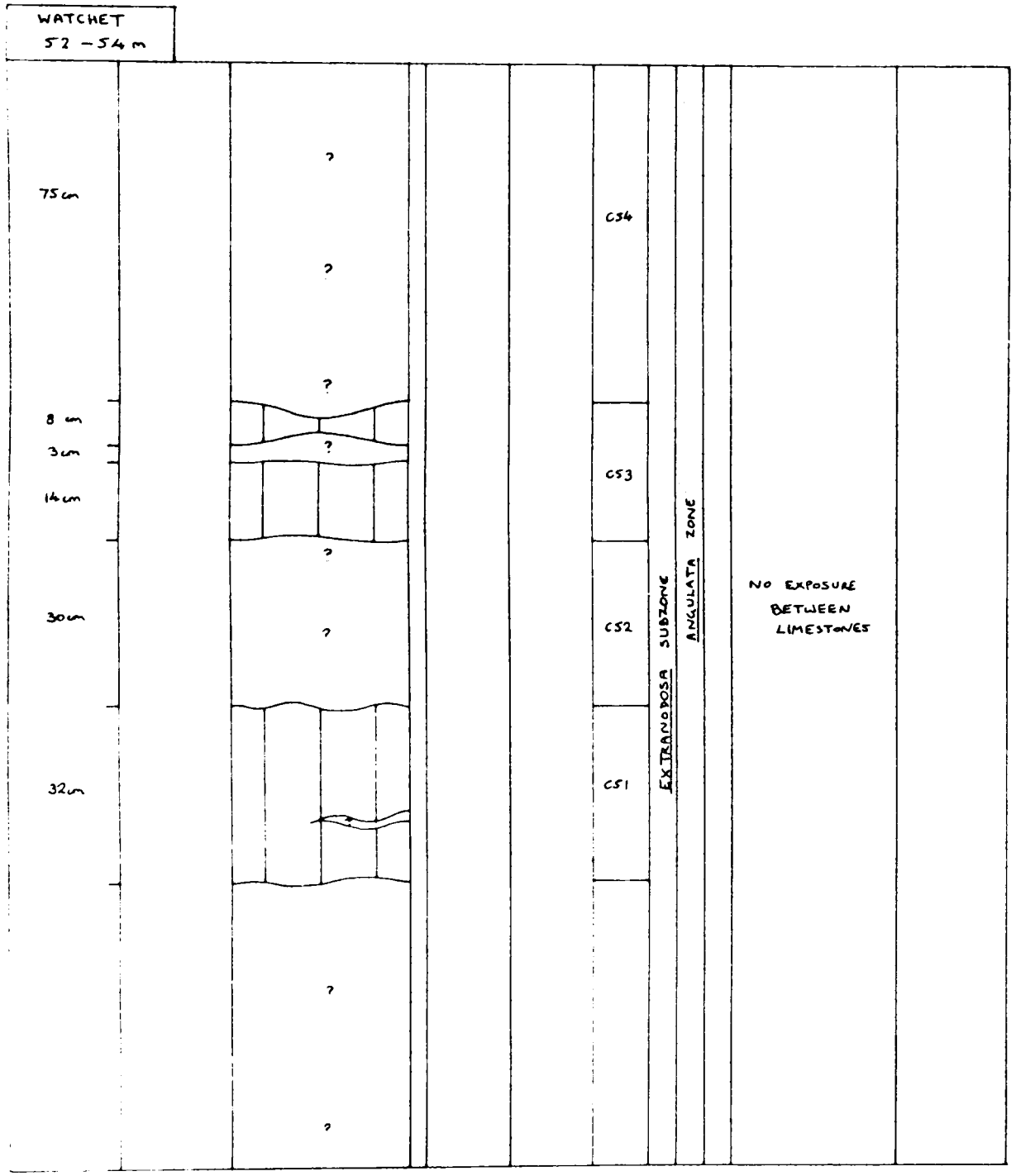
WATCHET
52 - 54 m
75cm
8 cm
3cm
14cm
30cm
32cm
CS4
CS3
CS2
CS1
EXTRANODOSA SUBZONE
ANGULATA ZONE
NO EXPOSURE
BETWEEN
LIMESTONES

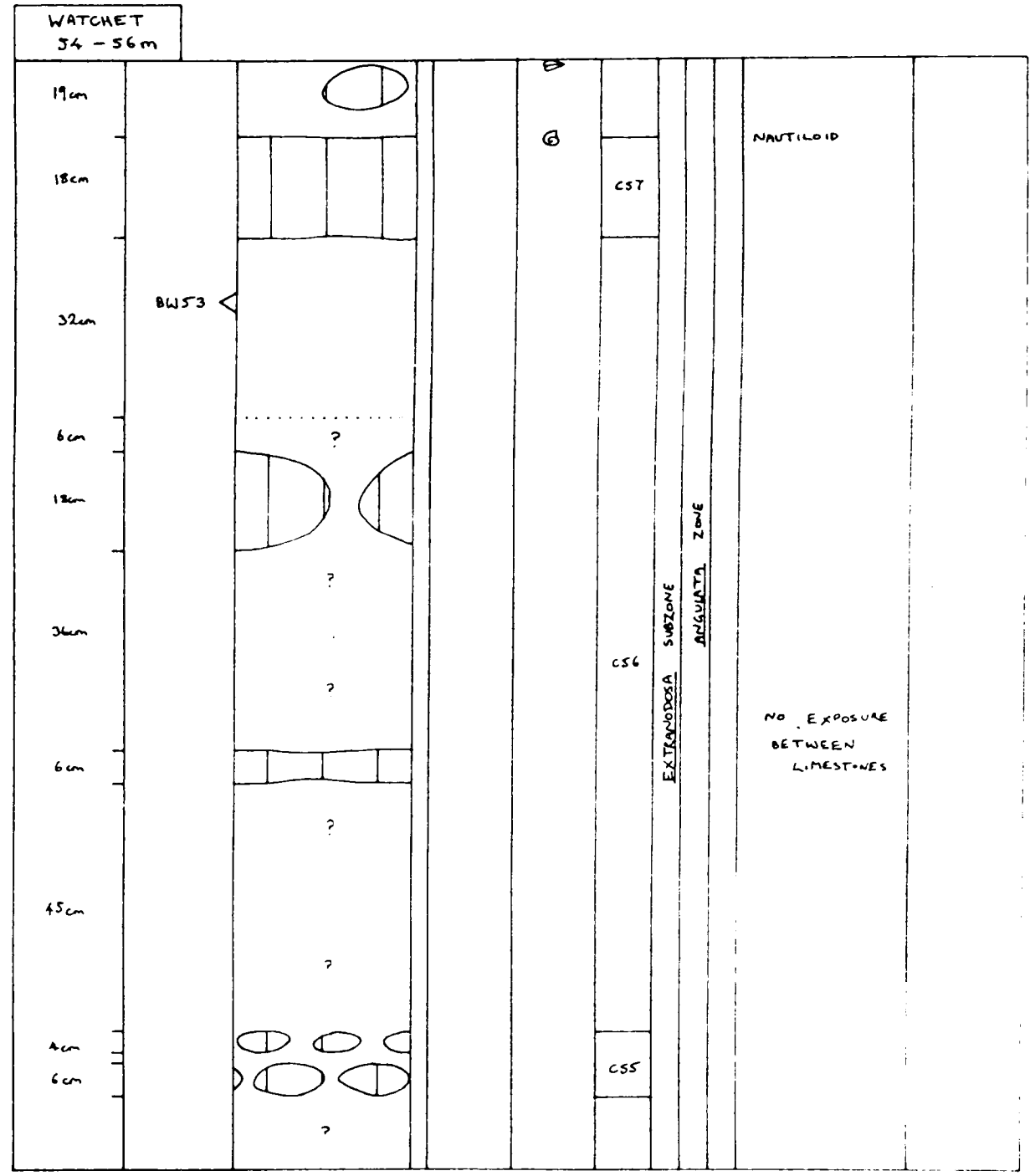
WATCHET
54 - 56m
19cm
18cm
32cm
6cm
13cm
36cm
6cm
45cm
4cm
6cm
BW53
CS7
CS6
CS5
EXTRANODOSA SUBZONE
ANGULATA ZONE
NAUTILOID
NO EXPOSURE
BETWEEN
LIMESTONES

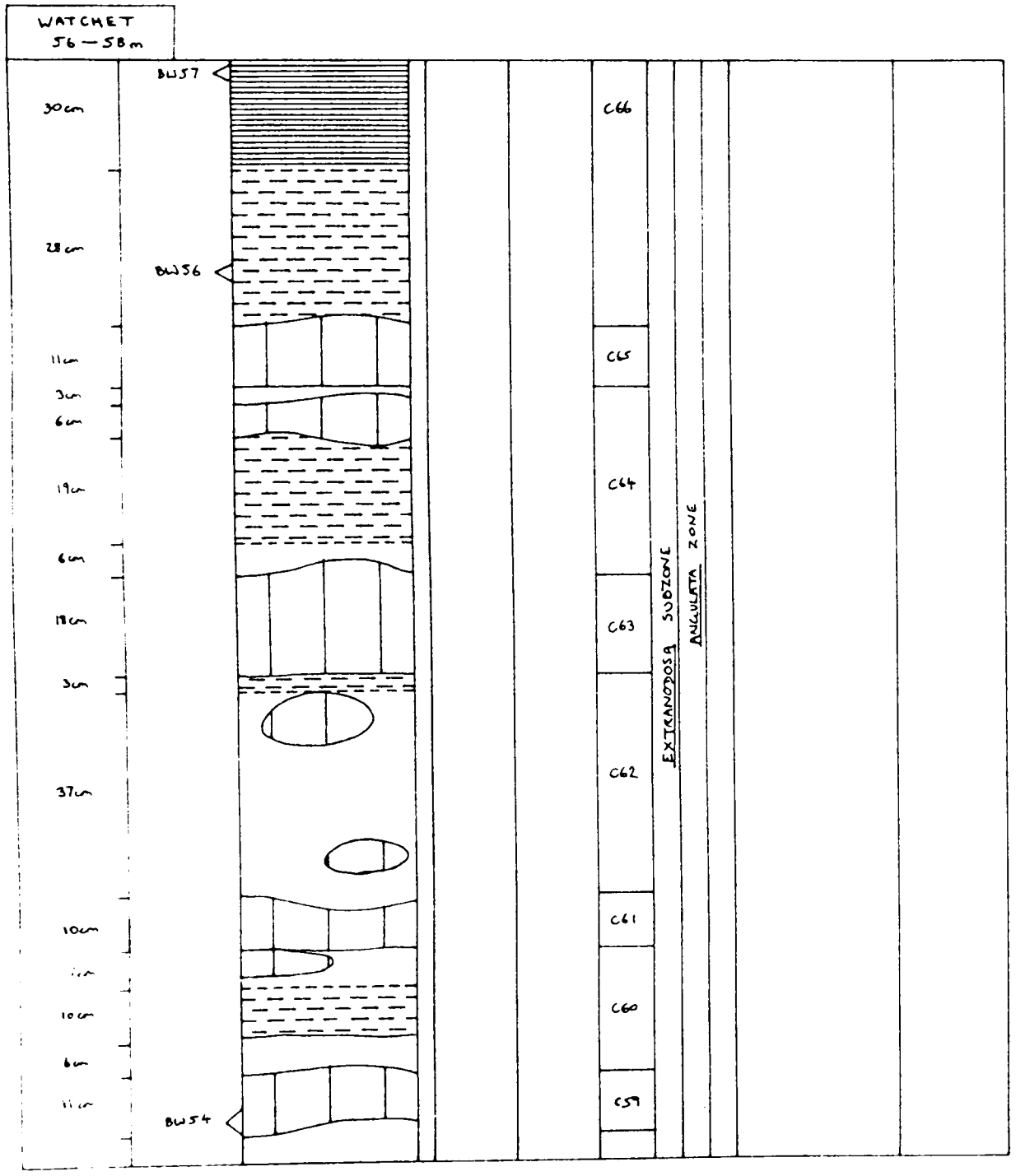
WATCHET
56 – 58m
BW57
BW56
BW54
30cm
28cm
11cm
3cm
6cm
19cm
6cm
18cm
3cm
37cm
10cm
10cm
6cm
11cm
C66
C65
C64
C63
C62
C61
C60
C59
EXTRANODOSA SUBZONE
ANGULATA ZONE

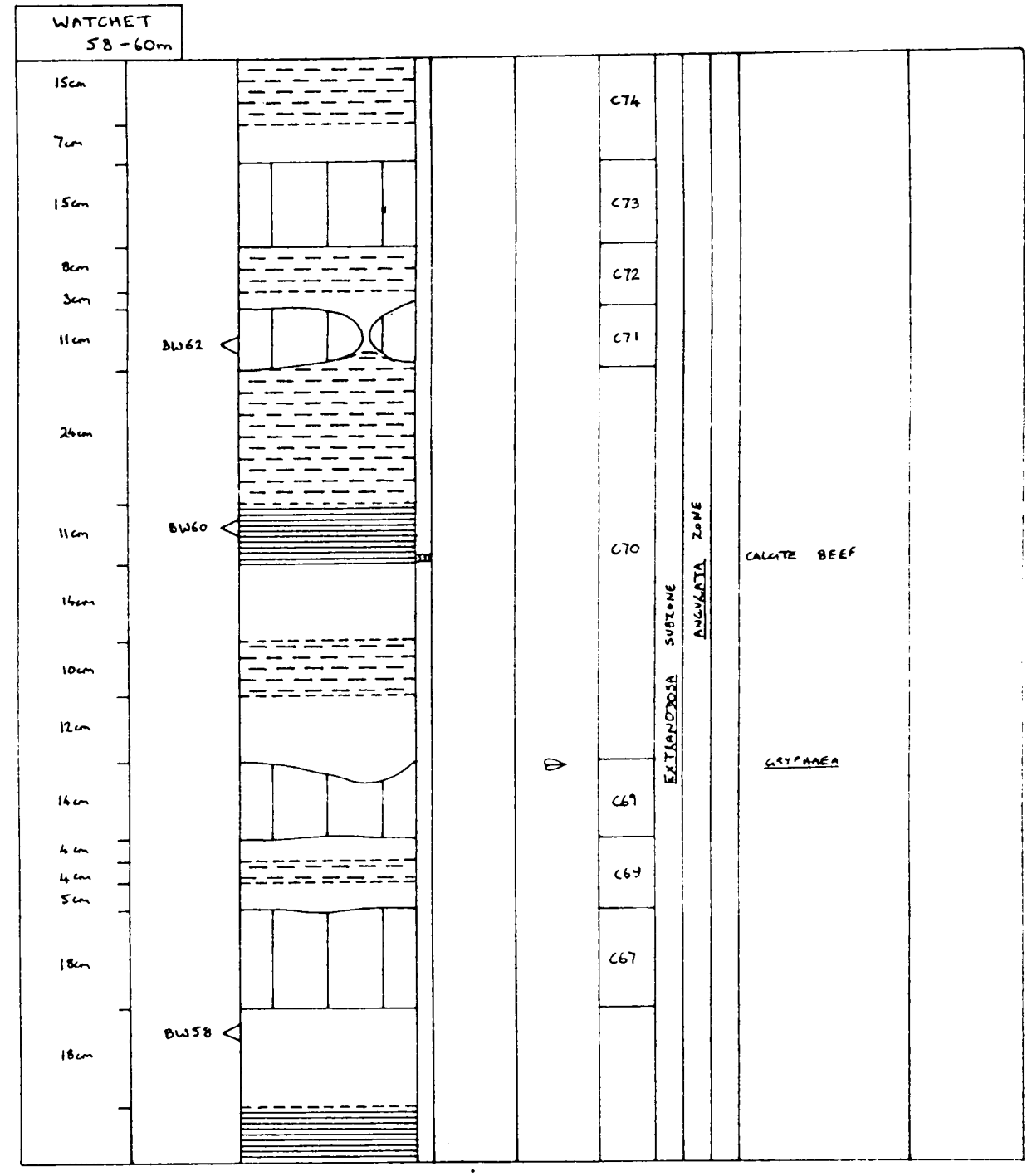
WATCHET
58 – 60m
BW62
BW60
BW58
15cm
7cm
15cm
8cm
3cm
11cm
24cm
11cm
14cm
10cm
12cm
14cm
4cm
4cm
5cm
18cm
18cm
C74
C73
C72
C71
C70
C69
C68
C67
EXTRANODOSA SUBZONE
ANGULATA ZONE
CALCITE BEEF
GREYAREA

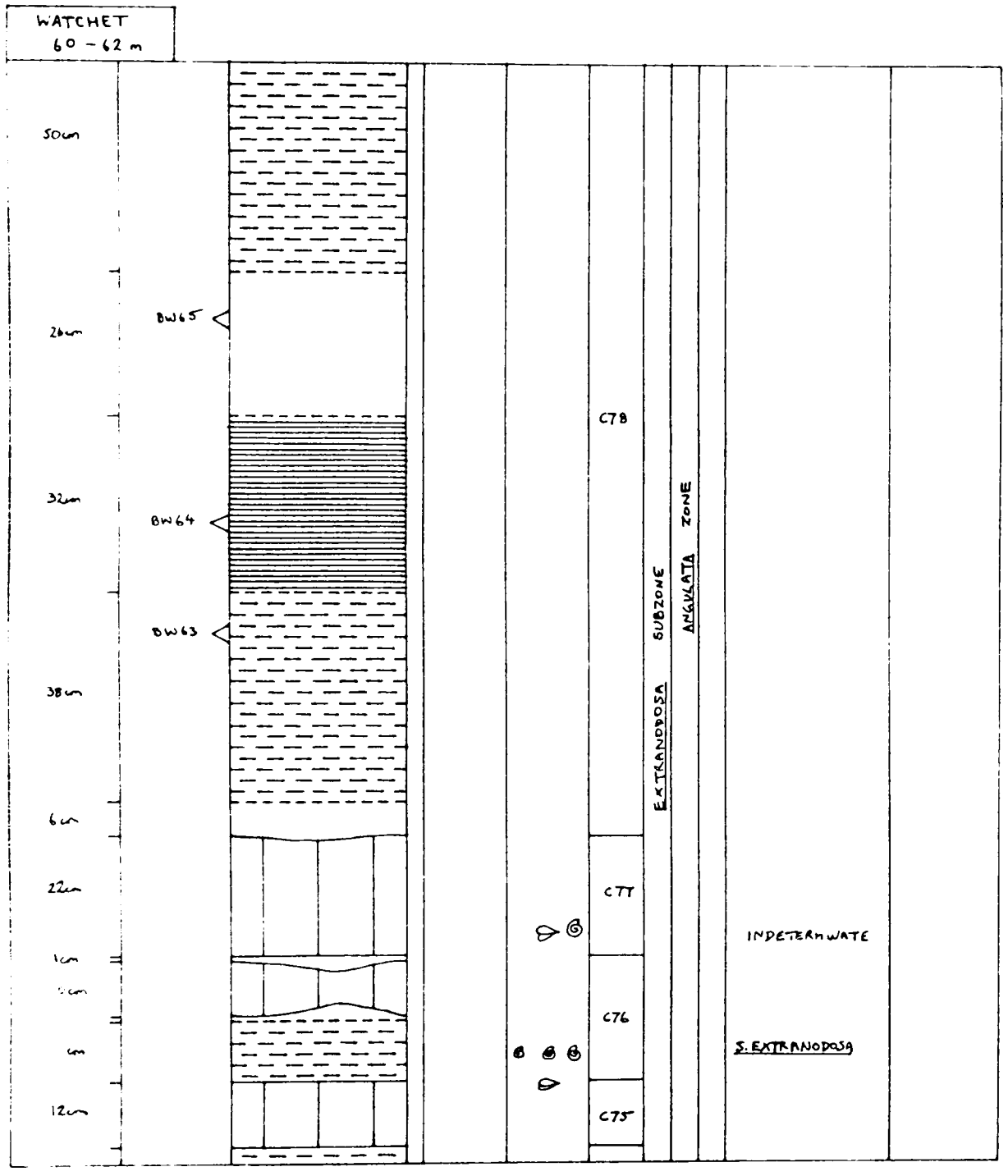
WATCHET
60 - 62 m
50cm
26cm
32cm
38cm
6cm
22cm
1cm
12cm
BW65
BW64
BW63
C78
C77
C76
C75
EXTRANODOSA SUBZONE
ANGULATA ZONE
INDETERMINATE
S. EXTRANODOSA

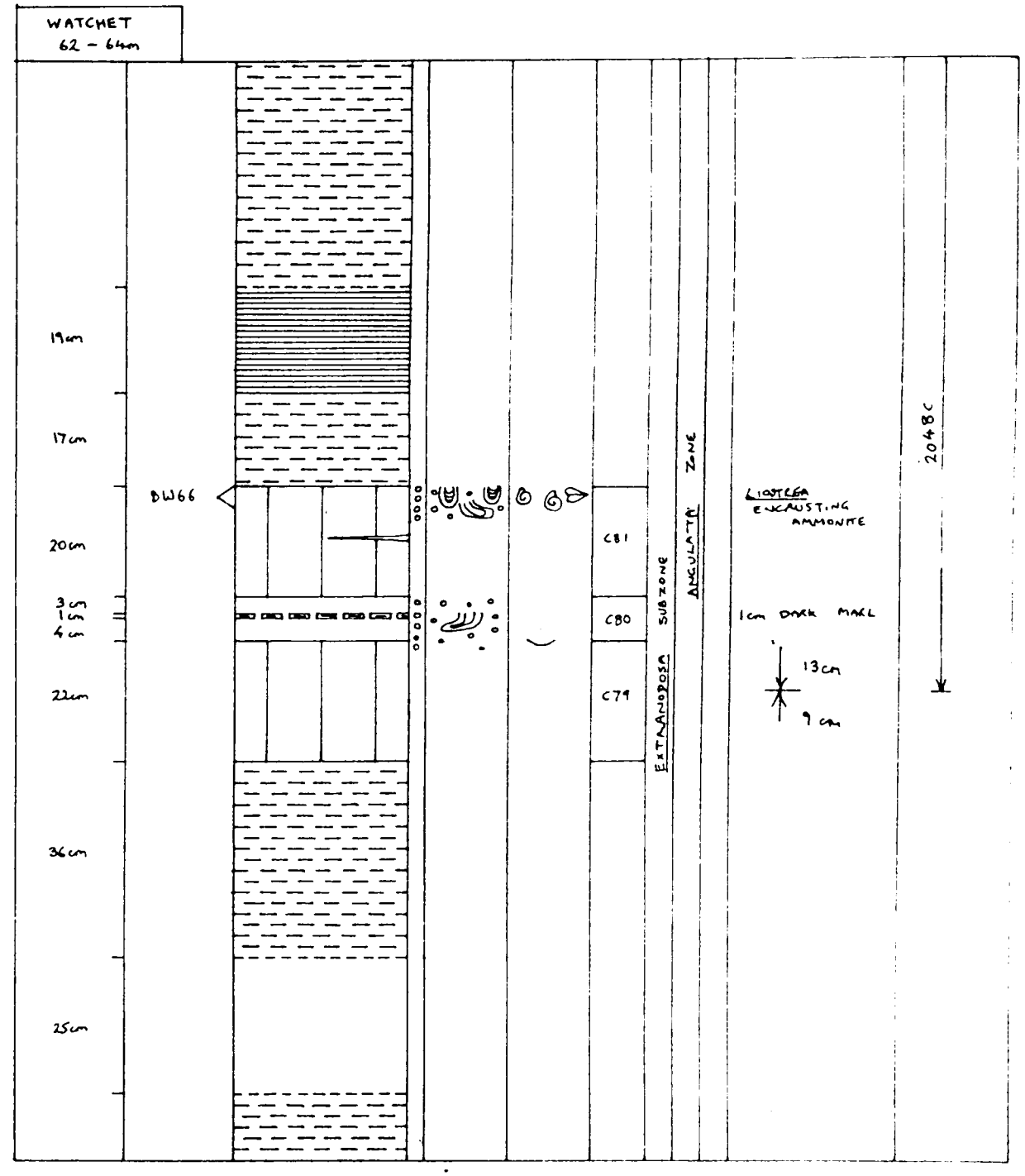
WATCHET
62 - 64m
19cm
17cm
20cm
3cm
1cm
4cm
22cm
36cm
25cm
BW66
C81
C80
C79
EXTRANODOSA SUBZONE
ANGULATA ZONE
LIOSTREA
ENCRUSTING
AMMONITE
1cm DARK MARL
13cm
9cm
2048C

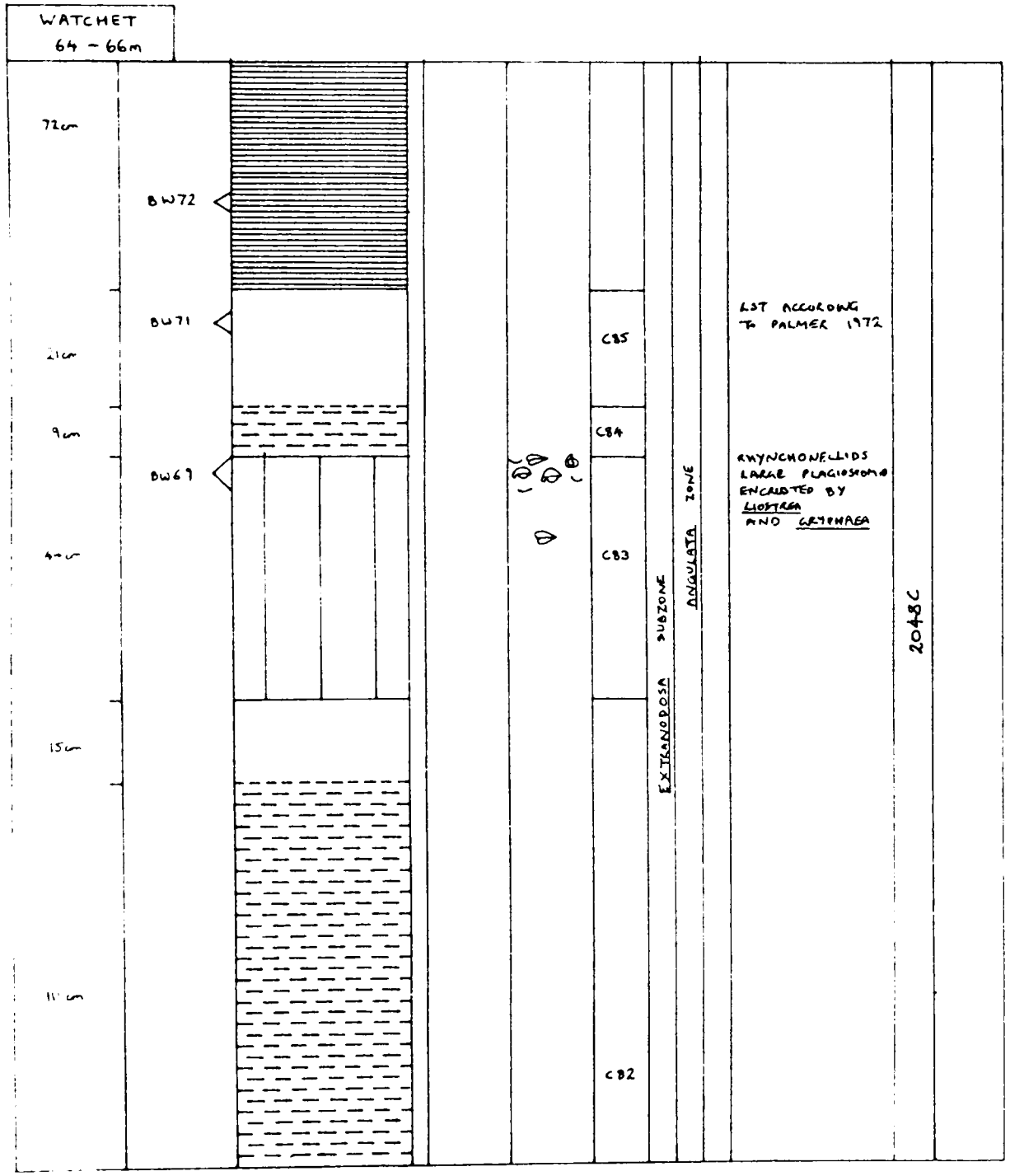
WATCHET
64 - 66m
72cm
BW72
BW71
21cm
9cm
BW69
40cm
15cm
11cm
C85
C84
C83
C82
EXTRANODOSA SUBZONE
ANGULATA ZONE
LOST ACCORDING TO PALMER 1972
RHYNCHONELLIDS LARGE PLAGIOSTOMA ENCRUSTED BY LIOSTREA AND GRYPHAEA
2048C

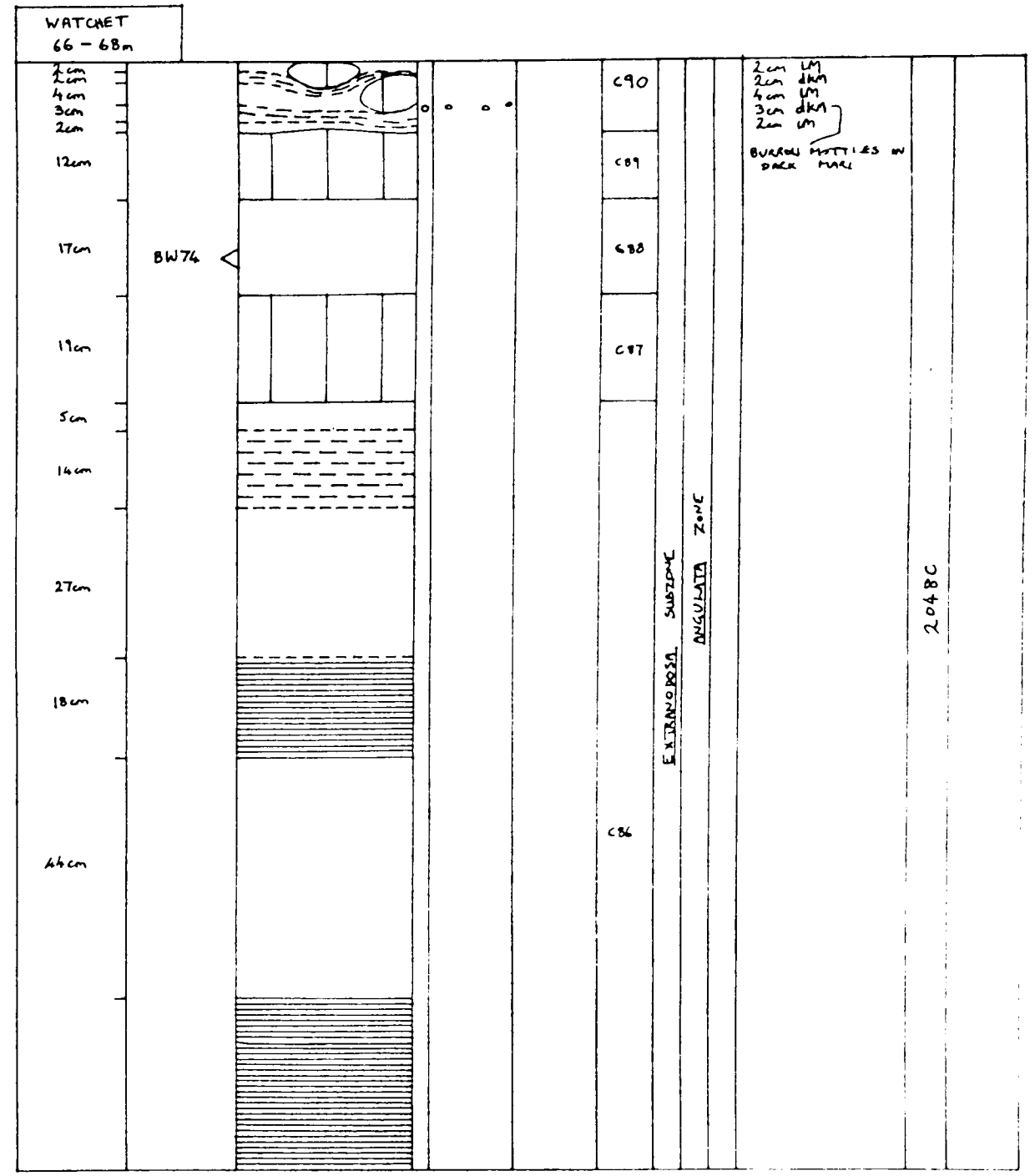
WATCHET
66 - 68m
2cm
2cm
4cm
3cm
2cm
12cm
17cm
19cm
5cm
14cm
27cm
18cm
44cm
BW74
C90
C89
C88
C87
C86
EXTRANODOSA SUBZONE
ANGULATA ZONE
2cm LM
2cm dkM
4cm LM
3cm dkM
2cm LM
BURROW MOTTLES IN DARK MARL
2048C

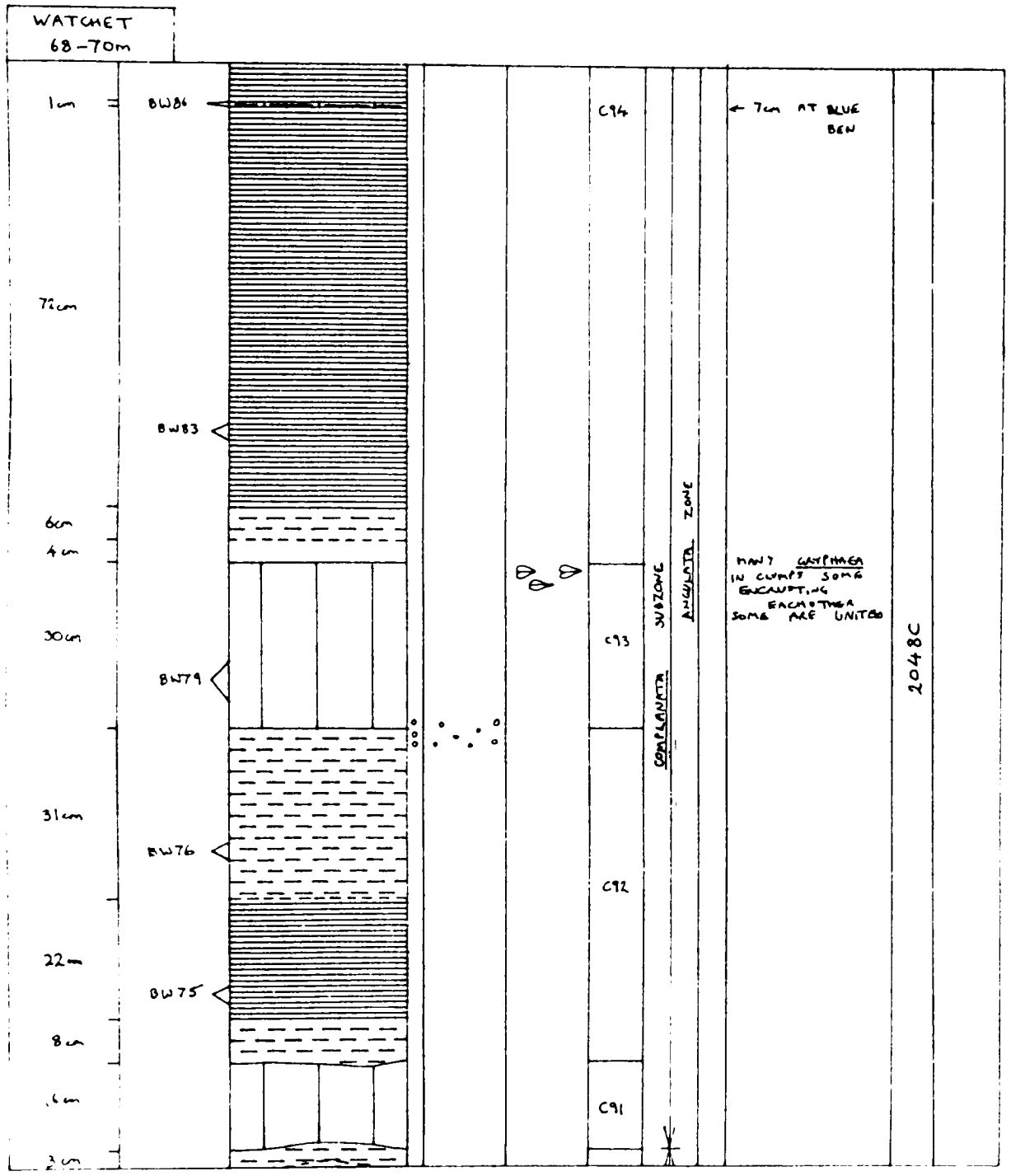
WATCHET
68-70m
1cm
BW86
72cm
BW83
6cm
4cm
30cm
BW79
31cm
BW76
22cm
BW75
8cm
.6cm
C94
C93
C92
C91
SUBZONE
COMPLANATA
ANGULATA ZONE
← 7cm AT BLUE BEN
MANY GRYPHAEA IN CLUMPS SOME ENCRUSTING EACH OTHER SOME ARE UNITED
2048C

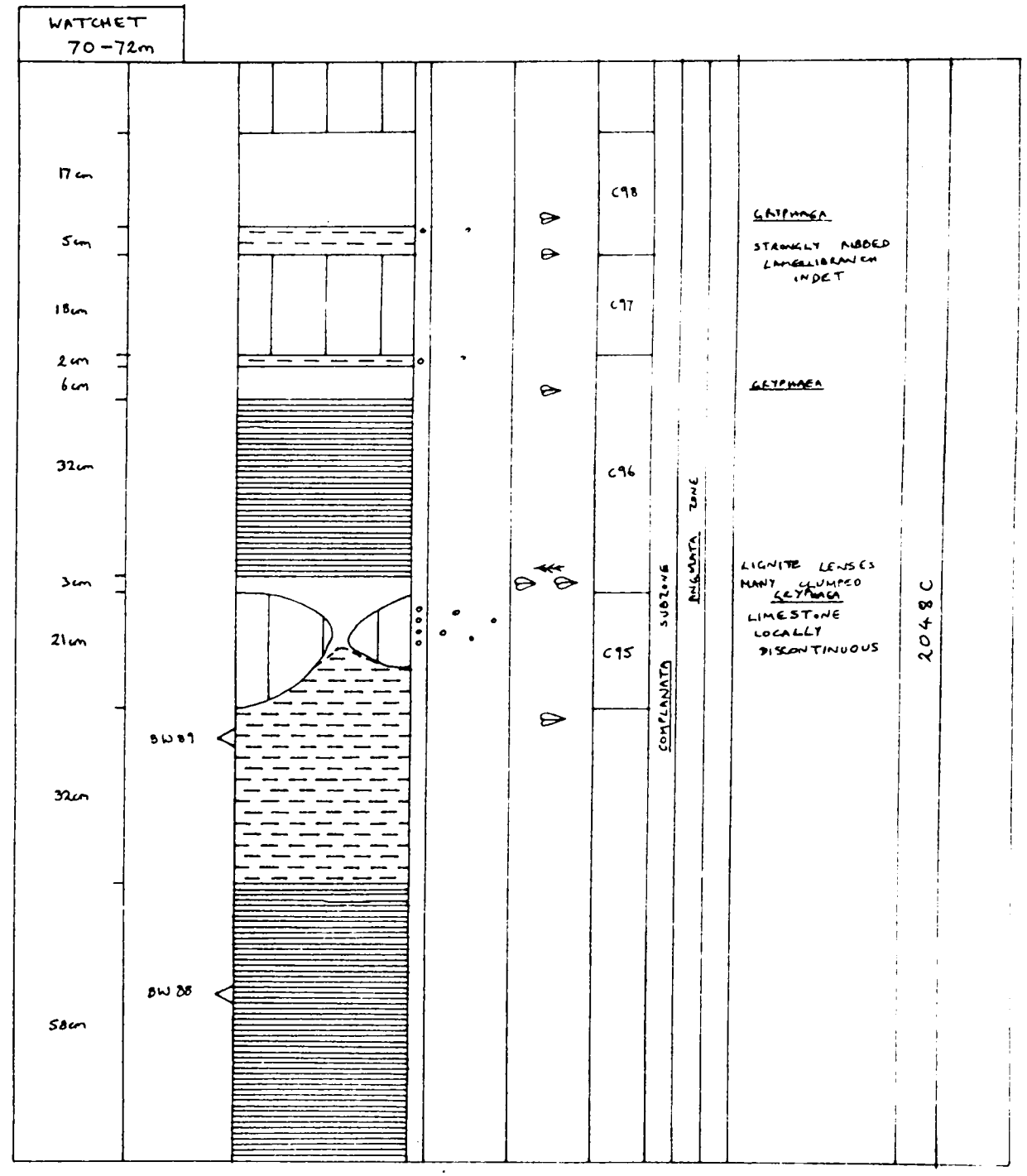
WATCHET
70-72m
17cm
5cm
18cm
2cm
6cm
32cm
3cm
21cm
BW89
32cm
BW88
58cm
C98
C97
C96
C95
SUBZONE
COMPLANATA
ANGULATA ZONE
GRYPHAEA
STRONGLY RIBBED LAMELLIBRANCH INDET
GRYPHAEA
LIGNITE LENSES
MANY CLUMPED GRYPHAEA
LIMESTONE LOCALLY DISCONTINUOUS
2048C

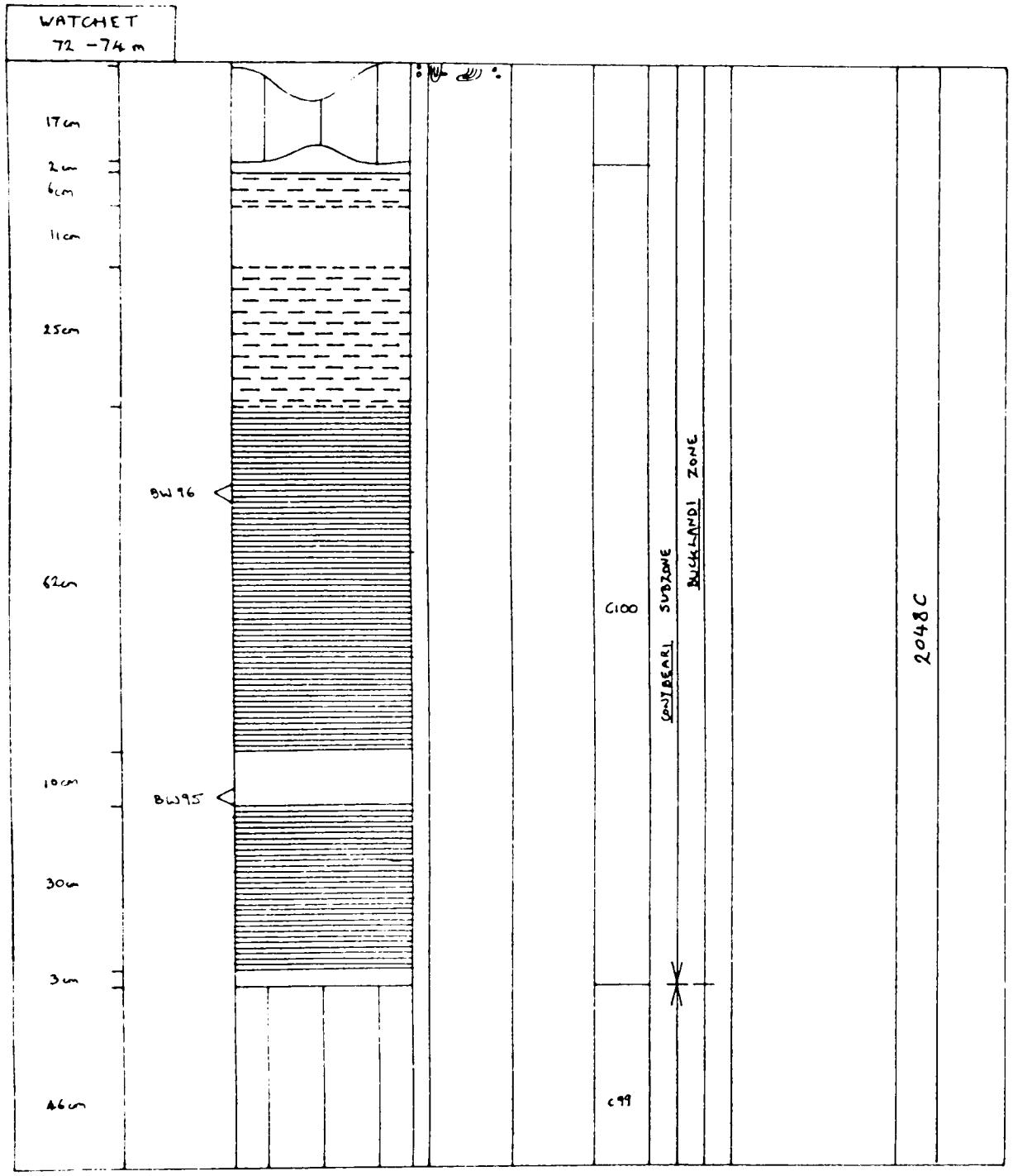
WATCHET
72 - 74 m
17cm
2cm
6cm
11cm
25cm
62cm
10cm
30cm
3cm
46cm
BW96
BW95
C100
C99
CONYBEARI SUBZONE
BUCKLANDI ZONE
2048C

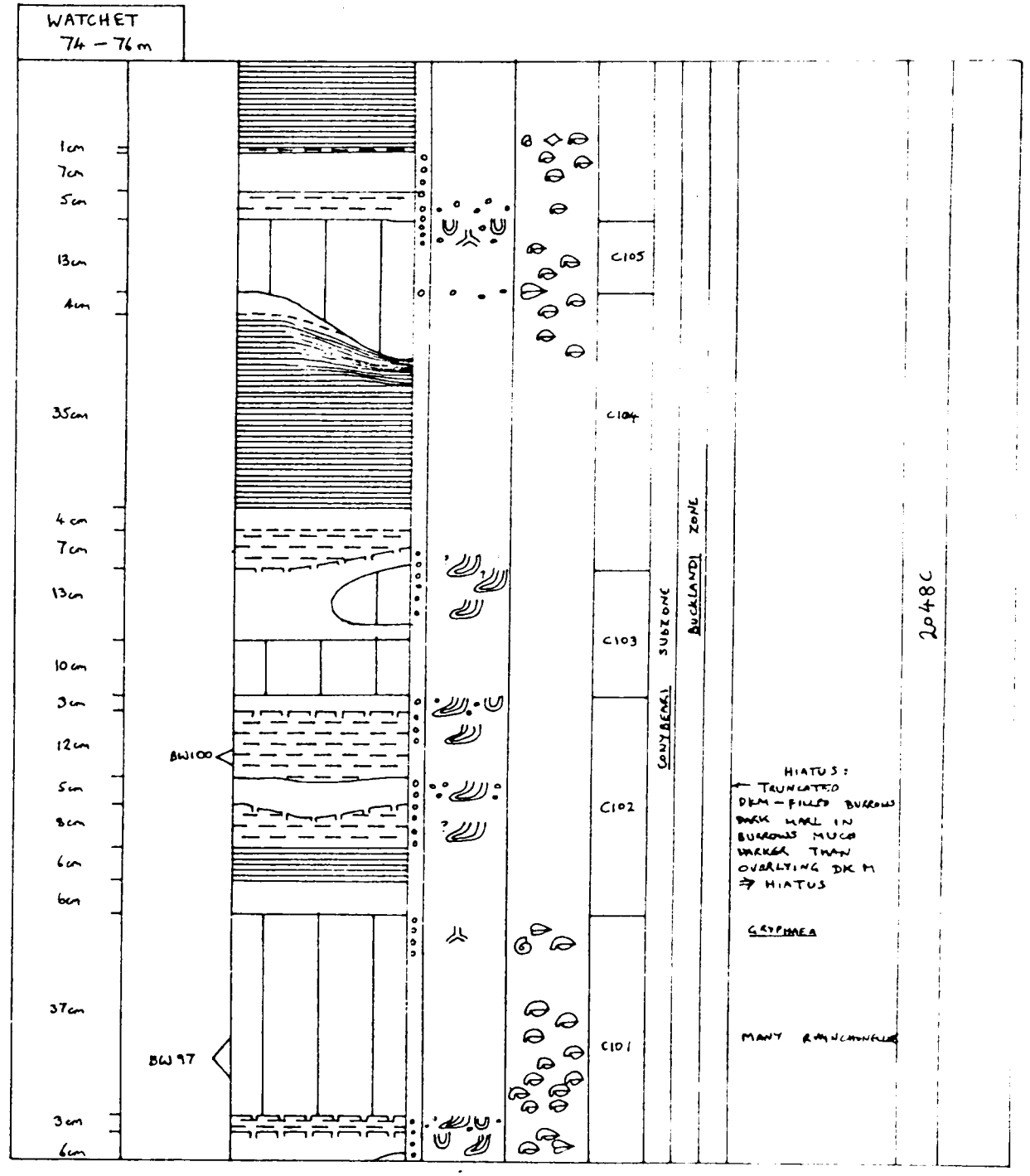
WATCHET
74 - 76 m
1cm
7cm
5cm
13cm
4cm
35cm
4cm
7cm
13cm
10cm
3cm
12cm
5cm
8cm
6cm
6cm
37cm
3cm
6cm
BW100
BW97
C105
C104
C103
C102
C101
CONYBEARI SUBZONE
BUCKLANDI ZONE
2048C
HIATUS:
← TRUNCATED
DKM-FILLED BURROWS
DARK MARL IN
BURROWS MUCH
DARKER THAN
OVERLYING DK M
⇒ HIATUS
GRYPHAEA
MANY RHYNCHONELLID

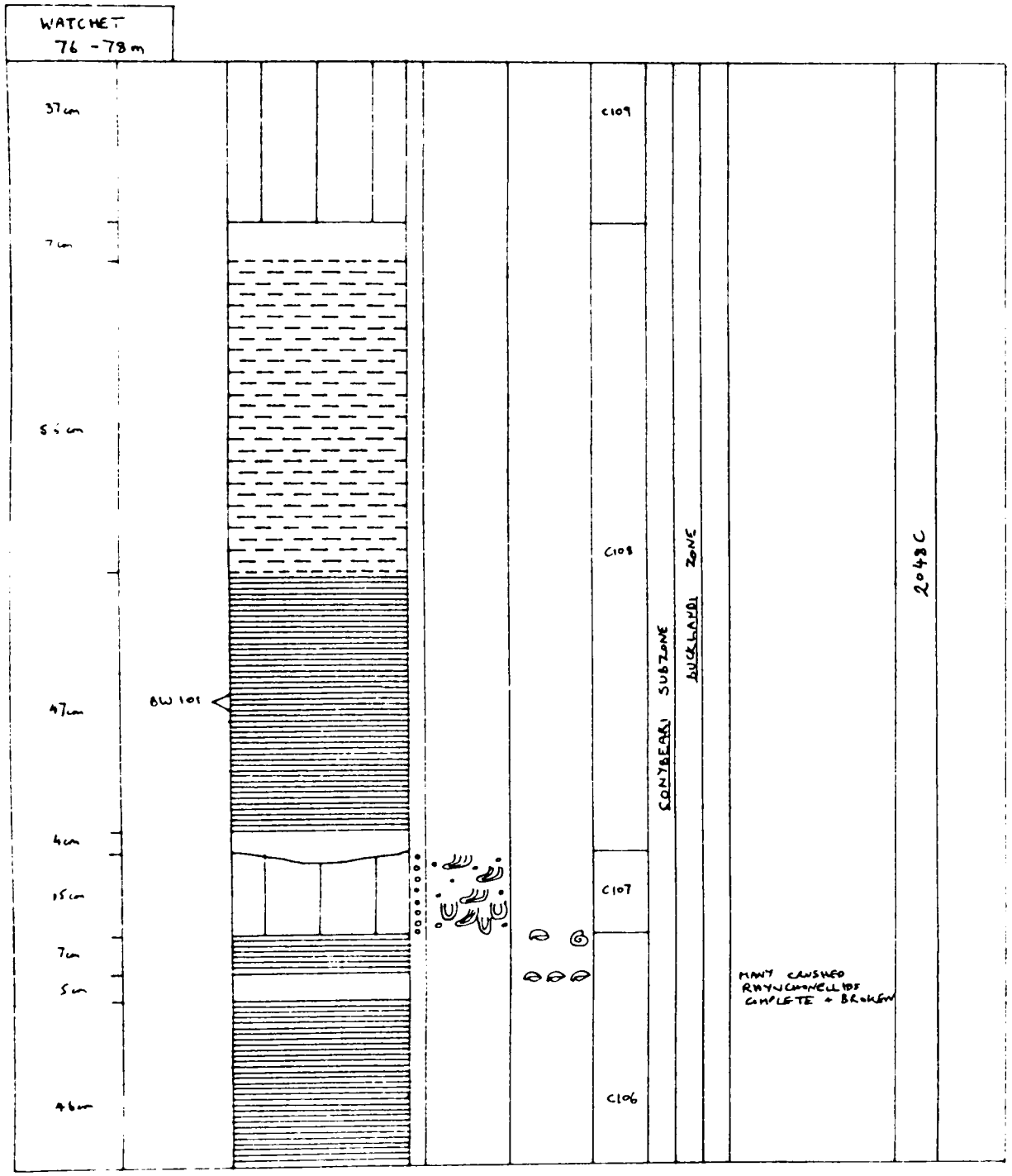
WATCHET
76 - 78 m
37cm
7cm
5cm
47cm
4cm
15cm
7cm
5cm
46cm
BW 101
C109
C108
C107
C106
CONYBEARI SUBZONE
AUCKLANDI ZONE
2048C
MANY CRUSHED
RHYNCHONELLIDS
COMPLETE + BROKEN

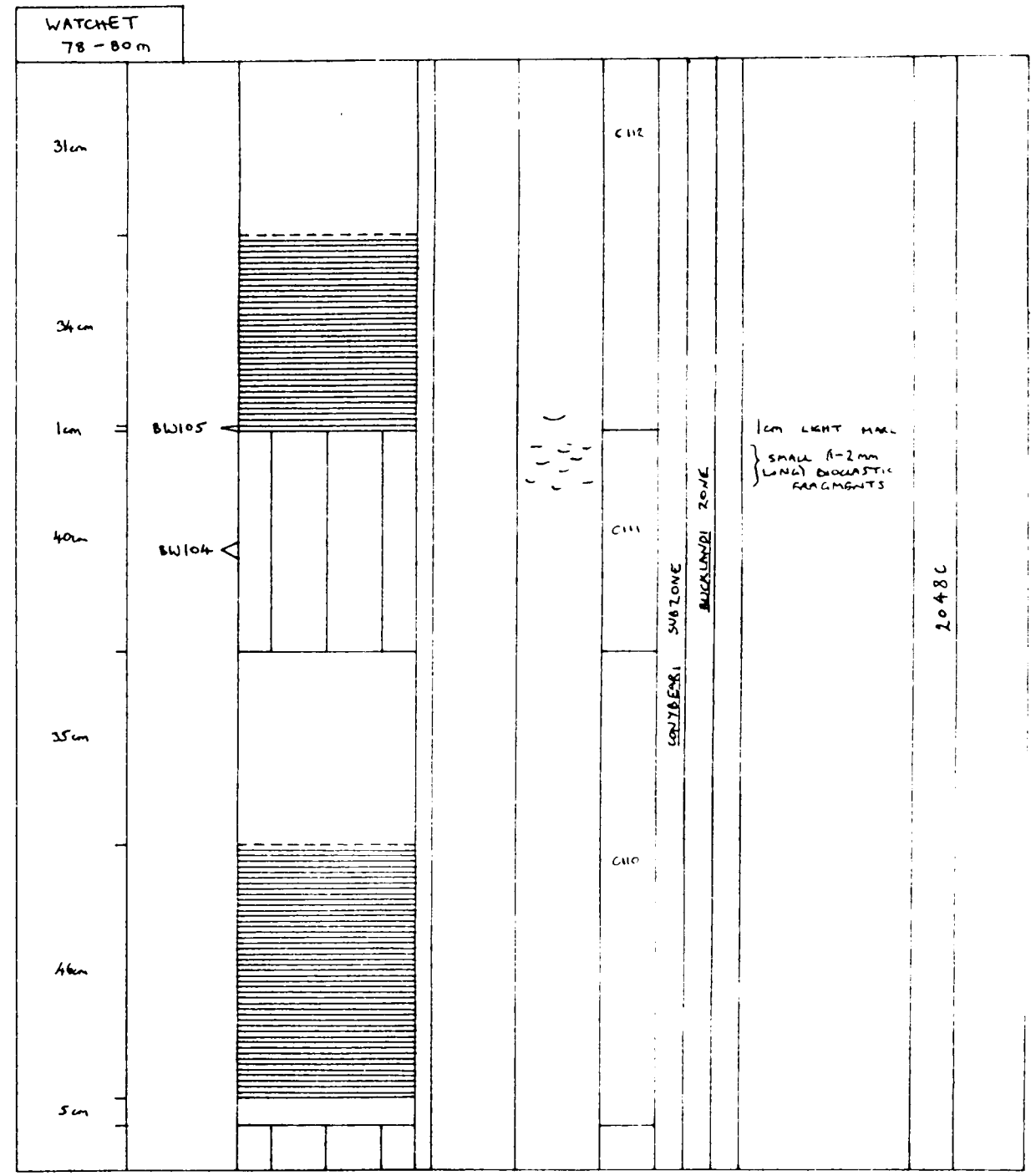
WATCHET
78 - 80 m
31cm
34cm
1cm
40cm
35cm
46cm
5cm
BW105
BW104
C112
C111
C110
CONYBEARI SUBZONE
AUCKLANDI ZONE
1cm LIGHT MARL
SMALL 1-2mm
LONG BIOCLASTIC
FRAGMENTS
2048C

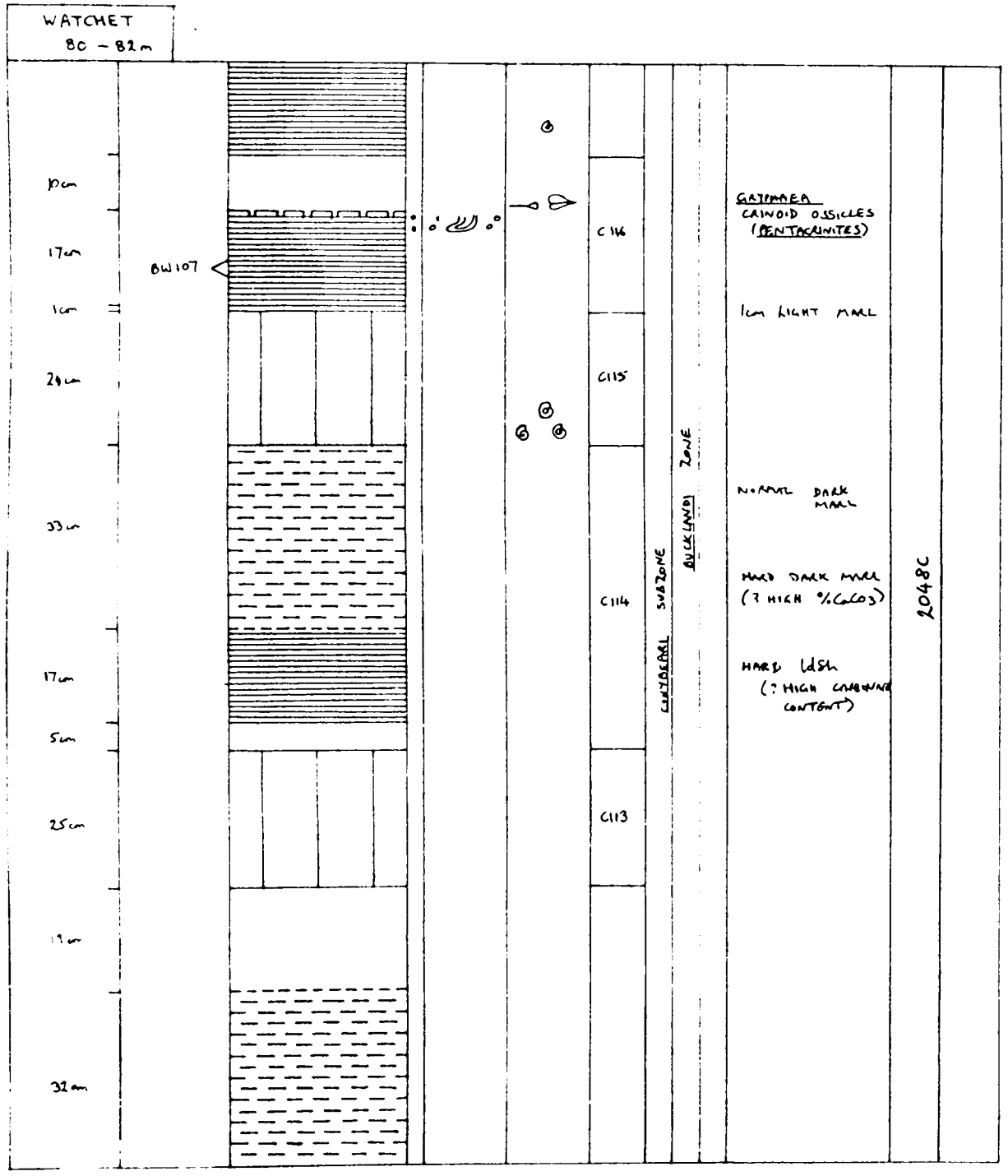
WATCHET
80 - 82m
BW107
C116
C115
C114
C113
CONYBEARI SUBZONE
BUCKLANDI ZONE
GRYPHAEA
CRINOID OSSICLES
(PENTACRINITES)
1cm LIGHT MARL
NODULE DARK MARL
HARD DARK MARL
(? HIGH % CaCO3)
HARD LdSh
(? HIGH CARBONATE CONTENT)
2048C

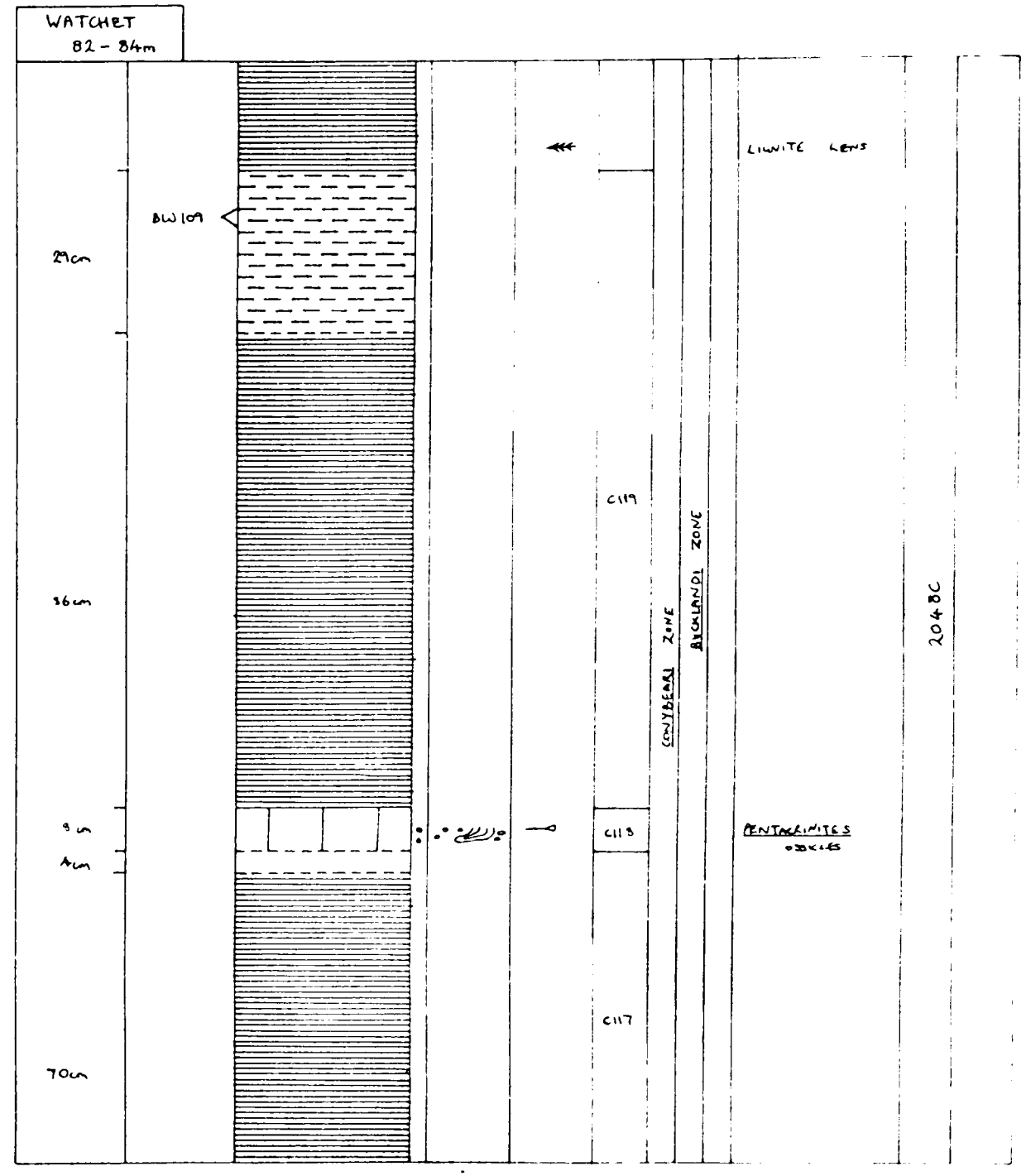
WATCHET
82 - 84m
BW109
C119
C118
C117
CONYBEARI ZONE
BUCKLANDI ZONE
LIGNITE LENS
PENTACRINITES
OSSICLES
2048C

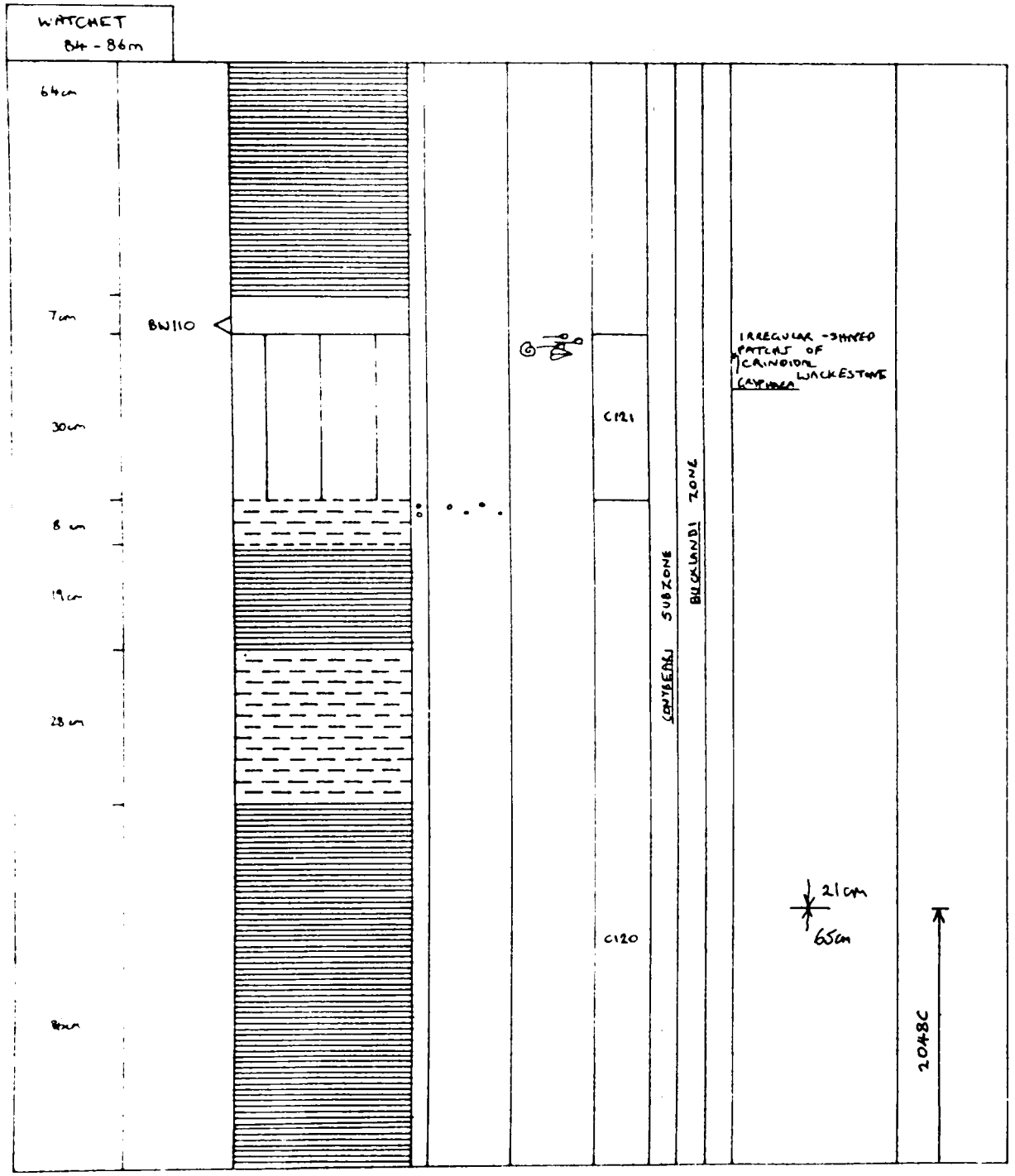
WATCHET
84 - 86m
64cm
7cm
30cm
8cm
19cm
28cm
8cm
BW110
C121
C120
CONTBEDAL SUBZONE
BUCKLANDI ZONE
IRREGULAR-SHAPED PATCHES OF CALNIOIDE WACKESTONE
21cm
65cm
2048C

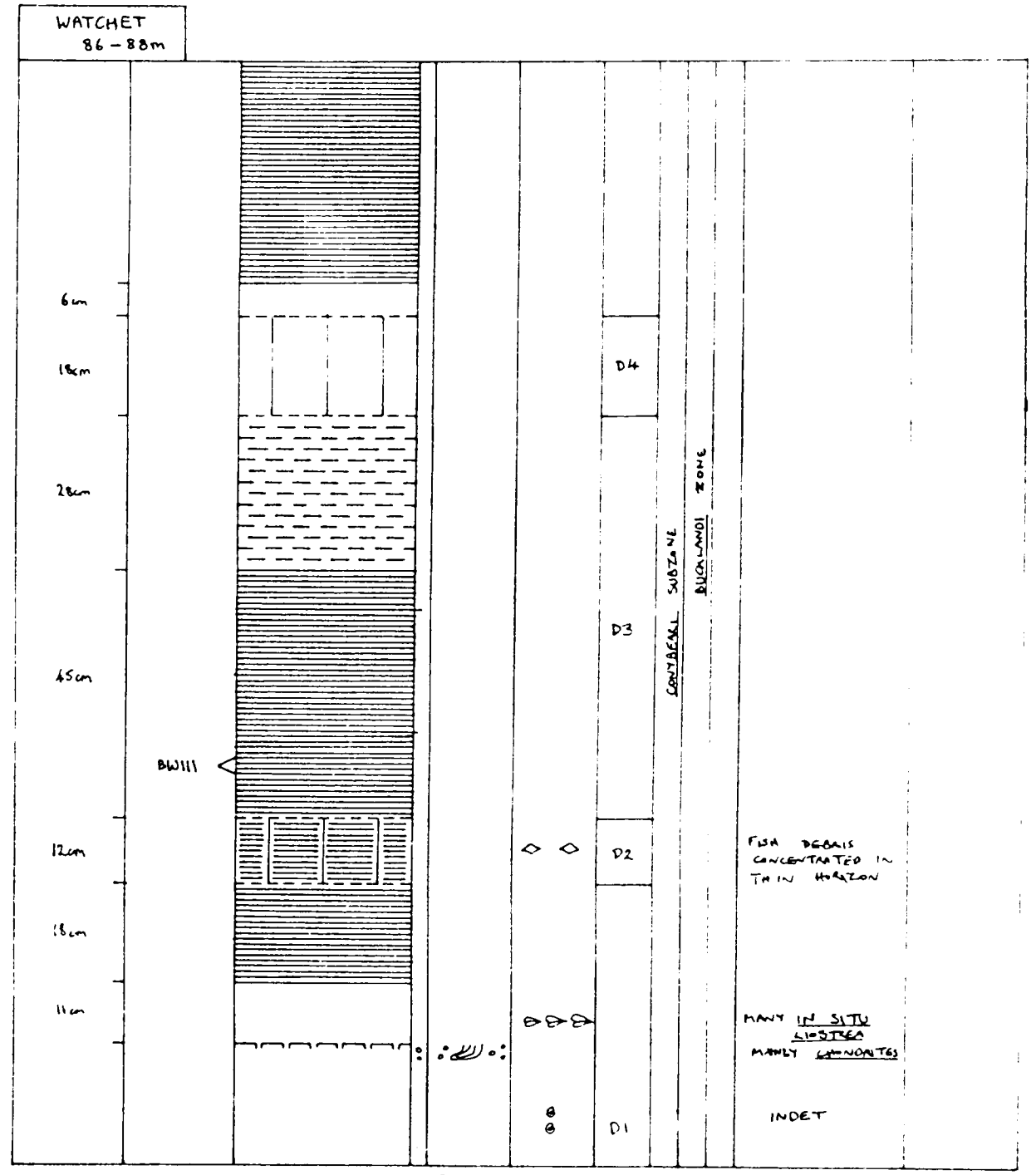
WATCHET
86 - 88m
6cm
19cm
28cm
45cm
12cm
18cm
11cm
BW111
D4
D3
D2
D1
CONTBEDAL SUBZONE
BUCKLANDI ZONE
FISH DEBRIS CONCENTRATED IN THIN HORIZON
MANY IN SITU LIOSTREA
MAINLY CALNIOIDES
INDET

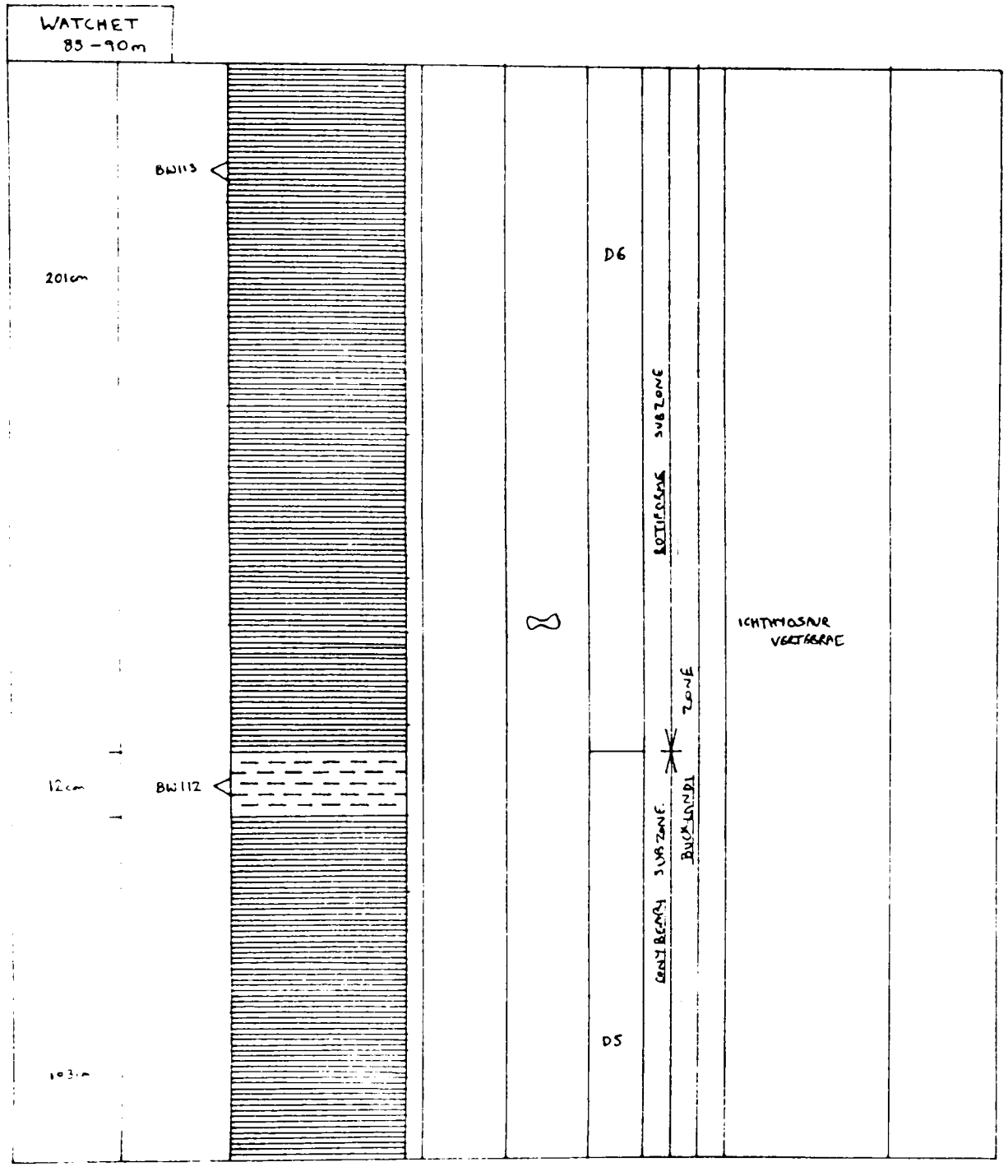
WATCHET
89 – 90m
BW113
201cm
D6
ROTIFORME SUBZONE
ICHTHYOSAUR VERTEBRAE
ZONE
12cm
BW112
BUCKLANDI
CONY BEARY SUBZONE
D5
103cm

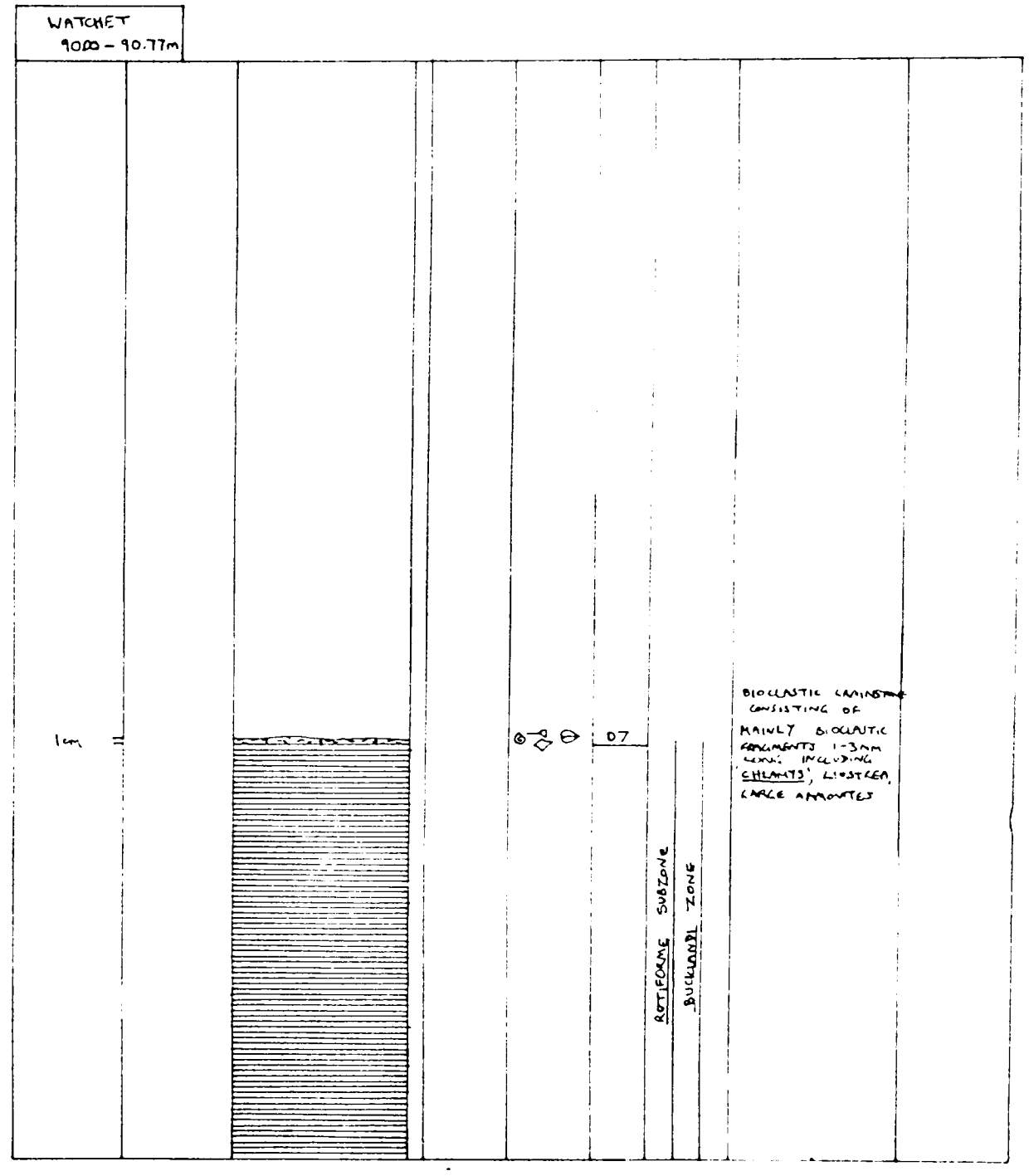
WATCHET
90.00 – 90.77m
1cm
D7
BIOCLASTIC LIMESTONE CONSISTING OF MAINLY BIOCLASTIC FRAGMENTS 1-3mm CONT. INCLUDING 'CHEMATS', LIOSTREA, LARGE AMMONITES
ROTIFORME SUBZONE
BUCKLANDI ZONE

2.3 Stratigraphic log for the basal Lias at Lavernock Point.

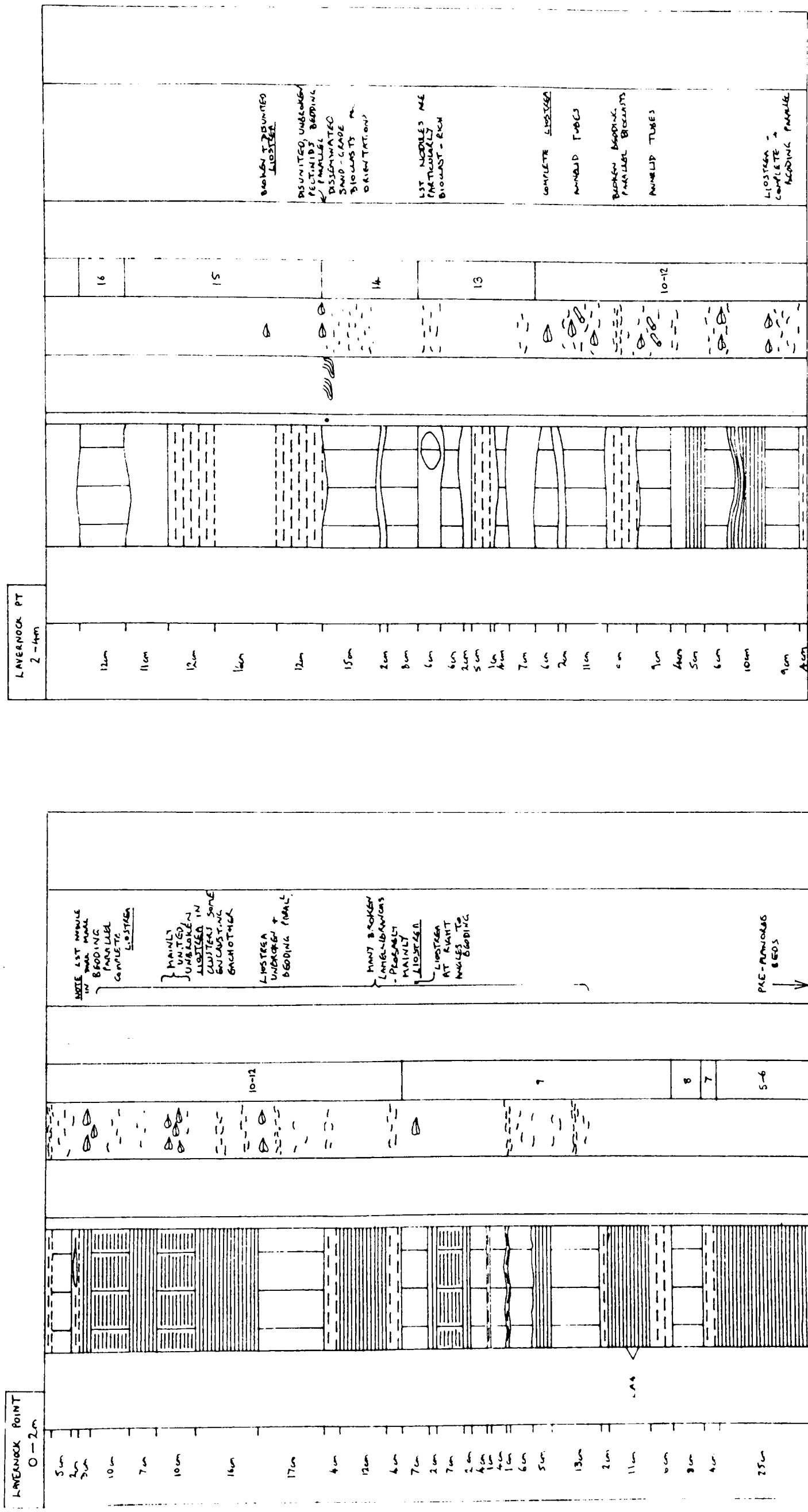

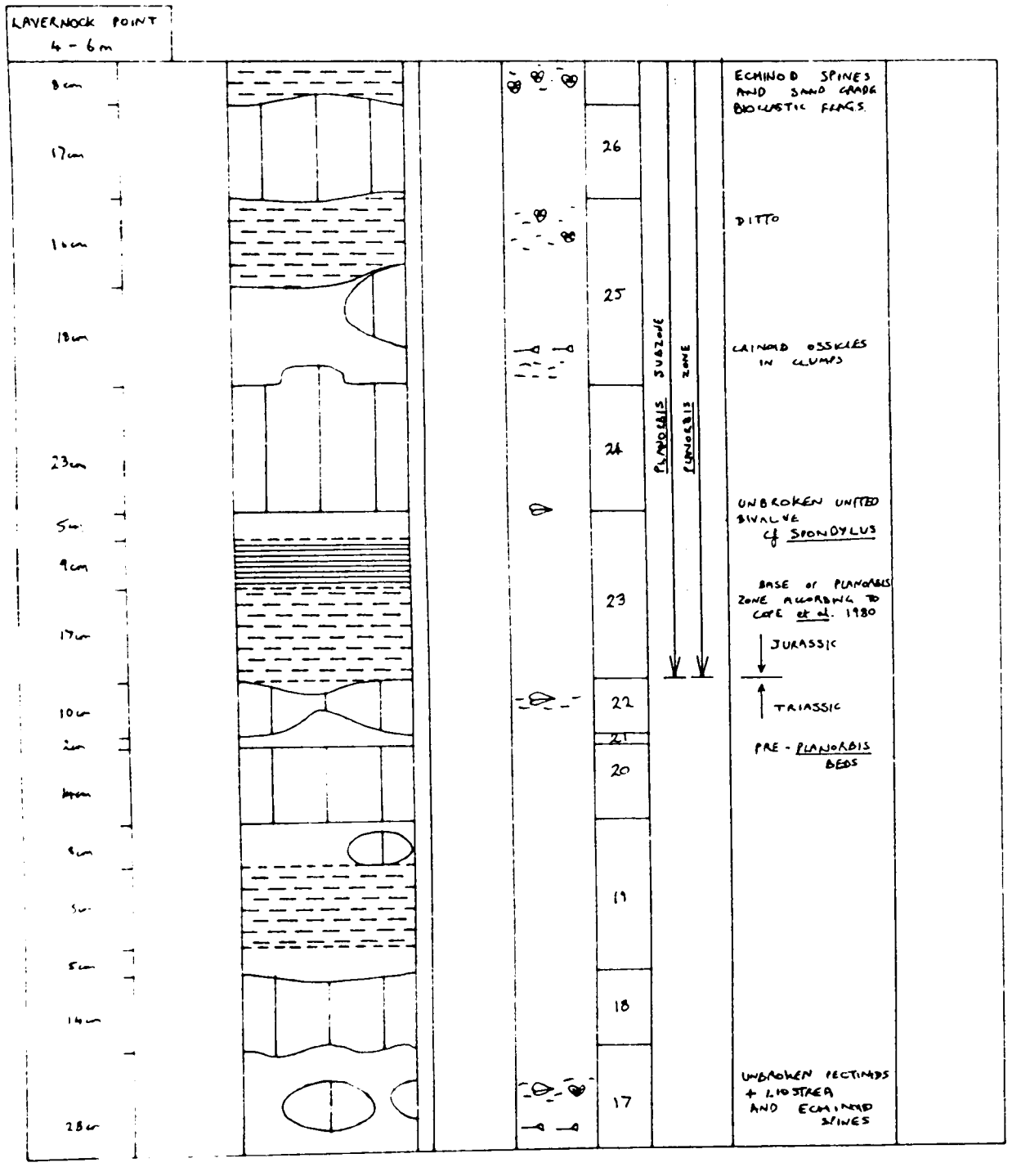
LAVERNOCK POINT
4 - 6m
8cm
17cm
16cm
18cm
23cm
5cm
9cm
17cm
10cm
2cm
4cm
9cm
5cm
5cm
14cm
28cm
26
25
24
23
22
21
20
19
18
17
PLANORBIS SUBZONE
PLANORBIS ZONE
ECHINOID SPINES AND SAND GRADE BIOCLASTIC FRAGS.
DITTO
CRINOID OSSICLES IN CLUMPS
UNBROKEN UNITED BIVALVE cf SPONDYLUS
BASE OF PLANORBIS ZONE ACCORDING TO COPE et al. 1980
JURASSIC
TRIASSIC
PRE - PLANORBIS BEDS
UNBROKEN PECTINIDS + LIOSTREA AND ECHINOID SPINES

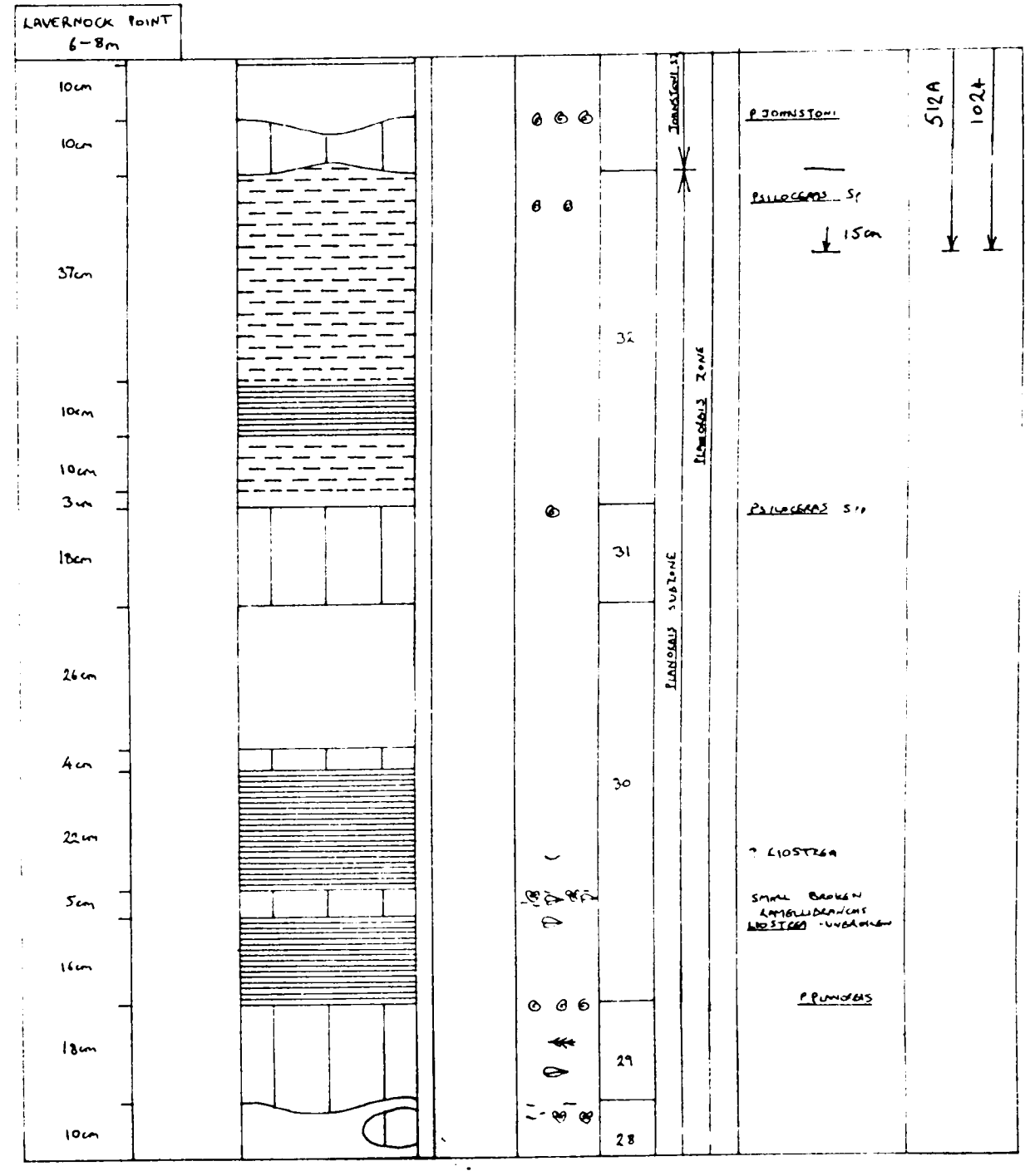
LAVERNOCK POINT
6-8m
10cm
10cm
37cm
10cm
10cm
3cm
18cm
26cm
4cm
22cm
5cm
16cm
18cm
10cm
32
31
30
29
28
JOHNSTONI
PLANORBIS SUBZONE
PLANORBIS ZONE
P. JOHNSTONI
PSILOCERAS Sp
15cm
PSILOCERAS Sp
? LIOSTREA
SMALL BROKEN RAMOLLIBRANCHS
LIOSTREA - UNBROKEN
P. PLANORBIS
512A
1024+

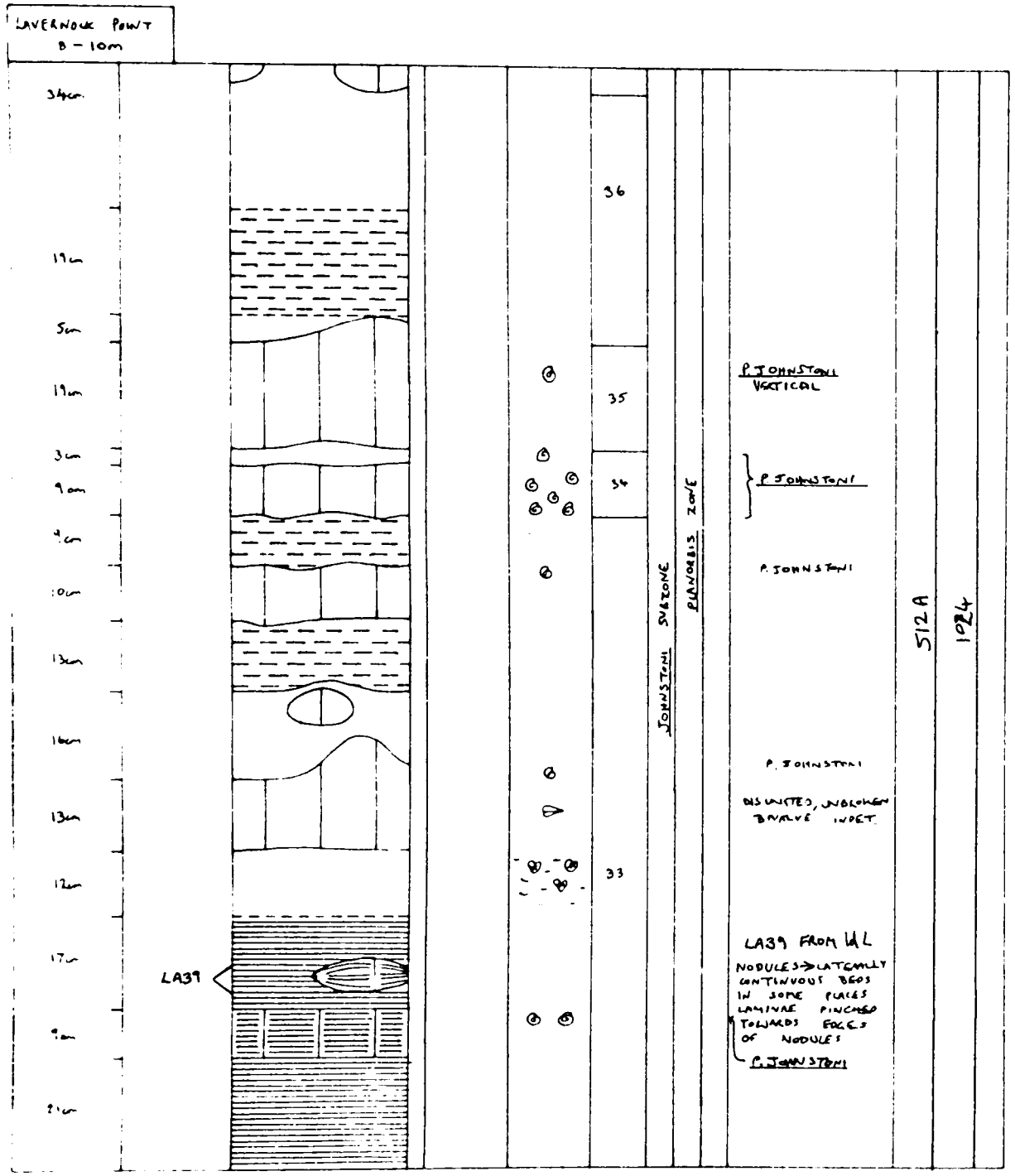
LAVERNOCK POINT
8 – 10m
34cm
19cm
5cm
19cm
3cm
9cm
4cm
10cm
13cm
16cm
13cm
12cm
17cm
9cm
21cm
LA39
36
35
34
33
JOHNSTONI SUBZONE
PLANORBIS ZONE
P. JOHNSTONI
VERTICAL
P. JOHNSTONI
P. JOHNSTONI
P. JOHNSTONI
DISUNITED, UNBROKEN BIVALVE INDET.
LA39 FROM W L
NODULES → LATERALLY CONTINUOUS BEDS IN SOME PLACES LAMINAE PINCHED TOWARDS FACES OF NODULES
P. JOHNSTONI
512A
1024

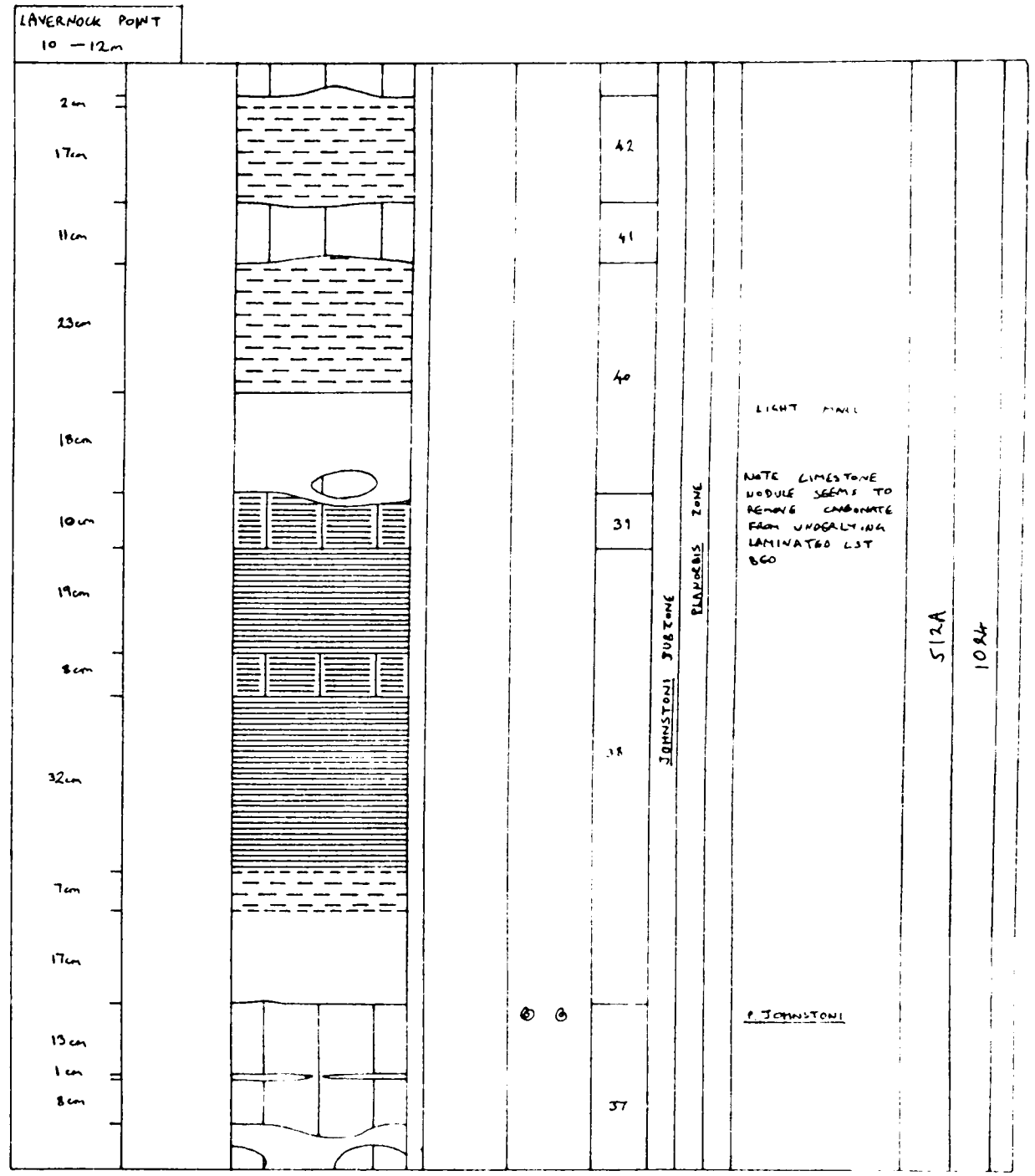
LAVERNOCK POINT
10 – 12m
2m
17cm
11cm
23cm
18cm
10cm
19cm
8cm
32cm
7cm
17cm
13cm
1cm
8cm
42
41
40
39
38
37
JOHNSTONI SUBZONE
PLANORBIS ZONE
LIGHT MARL
NOTE LIMESTONE NODULE SEEMS TO REMOVE CARBONATE FROM UNDERLYING LAMINATED LST BED
P. JOHNSTONI
512A
1024

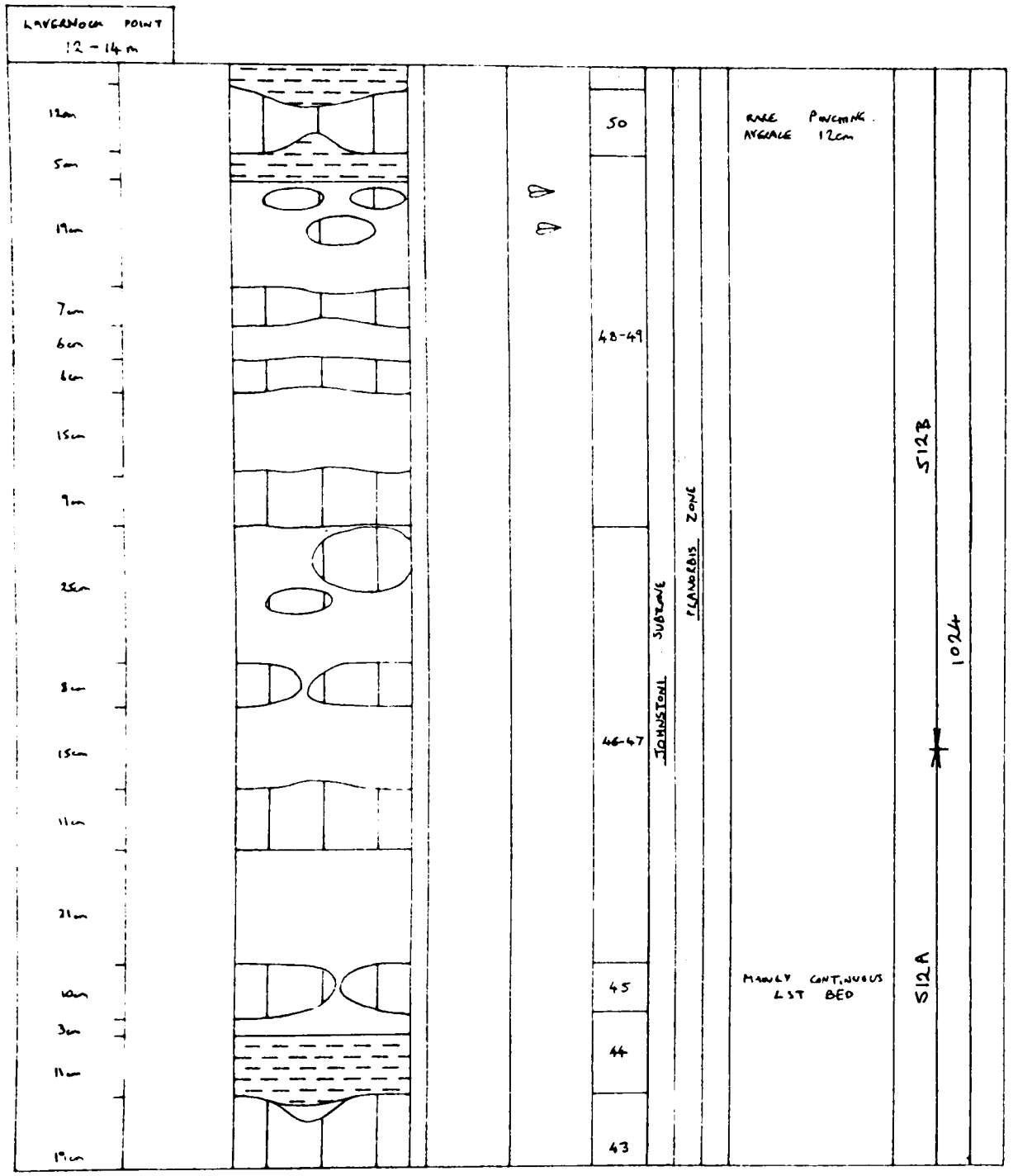
LAVERNOCK POINT
12 - 14 m
12cm
5cm
19cm
7cm
6cm
6cm
15cm
9cm
25cm
8cm
15cm
11cm
21cm
10cm
3cm
11cm
19cm
50
48-49
46-47
45
44
43
SUBZONE
JOHNSTONI
PLANORBIS ZONE
RARE PYCNOMK.
AVERAGE 12cm
MANLY CONTINUOUS
LST BED
512A
512B
1024

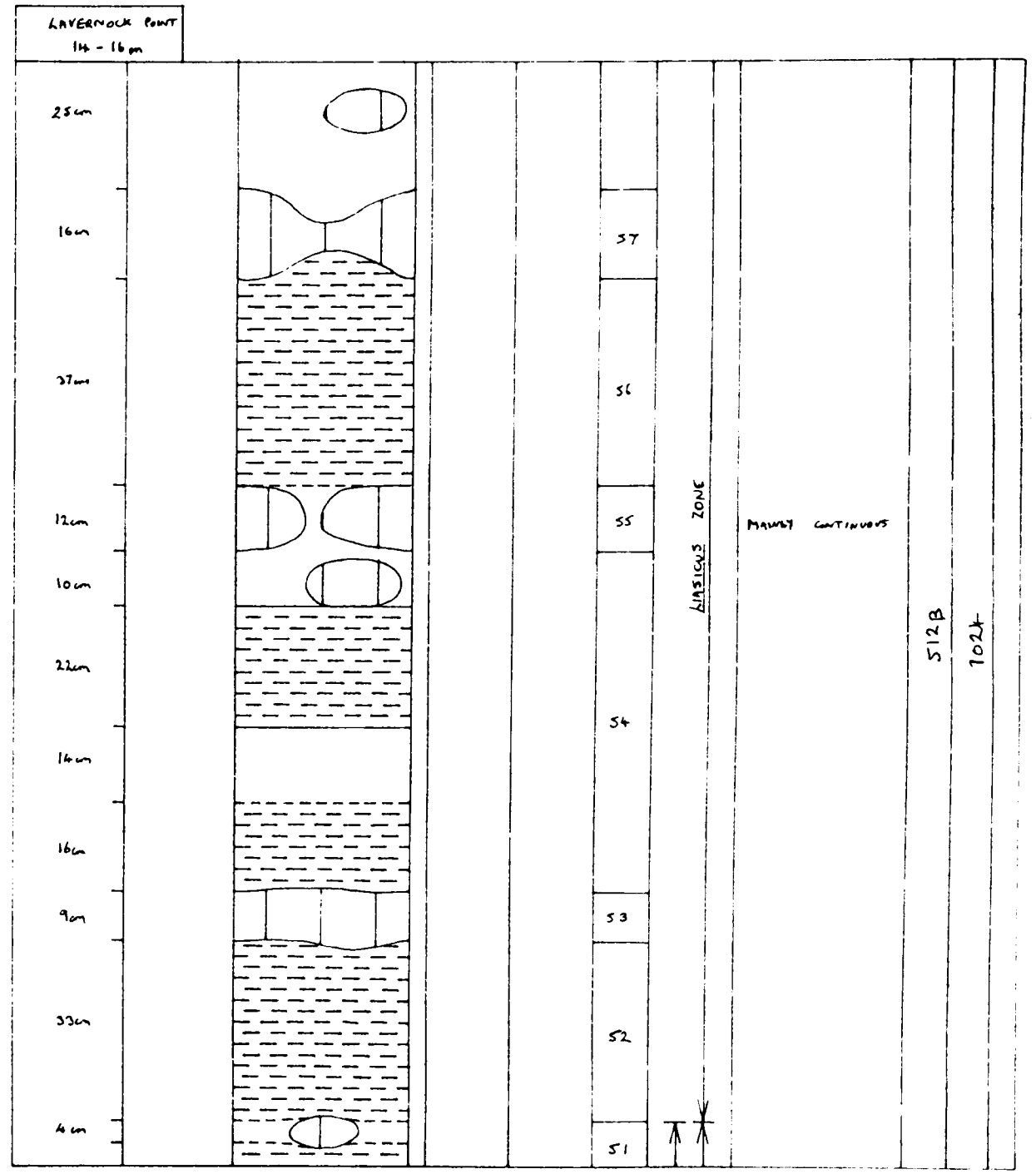
LAVERNOCK POINT
14 - 16 m
25cm
16cm
37cm
12cm
10cm
22cm
14cm
16cm
9cm
33cm
4cm
57
56
55
54
53
52
51
LIMSICUS ZONE
MANLY CONTINUOUS
512B
1024

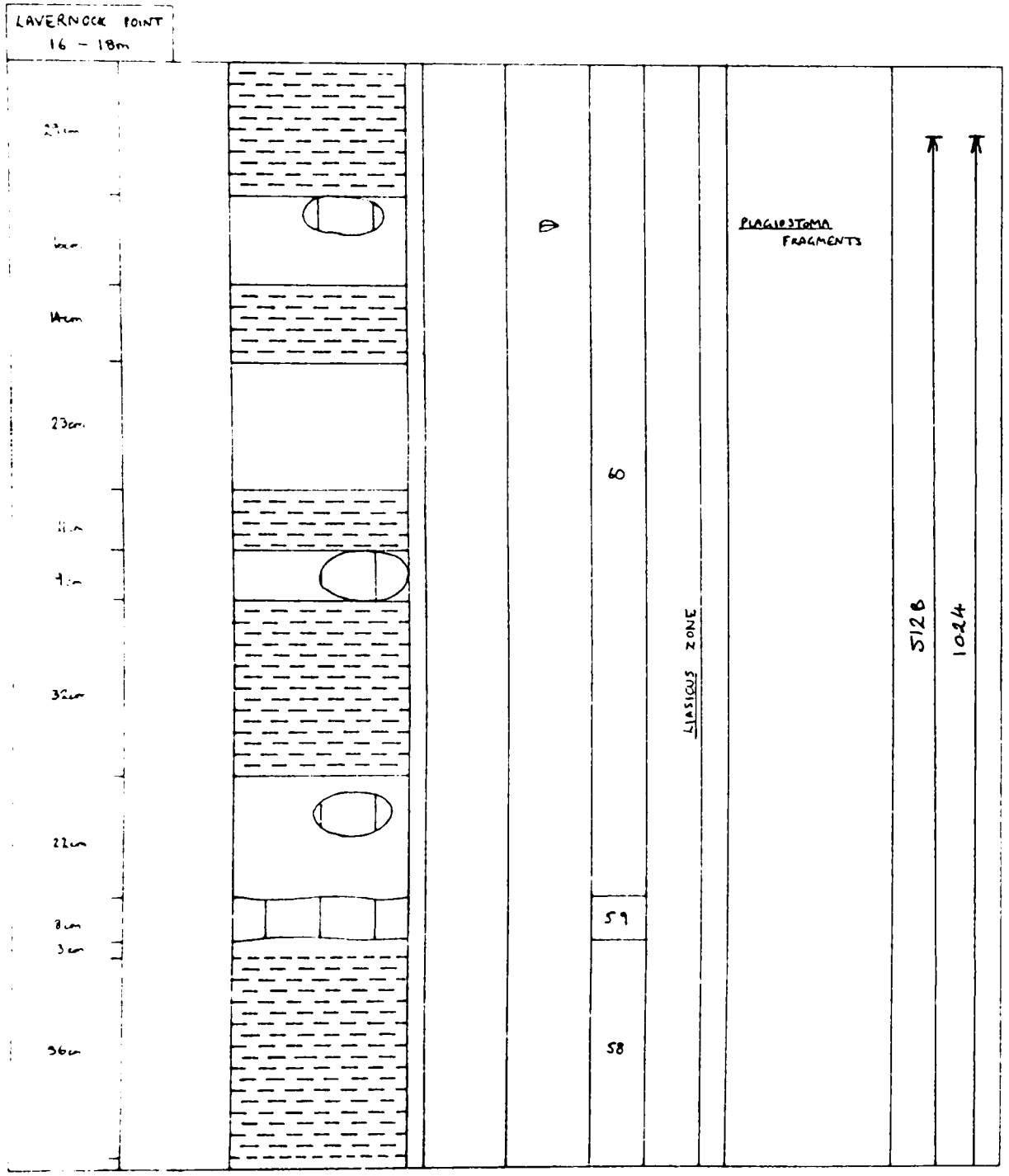
LAVERNOCK POINT
16 - 18m
23cm
14cm
23cm
11cm
7cm
32cm
22cm
8cm
3cm
36cm
60
59
58
LIASICUS ZONE
PLAGIOSTOMA
FRAGMENTS
512B
1024

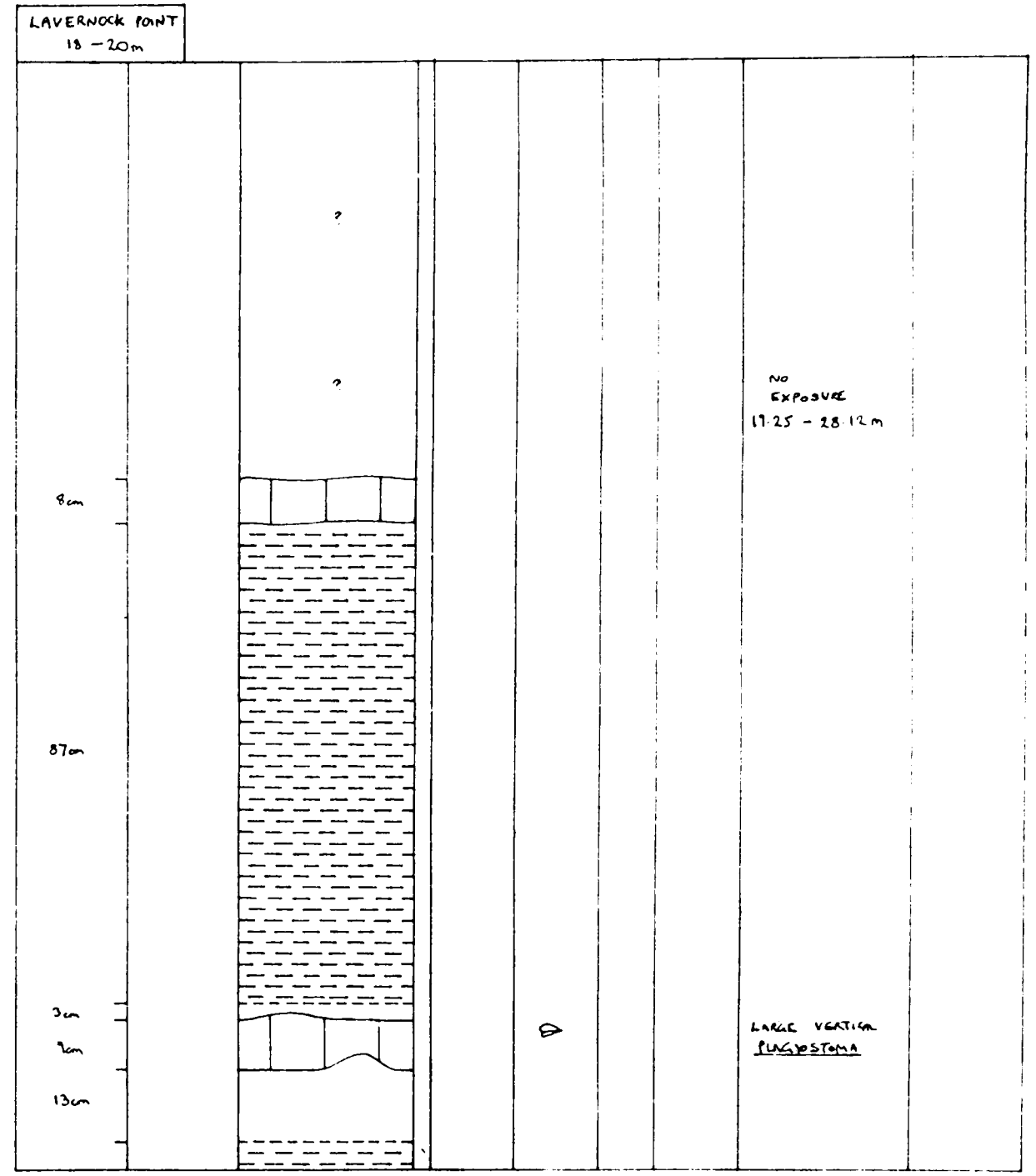
LAVERNOCK POINT
18 - 20m
?
?
8cm
87cm
3cm
7cm
13cm
NO
EXPOSURE
17.25 - 28.12m
LARGE VERTICAL
PLAGIOSTOMA

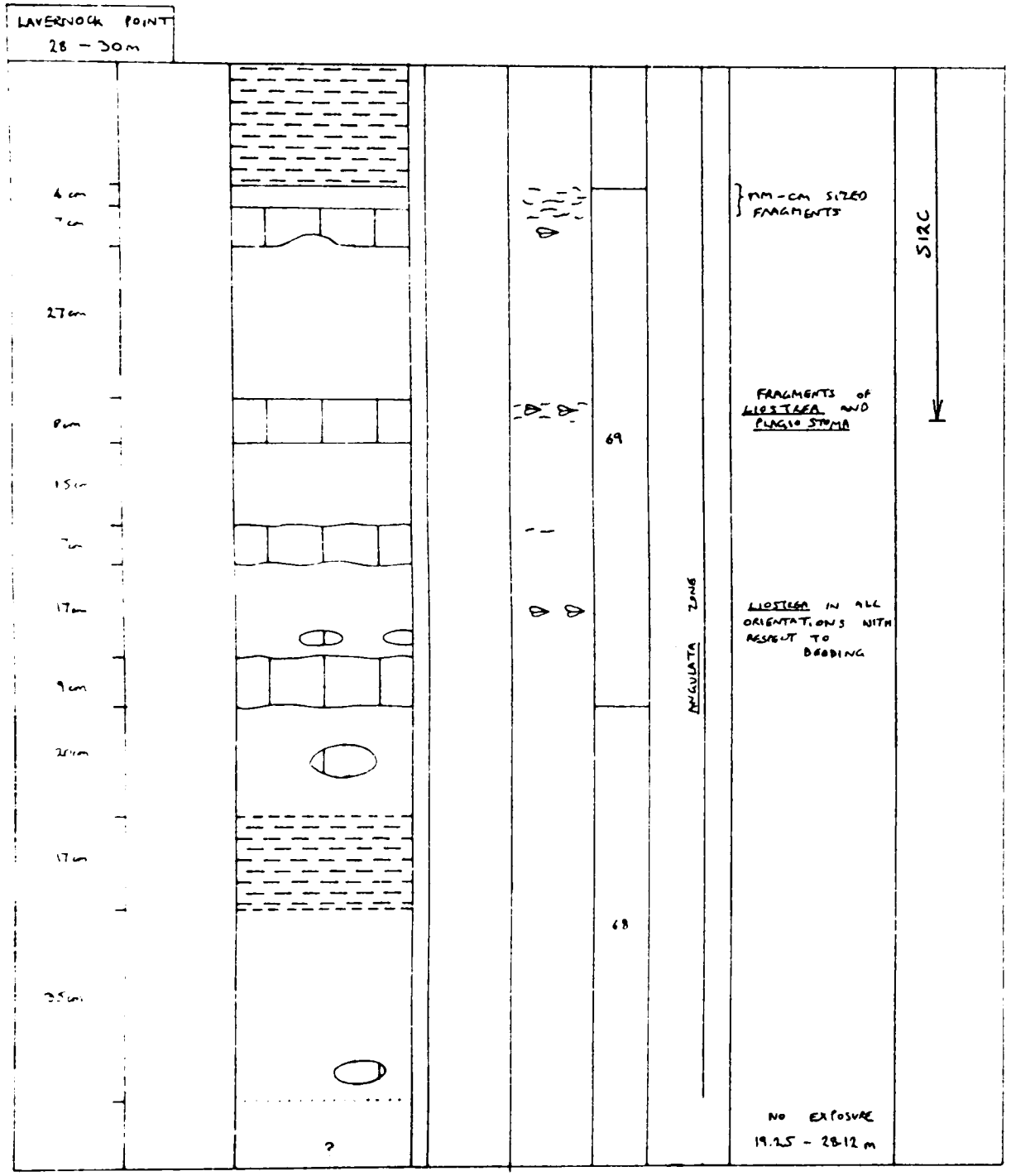
LAVERNOCK POINT
28 – 30m
4 cm
27cm
8cm
15cm
17cm
9cm
17cm
35cm
?
69
68
NEGULATA ZONE
mm-cm SIZED FRAGMENTS
FRAGMENTS of LIOSTREA AND PLAGIOSTOMA
LIOSTREA IN ALL ORIENTATIONS WITH RESPECT TO BEDDING
NO EXPOSURE
19.25 – 28.12 m
S12C

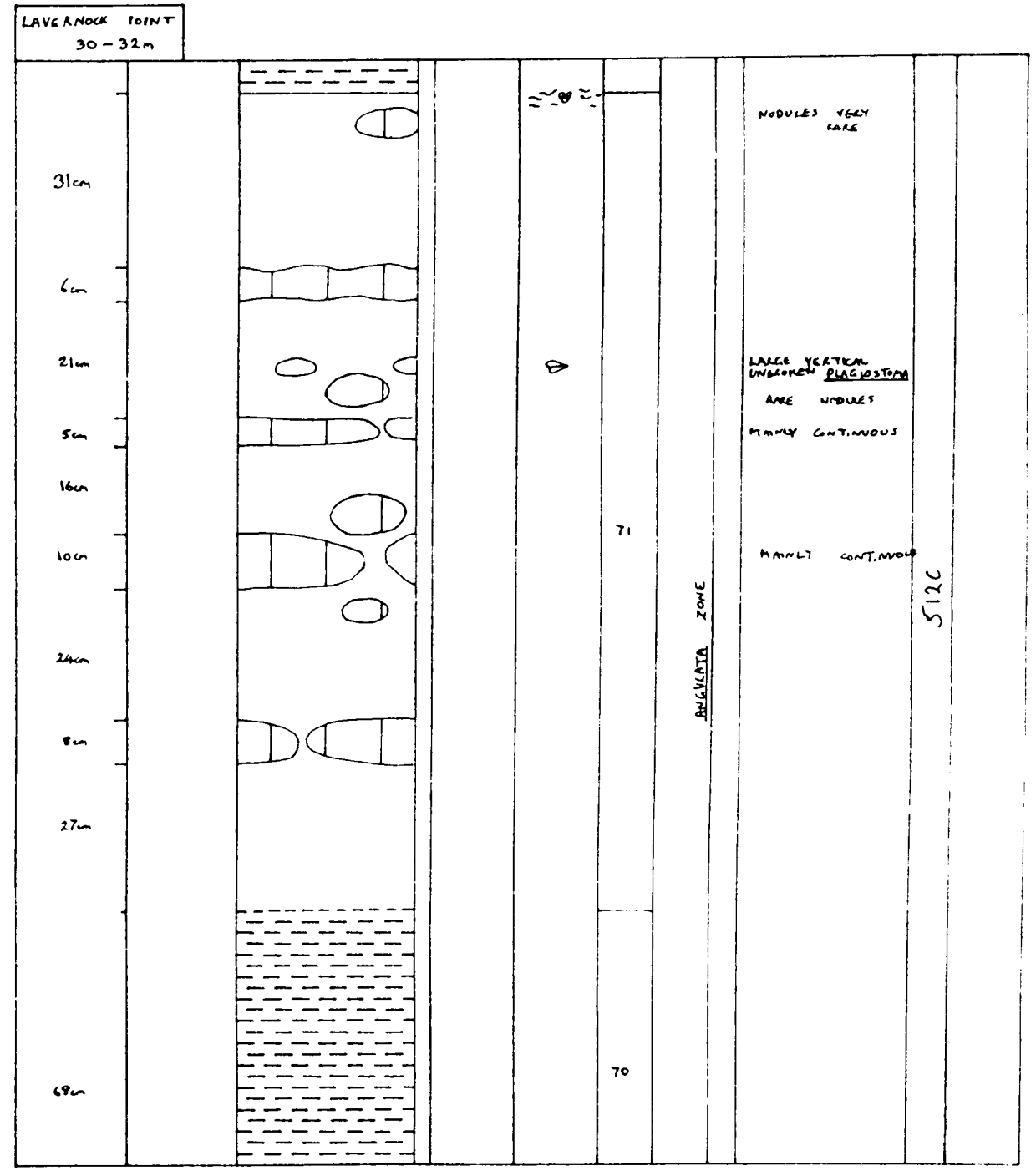
LAVERNOCK POINT
30 – 32m
31cm
6cm
21cm
5cm
16cm
10cm
24cm
8cm
27cm
68cm
71
70
NEGULATA ZONE
NODULES VERY RARE
LARGE VERTICAL UNBROKEN PLAGIOSTOMA
RARE NODULES
MANY CONTINUOUS
MANY CONTINUOUS
S12C

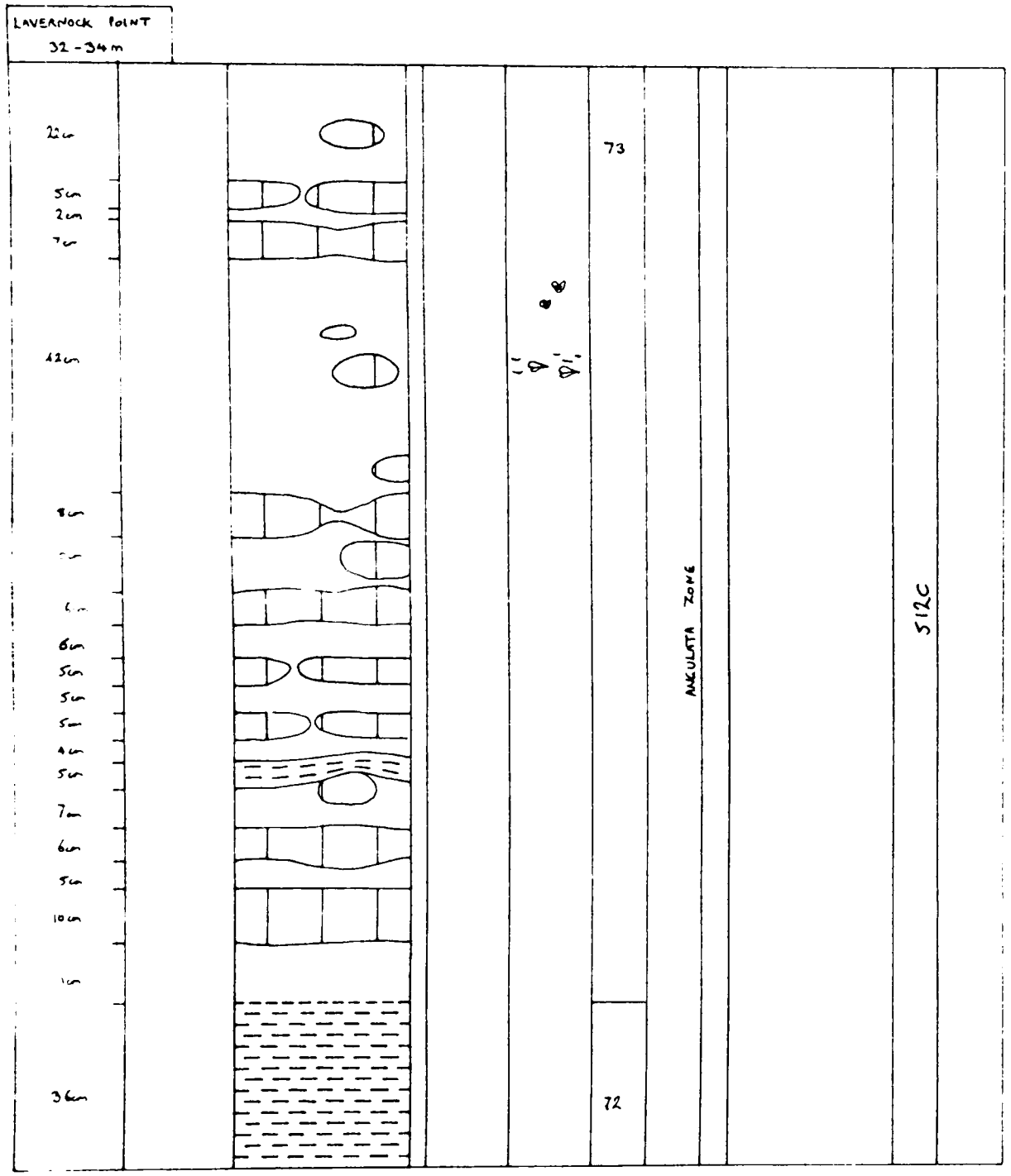
LAVERNOCK POINT
32 - 34 m
22cm
5cm
2cm
7cm
12cm
8cm
6cm
5cm
5cm
5cm
4cm
5cm
7cm
6cm
5cm
10cm
36cm
73
72
ANCULATA ZONE
S12C

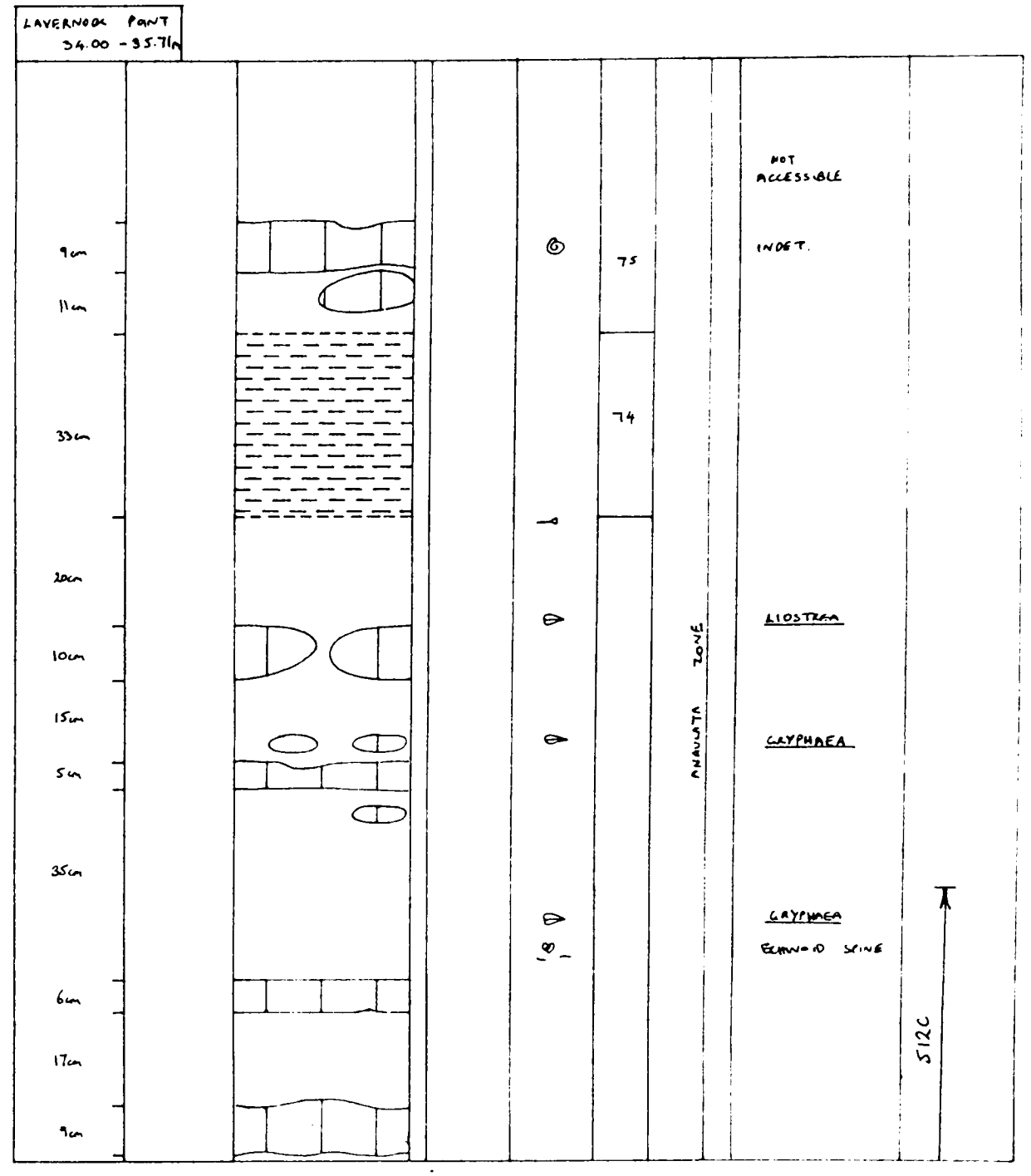
LAVERNOCK POINT
34.00 - 35.71m
9cm
11cm
33cm
20cm
10cm
15cm
5cm
35cm
6cm
17cm
9cm
75
74
ANAULATA ZONE
NOT ACCESSIBLE
INDET.
LIOSTREA
GRYPHAEA
GRYPHAEA
ECHINOID SPINE
S12C

2.4 Stratigraphic log for the basal Lias at Nash Point.

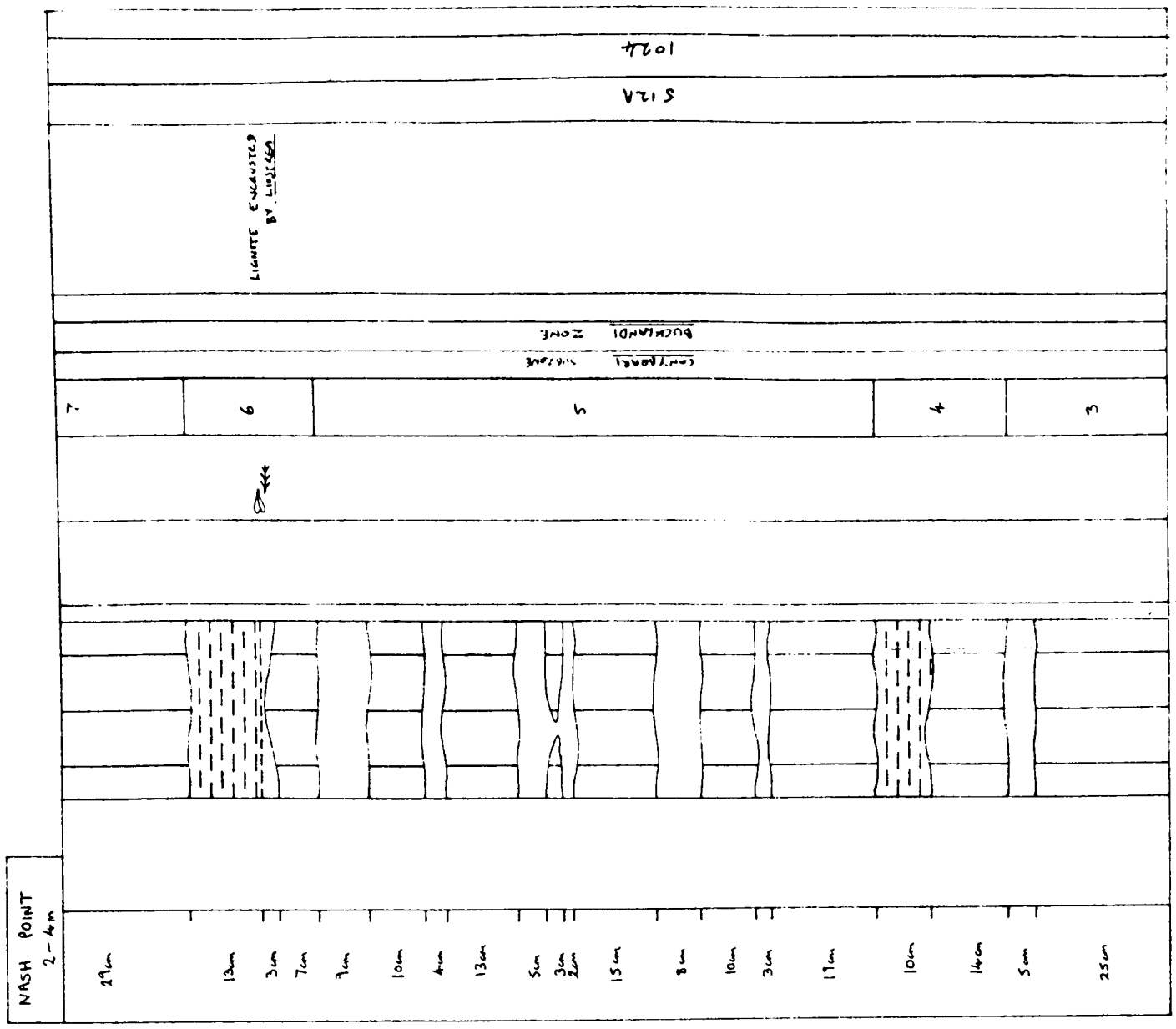

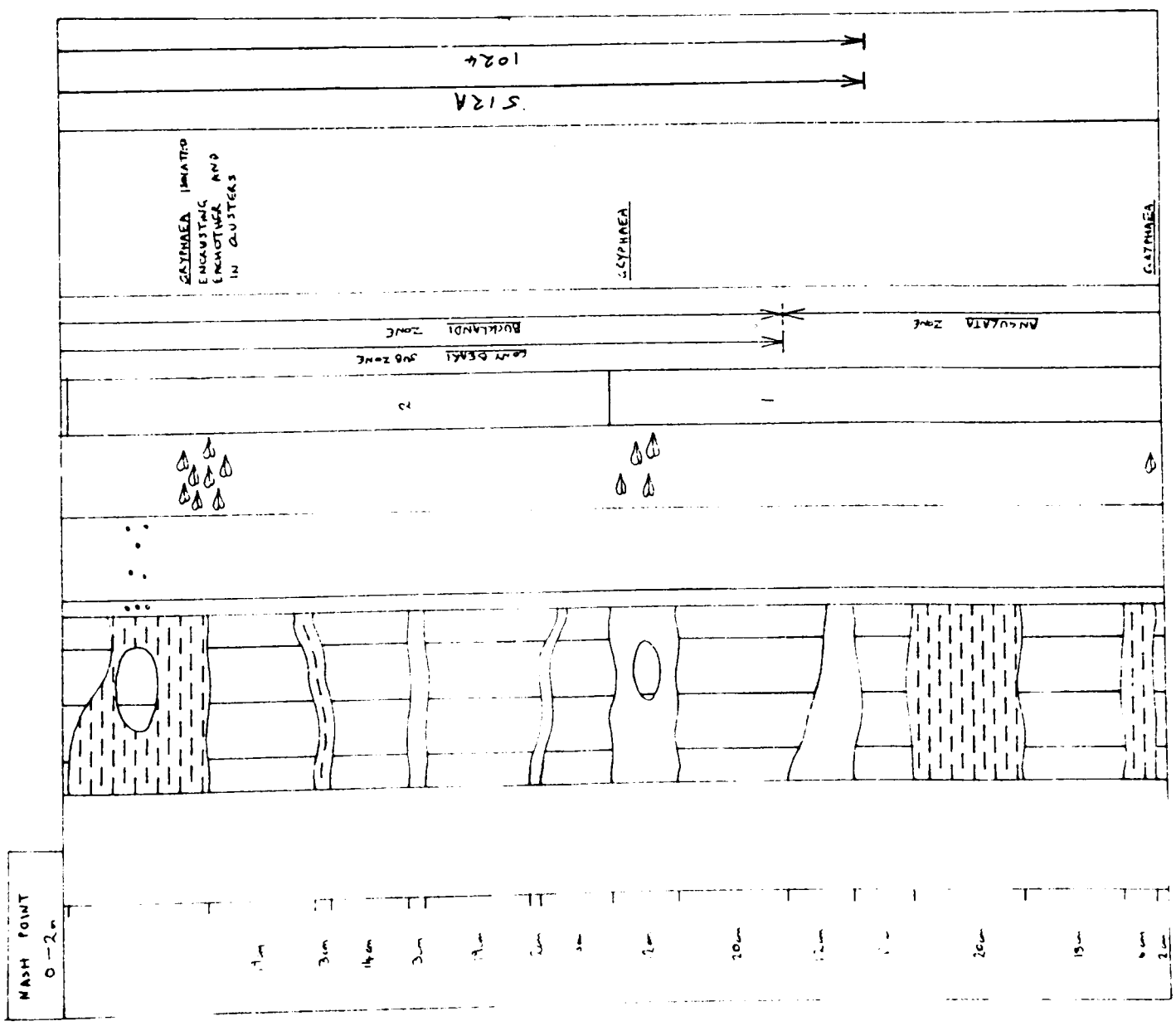

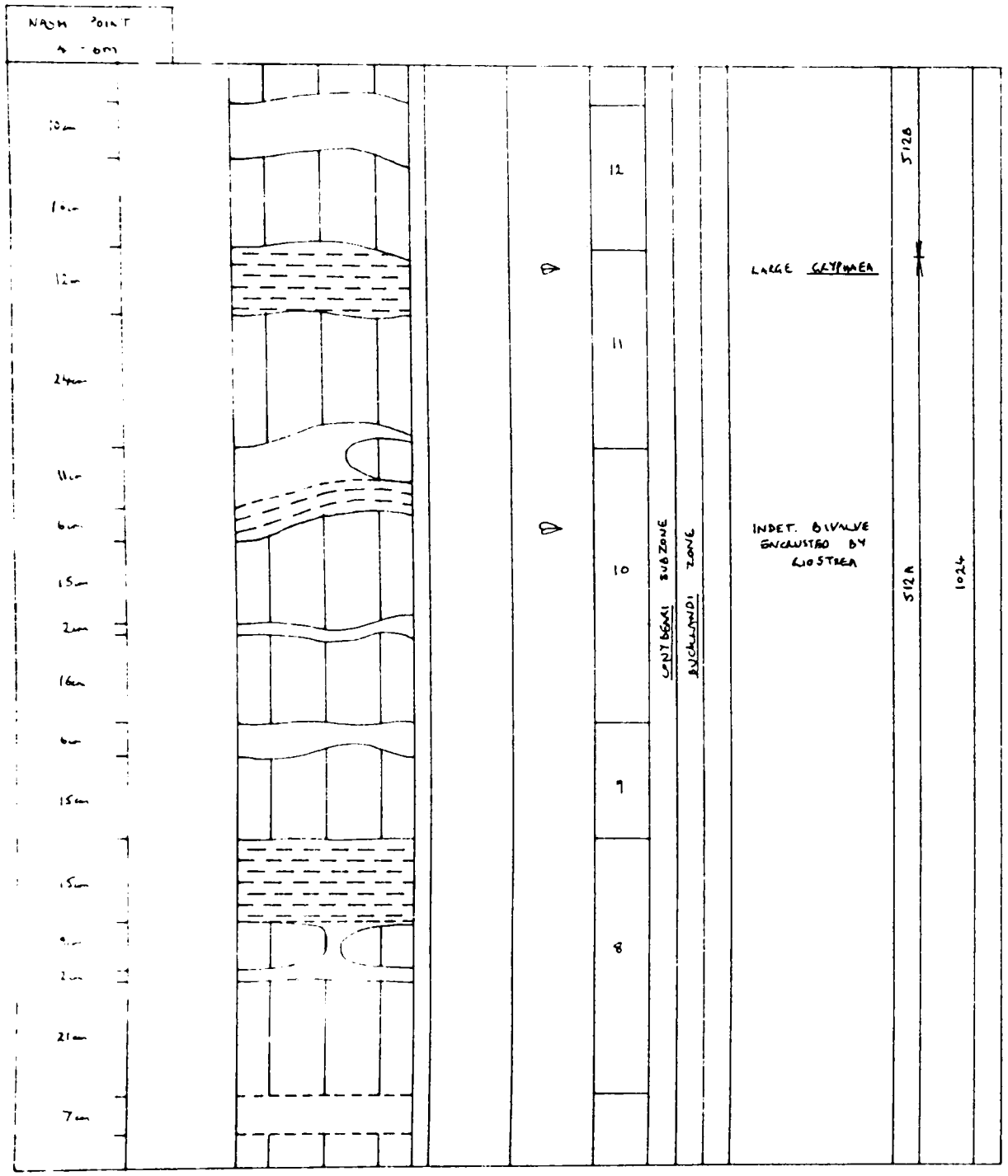
NASH POINT
4 - 6m
10cm
10cm
12cm
24cm
11cm
6cm
15cm
2cm
16cm
6cm
15cm
15cm
2cm
21cm
7cm
12
11
10
9
8
CONYBEARI SUBZONE
AUCKLANDI ZONE
LARGE GRYPHAEA
INDET. BIVALVE ENCRUSTED BY RIOSTREA
512B
512A
1024

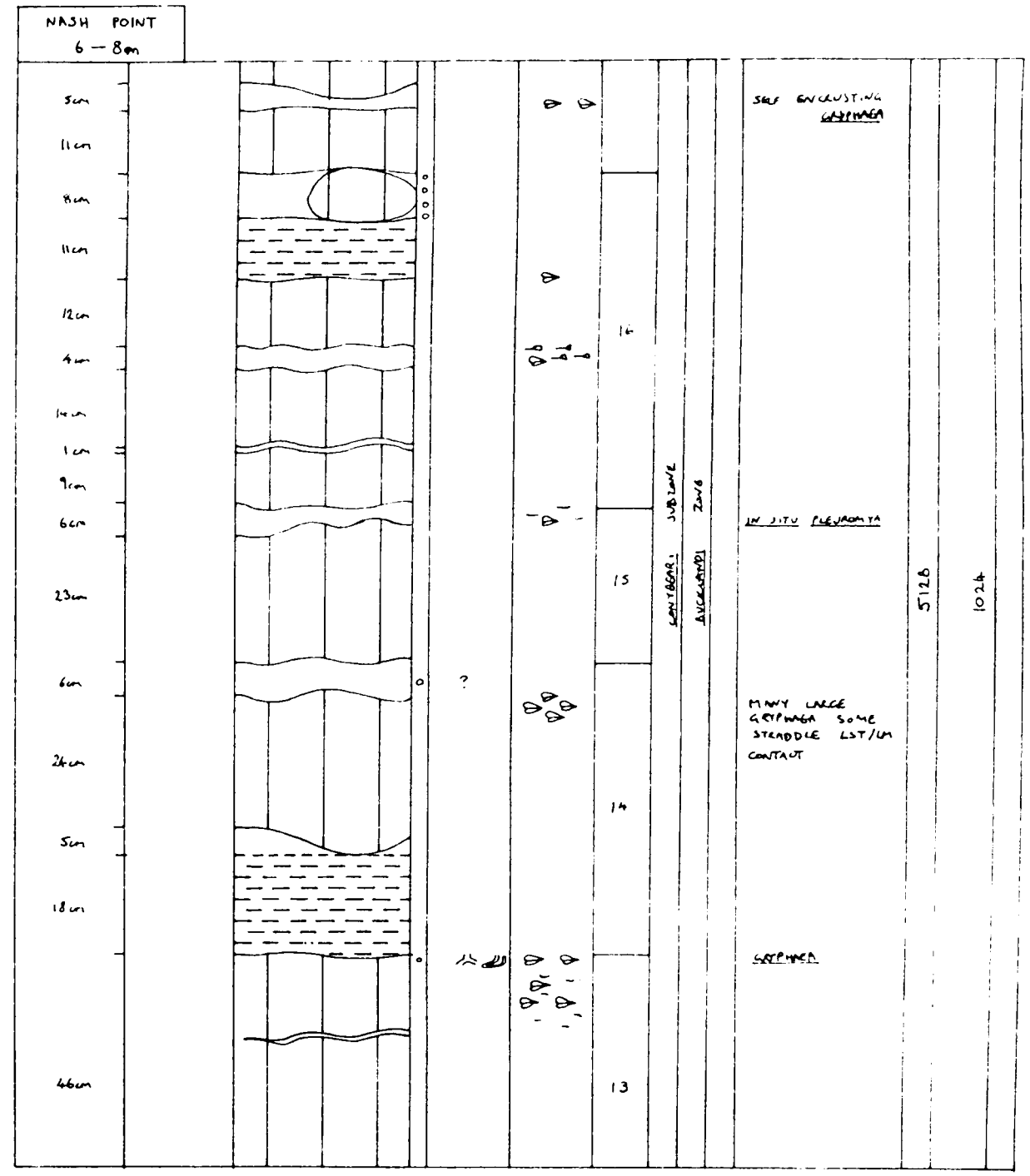
NASH POINT
6 - 8m
5cm
11cm
8cm
11cm
12cm
4cm
14cm
1cm
9cm
6cm
23cm
6cm
24cm
5cm
18cm
46cm
?
16
15
14
13
CONYBEARI SUBZONE
AUCKLANDI ZONE
SOLE ENCRUSTING GRYPHAEA
IN SITU PLEURIOMYA
MANY LARGE GRYPHAEA SOME STRADDLE LST/UM CONTACT
GRYPHAEA
512B
1024

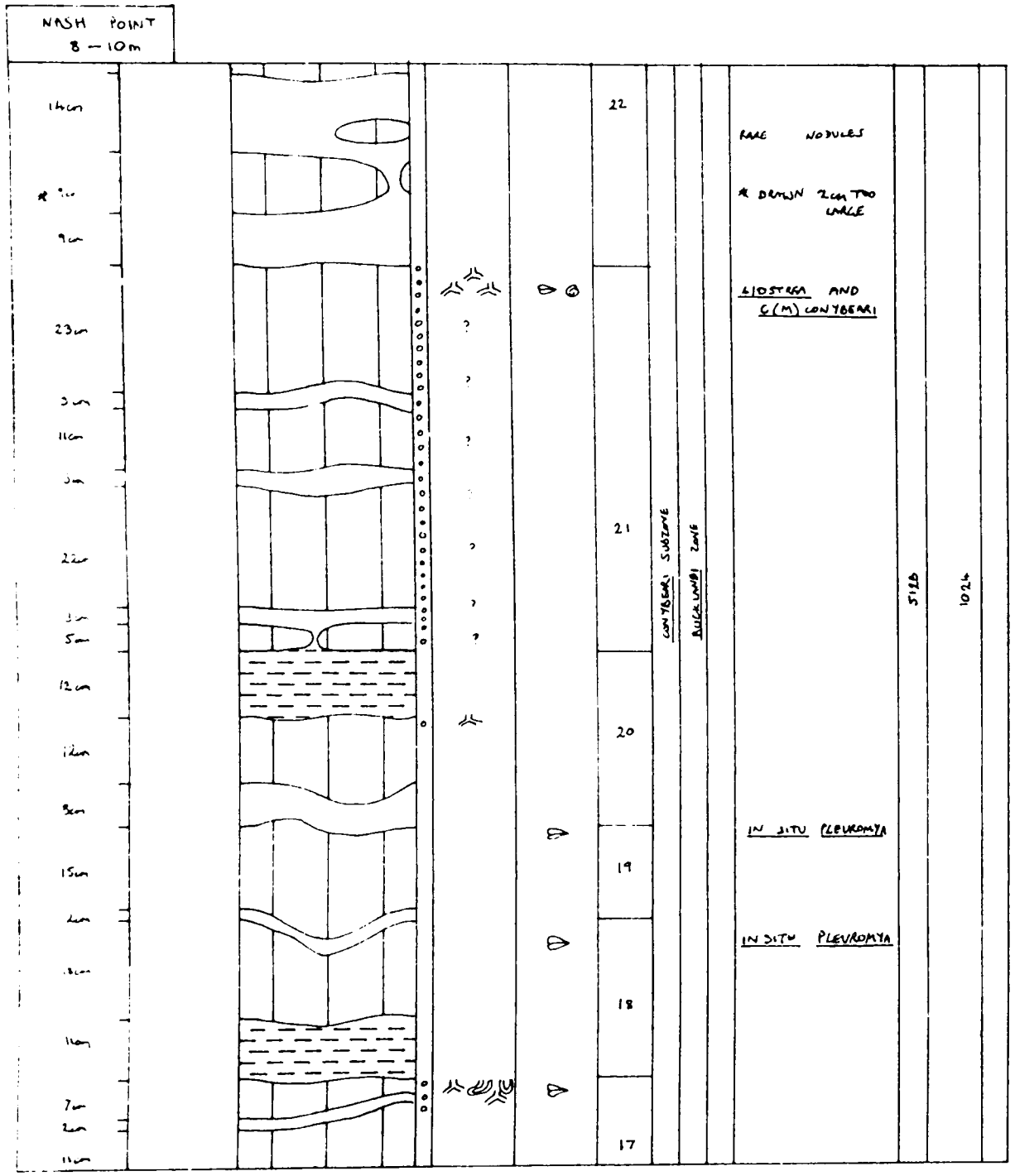
NASH POINT
8 – 10m
14cm
9cm
23cm
11cm
22cm
5cm
12cm
9cm
15cm
7cm
22
21
20
19
18
17
CONYBEARI SUBZONE
BUCKLANDI ZONE
RARE NODULES
DRAWN 2cm TOO LARGE
L/OSTREA AND C(M) CONYBEARI
IN SITU PLEUROMYA
IN SITU PLEUROMYA
512B
1024

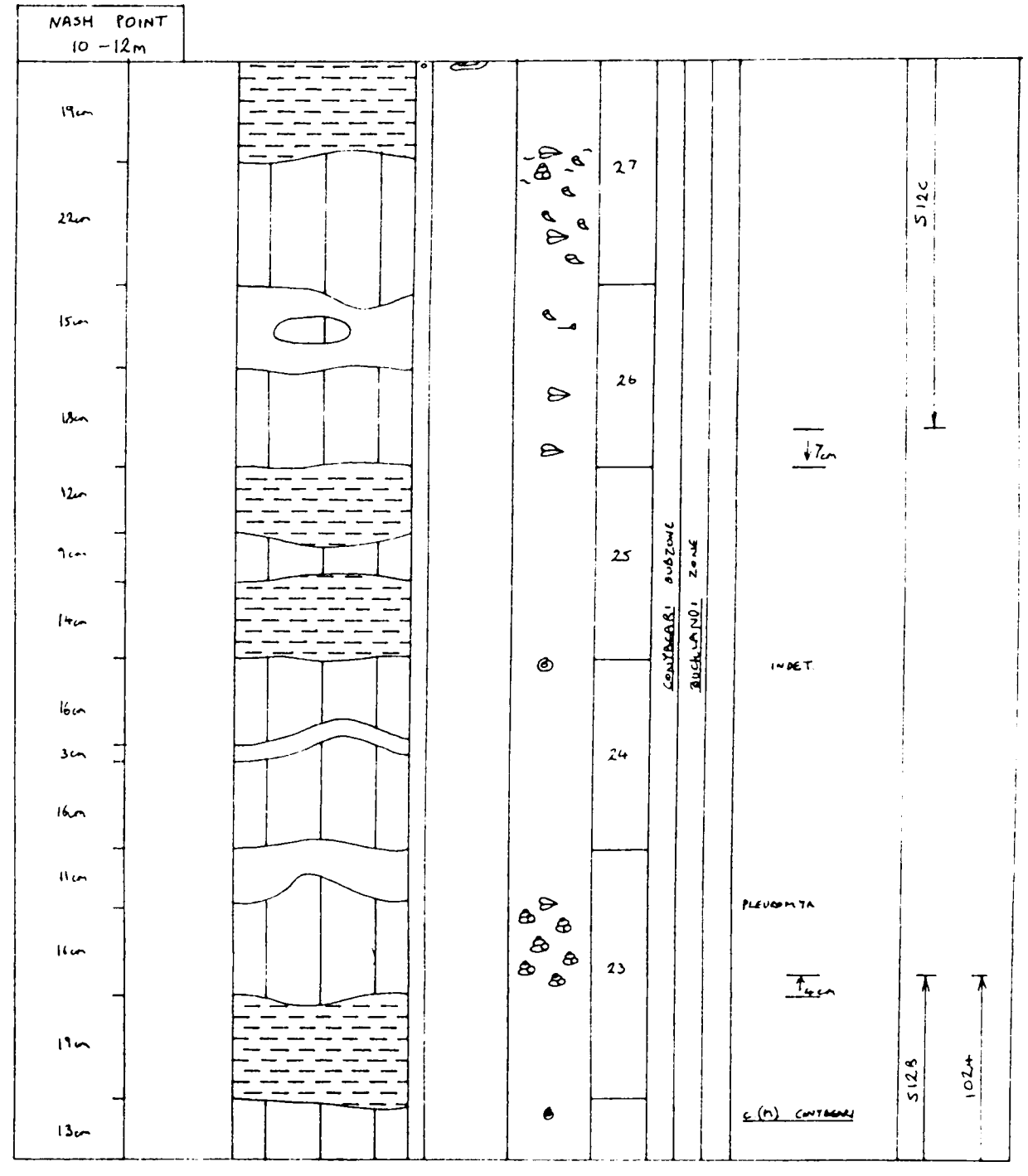
NASH POINT
10 – 12m
19cm
22cm
15cm
18cm
12cm
9cm
14cm
16cm
3cm
16cm
11cm
16cm
19cm
13cm
27
26
25
24
23
CONYBEARI SUBZONE
BUCKLANDI ZONE
7cm
INDET.
PLEUROMYA
4cm
C(M) CONYBEARI
512C
512B
1024

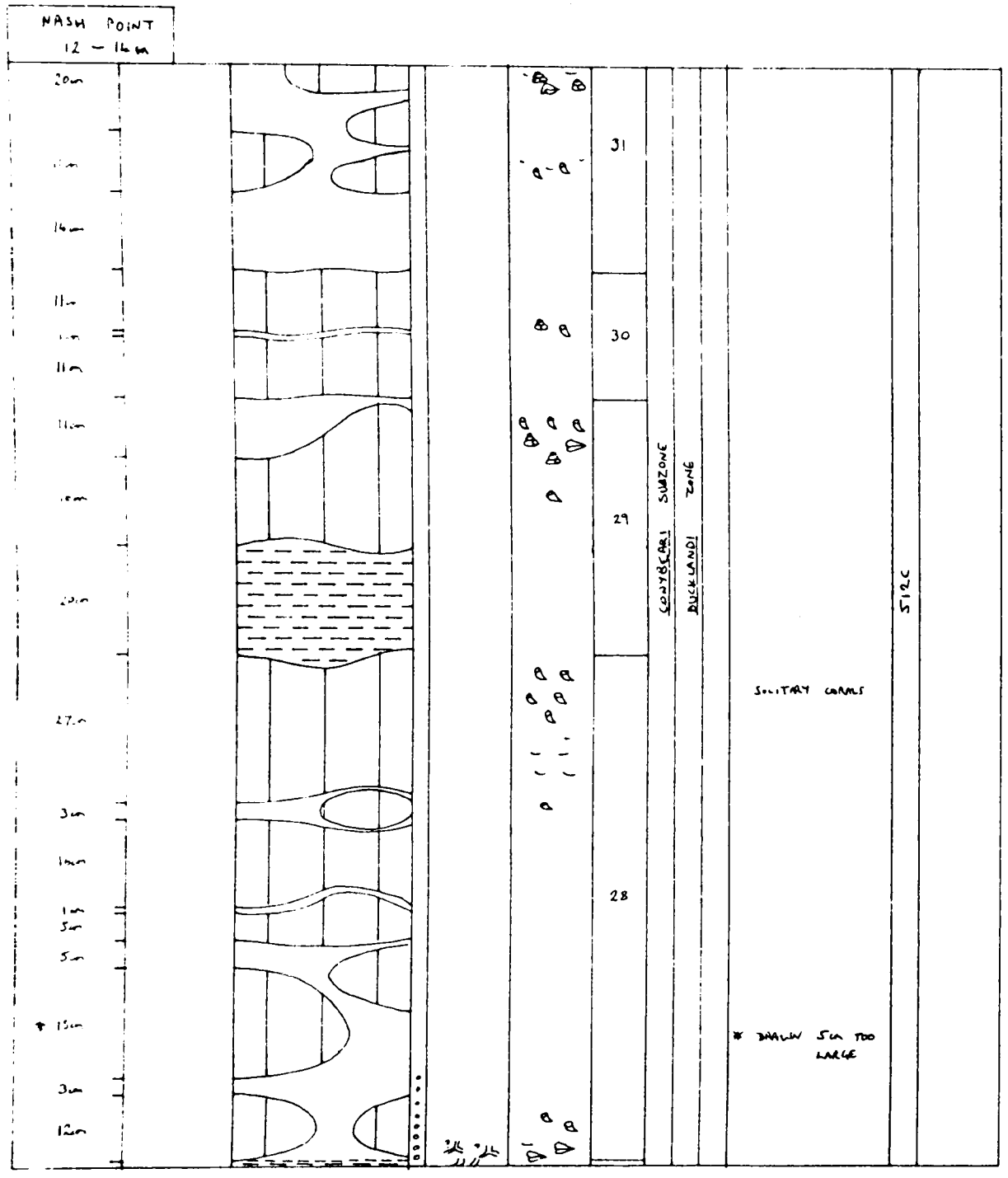
NASH POINT
12 – 14m
31
30
29
28
CONYBEARI SUBZONE
BUCKLANDI ZONE
SITE
SOLITARY CORALS
* DRAWN 5cm TOO LARGE

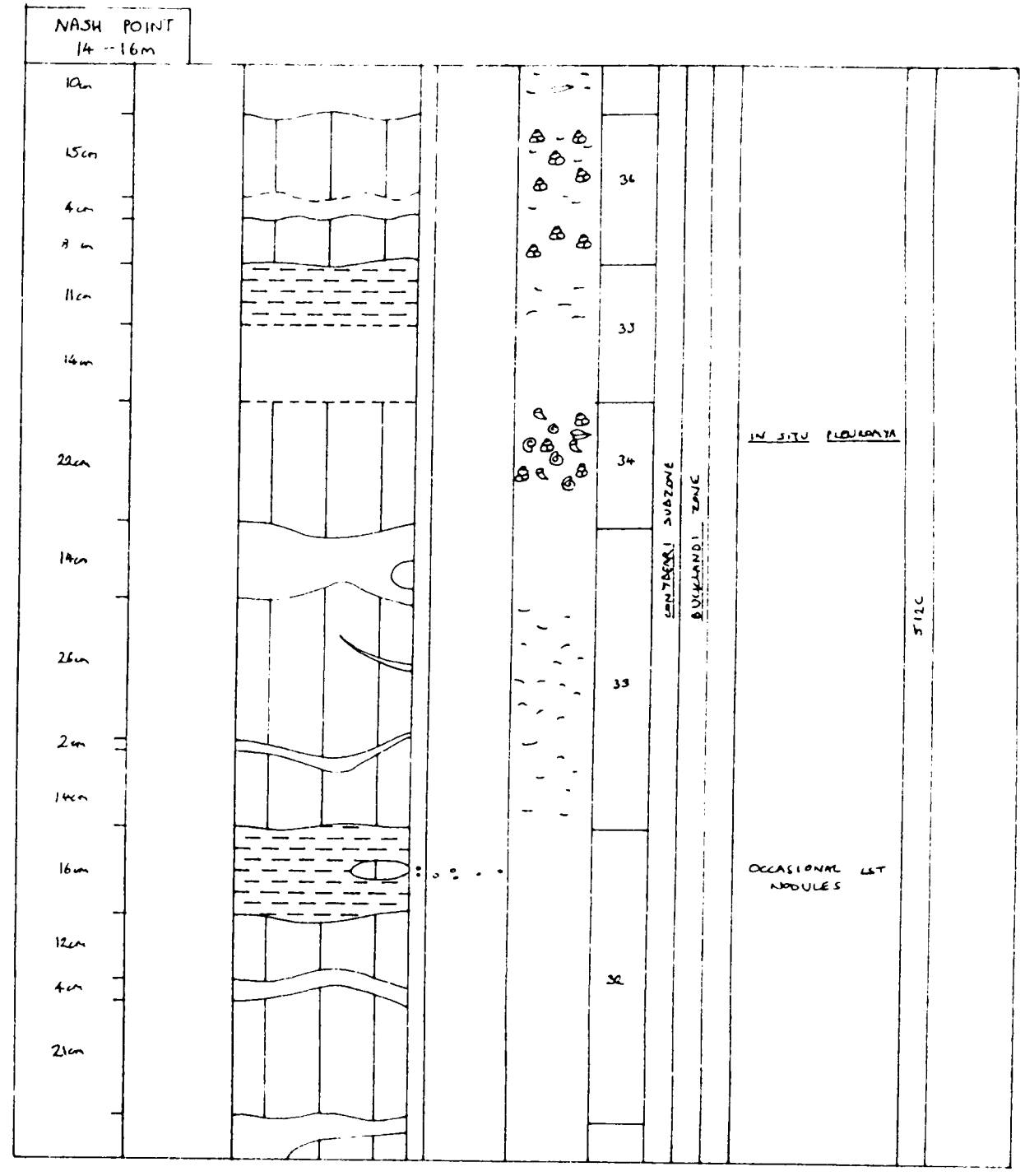
NASH POINT
14 – 16m
36
35
34
33
32
CONYBEARI SUBZONE
BUCKLANDI ZONE
IN SITU PLICATULA
OCCASIONAL LST NODULES
SITE

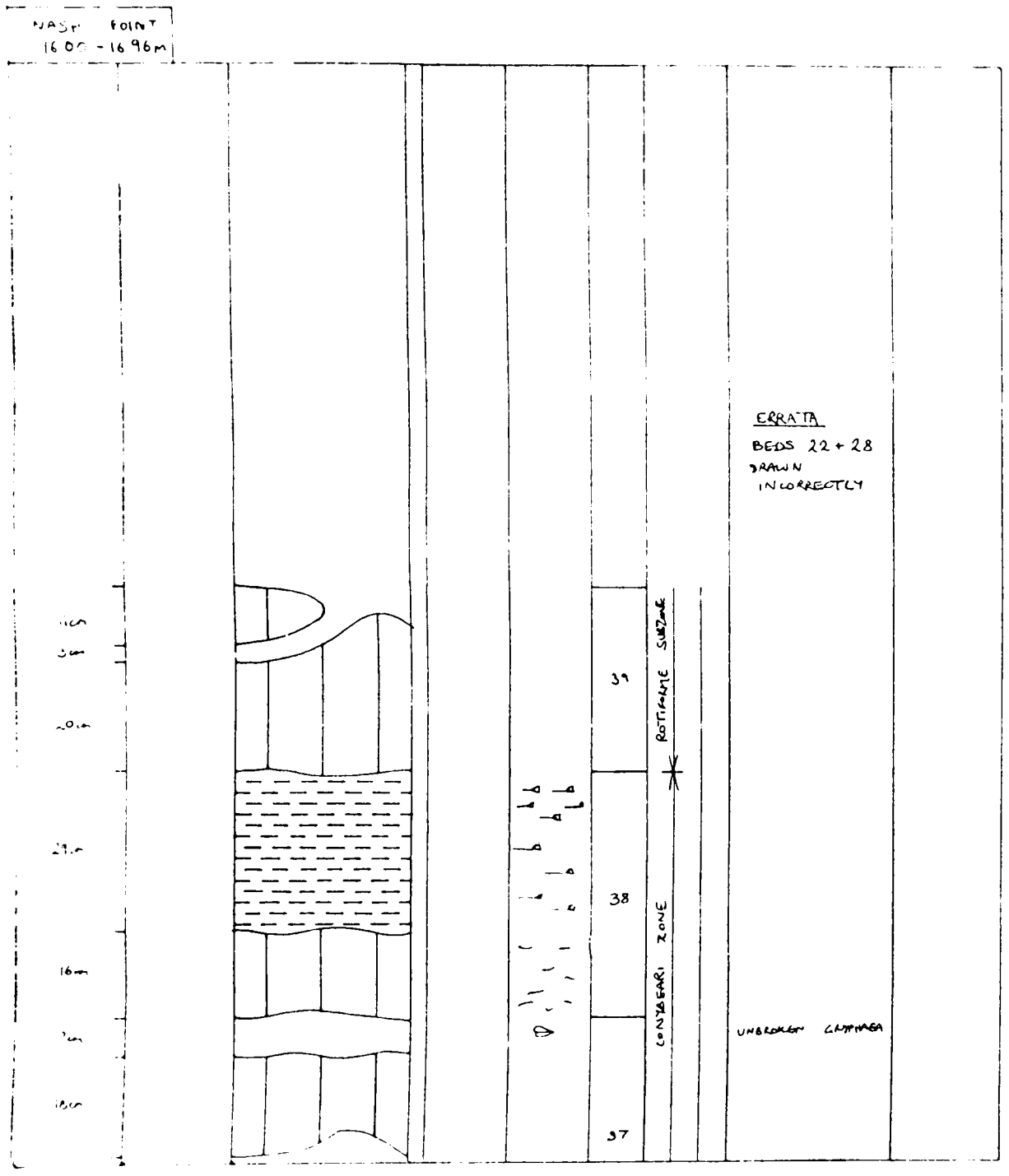
NASH POINT
16.00 - 16.96m
ERRATA
BEDS 22 + 28
DRAWN
INCORRECTLY
39
38
37
ROTIFANTE SUBZONE
CONYBEARI ZONE
UNBROKEN CLYMAGA

2.5 Stratigraphic log for the basal Lias at Long Itchington.

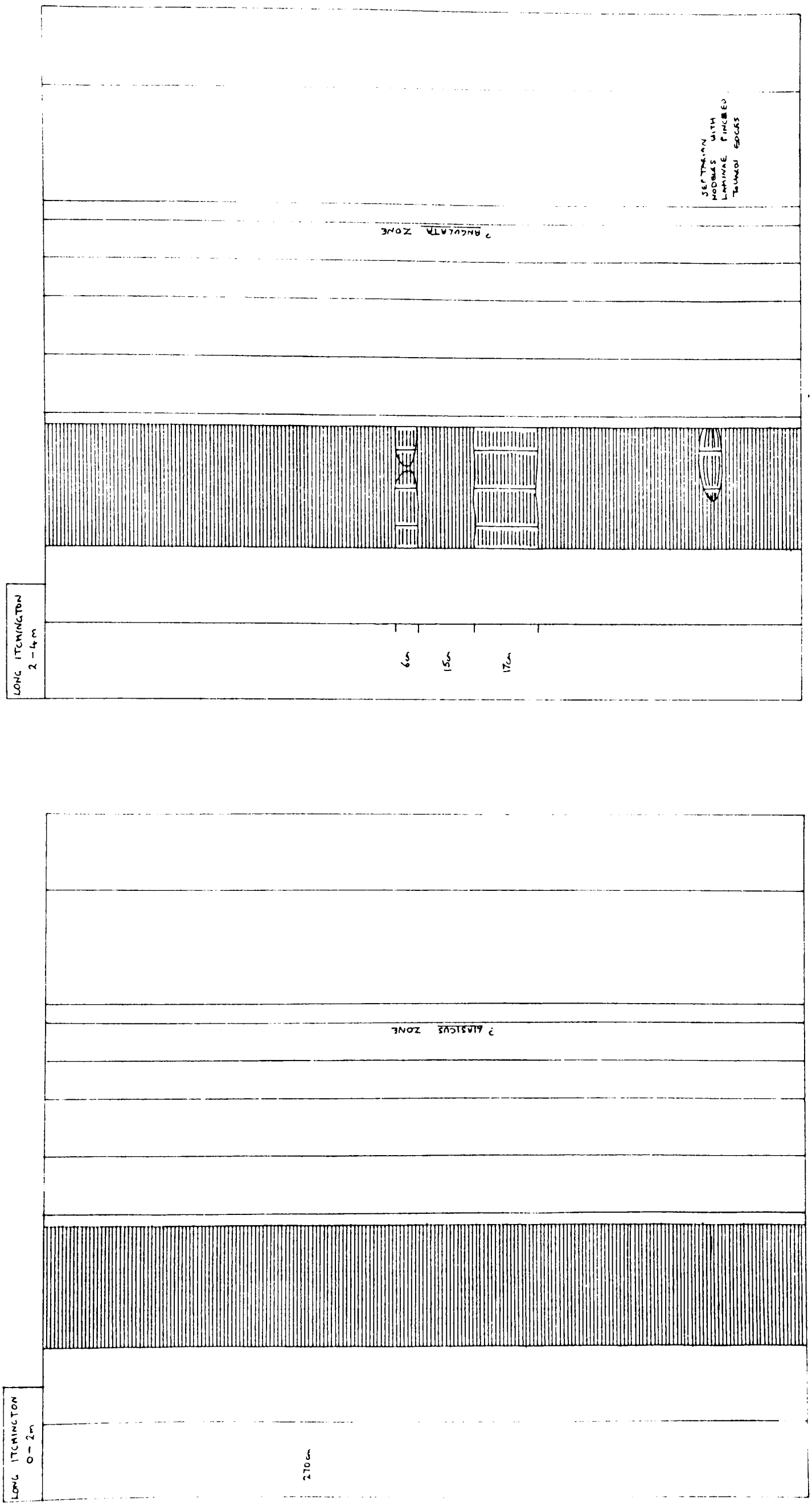

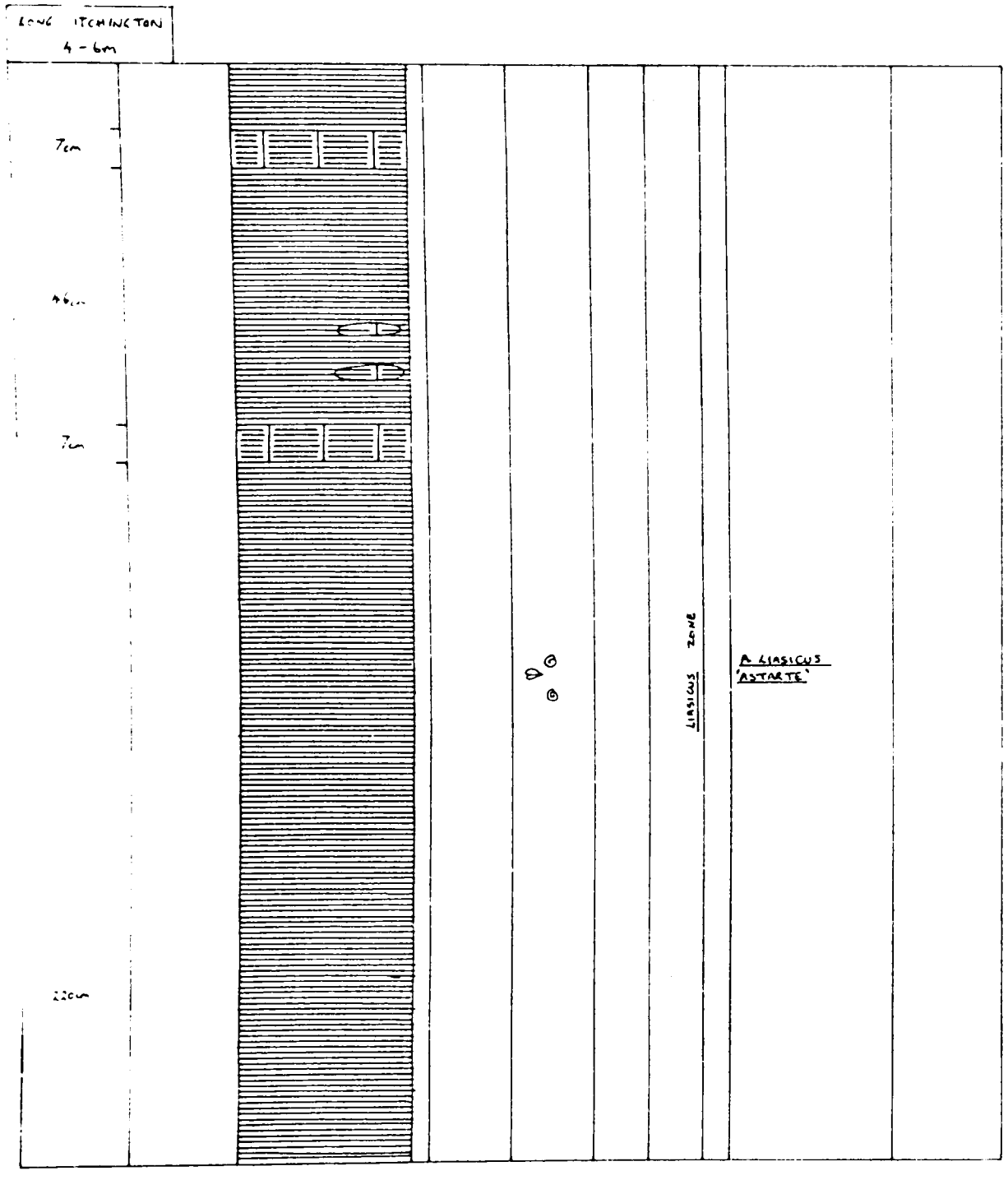
LONG ITCHINGTON
4 - 6m
7cm
7cm
220cm
LIASICUS ZONE
A. LIASICUS
'ASTARTE'

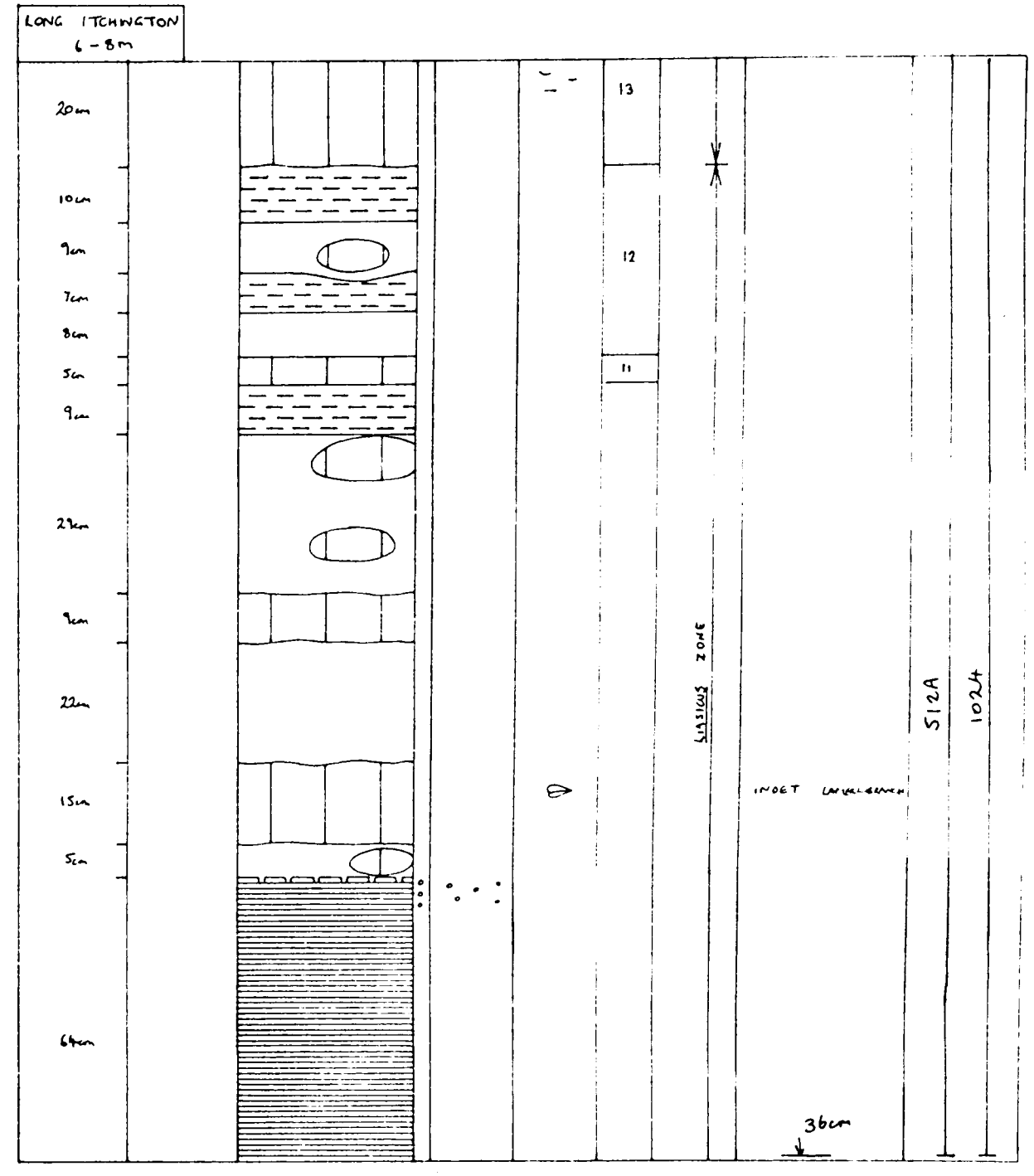
LONG ITCHINGTON
6 - 8m
20cm
10cm
9cm
7cm
8cm
5cm
9cm
22cm
9cm
22cm
15cm
5cm
64cm
13
12
11
LIASICUS ZONE
INDET
512A
1024
36cm

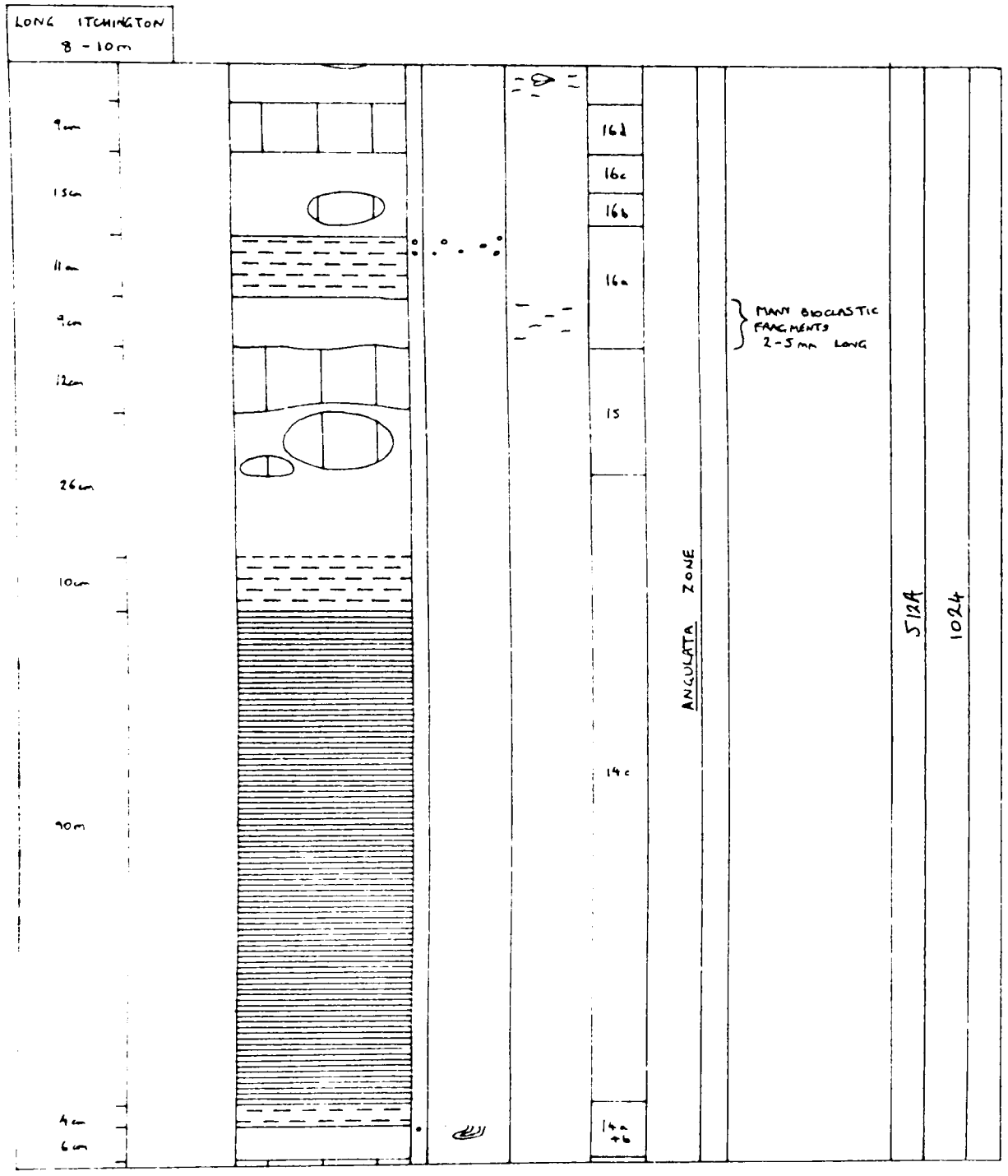
LONG ITCHINGTON
8 - 10m
9cm
15cm
11cm
9cm
12cm
26cm
10cm
90m
4cm
6cm
16d
16c
16b
16a
15
14c
14a
+b
ANGULATA ZONE
MANY BIOCLASTIC
FRAGMENTS
2-5mm LONG
512A
1024

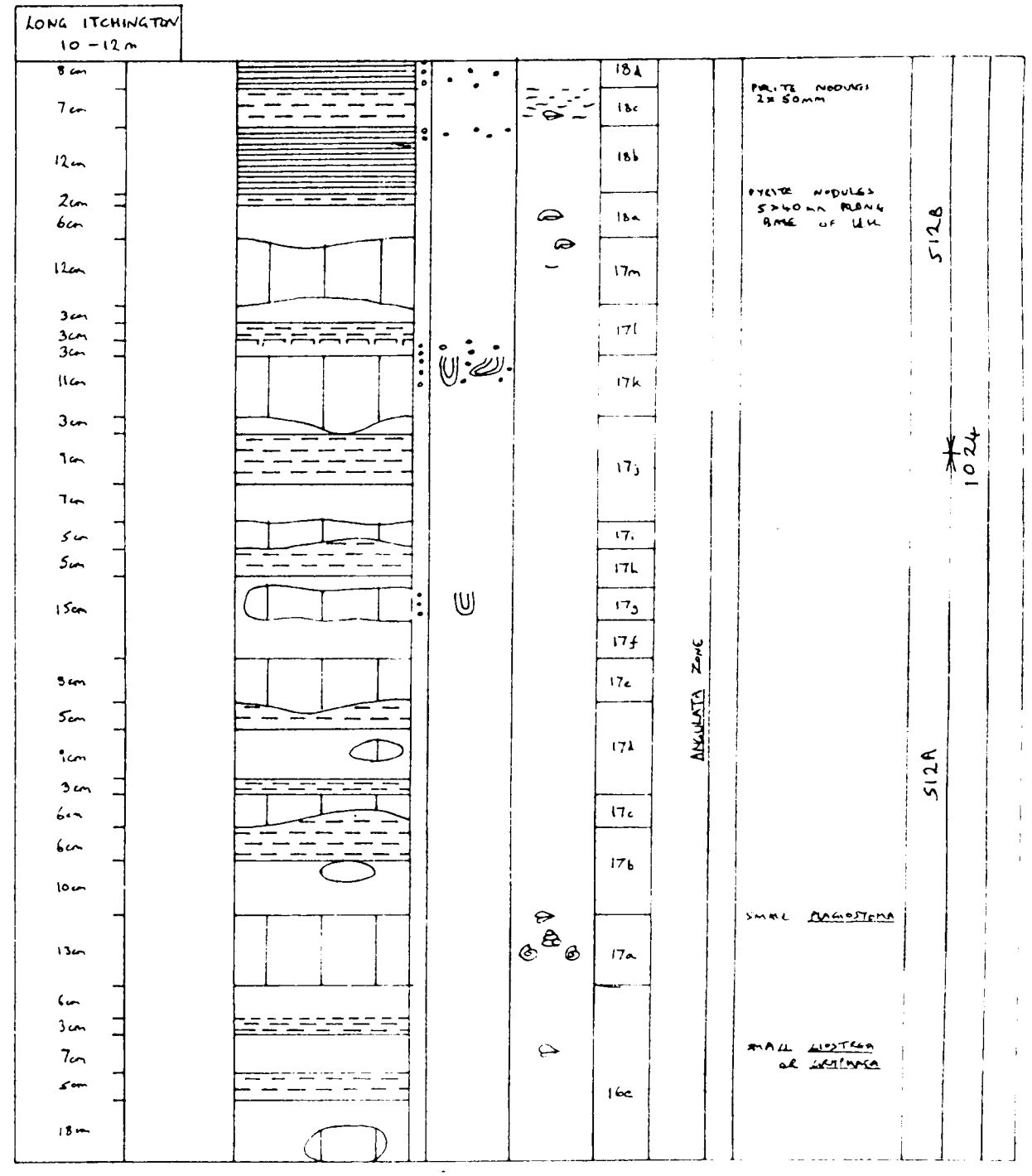
LONG ITCHINGTON
10 - 12m
8cm
7cm
12cm
2cm
6cm
12cm
3cm
3cm
3cm
11cm
3cm
9cm
7cm
5cm
5cm
15cm
9cm
5cm
9cm
3cm
6cm
6cm
10cm
13cm
6cm
3cm
7cm
5cm
18cm
18d
18c
18b
18a
17m
17l
17k
17j
17i
17h
17g
17f
17e
17d
17c
17b
17a
16e
ANGULATA ZONE
PYRITE NODULES
2x 50mm
PYRITE NODULES
5x40mm ALONG
BASE OF UNIT
SMALL ANGULATA
SMALL BIOSTRAT
OR LITHOLOGY
512B
1024
512A

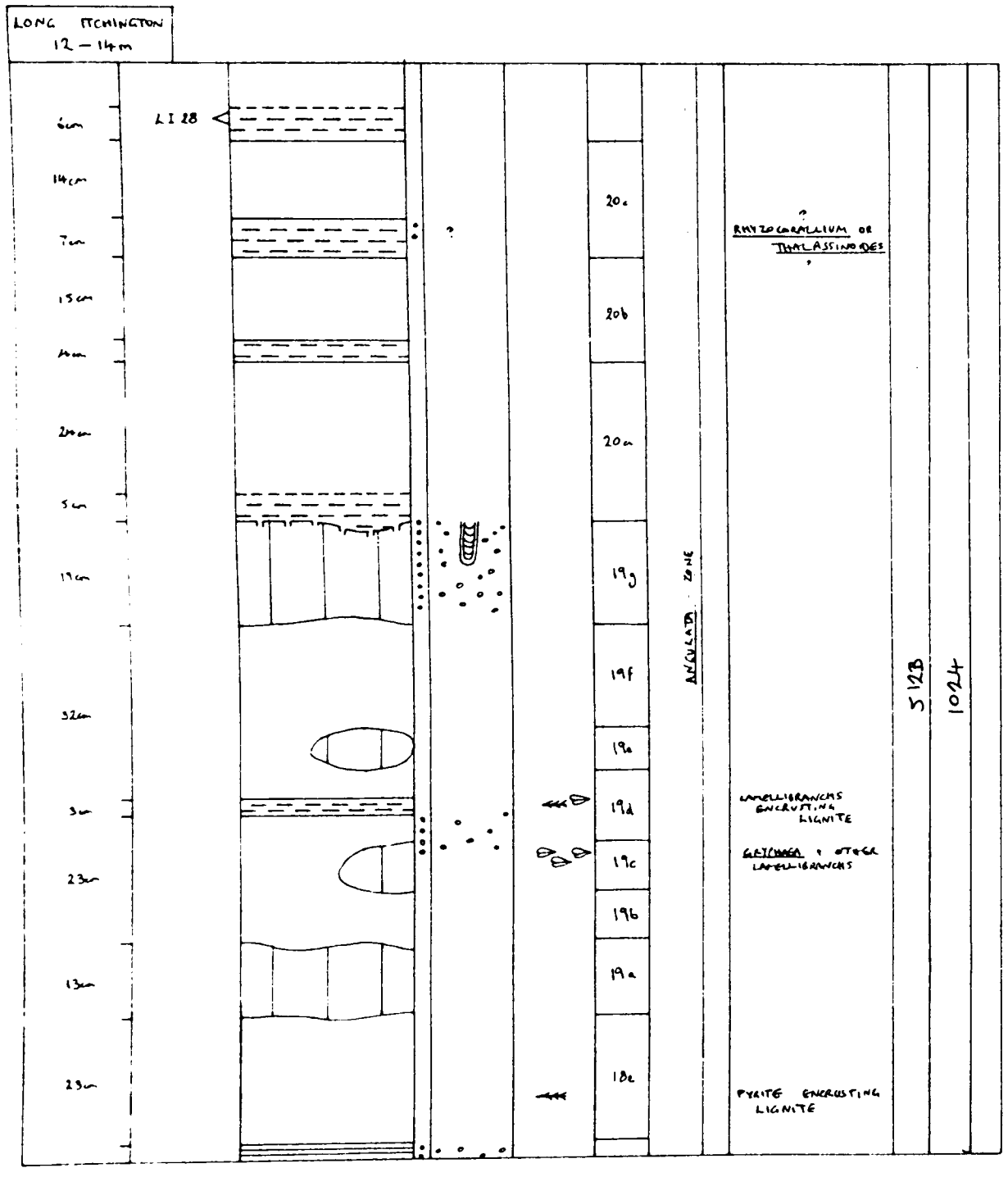
LONG ITCHINGTON
12 – 14m
6cm
14cm
7cm
15cm
4cm
20cm
5cm
17cm
32cm
3cm
23cm
13cm
23cm
LI 28
20c
20b
20a
19g
19f
19e
19d
19c
19b
19a
18e
ANGULATA ZONE
RHIZOCORALLIUM OR THALASSINOIDES
LAMELLIBRANCHS ENCRUSTING LIGNITE
GRYPHAEA + OTHER LAMELLIBRANCHS
PYRITE ENCRUSTING LIGNITE
512B
1024

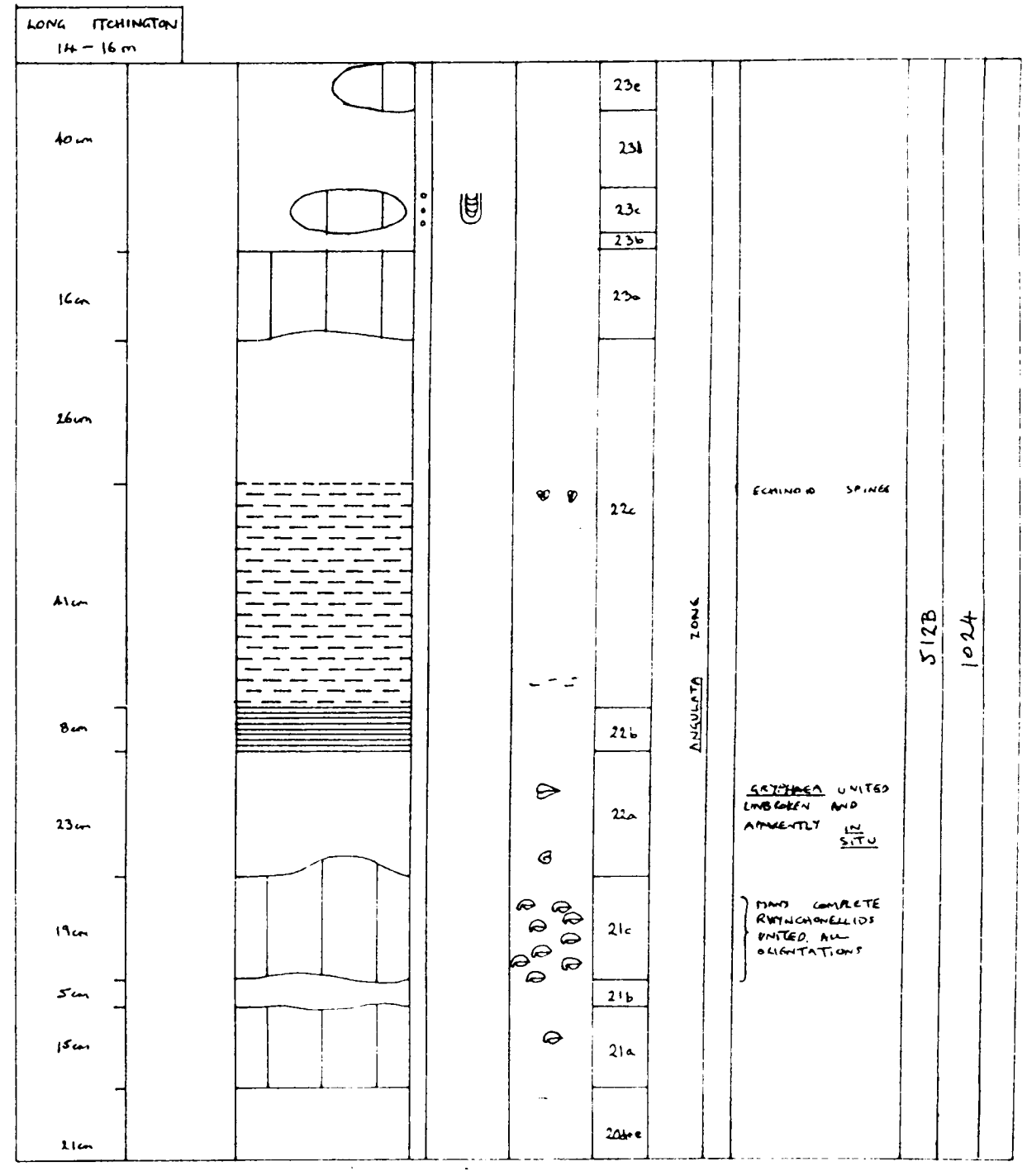
LONG ITCHINGTON
14 – 16m
40cm
16cm
26cm
41cm
8cm
23cm
19cm
5cm
15cm
21cm
23e
23d
23c
23b
23a
22c
22b
22a
21c
21b
21a
20d-e
ANGULATA ZONE
ECHINOID SPINES
GRYPHAEA UNITED UNBROKEN AND APPARENTLY IN SITU
MANY COMPLETE RHYNCHONELLIDS UNITED, ALL ORIENTATIONS
512B
1024

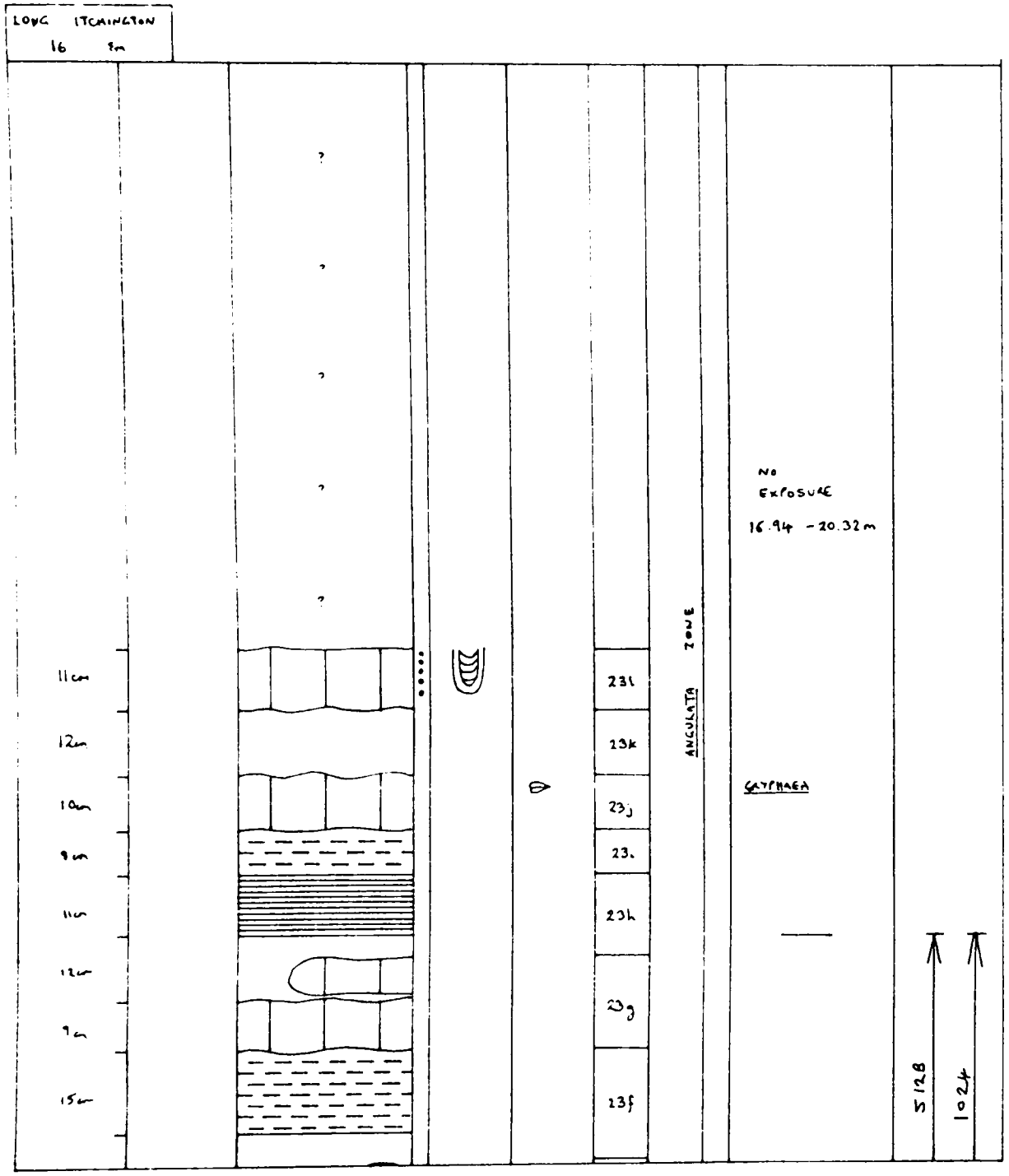
LONG ITCHINGTON
16 m
?
?
?
?
?
11cm
12cm
10cm
9cm
11cm
12cm
9cm
15cm
23l
23k
23j
23i
23h
23g
23f
ANGULATA ZONE
NO
EXPOSURE
16.94 - 20.32m
GRYPHAEA
5128
1024

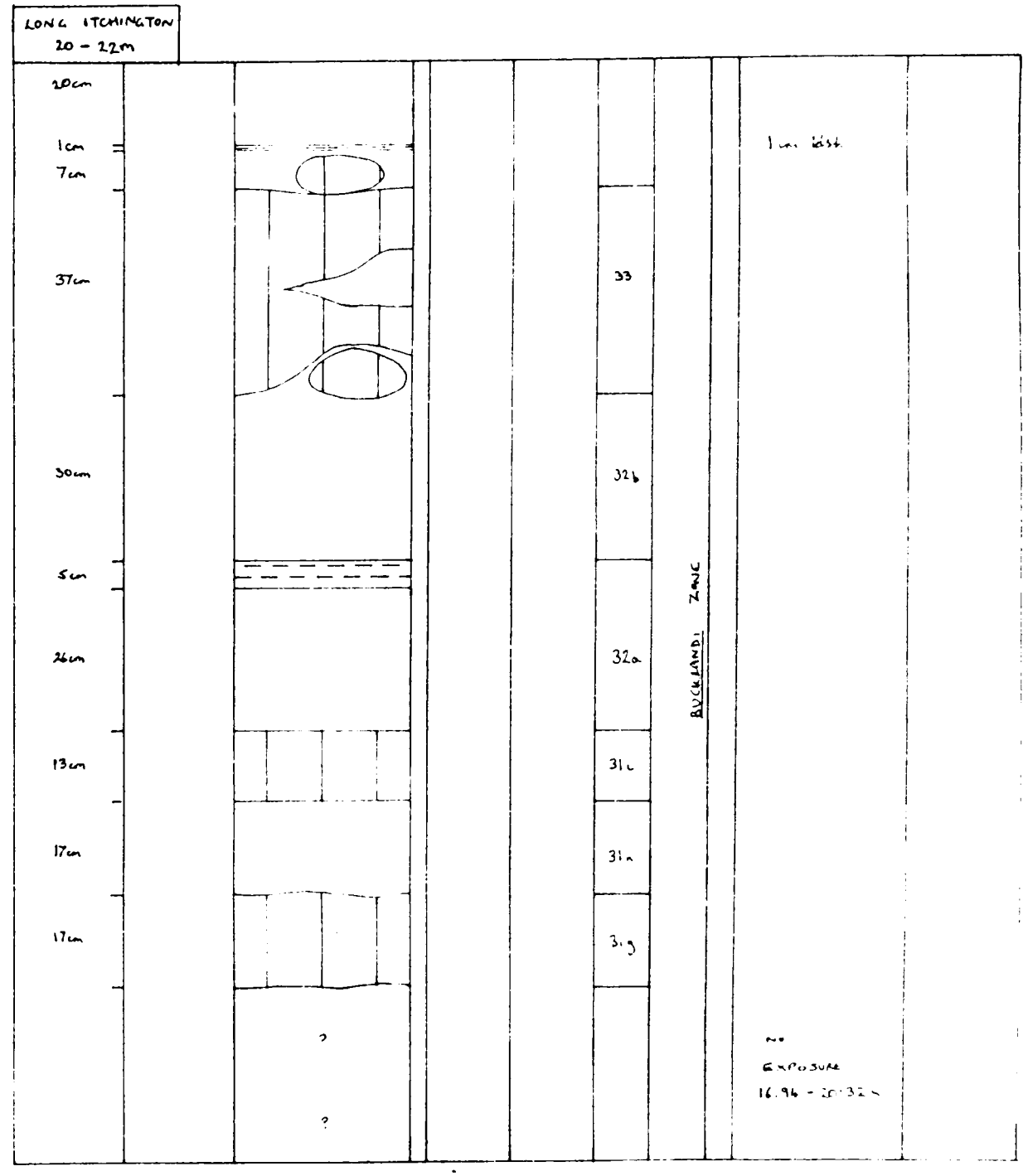
LONG ITCHINGTON
20 - 22m
20cm
1cm
7cm
37cm
30cm
5cm
26cm
13cm
17cm
17cm
33
32b
32a
31c
31a
31g
BUCKLAND. ZONE
1m lost
?
?
NO
EXPOSURE
16.94 - 20.32m

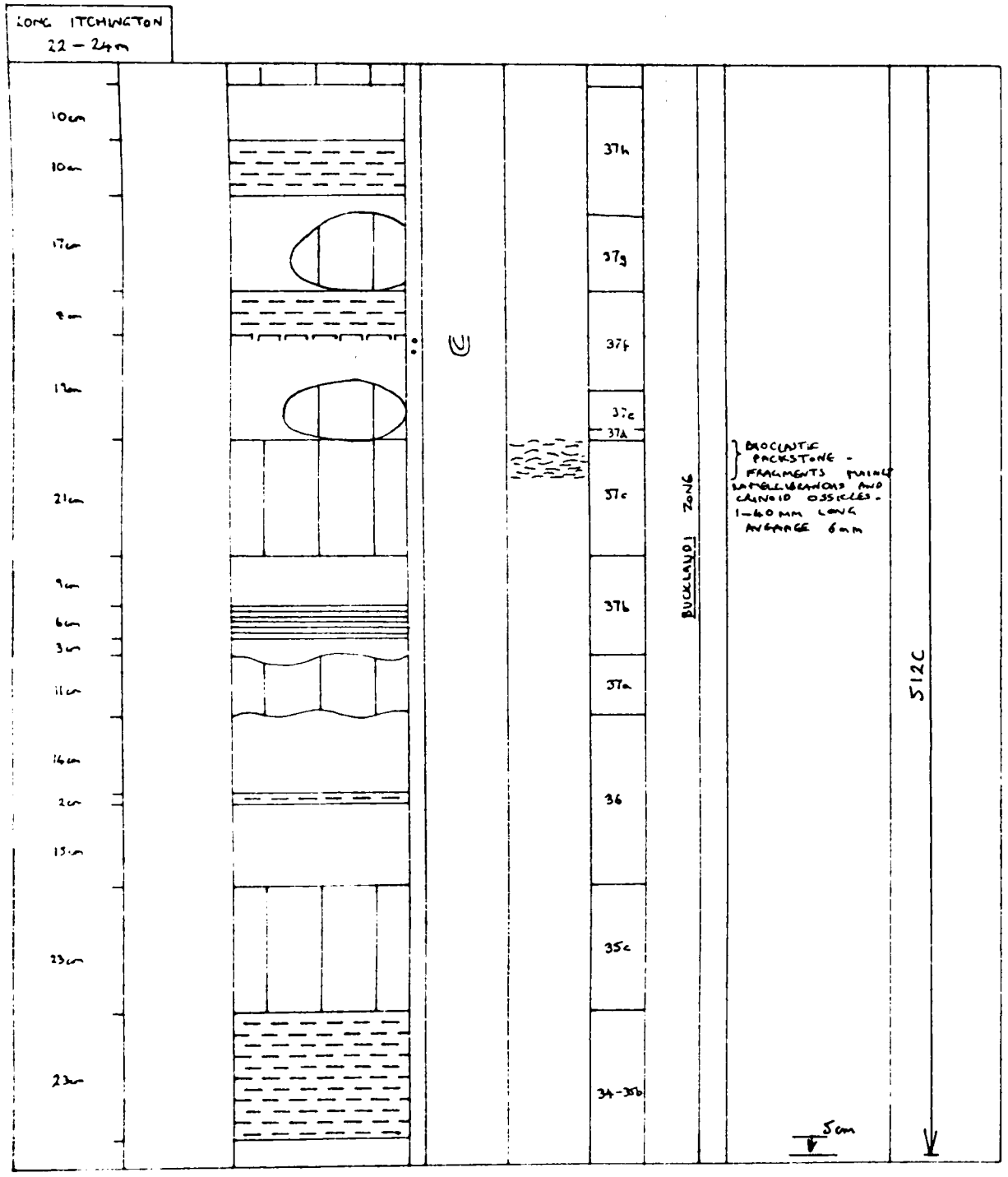
LONG ITCHINGTON
22 - 24m
10cm
10cm
17cm
8cm
12cm
21cm
9cm
5cm
3cm
11cm
16cm
2cm
13cm
23cm
23cm
37h
37g
37f
37e
37A
37c
37b
37a
36
35c
34-35b
BUCKLANDI ZONE
BIOCLASTIC PACKSTONE - FRAGMENTS FILINE BATELLIBRANCHS AND CRINOID OSSICLES - 1-60 MM LONG AVERAGE 6mm
5cm
512C

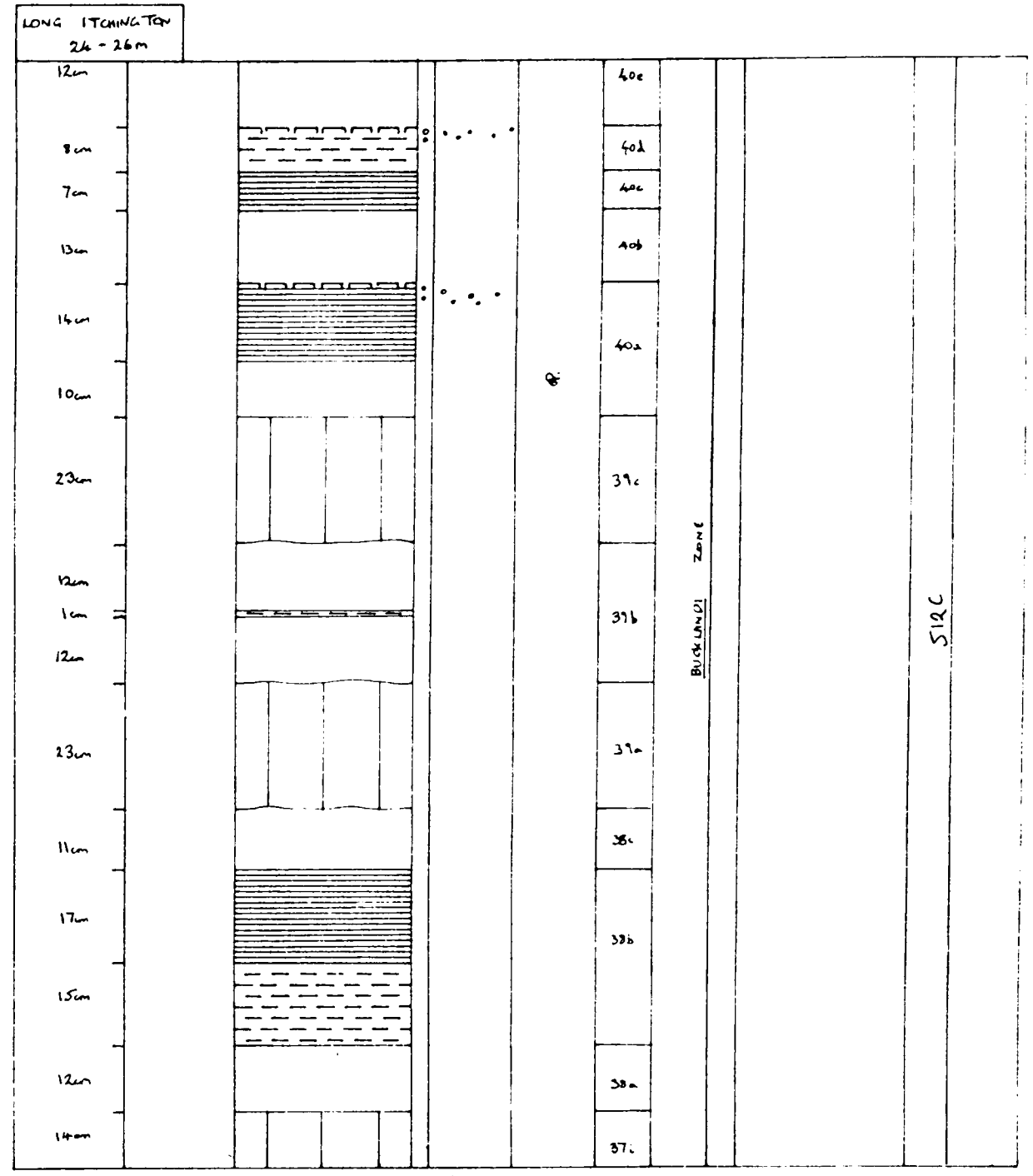
LONG ITCHINGTON
24 - 26m
12cm
8cm
7cm
13cm
14cm
10cm
23cm
12cm
1cm
12cm
23cm
11cm
17cm
15cm
12cm
14cm
40e
40d
40c
40b
40a
39c
39b
39a
38c
38b
38a
37c
BUCKLANDI ZONE
512C

APPENDIX FOR CHAPTER 3

GEOCHEMICAL METHODODOLOGY.

3.1 Bulk Sample Preparation.

All bulk samples were reduced to powder in the same way. 10-15 grams of rock were collected into polythene bags with a hammer and chisel from horizons 2cm thick at Lyme Regis and 3cm thick at Watchet. The specimens were crushed into pieces less than 3mm maximum length using a 6lb hammer and a metal plate. Marl and shale samples were ground for 10 minutes in a planetary ball-mill with agate pots (15g capacity). Limestone and laminated limestone samples were ground the same way, but for 15-20 minutes. Caking only occurred if the samples had not dried. The powders were stored in glass pots.

3.2 Gryphaea Specimen Preparation.

Specimen powders were only collected from left (lower) valves. Rock matrix was removed from the outer surface of the fossil using a dry tooth-brush and a steel pin. Powders were generated with a Burgess vibro-tool which has a vibrating tungsten carbide point. In most cases a point 1.5cm behind the umbo and along the median line was selected for drilling (position A on Fig 3.4H). In the case of specimens BLG12, 13, 17, 57 and 27 the umbos had been lost prior to or during collection so the normal position for drilling could not be used. Areas approximately 3 by 5mm on the outside of the shell were drilled, yielding 15-40mg of powder. The powder was stored in glass bottles.

Because Gryphaea grew its shell by adding successive growth layers to the inside of previous layers, the sampling mixed powder from several layers. Because of this and to allow Gryphaea specimens to be collected with the greatest possible stratigraphic resolution, no effort was made to select specimens of the same size/age.

3.3 Determination of %$CaCO_3$, %TOC and %FeS_2.

The Strohlein Coulomat 702 was used to determine total carbon or total sulphur in the rock powders. Unglazed porcellain 'boats' were pre-heated to 1000°C for 15-20 minutes and stored in a desiccator to remove organic matter and water.

To analyse for carbonate-carbon, 70mg of powder were weighed into each boat and heated at 450°C for 15 hours to remove organic matter from the sample without decomposing the carbonate. Analysis of each boat used the carbon setting on the Coulomat with the furnace at 1200°C. The carbonate was decomposed in a stream of pure oxygen yielding carbon dioxide and sulphur dioxide (from the pyrite) which was passed into a desiccating tube and then into a mixture containing urea designed to remove the sulphur dioxide. The carbon dioxide was dissolved by bubbling and stirring the gas into a solution with an accurately measured pH. Electrodes automatically passed an electric current through the solution to restore the pH value. The amount of electricity used was measured and provided the pH did not change too much the 'count number', reflecting the amount of electricity involved, was directly proportional to the amount of carbon dioxide dissolved. The pH was monitored and if it changed too rapidly then the stirrer was automatically turned off until the pH could be reset electrochemically. Once the rate of change of pH was below a certain limit, the count was stopped automatically and the next sample was inserted; the whole procedure took about 5 minutes. The count number was multiplied by 0.2 and divided by the weight in milligrams to yield the weight percent carbonate carbon. This was converted to the percent calcium carbonate assuming that virtually no dolomite was present (Sections 2.2, 2.3 and 2.6). The %TOC was determined in exactly the same way but without the step to remove organic

matter. The second value obtained equals carbonate carbon plus organic carbon so the %TOC was calculated by subtracting the two determinations.

The determination of the amount of pyrite was carried out by measuring the amount of sulphur in the rocks. About 50mg of powder was used and a little powdered tin added to act as a flux. The Coulomat was put on the sulphur setting and the furnace heated to 1350°C. This time the sulphur dioxide produced was not removed from the gas and the pH of the solution was chosen such that the sulphur dioxide dissolved but the carbon dioxide did not. This procedure took around 10 minutes per sample. The conversion factor used with the count number was 0.01 and the %sulphur determined and converted into pyrite using the formula FeS_2. (This formula was confirmed using XRD in Section 2.3.) It is assumed that no elemental sulphur was present in these powders. The sulphur values obtained might reflect a proportion of gypsum (detected by XRD Section 2.3). However, as there is no evidence for hypersalinity in the normal marine environment of the basal Lias, any gypsum can be assumed to represent the surface weathering product of pyrite.

3.4 Determination of %Fe/R and DOP/R.

As discussed in Section 3.4.2a these parameters are defined as: %Fe/R = %Fe/in pyrite + %Fe/soluble in HCl, and DOP/R = %Fe/pyrite ÷ %Fe/R. The sulphur measurement was used to calculate %Fe/pyrite. The hot HCl method of Berner (1970) extracts iron in the sediment that is able to react with hydrogen sulphide (Section 3.4.2a).

Approximately 100mg of sample powder was weighed into a conical flask and then 20ml of concentrated (11.5M) HCl added. The flask was placed on a pre-heated hot plate, brought up to boiling and allowed to

boil for 1 minute. The flask was removed and allowed to cool a little and the solution was gravity filtered into a volumetric flask (Whatman 42 filter paper, ϕ=2.7μm). The flask was washed-out into the funnel using deionized water. Then the filter paper was washed several times. The volume of solution was made up using deionized water.

A Perkin-Elmer 306 acetylene-air atomic absorbtion spectro-photometer was used to determine the iron concentration of the solutions by comparison with standards. If the concentration of iron lay outside the linear part of the calibration curve the solutions were diluted accordingly. The weight of sample, the dilution factor, and the iron concentration measured were converted into values of %Fe/HCl.

To check that pyrite is not dissolved in boiling concentrated HCl as assumed by Berner (1970), 97.1mg of powder from sample BL9 was mixed with 2.7mg of pure pyrite. The value of Fe/HCl for this sample was previously measured as 0.67%. Thus allowing for the proportion of sample, 0.65%Fe would be measured for the mixture if no pyrite had dissolved. After repeating the procedure above, 0.74%Fe was measured so 0.09%Fe must have come from dissolution of the added pyrite. The amount of iron present in the added pyrite is 1.26mg (using atomic weights) so 7.1% of the iron in the added pyrite was dissolved. Therefore the measured values of %Fe/HCl were overestimated by about 7%. However, as most iron in the value for Fe/R comes from pyrite this error can be discounted. For instance sample BL328 has the greatest proportion of Fe/R represented by Fe/HCl of all the samples analysed. The values in this case were measured as: Fe/HCl=0.14%, Fe/pyrite=0.37% and Fe/R=0.51%. If Fe/HCl was overestimated by 7%, the correct values should be: Fe/HCl=0.13% and Fe/R=0.50%. So the overestimation of Fe/R due to

the inaccuracies associated with the Fe/HCl measurement, is about 2‰ (negligible compared to net experimental error).

3.5 Determination of $\delta^{18}O$ and $\delta^{13}C$.

Analyses were conducted at the BGS Gray's Inn Road Laboratory in London. Dark marl and laminated shale powders were placed in a stream of oxygen in a plasma furnace for 15 hours to remove organic matter. 25 specimen powders including all rock types were treated as though substantial pyrite was present and would cause H_2S production during extraction. The extracted gases were passed over heated lead formate to remove H_2S before any further purification took place. However, no reaction with the lead formate occurred so this part of the procedure was abandoned. No subsequent preparations yielded H_2S according to the mass spectra.

Extraction of CO_2 from the carbonate followed the procedure of McCrea (1950). Outgassed phosphoric acid was reacted for 15 hours with the sample after equilibriation at 25.2°C in a water-bath. The liberated gas was passed through an acetone cold-trap (-90°C to remove water and phosphoric acid) into a liquid nitrogen cold-trap (-196°C). Keeping the nitrogen cold-trap filled, the gas collection vessel was evacuated to remove nitrogen gas, leaving the carbon dioxide frozen down in the trap. Analysis of the carbon dioxide was carried out with a Micromass 903 mass spectrometer. Two or three aliquots of the laboratory standard (MCS-8) were extracted and measured along with each sample series. The data were corrected for instrumental and isobaric effects using the methods of Craig (1957) and Deines (1970). The results were expressed in the del notation as permil deviation from the PDB standard:

$$\delta^{13}C = \left[\frac{Rc\ sample}{\ } - 1\right] * 1000 \text{ permil}, \qquad Rc = {}^{13}C/{}^{12}C,$$

$$\left[\text{Rc PDB}\right]$$

$$\delta^{18}O = \left[\frac{\text{Ro sample}}{\text{Ro PDB}} - 1\right] * 1000 \text{ permil}, \qquad Ro = {}^{18}O/{}^{16}O.$$

3.6 Reproducibility.

The determination of %C(in carbonate) and %C(total) -(used to determine %$CaCO_3$ and %TOC)-, and %S -(used to determine %FeS_2 and %Fe/pyrite)- involved repeated determinations for every sample. Values of %Fe/HCl (giving %Fe/R and DOP/R), $\delta^{18}O$, and $\delta^{13}C$ were repeated for 10% of the samples analysed. For repeated samples the quoted and plotted values are averages. The pairs of results can only be used to assess the maximum 'error' in reproducibility likely for a particular type of determination. For instance, if the largest difference in values for all the pairs of sulphur determinations was 0.4% sulphur, then the maximum 'error' would be quoted here as ±0.2%. This method is crude but it gives some idea of the reproducibility involved.

Many geochemical parameters used here are calculated from a combination of others (eg DOP/R = Fe/py ÷ Fe/R). The 'errors' for different types of determination have to be combined in these cases. The following general formulae have been used for this purpose:

Given three types of analytical determination: a, b and c, the maximum 'errors' associated are denoted: Ea, Eb & Ec.

If: $c = k * a$ (k = constant), then $Ec = k * Ea$,

If: $c = a \pm b$, then $Ec = \sqrt{\left((Ea)^2 + (Eb)^2\right)}$

If: $c = \frac{a}{b}$, then $Ec = \sqrt{\left((Ea \div \text{Mean of } a)^2 + (Eb \div \text{Mean of } b)^2\right)}$

On this basis the following values are meant to indicate the maximum errors associated with each type of analytical determination:

$CaCO_3$-------	<±1.58%	Fe/Rcf------	<±0.11%
TOCcf-------	<±0.25%	DOP/R-------	<±0.055
FeS_2cf------	<±0.23%	$\delta^{18}O$--------	<±0.14 permil
'Clay'cf-----	<±1.7%	$\delta^{13}C$--------	<±0.05 permil

APPENDIX FOR CHAPTER 4

COMPUTER PROGRAM FOR ILLUSTRATING TIME SERIES AND GENERATING WALSH POWER SPECTRA.

4.1 Listing of Program WPSPEC.

```
C
C             WPSPEC.FOR          GRAHAM  P. WEEDON
C
C   PROGRAM TO ILLUSTRATE TIME SERIES AND/OR GENERATE
C             WALSH POWER SPECTRA
C
C   WRITTEN IN FORTRAN TO RUN ON A VAX/VMS (VERSION V4.3) COMPUTER
C
C       TIME SERIES:
C     TIME SERIES ARE OBTAINED BY DIGITISING MEASURED STRATIGRAPHIC
C   SECTIONS. FIRST A FILE CALLED 'TSER.DAT' IS CREATED WITH FORMAT
C   (F5.0,1X,F6.2). THIS CONTAINS BED THICKNESS IN THE FIRST COLUMN
C   AND ROCK TYPE CODE (eg. LIMESTONE=+1, SHALE=-1) IN THE SECOND.
C
C       RUNNING WPSPEC:
C     ONCE WPSPEC.FOR IS STARTED THE DATA FROM TSER.DAT ARE READ INTO
C   ARRAY 'X'. WPSPEC.FOR IS DIMENSIONED TO ACCEPT UP TO 2000 LINES
C   IN TSER.DAT AND UP TO 17000 DATA POINTS. FOR EXAMPLE IF TSER.DAT
C   HAD 2 LINES: '  33. -1.0  ' & '   6.  1.0  ' THEN 39 POINTS
C   WOULD BE GENERATED. AFTER A VARIETY OF REMINDERS, THE NUMBER OF
C   POINTS, 'N', IS PRINTED ON THE SCREEN. THE PROGRAM CAN BE LEFT AT
C   THIS POINT IF THE NUMBER OF POINTS IS WRONG AND THE DATA FILE
C   NEEDS EDITING.
C
C   THE PROGRAM CONTINUES WITH THE OPTION TO ILLUSTRATE THE DATA/TIME
C   SERIES (SEE 'GENERATING HARD COPIES OF GRAPHS'). NEXT THERE IS AN
C   OPTION TO GENERATE POWER SPECTRA OR LEAVE THE PROGRAM. IF POWER
C   SPECTRA ARE TO BE GENERATED, THE TIME SERIES MUST HAVE THE NUMBER
C   OF POINTS (N) EQUAL TO AN INTEGER POWER OF 2 (ie. 2,4,8,16,.....
C   ...16384 - LIMITED BY THE DIMENSION STATEMENT).
C
C       ILLUSTRATING TIME SERIES:
C     THE PROGRAM GENERATES A GRAPHICAL OUTPUT FILE USING GHOST80
C   LIBFILE SUBROUTINES. THE FILE IS CALLED 'DEFAULT.GRD;1' (SEE
C   BELOW FOR HARDCOPIES OF GRAPHS).
C
C       GENERATING WALSH POWER SPECTRA:
C     FIRST THE NUMBER OF SAMPLES PER METRE IS REQUESTED ON THE
C   SCREEN. THE FORMAT IS F5.0, SO IF THE SAMPLE INTERVAL IS 1cm
C   FOR INSTANCE, THEN TYPE IN ' 100.'.
C     NEXT A SERIES OF OPTIONS ARE GIVEN. EACH OPTION ALLOWS THE
C   GENERATION OF A DIFFERENT OUTPUT FILE. THERE ARE 2 TYPES OF
C   FILE: A DATA FILE WITH A LIST OF 'POWER' AND CORRESPONDING
C   'CYCLES PER METRE' VALUES (eg. 'PSPEC.DAT'). OR A GRAPHICAL
C   OUTPUT FILE GENERATED USING GHOST80 LIBFILE SUBROUTINES
C   (eg. DEFAULT.GRD;1):
C
C  CONTENTS                    OUTPUT FILES
C                        DATA FILE          GRAPHICS FILE
C
C UNSMOOTHED POWER       PSPEC.DAT          DEFAULT.GRD;1
C   v. FREQ.
C  SMOOTHED POWER        SPEC.DAT           DEFAULT.GRD;1
C   v. FREQ.
C LOG10(SMOOTHED         LOGP.DAT           DEFAULT.GRD;1
C POWER) v. FREQ.
C
C     EACH TIME A SPECTRUM IS TO BE PLOTTED, THE AXES LIMITS ARE
C   REQUESTED ON THE SCREEN. THE PROGRAM SHOULD NOW FINISH WITH
C   'FORTRAN STOP' ON THE SCREEN.
C
C       STATISTICAL TESTS FOR POWER SPECTRA:
C     ALL THE POWER VALUES HAVE BEEN NORMALISED FOLLOWING
C   NOWROOZI (1967, SEE REFERENCES AT END OF PROGRAM). THUS
C   FISHER'S TEST FOR WHITE NOISE IS EASILY APPLIED USING
C   NOWROOZI'S TABLES (Nb. HIS VALUE 'm'  THE No. OF SPECTRAL
C   ESTIMATES WHICH   N/2 + 1). THE LOG10 POWER SPECTRA CAN BE USED
C   TO APPLY THE TEST FOR RED NOISE FOLLOWIING SCHWARZACHER 1975
C   (pp210-212)(Nb. DEGREES OF FREEDOM FOR SMOOTHED POWER=4 SEE
C   BEAUCHAMP 1975 p100).
C
C       GENERATING HARDCOPIES OF GRAPHS:
C     GRAPHICAL OUTPUT FILES OR 'GRIDFILES' CAN BE DUMPED AS
C   HARDCOPIES USING A 'CALCOMP 1012' GRAPHICS TERMINAL. FIRST
C   LOG-IN, MAKE SURE THE CALCOMP PLOTTER IS ON-LINE, TYPE
C   'C1012' AND THEN 'DEFAULT.GRD;1' AND THE SPECTRA OR TIME
C   SERIES SHOULD BE PLOTTED. NOTE THAT MANY GRAPHS CAN BE HELD
C   BY DEFAULT.GRD;1.
C
      PROGRAM WPSPEC
      DIMENSION A(2000),B(2000),X(17000),Y(17000),P(17000)
      DIMENSION W(17000),C(17000),D(17000),E(17000)
      DIMENSION F(17000),THICK(5000),G(17000)
```

```
C
C   SERIES OF NOTES LISTED ON SCREEN
C
      WRITE(*,5)
    5 FORMAT('                                          ')
      WRITE(*,5)
      WRITE(*,23)
      WRITE(*,10)
   10 FORMAT('        ***            PROGRAM TO            *** ')
      WRITE(*,15)
   15 FORMAT('        ***  ILLUSTRATE TIME SERIES OR    *** ')
      WRITE(*,20)
   20 FORMAT('        *** GENERATE WALSH POWER SPECTRA *** ')
      WRITE(*,23)
   23 FORMAT('        ************************************* ')
      WRITE(*,5)
      WRITE(*,5)
      WRITE(*,25)
   25 FORMAT('     NOTE : ')
      WRITE(*,28)
   28 FORMAT('    ********')
      WRITE(*,30)
   30 FORMAT('  1)READ COMMENT LINES IN WPSPEC.FOR .')
      WRITE(*,40)
   40 FORMAT('  2)TO GENERATE SPECTRA MAKE N=2**K, (K=INTEGER).')
      WRITE(*,45)
   45 FORMAT('  3)EXPERIMENTING WITH PERFECT SQUARE WAVES ? : ')
      WRITE(*,50)
   50 FORMAT('    REMEMBER THAT LOG10(0) IS IMPOSSIBLE !')
      WRITE(*,5)
      WRITE(*,5)
C
C   READ IN TIME SERIES DATA FROM TSER.DAT AND STORE AS STRING OF
C   VALUES IN ARRAY 'X' WITH 'N' POINTS
C
      OPEN(UNIT=1,FILE='TSER.DAT',FORM='FORMATTED',STATUS='OLD')
      READ(1,65,END=70)(A(I),B(I),I=1,2000)
   65 FORMAT(F5.0,1X,F6.2)
   70 NROWS=I-1
      J=0
      DO 80 I=1,NROWS
      DO 75 L=1,A(I)
      J=J+1
      X(J)=B(I)
   75 CONTINUE
   80 CONTINUE
      N=J
      WRITE(*,85)N
   85 FORMAT(1X,19HNUMBER OF POINTS  ,I5)
      WRITE(*,5)
C
C   OPTION TO LEAVE PROGRAM GIVEN SO THAT TSER.DAT CAN BE EDITED
C   TO CORRECT LENGTH IF NECESSARY.
C
      WRITE(*,90)
   90 FORMAT(' WANT TO ESCAPE FROM THE PROGRAM HERE ? YES=1, NO=0 ')
      READ(*,95)LMN
   95 FORMAT(I1)
      IF(LMN.EQ.1)GO TO 1000
      WRITE(*,5)
C
C   OPTION TO ILLUSTRATE TIME SERIES
C
      WRITE(*,100)
  100 FORMAT(' ILLUSTRATE TIME SERIES ? YES=1, NO=0 ')
      READ(*,95)LOPT
      WRITE(*,5)
      IF(LOPT.EQ.0)GO TO 200
      DO 110 L=1,N
      THICK(L)=L
  110 CONTINUE
C
C   PLOT TIME SERIES USING GHOST80 LIBFILE SUBROUTINES
C
      AN=N
      CALL PAPER(1)
      CALL PSPACE(0.1067,0.8933,0.436,0.564)
      CALL MAP(0.0,AN,-2.0,2.0)
      CALL PTJOIN(THICK,X,1,N,1)
      CALL GREND
  200 CONTINUE
C
C   OPTION TO GENERATE POWER SPECTRA OR LEAVE PROGRAM
C
      WRITE(*,202)
  202 FORMAT(' GENERATE POWER SPECTRA ? YES=1, NO=0 ')
```

```
      READ(*,95)LOT
      WRITE(*,5)
      IF(LOT.EQ.0)GO TO 1000
      AN=N
      K=((LOG10(AN)/LOG10(2.0))+0.5)
      WRITE(*,5)
C
C   SCREEN REQUEST TO ENTER No. OF SAMPLES PER METRE
C
      WRITE(*,205)
  205 FORMAT(' HOW MANY SAMPLES PER METRE ? (FORMAT=F5.0) ')
      READ(*,213)FS
  213 FORMAT(F5.0)
      WRITE(*,5)
      WRITE(*,5)
C
C  WALSH TRANSFORM FROM KANASEWICH  (1981)
C
      DO 300 I=1,K
      NN=2**(I-1)
      IF(I-1)220,220,260
  220 DO 240 J=1,N,2
      FF=X(J)
      X(J)=X(J)+X(J+1)
      X(J+1)=FF-X(J+1)
  240 CONTINUE
      IF(N-2)320,320,250
  250 GO TO 300
  260 L=2*NN
      J=0
      DO 280 MA=1,N,L
      MJ=NN+MA-1
      DO 280 MW=MA,MJ,2
      J=J+1
      W(J)=X(MW)+X(NN+MW)
      J=J+1
      W(J)=X(MW)-X(NN+MW)
      J=J+1
      W(J)=X(MW+1)-X(NN+MW+1)
      J=J+1
      W(J)=X(MW+1)+X(NN+MW+1)
  280 CONTINUE
      DO 290 JJ=1,N
  290 X(JJ)=W(JJ)
  300 CONTINUE
C
C  NORMALIZE TRANSFORM RELATIVE TO NO. OF SAMPLES
C
  320 DO 330 JK=1,N
  330 X(JK)=X(JK)/N
C
C  CALCULATE POWER SPECTRAL ESTIMATES FOLLOWING BEAUCHAMP (1975)
C
      P(1)=X(1)**2
      J=1
      MN=(N/2)+1
      DO 375 I=2,N-2,2
      J=J+1
      P(J)=(X(I)**2)+(X(I+1)**2)
  375 CONTINUE
      P(J+1)=(X(N)**2)
C
C  CALCULATE NORMALIZED SPECTRAL ESTIMATES FOLLOWING NOWROOZI (1967)
C
      TPSS=0.0
      DO 400 I=2,MN
      TPSS=TPSS+(P(I)**2)
  400 CONTINUE
      G(1)=P(1)
      DO 450 I=2,MN
      G(I)=(P(I)**2)/TPSS
  450 CONTINUE
C
C  CALCULATE CYCLES PER METRE FOR POWER VALUES
C
      Y(1)=0.0
      AN=N
      DO 500 J=2,MN
      AJ=J
      Y(J)=(100.0)/((AN/(0.01*FS))/(AJ-1.0))
  500 CONTINUE
      WRITE(*,505)
  505 FORMAT(' DO YOU WANT A PSPEC.DAT FILE ? YES=1, NO=0 ')
      READ(*,95)LMS
      WRITE(*,5)
      IF(LMS.EQ.0)GO TO 560
C
C   WRITE VALUES TO DATA FILE PSPEC.DAT
```

```
      OPEN(UNIT=2,FILE 'PSR-C.DAT',FORM='FORMATTED',STATUS='NEW')
      WRITE(2,510)N,TPSS
  510 FORMAT(1X,15HUNSMOOTHED  N    ,I4,3X,7HTPSS    ,E10.4)
      WRITE(2,525)
  525 FORMAT(2X,16HNORMALIZED POWER,2X,16HCYCLES PER METRE)
      WRITE(2,550)(G(J),Y(J),J=1,MN)
  550 FORMAT(6X,E10.4,11X,F8.4)
  560 WRITE(*,570)
  570 FORMAT(' PLOT UNSMOOTHED P v. FREQ ? YES=1, NO=0')
      READ(*,95)LMM
      IF(LMM.EQ.0)GO TO 600
C
C   SCREEN REQUEST FOR AXES LIMITS
C
      WRITE(*,575)
  575 FORMAT(' TYPE IN AXES LIMITS REQUIRED: ')
      WRITE(*,580)
  580 FORMAT(' ENTER MAX. FREQ. VALUE  (FORMAT=F6.2): ')
      READ(*,585)AFMAX
  585 FORMAT(F6.2)
      WRITE(*,590)
  590 FORMAT(' ENTER MAX. POWER VALUE  (FORMAT=F5.3): ')
      READ(*,595)APMAX
  595 FORMAT(F5.3)
      WRITE(*,5)
      WRITE(*,5)
C
C   PLOT SPECTRUM USING GHOST80 LIBFILE SUBROUTINES
C
      CALL PAPER(1)
      CALL PSPACE(0.10,0.58,0.10,0.40)
      CALL MAP(0.0,AFMAX,0.0,APMAX)
      CALL AXES
      CALL PTJOIN(Y,G,2,MN,1)
      CALL GREND
  600 CONTINUE
C
C   SMOOTH SPECTRUM USING A 3 POINT HANNING WINDOW (BEAUCHAMP 1975)
C
      NN = MN-1
      C(1) - P(1)
      C(2)=(0.5*P(2))+(0.5*P(3))
      DO 700 J=3,NN
      C(J)=(0.25*P(J-1))+(0.5*P(J))+(0.25*P(J+1))
  700 CONTINUE
      C(MN)=(0.5*P(MN-1))+(0.5*P(MN))
      TPSS=0.0
      DO 710 I=2,MN
      TPSS=TPSS + (C(I)**2)
  710 CONTINUE
      F(1) = C(1)
      DO 720 I=2,MN
      F(I)=(C(I)**2)/TPSS
  720 CONTINUE
      WRITE(*,722)
  722 FORMAT(' DO YOU WANT A SPEC.DAT FILE ? YES=1, NO=0')
      READ(*,95)LMT
      WRITE(*,5)
      IF(LMT.EQ.0)GO TO 780
C
C   WRITE VALUES TO DATA FILE SPEC.DAT
C
      OPEN(UNIT=2,FILE 'SPEC.DAT',FORM='FORMATTED',STATUS='NEW')
      WRITE(2,725)N,TPSS
  725 FORMAT(1X,13HSMOOTHED   N=,I4,1X,7H  TPSS=,E10.4)
      WRITE(2,750)
  750 FORMAT(4X,5HPOWER,11X,16HCYCLES PER METRE)
      WRITE(2,775)(F(K),Y(K),K=1,MN)
  775 FORMAT(3X,E10.4,10X,F8.4)
  780 WRITE(*,800)
  800 FORMAT(' PLOT SMOOTHED P v. FREQ ? YES=1, NO=0')
      READ(*,95)LMO
      IF(LMO.EQ.0)GO TO 900
C
C   SCREEN REQUEST FOR AXES LIMITS
C
      WRITE(*,575)
      WRITE(*,580)
      READ(*,585)BFMAX
      WRITE(*,590)
      READ(*,595)BPMAX
      WRITE(*,5)
      WRITE(*,5)
C
C   ON STEP PLOT
C
```

```
      CALL PAPER(1)
      CALL PSPACE(0.10,0.58,0.10,0.40)
      CALL MAP(0.0,BPMAX,0.0,BPMAX)
      CALL AXES
      CALL PTJOIN(Y,F,2,MN,1)
      CALL GREND
  900 CONTINUE
      WRITE(*,910)
  910 FORMAT(' DO YOU WANT A LOGP.DAT FILE ? YES=1, NO=0')
      READ(*,95)LMF
      WRITE(*,5)
      WRITE(*,925)
  925 FORMAT(' PLOT LOG10(P) v. FREQ ? YES=1, NO=0')
      READ(*,95)LMP
      IF(LMF.EQ.1)GO TO 950
      IF(LMP.EQ.0)GO TO 1000
C
C   SCREEN REQUEST FOR AXES LIMITS
C
      WRITE(*,575)
      WRITE(*,580)
      READ(*,585)CPMAX
      WRITE(*,940)
  940 FORMAT(' ENTER MIN. POWER VALUE (FORMAT=F5.1): ')
      READ(*,945)CPMIN
  945 FORMAT(F5.1)
      WRITE(*,5)
      WRITE(*,5)
C
C   CALCULATE LOG10(SMOOTHED POWER)
C
  950 D(1)=LOG10(F(1))
      DO 960 I=2,MN
      D(I)=LOG10(F(I))
  960 CONTINUE
      IF(LMF.EQ.0)GO TO 980
C
C   WRITE VALUES TO DATA FILE LOGP.DAT
C
      OPEN(UNIT=2,FILE='LOGP.DAT',FORM='FORMATTED',STATUS='NEW')
      WRITE(2,965)N
  965 FORMAT(9X,13HSMOOTHED    N=I4)
      WRITE(2,970)
  970 FORMAT(1X,11HLOG10 POWER,8X,16HCYCLES PER METRE)
      WRITE(2,975)(D(K),Y(K),K=1,MN)
  975 FORMAT(3X,F8.4,12X,F8.4)
      IF(LMP.EQ.0)GO TO 1000
  980 CONTINUE
C
C   GHOST80 PLOT
C
      CALL PAPER(1)
      CALL PSPACE(0.10,0.58,0.10,0.40)
      CALL MAP(0.0,CPMAX,CPMIN,0.0)
      CALL ANNOTP(1,0)
      CALL AXES
      CALL PTJOIN(Y,D,2,MN,1)
      CALL GREND
 1000 CONTINUE
C
C            REFERENCES
C
C   BEAUCHAMP 1975  'WALSH FUNCTIONS & THEIR APPLICATIONS', NO.3 IN
C                   'TECHNIQUES OF PHYSICS', ACADEMIC PRESS PP67-116
C
C   KANASEWICH 1981 'TIME SEQUENCE ANALYSIS IN GEOPHYSICS'
C                     HIGWELL PRINTING
C
C   NOWROOZI  1967  'TABLE FOR FISHER'S TEST OF SIGNIFICANCE IN HARMONIC
C                     ANALYSIS', GEOPHYS. J. R. AST. SOC. 12 PP517-520
C
C   SCHWARZACHER 1975  'SEDIMENTATION MODELS AND QUANTITATIVE
C                       STRATIGRAPHY'
C                       DEVELOPMENTS IN SEDIMENTOLOGY 19, ELSEVIER
C
      STOP
      END
```

APPENDIX FOR CHAPTER 5

PUBLICATIONS.

5.1 Weedon 1985 (Terra Cognita 5 p110).

PALAEOCLIMATIC INFORMATION FROM ANCIENT PELAGIC AND HEMIPELAGIC CYCLIC SEDIMENTS

G P WEEDON
Department of Earth Sciences Oxford University, Parks Road, Oxford OX1 3PR UK

Fourier power spectra applied to Pleistocene records of climatic change have revealed cycles that match the duration of changes in Earth's orbital parameters (precession, obliquity and eccentricity). Thus Milankovitch' theory of climatic change was supported. Similarly, power spectra for geochemical data and bedding-plane spacing in Jurassic and Cretaceous pelagic rocks have been used to suggest orbitally-forced climatic changes.

Walsh power spectra have been applied, for the first time, to cyclic sedimentary rocks. The rocks studied (Blue Lias Formation) are believed to represent hemipelagic deposition on the early Jurassic continental shelf of S.W. Britain. Three sediment types reflect cycles in bottom-water anoxia combined with changes in the clay-to-carbonate mud ratio. The spectra reveal four cycles with estimated durations of the modern orbital-precession (19 and 23Kyr) and obliquity (31 and 41Kyr) changes. The cyclicity is, provisionally, related to orbitally-forced changes in the volume of runoff from adjacent land-masses. The durations allow estimation of mean sedimentation rate at different localities. Net sedimentation rate can be calculated assuming that one ammonite zone represents 1Myr. The ratio of these two figures suggests that 70% of the sediment that could have accumulated was actually eroded or was never deposited, leaving hiatuses within the series.

The data used are simply measurements of the thickness of beds of different sediment-types; therefore Walsh power spectra can be generated very easily. The effects of bioturbation, hiatuses and diagenesis are readily allowed for during generation and interpretation of the spectra. This application provides a quick and relatively simple method for the extraction of palaeoclimatological, stratigraphic and, perhaps, diagenetic information from ancient pelagic and hemipelagic rocks.

Earth and Planetary Science Letters, 76 (1985/86) 321–335
Elsevier Science Publishers B.V. Amsterdam — Printed in The Netherlands

Hemipelagic shelf sedimentation and climatic cycles: the basal Jurassic (Blue Lias) of South Britain

G.P. Weedon

Department of Earth Sciences, University of Oxford, Parks Road, Oxford OX1 3PR (England)

Received May 23, 1985; revised version received August 22, 1985

The sedimentology, cyclicity and hiatuses of the Blue Lias Formation (basal Jurassic) were investigated at five localities in South Britain. Most carbonate mud, which is the dominant carbonate component, has been neomorphosed to microspar. However, carbonate mud was apparently supplied by coccoliths in zooplankton faecal pellets, suggesting hemipelagic sedimentation. Clay is assumed to have been supplied by rivers. The three sediment types involved reflect cyclic changes in bottom-water oxygenation levels combined with changes in the clay-to-carbonate mud ratio.

Walsh power spectra have been applied for the first time to measured sections in order to investigate the control of cyclicity. This application is analogous to palaeoclimatological studies of Pleistocene oxygen-isotope (ice-volume) records. The spectra show that 1 or 2 sedimentary cycles, of constant thickness, occur in four out of five sections, each of which represents several million years. The maximum possible duration of these cycles is too short for their generation by sea-level changes. Their regularity, stability and order of duration (tens of thousands of years) are consistent with the hypothesis of sedimentary cyclicity controlled by climatic change, itself forced by orbital changes in insolation (Milankovitch theory). The duration of both cycles recognised is less than 93,000 years (93 ka) and may record changes in orbital precession (21 ka) and obliquity (41 ka). Assuming that one ammonite zone represents 1 Ma, comparison of the longest-possible with the implied durations of the cycles, suggests that the sections are at best 20–40% complete. Loss of sediment may have occurred during winter storms or hurricanes. A model relating the sedimentary cycles to changes in the volume of runoff is proposed.

1. Introduction; orbital cycles and sedimentation

Since the classic paper by Hays et al. [1], Milankovitch theory has become a well established part of palaeoclimatic investigations (e.g. [2]). According to the theory changes in orbital parameters cause near-regular oscillations in the amount of radiation received at a given latitude and given time of year, and hence lead to climatic cycles ([3], and see Berger's paper in [4]). Cyclic variations in oxygen-isotope values and percentage carbonate within deep-sea cores have been ascribed to orbitally forced climatic changes as far back as the Miocene [5]. For times when no ice was present on the globe, for instance in the Triassic-Cretaceous, it has been speculated that certain cyclic marine and lacustrine rocks owe their cyclicity to a climatic control ([6,7], papers by de Boer, Olsen and Anderson in [4] and by Schwarzacher and Fischer in [8]). Barron et al. [9] showed, using a combination of geochemistry, sedimentology and General Circulation Model results, how cycles in the Greenhorn Formation of the North American Cretaceous probably recorded climatic cycles. An alternative approach towards demonstrating climatic control of sedimentation is the application of power spectral analysis [10]. Power spectra for Pleistocene data have been used to identify the role of orbital forcing because of its regularity and the characteristic duration of the orbital cycles [1]. The principal cycles involved are 100 ka (eccentricity), 41 ka (obliquity) and about 21 ka (precession) in duration [4].

In 1964 Schwarzacher [10] demonstrated regular cyclicity in limestone bed thickness for the Irish Carboniferous using power spectra. Carss and Neidell [11] suggested for Scottish cyclothems using a "marine" or "non-marine" classification that sedimentation was controlled glacio-eustatically or by local climatic cycles, in agreement with Schwarzacher's work.

The first application of power spectra to sedi-

0012-821X/86/$03.50 © 1986 Elsevier Science Publishers B.V.

ments formed on an ice-free globe was probably made by Dunn using geochemical data for the Kimmeridgian in South England [12]. This was continued for the Cretaceous in Italy (see de Boer in [4] and Schwarzacher and Fischer in [9]). All these studies indicated climatic control of cyclicity using Fourier power spectra. Walsh power spectra provide a fast method for the analysis of cyclic sections by using a coding system analogous to that of Carss and Neidell [11, fig. 4]. In this paper Walsh power spectra have been applied to Hettangian and Sinemurian rocks in South Britain (Fig. 1), using data measured along four coastal sections and within one active quarry. This application was made in order to investigate the possibility that their cyclicity was controlled climatically. The data used (which can be obtained from the author upon request) include a list of rock-type codes and thicknesses with the position of the spectral data (Fig. 1), bed numbers and ammonite zones. The zonal system used follows that of Dean et al. [13] and Cope et al. [14]. The zones and bed numbers were related to the measured data using [14] and the local stratigraphic descriptions [15–19].

Several rock types are interbedded on a centimetre-decimetre scale in tabular beds. They record cyclic changes in calcium carbonate, organic carbon contents and intensity of bioturbation. A long-standing controversy over the role of diagenesis complicates the picture of simple environmental changes as the sole cause of the cyclicity [20]. Diagenetic exaggeration of primary cyclicity is commonplace and does not prevent or invalidate spectral analysis [8,21]. However, a primary cyclicity must be demonstrated, otherwise application of power spectra for palaeoclimatic work is meaningless. For example, analysis of bedding-spacing would only reveal diagenetic processes if the bedding itself was solely diagenetic in origin. The recent work of House [7] uses a combination of logic and mathematical modelling. Unfortunately a subjective element enters this modelling and little effort was made to distinguish between di-

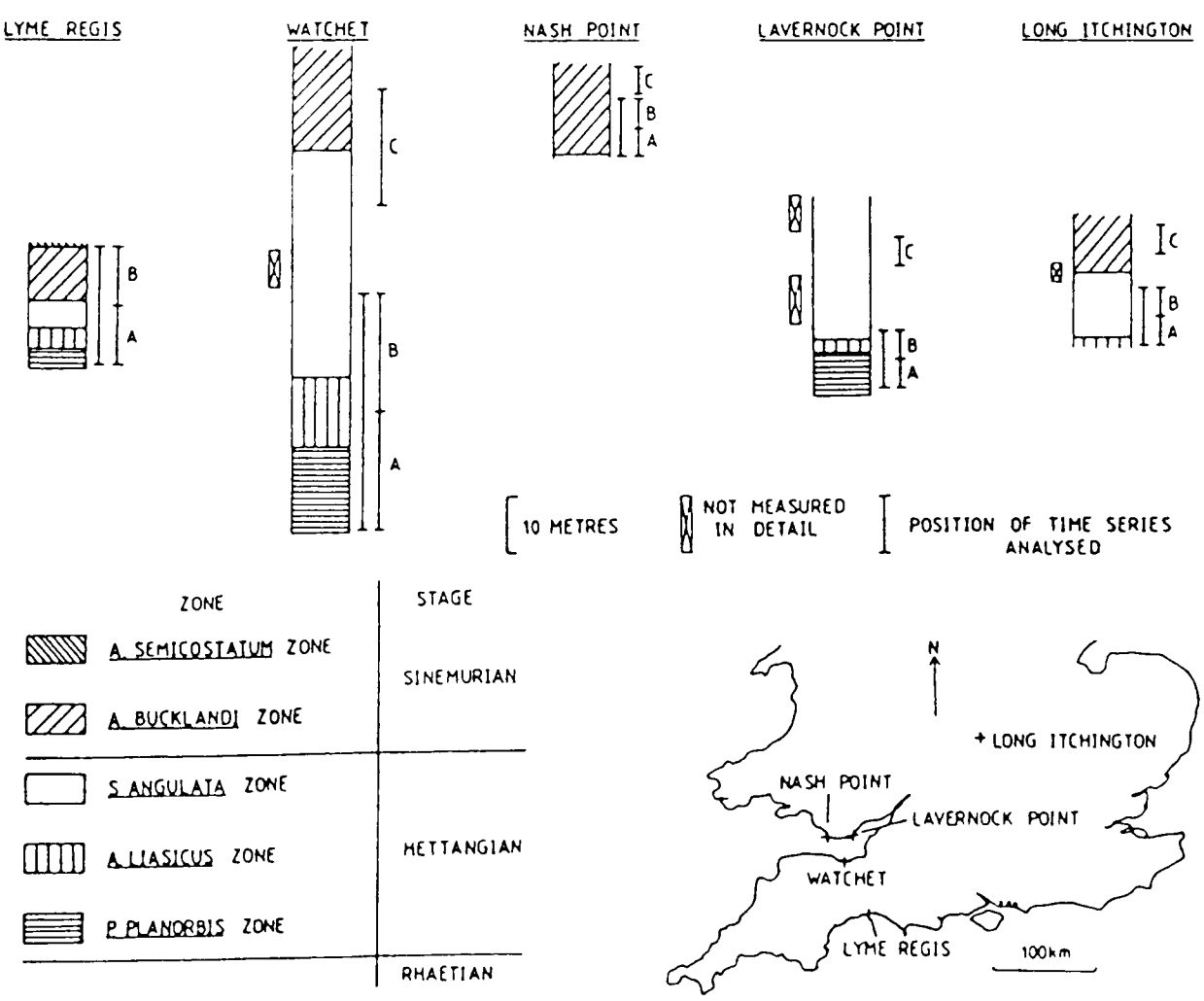

Fig. 1. Location of the sections measured and the time series obtained from them.

agenetic and primary cyclicity. In order to demonstrate the primary aspect of the cyclicity, the sedimentology and diagenesis is discussed here in some detail.

2. Description of rock types

In the field five rock types are recognised, viz. limestone, light- and dark-marl, laminated shale and laminated limestone, four of these are illustrated in Fig. 2. Light marls, dark marls and dark, laminated shales form beds from one to tens of centimetres thick which can be traced laterally for hundreds of metres and sometimes tens of kilometres [20]. The bed contacts are usually very sharp and planar. Limestone occurs as elliptical nodules enclosed by light marl or as beds with wavy or planar contacts. It is thought that the limestones formed during early diagenesis [20,22, 23]. Specifically limestone formation is believed to have been by calcite cementation of the pore spaces of light marl (Fig. 2). Laminated limestones are distinguished from limestones by internal lamination and a fetid odour. They are always enclosed by dark, laminated shales and usually have planar contacts; occasionally they occur in elliptical nodules with laminae passing inside. This rock type appears to represent dark, laminated shale cemented during diagenesis by analogy with the limestones. For a description of the fossils see [24–28]. A more detailed description of the different rock types given below, includes percentage calcium carbonate and organic carbon. Compositions were determined with a "Coulomat 702" for 15 g bulk samples from Lyme Regis and Watchet. 15 samples were analysed in duplicate for each

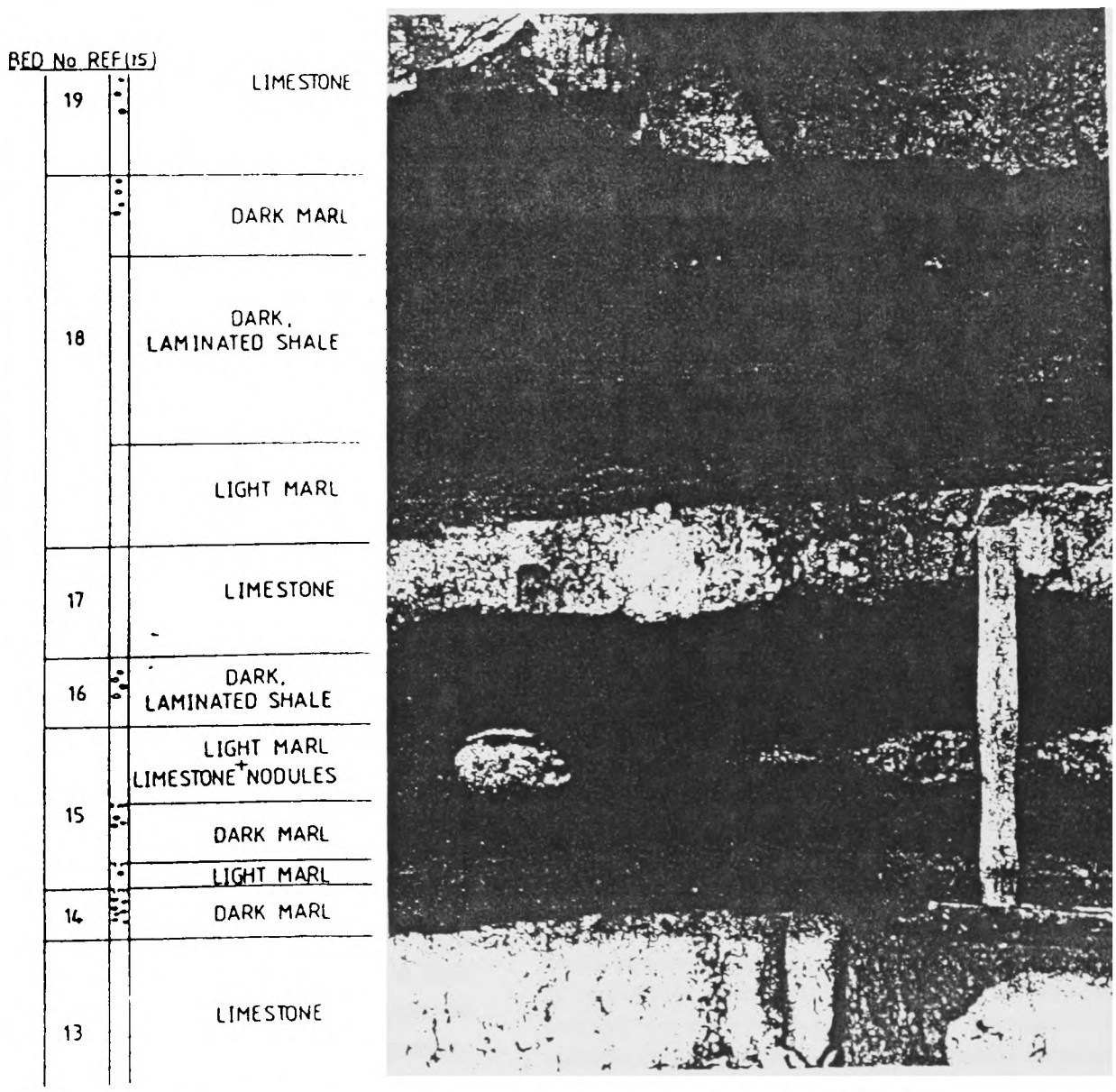

Fig. 2. Photograph of part of the *angulata* zone at Seven Rock Point, Lyme Regis. The hammer is 40 cm long.

rock type except the laminated limestone for which 6 samples were used

Light marl. Forming light blue/grey friable beds this rock type is dominated by calcite microspar and disseminated clay. The homogeneity in the field and under thin-section probably indicates complete bioturbation. Macro-fossils seem to be identical to those within the limestones except that benthos dominates due to the loss of ammonites during diagenesis (except for rare pyritized moulds). Scanning electron microscopy (SEM) of fractured surfaces reveals rare, isolated and poorly preserved coccoliths. Cathodoluminescence (CL) indicates that a large proportion of the carbonate is formed by ostracods. The ostracods are both united and disunited, form a wide range of sizes and are frequently self-supportive. Calcium carbonate: 35–57%, avg. 43%, organic carbon: 0.5–3.5%, avg. 1.3%.

Limestones. Limestones form homogeneous light blue/grey compact beds and nodules dominated by microspar with minor disseminated clay. Macrofossils are identical to those within the light marls excluding the ammonites which are a major component and are preserved as uncrushed calcite moulds [24]. SEM results are identical to those for light marls, confirming the work of Loughman [29]. CL indicates a very much lower proportion of ostracods relative to the light marls. However, within the limestones, the ostracods could only be detected by the presence of dull or non-luminescent internal matter, so in fact the proportion of ostracods present may well be higher than could be confidently inferred. Calcium carbonate: 64–89%, avg. 79%, organic carbon 0.3–1.1%, avg. 0.5%.

Dark marls. These form dark blue/grey friable beds which develop a crude fissility on weathering unlike the light marls. In thin-section most of the carbonate is present as elliptical microspar "blebs" 80 by 250 μm in cross-section on average with their long-axes parallel to bedding. The blebs are discrete or concentrated to form laminae a few diametres thick. They do not contain any type of calcite bioclasts, palynomorphs or silt-grade quartz. They are surrounded by clay and amorphous organic matter forming discontinuous laminae. The clay and amorphous organic laminae, but more importantly the discrete nature of the blebs and associated laminae, indicate a lack of bioturbation. Macrofossils seem to be identical to those found within the light marls. The SEM reveals many dense aggregates of well-preserved coccoliths (Fig. 3) [28]. The aggregates' size seems to be of the same order as that of the blebs. Occasionally individual coccolith rings can be seen to be partially engulfed by microspar crystals. CL reveals individual ostracods, not visible in transmitted light, which are embedded within organic matter and clay. Utilizing sections with burrow-fills of light marl within dark marl, the density of ostracods appears to be much lower in the dark marls. Calcium carbonate: 20–45%, avg. 33%, organic carbon: 1.0–6.5%, avg. 2.8%.

Dark, laminated shale. This rock-type is brown-black, well laminated and very fissile after weathering. Under thin-section the rock seems to be dominated by clay and organic laminae with rare microspar blebs. Macrofossils are dominated

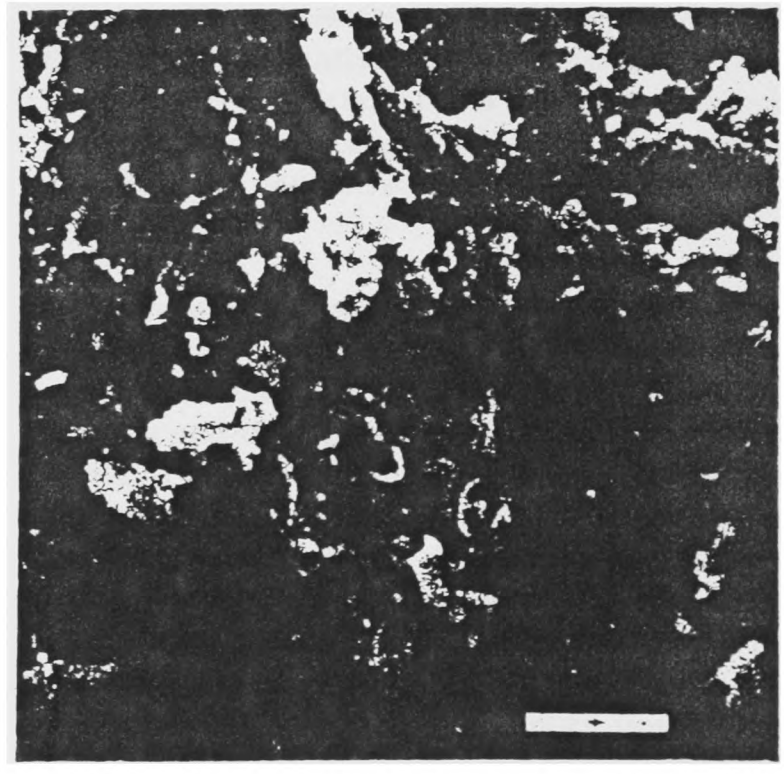

Fig. 3. Photomicrograph of a fractured surface of dark marl, basal *bucklandi* zone, Lyme Regis. A closely packed aggregate of coccoliths (centre) can be seen entirely surrounded by a clay- and organic-matter-rich matrix. Most aggregates observed are considerably larger, this picture may merely illustrate the tip of a normal sized aggregate (faecal pellet). The scale bar represents 10 μm.

by crushed ammonite moulds and restricted benthos [24]. SEM reveals the same coccolith aggregates found in the dark marls which are, however, considerably rarer. CL shows that the carbonate is predominantly present as discrete ostracods embedded within the clay and organics. They occur in all orientations, as united and disunited specimens, and in numbers approximating the dark marls. Calcium carbonate: 12–48% avg. 34%, organic carbon: 2.3–10.8%, avg. 5.7%.

Laminated limestones. This rock type is the rarest; occurring mainly within the *planorbis* zone; however, at Watchet it can be found sporadically at least into the *bucklandi* zone. It forms very dark blue/grey compact beds and nodules with a fetid odour when broken. The rock is dominated by microspar and disseminated clay with lamination formed by light microspar with vague pelloids, pyrite and sand-silt grade bioclastic fragments. Few complete bioclasts have been observed except for benthonic foraminifera. No definite ostracods can be identified from initial CL work. Calcium carbonate: 69–88%, avg. 82%, organic carbon: 0.7–3.0%, avg. 1.4%.

Burrow-mottling. Mottling occurs between light and dark marls, and this is preserved where limestones have formed. However, bed contacts usually remain sharp so burrowing must have been restricted. Dark marl fills burrows inside light marl beds and vice versa (Fig. 2). Mottling is dominated by *Chondrites*, but it also includes *Rhizocorallium, Diplocraterion, Arenicolites* and *Thalassinoides*. The dominance of *Chondrites* may indicate very low oxygen levels within the sediment during the transition between light and dark marls: thus explaining the restricted burrowing [30]. Very rarely, burrow-fills of light or dark marls are found at the tops of dark, laminated shale beds. However, where dark, laminated shale overlies one of the other rock types, no mottling occurs at the contact.

Hiatuses. Hiatuses are not apparent from biostratigraphy. At each locality, all the ammonite zones identified are present without gaps (using the local biostratigraphic descriptions and following [13–19]). Certain field observations, however, may indicate ubiquitous minor disconformities. For instance, horizons of burrows with dark marl fills can be found entirely enclosed within light marl beds with no sign of the dark marl bed which supplied the fill-material. At Lyme Regis, loose blocks of limestone occasionally show limestone intraclasts. One polished and peeled block from Lang's bed 25 of the basal *conybeari* Subzone, reveals a multiply bored and encrusted dome-shaped surface (3 cm high by > 13 cm long) underlain by intraclasts [15]. The bored and encrusted surface lies within limestone (originally light marl) and grades laterally into normal bioclastic mudstone. It is overlain by bioclastic packstone grading up into carbonate mudstone. The surface probably indicates erosion and at least a temporarily exposed hard substrate. Other features perhaps indicating hiatuses include anomalously thin beds (1–3 cm). All the sediment types are represented in these beds. They are traceable for up to hundreds of metres with sharp, gently undulating upper contacts; occasionally they are cut out laterally for approximately 20 m. Thin horizons of concentrated bioclasts may indicate winnowing or some form of sediment injection. The lack of obvious biostratigraphic gaps and of irregular contacts makes recognition of hiatuses very difficult. The observations described above have been made frequently even at the most expanded section studied (Watchet). Hiatuses may represent a significant loss of deposited sediment, therefore, they must be considered during analysis of measured sections.

3. Sedimentology and diagenesis

The size and composition of the coccolith aggregates and their presence within laminated sediments is believed to indicate an origin as zooplankton faecal pellets [31,32]. The microspar "blebs" are thought to represent neomorphosed aggregates when their common size, shape and occurrence are considered. The description of the coccoliths can be found in [28]. Loughman's SEM work was restricted to the limestones, but the lack of undoubted coccolith rings led to the belief that most of the microspar originated from green algae [29]. It is proposed here that most of the carbonate mud of the light marls and limestones is in fact coccolith material now largely neomorphosed to microspar.

The cause of the neomorphism may have been

water-films absorbed onto clay minerals [33,34]. The ubiquitous clay may be expected to have caused neomorphism of all the coccoliths. However, individual organic membranes and organic pellicles around faecal pellets may have protected the individual rings and aggregates observed (Fig. 3) [32,35]. In this model the organic matter contents are suggested as the controlling factor, explaining why so few coccoliths are observed within the light marls and limestones.

To have dominated local carbonate mud production, benthonic green algae would have required very shallow water for their high productivity [36]. Yet there is a lack of shallow-water criteria until the laterally equivalent coastal Sutton Stone and Southerndown Beds are encountered in South Wales [24,29,37]. For instance there is no evidence for exposure, micritic envelopes to bioclasts, ooids or stromatolites. Conversely pelagic elements are both common and diverse. They include ammonites, belemnites, large nekton such as the Ichthyosaurs, as well as coccolithophores, acritarchs and dinoflagellates [27]. Further it is considered very unlikely by the author that water still enough for low bottom-water oxygenation and the preservation of laminae could have been very shallow. Carbonate mud arriving in suspension was clearly only a minor source because such a low proportion of the microspar is present as disseminated, isolated crystals within the dark, laminated shale and dark marls. A certain amount of mud may have been generated by the activities of infauna when present, but it is contended here that most carbonate mud was supplied as coccolith aggregates.

The criteria for a primary cyclicity, which involved light and dark marl and dark, laminated shale, are essentially those of Hallam [20]. The burrow-mottling between light and dark marl is believed to be diagnostic of their primary distinction, particularly since both light marl burrow-fills within dark marl and vice versa are observed (Fig. 2), ([20], and Arthur et al. in [4]). Additionally dark marl preserves clay, organic and bleb-formed laminae and discrete blebs that would not have survived thorough bioturbation. Conversely the homogeneous light marls with intimately mixed clay and microspar probably do indicate ubiquitous burrowing. The rate *Chondrites* burrows penetrating the tops of dark, laminated shales also indicate a primary distinction of this sediment type from the others. Further, the lack of coccolith aggregates and blebs and the dominance of ostracod-rich carbonate, is thought here to represent a primary difference of this rock type and the dark marls. Nevertheless, it is possible that, quite apart from the limestone formation, there was some compositional exaggeration of these three rock types during diagenesis [20].

Early diagenesis led to carbonate cementation of pore spaces in the light marls and laminated shales thus producing limestones and laminated limestones and generating 5 rock types from 3 sediment types. The limestone nodules only formed within light marls (Fig. 2), and laminated limestone only within dark, laminated shales. This, and the way that the limestone beds are bedding parallel and only follow one stratigraphic horizon strongly suggests to the author that localization of cementation was controlled by primary compositions (cf. [21]).

Hallam showed that limestone bed thickness is constant, on average, regardless of the thickness of particular ammonite zones, i.e. it is independent of sedimentation rates. Additionally the number of limestones is reduced within thinner parts of a given zone [20]. These features do not have to be regarded as indicative of some rhythmic unmixing process independent of primary compositions. For instance, both observations can be explained if the main supply of carbonate for cementation was provided by dewatering fluids (cf. [29]). If the growth of a limestone was always terminated when porosity was reduced to a certain level, then higher sedimentation rates would have terminated growth earlier. But higher rates of compaction would have supplied carbonate from dewatering fluids faster, perhaps allowing faster cementation. If the two aspects of cementation, changing the time for growth and changing the rate of growth, cancelled each other then the average thickness of a limestone, once formed, would be constant and apparently independent of sedimentation rates. Additionally, the volume and average composition of the sediment supplying carbonate in dewatering fluids may have limited the number of limestones formed in a particular section. These ideas are merely intended to indicate that independent rhythmic unmixing need not apply. It is suggested here that cementation did occur during early di-

agenesis, but that it merely emphasised and was controlled by primary compositional variation.

Thus the three sediment types (pre-diagenetic) are considered to represent 3 distinct depositional environments. The deposition of light marl involved a rapid supply of carbonate mud, as zooplankton faecal pellets, relative to the supply of clay. Bottom waters were well oxygenated, which allowed thorough bioturbation. Dark marl deposition saw a reduction in the rate of supply of carbonate mud compared to clay, concurrently with the preservation of lamination and substantial organic matter. Clearly this records the development of anoxia within the sediment and perhaps a slight reduction in bottom-water oxygenation. During dark, laminated shale deposition a very low rate of supply of carbonate mud compared to clay, permitted ostracods to become the dominant carbonate component. Organic matter was preserved in large quantities with the lamination. The ostracods are associated with a dwarfed fauna, which indicates low bottom-water oxygenation. However, the numbers of ostracods suggest that the bottom water frequently contained at least low concentrations of oxygen, even if it was usually anoxic.

Environmentally the dark marls record intermediate conditions to the other two sediment types. "Hemipelagic shelf sedimentation" seems to be a reasonable classification for the rocks analysed considering the proportions of sediment composed of pelagic bioclasts and clay. Hiatus formation may have occurred during winter storms or hurricanes [29,38,39]. Since the cyclicity has been shown to be dominantly primary, the power spectra can be applied to test a hypothetical palaeoclimatic control.

4. Walsh power spectra: methodology

The details of the mathematics used can be found elsewhere [40,41]. Problems and procedure for the Fourier power spectral analysis of sedimentary rocks are discussed in [42]. A qualitative description of the generation of power spectra may help show that the method is straightforward and that geological application and interpretation is the most important aspect. There are four main steps in production of power spectra; generation of a time series (Fig. 4), the transform operation, power spectrum generation, and interpretation.

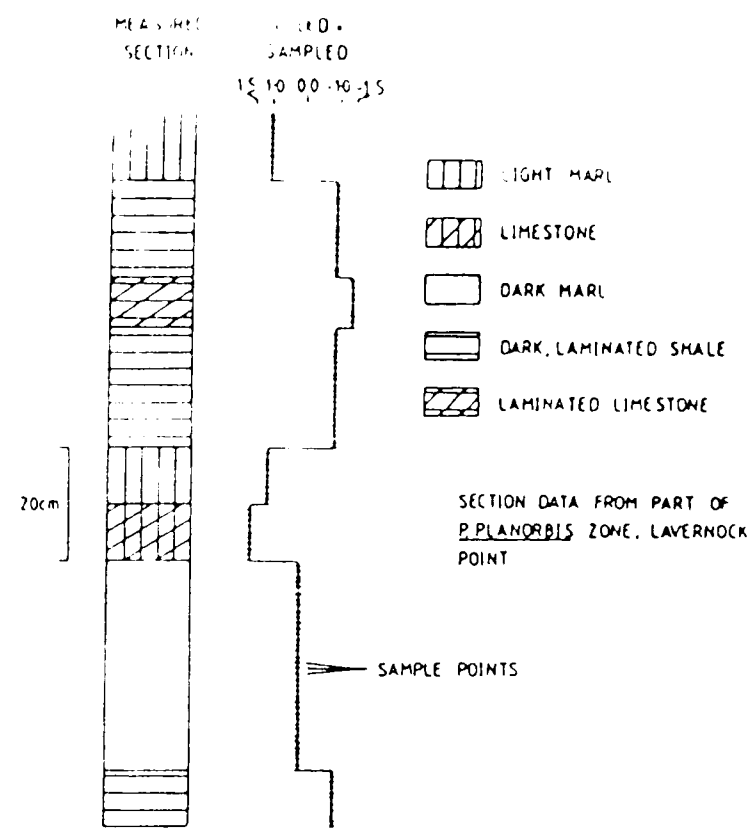

Fig. 4. Generation of time series from the measured sections.

The generation of power spectra requires data sets called "time series" which look like wavetrains. They are obtained by sampling at a constant interval along the length of measured sections (Fig. 4). To generate a time series for the present application requires numerical codes to distinguish the different sediment types. The numerical codes are somewhat arbitrary, but it is believed from the sedimentology that the light marl represents an environment most different from the dark, laminated shale. The dark marl is considered intermediate in the environmental extremes represented. The limestones represent an environment identical, or almost so, to the light marls. But because of their early diagenetic cementation they have not undergone the same degree of compaction as the light marls. In order to allow for this diagenetic distortion of the original thickness relationships, the limestones have been given a similar but different code to the light marls. Analogous reasoning applies to the coding of the laminated limestones and dark, laminated shales. Thus the codes used at all the localities were: limestone = +1.5, light marl = +1.0, dark marl = 0.0 and dark, laminated shales = −1.0, laminated limestone = −1.5. Experimentation with spectra

for Long Itchington, using the alternative values of +1.0, +0.5, 0.0, −0.5, −1.0 and of +1.0, +1.0, 0.0, −1.0, −1.0 respectively, showed no significant difference to the results obtained with the original codes. For example, in Fig. 7 spectra for Long Itchington using codes +1.0, +1.0, 0.0, −1.0, −1.0 have been plotted next to spectra generated using the code values preferred for the rest of the analyses (Fig. 4). The code values serve to generate a step-like wave-train of sediment code vs. cumulative bed thickness (Fig. 4). The power spectra are used to analyse the time series for dominant sedimentary cycles of different thicknesses.

Section measuring requires a rounding-up unit that is used consistently. In this case all beds were measured to the nearest centimetre. The sampling must accurately record the thinnest bed measured (1 cm), so that spurious low-frequency cycles are not generated by "aliasing". Therefore, in this case the sampling interval was 1 cm. In the present application a time series can be constructed by recording sediment codes every 1 cm along the measured section.

The time series are step-like or discontinuous rather than made of smooth curves; thus they are best decomposed into component square waves, Walsh functions, rather than sine and cosine waves; hence the Walsh rather than Fourier transform was used for the analysis [40]. One advantage of the Walsh transform is that computation is faster because only addition and subtraction is required [41]. Additionally, as the data used are discontinuous, they can be generated very quickly from measured sections (Fig. 4). Fourier spectra are best applied to continuous data such as geochemical values which, of course, require much more work for generation.

During the transform operation, a time series is regarded as a complicated wave-train that can be generated by the summation of many regular waves of different frequencies. Power spectra are plots of squared amplitude values, from the transform, for each different frequency component. Greater "power" can be regarded as indicating a more important role for a particular frequency component if it is used to recreate the time series.

The transform algorithm is taken from Kanasewich [41]. The estimates were generated from the transform and smoothed using a 3-point Hanning window following Beauchamp [40]. Power values are normalized for an application of Fisher's test for white noise [43]. Power is plotted linearly against frequency which is expressed in "cycles per metre". This constitutes the first application of Walsh power spectra to sedimentary rocks known to the author. Examples of Walsh power spectra for geomagnetic reversals and oxygen-isotope records can be found in papers by Negi and Tiwari [44,45].

The position of the time series used is shown in Fig. 1. The peaks not passing the 95% confidence level for the high-resolution spectra (figs. 5–7) are considered to be indistinguishable from white noise [43]. To test the stability of the remaining peaks the time series used for the high-resolution spectra were divided into two subsections and low-resolution spectra were generated [45]. Additional spectra have been generated where possible using time series of the same length as the subsections (Fig. 1). Thus for each locality a series of low-resolution spectra can, to a limited extent, be used to trace the development of peaks identified on the high-resolution spectra.

5. Walsh power spectra: results and interpretation

As can be seen from Figs. 5–7, there are peaks which pass the 95% confidence level on all the high-resolution spectra. Additionally the low-resolution spectra indicate reasonably stationary data. In each case one or two peaks pass the 95% confidence level and seem to be stable from the subsection spectra; although their power varies. Such peaks are interpreted as indicating a regular cyclicity in sedimentation and have been labelled with their respective cycle lengths in centimetres. They seem to be stable for between about 200 ka at Nash Point (most of a subzone), to about 4 Ma at Lyme Regis (4 zones). The regularity and stability of these cycles strongly suggests that sedimentation was controlled climatically [10]. A climatic explanation does not exclude the vertical change in power for particular cycles seen in Figs. 5–7, because Pleistocene sea-surface temperature data display similar changes for individual cycles [2]. However, before a climatic explanation can be accepted, some constraint on the duration of these regular sedimentary cycles is required.

The detection of stable peaks via the use of

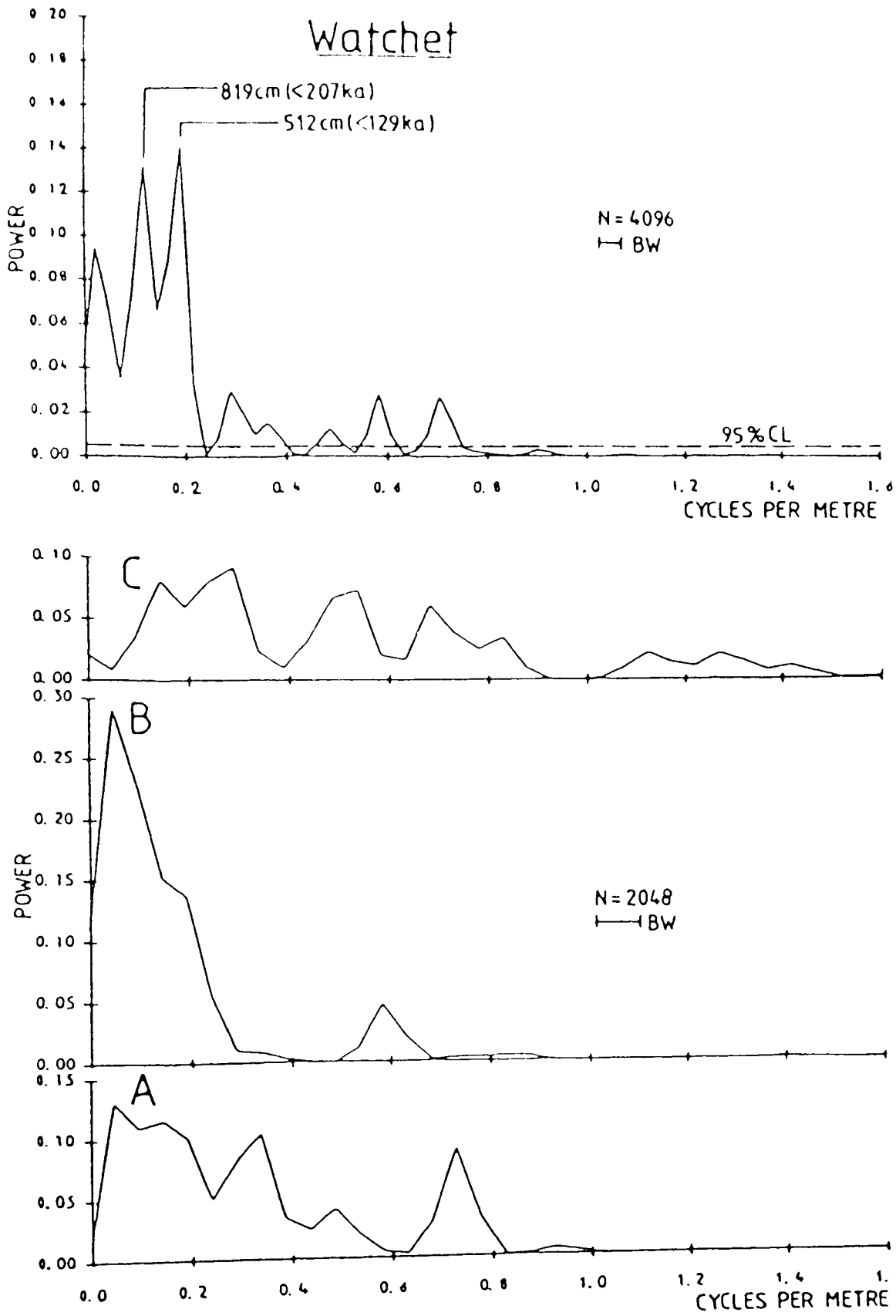

Fig. 5. Walsh power spectra for Watchet. The resolution is indicated by the bandwidth (BW). N = the number of points, or centimetres, in the time series used for each spectrum. 95%CL = 95% confidence level from Nowroozi [43].

subsections, indicates that sedimentation rates were near-constant at a given locality. If this were not the case, then a cycle of a particular length at the base of the section would have changed size so much by the top of the section that stable peaks would be absent. Perfectly constant sedimentation rates are not implied, however, because each peak on a spectrum is associated with a bandwidth implying a range of possible cycle lengths. Nevertheless, an estimation of sedimentation rates is a meaningful exercise.

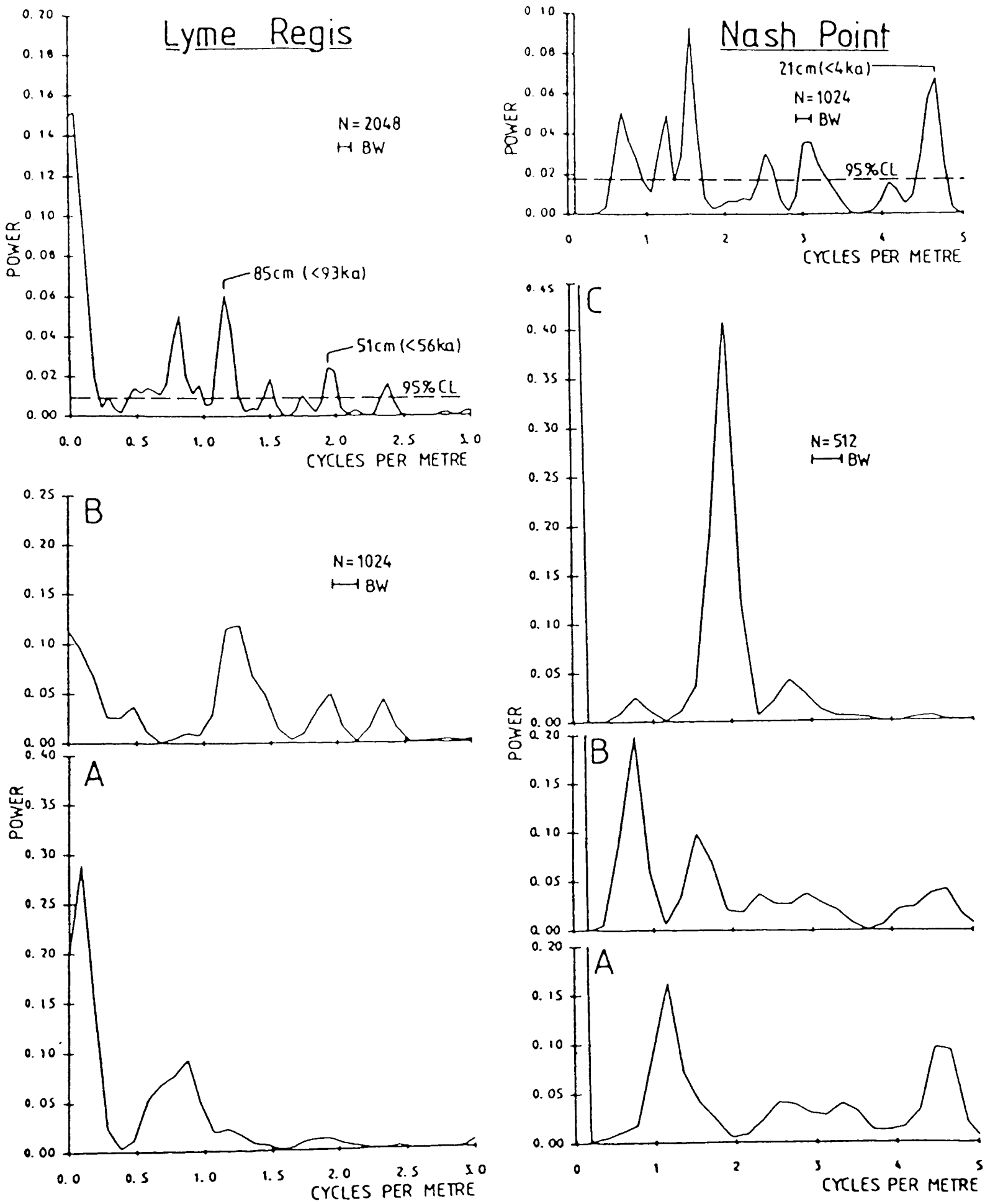

Fig. 6. Walsh power spectra for Lyme Regis and Nash Point.

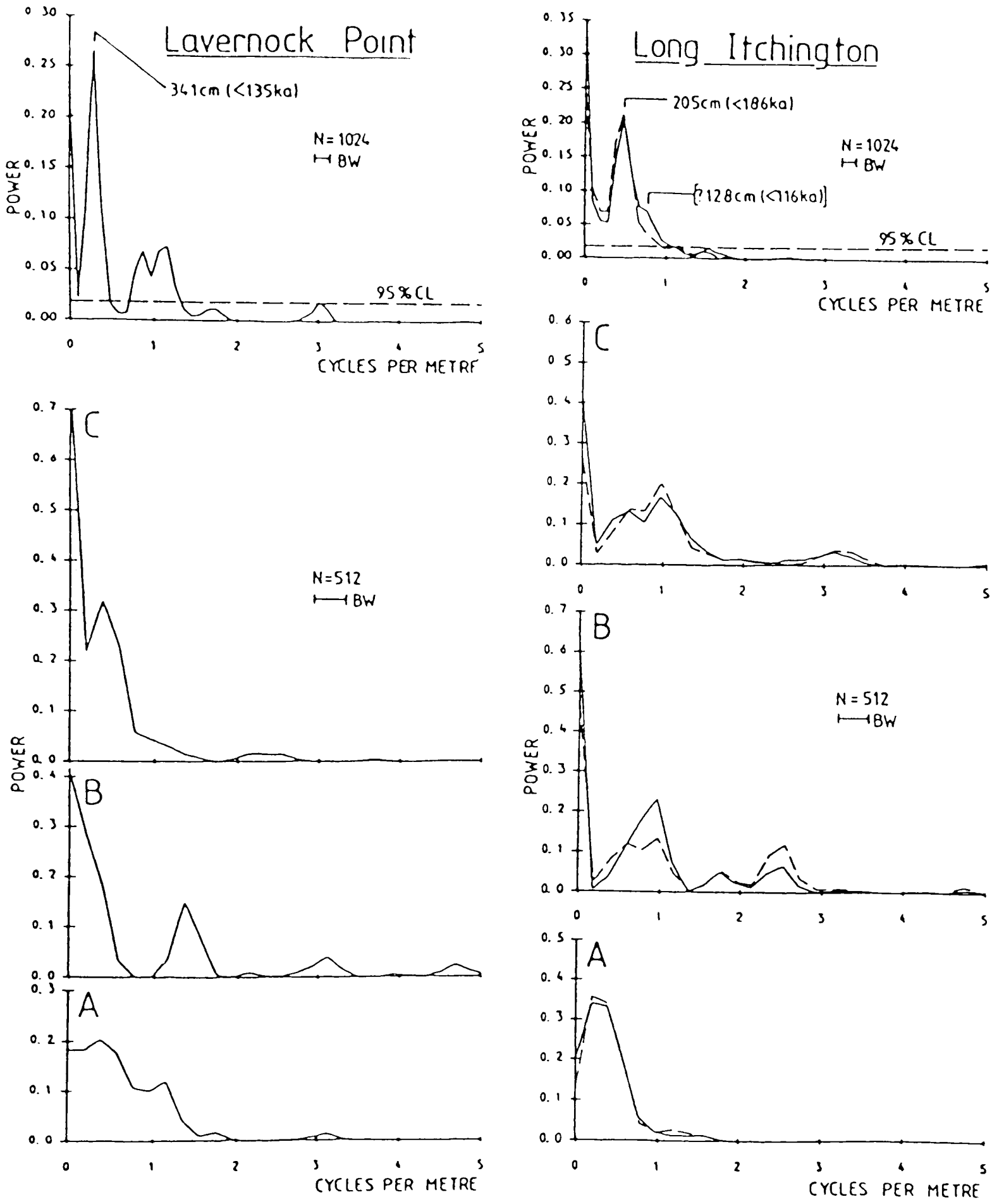

Fig. 7. Walsh power spectra for Lavernock Point and Long Itchington. The broken line spectra for Long Itchington were generated using codes: +1, +1, 0, −1, −1. All other spectra (continuous lines) were generated using the codes: +1.5, +1, 0, −1, −1.5.

Fig. 1 shows that the relative, as well as the absolute, thickness of ammonite zones changes between localities, suggesting a variation in the proportion of sediment missing at hiatuses. For constant sedimentation rate the thickest ammonite zone must be the most complete and should provide its best estimate. Thus sedimentation rates have been calculated for each location using the thickest zone and the assumption that one zone represents about 1 Ma (74 zones in 69 Ma according to Harland et al. [46], cf. [7]). These rates have been used to estimate the duration of different regular cycles as indicated in parentheses in Figs. 5–7. The durations are maximum limits as even the thickest zone is likely to be incomplete.

The maximum duration of all the regular cycles is shown to be about 200 ka. For an ice-free globe the maximum rate of sealevel change is about 1 cm/ka [6,47]. Therefore the largest range in sealevel during one sedimentary cycle would be 1 m. It is therefore considered very unlikely here that sealevel could have controlled the regular cyclicity although it may have affected sedimentation on a longer timescale [29,48,49]. It is proposed here that the regularity, persistence (millions of years), and order of duration (tens of thousands of years) of the cycles labelled in Figs. 5–7 can best be explained by climatic control of cyclicity. However, this cannot, as yet, be argued for Nash Point.

At Nash Point the cycle detected is given a maximum duration of 4 ka (Fig. 6). This section spans just one subzone of the three within the *bucklandi* zone. Being so short in duration, even if the sedimentation rate estimated is wrong by a factor of 2 or 3, it seems unlikely that the cycle detected represents one of the main orbital cycles. The low-resolution spectra show that this cycle is not stable for more than two thirds of the subzone. The Nash Point section is exceptional petrographically when compared to the other sections, but was included for completeness. There is an absence of dark, laminated shale and laminated limestone and abundant sand and silt grade bioclastic fragments and the estimated sedimentation rate is by far the largest calculated of all the localities studied. The exceptional sedimentology may reflect the proximity to the palaeo-shoreline [24,29,37]. The spectra for this section also indicate a substantial trend, or "zero" cycles per metre component, compared to the other locations. It remains possible that climate controlled sedimentation there, but the spectra may not demonstrate it because they represent too short a time span. Alternatively the trend may indicate a rapidly changing sedimentation rate or the local sedimentary processes may have masked the regular cycles.

The cycles identified at the other four locations do fit the climatic interpretation; the orbital components and durations may be identifiable. At Watchet and Lyme Regis 2 cycles have been detected (Figs. 5 and 6). The wavelength ratio of each pair of cycles is about 1.6, viz. 819 cm/512 cm and 85 cm/51 cm. This suggests that if climatically controlled, both pairs of cycles represent the same two orbital cycles. At Long Itchington (Fig. 7) as well as the main cycle of 205 cm, a cycle at 128 cm (indicated in parentheses) may also be present. This pair also have a wavelength ratio of 1.6. Unfortunately the cycle of 341 cm at Lavernock Point lies within the part of the spectrum with low wavelength resolution (Fig. 7). Thus it cannot be decided whether or not a cycle of (1.6 × 341) cm or of (341/1.6) cm is present. Nevertheless, it is postulated here that 2 cycles are involved at each locality and that the common wavelength ratio suggests that the same two orbital cycles were involved.

The most likely orbital cycles are 100 ka, 41 ka and 21 ka in duration following previous studies (see various authors in [4]). Yet cycles at 31 and 54 ka may be important components of Pleistocene data and other cycles are possible ([2,3] and Berger in [4]). The maximum duration for cycles at Lyme Regis is 93 ka. This suggests that the 41 and 21 (obliquity and precession) cycles are strongest candidates. The value of the common wavelength ratio suggests the same pair of the three main Pleistocene orbital cycles. Alternatively the 31 ka (obliquity) and 21 ka cycles would best explain the wavelength ratio. Of course the Jurassic obliquity and precession cycles may have had significantly different durations (but see [7]). The data used are considered here to be a "5-bit" representation of the variation of some climatic indicator, such as run-off. It is not certain that such a poor proxy-climatic record would correctly record wavelength ratios.

Therefore the best that can be inferred at present is: (a) two climatic cycles seem to have been involved; (b) their duration was probably less than

93 ka; (c) they probably represent one precession and one obliquity cycle; (d) they may have been 41 ka and 21 ka in duration. Notice that the sedimentation rates at Watchet exceeded those at Lyme Regis by between 4 and 10 times with no effect on the interpretation. Finally, if the cycle durations were 41 and ~~31~~ 21 ka then the maximum and implied durations can be compared. This indicates that at best the sections are 20–40% complete for a one million year interval (see [7]), which appears to be realistic for shelf sedimentation. Such a large proportion of missing section is surprising considering the results of the spectral analysis. However, rather than being very closely spaced throughout the sections, the hiatuses may in fact be present in clusters or at isolated horizons. In such a circumstance the hiatuses would separate packets of complete section and this could account for both the large loss of section and the detection of regular cyclicity.

6. Summary and conclusions

The basal Jurassic sedimentary rocks studied in South Britain accumulated in a hemipelagic shelf regime, with a palaeolatitude of about 35°N [50]. Carbonate mud was mainly supplied by coccoliths contained in zooplankton faecal pellets. Clay is believed to have been supplied by rivers. Cycles in bottom-water oxygenation, which affected organic carbon contents and the amount of bioturbation, were associated with changes in the clay-to-carbonate mud ratio. Walsh power spectra suggest that these cycles were climatically controlled and provide a rapid method for the palaeoclimatic analysis of measured sections. Two orbital cycles are implied, probably related to precession and obliquity, of perhaps 21 and 41 ka (or perhaps 21 and 31 ka).

The mechanism that related climatic and sedimentary cycles is unclear at present. The model used by Rossignol-Strick et al. [51] to explain the formation of Pleistocene sapropels in the Mediterranean may, however, provide an appropriate analogue following Barron et al. [9]. As an extension to this model, Rossignol-Strick [52] suggested that orbital-obliquity cycles indirectly influenced sapropel formation via a mechanism that did not involve ice. Through this analogy, orbitally forced changes in precipitation are related to the sedimentary cyclicity. During low runoff, clay supply may have been so slow that coccolithophore-derived carbonate dominated the sediment. Normal oxygenation allowed bioturbation and led to low organic carbon contents in the sediment. During high runoff, clay supply along with ostracod productivity may have increased relative to the supply of coccolithic carbonate. The surface productivity of coccolith- and of non-coccolith-producing algae may have increased with additional nutrients from the runoff water which indirectly accounts for higher numbers of ostracods. Bottom-water anoxia may have been caused by higher productivity combined with additional terrigenous organic matter and perhaps by density stratification related to a low-salinity surface wedge. The anoxia led to the deposition of laminated and organic carbon-rich sediment. This presumes that greater clay supply exceeded an increased coccolith supply. Comparison of the longest-possible and implied durations for the regular cycles, suggests that the sections are 20–40% complete at best. Sediment was perhaps removed during winter storms or hurricanes, leaving hiatuses in the sections. It is concluded that climatic processes dominated sedimentation at certain localities in the basal Jurassic of southern Britain.

Acknowledgements

I am indebted to H.C. Jenkyns for abundant suggestions, including the faecal pellet hypothesis, and help throughout this project. M.H. Worthington and W. Schwarzacher are thanked for their help with the power spectra. Inspiration to apply Walsh rather than Fourier power spectra was derived from [44] and M.H. Worthington. Permission to enter the Rugby Portland Cement Co. Southam works (Long Itchington) was granted by G. Benham which is greatly appreciated. Thanks are also due to C.F. Elders in particular, as well as J.D. Woodhead, and P.C. Jackson for their criticism of the manuscript. I should also like to thank C. Johnson for geochemical help and S. Baker for his help with the CL. This work was carried out during tenure of a NERC research studentship at Oxford University.

References

1 J.D. Hays, J. Imbrie and N.J. Shackleton, Variations in the Earth's orbit: pacemaker of the ice ages, Science 194 1121–1132, 1976.

2 W.F. Ruddiman, N.J. Shackleton and A. McIntyre, North Atlantic sea-surface temperatures for the last 1.2 million years, J. Geol. Soc. (London), in press

3 A.L. Berger, Support for the astronomical theory of climatic change, Nature 269, 44–45, 1977.

4 A. Berger, J. Imbrie, J. Hays, G. Kukla and B. Saltzmann, eds., Milankovitch and Climate: understanding the response to astronomical forcing, NATO ASI Ser. C 126, Reidel, Dordrecht, 1984.

5 T.C. Moore, N.G. Pisias and D.A. Dunn, Carbonate time series of the Quaternary and late Miocene sediments in the Pacific ocean: a spectral comparison, Mar. Geol. 46, 217–233, 1982.

6 L.A. Frakes, Climates Throughout Geologic Time, 310 pp., Elsevier, 1979.

7 M.R. House, Orbital cycles, sedimentary microrhythms, and a new approach towards an absolute time scale, Nature, in press.

8 G. Einsele and A. Seilacher eds., Cyclic and Event Stratification, Springer-Verlag, Berlin, 1982.

9 E.J. Barron, M.A. Arthur and E.G. Kauffman, Cretaceous rhythmic bedding sequences: a plausible link between orbital variation and climate, Earth Planet. Sci. Lett. 72, 327–340, 1985.

10 W. Schwarzacher, An application of statistical time series analysis to a limestone-shale sequence, J. Geol. 72, 195–213, 1964.

11 B.W. Carss and N.S. Neidell, A geological cyclicity detected by means of polarity coincidence correlation, Nature 212, 136–137, 1966.

12 C.E. Dunn, Identification of sedimentary cycles through Fourier analysis of geochemical data, Chem. Geol. 13, 217–232, 1974.

13 W.T. Dean, D.T. Donovan and M.K. Howarth, The Liassic ammonite zones and subzones of the North-West European Province, Bull. Brit. Mus. (Nat. Hist.), Geol. 4, No. 10, 435–505, 1961.

14 J.C.W. Cope, T.A. Getty, M.K. Howarth, N. Morton and H.S. Torrens, A correlation of Jurassic rocks in the British Isles, part one: Introduction and lower Jurassic, Geol. Soc. London, Spec. Rep. No. 14, 73 pp., 1980.

15 W.D. Lang, The Blue Lias of the Devon and Dorset coasts, Proc. Geol. Assoc. 35, 169–185, 1924.

16 C.P. Palmer, The lower Lias (lower Jurassic) between Watchet and Lilstock in North Somerset (United Kingdom), Newsl. Stratigr. 2, 1–30, 1972.

17 A.E. Trueman, The Liassic rocks of the Cardiff district, Proc. Geol. Assoc. 31, 93–107, 1920.

18 A.E. Trueman, The lower Lias (*bucklandi* zone) of Nash point, Glamorgan, Proc. Geol. Assoc. 41, 148–159, 1930.

19 R.G. Clements and members of the field studies in local geology class, The geology of Long Itchington Quarry (Rugby Portland Cement Co. Ltd., Southam Works), Percival Guildhall, Rugby and Department of Geology, University of Leicester, 1975.

20 A. Hallam, Origin of the limestone-shale rhythms in the Blue Lias of England: a composite theory, J. Geol. 72 157–169, 1964

21 W. Reiken, Epicontinental marl-limestone alternations: event deposition and diagenetic bedding (Upper Jurassic, Southwest Germany), in: Sedimentary and evolutionary cycles, Lecture Notes in Earth Sciences Vol. 1, pp. 127–162, U. Bayer and A. Seilacher, 1985.

22 H.S. Campos and A. Hallam, Diagenesis of English lower Jurassic limestones as inferred from oxygen and carbon isotope analysis, Earth Planet. Sci. Lett. 45, 23–31, 1979.

23 J.G. Gluyas, Early carbonate diagenesis within Phanerozoic shales and sandstones of the N.W. European shelf, Clay Miner. 19, 309–321, 1984.

24 A. Hallam, A sedimentary and faunal study of the Blue Lias of Dorset, Philos. Trans. R. Soc. London, Ser. B 243, 1–44, 1960.

25 A.R. Lord, Chapter on: The Jurassic part 1, Hettangian to Toarcian, in: A Stratigraphical Index of British Ostracoda, R.H. Bate and J.E. Robinson eds., Spec. Publ. Brit. Micropalaeontol. Soc., Geol. J., Spec. Issue 8, 189–212, 1978.

26 T. Barnard, Foraminifera from the lower Lias of the Dorset coast, Q.J. Geol. Soc. (London) 105, 347–388, 1949.

27 D. Wall, Microplankton, pollen and spores from the lower Jurassic in Britain, Micropalaeontology 11, 151–190, 1965.

28 G.B. Hamilton, Triassic and Jurassic calcareous nannofossils, in: A Stratigraphical Index of Calcareous Nannofossils, A.R. Lord, Brit. Micropalaeontol. Soc. Ser., pp. 17–39, 1982.

29 D.L. Loughman, A facies analysis of the Triassic/Jurassic boundary beds of the world: with special reference to North-West Europe and the Americas, Ph.D. Thesis, University of Birmingham, 1982 (unpublished).

30 R.G. Bromley and A.A. Ekdale, *Chondrites*: a trace fossil indicator of anoxia in sediments, Science 224, 872–874, 1984.

31 D.E. Hattin, Petrology and origin of fecal pellets in upper Cretaceous strata of Kansas and Saskatchewan, J. Sediment. Petrol. 45, 686–696, 1975.

32 S. Honjo, Coccoliths: production, transportation and sedimentation, Mar. Micropalaeontol. 1, 65–79, 1976.

33 R.G.C. Bathurst, Carbonate Sediments and Their Diagenesis, Developments in Sedimentology 12, Elsevier, Amsterdam, 1971.

34 R.L. Folk, Some aspects of recrystallization in ancient limestones, in: Dolomitization and limestone diagenesis—a symposium, L.C. Pray and R.C. Murray, eds., SEPM Spec. Publ. 13, pp. 14–48, 1965.

35 P.M. Burki, L.S.D. Glasser and D.N. Smith, Surface coatings on ancient coccoliths, Nature 297, 145–147, 1982.

36 M.D. Brasier, Microfossils, George Allen and Unwin, 1980.

37 F.J. Wobber, Sedimentology of the Lias (lower Jurassic) of South Wales, J. Sediment. Petrol. 35, 683–703, 1965.

38 K.M. Marsaglia and G. de V. Klein, The palaeogeography of Palaeozoic and Mesozoic storm depositional systems, J. Geol. 91, 117–142, 1983.

39 G.K. Pedersen, Thin, fine-grained storm layers in a muddy shelf sequence: an example from the lower Jurassic in the Stenlille 1 Well, Denmark, J. Geol. Soc. (London) 142, 357–373

40 K.G. Beauchamp, Walsh Functions and Their Applications, Techniques of Physics No. 3, 236 pp., Academic Press, 1975.

41 E.R. Kanasewich, Time sequence analysis in geophysics, Hignell Printing for University of Alberta Press, 1981.

42 W. Schwarzacher, Sedimentation Models and Quantitative Stratigraphy, Developments in Sedimentology 19, Elsevier, 1975.

43 A.A. Nowroozi, Table for Fischer's test of significance in Harmonic analysis, Geophys. J.R. Astron. Soc. 12, 512–520, 1967.

44 J.G. Negi and R.K. Tiwari, Matching long term periodicities of geomagnetic reversals and galactic motions of the solar system, Geophys. Res. Lett. 10, 713–716, 1983.

45 J.G. Negi and R.K. Tiwari, Periodicities of geomagnetic intensity and palaeomagnetic variations: a Walsh spectral approach, Earth Planet. Sci. Lett. 70, 139–147, 1984.

46 W.B. Harland, A.V. Cox, P.G. Llewellyn, C.A.G. Pickton, A.G. Smith and R. Walters, A Geologic Timescale, Cambridge Earth Science Series, Cambridge University Press, 1982

47 D.T. Donovan and E.J.W. Jones, Causes of world-wide changes in sealevel, J. Geol. Soc. (London) 136, 187–192, 1979.

48 D.T. Donovan, A. Horton and H.C. Ivimey-Cook, The transgression of the lower Lias over the London platform, J. Geol. Soc. (London) 136, 165–173, 1979.

49 A. Hallam, A revised sealevel curve for the early Jurassic, J. Geol. Soc. (London) 138, 735–743, 1981.

50 A.G. Smith, A.M. Hurley and J.C. Briden, Phanerozoic World Maps, 102 pp., Cambridge Earth Science Series, Cambridge University Press, 1981.

51 M. Rossignol-Strick, W. Nesteroff, P. Olive and C. Vergnaud-Grazzini, After the deluge: Mediterranean stagnation and sapropel formation, Nature 295, 105–110, 1982.

52 M. Rossignol-Strick, African monsoons, an immediate climate response to orbital insolation, Nature 304, 46–49, 1983.

5.3 Weedon 1987 and Hallam 1987 (Geology 15 pp92-94).

Comment and Reply on "Origin of minor limestone-shale cycles: Climatically induced or diagenetic?"

COMMENT

G. P. Weedon, *Department of Earth Sciences, University of Oxford, Parks Road, Oxford OX1 3PR, England*

Hallam's (1986a) paper prompts the following remarks, which mainly concern the basal part of the Lower Lias Formation of Britain (which includes the Blue Lias Member [Donovan and Kellaway, 1984]).

1. It has already been shown that it is meaningless to apply power-spectral analysis to limestone-shale sequences of a purely diagenetic origin (Weedon, 1986). However, a wide variety of textural, faunal, and field evidence supports the view that three sediment types were deposited on the seafloor of Britain in the earliest Jurassic (Hallam, 1964; Weedon, 1986). Early diagenesis enhanced the primary cyclicity by cementation of the most $CaCO_3$-rich parts of the light marls and laminated shales, producing homogeneous and laminated limestones (Hallam, 1964). Burrow-mottled contacts between limestone and dark marl are present at every locality, albeit rarely at some, so it is reasonable to assume that all limestones represent diagenetic exaggeration of carbonate-rich levels. More evidence for diagenetic enhancement of primary variations includes the observation that, if enclosed entirely by light marl, limestone beds and nodules always occupy the same horizon (Weedon, 1986). Evidence against independent rhythmic unmixing includes the correlation between percent $CaCO_3$ and percent TOC (carbonate-free) for the marls and shales (Le Riche, 1959).

2. The basal Lias limestones are argillaceous, which perhaps explains the poor preservation of coccoliths in this rock type (as shown for chalk by Hattin, 1975). Alternatively, neomorphic aggradation of the coccoliths may have been associated with the formation of the early diagenetic nodular limestones (Jenkyns, 1974, p. 257, 265). Coccolith preservation in the Kimmeridge Clay and ~~Kimmeridge~~ Chalk may reflect the absence of this process or the influence of organic films (Burki et al., 1982) in preventing aggradation, as proposed for the organic-rich parts of the basal Lias (Weedon, 1986).

The abundance of coccoliths in the marls and shales of the basal Lias suggests that coccoliths were the main precursor of the microspar. Green algae seem an unlikely source of most carbonate mud, given the proportion of pelagic fossils and the lack of shallow-water criteria (ooids, micrite envelopes, stromatolites, birdseyes, and mudcracks). Bacteria may have encouraged calcite precipitation by supplying carbonate ions for cementation. If the pH was generally lowered during cementation, then the only horizons to be cemented would have been those that were buffered; i.e., horizons with high primary carbonate contents.

3. If a few limestones were purely diagenetic in origin, they would randomize regular limestone-shale alternations related to orbital cycles (Sander's Rule, *in* Schwarzacher, 1975). Therefore, the peaks on the spectra for the Lower Lias (Weedon, 1986), which denote regularity, cannot result from few purely secondary limestones. The limestones and light marls, as a pair, represent an environment very different from that of the black laminated shales. This pair could represent the same (codes = +1 and +1) or slightly different (+1 and +1.5) environments. Either pair of codes yields the same spectral result, reflecting the way the Walsh transform is principally concerned with "zero-crossings" (Weedon, 1986, Fig. 7). Hallam (1986a) acknowledged that "the alternation of more calcareous bioturbated and less calcareous organic-rich laminated" horizons is consistent with Milankovitch-forcing. It is precisely this alternation that was analyzed spectrally (Weedon, 1986).

4. Hallam's (1986) statements concerning hiatuses are misleading. Evidence for many small gaps has been presented for many Liassic sections, including those at Avon (e.g., Donovan and Kellaway, 1984; Kent, 1936; Weedon, 1986). Hallam's (1986a) Figure 2B could be interpreted as evidence for more hiatuses in the left-hand column. My earlier suggestion, that large biostratigraphic gaps are absent when every ammonite zone is present, is probably erroneous, because the ammonite biostratigraphy was established inside the region in question (D. T. Donovan, 1986, personal commun.). Large gaps might yet be detected after further work on these rocks.

5. Hallam's (1986a) Figure 3, based on earlier work (Hallam, 1964), can be updated using recent literature; the simple linear relationship between number of limestones and thickness of zone is not supported. For example, at Watchet there are 13 limestone horizons (beds + nodule layers) in the *P. planorbis* zone, which is 15.73 m thick, and the *V. conybeari* subzone is 17.99 m thick and contains 14 limestone horizons (Palmer, 1972). The limestones at Watchet are identical to those described by Hallam (1964, 1986a).

The general rule that thicker developments of particular zones contain more limestones is easily explained. Expanded parts of particular zones had more beds available for cementation. Perhaps, more important, where there were higher sedimentation rates, each thicker light marl bed, for example, would have possessed more potential horizons for cementation. Power-spectral analysis is not invalidated by these considerations (see discussion of codes above).

I accept Hallam's (1964) view that the limestones are produced by diagenetic *enhancement* of primary cyclicity. Hallam's recent (1986a) arguments hinge on the nature of the limestones, which he convincingly showed to be diagenetic. The fact that the average thickness of diagenetic limestones in limestone-shale sequences remains constant regardless of sedimentation rate is important in this respect and seems to reflect some unexplained aspect of early diagenetic cementation in general. It is incorrect, however, to ignore the primary control on the formation of the limestones. The recent spectral analysis allowed for the influence of diagenesis, and it is reaffirmed that the primary cyclicity (laminated shale/burrowed marl) was produced by Milankovitch-forcing (Weedon, 1986).

ACKNOWLEDGMENTS

I thank H. C. Jenkyns for critically reading this manuscript.

5.3 Continued.

REPLY

A. Hallam, *Department of Geological Sciences, University of Birmingham, Birmingham B15 2TT, England*

Although my article (Hallam, 1986a) dealt with more than the Blue Lias, designated a formation rather than a member by the Geological Society of London Stratigraphic Committee (Cope et al., 1980), in this discussion it is right to concentrate on this formation because the correct interpretation of its depositional and diagenetic history has an important bearing on that of many other limestone-shale sequences.

1. There is no dispute that burrow-mottled limestone-marl contacts and alternations of bioturbated and organic-laminated sediment are evidence of primary environmental differences, but these phenomena are by no means ubiquitous; many limestone-shale alternations reveal no difference, after allowing for compaction, other than $CaCO_3$ content.

2. The origin of the calcite microspar in the limestones is certainly a problem, but I remain unconvinced of an origin from coccoliths, whose calcite might be expected to be comparatively resistant to dissolution. Are coccoliths really as abundant in the marls and shales as Weedon claims? One would like to have some knowledge of the volume ratio of coccoliths to indeterminate microspar before forming a firm conclusion on this important point. Where, moreover, is the evidence of progressive disintegration of coccoliths to microspar? The explanations put forward by Weedon for coccolith abundance in the [redacted] Chalk and Kimmeridge Clay are different, respectively invoking lack of clay or presence of organic films, and have to me the unpersuasive air of ad hoc hypotheses. Coccoliths (or ex-coccolith microspar) apart, the proportion of pelagic fossils in the Blue Lias is minimal, the formation is characterized by a rich and diverse benthos strongly indicative of deposition in the shallow neritic zone, probably not far from land.

3. There may be substantially more than a few purely diagenetic limestones. It is very hard to discriminate originally primary from secondary limestones in many cases, this was one of the principal points of my article. We know too little about diagenesis to be sure whether or not regular orbital-cycle alternations would be randomized. If one must depend upon the obvious primary alternations of limestone-marl pairs and organic-rich laminated shales, then most of the limestone-shale alternations of the Blue Lias must be excluded from spectral analysis, especially in the thicker sections such as Glamorgan.

4. That minor hiatuses are present, within the limit of resolution of ammonite chrons, is a fact I would not wish to deny, but it doesn't help Weedon's argument if there is no independent physical evidence for such hiatuses. To make my point most clearly, let us consider an extreme case. The *conybeari* Subzone of Glamorgan contains 61 limestone beds, and the same unit in neighboring Avon a mere 3; yet the physical appearance of the limestone-shale alternations is virtually identical. No doubt there are many hiatuses in the more condensed sequence, but physical evidence for them is lacking; whatever subtle indicators were originally present have been destroyed by diagenetic overprint. Clearly, the Avon sequence is most unsuitable for spectral or any other kind of analysis that aims at detecting a complete series of environmental signals. But the same problem arises with respect to the thicker and more fully studied correlative sequence in Dorset, and it cannot be excluded even for Glamorgan, because there are, no doubt, even thicker sequences elsewhere with more limestones.

5. I do not claim a simple linear relationship between number of limestones and zonal thickness, *independent of facies*. Thus, there is a widespread change in the Blue Lias of southern England and south Wales across the *Planorbis-Liasicus* Zone boundary from more calcareous to more argillaceous facies, a fact that I have interpreted as signifying a regional sea-deepening event (Hallam, 1960). The number of limestones per given stratigraphic thickness is consistently less in the *Liasicus* Zone than in the *Planorbis* Zone. As for Weedon's statement that "expanded parts of particular zones had more beds available for cementation," I fail to see how this lets him off the book.

In no sense do I wish to discourage quantitative research on stratal sequences that may reveal evidence of orbital cycles, but I think that alternations of bioturbated and laminated beds, signifying variations in degree of bottom-water oxygenation, are much more promising than limestone-shale alternations (Hallam, 1986b; Herbert and Fischer, 1986). There is a further difficulty that must not be underplayed, even when the complications of diagenesis can be discounted. In estimating cycle duration, Weedon makes the assumption that an ammonite zone represents 1 m.y. This assumption, also made by others, including myself, is based on substantial extrapolation from pathetically few reliable radiometric dates, and the recognition that the number of ammonite zones in the northwest European Jurassic roughly corresponds to the number of million years assigned to the Jurassic (Hallam, 1984; Hallam et al., 1985). The potential error is considerable, and the Blue Lias zones could signify a range in duration from as little as 0.5 m.y. to as much as 2 m.y. Therefore, estimates of duration will have a considerable bearing on which, if any, of the recognized orbital cycles are held responsible.

COMBINED REFERENCES CITED

Burki, P.M., Glaser, L.S.D., and Smith, D.N., 1982, Surface coatings on ancient coccoliths: Nature, v. 297, p. 145–147.

Cope, J.C.W., Getty, T.A., Howarth, M.K., Morton, N., and Torrens, H.S., 1980, A correlation of Jurassic rock in the British Isles. Part One: Introduction and Lower Jurassic: Geological Society of London Special Report 14, p. 1–73

Donovan, D.T., and Kellaway, G.A., 1984, Geology of the Bristol District, the Lower Jurassic rocks: London, Her Majesty's Stationary Office, 69 p.

Hallam, A., 1960, A sedimentary and faunal study of the Blue Lias of Dorset and Glamorgan: Royal Society of London Philosophical Transactions, v. 243, ser. B, p. 1–44.

—— 1964, Origin of the limestone-shale rhythm in the Blue Lias of England: A composite theory: Journal of Geology, v. 72, p. 157–169.

—— 1984, Relations between biostratigraphy, magnetostratigraphy and event stratigraphy in the Jurassic and Cretaceous, *in* Proceedings, International Geological Congress, 27th, Moscow: Utrecht, VNU Press, v. 1, p. 189–212.

—— 1986a, Origin of minor limestone-shale cycles: Climatically induced or diagenetic?: Geology, v. 14, p. 609–612.

—— 1986b, Role of climate in affecting Late Jurassic and Early Cretaceous sedimentation in the North Atlantic, *in* Summerhayes, C.P., and Shackleton, N.J., eds., North Atlantic palaeoceanography: Geological Society of London Special Publication 21, p. 277–281.

Hallam, A., Hancock, J.M., LaBrecque, J.L., Lowrie, W., and Channell, J.E.T., 1985, Jurassic to Paleogene: Part 1. Jurassic and Cretaceous geochronology and Jurassic to Paleogene magnetostratigraphy, *in* Snelling, N.J., ed., The chronology of the geological record: Geological Society of London Memoir 10, p. 118–140.

Hatton, D.E., 1975, Petrology and origin of fecal pellets in Upper Cretaceous strata of Kansas and Saskatchewan: Journal of Sedimentary Petrology, v. 45, p. 686–696.

Herbert, T.D., and Fischer, A.G., 1985, Milankovitch climatic origin of mid-Cretaceous black shale rhythms in central Italy: Nature, v. 321, p. 739–743.

Jenkyns, H.C., 1974, Origin of red nodular limestones (Ammonitico Rosso, Knollenkalke) in the Mediterranean Jurassic: A diagenetic model, *in* Hsü, K.J., and Jenkyns, H.C., eds., Pelagic sediments on land and under the sea: International Association of Sedimentologists Special Publication 1, p. 249–271.

Kent, P.E., 1936, The formation of the hydraulic limestones of the lower Lias: Geological Magazine, v. 73, p. 476–478.

Le Riche, H.H., 1959, The distribution of certain trace elements in the Lower Lias of Southern England: Geochimica et Cosmochimica Acta, v. 16, p. 101–122.

Palmer, C.P., 1972, The Lower Lias (Lower Jurassic) between Watchet and Lilstock in North Somerset (United Kingdom): Newsletters on Stratigraphy, v. 2, p. 1–30.

Schwarzacher, W.S., 1975, Sedimentation models and quantitative stratigraphy (Developments in Sedimentology 19): Amsterdam: Elsevier, 382 p.

Weedon, G.P., 1986, Hemipelagic shelf sedimentation and climatic cycles of the basal Jurassic (Blue Lias) of south Britain: Earth and Planetary Science Letters, v. 76, p. 321–335.

APPENDIX FOR CHAPTER 6

TIME SERIES FOR VARIOUS FORMATIONS.

6.1 Time series for the Boom Clay Formation, around Antwerp.

SAMPLE INTERVAL = 1cm

TOTAL THICKNESS MEASURED = 5891cm

CODES
SILT = +1.0
CALCAREOUS SILT = +0.5
BLACK CLAY = 0.0
CALCAREOUS CLAY = -0.5
CLAY " = -1.0

THICKNESS	CODE	TIME SERIES	BED NUMBER
55.	0.0		85a
68.	1.0		84
63.	-1.0		83
45.	0.0		82
45.	1.0		81
25.	-1.0		80
25.	0.0		79
10.	1.0		78
10.	0.5		77
210.	1.0		76
58.	0.0		75
13.	-0.5		74
125.	-1.0		73
20.	1.0		72
58.	-1.0		71
35.	1.0		70
8.	-1.0		69
28.	1.0	24/4	68
15.	0.5		67
23.	1.0		66
65.	-1.0		65
60.	0.0		64
220.	-1.0		63
23.	1.0		62
35.	-1.0		61 /61 /60 /59 /58
15.	1.0		57
88.	-1.0		56
55.	0.0		
45.	-1.0		
50.	0.0		
15.	-0.5		
47.	1.0		
86.	-1.0		
40.	0.0		
38.	-1.0		
21.	1.0		
35.	-1.0		
46.	0.0	30/16	
24.	-1.0		
21.	1.0		
19.	-0.5		
81.	-1.0		
16.	0.0		
21.	1.0		
64.	-1.0		
11.	-0.5		
54.	-1.0		
22.	0.0		
22.	1.0		
22.	0.0		
20.	-1.0		
8.	-0.5		
20.	-1.0		
25.	0.0		

2048B

VANDENBERGHE, 1978.

THICKNESS	CODE	TIME SERIES	BED NUMBER
25.	-1.0		55
83.	0.0		54
27.	1.0		53
22.	-1.0		52
75.	0.0		51
20.	1.0		50
84.	-1.0		49
15.	0.5		48
70.	-1.0		47
25.	0.0		46
30.	1.0		45
30.	-1.0		44
29.	0.0	16/13	43
40.	1.0		42
50.	-1.0		41
25.	0.0		40
30.	1.0		39
42.	-1.0		38
15.	0.0		37
5.	0.5		36
25.	1.0		35
10.	-1.0		34
55.	0.0		33
50.	1.0		32
43.	0.0		31
20.	1.0		30
30.	-1.0		29
10.	0.0		28
20.	1.0		27
10.	-1.0		26
10.	0.0		25
22.	1.0		24
37.	-1.0		23
22.	0.0		22
43.	1.0		21
25.	-1.0		20
10.	-0.5		19
25.	-1.0		18
40.	1.0		
35.	-1.0		
15.	0.0		
40.	1.0		
60.	-1.0		
40.	1.0		
35.	-1.0		
15.	0.0		
36.	1.0		
86.	-1.0	51/39	
65.	1.0		
77.	-1.0		
28.	0.0		
25.	1.0		
23.	-1.0		
30.	0.0		

2048A

4096

2048C

THICKNESS	CODE	TIME SERIES	BED NUMBER
20.	-1.0		
25.	1.0		
10.	0.5		17
25.	1.0		
110.	-1.0		16
65.	1.0		15
35.	-1.0		
10.	-0.5		14
35.	-1.0		
55.	1.0		13
60.	-1.0		12
55.	1.0		11
145.	-1.0		
10.	-0.5		10/9 IN VANDENBERGHE, 1978.
90.	1.0	51 / 39	8
40.	-1.0		7
70.	1.0		6
130.	-1.0		5
290.	1.0		4
45.	-1.0		3
284.	1.0		2

SAMPLE INTERVAL = 1 cm

TOTAL THICKNESS MEASURED = 16508 cm

CODES

UNDIFFERENTIATED MUDSTONE, CALCAREOUS MUDSTONE, HOMOGENEOUS CEMENTSTONE } = +1.0

BITUMINOUS MUDSTONE, LAMINATED CEMENTSTONE } = -1.0

OIL SHALE = -1.25

COCCOLITH LIMESTONE = -1.5

THICKNESS	CODE
34.	-1.25
442.	1.00
28.	-1.25
703.	1.00
39.	-1.25
534.	1.
54.	-1.25
483.	1.
23.	-1.25
8.	1.
101.	-1.25
35.	1.
94.	-1.25
42.	-1.5
23.	-1.25
87.	1.
35.	-1.25
105.	1.
111.	-1.
22.	-1.25
190.	1.
23.	-1.25
136.	1.
52.	-1.25
79.	1.
40.	-1.5
28.	-1.25
651.	1.
12.	-1.25
217.	1.
2.	-1.
60.	-1.5
2.	-1.
34.	-1.5
12.	1.
15.	-1.
19.	-1.25
12.	1.
11.	-1.25
75.	1.
25.	-1.25
15.	1.
18.	-1.25
58.	1.
13.	-1.25
67.	1.
7.	-1.25
31.	1.
20.	-1.25
37.	-1.
26.	-1.25
122.	1.
25.	-1.25
122.	1.

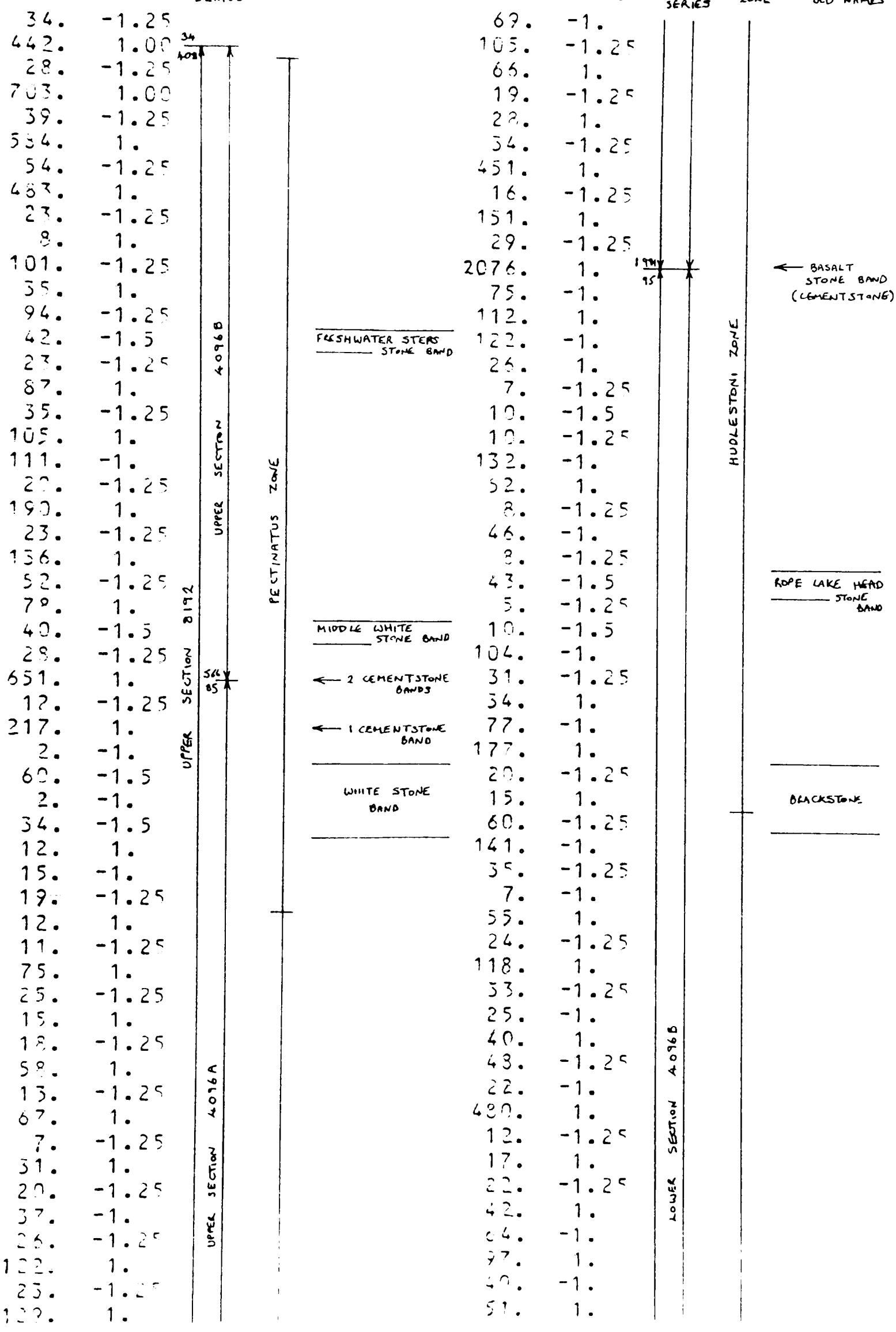

THICKNESS	CODE
69.	-1.
105.	-1.25
66.	1.
19.	-1.25
22.	1.
34.	-1.25
451.	1.
16.	-1.25
151.	1.
29.	-1.25
2076.	1.
75.	-1.
112.	1.
122.	-1.
26.	1.
7.	-1.25
10.	-1.5
10.	-1.25
132.	-1.
52.	1.
8.	-1.25
46.	-1.
8.	-1.25
43.	-1.5
5.	-1.25
10.	-1.5
104.	-1.
31.	-1.25
34.	1.
77.	-1.
177.	1.
20.	-1.25
15.	1.
60.	-1.25
141.	-1.
35.	-1.25
7.	-1.
55.	1.
24.	-1.25
118.	1.
33.	-1.25
25.	-1.
40.	1.
43.	-1.25
22.	-1.
480.	1.
12.	-1.25
17.	1.
22.	-1.25
42.	1.
64.	-1.
97.	1.
40.	-1.
51.	1.

THICKNESS	CODE
16.	-1.25
29.	-1.
10.	1.
25.	-1.
184.	1.
50.	-1.
55.	1.
15.	-1.25
90.	1.
62.	-1.
204.	1.
3.	-1.
90.	1.
5.	-1.
210.	1.
8.	-1.
23.	1.
6.	-1.
36.	1.
14.	-1.
62.	1.
106.	-1.
74.	1.
52.	-1.
110.	1.
35.	-1.25
107.	1.
25.	-1.25
312.	1.
48.	-1.
107.	1.
58.	-1.
22.	1.
25.	-1.25
22.	1.
21.	-1.25
40.	-1.
119.	1.
45.	-1.
12.	1.
14.	-1.
191.	1.
18.	-1.
90.	1.
9.	-1.
24.	1.
17.	-1.
18.	1.
41.	-1.
134.	1.
23.	-1.
90.	1.
21.	-1.
54.	1.

TIME SERIES: LOWER SECTION 8192 (15, 95)

ZONE: WHEATLEYENSIS ZONE; SCITULUS ZONE

BED NAMES: ← GREY LEDGE STONE BAND (CEMENTSTONE); ← CATTLE LEDGE STONE BAND (CEMENTSTONE)

THICKNESS	CODE
61.	-1.
43.	1.
22.	-1.
41.	1.
8.	-1.
90.	1.
48.	-1.
24.	1.
45.	-1.
113.	1.
62.	-1.
86.	1.
38.	-1.
38.	1.
35.	-1.
6.	-1.5
92.	-1.
29.	1.
34.	-1.
142.	1.
17.	-1.
67.	1.
35.	-1.25
55.	-1.
11.	-1.25
41.	-1.
209.	1.
15.	-1.
69.	1.
15.	-1.
59.	1.
40.	-1.
103.	1.
15.	-1.25
144.	-1.
36.	-1.25
63.	1.
55.	-1.25
79.	1.
22.	-1.
56.	1.

TIME SERIES: LOWER SECTION 4096A

ZONE: ELEGANS ZONE

BED NAMES: ← YELLOW LEDGE STONE BAND (LAMINATED CEMENTSTONE); ← BLAKE'S BED 41; BLAKE'S BED 42 (LAMINATED CEMENTSTONE)

6.3 Time series for the Toarcian section at Breggia Gorge.

SAMPLE INTERVAL = 1cm

TOTAL THICKNESS MEASURED = 1906cm

CODES

LIMESTONE = +1.0

SHALE = -1.0

THICKNESS	CODE
12.	1.00
27.	-1.00
7.	1.00
3.	-1.00
5.	1.00
3.	-1.00
8.	1.00
1.	-1.00
22.	1.00
6.	-1.00
4.	1.00
1.	-1.00
4.	1.00
8.	-1.00
7.	1.00
4.	-1.00
15.	1.00
3.	-1.00
5.	1.00
1.	-1.00
3.	1.00
1.	-1.00
2.	1.00
1.	-1.00
7.	1.00
4.	-1.00
9.	1.00
7.	-1.00
8.	1.00
7.	-1.00
3.	1.00
5.	-1.00
5.	1.00
12.	-1.00
14.	1.00
1.	-1.00
18.	1.00
2.	-1.00
3.	1.00
4.	-1.00
5.	1.00
10.	-1.00
7.	1.00
12.	-1.00
5.	1.00
5.	-1.00
14.	1.00
3.	-1.00
3.	1.00
1.	-1.00
5.	1.00
1.	-1.00
3.	1.00
1.	-1.00

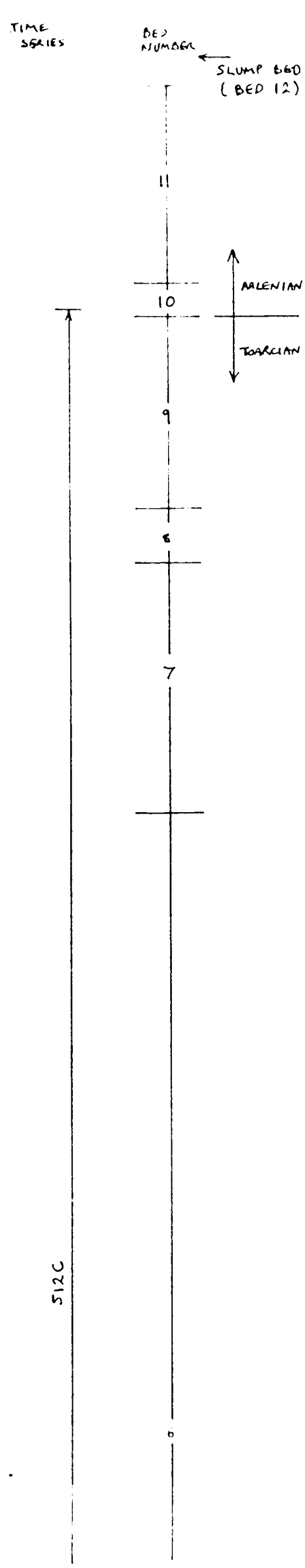

THICKNESS	CODE
1.	1.00
1.	-1.00
2.	1.00
1.	-1.00
7.	1.00
3.	-1.00
10.	1.00
1.	-1.00
3.	1.00
6.	-1.00
12.	1.00
1.	-1.00
10.	1.00
3.	-1.00
10.	1.00
5.	-1.00
4.	1.00
7.	-1.00
10.	1.00
7.	-1.00
10.	1.00
8.	-1.00
13.	1.00
11.	-1.00
4.	1.00
9.	-1.00
14.	1.00
10.	-1.00
13.	1.00
3.	-1.00
7.	1.00
1.	-1.00
4.	1.00
9.	-1.00
4.	1.00
10.	-1.00
9.	1.00
6.	-1.00
8.	1.00
1.	-1.00
23.	1.00
3.	-1.00
11.	1.00
6.	-1.00
14.	1.00
1.	-1.00
13.	1.00
2.	-1.00
11.	1.00
2.	-1.00
7.	1.00
4.	-1.00
7.	1.00
2.	-1.00

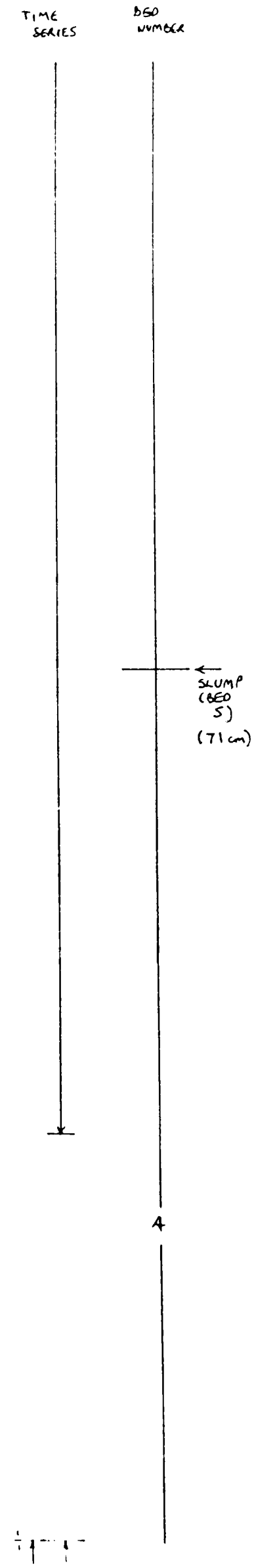

THICKNESS	CODE	TIME SERIES	BEV NUMBER
7.	1.00	5128	3
1.	-1.00		
10.	1.00		
2.	-1.00		
8.	1.00		
8.	-1.00		
6.	1.00		
9.	-1.00		
4.	1.00		
3.	-1.00		
9.	1.00		
11.	-1.00		
11.	1.00		
5.	-1.00		
10.	1.00		
5.	-1.00		
6.	1.00		
2.	-1.00		
1.	1.00		
13.	-1.00		
2.	1.00		
15.	-1.00		
2.	1.00		
6.	-1.00		
4.	1.00		
1.	-1.00		
6.	1.00		
9.	-1.00		
6.	1.00		
1.	-1.00		
1.	1.00		
4.	-1.00		
6.	1.00		
17.	-1.00		
3.	1.00		
18.	-1.00		
3.	1.00		
10.	-1.00		
4.	1.00		
4.	-1.00		
1.	1.00		
6.	-1.00		
2.	1.00		
8.	-1.00		
4.	1.00		
2.	-1.00		
7.	1.00		
5.	-1.00		
4.	1.00		
25.	-1.00		
2.	1.00		
1.	-1.00		
1.	1.00		
10.	-1.00		

THICKNESS	CODE	TIME SERIES	BEV NUMBER
2.	1.00	1024	5 5
3.	-1.00		
3.	1.00		
3.	-1.00		
2.	1.00		
3.	-1.00		
5.	1.00		
1.	-1.00		
4.	1.00		
5.	-1.00		
4.	1.00		
4.	-1.00		
4.	1.00		
13.	-1.00		
4.	1.00		
2.	-1.00		
2.	1.00		
3.	-1.00		
2.	1.00		
7.	-1.00		
2.	1.00		
2.	-1.00		
3.	1.00		
5.	-1.00		
2.	1.00		
3.	-1.00		
4.	1.00		
6.	-1.00		
4.	1.00		
4.	-1.00		
4.	1.00		
5.	-1.00		
7.	1.00		
10.	-1.00		
4.	1.00		
8.	-1.00		
5.	1.00		
13.	-1.00		
4.	1.00		
6.	-1.00		
8.	1.00		
4.	-1.00		
5.	1.00		
6.	-1.00		
4.	1.00		
16.	-1.00		
2.	1.00		
10.	-1.00		
9.	1.00		
2.	-1.00		
1.	1.00		
7.	-1.00		
2.	1.00		
1.	-1.00		

THICKNESS	CODE	TIME SERIES	BED NUMBER
3.	1.00	512A	2
4.	-1.00		
3.	1.00		
4.	-1.00		
2.	1.00		
3.	-1.00		
3.	1.00		
3.	-1.00		
4.	1.00		
3.	-1.00		
4.	1.00		
2.	-1.00		
6.	1.00		
1.	-1.00		
6.	1.00		
1.	-1.00		
5.	1.00		
1.	-1.00		
7.	1.00		
2.	-1.00		
4.	1.00		
3.	-1.00		
4.	1.00		
7.	-1.00		
6.	1.00		
3.	-1.00		
11.	1.00		
2.	-1.00		
5.	1.00		
4.	-1.00		
3.	1.00		
2.	-1.00		
5.	1.00		
6.	-1.00		
6.	1.00		
2.	-1.00		
10.	1.00		
4.	-1.00		
7.	1.00		
5.	-1.00		
7.	1.00		
5.	-1.00		
5.	1.00		
5.	-1.00		
4.	1.00		
4.	-1.00		
4.	1.00		
2.	-1.00		
7.	1.00		
3.	-1.00		
6.	1.00		
4.	-1.00		
7.	1.00		
4.	-1.00		

THICKNESS	CODE	TIME SERIES	BED NUMBER
5.	1.00		1
3.	-1.00		
5.	1.00		
5.	-1.00		
8.	1.00		
5.	-1.00		
8.	1.00		
6.	-1.00		
9.	1.00		
6.	-1.00		
11.	1.00		
3.	-1.00		
7.	1.00		
9.	-1.00		
6.	1.00		
6.	-1.00		
7.	1.00		
5.	-1.00		
8.	1.00		
7.	-1.00		
10.	1.00		
10.	-1.00		
8.	1.00		
11.	-1.00		
8.	1.00		
9.	-1.00		
7.	1.00		
7.	-1.00		
4.	1.00		
7.	-1.00		
11.	1.00		
8.	-1.00		
7.	1.00		
7.	-1.00		
7.	1.00		
7.	-1.00		
8.	1.00		
5.	-1.00		
16.	1.00		
14.	-1.00		
6.	1.00		
4.	-1.00		
6.	1.00		
14.	-1.00		
4.	1.00		
9.	-1.00		
6.	1.00		
9.	-1.00		
2.	1.00		
2.	-1.00		
4.	1.00		
4.	-1.00		

GRADATIONAL CONTACTS

6.4 Time series for the Upper Pliensbachian section at Breggia Gorge.

SAMPLE INTERVAL = 1mm

TOTAL THICKNESS MEASURED = 14341mm

CODES

LIMESTONE = +1.0

SHALES = -1.0

THICKNESS	CODE	TIME SERIES	BED No.	ZONES
115.	1.00		1115	TENUICOSTATUM ZONE
38.	-1.00		1114	
60.	1.00		1113	
2.	-1.00		1112	
105.	1.00		1111	
24.	-1.00		1110	
70.	1.00			
14.	-1.00		1109	
65.	1.00	30		
31.	-1.00	35	1108	
119.	1.00			
18.	-1.00		1107	
219.	1.00			
35.	-1.00		1106	
110.	1.00			
5.	-1.00		1105	
165.	1.00			
8.	-1.00			
193.	1.00		1104	
5.	-1.00			
49.	1.00		1103	
20.	-1.00			
117.	1.00		1102	
10.	-1.00			
119.	1.00		1101	
24.	-1.00			
64.	1.00		1100	
3.	-1.00			
185.	1.00		1099	
7.	-1.00			
58.	1.00			
20.	-1.00		1098	
54.	1.00			
9.	-1.00			
224.	1.00			
2.	-1.00		1097	
52.	1.00			
1.	-1.00		1096	
229.	1.00			
8.	-1.00		1095	
138.	1.00			
16.	-1.00		1094	
110.	1.00			
15.	-1.00		1093	
20.	1.00			
1.	-1.00			
165.	1.00		1092	
15.	-1.00			
116.	1.00		1091	
15.	-1.00			
230.	1.00		1090	
14.	-1.00			
37.	1.00		1089	
4.	-1.00		1088	

4096 C

SPINATUM ZONE

HAWSKERENSE SUBZONE

THICKNESS	CODE	TIME SERIES	BED No	ZONES
50.	1.00		1087	AMYRENUM SUBZONE
15.	-1.00		1086	
185.	1.00			
10.	-1.00		1085	
114.	1.00			
11.	-1.00		1084	
85.	1.00			
2.	-1.00			
30.	1.00			
1.	-1.00		1083	
59.	1.00			
1.	-1.00			
111.	1.00		1082	
10.	-1.00			
180.	1.00			
6.	-1.00		1081	
75.	1.00			
3.	-1.00		1080	
257.	1.00	54 203		
25.	-1.00		1079	
47.	1.00			
15.	-1.00		1078	
251.	1.00			
15.	-1.00		1077	
72.	1.00			
14.	-1.00			
64.	1.00		1076	
22.	-1.00			
56.	1.00			
10.	-1.00			
224.	1.00			
22.	-1.00		1075	
105.	1.00			
28.	-1.00			
77.	1.00		1074	
20.	-1.00			
41.	1.00			
5.	-1.00			
40.	1.00			
10.	-1.00			
45.	1.00			
10.	-1.00			
67.	1.00			
12.	-1.00		1073	
78.	1.00			
18.	-1.00			
57.	1.00			
10.	-1.00			
35.	1.00			
15.	-1.00			
35.	1.00			
31.	-1.00			
35.	1.00		1072	
10.	-1.00			

Thickness	Polarity	Time Series	Sec. No.	Zone	Zone
50.	1.00	4096B		Marcak/Tatum Zone	Gibbosus Subzone
13.	-1.00				
139.	1.00		1071		
13.	-1.00				
25.	1.00				
5.	-1.00				
45.	1.00		1070		
15.	-1.00				
35.	1.00				
12.	-1.00				
206.	1.00				
10.	-1.00		1069		
50.	1.00				
20.	-1.00				
35.	1.00				
11.	-1.00		1068		
305.	1.00				
35.	-1.00		1067		
285.	1.00				
18.	-1.00		1066		
40.	1.00		1065		
38.	-1.00		1064		
50.	1.00		1063		
43.	-1.00		1062		
128.	1.00				
30.	-1.00		1061		
160.	1.00				
27.	-1.00		1058-1060		
53.	1.00		1059		
18.	-1.00		1058		
73.	1.00		1057		
60.	-1.00		1056		
58.	1.00		1055		
45.	-1.00		1054		
315.	1.00		1053		
36.	-1.00		1052		
175.	1.00				
74.	-1.00		1051		
70.	1.00				
28.	-1.00		1050		
105.	1.00		1049		
34.	-1.00		1048		
225.	1.00		1047		
17.	-1.00		1046		
51.	1.00				
93.	-1.00		1045		
71.	1.00				
39.	-1.00		1044		
88.	1.00				
45.	-1.00		1043		
70.	1.00				
47.	-1.00		1042		
78.	1.00				
34.	-1.00		1041		
			1040		
			1039		
			1038		

72
143

Thickness	Polarity	Time Series	Sec. No	Zone	Zone
77.	1.00	4096A	1037		Subnodosus Subzone
4.	-1.00		1036		
379.	1.00		1035		
51.	-1.00		1034		
61.	1.00		1033		
10.	-1.00		1032		
127.	1.00		1031		
31.	-1.00		1030		
42.	1.00		1029		
32.	-1.00		1028		
86.	1.00		1027		
45.	-1.00		1026		
98.	1.00		1025		
22.	-1.00		1024		
268.	1.00		1023		
120.	-1.00		1022		
139.	1.00				
14.	-1.00		1021		
181.	1.00				
20.	-1.00				
41.	1.00		1020		
50.	-1.00				
46.	1.00		1019		
57.	-1.00		1018		
62.	1.00		1017		
9.	-1.00		1016		
212.	1.00		1015		
35.	-1.00		1014		
87.	1.00		1013		
29.	-1.00		1012		
67.	1.00		1011		
18.	-1.00		1010		
88.	1.00		1009		
33.	-1.00		1008		
143.	1.00		1007		
27.	-1.00		1006		
42.	1.00		1005		
12.	-1.00				
45.	1.00		1004		
20.	-1.00		1003		
38.	1.00				
8.	-1.00		1002		
284.	1.00				
18.	-1.00		1001		
440.	1.00				
90.	-1.00		1000		
100.	1.00		999		
20.	-1.00				
190.	1.00		998		

43
2

Darnel Zone

6.5 Time series for the Middle Pliensbachian section at Breggia Gorge.

SAMPLE INTERVAL = 1 cm

TOTAL THICKNESS MEASURED = 1731 cm

CODES
LIMESTONE = +1.0
MARL = 0.0
SHALE = -1.0

THICKNESS	CODE	TIME SERIES	BED No	ZONE
4.	-1.00			
29.	1.00	27/2		
1.	-1.00			
4.	1.00			
1.	-1.00			
13.	1.00			
1.	-1.00			
3.	1.00		982	
1.	-1.00			
6.	1.00			
2.	-1.00			
15.	1.00			
1.	-1.00			
8.	1.00			
16.	-1.00		981	
36.	1.00	512C	980	
10.	-1.00		979	
36.	1.00		978	
7.	-1.00		977	
42.	1.00		976	
17.	-1.00		975	
25.	1.00			
39.	0.00		974	
41.	1.00			
14.	-1.00		973	
38.	1.00		972	
10.	-1.00		971	
35.	1.00		970	
17.	-1.00		969	
42.	1.00		968	
7.	-1.00		967	
51.	1.00	22/23		
3.	-1.00			
22.	1.00		966	
2.	-1.00			
37.	1.00	20/17		
12.	-1.00		965	
40.	1.00		964	
11.	-1.00		963	
38.	1.00		962	
7.	-1.00		961	
38.	1.00		960	
5.	-1.00		959	
39.	1.00		958	
13.	-1.00		957	
37.	1.00		956	
7.	-1.00		955	
5.	1.00	512B		
2.	-1.00		954	
38.	1.00			
8.	-1.00		953	
22.	1.00			
2.	-1.00		952	
20.	1.00			

THICKNESS	CODE	TIME SERIES	BED No	ZONE
6.	-1.00		951	
51.	1.00			
1.	-1.00			
39.	1.00			
8.	-1.00		950	
21.	1.00			
1.	-1.00			
20.	1.00			
11.	-1.00	4/7	949	
41.	1.00	1024	948	
14.	-1.00		947	
15.	1.00			
8.	0.00		946	
19.	1.00			
14.	-1.00		945	
71.	1.00			
17.	0.00		944	
15.	1.00			
3.	-1.00		943	
29.	1.00		942	
10.	-1.00		941	
25.	1.00			
2.	-1.00	512A	940	
15.	1.00			
9.	-1.00		939	
20.	1.00			
1.	-1.00		938	
19.	1.00			
11.	-1.00		937	
43.	1.00		936	
8.	-1.00		935	
58.	1.00		934	
5.	-1.00			
2.	1.00		933	
3.	-1.00			
13.	1.00			
8.	0.00			
10.	1.00	7/3	932	
3.	0.00			
23.	1.00			
16.	-1.00		931	
34.	1.00			
9.	-1.00		930	

MARGARITATUS ZONE

DAVOEI ZONE

IBEX ZONE

6.6 Time series for the Belemnite Marls, Charmouth.

SAMPLE INTERVAL = 1 cm

TOTAL THICKNESS MEASURED = 1067 cm

CODES

ARGILLACEOUS	CALCILUTITE	= +1.0
CALCAREOUS	CLAY	= 0.0
BITUMINOUS	SHALE	= -1.0

THICKNESS	CODE
9.	1.00
10.	0.00
5.	1.00
8.	0.00
6.	1.00
32.	-1.00
21.	1.00
16.	0.00
10.	1.00
43.	-1.00
7.	1.00
11.	0.00
43.	1.00
12.	0.00
9.	1.00
25.	0.00
7.	1.00
11.	0.00
7.	1.00
9.	0.00
6.	1.00
15.	0.00
13.	1.00
7.	0.00
11.	1.00
9.	0.00
19.	1.00
12.	0.00
13.	1.00
13.	0.00
14.	1.00
12.	0.00
11.	1.00
9.	-1.00
3.	0.00
12.	1.00
5.	0.00
12.	-1.00
3.	0.00
22.	1.00
10.	0.00
24.	1.00
24.	0.00
26.	1.00
10.	-1.00
25.	1.00
6.	0.00
22.	1.00
16.	0.00
8.	1.00
31.	0.00
33.	-1.00
14.	1.00
18.	0.00

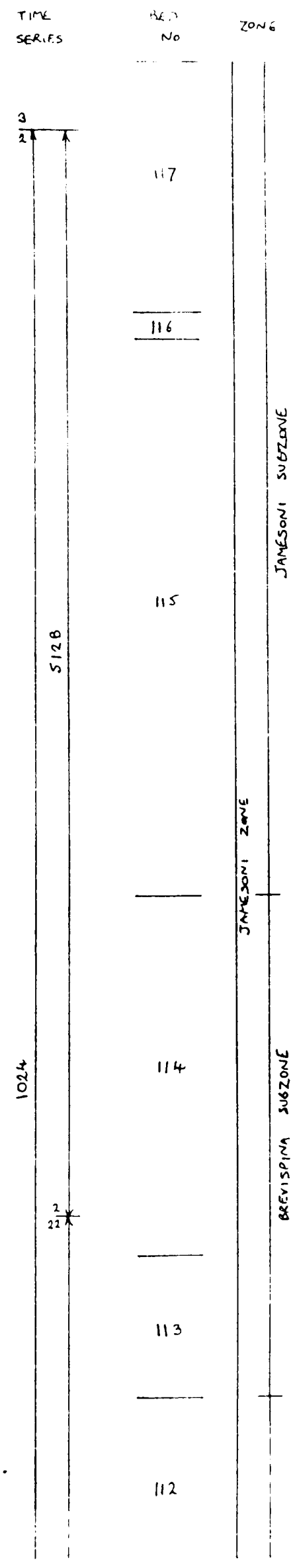

THICKNESS	CODE
8.	1.00
22.	0.00
20.	1.00
18.	0.00
16.	1.00
35.	0.00
36.	1.00
8.	0.00
15.	-1.00
31.	0.00
15.	-1.00
10.	1.00
44.	0.00

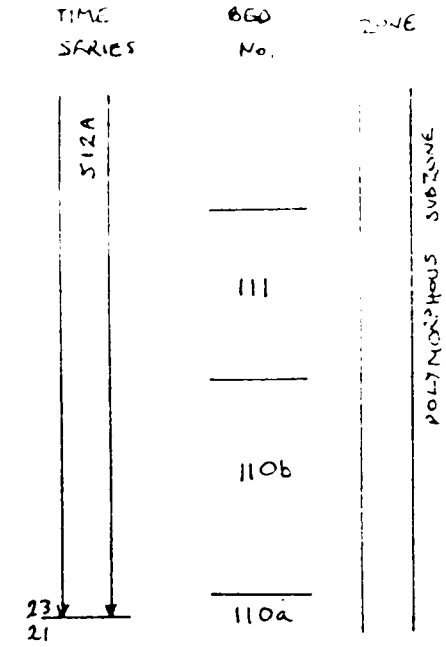

6.7 Time series for the 'Siliceous Shales', Robin Hood's Bay.

SAMPLE INTERVAL = 1cm

TOTAL THICKNESS MEASURED = 1236 cm

CODES

ARGILLACEOUS SANDSTONE = +1.0

SILTY SANDSTONE = 0.0

SILTY SHALES / MUDSTONES = -1.0

THICKNESS	CODE
60.	-1.00
14.	0.00
85.	-1.00
16.	0.00
32.	-1.00
8.	0.00
23.	-1.00
5.	0.00
18.	-1.00
7.	1.00
4.	-1.00
17.	1.00
102.	-1.00
10.	0.00
4.	-1.00
15.	1.00
58.	0.00
34.	-1.00
10.	0.00
18.	-1.00
7.	1.00
11.	0.00
8.	1.00
11.	0.00
11.	1.00
40.	-1.00
76.	0.00
19.	-1.00
40.	0.00
1.	1.00
14.	-1.00
17.	0.00
131.	-1.00
9.	0.00
56.	1.00
30.	0.00
72.	1.00
1.	-1.00
19.	0.00
100.	-1.00
21.	0.00
2.	-1.00

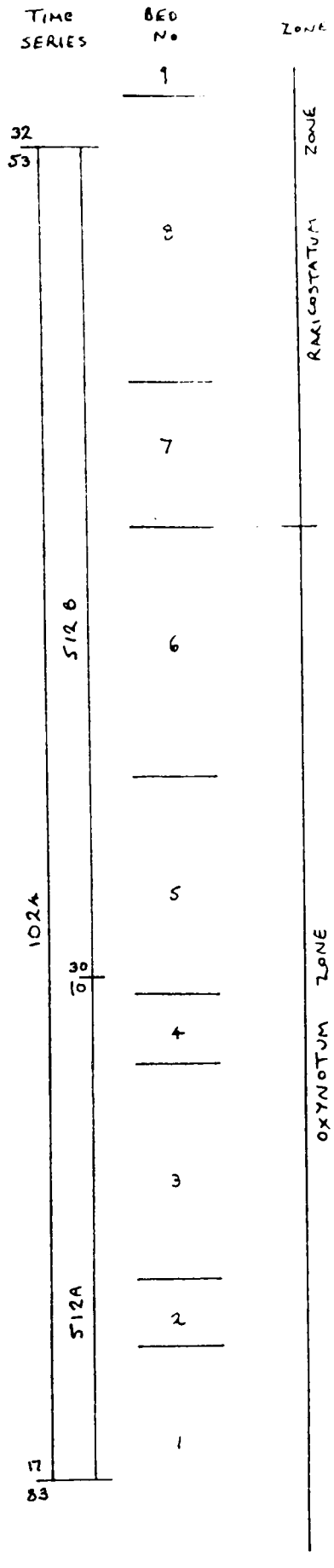

FROM SELLWOOD, 1970

6.8 Time series for the Upper Birkhill Shales, Dob's Linn.

SAMPLE INTERVAL = 1mm

TOTAL THICKNESS MEASURED = 7291mm

THICKNESS MINUS PYROCLASTIC CLAYSTONE = 4998mm

CODES:
GREY MUDSTONE = +1.0
BLACK MUDSTONE −1.0

PYROCLASTIC CLAYSTONE BEDS NOT INCLUDED BELOW

THICKNESS	CODE
6.	-1.00
44.	1.00
54.	-1.00
591.	1.00
30.	-1.00
12.	1.00
1.	-1.00
2.	1.00
1.	-1.00
135.	1.00
1.	-1.00
7.	1.00
41.	-1.00
4.	1.00
2.	-1.00
125.	1.00
1.	-1.00
4.	1.00
1.	-1.00
2.	1.00
1.	-1.00
13.	1.00
1.	-1.00
1.	1.00
43.	-1.00
9.	1.00
1.	-1.00
1.	1.00
1.	-1.00
1.	1.00
1.	-1.00
17.	1.00
1.	-1.00
26.	1.00
4.	-1.00
75.	1.00
44.	-1.00
719.	1.00
15.	-1.00
39.	1.00
10.	-1.00
9.	1.00
1.	-1.00
9.	1.00
19.	-1.00
10.	1.00
5.	-1.00
131.	1.00
7.	-1.00
39.	1.00
83.	-1.00
9.	1.00
180.	-1.00
154.	1.00

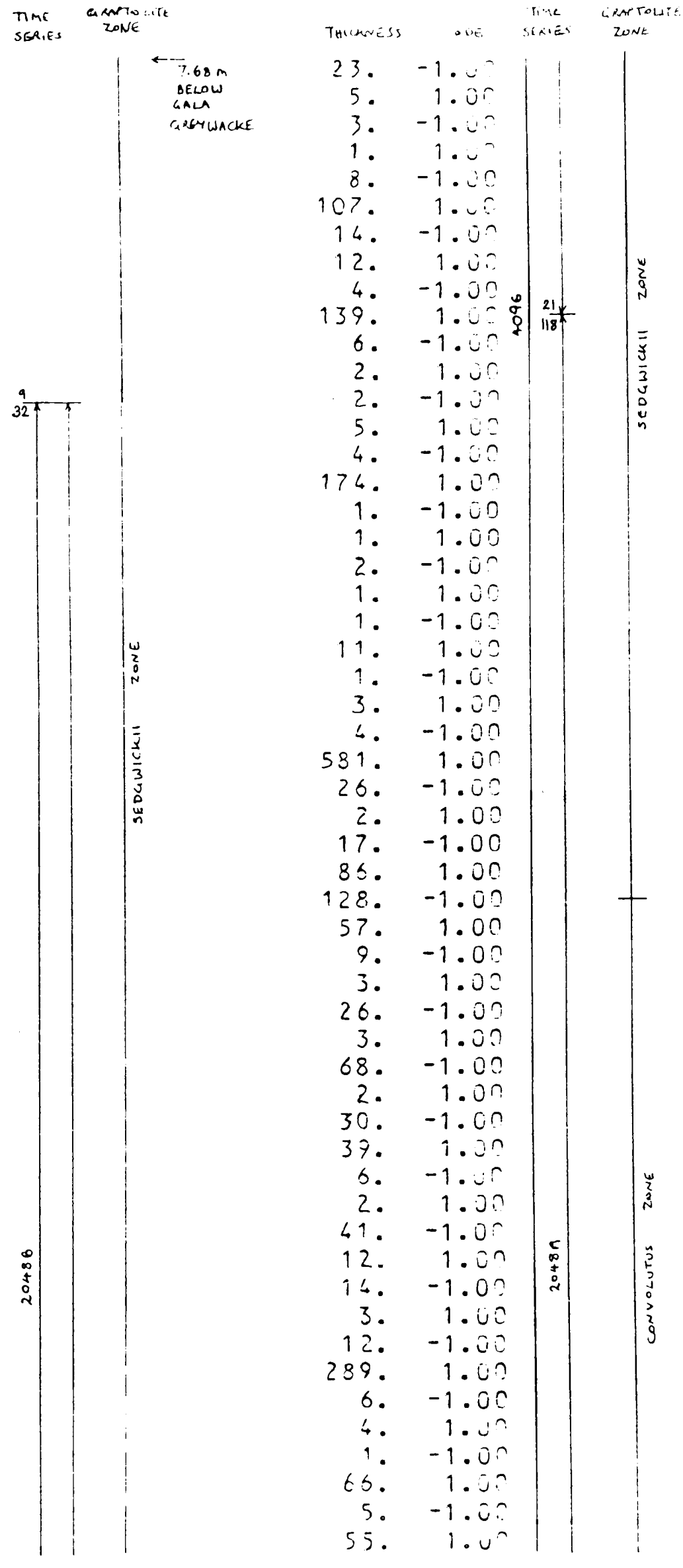

THICKNESS	CODE
23.	-1.00
5.	1.00
3.	-1.00
1.	1.00
8.	-1.00
107.	1.00
14.	-1.00
12.	1.00
4.	-1.00
139.	1.00
6.	-1.00
2.	1.00
2.	-1.00
5.	1.00
4.	-1.00
174.	1.00
1.	-1.00
1.	1.00
2.	-1.00
1.	1.00
1.	-1.00
11.	1.00
1.	-1.00
3.	1.00
4.	-1.00
581.	1.00
26.	-1.00
2.	1.00
17.	-1.00
86.	1.00
128.	-1.00
57.	1.00
9.	-1.00
3.	1.00
26.	-1.00
3.	1.00
68.	-1.00
2.	1.00
30.	-1.00
39.	1.00
6.	-1.00
2.	1.00
41.	-1.00
12.	1.00
14.	-1.00
3.	1.00
12.	-1.00
289.	1.00
6.	-1.00
4.	1.00
1.	-1.00
66.	1.00
5.	-1.00
55.	1.00

THICKNESS	ODE	TIME SERIES	CONTOUR ZONE
2.	-1.00		
32.	1.00		
1.	-1.00		
8.	1.00		
3.	-1.00		
2.	1.00		
7.	-1.00		
10.	1.00		
41.	-1.00		
3.	1.00		
10.	-1.00		

FLOWERS
BLUE LIAS